Pathogenic impact of immune-related cells in Batten disease

Kühl, Thomas

Awarding institution:
King's College London

Title: Pathogenic impact of immune-related cells in Batten disease

Author: Thomas Kühl

Pathogenic impact of immune-related cells in Batten disease

Thesis submitted for the degree of

Doctor of Philosophy

Thomas G. Kühl

Department of Neuroscience

Institute of Psychiatry

King's College London

2012

Abstract

The neuronal ceroid lipofuscinoses (NCLs or Batten disease) are inherited neurodegenerative diseases of children. In all types of NCL glial activation, the innate immune response of the brain, precedes neurodegeneration. However, it is unclear whether adaptive immune responses are also involved in these diseases, or if they directly contribute to disease pathogenesis. Therefore, we examined the role of adaptive immune cells in mouse models of Infantile NCL (*Ppt1*$^{-/-}$ mice) and Juvenile NCL (*Cln3*$^{-/-}$ mice) by identifying, localising, and subsequently genetically removing immune components.

Characterising the adaptive immune response within *Ppt1*$^{-/-}$ and *Cln3*$^{-/-}$ mice, we revealed evidence for progressive CNS infiltration by different classes of T-cells in both forms of NCL. To analyse the pathogenic impact of these lymphocytes, we crossbred *Ppt1*$^{-/-}$ mutants with mice deficient in Rag-1, which lack T- and B-lymphocytes. Disease progression was significantly delayed in immune deficient *Ppt1*$^{-/-}$/*Rag-1*$^{-/-}$ mice, which displayed ameliorated neuroinflammation and neuron loss. We also crossed our Infantile and Juvenile NCL mouse models with mice deficient in sialoadhesin (Sn), a binding protein found on macrophages and microglia, and is involved in pro-inflammatory T-cell regulation. Disease progression was also slowed down, with significantly increased neuron survival in both *Sn* deficient NCL mice. However, contrasting effects on glial activation were observed between *Ppt1*$^{-/-}$/*Sn*$^{-/-}$ and *Cln3*$^{-/-}$/*Sn*$^{-/-}$ mice. Whereas glial activation was only marginally attenuated in *Cln3*$^{-/-}$/*Sn*$^{-/-}$ mice, significantly decreased microglial activation and enhanced astrocytosis were observed in *Ppt1*$^{-/-}$/*Sn*$^{-/-}$ mice. These latter findings suggest an unexpected link between macrophage-expressed Sn and astrocytosis in *Ppt1*$^{-/-}$ mice.

Taken together, our findings prove that adaptive immune cells and sialoadhesin each appear to contribute to disease progression in Infantile and Juvenile NCL mice. Therefore, both immune components could prove to be suitable therapeutic targets for these fatal disorders.

Statement of originality

All histological, qualitative and quantitative analyses of neuropathology in the brains of *Ppt1*$^{-/-}$, *Cln3*$^{-/-}$, *Ppt1*$^{-/-}$/*Rag-1*$^{-/-}$, *Ppt1*$^{-/-}$/*Sv*$^{-/-}$, *Cln3*$^{-/-}$/*Sv*$^{-/-}$ and corresponding control mice presented in this thesis were performed at the Pediatric Storage Disorders Laboratory (PSDL), Institute of Psychiatry (IoP) by Thomas Kühl, under the supervision of Prof. Jonathan Cooper and Dr. Brenda Williams. In parallel, pathology in the retinae and optic nerves from the same mice was assessed by our collaborators Janos Groh and Prof. Rudolf Martini (University of Würzburg, Germany), whose advice on immunology was also essential for this project.

All molecular analyses of mouse genotypes were carried out at the Institute of Psychiatry (IoP) by Thomas Kühl, Dr. Andrew Wong or Michael Licudi, or by our collaborators in Würzburg.

Cross breeding and tissue harvesting from *Ppt1*$^{-/-}$, *Ppt1*$^{-/-}$/*Sv*$^{-/-}$, *Ppt1*$^{-/-}$/*Rag-1*$^{-/-}$ and corresponding control (*Rag-1*$^{-/-}$, *Sv*$^{-/-}$ and WT) mice was carried out in the Biological Services Unit, at the James Black Centre, Denmark Hill, London by Thomas Kühl and Dr. Andrew Wong. Additional *Ppt1*$^{-/-}$ tissue was supplied by Prof. Mark Sands, University of Washington Medical School, St Louis, MO, USA. Tissue from *Cln3*$^{-/-}$, *Cln3*$^{-/-}$/*Sv*$^{-/-}$ and additional *Ppt1*$^{-/-}$/*Rag-1*$^{-/-}$, *Ppt1*$^{-/-}$/*Sv*$^{-/-}$ and *Sv*$^{-/-}$ mice was generated in Würzburg.

All animal procedures were carried out in accordance with Institutional and UK Animals (Scientific Procedures) Act (1986) guidelines or under the guidance of the respective local university committee on animal use (if procedures were performed by collaborators outside the UK).

This studentship was generously funded by the NCL Stiftung, the Batten Disease Support and Research Association (BDSRA) and the Batten Disease Family Association (BDFA).

Publication arising from this thesis

J Groh, **TG Kühl**, S Duckett, CW Ip, M Mirza, T Langmann, JD Cooper, R Martini (2013) Immune cells perturb axons and impair neuronal survival in a mouse model of Infantile Neuronal Ceroid Lipofuscinosis, *Brain*, in press.

Acknowledgements

As the journey of my PhD comes to an end, I would like to take this opportunity to reflect upon this remarkable time in my life. Yes, finally, I conquered the long and sometimes windy path over the 'PhD-mountain'. Indeed, doing a PhD is a bit like hiking through a mountainous landscape. You start off with a big backpack full of energy and excitement driven by the desire to discover new things, hoping to widen yours and everybody's horizon, but also determined to enjoy yourself. The path is long, with a lot of ups and downs, sometimes you are blessed with sunshine, other times thunderstorms bring a downpour of rain and you wish you could turn around. However, you are the privileged one who can explore new territory and engross yourself in some of the most stunning and breath-taking sceneries along the way. Even better, at the end, after you finally reach the other side of the 'PhD-mountain', you can not only look back on priceless memories that last forever, but also move closer to your goal of gaining greater knowledge and helping people. Nevertheless, as mountains can be very dangerous, you have to be constantly careful and make sure you never walk alone. Therefore, I am grateful for all the people who accompanied me on my path. I want to thank all those, who joined me on this adventure no matter if it was only for a short period or throughout the whole trip. But special thanks go to several particular 'mountaineers'.

First of all, my sincere thanks go to my two 'mountain guides' and supervisors, Jonathan Cooper and Brenda Williams, for ensuring a safe journey without any big missteps. I could not have done it without you both! But particularly, a big thank you to Jon for constantly pointing me into the right direction, helping me to overcome steep slopes by pulling me up with a vital rope and of course also for introducing me to the Southampton football club ('The Saints').

I owe a big thank you to all the past and current PSDL members for making my PhD such a great experience. It was my biggest pleasure to work with them all, to share many laughing moments together and most of all, to be converted into a chocolate and cake addict. Not only were they excellent colleagues, but I am now also proud to call many of them my friends. In particular, I want to give many thanks to my two former 'PhD buddies': Sybille Dihanich ('Miss Dinacchi') for all her Austrian influence, kindness and support throughout my PhD! Sybille not only made me always

feel very welcome in the PSDL, but also introduced me to one of my favourite songs! And Sarah Pressey (the 'bowling queen') for all her support, constant help and, of course, singing microscope room sessions! A huge thank you also goes to Andrew Wong (the 'rescuer with an iPhone') who not only helped me with all mouse related parts of this study or supplied me with scientific advice, but also shared the trendiest corner of the PSDL with me. To Lotta Parviainen (the 'mother of the astrocytes') who with her charm, sarcasm and cheekiness kept me entertained. To Helen Brooks (the 'beauty magazine addict') who loves her crayons, stem cells and always had a kind word for me, even while learning 'coffee break French' in the microscope room. To Yewande Pearse (the 'cerebellum of the PSDL') who represents the next generation of trendy PhD students with her constantly happy smile on her face. To Michael Licudi ('Mike Lucchidi') who generously assisted our work in the PSDL with a flavour of heavy metal. To Federica Buonocore ('Lisa') who was always there for me during my PhD and demonstrated compelling passion for PCRs. To Ahad Rahim ('Mr UCL') who delighted us with occasional visits, countered my humour well and told us stories about dining with Chris Martin. To Megan O'Hare ('Miss Oh hair') who prefers drosophila over mouse brains and entertained our lunch breaks with quirky conversations. To our Finnish friends who visited the PSDL several times over the years and introduced the famous 'cheese and wine' events: Mervi Kuronen ('Miss Capoeira') with whom I was allowed to philosophise about the world and its purpose on several occasions, Mia Schmiedt (the 'horse whisperer') who probably has the kindest heart of the whole of Finland and Germany together. Furthermore, special thanks also to the 'army' of Master Students who passed through, too many to mention, but each one of them contributed his/her part to make my PhD a great experience. Special mention is due to Scott Nelson ('superman') who taught me how to eat a whole chicken for lunch and changed my life in London by selling his bike to me, to Klemens Höfer ('Millhouse') who introduced me to 'Mundl' and the Austrian accent, to Srishti Mukherji ('Sushi' or 'Halfshiva'), Sarmi Sri ('Salami' or 'Mobile queen'), Ewelina Lenartowicz ('Polish tornado'), Hemanth Ramesh ('Big Srishti') and Steven Duckett ('The survivor') who all helped and supported me over the finish line with fun conversations and much appreciated motivation.

Furthermore, I want to give my infinite thanks to all my friends here in London and at home in Switzerland. They were the true pillars and foundation of this work by

constantly believing in me, giving me joy in life, keeping me on the right path and most of all being there for me. These include here in London Gareth Whatmore ('Mr Bolu'), Samuel Adams ('Netcrawler'), Doug Richardson ('Skippy'), Vanessa Cretoux ('Frenchy'), Nabs Allybokus ('Nabyliia'), Carla Cheetham ('Crazy Cheetham') and in Switzerland, most of all, Dominik Leitner ('s Mathegenie'), David Mäder ('dr Steinerschüler'), Samuel Burckhardt ('Sämu') and many more…

This leaves me to thank the closest people in my life who not only tolerated all the ups and downs of this PhD but who supported me with their deepest love. I owe eternal thanks to my mother ('Mummy Cool') who helped me with proof reading and gave me continuous guidance and to my father ('Daddy Cool') who always believed in and supported me. They are the best parents one could wish for! I also want to thank my brother Richard ('Bruederhärz') who not only inspired me, but in whom I can trust no matter what. And finally, I want to thank Gina Plummer ('Princess Plummy') for her never-ending patience and her unconditional love that gave me strength and happiness throughout my PhD.

Thus, with all these precious mountain experiences and dear companions in my heart and mind, my journey over the 'PhD-mountain' ends here. As usual in mountainous landscapes, once you have conquered one mountain, there are always new summits in front of you. But it is time for me to pass on the baton to the next adventurers who can lead us over the remaining mountains. I wish them luck and success, because this great journey is not yet finished and the overall purpose still awaits completion. I wholeheartedly hope and have faith that one day this journey will lead to an open space where there are no mountains left to climb, and where we can sow our collected knowledge on fertile soil to convert it into a fruitful harvest from which generations to come will be able to reap.

In this sense, I want to thank all the families who gave me the opportunity, the trust and the privilege to help and be part of this joint journey in seeking a cure to combat Batten disease.

'Learn from yesterday, live for today, hope for tomorrow.'

Albert Einstein

'Lasciate ogne speranza, voi ch'entrate'

Dante Alighieri

La Divina Commedia, Canto III, line 9

Table of Contents

Table of Figures

List of Tables

List of Abbreviations

A	Adenine
AAD	Anterior amygdaloid area
AAV	Adeno-associated virus
AC	Anterior commissural nucleus
AD	Anterodorsal thalamic nucleus
AHipM	Amygdalohippocampal area
AID/V	Agranular insular cortex, dorsal/ventral
ALS	Amyotrophic lateral sclerosis
AM	Anteromedial thalamic nucleus
AMPA	2-amino-3-(3-hydroxy-5-methyl-isoxazol-4-yl)propanoic acid
ANCL	Adult neuronal ceroid lipofuscinoscis
ANOVA	Analysis of variance
APC	Antigen presenting cell
APir	Amygdalopiriform transition area
asf	Area sampling fraction
ATP	Adenosine-5'-triphosphate
ATP13A2	Probable cation-transporting ATPase 13A2
AuD/V	Secondary auditory cortex, dorsal/ventral
Au1	Primary auditory cortex
AV	Anteroventral thalamic nucleus
AVDM/VL	Anteroventral thalamic nucleus, dorsomedial/ventrolateral part
BBB	Blood brain barrier
B-cell	Bursa-derived cell (in mammals: bone-marrow-derived), lymphocyte
BCR	B-cell receptor
BLA	Basolateral amygdaloid nucleus
BMT	Bone marrow transplantation
B220	CD45R B-cell isoform with 220 kDa weight
C	Cytosine
CAM	Cell adhesion molecules
CA1-3	Cornu Ammonis 1-3, subfield of the hippocampus
Ca^{2+}	Calcium
CD	Cluster of differentiation
CD x	CD-antigen x (x = 4, 8, 45, 68, etc.)
CE	Coefficient of error
CeC/M	Central amygdaloid nucleus, capsular part/medial division
ClC	Central nucleus of the inferior colliculus
Cig1/2	Cingulate cortex area 1/2
CLCN6	Chloride transport protein 6
CLC7	Chloride channel 7
CLN1-14	Ceroid-lipofuscinosis, neuronal 1-14 gene/protein
CTSD	Cathepsin D
CTSF	Cathepsin F
CM	Central medial thalamic nucleus
CNS	Central nervous system
CSF	Cerebrospinal fluid

CVO	Circumventricular organs
C57Bl	C57 black 6 mouse strain
DAB	3,3 – diaminobenzidine tetrahydrochloride
DC	Dendritic cells
DEn	Dorsal endopiriform nucleus
DG	Dentate gyrus
DNA	Deoxyribonucleic acid
DNAJC5	DnaJ homolog subfamily C member 5 gene/protein
DPX	Di-n-butyl Phthalate in Xylene
EAE	Experimental autoimmune encephalomyelitis
ECIC	External cortex of the inferior colliculus
Eo	Eosinophil
ER	Endoplasmic reticulum
ERT	Enzyme replacement therap
ES	Embryonic stem cell
FACS	Fluorescence-activated cells sorting
F1/2	First/second filial generation
F4/80	F4/80 glycoprotein
G	Guanine
GABA	γ-aminobutyric acid
GFAP	Glial fibrillary acidic protein
GAGs	Glycosaminoglycans
GFP	Green fluorescent protein
GM1/2	Monosialic ganglioside 1/2
GRB2	Growth factor-receptor-bound protein 2
GRN	Granulin gene/protein
GP	Globus pallidus
HDB	Nucleus of the horizontal limb of the diagonal band
HLDA	Human leukocyte differentiation antigens workshop
HSC	aematopoietic stem cell
hsf	Height sampling fraction
huNSCs	Human neural stem cell
ICAM-1	Intercellular adhesion molecule 1
IF	Intermediate filament
IFN-α/γ	Interferon-alpha/gamma
IGF	Insulin-like growth factor
IgG/M	Immunoglobulin G/M
IgSF	Immunoglobulin superfamily
IgV	V-like immunoglobulin domain
IL-x	Interleukin-x (x = 1β, 10, 12, 17, 35 etc.)
I.M.S.	Industrial methylated spirits
INCL	Infantile neuronal ceroid lipofuscinosis
IPACM/L	Interstitial nucleus of posterior limb of anterior commissure, medial/lateral part
ISF	Interstitial fluid
ITIM	Immunoreceptor tyrosin-based inhibitory motif
JNCL	Juvenile neuronal ceroid lipofuscinosis

KCTD7	Potassium channel tetramerisation domain containing 7
KO	Knockout
LAMP	Lysosomal-associated membrane protein
LEnt	Lateral entorhinal cortex
LDTg	Laterodorsal tegmental nucleus
LIMP2	Lysosomal integral membrane protein 2
LINCL	Late Infantile neuronal ceroid lipofuscinosis
LGP	Lateral globus pallidus
LGNd	Dorsal lateral geniculate nucleus
LFA-1	Lymphocyte function-associated antigen 1
LO	Lateral orbital cortex
LPLR/MR	lateral posterior thalamic nucleus, laterorostral/mediocaudal part
LPS	Lipopolysaccharide
MAG	Myelin-asociated glycoprotein
MCPO	Magnocellular preoptic nucleus
MD	Mediodorsal thalamic nucleus
MDM/L	Mediodorsal thalamic nuclei, medial/lateral part
Med	Medulla of lymph node
MFSD8	Major facilitator superfamily domain containing 8
MG	Medial geniculate nucleus
MGV/D/M	Medial geniculate nucleus, ventral/dorsal/medial part
MGL1	Macrophage galactose-type lectin
MHC	Major histocompatibility complex
MI	Mitral cell layer of the olfactory bulb
MMP	Matrix metalloproteinase
MPS	Mucopolysaccharidosis
MR	Mannose receptor
mRNA	Messenger ribonucleic acid
MZM	Marginal zone metallophilic
M-6-P	Mannose-6-phosphate
M1/2	Motor cortex 1/2
M6PR	Mannose 6-phosphate receptor
NCAM	Neural Cell Adhesion Molecule
NeuN	Neuronal nuclei protein/marker
NK	Natural killer cell
NKT/iNKT	Natural killer T-cell/invariant (TCR) natural killer T-cell
NMDA	N-Methyl-D-aspartate
NO	Nitric oxide
NPC	Neuroprogenitor cell
NPC1	Nieman-Pick disease, type 1
PAMP	Pathogen-associated molecular pattern
PBS	Phosphate buffered Saline
PCR	Polymerase chain reaction
PECAM-1	Platelet endothelial cell adhesion molecule
PFA	Paraformaldehyde
Pir	Piriform cortex
PLP	Proteolipid protein

PMCo	Posteromedial cortical amygdaloid nucleus
Pn	Pontine nuclei
PO	Posterior thalamic nuclei
Ppt1	Palmitoyl protein thioesterase 1
PRR	Pattern recognition receptor
Pr5VL	Principal sensory trigeminal nucleus
PSDL	Pediatric Storage Disorders Laboratory
PSGL-1	P-selectin glycoprotein ligand 1
PTP	Protein tyrosine phosophatase
PTPRC	Protein tyrosine phosphatase receptor type C
RAG1/2	Recombination activating gene 1/2
RANTES	Regulated and normal T-cell expressed and secreted protein
Re	Reuniens thalamic nucleus
RER	Rough endoplasmic reticulum
ROI	Region of interest
RMC	Red nucleus, magnocellular part
RPC	Red nucleus, parvicellular part
RSA/G	The retrosplenial (a)granular cortex
RtTg	Reticulotegmental nucleus of the pons
SEM	Standard error of the mean
Sema-3A	Semaphorin class 3A
SER	Sheep erythrocyte receptor
SGSH	N-sulphoglucosamine sulphohydrolase
Siglec	Sialic-acid binding immunoglobulin-like lectin
Sn	Sialoadhesin
SNAP	Soluble NSF (N-ethylmaleimide-sensitive factor) attachment protein
SNARE	SNAP receptor
SS	Subcapsular sinus
ssf	Section sampling fraction
SYT7	Synaptotagmin-7
S1BF	Primary somatosensory barrel field
S1HL/S1FL	Primary somatosensory cortex, hind-/forelimb region
S2	Secondary somatosensory cortex
T	Thymine
T-cell	Thymus-derived cell
TBS(-T)	Tris buffered saline (with triton)
TCR	T-cell receptor
Th1/2	T-helper cell 1/2
Th17	T-helper cell producing IL-17
TIBDC	The International Batten Disease Consortium
TGF- β	Transforming growth factor β
TNF-α	Tumour necrosis factor α
TNG	Trans-Golgi-network
TPP1/2	Tripeptidyl-peptidase 1/2
Tris	Tris-(hydroxymethyl)-aminomethane
V-ATPase	Vacuolar-type H^+-ATPase
VCAM-1	Vascular cell adhesion molecule 1

V(D)J	Variable diverse and joining genes
VEn	Ventral endopiriform nucleus
Vim	Vimentin
VL	Ventrolateral thalamic nucleus
VLA-1	Very late antigen 1 (integrin on leukocytes)
VLL	Ventral nucleus of lateral lemniscus
VP	Ventral pallidum
VPM/VPL	Ventral posteromedial and posterolateral thalamic nucleus
V1	Visual cortex
WT	Wildtype
129/Sv	129 mouse sub-strain with steel mutation
μMT	Heavy chain μ of immunoglobulin M gene
-/-	Mutant

Chapter 1

Introduction

The neuronal ceroid lipofuscinoses (NCLs) are a group of recessively inherited lysosomal diseases that affect mainly children (Santavuori, 1988). The NCLs are collectively considered to be the most common inherited neurodegenerative storage disorders of childhood (Haltia, 2006; Jalanko and Braulke, 2009). They are now classified as lysosomal storage disorders (LSDs), which characteristically due to a specific monogenetic defect, impact the function of the endosomal/lysosomal system (Neufeld, 1991; Schultz *et al.*, 2011). The NCLs in particular have widely varying ages of onset, rates of progression and underlying disease mechanisms, but ultimately lead to similar clinical manifestations (Cooper, 2010). The neuropathological features of the different forms of NCLs have been systematically characterised in animal models, and well-defined landmarks of disease progression have been identified (Bible *et al.*, 2004; Pontikis *et al.*, 2004; Oswald *et al.*, 2005; Pontikis *et al.*, 2005; Kielar *et al.*, 2007; Partanen *et al.*, 2008; von Schantz *et al.*, 2009; Kuronen *et al.*, 2012; Schmiedt *et al.*, 2012), with early glial activation and selective neuron loss in the thalamocortical system being identified as key pathologies. Whereas the innate immune response in terms of this glial activation has been well characterised (Pontikis *et al.*, 2005; Kielar *et al.*, 2007), the role of the adaptive and peripheral immune responses in the NCLs have so far been overlooked. Inspired by recent evidence of the presence and putative role of adaptive immune cells in NCL disease pathogenesis (Macauley *et al.*, 2011; Seehafer *et al.*, 2011), we created immune deficient INCL (*Ppt1*$^{-/-}$) and JNCL (*Cln3*$^{-/-}$) mice. This was achieved by crossing our NCL mouse models with mice deficient in Rag-1, which is essential for the maturation of T- and B-cells, and also by crossing with mice deficient in sialoadhesin (Sn), a T-cell activating binding protein expressed on macrophages, and subsequently characterising the impact of these immune deficiencies in the resultant double knockout (*Ppt1*$^{-/-}$/*Rag-1*$^{-/-}$, *Ppt1*$^{-/-}$/*Sn*$^{-/-}$ and *Cln3*$^{-/-}$/*Sn*$^{-/-}$) mice. As such, this thesis provides new insights into the role of adaptive immune cells and macrophages in the pathogenesis of two NCL forms, and potentially lays the foundation for treatment strategies targeting the immune system in NCLs.

1.1 Lysosomal storage disorders (LSDs)

Since the discovery of the lysosome (De Duve *et al.*, 1955), it took about 10 years for the concept of LSDs to become established (Hers, 1965), and defined as being a group of inherited disorders all displaying an intra-lysosomal accumulation of undegraded material or catabolic products (Hers, 1972). Over 70 different LSDs have been

identified and these have been intensively studied and characterised over the years (Neufeld, 1991; Lachmann, 2010; Schultz *et al.*, 2011). Although individually rare, the LSDs have a collective incidence of approximately 1 in 7,700 live births (Meikle *et al.*, 1999), and therefore place a significant burden on health systems worldwide. However, this number is probably an underestimate because many LSDs remain undiagnosed due to their variable and heterogeneous clinical presentation. An important consequence of investigating the LSDs is that this has enriched our knowledge about lysosomal function and its involvement in general cell biology.

a) The lysosomal proteins and pathways

The lysosome is a membrane bound acidic organelle in which the cell recycles and degrades macromolecules via a variety of acid hydrolases (De Duve, 1963). For this degradation to function properly two processes are essential: firstly, a correct delivery of proteins destined to be degraded via the endocytic pathway and secondly, proper sequestering of the lysosomal hydrolases necessary for this process (Kornfeld and Mellman, 1989; Mellman, 1996).

Macromolecules destined for lysosomal degradation can either reach the lysosome via endocytosis from the extracellular environment, or by intracellular routes from within the cytosol (Zhang *et al.*, 2009). Proteins from the extracellular space can enter the cell either via endocytosis or phagocytosis, depending on the nature of the protein (Dunina-Barkovskaya, 2004; Doherty and McMahon, 2009; Flannagan *et al.*, 2012). Receptor mediated endocytosis is a common process for internalising a variety of substances, and occurs after binding to specific cell surface receptors (Goldstein *et al.*, 1985). This kind of internalisation relies most commonly on a clathrin mediated vesicular process (Doherty and McMahon, 2009), whereas phagocytosis is mediated by phagosome creation (Flannagan *et al.*, 2012). However, both vesicular structures end up fusing with endosomes, and eventually with lysosomes. In contrast, proteins from the cytosol reach the lysosome via the process of autophagy (Stromhaug and Klionsky, 2001; Levine and Klionsky, 2004), or after normal protein synthesis from the endoplasmic reticulum (ER) via the Golgi apparatus (Braakman and Bulleid, 2011).

In addition, to guarantee the correct degradation of macromolecules in the lysosome, soluble hydrolases have to be delivered to the lysosomal lumen. After protein synthesis, these hydrolases that are destined for the lysosomal lumen become tagged with mannose oligosaccharide side chains as they are trans-located into the ER lumen

(Helenius and Aebi, 2001). This is part of the sorting and control mechanism to guarantee correctly folded proteins. Furthermore, hydrolases that are targeted for the lysosome have to be linked to mannose-6-phosphate (M-6-P) residues (Kaplan *et al.*, 1977). If misfolding occurs, the proteins are directly degraded in the ER (Gething and Sambrook, 1992), otherwise correctly folded proteins are transported to the Golgi apparatus (Saraste and Kuismanen, 1992). In the Golgi apparatus, proteins that will be targeted to the lysosome are recognized by the M-6-P receptor, by which lysosomal hydrolases are segregated from other proteins (Kornfeld and Mellman, 1989; Kornfeld, 1992). These proteins are transported along the trans-Golgi-network (TNG) to the pre-lysosomal compartment and/or endosome where the low pH dissociates the receptor and enzyme, after which the M-6-P receptor is recycled to the Golgi network (Dell'Angelica and Payne, 2001).

In stark contrast to these soluble lysosomal proteins, the trafficking of lysosomal membrane proteins does not depend on M-6-P receptors, but instead upon a tyrosine-based and/or dileucine-based sorting signal at the cytoplasmic domain of the protein (Peters *et al.*, 1990; Braulke and Bonifacino, 2009). Lysosomal membrane proteins have been shown to reach the lysosome by two pathways: either directly or indirectly (Kornfeld and Mellman, 1989; Hunziker and Geuze, 1996). In the direct pathway lysosomal membrane proteins are transported directly to early or late endosomes and then subsequently to lysosomes. In the indirect pathway, these proteins are instead transported to the plasma membrane of the cell surface where they are internalised into early endosomes and eventually delivered to the endosomes and lysosomes (Braulke and Bonifacino, 2009). Once these lysosomal membrane proteins have correctly reached the lysosome they are crucial for the acidification of the lysosomal lumen, transport of molecules across the lysosomal membrane and mediating membrane fusion (Saftig and Klumperman, 2009).

b) Lysosomal function

Originally the lysosome was only regarded as the waste disposal and recycling machinery of the cell (Kornfeld and Mellman, 1989). However, with increasing research into intracellular trafficking, the lysosome is now seen as a more dynamic organelle that contributes to a variety of intracellular cell processes. Indeed, apart from being the final destination of the endosomal/lysosomal pathway after endocytosis, phagocytosis or autophagy of molecules targeted for destruction or recycling, the

lysosome has been shown to be the centre of many cellular functions (see **Figure 1**) (Luzio *et al.*, 2007; Walkley, 2007; Saftig and Klumperman, 2009). These include cellular recycling and repair, homeostatic control (Stinchcombe and Griffiths, 1999), in particular cholesterol homeostasis (Chang *et al.*, 2006), cell surface receptor down regulation (Carpentier *et al.*, 1985), bone and tissue remodelling, cell death (Guicciardi *et al.*, 2004), cell signalling and inactivation of pathogenic organisms (Saftig and Klumperman, 2009). Furthermore, lysosomes are also involved in cell-specific functions like the correct loading of major histocompatibility complex (MHC) class II molecule receptor with peptides, before enabling antigen presentation at the cell surface of T-cells (Raposo *et al.*, 2002), or secretory vesicle formation in cytotoxic T-cells at the immunological synapse (Luzio *et al.*, 2007). Taken together, the endosomal/lysosomal system is essential for correct protein sorting and trafficking within each cell of the body. This becomes even more significant in highly polarized cells like neurons of the central nervous system (CNS).

c) Lysosomes in neurons

As in every other cell in the body, all the basic lysosomal functions mentioned above are also essential for the long term survival of neurons and the crosstalk within, and between, cells of the CNS (Nixon and Cataldo, 1995). However, neurons above all other cell types have a fundamental need for a functional endosomal/lysosomal system, and in particular for endocytosis (Parton and Dotti, 1993). The considerable spatial separation of the cell soma, where most proteins are made, and synapses means that a functioning vesicular and protein trafficking system is critically required for neuronal function (Lasiecka and Winckler, 2011). Furthermore, after neurotransmitter release at the synapse, a series of rapid endocytic events are needed to maintain synaptic vesicle numbers (Murthy and Stevens, 1998). Indeed, neurons also rely on endocytosis to mediate communication with peripheral tissues, which may be essential for survival (Sofroniew *et al.*, 2001). Many different hormones and growth factors from the extracellular space regulate neuronal function and activity by triggering intracellular signals (Howe *et al.*, 2001; Schlett, 2006; Ascano *et al.*, 2012), and all depend on precise intracellular trafficking.

Besides these necessities imposed by neuronal morphology and function, some specific features of lysosomal involvement in neurobiology should also be considered. These processes all start during brain development, when late endosomes/lysosomes

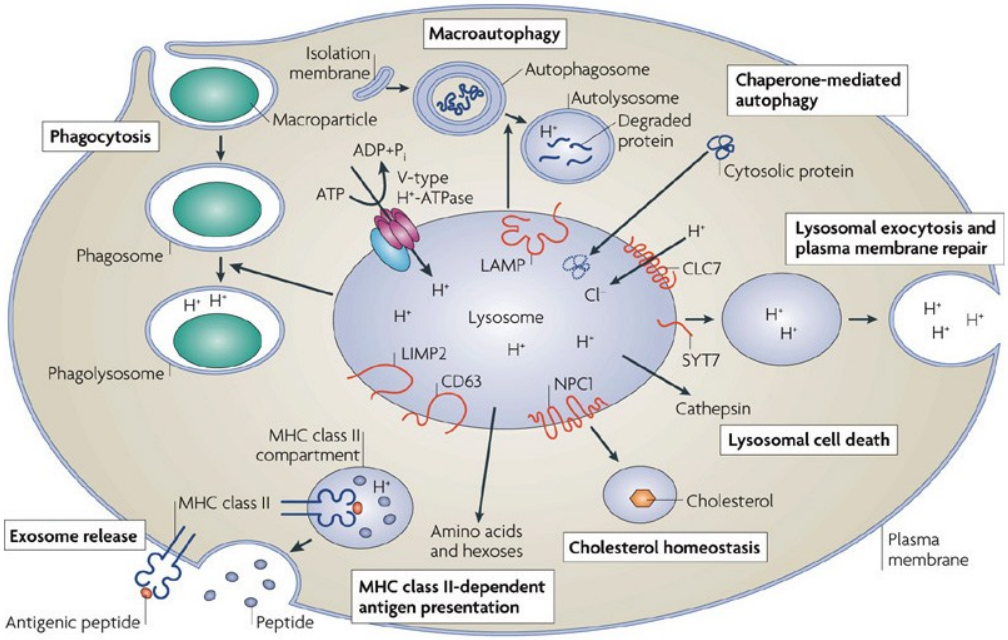

Figure 1. The numerous functions of the lysosome. As a central organelle within a cell, the acidic compartment (H+ of the lysosome is created by V-type H+-ATPase activity which ensures optimal conditions for lysosomal hydrolases). The lysosome is involved in various pathways: During macro-autophagy, lysosomal fusion with autophagosomes is essential for the turnover of cytoplasmic components. Essential for adaptive immune responses, major histocompatibility complex (MHC) class II dependent antigen presentation and exosome release depend on lysosomal proteases and membrane proteins. Fusion of the lysosome with phagosomes is required for successful phagocytosis in pathogen defence processes. Furthermore, exocytosis, plasma membrane repair, chaperone-mediated autophagy, lysosomal cell death all rely on functional lysosomal activity. Several lysosomal (transport) processes are regulated by membrane bound lysosomal proteins including lysosome-associated membrane proteins (LAMPs), lysosome-integrated membrane protein (LIMP2), chloride channel 7 (CLC7), synaptotagmin 7 (SYT7) and cluster of differentiation molecule 63 (CD63 The deficiency of the membrane protein Niemann-Pick C1 (NPC1) leads to cholesterol accumulation, suggesting its involvement in cholesterol homeostasis, amongst several other proposed functions. Reproduced from (Saftig and Klumperman, 2009).

play an essential role in neurite outgrowth and arborisation by adding new membranes to developing neurite extensions (Arantes and Andrews, 2006), or by guaranteeing vesicular protein trafficking during axonal and dendritic growth (Sann *et al.*, 2009). Whereas lysosomes are essential for axonal growth, they have also been shown to be a central feature of synapse elimination, via their degradative activity during the process of axon pruning (Song *et al.*, 2008). Studies in Niemann-Pick disease, another LSD, revealed the key role of the lysosome in cholesterol homeostasis, which is necessary for the maintenance of synaptic structure and function and effective neurotransmission (Mitter *et al.*, 2003; Wasser *et al.*, 2007), and last but not least, the lysosome is important for effective autophagy and mitochondrial turnover in neurons (Settembre *et al.*, 2008; Batlevi and La Spada, 2011; Marino *et al.*, 2011). When neurons

age it has been suggested that lysosomes can inhibit or induce neuronal death via lysosomal rupture or permeabilization, which is comprised in the so-called 'mitochondrial–lysosomal axis theory of aging' (Yamashima and Oikawa, 2009; Terman *et al.*, 2010).

It may not come as a surprise, with so many crucial functions for the lysosome in healthy neurons that altered lysosomal function has been described as a cause of many neurodegenerative disorders. Apart from LSDs, lysosomal dysfunction has been considered in relation to Alzheimer disease, in which disturbances of the endosomal/lysosomal pathways are one of the earliest known manifestations of Alzheimer disease (Nixon and Cataldo, 2006). Likewise, in Parkinson disease the disease-associated mutant α-synuclein can inhibit autophagy-lysosomal pathways in neurons (Pan *et al.*, 2008). Furthermore, anterograde lysosomal transport seems to be a key factor in motor neuron degeneration (Lim and Kraut, 2009). Therefore, lysosomal dysfunction could perhaps be used as an early marker for axon degeneration and, *vice versa*, the proper maintenance of lysosomal transport function could be potentially therapeutic for many neurodegenerative disorders (Zheng *et al.*, 2010). Moreover, other candidates for neurodegenerative disorders with lysosomal involvement include frontotemporal dementia (Lee *et al.*, 2007a) and amyotrophic lateral sclerosis (ALS) (Filimonenko *et al.*, 2007). Nevertheless, the prime examples of neuronal dysfunction due to endosomal/lysosomal pathway disruptions are of course the LSDs themselves. Given the complexity of lysosomal functions, together with the highly polarized and long-distance nature of neurons and their projections, a pronounced neurological component is a common pathological feature in most LSDs (Scriver *et al.*, 2001; Walkley, 2009).

d) Neurodegeneration in LSDs

About three quarters of LSDs show CNS pathology as a hallmark, and these disorders are considered the most common cause of paediatric neurodegeneration (Vitner *et al.*, 2010; Schultz *et al.*, 2011). Yet, the actual cause of neuronal death is a topic that has been debated for many years. Whereas originally, the storage material itself was thought to be the main cause and driving force of cell death (Desnick *et al.*, 1976), the key contributor to the pathogenesis of LSDs is now considered to be a consequence of the deficiencies in the endosomal/lysosomal system (Walkley and Vanier, 2009). The loss of gene function may cause both primary and secondary damage to cells and

tissues, with storage material contributing directly or indirectly to pathogenesis. In addition, various secondary pathological cascades as a downstream consequence of the loss of lysosomal function and/or storage accumulation are likely to contribute and accelerate pathogenesis. The pathological cascades will inevitably vary between each form of LSDs, as a consequence of different gene deficiencies. In many LSDs the storage material accumulates as a direct cause of the gene deficiency and is likely to have upstream effects on pathogenesis (e.g. in several sphingolipidoses Tay Sachs disease or gangliosidoses like Mucopolysaccharidosis (MPS) type I) and this situation is further complicated by the accumulation of secondary molecules that may also have pathological consequences (Futerman and van Meer, 2004). However, in the NCLs, with very little known about the normal function of the deficient genes it is harder to link storage material accumulation to downstream pathology. This issue is made more complicated by the finding that while storage material accumulation is widespread within the CNS (Haltia, 2003), neuron loss is relatively selective (Pontikis *et al.*, 2005; Cooper *et al.*, 2006; Kielar *et al.*, 2007), and there does not appear to be a direct correlation between these events. However, secondary downstream events caused by storage accumulation could still indirectly influence disease pathogenesis and have to be considered in interpreting disease mechanisms. It is important to disentangle such primary and secondary pathogenic events when considering therapeutic strategies, as certain events are probably only secondary downstream consequences of primary causes of gene deficiency, and the 'wrong' therapeutic targets will not be able to reverse neurodegenerative processes *per se* (Walkley and Vanier, 2009).

e) Clinical features of LSDs

The LSDs are classically childhood disorders, with some rarer adult onset forms, as for example CLN4 disease/Kufs disease (see below and **Table 1**; (Rapola, 1994; Goebel, 1995; Schultz *et al.*, 2011)). All LSDs are monogenetic with the vast majority of disease-causing mutations inherited in an autosomal recessive fashion (Winchester *et al.*, 2000), except for Fabry disease and Mucopolysaccharidosis (MPS) type II (Hunter syndrome) which are X-linked (Desnick *et al.*, 1989; Hopwood *et al.*, 1993a), and the autosomal dominant inherited CLN4 disease (originally associated with Kufs Disease, Parry type) (Nijssen *et al.*, 2003; Benitez *et al.*, 2011; Velinov *et al.*, 2012). These genetic defects may include lysosomal hydrolases, lysosomal membrane proteins or proteins expressed elsewhere in the endosomal/lysosomal system resulting in heterogeneous clinical outcomes (Winchester *et al.*, 2000; Walkley, 2009).

Nevertheless, common clinical manifestations can be described: normal early development is followed by developmental delay, leading to motor deficits often accompanied by loss of vision continuing through to a later stage when neurological symptoms arise with seizures, dementia, behavioural changes, and eventually premature death (Wraith, 2004). However, different forms of LSDs show large discrepancies in age of onset, severity and which organs are affected, due to the distinct genetic differences between them and other unidentified reasons (Beck, 2001; Wilcox, 2004). One explanation can be found in the fact that in each disease-causing gene, numerous mutations can result in different molecular consequences and clinical manifestations. As such, often no straightforward genotype-phenotype correlation can be observed in each specific form of LSD (Mole *et al.*, 2011). Typical examples include the neuronal ceroid lipofuscinoses (NCLs), in which patients with mutations in the same disease-causing gene typically show heterogeneous ages of onset and rates of progression (see NCL classification in **Table 1**).

1.2 Neuronal Ceroid Lipofuscinoses (NCLs)

The NCLs are considered to be the most common inherited neurodegenerative storage disorders of childhood (Goebel, 1995; Jalanko and Braulke, 2009), with an incidence of up to 1 in 12,500 live births in Scandinavian countries and 1:100,000 worldwide (Santavuori, 1988; Kyttala *et al.*, 2006; Jalanko and Braulke, 2009). Despite the first observation of NCL cases by Dr Otto Stengel in 1826 (Brean, 2004), these diseases are more commonly called Batten disease after the British paediatrician Frederick Batten who reported Juvenile NCL cases in 1903 (Zeman and Dyken, 1969).

a) Classification of the NCLs

Since the discovery of the first genes causing NCL in 1995 (Lerner *et al.*, 1995; Vesa *et al.*, 1995), roughly 400 mutations have been described in thirteen different genes. Traditionally the classification of the NCLs has always been by age of onset, which grouped the diseases into four main categories: Infantile NCL (INCL), Late-infantile NCL (LINCL), Juvenile NCL (JNCL) and Adult NCL (ANCL) (Goebel *et al.*, 1999). However, progress in identifying the genetic basis of these disorders made it possible to classify them according to the disease-causing gene (Cooper, 2003; Mole, 2004; Siintola *et al.*, 2006; Jalanko and Braulke, 2009). Subsequent years have seen the identification of an increasing number of mutations and variant forms of NCL (Siintola *et al.*, 2006; Jalanko and Braulke, 2009) (see NCL mutation database

http://www.ucl.ac.uk/ncl/mutation.shtml). Whereas for most NCL genes a characteristic disease phenotype is associated with a complete loss of gene function, additional 'milder' cases with some remaining gene function and with delayed disease onset and/or progression added complexity to the classification system (Lake and Cavanagh, 1978; Santavuori *et al.*, 1982). Therefore, recently a new nomenclature has been proposed based upon combining the genetic defect with the age of onset (see **Table 1**). However, in everyday practice the classical nomenclature is still in use. Likewise, in this study any notation of a NCL disease will always refer to a complete loss of function mutation and for that reason, we will stick to a simplified 'classical' description based on the age of onset ('Infantile NCL' instead of 'CLN1 disease, infantile' or 'Juvenile NCL' instead of 'CLN3 disease, juvenile'). The studies described in this thesis focus upon two of the three most common forms of NCL: Infantile NCL (INCL/CLN1) and Juvenile NCL (JNCL/CLN3). Hence these two forms shall be summarised in more detail.

b) Infantile NCL (INCL/CLN1)

Infantile NCL (INCL) is a rare disease form (~1:2,000,000 live births worldwide), but it has a particularly high incidence in the Finnish population (~1 in 20,000 live births) (Santavuori, 1988; Mole *et al.*, 2011). INCL is caused by mutations in the *CLN1* gene which encodes a soluble lysosomal enzyme, palmitoyl protein thioesterase 1 (PPT1) (Vesa *et al.*, 1995). So far, 49 different mutations have been identified for *PPT1* with missense mutations (23 of 49) being the most prominent (*http://www.ucl.ac.uk/ncl/mutation.shtml*). The biochemical function of PPT1 is mainly to cleave palmitate or fatty acyl chains from proteins and peptides (Camp and Hofmann, 1993; Camp *et al.*, 1994), whereas the exact cellular function *in vivo* still remains elusive. PPT1/Ppt1 has been shown to participate in several cellular processes including endocytosis (Ahtiainen *et al.*, 2006), apoptosis (Cho and Dawson, 2000; Tardy *et al.*, 2009), vesicular trafficking and synaptic function (Lehtovirta *et al.*, 2001; Virmani *et al.*, 2005; Kim *et al.*, 2008). Consistent with these suggestions, additional cellular localisations of PPT1/Ppt1 have been described in axonal varicosities and presynaptic terminals of neurons (Heinonen *et al.*, 2000; Ahtiainen *et al.*, 2003; Virmani *et al.*, 2005). Furthermore, PPT1 transport along the endosomal/lysosomal pathways is suggested to be mediated by the mannose-6-phosphate receptor (M6PR) (Hellsten *et al.*, 1996; Verkruyse and Hofmann, 1996). In mice and rats, Ppt1 protein expression can be expressed during developmental stages and has been associated with neuronal

Table 1. New classification nomenclature of the neuronal ceroid lipofuscinoses (NCLs). All diseases listed are autosomal recessive disorders unless marked differently. Adapted from (Williams and Mole, 2012) and (Mole *et al.*, 2011).

Biological function	Gene (Location)	Protein	Diseases
Soluble lysosomal enzyme deficiencies	*CTSD* *CLN10* (11p15.5)	Cathepsin D Soluble lysosomal enzyme (Aspartyl protease)	CLN10 disease, congenital CLN10 disease, late infantile CLN10 disease, juvenile CLN10 disease, adult
	PPT1 *CLN1* (1p32)	Palmitoyl protein thioesterase 1, PPT1 Soluble lysosomal enzyme	CLN1 disease, infantile CLN1 disease, late infantile CLN1 disease, juvenile CLN1 disease, adult
	TPP1 *CLN2* (11p15)	Tripeptidyl peptidase 1, TPP1 Soluble lysosomal enzyme	CLN2 disease, late infantile CLN2 disease, juvenile
	CTSF *CLN13* (11q13)	Cathepsin F Soluble lysosomal enzyme (Cysteine protease)	CLN13 disease, adult Kufs type B
Non-enzyme deficiencies (functions of identified proteins generally poorly understood at the current time)	*CLN3* (16p12)	Transmembrane protein of unknown function	CLN3 disease, juvenile
	CLN5 (13q21)	Soluble, lysosomal glycoprotein of unknown function	CLN5 disease, late infantile CLN5 disease, juvenile CLN5 disease, adult
	CLN6 (15q21-23)	Transmembrane protein, ER, unknown function	CLN6 disease, late infantile CLN6 disease, adults Kufs type A
	MFSD8 *CLN7* (4q28.1-28.2)	Major facilitator superfamily domain-containing protein 8, Transmembrane protein, Putative endolysomal transporter	CLN7 disease, late infantile
	CLN8 (8p23)	Transmembrane protein, ER, ER-Golgi intermediate complex, unknown function	CLN8 disease, late infantile CLN8 disease, EPMR
	DNAJC5 *CLN4* (20q13.33)	Soluble cysteine string protein	CLN4 disease, adult autosomal dominant
	GRN *CLN11* (17q21.32)	Progranulin	CLN11 disease, adult Heterzygous mutations cause frontotemporal lobar dementia
	ATP13A2 *CLN12* (1p36)	P-type ATPase	CLN12 disease, juvenile Mutations also cause Kufor-Rakeb syndrome
Others: those whose classification is uncertain because of incomplete diagnostic investigations or absence of confirmed gene/mutation designation, or where NCL is rare or minor mutation-specific phenotype	*KCTD7* *CLN14* (7q11.12)	Potassium channel tetramerization domain-containing protein 7	CLN14 disease, infantile Mutations also cause progressive myoclonic epilepsy-3
	CLN9?	Mutations not yet defined in any gene	Juvenile variants
	CLCN6 (1p36)	Mutations not yet found on both disease alleles in human disease	Chloride transport defect, adult onset
	SGSH (17q25.3)	Mutations usually cause MPSIIIA	Adult onset
	?	Mutations not yet defined in any gene	Congenital, infantile variants
	?	Mutations not yet defined in any gene	Late infantile variants
	?	Mutations not yet defined in any gene	Late onset/adult variants including some adult Kufs type B

maturation (Isosomppi *et al.*, 1999; Heinonen *et al.*, 2000). The clinical manifestations of Infantile NCL normally appear between 6-12 months of age, followed by loss of vision and speech, cognitive decline, microcephaly and seizures leading to premature death between 9-13 years of age (Santavuori, 1988; Santavuori *et al.*, 1993; Santavuori *et al.*, 2000).

c) Juvenile NCL (JNCL/CLN3)

Juvenile NCL (JNCL) is the most common form of NCL worldwide with the highest incidence in Scandinavia (~ 1 in 15,000-50,000) (Mole *et al.*, 2011). JNCL is caused by mutations in the *CLN3* gene, which encodes for a conserved transmembrane protein of unknown function (The International Batten Disease Consortium (TIBDC), 1995; (Lerner *et al.*, 1995)). To date, 50 mutations have been discovered in *CLN3*, but interestingly, 85-90% of all JNCL cases share the same mutation caused by a 1kb deletion. (*http://www.ucl.ac.uk/ncl/mutation.shtml*) (Lerner *et al.*, 1995). Expression of CLN3 in human tissue is widespread in many organs (lung, liver, muscle, kidney etc.) (TIBDC, 1995). In the CNS, CLN3 expression levels are not particularly high, but constitutively expressed and therefore CLN3 is suggested to incorporate 'housekeeping' cell functions (Mole *et al.*, 2011). The structure of CLN3 has been defined as a type III transmembrane protein with six membrane-spanning domains and cytosolic facing N- and C-termini (Kyttala *et al.*, 2004), which indicate possible functions in luminal environment changes or modulation of other membrane proteins (e.g. ion channels) (Mole *et al.*, 2011). For largely technical reasons CLN3 has been assigned to many intracellular compartments, with the most favourable localisation currently being in the endosomal/lysosomal system trafficking through ER and Golgi apparatus (Kida *et al.*, 1999; Haskell *et al.*, 2000; Kyttala *et al.*, 2004). Further locations have been reported in the synaptosomal fraction of the mouse brain and the early endosomes of neurons (Luiro *et al.*, 2001; Kyttala *et al.*, 2004; Storch *et al.*, 2007), in the Golgi apparatus (Codlin and Mole, 2009), a small fraction (~10 %) in the plasma membrane (Mao *et al.*, 2003; Storch *et al.*, 2007), and also in membrane lipid raft preparations (Rakheja *et al.*, 2004). However, the exact cellular function of CLN3 still remains elusive. No known protein is homologous to CLN3, but its topology is suggestive of a membrane transporter function (Mole *et al.*, 2011). It is postulated that CLN3 is involved in lysosomal acidification (Pearce *et al.*, 1999; Padilla-Lopez and Pearce, 2006), mitochondrial function (Palmer *et al.*, 1992; Jolly *et al.*, 2002; Fossale *et al.*, 2004), intracellular trafficking via interactions with the cytoskeleton (Uusi-Rauva *et*

al., 2008; Getty *et al.*, 2011), membrane fusion and synaptic vesicle transport (Luiro *et al.*, 2001; Fossale *et al.*, 2004; Kama *et al.*, 2007), autophagy (Cao *et al.*, 2006; Cotman and Staropoli, 2012), developmental cell polarity and proliferation processes (Tuxworth *et al.*, 2009; Weimer *et al.*, 2009), as well as Ca^{2+} level regulation (Chang *et al.*, 2007; An Haack *et al.*, 2011). Furthermore, CLN3 has been suggested to take on a protective role against apoptosis (Puranam *et al.*, 1999; Persaud-Sawin and Boustany, 2005). In JNCL patients clinical manifestations usually begin with visual impairment between 4-7 years of age, leading to blindness caused by retinal degeneration at 5-10 years, proceeded by mental deterioration, epilepsy and motor deficits, and premature death at a mean age of 24 years (Williams *et al.*, 2006; Jalanko and Braulke, 2009; Mole *et al.*, 2011).

d) NCL animal models

The discovery of the molecular basis of most disease-causing genes (TIBDC, 1995) has laid the foundation for developing genetically accurate models of NCL (Cooper *et al.*, 2006; Jalanko and Braulke, 2009). A series of animal models have been established over the years to investigate NCL pathogenesis. These models range from yeast (Pearce and Sherman, 1998; Pearce *et al.*, 1999; Kama *et al.*, 2007), nematode worms (de Voer *et al.*, 2005; Phillips *et al.*, 2006), *Drosophila* (Tuxworth *et al.*, 2009), to zebrafish (Cooper *et al.*, 2006). But, as in many other disorders, the most commonly used models are genetically engineered mutant mice (reviewed by (Cooper *et al.*, 2006)), but a series of spontaneous mutants in larger animal species including dogs and sheep have also been identified (Melville *et al.*, 2005; Tammen *et al.*, 2006). Each model system has its own advantages and disadvantages. Whereas for example, yeast is very useful for investigating biochemical and cellular pathways (Codlin and Mole, 2009), *Drosophila* is the best-characterised tool for single gene – cell interactions (Bier, 2005; Marsh and Thompson, 2006). Zebrafish are ideal for drug screening with their transparent bodies (Sukardi *et al.*, 2011), although larger animal species more closely resemble the human brain (Mole *et al.*, 2011). In this study we focused only on mouse models of Infantile and Juvenile NCL (see summary in **Table 2**). Numerous mouse models with differently constructed mutations on several background strains have been created. It is important to note that discrepancies in mutations as well as strain backgrounds can dramatically modify disease phenotypes in the mice (de la Hoz *et al.*, 2003; McLin and Steward, 2006; Adams *et al.*, 2010; Finn *et al.*, 2010; Kousi *et al.*, 2012). Therefore, it is of uppermost importance that reliable comparisons can only be

made between mice of the same background strain (Mole *et al.*, 2011). Nowadays, most commonly used are mice on the C57Bl/6 strain background, although earlier studies also utilised 129Sv strains of mice.

Table 2. Overview of mouse models of Infantile and Juvenile NCL. Adapted from (Cooper *et al.*, 2006)

Animal model	Genetic mutation	Onset of neurological signs	Mortality	Originating references
Infantile NCL (CLN1)				
Ppt1$^{-/-}$ mouse	Exon 9 insertion + termination codon at Val281	2 months	~ 8 months	(Gupta *et al.*, 2001)
Ppt1$^{\Delta ex4}$ mouse	Exon 4 deletion	4 months	~ 6.5 months	(Jalanko *et al.*, 2005)
Juvenile NCL (CLN3)				
Cln3$^{-/-}$ mouse	Exons 1-6 replacement insertion	2 months	~ 20 months	(Mitchison *et al.*, 1999)
Cln3$^{\Delta ex7/8}$ knock-in mouse	Exons 7-8 deletion	4 months	~ 20 months	(Cotman *et al.*, 2002)
Cln3 knockout mouse	Exons 7-8 replacement insertion	3 months	~ 20 months	(Katz *et al.*, 1999)
Cln3 'reporter' mouse	Exons 1-8 deletion and β-gal insertion	1 month	~ 20 months	(Eliason *et al.*, 2007)

Non-human model systems serve two main purposes. First of all, the investigation of the functional consequences of each gene mutation and the underlying disease mechanisms of each NCL form can be conducted. When compared to studies on *post mortem* tissue from NCL patients, a main advantage of these model systems is the possibility of obtaining important information about progressive pathogenesis, even from before the onset of overt disease manifestations. Secondly, animal models provide a controlled system for systematic and accurate assessment of therapeutic interventions in an ethically acceptable manner. Therefore, they are vital in paving the way towards successful pre-clinical therapies and eventually clinical trials in humans (Cooper *et al.*, 2006; Mole *et al.*, 2011).

1.3 Therapeutic approaches for Infantile and Juvenile NCL

Several therapeutic approaches have been tested in mouse models of INCL and JNCL (see **Table 2**). To successfully treat each of the NCL forms, the basic biology of the deficient proteins has to be considered. As described above, PPT1 has been shown to be a soluble late-endosomal/lysosomal protein that can diffuse throughout and between cells (Hellsten *et al.*, 1996; Verkruyse and Hofmann, 1996). CLN3 is a hydrophobic integral membrane protein of so far disputed location and function in the cell (Janes *et al.*, 1996; Kaczmarski *et al.*, 1999; Mao *et al.*, 2003). This difference in solubility and the so-called principle of 'cross-correction' (see next **section 1.3a**) define which therapeutic approaches are suitable for each form of NCL.

a) Principle of cross-correction

As mentioned above, some proteins, including PPT1, are glycosylated during trafficking throughout the rough endoplasmic reticulum (RER) to the Golgi to guarantee efficient transport to the lysosomal compartment or for cell secretion. These proteins can be recognized by the mannose 6-phosphate/IGF II receptor (M6PR) (Achord *et al.*, 1978; Kornfeld, 1992). As M6PR is also expressed on the cell surface where it mediates endocytosis and trafficking to the lysosomal compartment of glycosylated proteins (Hawkes and Kar, 2004; Coutinho *et al.*, 2012), extracellular PPT1 can bind to this receptor and reach its correct location within the cell (Sands and Davidson, 2006; Wong *et al.*, 2010). This mechanism provides the enticing possibility that, as long as the missing protein can be introduced into the extracellular space in some fashion (either via secretion from other cells or via direct injection), it could correct the diseased phenotype of a *Ppt1* deficient cell. This principle was termed 'cross-correction' and is particularly important in enzyme replacement and gene therapy approaches (Fratantoni *et al.*, 1968; Sands and Davidson, 2006). However, these molecular mechanisms are not relevant for proteins like CLN3 which are integral membrane bound proteins and cannot be secreted to cross-correct neighbouring deficient cells.

By capitalising on the knowledge of possible cross-correction, several therapies have been tested with promising or less promising effects on experimental model systems. These include experimental therapeutic approaches including enzyme replacement therapy (ERT) and gene therapy (Griffey *et al.*, 2004; Hu *et al.*, 2012). Furthermore, cell based therapies like bone marrow transplantation (BMT), *ex vivo* gene therapy or

neuronal stem cell therapies have increased the understanding of cellular contribution to disease amelioration (Lake *et al.*, 1997; Zheng *et al.*, 2003; Tamaki *et al.*, 2009). Additionally, small molecule therapies including glutamate receptor antagonists and chemical chaperones resulted in some moderate effects upon NCL disease progression (Sleat *et al.*, 1999; Dawson *et al.*, 2010; Kovacs *et al.*, 2011), whereas dietary therapies had limited success (Santavuori *et al.*, 1989; Wei *et al.*, 2011), and encouraging storage material degradation did not seem to affect disease outcome in patients or mice (Zhang *et al.*, 2001). Last but not least, immune modulatory or combinational therapies have recently also been attempted (see **Chapter 7** for more detail and (Seehafer *et al.*, 2011; Macauley *et al.*, 2012)). As beneficial therapies are the main goal of the studies presented in this thesis, in the following sections the benefits and implications of each therapeutic strategy shall be discussed in relation to Infantile and Juvenile NCL.

b) Enzyme replacement therapy (ERT)

Based on the possibility of cross-correction, straightforward administration of the missing enzyme seems the ideal solution for INCL, but is clearly not applicable to JNCL. ERT studies in other non-neuropathic lysosomal disorders, for example Gaucher disease (Barton *et al.*, 1991; Beutler *et al.*, 1991), Fabry disease (Eng *et al.*, 2001) or the mucopolysaccaridoses (MPSs) greatly reduced disease symptoms (Kakkis *et al.*, 2001; Harmatz *et al.*, 2004), but so far ERT does not appear to have a beneficial influence on LSDs with CNS involvement. A major problem is the delivery method of the enzyme with intravenously injected (lysosomal) enzymes prevented from accessing the CNS by the blood brain barrier (BBB), whereas direct intracranial injections, in addition to being very invasive, run the risk of provoking an immune response and neutralisation of the delivered enzyme by antibodies (Harmatz *et al.*, 2004; Linthorst *et al.*, 2004). A recent study focused on PPT1 intravenous delivery to Infantile NCL mice (Hu *et al.*, 2012), and treated mice showed marked reduction in visceral storage, but PPT1 could only reach the brain if it was delivered neonatally before the BBB forms properly. As such, ERT with PPT1 may have potential in treating visceral pathology, even when administered at later time points, but other strategies will be needed for the CNS.

c) Gene therapy

By definition gene therapy manipulates gene expression in diseased cells or organisms to achieve therapeutic benefit (Mole *et al.*, 2011). The most commonly used tools to

achieve this goal are viral vectors. Besides retrovirus and adenoviruses, the use of adeno-associated viruses (AAVs) has shown promising results. Their non-pathogenic nature in humans plus their ability to transduce non-replicating cell types like neurons make them well suited for CNS gene therapy (McCown, 2005). Since gene therapy is also based on the principle of cross-correction, this approach has its main potential in treating enzyme deficient forms of NCL, including INCL. In JNCL it would only be beneficial if every cell could be transfected (and therefore genetically corrected), which is unlikely. In Infantile NCL, successful PPT1 gene delivery has been performed after intracranial injections of an AAV2 vector expressing PPT1 in new-born *Ppt1*$^{-/-}$ mice (Griffey *et al.*, 2004). However, other than reduced storage material in the brain, alongside improved neuropathology and behaviour, AAV2-PPT1 had no impact upon the lifespan of these mice (Griffey *et al.*, 2006). Nevertheless, two recent studies in *Ppt1*$^{-/-}$ mice using a newer and more efficient AAV2/5 vector have demonstrated significant motor function and lifespan improvements, alongside significantly reduced neuroinflammation and brain pathology (Macauley *et al.*, 2012; Roberts *et al.*, 2012). These gene therapy approaches represent the best single treatment of INCL mice so far (with an improvement of 19 weeks or 54% in lifespan). Furthermore, these treatments were used as control groups in combinational therapeutic studies, which shall be discussed in more detail in **Chapter 7**, but which produced even greater therapeutic effects. As a side note, the most promising gene therapy studies, in any form of NCL, have been conducted in Late Infantile NCL (Sondhi *et al.*, 2007) which led to clinical trials I and II (in progress) in humans (Worgall *et al.*, 2008). However, gene therapy may soon be revolutionised by the delivery of capsid-modified vector (and hence enzyme) into the CNS via intravenous injections using the therapeutic principle of 'phage panning', with which disease specific peptide patterns on endothelial cells are identified and used to modify the viral capsid to overcome the BBB (Chen *et al.*, 2009). First tests in a Late Infantile NCL canine model system resulted in improved motor behaviour and decreased disease symptoms (Davidson, 2012; Wininger, 2012) and further developments will be awaited with interest.

d) Bone marrow transplantation (BMT)

The principle behind BMT is the donation of healthy haematopoietic stem cells (HSCs) to diseased patients (Mole *et al.*, 2011). HSCs can develop into all types of immune cells, lymphocytes, macrophages and particularly into microglia. Therefore, these cell types could potentially act as vehicles to deliver the missing enzyme into the

CNS. This possibility seems attractive for enzyme deficient forms of NCL. Successful BMT has been conducted in patients with lysosomal storage disorders such as MPS I that primarily affect the viscera and have little CNS involvement (Hopwood *et al.*, 1993b), and the life quality of these patients was significantly improved. However, attempts of BMT in Late Infantile NCL (Lake *et al.*, 1997), Infantile (Lonnqvist *et al.*, 2001; Macauley *et al.*, 2012) and Juvenile NCL (Lake *et al.*, 1997) have not been successful due to limited CNS migration of HSCs and only low levels of enzyme secretion. Therefore, this approach, so far, seems unsuitable for either Infantile or Juvenile NCL, but does show potential when part of a combination therapy with gene transfer (see **Chapter 7**).

e) *Ex vivo* gene therapy

As a mix of gene therapy and BMT, another approach tries to amplify the enzyme secretion of HSCs via *ex vivo* gene therapy to enhance gene expression of the donor cells before subsequent transplantation into the recipient mice/patients. This approach has proved to be successful in neuropathic LSDs like MPS I (Zheng *et al.*, 2003) or a metachromatic leukodystrophy (Biffi *et al.*, 2004). In addition to traditional BMT, enzyme overexpressing HSCs cells have also been directly implanted into the ventricles of the brain of a MPSVII mouse model, which overcomes the necessity HSCs to migrate into the CNS (Sakurai *et al.*, 2004). All of these examples resulted in improved behavioral and ameliorated brain pathology. However, this strategy has not yet been applied to any form of NCL, but could be an encouraging method for the future.

f) Stem cell therapy

Apart from HSCs, other cell-mediated therapies have been attempted via the implantation of neuroprogenitor cells (NPCs) into the brain of mice or patients. These cells have the potential to develop into neurons or glial cells. They are not only potentially able to become functional cells which can build connections with existing neurons, but first and foremost could also function as a long-term living enzyme delivery pool within the brain (Mole *et al.*, 2011). Stem cell therapy has recently been investigated in Infantile NCL where researchers transplanted human neural stem cells (huNSCs) into immune deficient NSCID *Ppt1*$^{-/-}$ mice (Tamaki *et al.*, 2009). Early transplantation led to improved motor performance, significant neuroprotection and decrease of autofluorescent storage material (Tamaki *et al.*, 2009). Detailed

characterization of the fate of the transplanted stem cells showed that most huNSCs did not develop into functional neurons. Nevertheless, many of the transplanted cells persisted in a relatively undifferentiated state and were capable of secreting the missing PPT1 enzyme. As a consequence, this approach is probably more promising for soluble enzyme deficient disorders for which long-term viable enzyme secretion is needed. Therefore, since little cell replacement was seen after such transplants this method does not seem applicable for Juvenile NCL treatment, but this remains untested experimentally. Due to the common development of tumors in NSCID mice (Leblond *et al.*, 1997; Nishimura *et al.*, 1999; Huang *et al.*, 2011), no lifespan analysis could be performed in this study. However, the time of sacrifice of the mice with the highest dose transplantation was 188 days, whereas untreated mice in this study had a life expectancy of about 162 days (Tamaki *et al.*, 2009). Thus, this proof of principle study demonstrated the therapeutic benefit of stem cells for Infantile NCL, which led to the initiation of a clinical phase I safety trial in INCL and LINCL patients (see *http://www.stemcellsinc.com/therapeutic-programs/clinical-trials.htm* for more information). The results of this phase I trial showed no safety concerns, but unfortunately an anticipated phase II trial has been suspended by the sponsoring company for unknown reasons. However, this approach seems to have great potential for the future, at least for Infantile NCL disease.

g) Chemical chaperones

A completely different therapeutic approach potentially has some benefits for certain types of Infantile NCL (Dawson *et al.*, 2010). Based on the assumption that the genetic mutation might lead to a misfolding and not a complete eradication of the encoded protein, chemical chaperones could facilitate the correct folding and consequent trafficking of the mutated protein. This approach has showed promising results in other LSDs like Fabry or Gaucher disease (Fan *et al.*, 1999; Sawkar *et al.*, 2005). Unfortunately, the majority of NCL forms are the consequence of a null mutation or a mutation in the active site of the enzyme which rules out this chaperone approach. Nevertheless, in some mutations of PPT1 where a missense mutation creates only a misfolded and unstable protein, chaperones have been proven to double enzyme activity in patient lymphoblasts (Dawson *et al.*, 2010), although it is unclear whether this would also work *in vivo*. This approach may also be beneficial for a subset of other NCL forms, even in membrane-bound deficiencies. But this is unlikely to work for Juvenile NCL due to the nature of its most common mutation (1kb deletion

mutation). Furthermore, the difficulties of this approach lie in the identification of a compound and its direct targeting in the host cells to the ER where protein folding takes place (Mole *et al.*, 2011).

h) Stop codon read-through therapies

Since many mutations are caused by premature stop codons of the transcriptional gene (McCaughan *et al.*, 1995), inducing the read-through of these mutations, a mechanism that also exists in natural circumstances, could theoretically recover protein translation. Several antibiotics are known to promote stop codon read-through and have been tested and shown to function in fibroblasts from Hurler disease or Late Infantile NCL patients (Sleat *et al.*, 1999; Keeling *et al.*, 2001). There have been successful clinical trials of this approach for cystic fibrosis (Wilschanski *et al.*, 2003), and safety assessments in healthy controls (Hirawat *et al.*, 2007). This approach could be of importance for some forms of NCL, for example, a large percentage (40% of 29) of PPT1 mutations in families affected by INCL encode for a stop mutation (Das *et al.*, 1998). Similar values were seen in a survey of 58 families affected by Late Infantile NCL (28%) (Sleat *et al.*, 1999). In the Juvenile form of NCL roughly 85% of all cases result from a truncation of the CLN3 protein by a premature stop codon mutation which leads to the classical JNCL phenotype (see **section 1.2c** above and (Haskell *et al.*, 2000)). Therefore, JNCL could be even more suitable for this therapeutic approach. However, the use of antibiotics brings with it potential side effects of toxicity and other off target effects. For this reason, this approach has not been followed up seriously for any form of NCL. Although it may have theoretical potential, in reality its usage still leaves room for doubt.

i) Receptor modulation

The findings that elevated glutamate levels are present in Juvenile NCL brains (Pears *et al.*, 2005), and that *Cln3* deficient neurons show vulnerability to AMPA-mediated neurotoxicity (Kovacs *et al.*, 2006) have led to the idea that a targeted blocking of the glutamate receptor via an AMPA antagonist could have beneficial consequences (Cooper *et al.*, 2006). Indeed, studies on 1 month and 6-7 month old *Cln3* deficient mice showed clear motor function improvements after administration of an AMPA antagonist (Kovacs and Pearce, 2008; Kovacs *et al.*, 2011). Recent findings indicated a glutamate receptor alteration is also present in *Ppt1*$^{-/-}$ neurons. A down-regulation of AMPA receptors in favor of a hyper-function of the NMDA receptor was observed in

Ppt1$^{-/-}$ cerebellar granule cell cultures (Finn *et al.*, 2012). Based on the observation of a disrupted glutamatergic function in *PPT1/Ppt1* deficient cells and mice (Sitter *et al.*, 2004; Ahtiainen *et al.*, 2007), possible therapeutic targets for INCL mice include NMDA receptor antagonists or positive modulation of AMPA receptor function. Therefore, this approach may be promising in the future for both the Infantile as well as the Juvenile form of NCL.

j) Immune modulatory therapies

The involvement of the immune system in NCLs has gained more and more attention in the last years leading to therapeutic approaches in which the immune system is modulated (Chattopadhyay *et al.*, 2002a; Seehafer *et al.*, 2011). As main focus of this thesis, they shall be discussed in **Chapter 7** in the context of the findings presented in this study.

k) Other therapeutic approaches

Since the discovery of the NCLs the accumulation of storage material within cells was assumed to directly kill neurons. However, several studies addressing this issue have not shown any significant improvement in neuron survival after a reduction of the storage load in these cells, and neuronal loss does not appear to correlate directly with the accumulation of these waste products (Palmer *et al.*, 2002; Bible *et al.*, 2004; Griffey *et al.*, 2004; Oswald *et al.*, 2005; Cooper, 2010).

Another strategy addressed the neurodegenerative mechanisms that may operate in the NCLs itself. After it has been shown that the non-opioid analgesic substance flupirtine disrupt chemically induced apoptosis of NCL neurons in tissue culture (Dhar *et al.*, 2002), several families administered flupirtine to their affected patients. However, no positive effects were seen, which emphasizes the fact that simply attempting to rescue dysfunctional neurons does not improve disease course and the restoration of the deficient protein is likely to be of greater importance (Cialone *et al.*, 2011; Mole *et al.*, 2011).

Furthermore, it has been shown that antioxidant mechanisms are apparently impaired (Westermarck *et al.*, 1997), and a reduction of polyunsaturated fatty acids is present in JNCL patients (Bennett *et al.*, 1994). However, giving antioxidant or other food supplements to correct these phenotypes does not appear to have any distinct effects on JNCL disease progression in patients (Santavuori *et al.*, 1989; Mole *et al.*, 2011). In

contrast, a recent study in *Cln3*$^{-/-}$ lymphoblasts demonstrated the reduction of ER stress and apoptosis markers after treatment with the anti-oxidant resveratrol (Yoon *et al.*, 2011). Likewise, in *Ppt1*$^{-/-}$ mice the reduction of mitochondrial and oxidative stress via application of resveratrol as a food supplement increased lifespan by roughly 6 % (Wei *et al.*, 2011). While not a cure in itself, this method is under consideration to be used in conjunction with other therapeutic approaches, such as gene therapy, as a means to boost their efficacy (JD Cooper, personal communication).

I) Combination therapies

All the above mentioned therapeutic approaches so far only partially ameliorated the outcome of INCL and JNCL (see **Table 3** for overview). Therefore, performing combination therapies has been postulated to potentially enhance the efficacy of each single approach. This aspect shall also be discussed in more detail in **Chapter 7**, in the context of the findings of our studies.

Table 3. Overview of therapeutic approaches and their suitability for Infantile and Juvenile NCL. Signs: ✓= therapy suitable and tested, (✓)? = therapy potentially suitable but not tested yet in INCL resp. JNCL, × = therapy not suitable, × (✓) = therapy only hypothetically possible so far. (×)? = therapy tested but not suitable so far.

	Infantile NCL (CLN1)	Juvenile NCL (CLN3)
Enzyme replacement therapy (ERT)	✓	×
Gene therapy	✓	×(✓)
Bone marrow transplantation (BMT)	(×)?	×
Ex vivo gene therapy	✓	×(✓)
Stem cell therapy	✓	×
Chemical chaperone therapy	(✓)?	×
Stop codon read through therapy	(✓)?	(✓)?
Receptor modulation therapy	(✓)?	✓
Anti-oxidant therapy	✓	(×)?
Immune modulation therapy	✓	✓
Combination therapy	✓	(✓)?

1.4 NCL Pathogenesis

Despite their wide genetic heterogeneity, all NCL patients show relatively similar clinical phenotypes with blindness, epilepsy and mental impairment invariably leading to premature death (Haltia, 2003; Goebel and Wisniewski, 2004; Jalanko and Braulke, 2009). Likewise, broad similarities can be found in the pathological phenotypes of the different forms of NCL. Being considered LSDs, all NCL forms show intra-lysosomal accumulation of autofluorescent material in neural and peripheral tissue (Haltia, 2003, 2006). Furthermore, *post mortem* tissue from NCL patients revealed pronounced

neuron loss and glial activation (Suzuki *et al.*, 1968; Haltia *et al.*, 1973a; Cooper, 2003; Tyynela *et al.*, 2004; Weimer *et al.*, 2009). Similar to the findings in humans, NCL mouse models have demonstrated wide similarities between all forms of NCL, although marked differences between nature and timing of disease phenotypes have also become increasingly apparent (Cooper *et al.*, 2006; Cooper, 2010). Common features across all NCL subtypes include, apart from the autofluorescent storage material, an early glial response (Pontikis *et al.*, 2004; Cooper *et al.*, 2006; Kay *et al.*, 2006; Macauley *et al.*, 2009), synaptic pathology (Kim *et al.*, 2008; Partanen *et al.*, 2008; Kielar *et al.*, 2009) and selective neuron loss (Mitchison *et al.*, 2004; Pontikis *et al.*, 2005; Cooper *et al.*, 2006; Kielar *et al.*, 2007). These pathological landmarks in mouse models of NCL are useful for comparing the extent of disease progression between each NCL form, but are also crucial for evaluating therapeutic efficacy (Cooper *et al.*, 2006; Shacka, 2012).

a) Storage material

Giving the NCLs their name, the autofluorescent storage material that accumulates in every cell was first described as being similar to ceroid and lipofuscin (Zeman and Dyken, 1969). However, we know now that the major component of the storage material in the NCLs is subunit C of the mitochondrial ATP synthase (Palmer *et al.*, 1992), except in Infantile and Congenital NCL where sphingolipid activating proteins (saposins) A and D accumulate instead (Tyynela *et al.*, 1993). For a long time it was assumed that the storage material itself contributes to pathogenesis and the neurodegeneration in the NCLs as often seen in other LSDs (Suzuki, 1998; Walkley, 2009; Parkinson-Lawrence *et al.*, 2010). However, recent studies have suggested that there is no direct relationship or spatiotemporal link between the storage material and the pathogenesis of NCL (Cooper, 1990; Cooper *et al.*, 2006). These findings were supported by other studies in which pharmacological induction or therapeutic reduction of the storage material had no significant effect on neuron survival or lifespan (Ivy *et al.*, 1984; Griffey *et al.*, 2006). However, secondary effects as a consequence of storage accumulation upon pathogenesis on cellular level and intercellular level cannot be completely ruled out because the normal substrate and/or location of the deficient protein are for most of the NCLs so far unknown. Therefore, although storage material accumulation does not seem to be the primary cause of neuron loss, or cannot be directly linked with it, downstream cues resulting from this

storage may possibly influence other mechanisms including inflammation or leukocyte migration.

b) Neuron loss

Based on the first observations in human *post mortem* tissue, neuron loss was thought to be a widespread and homogenously distributed throughout the NCL brain (Haltia *et al.*, 1973a; Hofmann *et al.*, 1999). However, after studying mouse models, it has become apparent that neuron loss actually shows regional specific selectivity in the majority of NCL mice (reviewed in (Mitchison *et al.*, 2004; Cooper *et al.*, 2006)), and similar data can also be seen in human JNCL cases (Tyynela *et al.*, 2004). This selectivity is particularly evident in the early stages of the disease leading to more widespread neuron loss at the end stage of the disease (Cooper, 2010). Several studies demonstrated an increased vulnerability of GABA-ergic interneurons both in human cases, as well as in animal models of NCL (Cooper *et al.*, 1999; Bible *et al.*, 2004; Pontikis *et al.*, 2004; Tyynela *et al.*, 2004; Oswald *et al.*, 2008). Interneurons in different subfields of the hippocampus seem to be especially affected (Bible *et al.*, 2004; Mitchison *et al.*, 2004; Tyynela *et al.*, 2004), as are for example, pyramidal neurons in the hippocampal CA2 and CA3 sub-regions in JNCL (Tyynela *et al.*, 2004). Furthermore, the thalamocortical system of the brain has emerged to be a particular pathological target in all forms of NCL. Even though pronounced cortical atrophy can be observed at the end stage of the disease, it has been consistently demonstrated that neuron loss starts in the thalamus of most forms of NCL (Pontikis *et al.*, 2005; Weimer *et al.*, 2006; Kielar *et al.*, 2007; Partanen *et al.*, 2008), except in *Cln5*$^{-/-}$ mice where a reverse order of neuron loss has been observed, starting in the cortex and only subsequently reaching the thalamus (von Schantz *et al.*, 2009). Another cell specific neurodegeneration has been reported in the cerebellum of *Cln3*$^{-/-}$ mice where Purkinje cells, but not granule cells, die off first and foremost (Weimer *et al.*, 2009), and similar data are seen in murine INCL (Macauley *et al.*, 2009). Interestingly, even though most of these studies were conducted in mouse models, studies in more complex brains like sheep models and human cases reveal similar phenotypes, but these appear to be much more severe (Oswald *et al.*, 2005; Oswald *et al.*, 2008; Cooper, 2010).

However, the fundamental question of which mechanisms are responsible for neuronal death in NCLs is still unanswered. As suggested in other neurodegenerative diseases, neuronal death can probably not only be described in terms of an apoptotic

vs. necrotic dichotomy (Graeber and Moran, 2002). Likewise, the NCLs probably display a variety of cell death mechanisms. Apoptotic events have been suggested to cause cell death in INCL as well as JNCL (Lane *et al.*, 1996; Gupta *et al.*, 2001; Kim *et al.*, 2006), but the evidence is not compelling, as reviewed in (Mitchison *et al.*, 2004). These apoptotic events have been linked to ER, mitochondrial and oxidative stress in INCL (Kim *et al.*, 2006; Zhang *et al.*, 2006). Additionally, autophagy coincides with cell death in JNCL (Persaud-Sawin and Boustany, 2005; Cao *et al.*, 2006; Chang *et al.*, 2011) and glutamate mediated excitotoxicity has also been reported in INCL and JNCL model systems (Kovacs *et al.*, 2006; Finn *et al.*, 2011, 2012). Furthermore, calcium dependent alterations have been postulated to induce cell death in JNCL (Chang *et al.*, 2007; Chang *et al.*, 2011). However, besides all these mainly cell intrinsic events, other pathological changes in the brain, such as synaptic alterations and glial activation precede, and therefore possibly also influence, neuron loss (reviewed in (Cooper *et al.*, 2006)).

c) Synaptic changes

The first key phenotype that has been shown in several NCL forms to predict subsequent neuron loss is early synaptic pathology. These changes include anterograde transport defects and postsynaptic receptor reductions (Rinne *et al.*, 2002; Weimer *et al.*, 2007), rearrangement of presynaptic compartments, impaired recycling of synaptic vesicle components, altered SNAP/SNARE complex formation and synapse elimination (Kim *et al.*, 2008; Partanen *et al.*, 2008; Kielar *et al.*, 2009). These changes in distribution of synaptic proteins are often supplemented by axonal pathology (Partanen *et al.*, 2008; Kielar *et al.*, 2009). The exact impact of such synaptic changes on neuron loss is currently still unknown. However, these synaptic changes follow the same temporal and regional specific pathways as the subsequent neuron loss, starting first in the thalamus and only later occurring in the cortex (Partanen *et al.*, 2008; Kielar *et al.*, 2009). Therefore, it seems possible that a direct relationship may exist between these two disease phenotypes.

d) Glial activation

The second key feature of NCL pathogenesis and very reliable predictor of subsequent neurodegeneration is glial activation. Glial activation is uniformly present in all forms of NCL (Cooper, 2003; Cooper *et al.*, 2006; Shacka, 2012) and represents the initial response of the innate immune system. Work in CLN6 sheep models

demonstrated that glial up-regulation even occurs prenatally (as early as 40 to 20 days before birth) (Kay *et al.*, 2006). Likewise, in a variety of LSDs there is emerging evidence for an early immune response, which highlights the importance of the immune system in these diseases (Allen *et al.*, 1997; Wada *et al.*, 2000; Jeyakumar *et al.*, 2003; Pontikis *et al.*, 2004; Kielar *et al.*, 2007).

1.5 Immune system

Throughout the body inflammation has two general purposes. On the one hand, there is tissue homeostasis via removing dead cells, promoting the death of damaged cells and wound healing (Lo *et al.*, 1999; Elward and Gasque, 2003). On the other hand, inflammation serves as defence against pathogens via production of cytotoxic substances, of chemokines to recruit specific immune cells and of cytokines to coordinate immune responses and alter resident vascular or tissue cells (Rosenberg, 2002; Carson *et al.*, 2006b; Rivest, 2009).

Immune responses can be divided into two main parts the (unspecific) innate immune response and the (specific) adaptive immune response (Abbas and Lichtman, 2011). Each of the immune responses is the product of complex interactions between various types of immune cells, which are collectively called 'leukocytes' or 'white blood cells' (Abbas and Lichtman, 2011). Immune cells are distinguished via expression of immunologically active proteins on the cell surface, referred as 'cluster of differentiation' (CD) molecules (Bernard and Boumsell, 1984b). Being mainly integral membrane proteins with one or more transmembrane domain, CD molecules act as ligands and receptors on leukocytes (Koubek, 2008). The original CD nomenclature was devised by the Human Leukocyte Differentiation Antigens Workshop (HLDA) in 1984 (Bernard and Boumsell, 1984a), and since then new molecules have been steadily discovered and included. To date, over 350 different CD molecules have been identified and are commonly used to identify and distinguish between classes of adaptive immune cells (Zola *et al.*, 2007; Koubek, 2008).

Simplistically, in the case of an acute inflammation in the tissues of the body periphery, the innate immune response is initiated with the activation of mainly tissue resident dendritic cells and macrophages (Steinman, 1991; Abbas and Lichtman, 2011; Ingersoll *et al.*, 2011). These immune cells express so called 'pattern recognition to as receptors' (PRRs) that traditionally recognise foreign antigens on pathogens, referred

'pathogen-associated molecular patterns' (PAMPs) (Janeway, 1989; Medzhitov and Janeway, 1997). As a consequence, dendritic cells and macrophages on the one hand, release pro-inflammatory cytokines and chemokines to activate other innate immune cells (like neutrophils, natural killer cells, mast cells, basophil or eosinophil), but on the other hand, often also initiate the adaptive immune response consisting of T- and B-cells (Iwasaki and Medzhitov, 2010; Schenten and Medzhitov, 2011). Dendritic cells and macrophages, and also B-cells, are capable of displaying antigens, after phagocytosis or receptor mediated endocytosis, on MHC molecules to naïve T-cells and therefore, are often referred to as 'professional antigen presenting cells' (APCs) (Mellman *et al.*, 1998; Murtaugh and Foss, 2002; Abbas and Lichtman, 2011). Depending on the type of tissue disturbance, the immune response results in the recruitment of different immune cells. Whereas for example, soluble pathogens in the blood system result in complement activation and antibody production by B-cells (Nielsen and Leslie, 2002; Mix *et al.*, 2006; Abbas and Lichtman, 2011; Trouw and Daha, 2011), T-cell based immune responses are required for the effective clearance of intracellular microbes, for example during virus infections (Wiesel *et al.*, 2009; Kennedy, 2010; Abbas and Lichtman, 2011; Kreijtz *et al.*, 2011; Zeromski *et al.*, 2011).

a) Neuroinflammation

Since the brain is considered an immune privileged organ (Galea *et al.*, 2007a), specific cell types and immune reactions lead to distinctive immune responses. Astrocytes and microglia take over the role of the innate immune system by carefully monitoring their surroundings, and in case of disturbance or injury, activate and recruit other (including adaptive) immune cells (Garden and Moller, 2006; Sofroniew and Vinters, 2010). These complex interactions between the immune and nervous system that occur in the brain are comprised in what is termed 'neuroinflammation' (Czirr and Wyss-Coray, 2012).

Neuroinflammation occurs in two stages: The activation of the innate immune responses results from the interactions between neurons and astrocytes and microglia, which accurately regulate and monitor the physiological brain environment (Garden and Moller, 2006; Sofroniew and Vinters, 2010). Microglial activation is a common feature in most forms of NCL (Haltia, 2003), but is also apparent in other lysosomal disorders, for instance Sandhoff disease (Wada *et al.*, 2000), MPSI and IIIB (Ohmi *et al.*, 2003) or neurodegenerative disorders like Krabbe disease (Suzuki, 2003) – to

mention only a few examples. Astrocytosis is similarly a prominent feature in the NCLs (Tyynela *et al.*, 2004), but is also seen for example in Niemann-Pick disease type C (German *et al.*, 2002).

In chronic (as seen in the NCLs) or persistent brain damage or insults, these cellular activations can lead to disruption of the BBB and the recruitment of the adaptive immune responses via pro-inflammatory cytokine release (Finsen and Owens, 2011; Ransohoff and Brown, 2012). In this second stage of neuroinflammation this transition to an adaptive immune response results in a subsequent arrival of systemic effector cells (T-cell, B-cells, NK, macrophages, monocytes), facilitating either cell death or cell survival (Amor *et al.*, 2009). Leukocyte infiltration has been observed in mouse models of LSDs like globoid cell leukodystrophy (Wu *et al.*, 2000), Sandhoff disease (Jeyakumar *et al.*, 2003), and also Juvenile and Infantile NCL (see **Chapter 3** and (Lim *et al.*, 2007b; Macauley *et al.*, 2011)). The adaptive immune cell response may arise from primary glial activation and/or neurodegenerative processes in these childhood disorders. Additionally, neuroinflammation may also be a secondary consequence of lysosomal storage, as has been seen for example in Sandhoff disease (Jeyakumar *et al.*, 2003). The degree of these immune responses are defined by either the extent of glial activation, the presence of auto-antibodies and/or antigenicity of storage material or by-products of neuronal degradation (Lim, 2011).

b) Immune privilege of the brain

As an important feature to understand neuroinflammation, the specific immune properties and privileges of the brain have to be explained. For a long time the brain has been regarded as an organ of complete immune privilege, but these assumptions have been challenged over the years. Nowadays, it is thought that the immune privilege is an active and relative process that is only confined to the CNS parenchyma (Galea *et al.*, 2007a). Other compartments of the brain, including the ventricles containing the choroid plexus, the cerebrospinal fluid (CSF), circumventricular organs (CVO) and the meninges have shown similar immune reactivity to the periphery (Mason *et al.*, 1986; Andersson *et al.*, 1992; Matyszak and Perry, 1996a; Blond *et al.*, 2002). Therefore, the supposed immunological privilege of the brain appears to be relative. Immune responses in the brain can be divided into an afferent (= sensing) and an efferent (= effector) arm. Only the afferent arm of the CNS immune system seems to be privileged and restricted (Galea *et al.*, 2007a), i.e. it is mainly reliant on

transport of a soluble (auto) antigen to the cervical lymph nodes (Yamada *et al.*, 1991; Kida *et al.*, 1993; Weller *et al.*, 1993), or alternatively the cellular migration of T-cells (Goldmann *et al.*, 2006) or dendritic cells (DC) from the CSF (Hatterer *et al.*, 2006) and/or even the brain parenchyma (Gottfried-Blackmore *et al.*, 2009; Felger *et al.*, 2010) to the cervical lymph nodes. The efferent arm is definitively active and systemic cells can enter the brain parenchyma under surveillance or non-pathological conditions (Hickey, 2001), but especially in the case of inflammation they can do so without any hindrance, as long as the right binding partners or receptors are up-regulated in the brain (endothelial cells, antigen presenting cells) (Greenwood *et al.*, 2002).

c) Blood brain barrier (BBB)

One of the main features of the 'immune privilege' in the CNS is the BBB. It results from the selectivity of tight junctions of endothelial cells of brain capillaries, which are surrounded and supported by perivascular pericytes and the endfeet of astrocytes (Abbott *et al.*, 2010). The role of pericytes in BBB function is not well studied and the role of astrocytes is controversial (see **section 1.6a** below), but all three cell types result in a diffusion barrier that controls the permeability and entry of substances and cells on the basis of polarity and size into the brain (Ballabh *et al.*, 2004; Abbott *et al.*, 2006). Furthermore, there are three main interfaces of the BBB. In the brain and spinal cord of all mammals the main 'classical' interface is formed by cerebrovascular endothelial cells between blood and brain interstitial fluid (ISF), secondly by the choroid plexus epithelium between blood and the ventricular CSF, and thirdly by the arachnoid epithelium between blood and subarachnoid CSF (Abbott *et al.*, 2006) (see **Figure 2**). But the BBB is not fixed and can be modulated and regulated according to physiological and pathological state (Abbott, 2005). Therefore, it is important to consider these features of the BBB when interpreting experimental data and directing therapeutic approaches into the brain.

1.6 Innate immune responses in the brain

Besides dendritic cells and infiltrated macrophages from the systemic circulation, the main two cell types of the innate immune system of the brain are astrocytes and microglia. Each of the two has its specific roles and functions in the brain under healthy, as well as inflammatory conditions (Garden and Moller, 2006; Sofroniew and Vinters, 2010). Their activation is a characteristic feature of NCL pathology (Oswald *et*

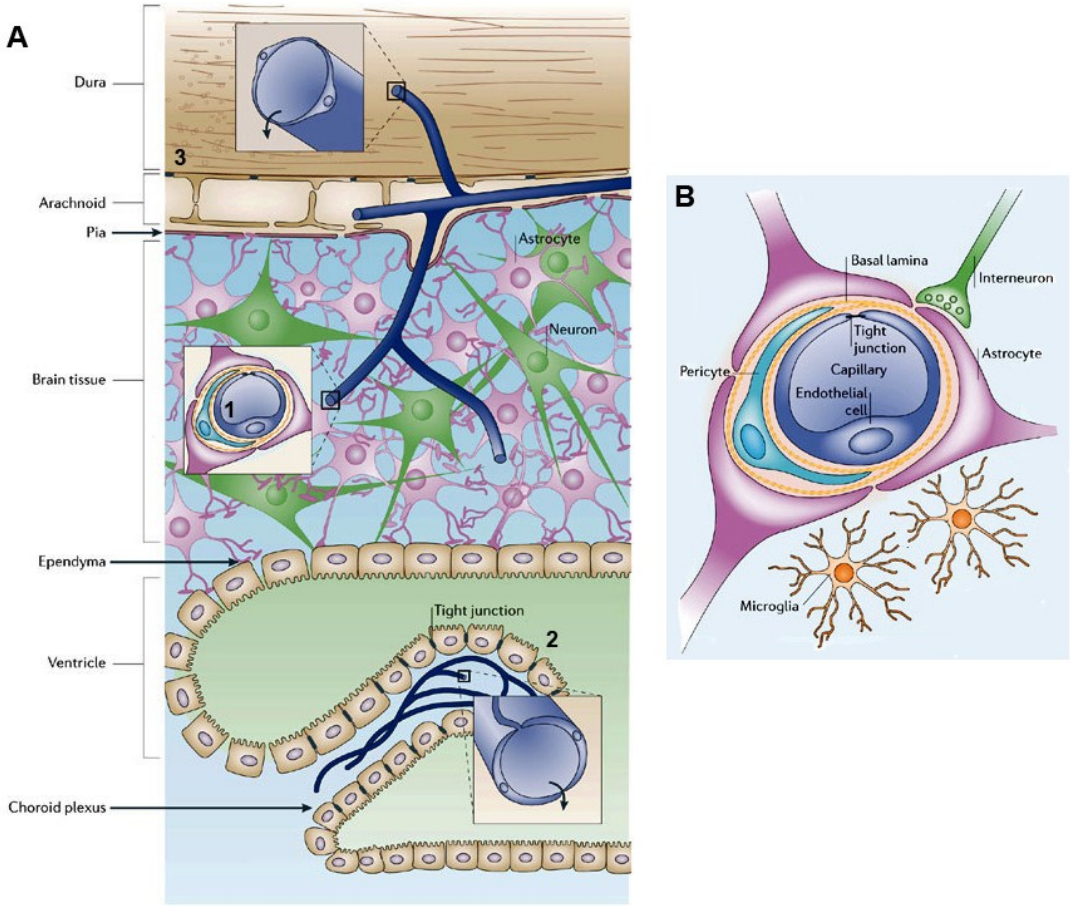

Figure 2. Location of barrier sites in the CNS and the blood brain barrier (BBB). (A) There are three main barrier sites with interfaces between blood and neural tissue or fluid spaces in the CNS: (1) the cerebrovascular endothelial cells of the BBB between blood and brain interstitial fluid (ISF), (2) the choroid plexus epithelium between blood and cerebrospinal fluid (CSF) and (3) the arachnoid epithelium as the middle layer of the meninges between blood and subarachnoid CSF. At each site tight junctions reduce the permeability of paracellular pathways of molecular substances and cell migration. (B) Schematic illustration of the BBB. The barrier is formed by capillary endothelial cells surrounded by the basal lamina, pericytes and the endfeet of astrocytes. Tight junctions between the endothelial cells provide the main barrier function. Astrocytes provide a cellular link to neurons (not shown). Microglia are also in close proximity to the BBB. Adapted from (Abbott *et al.*, 2006).

al., 2005; Pontikis *et al.*, 2005; Kay *et al.*, 2006; Kielar *et al.*, 2007; von Schantz *et al.*, 2009; Kuronen *et al.*, 2012; Schmiedt *et al.*, 2012; Thelen *et al.*, 2012), and therefore shall be described in more detail.

a) Astrocytes

The entire CNS is contiguously covered in a non-overlapping manner by astrocytes (Nedergaard *et al.*, 2003; Halassa *et al.*, 2007b). Once regarded as the 'glue of the brain', nowadays numerous functions have been assigned to astrocytes in the healthy brain (see review (Sofroniew and Vinters, 2010)). During brain development, astrocytes are

thought to be important for the formation of synapses and induction of neurite pruning (Christopherson *et al.*, 2005; Stevens *et al.*, 2007; Barres, 2008). In the adult brain, astrocyte processes envelop essentially all synapses, where they perform crucial maintenance functions related to fluid, ion, pH and transmitter homeostasis at the synaptic cleft (Simard and Nedergaard, 2004; Obara *et al.*, 2008). Via their high expression of neurotransmitter transporters astrocytes can rapidly clear the synaptic clefts of excessive glutamate, GABA or glycine (Sattler and Rothstein, 2006; Seifert *et al.*, 2006). In this context, there is supporting evidence that astrocytes are directly involved in synaptic transmission and alter neuronal excitability by release of synaptic active molecules, so called 'gliotransmitters' (Nedergaard *et al.*, 2003; Shigetomi *et al.*, 2008). This idea gave rise to the hypothesis of the 'tripartite synapse' postulating that astrocytes exchange information, respond to and regulate synaptic activity of neurons at the synapses (Halassa *et al.*, 2007a; Perea *et al.*, 2009). These processes are linked to a form of astrocyte excitability mediated via regulated increases in intracellular calcium concentrations (Cornell-Bell *et al.*, 1990; Charles *et al.*, 1991), which can even be propagated to neighbouring astrocytes and create an internal communication network between astrocytes via Ca^{2+} waves (Volterra and Meldolesi, 2005). Furthermore, the release of growth factors, as seen during development (Barres, 2008), astrocyte regulation of blood flow (Gordon *et al.*, 2007; Iadecola and Nedergaard, 2007), and the direct contribution of astrocytes to CNS energy metabolism have been demonstrated in the adult brain (Brown and Ransom, 2007). The latter contribution is made possible because astrocytes can interlink blood and neurons via their processes, and therefore their uptake of glucose from the blood can directly enable the transfer of energy metabolites to neuronal cells (Brown *et al.*, 2004; Pellerin *et al.*, 2007). Last but not least, astrocytes are involved in the formation of the BBB along with endothelial cells and perivascular pericytes (see **section 1.5c** above). Whether astrocytes take on the function of the actual barrier or not, or whether it is only the tight junctions between the endothelial cells that are responsible for the selectivity, is still disputed (Ballabh *et al.*, 2004; Haseloff *et al.*, 2005; Saunders *et al.*, 2008). Nevertheless, astrocytes have been shown to influence BBB permeability, particularly in the state of inflammation (Beck *et al.*, 1984; Abbott, 2005).

Under inflammatory conditions, astrocytes play a role in innate immune responses, responding by their activation and hypertrophy (Perry *et al.*, 1992; Farina *et al.*, 2007).

This astrocytosis or reactive gliosis is easily identified by astrocytes developing thickened fibrous processes (Luse, 1958; Graeber and Kreutzberg, 1986). Up-regulation of intermediate filament (IF) proteins, in particular glial fibrillary acidic protein (GFAP), by reactive astrocytes is perhaps the best known hallmark of astrocytosis and an important histopathological sign of CNS injury (Eng *et al.*, 1971; Raivich *et al.*, 1999; Pekny and Nilsson, 2005). Astrocytes display a wide range of receptors involved in innate immunity, including Toll-like, mannose and scavenger receptors (Husemann and Silverstein, 2001; Sasaki *et al.*, 2001; Bsibsi *et al.*, 2002; Liu *et al.*, 2004; Farina *et al.*, 2005; Farina *et al.*, 2007; Hanke and Kielian, 2011). Even nucleotide-binding oligomerization domains and components of the complement system can be found on astrocytes (Gasque *et al.*, 2000; Sterka *et al.*, 2006). Especially after activation, astrocytes are also able to secrete soluble mediators that have an impact on both innate and adaptive immune responses (Dorf *et al.*, 2000; Ambrosini and Aloisi, 2004; Farina *et al.*, 2007).

The exact influence of astrocytosis upon neuron survival has been debated at length. It becomes increasingly apparent that astrocytosis is not an 'all or nothing' process with only one consequence, but instead can have neuroprotective as well as neurotoxic effects in the brain (see reviews (Sofroniew, 2009; Sofroniew and Vinters, 2010)). Astrocytosis occurs as a response to a wide variety of CNS disturbances including injury and disease (Faulkner *et al.*, 2004; Myer *et al.*, 2006; Drogemuller *et al.*, 2008). These responses display a graded spectrum of molecular signals and altered gene expression, which lead to astrocyte hypertrophy and various effects on neurons (Eddleston and Mucke, 1993; John *et al.*, 2005; Lovatt *et al.*, 2007; Cahoy *et al.*, 2008; Daginakatte *et al.*, 2008). Moreover, different diseases, different stages of disease progression, and different brain locations result in various outcomes, suggesting that these astrocyte responses are very much context dependent (Wilhelmsson *et al.*, 2006; Hewett, 2009; Sofroniew, 2009; Yeh *et al.*, 2009). The traditional view of astrocytosis being negative *per se* (Ramon y Cajal, 1928) has been revised in recent years with several studies describing protective roles for astrocytosis, for example via uptake of extracellular glutamate (Rothstein *et al.*, 1996), BBB repair (Bush *et al.*, 1999), reduction of inflammatory spread (Faulkner *et al.*, 2004; Li *et al.*, 2008) and others (see review (Sofroniew and Vinters, 2010) for further details/examples). However, at the same time other studies have attributed detrimental roles to astrocytosis by compromising BBB integrity (Argaw *et al.*, 2009), and also exhibiting an increased inflammatory

response and immune cell infiltration via cytokine release (Brambilla *et al.*, 2009), reducing neuronal regeneration (Wilhelmsson *et al.*, 2004), releasing excitotoxic glutamate (Takano *et al.*, 2005) or even contributing to seizure genesis (Tian *et al.*, 2005). All in all, astrocytes can take on several functions and have heterogeneous roles in the healthy and diseased brain, which should be considered in the context of the NCLs.

b) Microglia

The role of microglial cells in neurologically normal brains ranges from apoptotic cell removal and induction of cell death (Bessis *et al.*, 2007; Streit and Xue, 2009), extensive tissue remodeling (Pollard, 2009) to axon guidance in white matter during development (Milligan *et al.*, 1991). Microglia are also thought to act as synaptic sensors and may be involved in synaptogenesis and synapse degeneration (Bessis *et al.*, 2007; Wake *et al.*, 2009). However, the main roles of microglia are in surveillance by monitoring their immediate proximity in the brain. Microglia are very mobile and constantly surveying the brain which enables them to quickly respond to any disturbance (Kreutzberg, 1996; Hailer *et al.*, 1997; Stence *et al.*, 2001). This has been shown *in vitro*, and in histological studies, but also recently in the living brain via two-photon microscopy (Nimmerjahn *et al.*, 2005). These properties have given microglia the reputation of being the 'brain's immune system' (Graeber and Streit, 1990).

Accordingly, innate immune responses within the CNS largely involve microglial activation (Perry and Gordon, 1988; Kreutzberg, 1996). Once a threat has been identified microglial cells respond quickly to destroy the infectious agents before they damage neural tissue (Stoll and Jander, 1999). As part of this stimulation process microglia transform from their quiescent ramified morphology into activated microglia (Ransohoff and Perry, 2009). But in extreme cases of inflammation or brain injury, they further transform into brain macrophages (Raivich *et al.*, 1999; Streit, 2002; Hanisch and Kettenmann, 2007), which act as phagocytic cells in the CNS (Perry and Gordon, 1988). Since antibodies cannot cross the BBB due to their large size (Seitz *et al.*, 1985; Azzi *et al.*, 1990; Dai *et al.*, 2002), microglia must be able to recognise antigens, incorporate them, and act as antigen-presenting cells (via MHC II) to activate the adaptive immune system and recruit T-cells (Fischer and Reichmann, 2001; Kim and de Vellis, 2005). In addition, microglial cells are increasingly recognised to play an important role in inflammatory responses within the CNS via the secretion of

cytokines, chemokines and trophic factors (Lee *et al.*, 1993; Presta *et al.*, 1995; Elkabes *et al.*, 1996; Hanisch, 2002; Lee *et al.*, 2002; Kim and de Vellis, 2005). This pro-inflammatory release of chemotactic substances by activated microglia seems to be crucial for immune responses in the CNS (Thomas, 1992; Garden and Moller, 2006). However, whereas several studies have demonstrated that microglia are fundamentally neuroprotective and have beneficial effects on neuronal survival (Neumann *et al.*, 2006; Gowing *et al.*, 2008; Hines *et al.*, 2009), in other studies microglia often contribute directly to the pathogenesis of a variety of neurodegenerative diseases (Dickson *et al.*, 1991; Kreutzberg, 1996; Gonzalez-Scarano and Baltuch, 1999; Lobsiger and Cleveland, 2007).

Therefore, microglial activation should perhaps be considered as a 'double-edged sword' in neurodegenerative diseases, depending on the extent and stage of disease progression, microglia may be initially neuroprotective and subsequently exert a negative effect on neuron survival. There is a precedent for this happening in amyotrophic lateral sclerosis (ALS) (Fendrick *et al.*, 2007), where motor neuronal death was linked to microglial dysfunction, attributing neurodegeneration to a loss of microglial-mediated neuroprotection. These properties are consistent with the theory of functional 'microglial plasticity' (Streit *et al.*, 1988), which proposes that not only resting or activated microglia are present in the brain, but rather a mix of several subpopulations of macrophage-like cells expressing different genes and cytokines. Just as macrophages outside the CNS originally have been identified as classical (M1) or alternative (M2) activated macrophages (Gordon, 2003), similarly different activation states have also been identified for microglia (Michelucci *et al.*, 2009). However, the strict definition of these two activation states of macrophages becomes increasingly blurred by the discovery of intermediate activation states (Mosser and Edwards, 2008), and microglia can also adopt different phenotypes depending on various stimuli and secondary challenges (Hanisch and Kettenmann, 2007; Colton and Wilcock, 2010). There is even evidence of regionally specific activation within the brain (Choi *et al.*, 2012). This issue is exacerbated by the ambiguity of contemporary microglial markers, as typified by CD68 or F4/80. Such commonly used microglial markers are only cell specific to the extent that they do not label other glial cells or neurons, but are unable to discriminate microglia from peripheral macrophages. This ambiguity had to be considered when interpreting microglial staining results in our experiments on NCL brains, but this matter will be discussed in more detail in **Chapter 7**.

1.7 Adaptive immune responses in the brain

As a second part of the immune system, the adaptive immune response consists of two major types of immune cells, T- and B-cells (collectively known as lymphocytes) (Abbas and Lichtman, 2011). These cell types guarantee a more specific immune response against pathogens or antigens in the body, as well as in the brain. One main advantage of this system is that the adaptive immune response can not only target and clear pathogens more efficiently, it also supplies memory cell functions that enable rapid responses to re-occurring infections (Lefrancois, 2006; Abbas and Lichtman, 2011; Masopust and Picker, 2012). The antigen specificity of T- and B-cells is accomplished by the display of a large diversity of cell surface receptors, which can bind to an unlimited number of antigens (Boudinot *et al.*, 2008; Jhunjhunwala *et al.*, 2009). For successful activation of lymphocytes, T-cell and B-cell receptors (TCR and BCR) have to recognise antigens bound to MHC molecules on APCs (mainly dendritic cells, macrophages and B-cells) (Mondino and Jenkins, 1994; Medzhitov and Janeway, 1998; Dustin, 2008; Abbas and Lichtman, 2011), besides several other co-stimuli (Fathman and Lineberry 2007; Mor et al. 2007). This complex is often referred to as the 'immunological synapse' (Bromley *et al.*, 2001; Sims and Dustin, 2002). To generate the necessary variation of antigen-recognition regions, genes of TCR and BCR are assembled via a so called 'V(D)J recombination' which is directed by the lymphocyte-specific recombinases RAG-1 and RAG-2, and ubiquitously expressed DNA repair proteins (Bassing *et al.*, 2002). Recombination-activating gene-1 and 2 (RAG-1 or RAG-2) proteins cleave the DNA at well-conserved recombination signal sequences (RSSs) that flank variable (V), diversity (D) and joining (J) TCR gene segments (Schatz *et al.*, 1989; Oettinger *et al.*, 1990; Schlissel *et al.*, 1993). Subsequently, the ends of the recombination signals (RS) are joined precisely, while coding ends are modified, rearranged and resolved by non-homologous end joining (Tonegawa, 1983). The V(D)J recombination takes place in the primary lymphoid tissue (thymus for T-cells and bone marrow for B-cells), after which a stringent selection process of TCR/BCR specificity against MHC molecules and auto-antigens determines the survival of functional adaptive immune cells (Hardy *et al.*, 2000; Starr *et al.*, 2003). Released from the thymus/bone marrow into the body periphery, B-cells and T-cells are potent antigen recognising cells, with a high concentration of lymphocytes found in the lymph and lymphoid tissues like the spleen or lymph nodes (Crivellato *et al.*, 2004;

Abbas and Lichtman, 2011; Boehm *et al.*, 2012). As one of the main focuses of this thesis it is important to consider T-cells in more detail.

a) T cells

Various subsets of T-cells exist with different functions, but each can be distinguished via their expression of different CD molecules. The main distinction is made between CD8+ve T-cells, also known as 'cytotoxic T-cells', and CD4+ve T-helper cells (Abbas and Lichtman, 2011). CD8 is a transmembrane glycoprotein that acts as a co-receptor for the TCR during interactions at the immunological synapse (Miceli and Parnes, 1991; Abbas and Lichtman, 2011; Laugel *et al.*, 2011). Antigen specific binding of peptides displayed on the major histocompatibility complex (MHC) molecule class I proteins by both receptors (TCR and CD8) initiates CD8+ve T-cell activation (Engleman *et al.*, 1981; Meuer *et al.*, 1982; Norment and Littman, 1988; Connolly *et al.*, 1990). Most nucleated cells express MHC I molecules on which endogenous (possibly foreign) peptides are displayed for potential activation of CD8+ve T-cells (Germain, 1994; Abbas and Lichtman, 2011). Additionally, some APCs, in particular dendritic cells, can also activate CD8+ve T-cells after digestion of extracellular antigens and peptide presentation on MHC I, in a process called 'cross-presentation' (Brossart and Bevan, 1997; Amigorena and Savina, 2010; Joffre *et al.*, 2012). The main function of activated CD8+ve T-cells is to induce apoptosis (Shresta *et al.*, 1998; Trapani *et al.*, 2000) of virus or pathogen infected, damaged or dysfunctional nucleated cells after identifying specific antigenic peptides bound to MHC class I molecules (Townsend and Bodmer, 1989; Cohen *et al.*, 1992; Germain, 1994; Page *et al.*, 1998). Cytotoxic T-cells initiate death cascades, either via Fas Ligand (FasL)-Fas interactions at the cell surface, or release secretory proteins from lysosome-like compartments which are referred to as lytic granules (Peters *et al.*, 1991; Suda *et al.*, 1995). Additionally, CD8+ve T cells are capable of producing pro-inflammatory and regulatory cytokines (Koide and Engleman, 1990; Salgame *et al.*, 1991; Ciubotariu *et al.*, 1998; Filaci *et al.*, 2004).

CD4 is, like CD8, a glycoprotein that assists the TCR as a co-receptor while recognising MHC class II molecules on the surface of APCs (Janeway, 1991; Abbas and Lichtman, 2011). MHC II molecules display (via phagocytosis or receptor mediated endocytosis) internalised and processed extracellular antigens that can initiate T-helper cell activation after successful recognition by CD4 and TCR. (Schwartz *et al.*, 1978; Germain, 1994; Abbas and Lichtman, 2011). CD4+ve T-helper cells facilitate

antibody production via B-cell activation, enhance macrophage activity and recruit other immune cells (like neutrophils, eosinophils, basophils) to inflammation sites (Zhu and Paul, 2008; Abbas and Lichtman, 2011). In general, CD4+ve T-helper cells are important for the coordination of the immune response via the production of various cytokines and chemokines (Germain, 1994; Zhu and Paul, 2008; Zhu and Paul, 2010). Traditionally, it was thought that CD4+ve T-helper cells are essential for the activation and proliferation of CD8+ve T-cells (Bach *et al.*, 1977; Keene and Forman, 1982; Guerder and Matzinger, 1989). However, the prevailing view is currently that CD4+ve T-cells can be dispensable for CD8+ve T-cell expansion, but generally facilitate proliferation and activation of CD8+ve T-cell responses indirectly via dendritic cell differentiation, which in turn promotes CD8+ve T-cell activation (reviewed in (Castellino and Germain, 2006)). Furthermore, CD4+ve T-cells are required for the generation of CD8+ve memory T-cells (Janssen *et al.*, 2003; Shedlock and Shen, 2003). CD4+ve T-helper cells themselves can be divided into Th1 and Th2 cells (Mosmann *et al.*, 1986), depending on cells they interact with and the cytokines that they release (Romagnani, 1997; Dong and Flavell, 2001). Th1 cells provide immunity against intracellular pathogens or disturbances. Therefore, they promote cellular immune responses by maximising the killing efficacy of macrophages and assist in priming of CD8+ve T-cells (Mosmann and Coffman, 1989; Paul and Seder, 1994). In contrast, Th2 cells provide immunity against extracellular pathogens by binding to B-cells and accelerating the humoral immune response via increased antibody production (Mosmann and Coffman, 1989; Paul and Seder, 1994). Furthermore, in recent years, CD4+ve T-regulatory cells, as well as Th17 cells have been identified (Sakaguchi, 2004; Harrington *et al.*, 2005). In contrast to other effector T-cells, which are suggested to begin with pro-inflammatory cytokine expression and switch later in their life-cycle to inhibitory cytokines (Zhu and Paul, 2008; Zhu and Paul, 2010; Cope *et al.*, 2011), CD4+ve T-regulatory cells exhibit solely an anti-inflammatory role in the immune response (Sakaguchi, 2000; Shevach, 2002). This is mainly via transforming growth factor β (TGF-β), interleukin-10 (IL-10) and interleukin-35 (IL-35) release (Li *et al.*, 2006; Collison *et al.*, 2007; Rubtsov *et al.*, 2008). On the other hand, CD4+ve Th17 cells characteristically produce interleukin 17 (IL-17) and have been originally assigned to a pathogenic role in autoimmune diseases (Harrington *et al.*, 2005; Stockinger and Veldhoen, 2007). However, in recent years Th17 cells have been shown to have their own effector and regulatory functions,

particularly in the host defence against bacteria and fungi (Weaver *et al.*, 2006), and therefore, illustrate an example of the recently suggested functional plasticity of immune responses as an intrinsic factor of T-helper cells (Zhu and Paul, 2010; Hirota *et al.*, 2011; Larsen *et al.*, 2011). Last but not least, to confuse matters even more, cytotoxic abilities of CD4+ve T-cells have also been identified. Cytotoxic CD4+ve T-cells can induce apoptosis either via FasL-Fas interactions with target cells or via granzymes and perforin release (Hahn *et al.*, 1995; van de Berg *et al.*, 2008). Controversially, in humans these processes seem to happen in an antigen- and MHC-independent manner, whereas in mice they mainly happen in a MHC II-dependent manner (Soghoian and Streeck, 2010). However, the cytotoxic functions of CD4+ve T-cells have been suggested to be important as an immunomodulatory process for eliminating activated MHC II expressing target cells (APCs) or other T-cells (Hahn *et al.*, 1995; van de Berg *et al.*, 2008). But more commonly, cytotoxic CD4+ve T-cells have been associated with viral infections where they can assist the clearance of virus-infected cells, and furthermore, may be generated through repeated antigen stimulation in chronic infections (Brown, 2010; Soghoian and Streeck, 2010). Therefore, cytotoxic CD4+ve T-cells putatively represent another example of the suggested functional plasticity of CD4+ve lymphocytes (Appay, 2004; Brown, 2010; Zhu *et al.*, 2010), that is discussed above.

In many neurodegenerative diseases CD4+ve T-helper cells have been identified as contributing to pathogenesis, including for example multiple sclerosis (Stadelmann *et al.*, 2011), Parkinson (Brochard *et al.*, 2009) and Alzheimer disease (Heneka and O'Banion, 2007) amongst many others. Likewise, CD8+ve cytotoxic T-cells have also often been identified as making a harmful contribution to disease pathogenesis. Rasmussen's Encephalitis is a classic example of cell based epilepsy and a MHC-I related disease in which CD8+ve cytotoxic T-cells are directly associated with brain pathogenesis (Bien *et al.*, 2002). Furthermore, CD8+ve T-cells also play a major role in ALS (Holmoy, 2008), where they are found in the precentral gyrus (Kawamata *et al.*, 1992) and cortico-spinal tracts (Troost *et al.*, 1990), or in perivascular distributions in the parietal cortex and hippocampus of Alzheimer disease patients (Itagaki *et al.*, 1988; Town *et al.*, 2005).

b) T cells in the brain

Because of the seclusion of the brain from the body periphery by means of specialised

structures like the BBB, meninges and/or ventricular system, the entry of lymphocytes into the brain is not as straight forward as in other organs of the body (Galea *et al.*, 2007a; Engelhardt, 2008). Thus, three main preferred routes of leukocytes into the brain have been described: Firstly, via the choroid plexus into the ventricles and CSF; secondly, via the blood system of the meninges into the subarachnoid space; or thirdly, directly from cerebral blood vessels via the perivascular space into the brain parenchyma (see **Figure 3**) (Ransohoff *et al.*, 2003; Wilson *et al.*, 2010). Compared to the first two pathways, the latter requires the lymphocytes to cross the tightly regulated vascular endothelium of the BBB (Ransohoff *et al.*, 2003; Owens *et al.*, 2008). On a side note, T-cells are thought to exit the brain via the same pathways along which the CSF drains: they get back into the blood system via arachnoid villi and granulations at the major venous sinuses (see **Figure 3**) (Ransohoff *et al.*, 2003; Johanson *et al.*, 2008; Wilson *et al.*, 2010).

As a first requirement for crossing the BBB, T-cells (or leukocytes in general) have to exit blood vessels, a process termed 'extravasation'. This is a tightly regulated event that involves the interaction of molecular cues between the endothelial and immune cells. A precise sequence of steps controlled by adhesion molecules and activation factors has been characterised and summarised into a so-called 'multistep paradigm' (Butcher, 1991; Springer, 1994). Classically, four simplified steps of transmigration have been defined: Firstly, T-cells are captured and roll along the endothelial wall, partly via the help of selectins (L-selectin, P-selectin and E-selectin (Kansas, 1996) which interact with P-selectin glycoprotein ligand 1 (PSGL1) and other glycosylated ligands (McEver and Cummings, 1997)) and also by means of integrins that bind members of the immunoglobulin family (Ley *et al.*, 2007; Constantin, 2008). As second step, the immune cells characteristically become activated by chemokines (or other chemoattractants) that have been released either from the brain parenchyma or are presented on glycosaminoglycans (GAGs) on the endothelial cells (Johnson *et al.*, 2005). These chemokines interact with G-protein coupled receptors to activate intracellular signalling leading to leukocyte integrin activation (so called 'inside-out signalling') (Simon *et al.*, 1991; Laudanna *et al.*, 2002; Kinashi, 2005). As a third step, the immune cells arrest, due to binding of the activated integrins (most studied are 'lymphocyte function-associated antigen 1' (LFA1) and 'very late antigen 4' (VLA4)) to immunoglobulin superfamily members like 'intercellular adhesion molecule' (ICAM-1) and 'vascular cell-adhesion molecule 1' (VCAM1), expressed by endothelial cells ('so

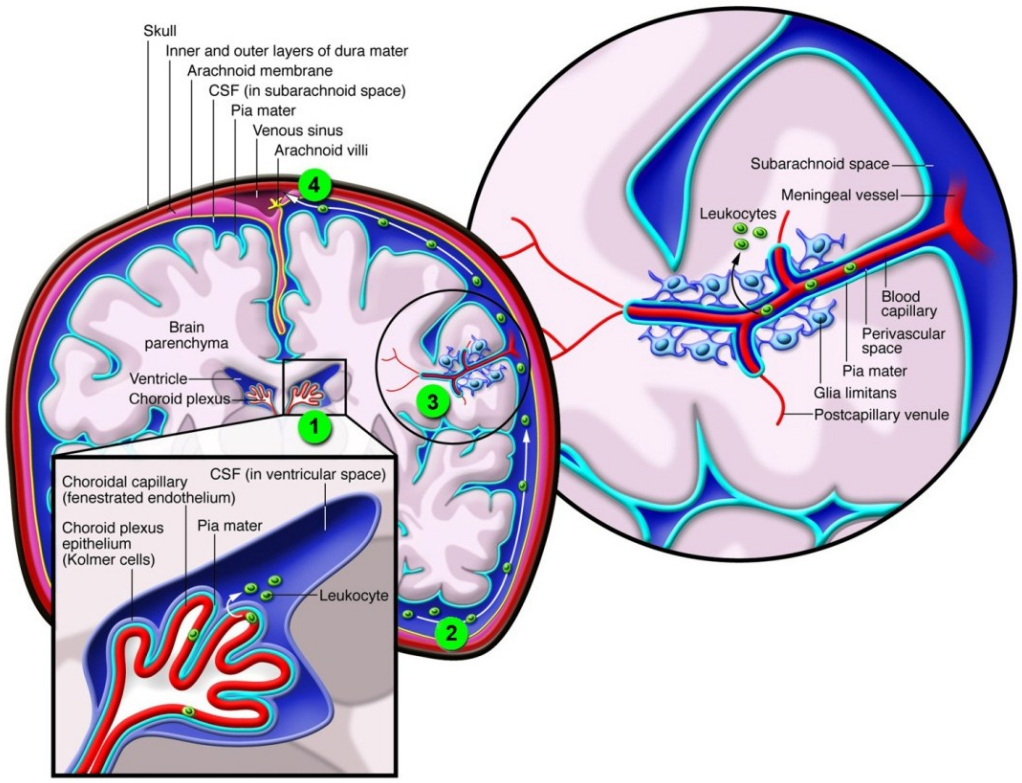

Figure 3. Schematic illustration of the brain showing the routes of leukocyte entry and traffic. The brain is surrounded by the skull and the three layers of the meninges: dura mater, arachnoid membrane and pia mater. Between the latter two, the subarachnoid space contains the cerebrospinal fluid (CSF), which is produced by the epithelium cells of the choroid plexus within the ventricles. From there the CSF circulates around the brain parenchyma and drains into the blood/venous sinus via arachnoid villi. Meningeal blood vessels extend from the subarachnoid space over the pia mater creating the perivascular space (also known as 'Virchow-Robin space'). Arterial branches divide into capillaries to supply blood deep inside the brain parenchyma. Leukocytes can enter the CSF via the choroid plexus (1), the blood veins in the meninges (2) or directly to the parenchyma via blood capillaries within the brain (3). In the latter case, leukocytes have to migrate over the tightly regulated vascular endothelium as part of the blood brain barrier (BBB), crossing the subarachnoid space, pia mater and glia limitans. Leukocytes can circulate and exit the brain via pathways of the flowing CSF ending up in the venous sinus (4). Adapted from (Wilson *et al.*, 2010)

called 'outside-in signalling') (Campbell *et al.*, 1996; Campbell *et al.*, 1998). Finally, these steps lead to 'diapedesis' or transmigration. Recent research has defined additional steps: capture (or thethering), slow rolling, adhesion strengthening and spreading, intravascular crawling and paracellular or transcellular transmigration (Feng *et al.*, 1998; Engelhardt and Wolburg, 2004; Ley *et al.*, 2007). Having successfully penetrated the endothelial-cell barriers, leukocytes migrate through the endothelial basement membrane and, most commonly, the pericyte sheath to reach the perivascular space (Ley *et al.*, 2007). Interestingly, leukocyte extravasation only occurs in post-capillary venules where less strong shearing forces of the blood flow act on the leukocytes and more favourable anatomic features (like the separation of glia limitans

and the endothelial layer) promote cell migration as opposed to the environment of (arterial) capillaries (Lewinsohn *et al.*, 1987; Carlos and Harlan, 1994; Engelhardt and Ransohoff, 2005; Bechmann *et al.*, 2007).

On a side note, these distinct differences between blood vessels can lead to confusion when referring to the term 'BBB' in the context of leukocyte infiltration. On the one hand, the term 'BBB' physiologically refers to the ability of the vascular segment of the capillaries to regulate diffusion of solutes, but on the other hand, in the context of neuroinflammation, the term refers to the postcapillary venules from which leukocytes migrate into the CNS (Bechmann *et al.*, 2007; Owens *et al.*, 2008). Likewise, the term 'BBB permeability' can encompass soluble diffusion and/or cellular migration into the brain.

Nevertheless, the vasculature will also differ between CNS compartments which will influence immune cell entry (Owens *et al.*, 2008). For example, the fenestrated endothelium of the choroid plexus and circumventricular organs or the mono-layer structure of blood vessels in the meninges allow easier access of leukocytes to the CSF, compared to the double membrane barrier present in the brain parenchyma (Wilson *et al.*, 2010).

However, in all steps the endothelial cells play a crucial role, depending on their state of activation (under physiological or inflammatory conditions) different ligands and cell adhesion molecules are expressed, which control selective leukocyte (or in particular T-cell) transmigration (Carlos and Harlan, 1994; Springer, 1994; Fabbri *et al.*, 1999). Yet, leukocytes themselves can also alter vascular properties (Dahlen *et al.*, 1981). Generally, successful immune cell migration into the CNS varies depending on the immune subtype, the condition of the migrating cell, the state of the neural parenchyma and the endothelial cells (Hickey, 1999).

Furthermore, as a second step after migrating into the perivascular space, T-cells have to cross the glia limitans, which consists primarily of the parenchymal basement membrane and astrocytic endfeet, to reach the brain parenchyma. Whereas chemokines and integrins have been suggested to exert the major influence upon leukocyte extravasation (Campbell *et al.*, 1996; Johnson *et al.*, 2005), matrix metalloproteases have been shown to play a crucial role for the migration across the glia limitans as second barrier (Toft-Hansen *et al.*, 2006). This migration process is

tightly regulated by astrocytes via the secretion of chemokines and/or overall changes to the BBB permeability (Ransohoff *et al.*, 2003; Farina *et al.*, 2007). Thus, leukocytes (like T-cells) often remain in the perivascular space in the absence of favourable parenchymal conditions like on-going neuroinflammation (Owens *et al.*, 2008).

With regard to T-cells, the current consensus view proposes that it is mainly activated T-cells that enter the brain parenchyma (Wekerle *et al.*, 1986; Hickey *et al.*, 1991; Neumann and Wekerle, 1998; Carrithers *et al.*, 2002), apart from CD4+ve T-memory cells that survey the brain under healthy conditions (Kivisakk *et al.*, 2003; Goverman, 2009). Interestingly, each subset of T-cells has been suggested to utilise a different route of entry. Whereas CD4+ve T-cells rely on APCs and their MHC II expression in the perivascular space to successfully enter the brain parenchyma (Ransohoff *et al.*, 2003; Greter *et al.*, 2005; Becher *et al.*, 2006), antigen-specific CD8+ve T-cells have been shown to gain entry independent of APCs, but via the expression of MHC I molecules upon cerebral endothelial cells (Galea *et al.*, 2007b; Melzer *et al.*, 2009).

Nevertheless, how and where these T-cells are primed or activated to become able to enter the brain is a highly debatable point. Some authors suggest that the activation of T-cells occurs in the deep cervical lymph nodes by APCs (Yamada *et al.*, 1991; Ling *et al.*, 2003; Karman *et al.*, 2004; Hatterer *et al.*, 2006), while others favour perivascular priming or activation in the meninges, CSF or choroid plexus (Fischer and Reichmann, 2001; Greter *et al.*, 2005; Serafini *et al.*, 2006). Moreover, it has even been proposed that T-cell activation occurs directly in the brain parenchyma itself by APCs during normal CNS surveillance, or even after entry as naïve T-cells (Becher *et al.*, 2000; Krakowski and Owens, 2000; Greter *et al.*, 2005; McMahon *et al.*, 2005; Bailey *et al.*, 2007; Zozulya *et al.*, 2009; Jain *et al.*, 2010). In the particular case of chronic or autoimmune related inflammation, as often seen in neurodegenerative diseases including the NCLs (DeLegge and Smoke, 2008; Amor *et al.*, 2009; Goverman, 2009; Lynch and Mills, 2011), the activation of T-cells may be mediated via soluble antigen drainage into the cervical lymph nodes (Cserr *et al.*, 1992). However, even after activation, effector T-cells have to be re-activated either in the CSF or brain parenchyma after entry (Shrikant and Benveniste, 1996; Aloisi *et al.*, 2000b), due to short-lived activation and lifespan of these cells (Bauer *et al.*, 1998).

Once in the brain parenchyma T-cells face a variety of challenges, with the largest being to avoid death by apoptosis. All cells in the CNS express Fas ligand (FasL) and

infiltrating Fas-positive T-cells can experience apoptosis irrespective of antigen specificity (Bauer *et al.*, 1998; Bechmann *et al.*, 1999; Choi and Benveniste, 2004). Therefore, in order to survive, infiltrating lymphocytes have to recognise their specific antigen on MHC molecules in the brain (Shrikant and Benveniste, 1996; Aloisi *et al.*, 2000a; Melzer *et al.*, 2009). In the healthy CNS MHC expression is minimal, but under inflammatory conditions CNS MHC expression is markedly up-regulated (Shrikant and Benveniste, 1996; Neumann *et al.*, 1997; Kimura and Griffin, 2000; Neumann, 2001; Olson *et al.*, 2001). Furthermore, the CNS microenvironment is rather hostile for adaptive immune cells as, under normal conditions, both astrocytes and microglia help sustain an anti-inflammatory environment in the brain (Garden and Moller, 2006; Melzer *et al.*, 2009; Sofroniew and Vinters, 2010). Astrocytes have been shown to inhibit T-cell proliferation and induce T-regulatory cells (Meinl *et al.*, 1994; Trajkovic *et al.*, 2004). Likewise, microglia can negatively regulate T-cell activation and cytokine production (Kwidzinski *et al.*, 2005; Magnus *et al.*, 2005), and last but not least, neurons have also been shown to influence T-cells in their proximity (Liu *et al.*, 2006).

1.8 Neurons can influence immune cells

Neurons are very sensitive to their milieu and once their health is compromised, they do not have an inherent capacity to regenerate. In the crosstalk between different CNS cell types, neurons have always been considered as passive victims of reactions and/or insults from astrocytes (Farina *et al.*, 2007) or microglia (Hanisch and Kettenmann, 2007). However, recent studies have elucidated that neurons actually play a larger role than previously appreciated in controlling both innate and adaptive immune responses in the CNS (Biber *et al.*, 2007; Levite, 2008).

Whereas the innate immune response (consisting of dendritic cells and macrophages in the meninges or the perivascular space (Matyszak and Perry, 1996b; McMenamin, 1999; Bechmann *et al.*, 2001; McMenamin *et al.*, 2003), and of astrocytes and microglia inside the parenchyma) is very sensitive to microclimate changes, the adaptive immune cell activation in the brain is harder to provoke and is usually avoided for as long as possible (Garden and Moller, 2006; Melzer *et al.*, 2009; Sofroniew and Vinters, 2010). Under normal healthy conditions, this relative retention of adaptive immune responses is controlled in the first instance by the BBB, by the absence of draining lymphatic vessels in the brain and by ensuring that astrocytes and microglia have a poor antigen presenting capacity (Carson *et al.*, 2006a). However, T-cells routinely enter the

parenchyma in an activated state to perform their surveillance function (Kivisakk *et al.*, 2003; Engelhardt and Ransohoff, 2005) see also **Chapter 3**). Therefore, maintaining glial cells as inefficient at antigen presentation is of major importance to avoid provoking unnecessary immune responses. As a consequence, neurons have developed ways to modify or influence these activation processes. On the one hand, neurons can suppress or down-regulate (micro)glial activation in a contact-independent manner via neurotransmitters, neurotrophins, neuropeptides or cytokines (Pavlov and Tracey, 2004; Reinke and Fabry, 2006; Biber *et al.*, 2007; Levite, 2008). These processes take place predominantly in the perivascular space and are essential to keep the integrity of the brain and BBB under healthy conditions. Alternatively, after an insult or on-going inflammation, direct contact-dependent interactions between neurons, glia and T-cells become more important. Presently, three important interactions are recognised (Tian *et al.*, 2009). Firstly, neurons can down-regulate the APC properties of glial cells and suppress for example the nitric oxide (NO) or tumour necrosis factor-α (TNF-α) release of microglia via cell-cell receptor interactions (e.g. NCAM or CD22) (Chang *et al.*, 2000; Mott *et al.*, 2004). These mechanisms potentially allow stressed neurons to protect themselves from further microglial damage (Minghetti *et al.*, 2005). Secondly, it has been suggested that neurons are directly able to suppress T-cell activation via cell adhesion molecules (i.e. cadherins) (Grundemann *et al.*, 2006; Ito *et al.*, 2006), and also to change the Th1 and Th2 balance of T-cells (Liu *et al.*, 2006; Dittel, 2008), although direct evidence for this is rather limited. Last but not least, neurons (as well as glial cells) express Fas Ligand, which can promote apoptosis of activated T-cells (Bechmann *et al.*, 1999; Choi and Benveniste, 2004). Additionally, stressed neurons can secrete a protein called Sema-3A to induce apoptosis of activated microglia after binding to the microglial neuropilin-1 and plexin-1 receptor complex (Majed *et al.*, 2006). Furthermore, direct interaction with apoptotic neurons forces microglia to release anti-inflammatory cytokines and neuroprotective agents, and to simultaneously reduce the secretion of nitric oxide and pro-inflammatory proteins (Minghetti *et al.*, 2005). Interestingly, many cell adhesion molecules (CAMs) (like cadherins) are also involved in synaptic plasticity and are strongly expressed on neurons in regions of neurogenesis and on neuronal stem cells (Tai *et al.*, 2008; Tian *et al.*, 2009). CAMs not only administer normal regeneration processes in these regions, but at the same time are proposed to ensure that the inflammatory response is kept to a minimum (Pluchino *et al.*, 2005; Ben-Hur, 2008).

In summary, with the secretion of different neuroprotective substances, as well as direct cell-cell interactions, neurons have the ability to influence both glial cells and T-cells to enhance a neuroprotective environment and to reduce the likelihood of adaptive immune responses.

Finally, it should be mentioned that neurons can also enhance inflammatory responses under certain circumstances, for example after injury to accelerate innate immune responses and clearance of cell debris (Rubartelli and Lotze, 2007; Pais *et al.*, 2008; Tian *et al.*, 2009). This raises the question of what determines which direction this neuronal influence will tilt, to either suppress or promote inflammation. Moreover, it could be speculated that neurons also take on different roles during the progression of neurodegenerative disorders like the LSDs. As such, this possibility shall be considered when interpreting our findings on the NCLs in **Chapter 7**.

1.9 Lysosomes in immune cells

As described above (see **section 1.1b**), the lysosome is involved in a variety of intracellular processes (Saftig and Klumperman, 2009). Therefore, it is not surprising that any dysfunction in the complex endosomal/lysosomal pathways due to protein deficiency could lead to numerous functional consequences in a range of cell types (as for example described in neurons above in **section 1.1c**). However, immune cells in particular, with their many varied interactions with antigens and other (immune) cells, seem especially prone to such functional alterations. This hypothesis is supported by several findings of immune irregularities in the LSDs and in some forms of NCL (Castaneda *et al.*, 2008).

Firstly, the accumulation of lysosomal storage material is evident in immune cells in many LSDs (Aula *et al.*, 1975; Bruck *et al.*, 1991; Kieseier and Goebel, 1994). Before genetic tools became available, the storage inclusions in T-cells in the blood periphery were used as a reliable diagnostic tool for the NCLs (Dolman *et al.*, 1980; Bruck *et al.*, 1991). In Late Infantile NCL 12-21%, and in Juvenile NCL 20-70% of lymphocytes, are reported to contain vacuolated inclusions (Dolman *et al.*, 1980; Ikeda *et al.*, 1982; Kimura and Goebel, 1988). However, a direct effect of such storage material on function of these immune cells has still to be unambiguously shown. Studies addressing this issue, after deriving leukocytes from peripheral blood monocytes from NCL patients, did not reveal any differences in reactive oxygen species, cytokine

production or cell proliferation compared to control cells (Kieseier *et al.*, 1997). Nevertheless, an increase in apoptotic cell death and cellular turnover was detected in NCL-patient derived leukocytes (Kieseier *et al.*, 1997). However, certain immune cell functions do require a properly functional lysosome, which could be impaired in the NCLs. Lysosomes are particularly involved in antigen presenting functions via MHC I and MHC II receptors, cytotoxic T-cell functions and natural killer T-cell development (reviewed in (Castaneda *et al.*, 2008)).

Via MHC I molecules the majority of nucleated cells present endogenous peptide antigens to the immune system, in particular CD8+ve T-cells, providing a powerful surveying tool for the immune system to recognise viral infected, transformed or diseased cells (Germain, 1994; Davis *et al.*, 1998). Although the majority of degradation of the endogenous proteins destined for MHC I presentation occurs in the cytosol by the proteasome (Tanaka *et al.*, 1997), a lysosomal enzyme (TPPII) has been shown to also independently generate epitopes for MHC I (Seifert *et al.*, 2003), therefore suggesting a role of the endosomal/lysosomal pathways in MHC I peptide presentation. As such, these mechanisms could be affected in LSDs and NCLs, as for example an altered MHC I expression has been shown in Gaucher disease (Balreira *et al.*, 2005).

More obviously the lysosome is directly involved in cleavage of antigens and their loading onto MHC II proteins (Watts, 2001; Schmid and Munz, 2005). MHC II expression is normally only found in professional APCs, including macrophages, dendritic cells, activated T- and B-cells (Drozina *et al.*, 2005). Generally, these cell types present their antigens displayed on MHC II molecules to CD4+ve T-helper cells, the main regulators of the immune system (Germain and Margulies, 1993; Zhu and Paul, 2008). To date, no direct evidence for these processes being altered has been reported in any LSD. Nevertheless, alterations in pH (Bach *et al.*, 1999; Virmani *et al.*, 2005; Yanagawa *et al.*, 2007), oxidation/reduction states (Deganuto *et al.*, 2007), protein sorting (Cooper, 2003; Fraldi *et al.*, 2010), and of course storage accumulation, have been demonstrated in several LSDs. Each of these factors alone, or in combination, could have considerable potential to modify antigen processing in the lysosome and therefore the APC functions of immune cells.

Another involvement of lysosomes in immune cell function is in their control of CD8+ve cytotoxic T-cell activity. As described previously (see **section 1.7a**), cytotoxic

T-cells can recognise foreign or transformed cells via MHC I molecule interactions (Townsend and Bodmer, 1989; Abbas and Lichtman, 2011), and can induce cell apoptosis via FasL-Fas interactions at the cell surface or the release of lytic granules (Peters *et al.*, 1991; Suda *et al.*, 1995; Page *et al.*, 1998). The delivery of FasL to the cell surface and the secretion of lytic granules are carefully regulated by the lysosome, and drugs that increase the pH of the lysosomal compartment have been shown to block cytotoxic T-cell activity (Kataoka *et al.*, 1994). As already mentioned, lysosomal pH is altered in a subset of LSDs (Bach *et al.*, 1999; Yanagawa *et al.*, 2007) including the NCLs (Virmani *et al.*, 2005), and it is possible that cytotoxic T-cell functions are deficient as well. Furthermore, it has been shown that during the secretory process of CD8+ve T-cells, storage material in LSDs ends up in the extracellular space (Klein *et al.*, 2005a). Similar events and storage clearance have been proposed as a general consequence of plasma membrane repair and exoctytosis (Medina *et al.*, 2011). Speculatively, such secretory events could also be important in the induction of autoimmune responses (Castaneda *et al.*, 2008).

Last but not least, the accumulation of storage material has been proposed to alter natural killer T-cell (NKT) development in the thymus (Godfrey *et al.*, 2006; Castaneda *et al.*, 2008). Most NKT cells are a subset of T-cells, which are characterised by a partially invariant T-cell receptor and they are mainly involved in regulatory functions of the immune response via the production of various cytokines (van der Vliet *et al.*, 2004). NKTs recognise lipids and glycolipids mainly via CD1d molecules that are expressed on the surface of cells, similar to the expression of MHC molecules (Brigl and Brenner, 2004). For the correct development of these cells in the thymus, lysosomes have to appropriately load the CD1d protein in the thymus (MacDonald, 2002), and in the complete absence of CD1d NKT cells do not develop (Mendiratta *et al.*, 1997). Similarly, reduced levels of NKT cells have been described in various LSD mouse models, which has been linked to incorrect processing and presentation of antigen by CD1d protein (Daly *et al.*, 2000; Gadola *et al.*, 2006). However, similar events have not yet been reported in the NCLs, but it would indeed be quite likely. Nevertheless, the direct effect of such impairments on the maturation and development of the immune system and response is still unknown in these disorders.

Furthermore, such lysosomal deficiencies are likely to affect not only the classical immune cells, but also glial cells as part of the innate immune response. The same

potential impairments of MHC II and MHC I dependent antigen presentation are valid for dendritic cells, macrophages, microglia and astrocytes. There is also emerging evidence for general glial dysfunction in both INCL and JNCL (Dihanich, 2010; Milà, 2012; Parviainen, 2012) which shall be discussed below (see **section 1.10a**).

In summary, although there are several potential links and correlations between endosomal/lysosomal deficiencies and altered adaptive immune cell function, the exact consequences of such altered immune responses on the pathogenesis of LSDs, including the NCLs, remains unclear. However, these possible alterations should be kept in mind while investigating disease progression and pathogenesis, as it is certainly plausible that defects in the lysosomal system may also directly affect immune responses in the NCLs.

1.10 Immune responses in Infantile and Juvenile NCL

All forms of NCL display pronounced innate immune responses within the brain, including both astrocytosis and microglial activation. Glial responses have been reported in most neurodegenerative disorders ranging from Alzheimer and Parkinson disease, to trauma or ischemia (Neumann, 2001; Rogers *et al.*, 2007), and also in other lysosomal storage disorders (Jeyakumar *et al.*, 2003; Ohmi *et al.*, 2003).

Gliosis can be found in *post mortem* tissue of individuals who succumbed to JNCL (Braak and Goebel, 1978, 1979; Tyynela *et al.*, 2004), and in other forms of NCL (Haltia *et al.*, 1973a; Haltia *et al.*, 1973b; Tyynela *et al.*, 1997; Tyynela *et al.*, 2004). Analogous innate inflammatory responses can be seen in mouse models of various forms of NCL (Oswald *et al.*, 2005; Cooper *et al.*, 2006; Kay *et al.*, 2006; von Schantz *et al.*, 2009; Kuronen *et al.*, 2012; Schmiedt *et al.*, 2012; Thelen *et al.*, 2012), similarly in Juvenile or Infantile NCL (Bible *et al.*, 2004; Pontikis *et al.*, 2004; Pontikis *et al.*, 2005; Kielar *et al.*, 2007; Macauley *et al.*, 2009; Weimer *et al.*, 2009; Macauley *et al.*, 2011)

As in human INCL, at the end stage of the disease, *Ppt1*$^{-/-}$ mice display a widespread and pronounced neuron loss and glial activation in the cerebellum, the cortex and numerous subcortical regions (Gupta *et al.*, 2001; Bible *et al.*, 2004; Kielar *et al.*, 2007; Macauley *et al.*, 2009). However, in the course of disease progression a distinct regional and cellular selectivity can be observed, especially within the thalamocortical system (Kielar *et al.*, 2007), and in the cortex and hippocampus at the end stage of the disease (Bible *et al.*, 2004). Moreover, as mentioned above, in *Ppt1*$^{-/-}$ mice, an early localized

astrocytosis precedes neuron loss, with subsequent microglial activation in the thalamocortical system from 3 months onwards and in the cerebellum from 1 month onwards (Kielar *et al.*, 2007; Macauley *et al.*, 2009). These inflammatory responses are complemented by early up-regulation of inflammatory genes and mediators (Qiao *et al.*, 2007; Saha *et al.*, 2008), which can recruit peripheral immune cells to the brain (Zhang *et al.*, 2007). Nonetheless, the adaptive immune responses involved in Infantile NCL have not been investigated so far, even though the first indications of immune cell infiltration have recently been reported, albeit briefly (Macauley *et al.*, 2011).

Astrocytosis and microglial activation also occur in *Cln3* deficient mice, but in a much more subtle manner (Pontikis *et al.*, 2004; Pontikis *et al.*, 2005). In the cerebellum, GFAP and F4/80 glial up-regulation have already been observed in *Cln3*$^{-/-}$ mice 7 days after birth (Weimer *et al.*, 2009), or at 3 months of age in *Cln3* knock-in mice (Herrmann *et al.*, 2008b). From 5 months onwards a clear astrocytosis and microglial cell activation was detected in the forebrain of *Cln3*$^{-/-}$ mice (Pontikis *et al.*, 2004). These findings were confirmed in 12 month old *Cln3* knock-in mice (Pontikis *et al.*, 2005), and in the oldest (19 month old) *Cln3* knock-in mice analysed so far (Herrmann *et al.*, 2008b). As in other forms of NCL, this glial activation is predominantly seen in the cerebellum and the thalamocortical system, and is followed by subsequent selective neuron loss (Pontikis *et al.*, 2004; Pontikis *et al.*, 2005; Weimer *et al.*, 2009). However, these glial responses in JNCL mice appear to be atypical with incomplete morphological transformation of glial cells (see **section 1.10a** below) (Pontikis *et al.*, 2004; Tyynela *et al.*, 2004; Pontikis *et al.*, 2005; Dihanich, 2010; Parviainen, 2012). Furthermore, specific to JNCL pathogenesis, and not observed in other NCL forms so far, JNCL patients and *Cln3*$^{-/-}$ mice demonstrate an early autoimmune response (Chattopadhyay *et al.*, 2002a; Chattopadhyay *et al.*, 2002b; Castaneda and Pearce, 2008). The presence and deposition of autoantibodies in the JNCL brain has been described (Lim *et al.*, 2007b), and immunosuppressive drugs or genetic deletion of B-cells proved their direct influence on JNCL pathogenesis ((Seehafer *et al.*, 2011) and **Chapter 7**). However, apart from this presence of autoantibodies the involvement of adaptive immune cells has not been investigated in Juvenile NCL.

To date, it is not known what triggers immune cell activation in the CNS. The glial response in other more chronic diseases is thought to be triggered variously by abnormal β-amyloid protein accumulation or initial neuronal loss/brain injury (Stoll

and Jander, 1999; Minagar *et al.*, 2002). In the NCLs, glial responses are most likely triggered as a consequence of the gene deficiency itself, and disturbances in cell homeostasis resulting in a slow onset of excitotoxicity in selective neuron populations of the brain (Das *et al.*, 2001; Luiro *et al.*, 2006). Subtle neuronal homeostatic changes could already warn surveillance cells like microglia and astrocytes to induce an inflammatory response. To mention only a few such changes (see **section 1.2b** and **section 1.2c** above): ER and oxidative stress and misfolded protein responses (Kim *et al.*, 2006; Zhang *et al.*, 2006), compromised lipid metabolism and trafficking (Ahtiainen *et al.*, 2007; Lyly *et al.*, 2008), disturbances in autophagic pathways (Cao *et al.*, 2006) or calcium homeostasis (Chang *et al.*, 2007). Similarly, early synaptic pathology (Virmani *et al.*, 2005; Song *et al.*, 2008; Kielar *et al.*, 2009), or excitotoxicity via increased glutamate levels (Chattopadhyay *et al.*, 2002a; Pears *et al.*, 2005) may also contribute to the initiation of immune reactions in the brain. In any case, innate immune reactions are always present in NCL brains. In addition to these well-characterised innate immune responses, the adaptive immune responses shall be investigated in this thesis and the impact of each immune response upon neurodegeneration discussed in **Chapter 7**.

a) Glial dysfunction in INCL and JNCL

Another important aspect to consider is the entire idea of 'gliodegeneration', according to which glial cells are dysfunctional and consequently cause neurodegeneration (Croisier and Graeber, 2006). Although mainly referred to in aging and age-dependent disorders (Streit and Xue, 2009), dysfunctional glia may also play a role in the NCLs. There is *in vitro* evidence that the biology of astrocytes is compromised in both JNCL and INCL, and in JNCL that these changes may exert a negative influence on neuron health (Dihanich, 2010; Milà, 2012; Parviainen, 2012). Pure microglial cultures derived from *Cln3* deficient mice also show an impaired morphological response to stimulation and a series of specific alterations in cytokine release, yet retain normal phagocytic properties (Dihanich, 2010). Furthermore, similar results have been obtained for *Cln3*$^{-/-}$ astrocytes, which show a broader range of functional defects. They also show an impaired morphological response to stimulation, marked cytoskeletal abnormalities and pronounced secretion defects. These defects extend to a dramatic reduction in glutathione secretion, the major anti-oxidant in the brain (Dringen, 2000; Fernandez-Fernandez *et al.*, 2012), together with evidence for altered internal calcium responses (Parviainen, 2012). Most intriguingly, mutant glia appear to directly harm the survival of both healthy and mutant neurons

when co-cultured with primary cortical neurons, but this can be ameliorated by substituting wildtype glia, suggesting that a therapeutic benefit can be gained by treating glia alone.

Likewise, first indications from cell culture experiments on *Ppt1*$^{-/-}$ astrocytes suggest that they display also abnormalities (Milà, 2012). Under basal conditions they already resemble stimulated astrocytes and morphologically only partly respond to stimulation (Milà, 2012). Nevertheless, further detailed characterisation of *Ppt1*$^{-/-}$ glial cells is still required. However, if glial dysfunction can be confirmed in both INCL and JNCL mice, a direct comparison of glial defects in these mice may reveal the role of each deficient protein (Ppt1 and Cln3) in the different types of glia. Secondly it may also give us clues as to where the initial pathological symptoms arise: in astrocytes, or microglia or neurons, or indeed a combination of these cell types.

1.11 Modification of immune responses

The field of neuroinflammation has gained increasingly more interest in recent years, in particular in the context of neurodegenerative diseases. There are potentially convergent mechanisms between classical inflammatory diseases like multiple sclerosis, which demonstrate neurodegenerative features, and classical neurodegenerative disorders like Alzheimer disease, Parkinson disease or the NCLs which show increasing evidence of the pathogenic role of inflammation (Zipp and Aktas, 2006; Aktas *et al.*, 2007; Infante-Duarte *et al.*, 2008; Lim, 2011).

Both innate and adaptive inflammatory responses can lead to, or possibly be caused by, neurodegeneration. To determine the answer to such a 'chicken or egg' question will be crucial for any successful treatment of these diseases. This relationship will very likely vary between disease types and at different stages of disease progression. However, potential confounders of neuroinflammation will also have to be considered. An acute systemic inflammation can increase brain pathology and neuroinflammation (Perry, 2004; Holmes *et al.*, 2009). Alternatively impaired immune cells may contribute directly to disease pathology (Gadola *et al.*, 2006). As discussed above, this is particularly likely in lysosomal storage disorders like the NCLs, because the lysosome has been shown to be involved in antigen presenting mechanisms (see **section 1.9** above and (Hsing and Rudensky, 2005)).

It will be essential to define the pathogenic role of each immune response (and con-

founding factors) to develop effective treatments. Indeed, each part of the immune response can have different implications for disease progression. In this thesis we investigate the role of adaptive immune cells, as well as the role of an immune regulatory protein called sialoadhesin that is expressed on macrophages. By knocking out either, an essential enzyme for T- and B-cell maturation called RAG-1, or sialoadhesin in NCL mice, we aimed to identify the exact role of these two immune responses in the disease pathogeneses and establish a further link between neurodegenerative disorders and neuroinflammation. Hence, the properties and functions of the proteins RAG-1 and sialoadhesin will be defined in more detail.

a) RAG-1

V(D)J rearrangement is an essential process during the maturation of B- and T-lymphoid cells and is activated by enzymes called recombination-activating gene-1 and -2 (RAG-1 and RAG-2) (see also **section 1.7** above and (Schatz *et al.*, 1989; Oettinger *et al.*, 1990). Their first identification was *ex vivo* in fibroblasts and both proteins are required for a successful execution of V(D)J recombination (Oettinger *et al.*, 1990). They are lymphoid specific enzymes that carry out the cutting of DNA after the initial recognition of RSSs, whereas the other processes are linked to ubiquitously expressed DNA repair molecules (Schlissel *et al.*, 1993). RAG-1 and RAG-2 are sufficient to induce V(D)J recombination activity when expressed in non-lymphoid cells (Schatz *et al.*, 1989; Oettinger *et al.*, 1990). Mice lacking Rag-1 or Rag-2 are completely defective in V(D)J recombination, and therefore contain no mature B or T cells (Mombaerts *et al.*, 1992; Shinkai *et al.*, 1992). These mice show no other overt defects, indicating that *Rag* genes are lymphocyte specific and only expressed in T- and B-cells. Therefore *Rag-1* and *Rag-2* deficient mice have become useful model systems for studying adaptive immune responses and have been used in several studies in numerous disease settings (Matthews *et al.*, 2002; Bieber *et al.*, 2003; Berghoff *et al.*, 2005; Ip *et al.*, 2006). An additional advantage of *Rag-1* or *Rag-2* deficient mice is that after cell specific re-constitution of subsets of T-cells or B-cells (via BMT for example), the direct impact of a specific adaptive immune cell type on disease progression can be investigated (Sun *et al.*, 2001; Ip *et al.*, 2006; Dimayuga *et al.*, 2011). For the same reasons, the crossbreeding of *Rag-1* deficient mice with NCL mouse models represents an ideal means to investigate the role of adaptive immune cells in the pathogenesis of different forms of NCL.

b) Sialoadhesin (Sn)

Sn was first described in 1985 as a non-phagocytic sheep erythrocyte receptor (SER) on resident bone marrow macrophages (Crocker and Gordon, 1985, 1986). The production of a monoclonal antibody four years later was essential for the characterisation (Crocker and Gordon, 1989), purification (Crocker *et al.*, 1991) and eventually molecular cloning of this gene, which led to the renaming of the receptor to Sn (Crocker *et al.*, 1994). Thus, Sn was defined as a sialic-acid dependent macrophage adhesion molecule as a member of the immunoglobulin superfamily (IgSF) with an extracellular region of 17 immunoglobulin domains (Crocker *et al.*, 1994). Since they are used by antibodies and T-cell receptors these immunoglobulin domains make use of the structural diversity of glycans in their recognition function and can bind to a vast number of molecules (Williams and Barclay, 1988; Powell and Varki, 1995; Angata and Brinkman-Van der Linden, 2002). Sn is a well conserved protein in mammals and belongs to a subset of the immunoglobulin superfamily called 'siglecs' (sialic-acid binding immunoglobulin-like lectins) (Kelm *et al.*, 1994). All siglecs are transmembrane proteins that contain extracellular V-like immunoglobulin (IgV) domains, which bind sialic acids and a variable number (16 in the case of Sn) of C2-type immunoglobulin (IgC2) domains (see **Figure 4**, (Crocker *et al.*, 1998)). Intracelluar tyrosine based signalling motifs are common in most siglecs, but interestingly Sn lacks these signalling motifs in its cytoplasmic tail suggesting a predominant role in cell-cell interactions rather than in cell signalling (Crocker, 2002).

To date, 15 different siglecs have been identified in humans and 9 in mice, while most of them can be found on haemotopoietic and immune cells (Pillai *et al.*, 2012). Apart from resting T-cells, in mice and humans most immune cells express at least one siglec, or sometimes even several (Crocker *et al.*, 2007) (see **Figure 4**). The exact role of siglecs is still unknown, but it is assumed that their recognition of sialic acid/sialylated glycans is important to regulate adhesion, cell signalling and endocytosis (Crocker and Varki, 2001; Crocker, 2002; Varki and Angata, 2006), and especially in regulating innate and adaptive immune cells. Siglecs are able to regulate the functions of innate and adaptive immune cells via sialic acid compounds, which are modified during immune cell development and activation (Pillai *et al.*, 2012), as for example the regulation of cell proliferation or cell survival (Vitale *et al.*, 1999; Nutku *et al.*, 2003; von Gunten *et al.*, 2005). Furthermore, a role for siglecs as self and non-self recognition molecules is now emerging (as reviewed in (Paulson *et al.*, 2012)). Siglecs

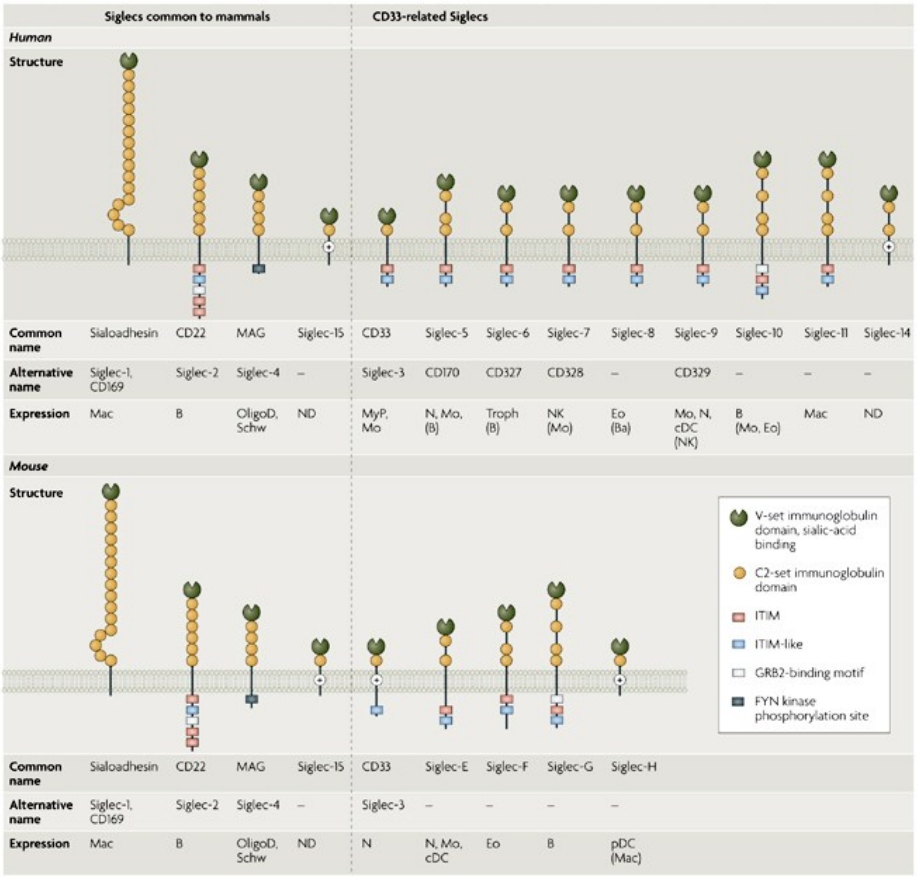

Figure 4. Siglec proteins in humans and mice. Sialic-acid-binding immunoglobulin-like lectins (siglecs) are type 1 membrane proteins and consist of an amino-terminal V-set immunoglobulin domain, which recognises sialic acid, and varying numbers of C2-set immunoglobulin domains. According to their evolutionary conservation and sequence similarity, they can be divided into "common siglecs" and "CD33-related siglecs". CD33-related siglecs show high sequence similarity in their extracellular regions and often contain conserved tyrosine-based signalling motifs in their cytosolic domains, but differ in composition between species. In contrast, sialoadhesin, CD22, myelin-asociated glycoprotein (MAG) and siglecs-15 exhibit lower sequence similarity, but represent orthologues in all mammals examined. Siglecs are expressed on various immune cells. To date, 15 human and 9 murine siglecs have been identified (human siglecs-12 and siglecs-16 are not shown). B = B cells, Ba = basophils, cDCs = conventional dendritic cells, Eo = eosinophils, GRB2 = growth factor-receptor-bound protein 2, ITIM = immunoreceptor tyrosin-based inhibitory motif, Mac = macrophages, Mo = monocytes, MyP = myeloid progenitors, N = neutrophils, ND = not determined, NK = natural killer cells, OligoD = oligodendrocytes, pDCs = plasmacytoid dendritic cells, Schw = schwann cells, Troph = trophoblasts. Reproduced from (Crocker et al., 2007).

utilise the fact that all mammalian cells express glycolipids and glycoproteins, to which they can bind via sialic acid containing glycans, and hence recognise 'self' (Ohtsubo and Marth, 2006; Crocker *et al.*, 2007). Therefore, most siglecs are believed to carry out an immune inhibitory role and have often been linked to autoimmune responses (Paulson *et al.*, 2012; Pillai *et al.*, 2012).

However, in contrast to all other siglecs, Sn (also known as siglec-1 or CD169) is thought to act as a pro-inflammatory binding protein of macrophages. Its special role compared to the other siglecs is also supported by its unique structure, with a lack of

intracellular and the extended extracellular domains (see **Figure 4**) (Crocker *et al.*, 1994). Sn is expressed under normal conditions on macrophages in lymphoid tissues (particularly in spleen, lymph nodes) and adrenal gland (Dijkstra *et al.*, 1985; Crocker and Gordon, 1986; van den Berg *et al.*, 2001). In the brain Sn immunoreactivity is normally only found on macrophages in the meninges or choroid plexus (Perry *et al.*, 1992). However, under inflammatory conditions, Sn expression is rapidly up-regulated and found on macrophages at sites of inflammation in body tissue of both humans and rodents (van den Berg *et al.*, 1992; Hartnell *et al.*, 2001), but also on infiltrated macrophages and on nearby microglia in the brain (Perry *et al.*, 1992). It has been shown that mainly interferon-α (IFN-α), but also other glucocorticoid, cytokines and inflammatory stimuli can up-regulate Sn expression on macrophages (van den Berg *et al.*, 1996; York *et al.*, 2007). The exact function of Sn is still debatable, but since it is exclusively expressed on macrophages and displays cell-cell interaction properties, a role in endocytic or phagocytic processes has been postulated (Jones *et al.*, 2003; Delputte *et al.*, 2011). Sn can mediate interactions with immune cells in both sialic acid-dependent, but also sialic acid-independent, manner. Whereas for example CD43 on T-cells is a putative Sn ligand in a sialic acid-dependent manner (van den Berg *et al.*, 2001), Sn has also been shown to bind to the mannose receptor of several myeloid cells, and other lectin receptors (MGL1) in an sialic acid-independent manner (Martinez-Pomares *et al.*, 1996; Kumamoto *et al.*, 2004). Furthermore, Sn has been shown to facilitate interactions with various (sialylated) pathogens including bacteria (Jones *et al.*, 2003; Heikema *et al.*, 2010), viruses (Rempel *et al.*, 2008; Seyerl *et al.*, 2010; Van Breedam *et al.*, 2010) and even parasites (Monteiro *et al.*, 2005). However, most strikingly recent studies have demonstrated the involvement of Sn+ve macrophages in lymphocyte activation and regulation of T- and B-cell responses (reviewed in (Martinez-Pomares and Gordon, 2012)), suggesting their importance in antigen presentation and self vs. non-self recognition in the spleen or lymph nodes (see **next section 1.11c** and (Junt *et al.*, 2007; Miyake *et al.*, 2007; Backer *et al.*, 2010; McGaha *et al.*, 2011). To what extent Sn itself is involved as a ligand in these processes, is still controversial (Revilla *et al.*, 2009; Klaas and Crocker, 2012). However, recent studies with *Sn* deficient mice have confirmed its role as a regulator of adaptive immune cells, particularly in the context of neurodegenerative disorders, resulting in decreased (CD8+ve) T-cell activation and infiltration as well as overall disease amelioration (Jiang *et al.*, 2006; Kobsar *et al.*, 2006; Ip *et al.*, 2007). As a consequence, Sn has gained

interest as a potential target for immunotherapy, on the one hand, by specifically targeting antigens or drugs to macrophages or on the other hand, by specifically blocking Sn and its function as an immune system regulator (Halkes *et al.*, 2003; Ducreux *et al.*, 2009; O'Reilly and Paulson, 2009; Kratzer *et al.*, 2010; De Baere *et al.*, 2011; Delputte *et al.*, 2011). To highlight the potential role of Sn in the body and putatively in the brain, the specific role of Sn expressing macrophages will be addressed in more detail.

c) Sialoadhesin positive macrophages

In general, macrophages act as one of the first frontiers of the body's innate immune system. They are essential for phagocytic cell clearance, as well as presenting antigens to B- and T-cells via MHC II molecules (Badwey and Karnovsky, 1980; Unanue, 1984; Abbas and Lichtman, 2011). In the rest of the body, as well as in the brain, macrophages are distinguishable by their expression of different receptor and binding molecules, such as mannose receptor (MR) and PECAM-1 for example (Watt *et al.*, 1995; Takahashi *et al.*, 1998; Gordon and Taylor, 2005). The expression of different receptors depends on tissue location and activation status (Gordon *et al.*, 1995). Therefore, each subset of macrophages represents a functional specialization, as for example also Sn+ve macrophages.

Three types of Sn+ve macrophages can be found systemically in mice: marginal zone metallophilic (MZM) macrophages in spleen, and subcapsular sinus (SS) and medullary (Med) macrophages in lymph nodes (Crocker and Gordon, 1989). In the spleen, as well as in the lymph node, Sn+ve macrophages are strategically (and ideally) located at the cross-road between blood and lymph to activate adaptive immune cells (Martinez-Pomares and Gordon, 2012). Sn+ve macrophages have been shown to be involved in three main regulatory processes in which Sn putatively plays a role: T-cell activation, B-cell priming and self *vs.* non-self discrimination (Umansky *et al.*, 1996; Junt *et al.*, 2007; Miyake *et al.*, 2007).

First of all, direct cell-cell contacts between Sn+ve macrophages and T-cells have been suggested in previous studies where cluster formations of Sn+ve macrophages and CD8+ve T-cells were observed in the body periphery (Muerkoster *et al.*, 1999), and speculatively also in the brain (Ip *et al.*, 2007). The molecular structure of Sn would favour possible direct cell-cell interactions, which was supported by the finding of a putative Sn counter-receptor on T-cells, called CD43 (van den Berg *et al.*, 2001).

Secondly, although dendritic cells are regarded as the master antigen presenting cells (Segura and Villadangos, 2009), the ideal location of Sn+ve macrophages in the spleen and lymph nodes where they are in constant contact with blood and lymph drainage, would place them at an ideal antigen presenting cell frontier. Because cell-free antigens reach the lymph nodes hours before migratory DCs arrive, Sn+ve macrophages could evaluate, capture, process incoming material and eventually present it to lymphocytes more quickly (Martinez-Pomares and Gordon, 2012). Indeed, Sn+ve macrophages have been described as having antigen-presenting functions. They have been shown to act as APCs to B-cells (Carrasco and Batista, 2007; Junt *et al.*, 2007; Gonzalez *et al.*, 2011), CD4+ve cells (Umansky *et al.*, 1996) and iNKT cells (Barral *et al.*, 2010) via complement/MHC II/CD1b pathways. Furthermore, recent findings have shown that Sn+ve macrophages in the spleen also transfer, or cross-present, antigen to CD8+ve dendritic cells, which then activate CD8+ve T-cells via MHC I receptors (Harshyne *et al.*, 2001; Backer *et al.*, 2010). Indeed, in the lymph nodes Sn+ve macrophages even present dead cell debris (as antigen) directly to CD8+ve T-cells and activate their immune responses (Asano *et al.*, 2011).

Thirdly, Sn+ve macrophages in the spleen have been postulated to be involved in recognition and discrimination of self and non-self of apoptotic cell associated antigens (Klaas and Crocker, 2012). There is a fine line between this discrimination, binding protein expression and the carefully regulated phagocytosis, all of which are essential for a correct immune response. Sn+ve macrophages must determine which antigens to oppose B-cells, and which ones to take up and render cryptic to the immune system. Malfunctions of these phagocytic processes, or of putative antigen discrimination via Sn, could lead to a breakdown in tolerance and development of autoimmune responses. Such processes are postulated for systemic sclerosis (York *et al.*, 2007) and this could possibly be the case in Juvenile NCL since the CLN3 protein is thought to function in the ER-Golgi (Cotman and Staropoli, 2012), as well as endocytotic pathways (Uusi-Rauva *et al.*, 2008). Depletion of Sn+ve macrophages in other model systems has led to increased autoimmune responses, including T-cell activation and pro-inflammatory cytokine production, by suppressing the tolerance towards apoptotic cells (Miyake *et al.*, 2007; McGaha *et al.*, 2011). The suppression of immune responses to cell-associated antigens also normally involves CD8+ dendritic cells in the spleen, which selectively capture apoptotic cells. However, this mechanism seems orchestrated by Sn+ve macrophages (Miyake *et al.*, 2007). Therefore, Sn

deficiency on macrophages results in malfunctioning apoptotic cell engulfment by CD8+ dendritic cell, which leads to increased (auto-)immune reactivity.

However, the involvement of the binding protein Sn itself in each of these processes has not yet been unambiguously demonstrated (Revilla *et al.*, 2009; Klaas and Crocker, 2012). Nevertheless, because Sn+ve macrophages in the spleen and lymph nodes are considered as potential gatekeepers of adaptive immunity, it is likely that Sn itself plays a role in the regulation of these processes, including immune activation and facilitating the distinction between self- and non-self-antigens (Klaas and Crocker, 2012). This is of particular interest as similar reactions may also occur in the brain. But how, and if, these events in the periphery influence the brain has not yet been determined.

1.12 Overall aim

The first aim of this thesis was to investigate the nature and extent of adaptive immune responses in the brains of Infantile and Juvenile NCL mice. We wanted to characterise, in particular, the relative timing of T-cell infiltration in relation to other well described features of the innate immune response and neurodegeneration of both forms of NCL.

Furthermore, we strived to identify the influence of adaptive immune cells upon the pathogenesis of Infantile NCL by genetically removing adaptive immune components. By comparing characteristic features of glial activation and neuron loss in *Ppt1*$^{-/-}$ mice to immune deficient *Ppt1*$^{-/-}$/*Rag-1*$^{-/-}$ mice, we aimed to determine whether the adaptive immune system acts as a pathogenic or beneficial contributor to disease progression.

As a second goal of this thesis, we wanted to characterise the role of Sn, a binding protein of inflammatory macrophages, on disease progression in Infantile and Juvenile NCL. Recent studies have demonstrated the regulatory and often pro-inflammatory role of Sn on adaptive immune responses in the brain (Jiang *et al.*, 2006; Kobsar *et al.*, 2006; Ip *et al.*, 2007). Therefore, by genetically creating and characterising *Sn* deficient Infantile NCL (*Ppt1*$^{-/-}$/*Sn*$^{-/-}$) as well as Juvenile NCL (*Cln3*$^{-/-}$/*Sn*$^{-/-}$) mice, we wanted to identify the putative pathogenic role of Sn and Sn+ve macrophages/microglia on disease progression in both Infantile and Juvenile NCL.

In summary, this thesis will not only provide detailed characterisation of the involvement of adaptive immune responses in Infantile and Juvenile NCL, but also assess, as proof of principle, the potential and suitability of two different (adaptive) immune system manipulations as possible immune modulatory therapies for Infantile and Juvenile NCL.

Chapter 2

Material and methods

This thesis examines the impact of immune-related cells on NCL disease progression. The differences between normal diseased NCL mice, immunodeficient NCL mice and their corresponding control mice have been investigated using immunohistochemistry, stereology and other quantitative morphological techniques.

2.1 Mice

In total 8 different genotypes of mice have been used in this thesis (see **Table 4**). These include NCL mouse models (*Ppt1*$^{-/-}$, *Cln3*$^{-/-}$), immunocompromised double knockout NCL mice (*Ppt1*$^{-/-}$/*Rag-1*$^{-/-}$, *Ppt1*$^{-/-}$/*Sn*$^{-/-}$ and *Cln3*$^{-/-}$/*Sn*$^{-/-}$) and the corresponding control mice (wildtype (WT), *Rag-1*$^{-/-}$ and *Sn*$^{-/-}$). As detailed below, several laboratories kindly supplied us with these mice. All *Ppt1*$^{-/-}$ mouse studies were performed using mice maintained on the C57BL/6 background while *Cln3*$^{-/-}$ mice were bred either on a C57BL/6 background (pure *Cln3*$^{-/-}$ mice in **Chapter 3**), or on a 129/Sv (control *Cln3*$^{-/-}$ mice in **Chapter 6**) and a mixed C57BL/6 / 129/Sv background (*Cln3*$^{-/-}$/*Sn*$^{-/-}$). All animal procedures were carried out in accordance with Institutional and UK Animals (Scientific Procedures) Act (1986) guidelines or under the guidance of the respective local university committee on animal use (if procedures were performed by collaborators outside the UK).

a) *Ppt1*$^{-/-}$ mice

The *Ppt1* deficient mice (*Ppt1*$^{-/-}$) used in this study were kindly supplied from Washington University, USA. These mice were originally generated using homologous recombination to produce a null mutation, which eliminates the last exon in the coding sequence of *Ppt1* (see **Table 2** in **Chapter 1**, (Gupta *et al.*, 2001)), and were subsequently bred onto C57BL/6 mouse background. In humans mutations in the *CLN1/PPT1* gene cause Infantile NCL, and similar disease phenotypes can be seen in these mice. They develop a characteristic accumulation of osmiophilic storage material, display marked neurodegeneration and glial up-regulation, visual, motor and cognitive deficits and develop spontaneous seizures, which eventually lead to premature death around 8 to 8.5 months (Gupta *et al.*, 2001; Bible *et al.*, 2004; Griffey *et al.*, 2004; Griffey *et al.*, 2005). Previously the laboratory has characterised the onset and progression of pathological changes in these mice (Kielar *et al.*, 2007), and in this thesis the same well-defined age groups of 1, 3, 5 and 7 months of age were collected, together with age-matched C57BL/6 control mice (n=5 for each age group).

b) Cln3$^{-/-}$ mice

The most commonly used *Cln3* deficient (*Cln3*$^{-/-}$) mouse strain was originally generated as a null mutant by targeted disruption of the *Cln3* gene (Mitchison *et al.*, 1999). These authors replaced the start codon and the first six exons with a neo cassette and the resulting mice were ultimately backcrossed onto a C57BL/6 background. Previous studies using *Cln3*$^{\Delta ex1\text{-}6}$ mice were mainly conducted on the 129/Sv background strain, whereas this study also included besides *Cln3*$^{\Delta ex1\text{-}6}$ mice on 129/Sv (in **Chapter 6**), for the first time also *Cln3*$^{\Delta ex1\text{-}6}$ mice on C57BL/6 background (in **Chapter 3**). However, recent unpublished findings suggest no overt differences between *Cln3*$^{\Delta ex1\text{-}6}$ mice on C57BL/6 or 129/Sv background (JD Cooper, personal communication). Therefore, mice on a mixed C57BL/6 and 129/Sv background strain (as used for **Chapter 6**, see **section 2.1f** below) are not likely to show overtly different phenotype aberrations compared to congenic mice, and based on previous investigations in these mice similar phenotypes will be assumed for each *Cln3*$^{-/-}$ mouse strain used in this study (JD Cooper, personal communication). Nevertheless, it has to be kept in mind that strain specific alterations may influence immune functions and treatment responsiveness (van der Spoel *et al.*, 2008; Sellers *et al.*, 2012). Congenic 129/Sv *Cln3*$^{\Delta ex1\text{-}6}$ mice demonstrate early glial up-regulation in the cerebellum already at 1 week of age, followed by motor deficits from 2 weeks onwards leading to significant neuron loss at 6 months of age in the cerebellum (Kovacs *et al.*, 2006; Weimer *et al.*, 2009). Thalamocortical pathology is evident at 5 months of age with initial glial up-regulation leading to optic nerve pathology at 1 year of age and specific interneuron loss at 14 months of age in the hippocampus (Sappington *et al.*, 2003; Pontikis *et al.*, 2004). In general, *Cln3*$^{\Delta ex1\text{-}6}$ mice survive for up to 22 months (Mitchison *et al.*, 1999; Cooper *et al.*, 2006). To investigate the adaptive immune cell infiltration 6.5, 12 and 21 month old C57BL/6 *Cln3*$^{-/-}$ mice have been used in **Chapter 3**. These three age groups were chosen to examine the temporal course of disease manifestations representing mice at early (6.5 months), middle (12 months) and end stage (21 months) of disease progression. These mice have been bred and housed in an animal facility at University College London (UK). For the sialoadhesin (Sn) deficient knockout experiments in **Chapter 6**, 18 month old 129/Sv *Cln3*$^{-/-}$ mice were used as control animals which were generously supplied by our collaborators in Prof. R Martini's laboratory at the Department of Neurology, Julius-Maximilians-University Würzburg, Germany.

c) *Rag-1*$^{-/-}$ mice

The *Rag-1* deficient (*Rag-1*$^{-/-}$) mice used in this study were generously supplied by our collaborators in Würzburg, Germany, but are also commercially available (*http://jaxmice.jax.org/strain/002216.html*). These *Rag-1*$^{-/-}$ mice were originally created by introducing a null mutation in the *Rag-1* via gene targeting in embryonic cells resulting in a 1356 dp deletion in the 5' end of the coding sequence of *Rag-1* (Mombaerts *et al.*, 1992). Although originally crossed onto 129Sv background, this study used congenic C57BL/6 *Rag-1*$^{-/-}$ mice after being backcrossed with C57BL/6 mice for six to eight generations. Besides greatly diminished lymphoid organs, *Rag-1*$^{-/-}$ mice show no overt brain pathology, or other pronounced phenotypes other than lacking mature T- and B-cells (Mombaerts *et al.*, 1992). In non-sterile conditions, their life expectancy can be restricted to approximately 1 year as these mice potentially display *Pneumocystis carinii* pneumonia and thoracic or abdominal abscesses (Mombaerts, 1995). Furthermore, compared to the adaptive immune deficient alternative, the SCID-mice which spontaneously can produce low levels of functional T- and B-cells (a process described as "leaky") at increased age (Bosma *et al.*, 1983; Schuler *et al.*, 1986; Bosma *et al.*, 1988; Bosma and Carroll, 1991), so far no "leakage" of functioning adaptive immune cells has been detected in *Rag-1*$^{-/-}$ mice. Thus, *Rag-1*$^{-/-}$ mice represent a consistent and unambiguous way to investigate the impact of adaptive immune deficiency.

d) *Sn*$^{-/-}$ mice

The sialoadhesin deficient (*Sn*$^{-/-}$) mice used in this study were generously supplied by Prof. P Crocker at the College of Life Sciences, University of Dundee, Scotland. Originally the mutation was created in embryonic stem (ES) cells by inserting a neomycin resistance gene expression cassette, via homologous recombination, in exon III which encodes the second immunoglobulin-like domain of *Sn*. Subsequently, the resulting chimeric mice were backcrossed to C57BL/6 mice for at least 8 generations (Oetke *et al.*, 2006). These mice have also been previously used by our collaborators in Würzburg (Kobsar *et al.*, 2006; Ip *et al.*, 2007). In comparison to *Rag-1* deficient mice, *Sn*$^{-/-}$ mice show a much more subtle immune deficiency. Under normal specific pathogen-free conditions, *Sn*$^{-/-}$ mice are viable and fertile and do not reveal gross alterations from wildtype mice, except for alterations in T-cell subpopulations (slightly more CD8+ve T-cells have been found in *Sn*$^{-/-}$ mice than in wildtype mice, while CD4+ve T-cell populations are unaltered) and a decrease in CD45+ve (i.e. B220+ve)

cells in spleen and lymph nodes. Furthermore in the spleen, a small decrease in follicular B-cells, but an increase in marginal zone B cells could be observed, which reflects itself in lower immunoglobulin M (IgM) but unaltered immunoglobulin G (IgG) levels in the serum of *Sn*$^{-/-}$ mice (Oetke *et al.*, 2006). As such, their relatively mild phenotype suggests Sn is more involved in immune system regulation than in steady-state hematopoiesis.

e) *Ppt1*$^{-/-}$*/Rag-1*$^{-/-}$ and *Ppt1*$^{-/-}$*/Sn*$^{-/-}$ double knockout mice

To ensure the required supply of mice, both NCL double knockout strains were simultaneously created by our collaborators, as well as in our own animal facility. As an initial step, homozygous *Ppt1*$^{-/-}$ mice were crossbred with *Rag-1*$^{-/-}$ or *Sn*$^{-/-}$ mice respectively, resulting in heterozygous offspring for both genes (F1). These heterozygous mice were then further interbred to generate the initial double mutants (F2) as future colony founders. Since this is the first time such mice have been generated, no information about survival and brain morphology is known so far.

f) *Cln3*$^{-/-}$*/Sn*$^{-/-}$ double knockout mice

These mice were kindly supplied by our collaborators, in Würzburg, Germany. However, due to lack of time and resources, *Sn*$^{-/-}$ mice on C57Bl/6 background have been crossbred with *Cln3*$^{\Delta ex1\text{-}6}$ on 129/Sv background, resulting in a mixed background double mutant *Cln3*$^{-/-}$/*Sn*$^{-/-}$ mouse strain. Even though, mixed background breeding can bias data, the experiments were nevertheless conducted as a proof of principle study. This is again the first time such mice have been created, thus no information exists yet about their survival and pathology.

g) Wildtype mice

All wildtype (WT) mice used in this study were animals on C57BL/6 background and have been originally created by breeding heterozygous *Ppt1*$^{+/-}$ mice. But the same WT mice are also commercially available (*http://jaxmice.jax.org/strain/000664.html*). Average survival age is around 27-28 months (Crawley, 2007). Mice have been bred and housed either in our own animal facility at King's College London (UK) or at our collaborators facilities in Würzburg, Germany and subsequently shipped to the Pediatric Storage Disorders Laboratory (PSDL), Institute of Psychiatry for histological analysis.

Table 4. Overview of mice used in this thesis. A total of 9 different mouse populations have been used, supplied and bred in various laboratories. Abbreviations: PSDL = Pediatric Storage Disorders Laboratory, London, United Kingdom; Würzburg = Laboratory of Prof. R Martini Department of Neurology, Julius-Maximilians-University; Washington = Laboratory of Prof. M Sands at Washington University Medical School, USA; Dundee = Laboratory of Prof. P Crocker at College of Life Sciences, University of Dundee, Scotland, ND= not (yet) defined.

Animal model	Genetic mutation	Background strain	Onset of neurological signs	Mortality	Original mouse source	Breeding	References
Wildtype	None	C57BL/6	None	~ 27-28 months	PSDL	PSDL	http://jaxmice.jax.org/strain/000664.html
Ppt1$^{-/-}$ mouse	Exon 9 insertion + termination codon at Val281	C57BL/6	2 months	~ 8 months	Washington	PSDL	(Gupta *et al.*, 2001)
Cln3$^{-/-}$ mouse	Exons 1-6 replacement insertion	C57BL/6 (Chapter 3) 129/Sv (Chapter 6)	2 months	~ 20-22 months	UCL Würzburg	PSDL Würzburg	(Mitchison *et al.*, 1999)
Sn$^{-/-}$ mouse	Exon III replacement insertion	C57BL/6	None	~ 27-28 months	Dundee	PSDL	(Oetke *et al.*, 2006)
Rag-1$^{-/-}$ mouse	Exon II 1356 dp replacement insertion	C57BL/6	None	Sterile: ~ 27-28 months non-sterile: ~ 12 months	Würzburg	PSDL Würzburg	(Mombaerts *et al.*, 1992)
Ppt1$^{-/-}$*/Rag-1*$^{-/-}$ mouse	Both single mutations (see above)	C57BL/6	ND	ND	PSDL Würzburg	PSDL Würzburg	Created in PSDL
Ppt1$^{-/-}$*/Sn*$^{-/-}$ mouse	Both single mutations (see above)	C57BL/6	ND	ND	PSDL Würzburg	PSDL Würzburg	Created in PSDL and Würzburg
Cln3$^{-/-}$*/Sn*$^{-/-}$ mouse	Both single mutations (see above)	Mixed 129/Sv / C57BL/6	ND	ND	Würzburg	Würzburg	Created in Würzburg

h) Determination of genotype

To determine and verify the genotype of mice several polymerase chain reactions (PCRs) were performed and reaction products run on agarose gels (see example **Figure 5**) using primers below. For each characterisation a triple primer approach has been used with each time a common, WT and knockout/neomycin primer (Distributor: Sigma, UK):

Ppt1 genoptyping: Common forward (PG59): GTACATAGTTCATGCTCAGCC, reverse WT (PG60): CTGCTAGGTACCTCTAGAGGG and reverse *Ppt1* allele primer (S125): GATTGGGAAGACAATAGCAGGCATGC, resulting in a 448 bp product for the WT allele and a 420 bp product for the mutated *Ppt1* allele.

Cln3 genotyping: Common (Ex1f): TGTATAGCAGACAGCGGAACC, reverse WT (M6R): CACTCCGACTATCCAACCGA and reverse *Cln3* allele primer (NIHNeo3): TCGCCTTCTTGACGAGTTCT, resulting in a 380 bp product of WT allele and a 580-bp product for the mutated *Cln3* allele.

Rag-1 genotyping: Common (oIMR1746): CCGGACAAGTTTTTCATCGT, forward WT (oIMR1746): GAGGTTCCGCTACGACTCTG reverse *Rag-1* allele primer: TGGATGTGGAATGTGTGCGAG, resulting in a 474-bp product for WT allele and a 530-bp product for the mutated *Rag-1* allele.

Sn genotyping: Common forward (SND1F3): CACCACGGTCACTGTGACAA; reverse WT (SND2R2): GGCCATATGTAGGGTCGTCT and reverse *Sn* allele primer (Neo): CGTTGGCTACCCGTGATATTGC. This resulted in a 468-bp product for WT allele and a 1729-bp product for the mutated *Sn* allele.

2.2 Processing of brain tissue

All mice were anesthetized with "Euthatal" (200mg sodium pentobarbital/ml, Merial Animal Health Ltd, UK) and transcardially perfused with Phosphate buffered Saline (PBS: 50 mM Phosphate buffered Saline, with $MgCl_2$ and $CaCl_2$, pH 7.4, D8662, Sigma Gillingham, Dorset, UK) and 4% paraformaldehyde in 0.1 M Sodium Phosphate buffer, pH = 7.4 (PFA). All brains were carefully dissected at each required time point and then immersion fixed for at least 24 hours in 4% PFA and subsequently, cryoprotected in a solution of 30% sucrose in Tris buffered saline (TBS: 50 mM Tris, pH 7.6, 150 mM NaCl). Before further processing, each brain was

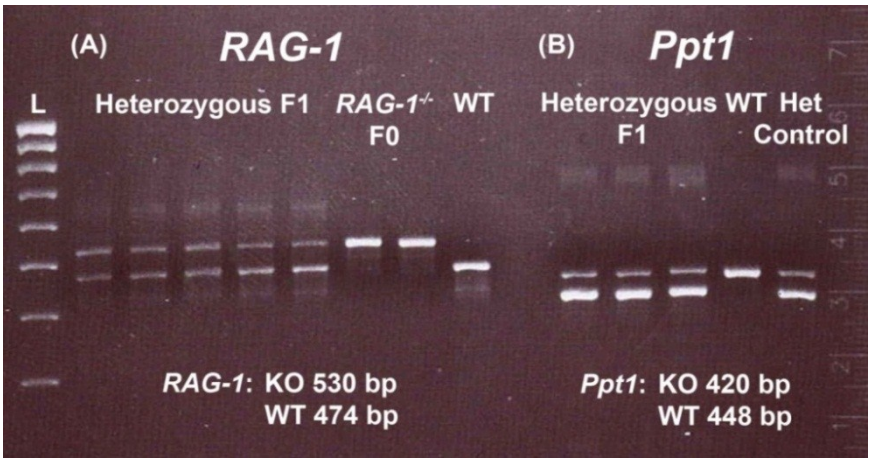

Figure 5. Genotyping example: *Rag-1*$^{-/-}$ and *Ppt1*$^{-/-}$ mice. Via polymerase chain reaction (PCR) different genotypes of mice can be identified. *Rag-1* PCR and *Ppt1* PCR products have been run on the same gel. (A) Due to their different sized reaction products, the wildtype (WT) *Rag-1* allele (474 bp) shows up as a lower band than the knockout (KO) *Rag-1* allele (530 bp). (B) In contrast, in the *Ppt1* PCR reaction the wildtype *Ppt1* allele (448 bp) is seen with a higher band than the knockout allele (420bp). Heterozygous individuals can be readily identified as bearing both wild type and mutant alleles. L = control ladder, Het = heterozygous individual, WT = wildtype, F0, F1 = Breeding generations.

weighed after separating any remaining spinal cord from the brainstem at a consistent level (along the rostral end of the cerebellum). Next, the cerebellum was cut off coronally and the hemispheres separated with a clean, straight cut using a razorblade (see **Figure 6**). Between each step the weights of the brain parts were recorded. This thesis concentrates upon well-defined pathological changes that occur within the forebrain, and the cerebellum was retained for future analysis.

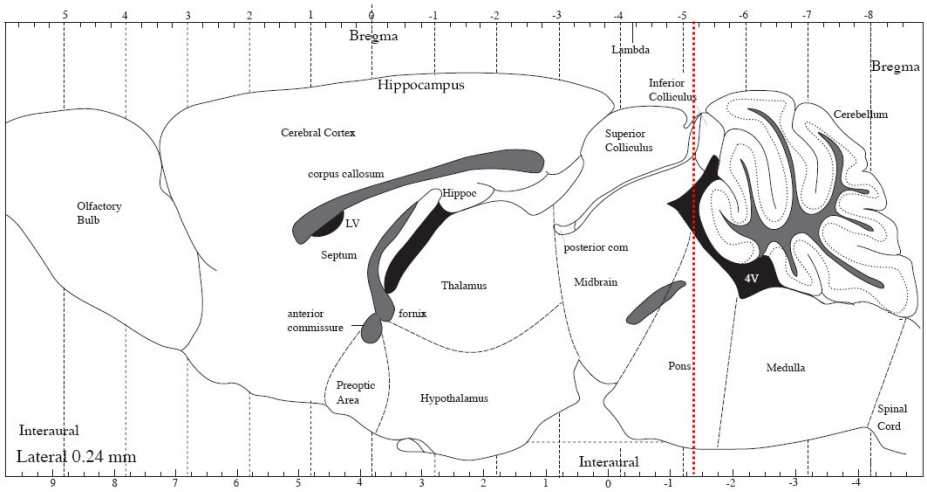

Figure 6. Schematic sagittal section of the mouse brain. Areas indicated according to schematic distinction in Paxinos and Franklin atlas. Ventricles are shown in black. The position of skull marks (bregma, lambda and interaural) are indicated. Red line indicates coronal separation of cerebellum. Only mid- and forebrain have been analysed and looked at in this study, including the regions such as the thalamus, hippocampus and cortex where the most prominent pathology occurs in *Ppt1* and *Cln3* deficient mice (Bible *et al.*, 2004; Pontikis *et al.*, 2004; Pontikis *et al.*, 2005; Kielar *et al.*, 2007). Adapted from (Paxinos and Franklin, 2001).

Subsequently, all brains were cut coronally into 40µm thick sections on a Leitz 1321 freezing microtome (Microm HM 430/Carl Zeiss Ltd, Cambrigde, UK) (Bible *et al.*, 2004; Pontikis *et al.*, 2004; Kielar *et al.*, 2007) and stored in 96 well plates containing an anti-freeze cryoprotectant solution (TBS/30 % ethylene glycol/15% sucrose/0.05 % sodium azide) at 4 ºC (see **Figure 7**).

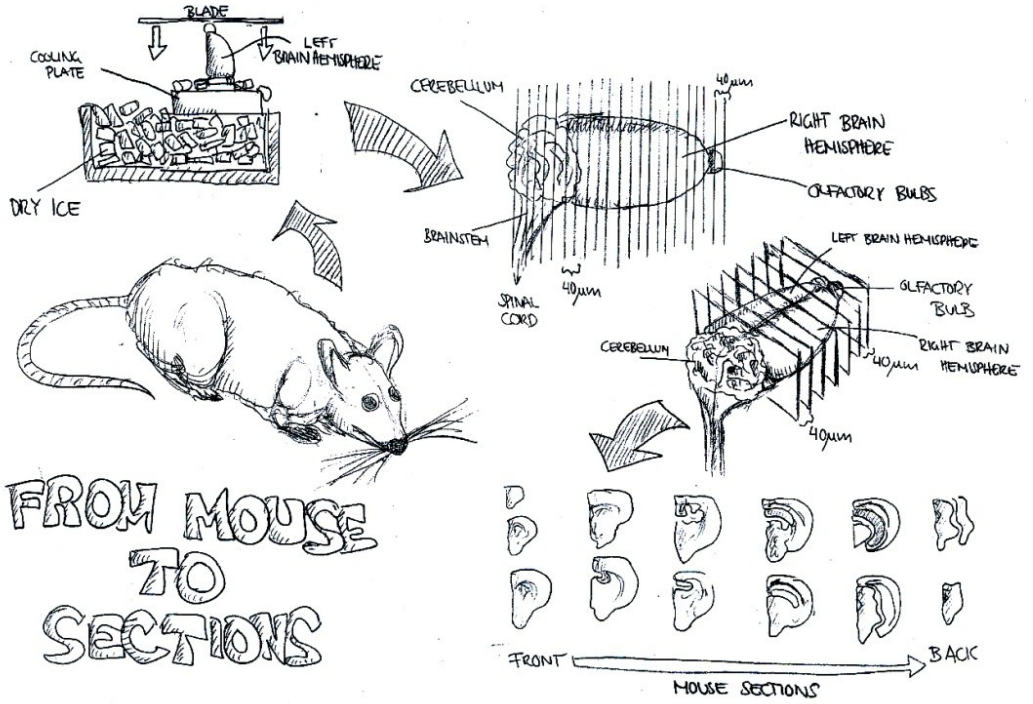

Figure 7. Schematic illustration how mouse sections are produced. After freezing the brains with dry ice, 40 µm sections are cut on a microtome and collected in 96 well plates containing an anti-freeze cryoprotectant solution (TBS/30 % ethylene glycol/15% sucrose/0.05 % sodium azide), in which they can be stored at 4 ºC until further processing.

2.3 Immunohistochemistry

To determine the degree of astrocytosis and microglial activation, 1 in 6 series of sections were stained for glial fibrillary associated protein (GFAP, 1:4,000, Dako, Ely, Cambridgeshire, UK) or the microglial marker CD68 (1:2,000, Serotec, Oxford, UK). In addition, immune cell and lymphocyte infiltration was assessed by staining for CD45 (1:250 Serotec), CD169 (1:100, Serotec), CD8 (1:100, Serotec) and CD4 (1:35, Serotec) (see **Table 5**). Immunohistochemical staining for each antigen was generally conducted in the same manner (see **Figure 8**), except for slightly modified protocols for CD8 and CD4 (see paragraph below).

Sections were incubated in 1 % H_2O_2 in TBS for 30 minutes to quench endogenous peroxidase activity, subsequently rinsed in TBS, and then blocked with 15% normal serum in TBS-T (TBS containing 0.3% Triton X-100) for 45 minutes. Next, sections

Table 5. Overview of antibodies used for immunohistochemistry. (Conc = concentration, rab = rabbit, GFAP = glial fibrillary acidic protein, CD = cluster differentiation antigen)

Marker for	1st Antibody	Company & Product code	Conc	2nd Antibody (for DAB)
Astrocytes	rab α GFAP	Dako Z0334	1:4,000	swine α rab, 1:1,000, Dako
Microglia	rat α CD68	Serotec MCA1957	1:2,000	rab α rat, 1:1,000, Vector
Cytotoxic T-cells	rat α CD8	Serotec MCA609G	1:100	rab α rat, 1:1,000, Vector
T-helper cells	rat α CD4	Serotec MCA1767	1:35	goat α rat, 1:1,000, Vector
Leukocytes	rat α CD45	Serotec MCA1031GA	1:250	rab α rat, 1:1,000, Vector
Sialoadhesin	rat α CD169	Serotec MCA884	1:100	rab α rat, 1:1,000, Vector

were incubated overnight at 4 ºC with the appropriate concentration of primary antibody diluted in TBS-T and 10 % normal serum. On the following day, sections were rinsed in TBS and incubated in TBS-T and 10% normal serum for 2 hours at room temperature containing the appropriate concentration of biotinylated secondary antisera (1:1,000, Vector Laboratories, Peterborough, UK) was added. After washing anew, sections were incubated for 2 hours in TBS with avidin-biotin peroxidase complex (Vestastain Elite ABC kit, Vector Laboratories), prepared at least 30 minutes before use. With a subsequent wash in TBS, immunoreactivity was visualised by incubation in 0,05% 3,3 – diaminobenzidine tetrahydrochloride HCl (DAB, Sigma) and 0.001% H_2O_2 in TBS for a precise predetermined time (up to 15 minutes, depending on antigen) that represents saturation for this reaction. Staining was stopped by adding ice-cold TBS and rinsed several times, before sections were mounted onto microscope slides, air-dried overnight, rinsed in 100% industrial methylated spirits (I.M.S.) and cleared in xylene for at least 30 minutes, before being coverslipped with DPX [p-xylene-bis(pyridinium bromine)] (VWR, Lutterworth, Leicestershire, UK).

To ensure reproducibility, each antigen was developed for exactly the same time and for each antigen mice from each age group were stained simultaneously as one batch rather than separately.

For the lymphocytic antigens CD8 and CD4 two amendments to the above protocol were made due to an initial appearance of variable amounts of background staining (punctate dots of immunoreactive deposits that were most pronounced within the white matter, of both mutant and control wildtype mice). Firstly, a higher

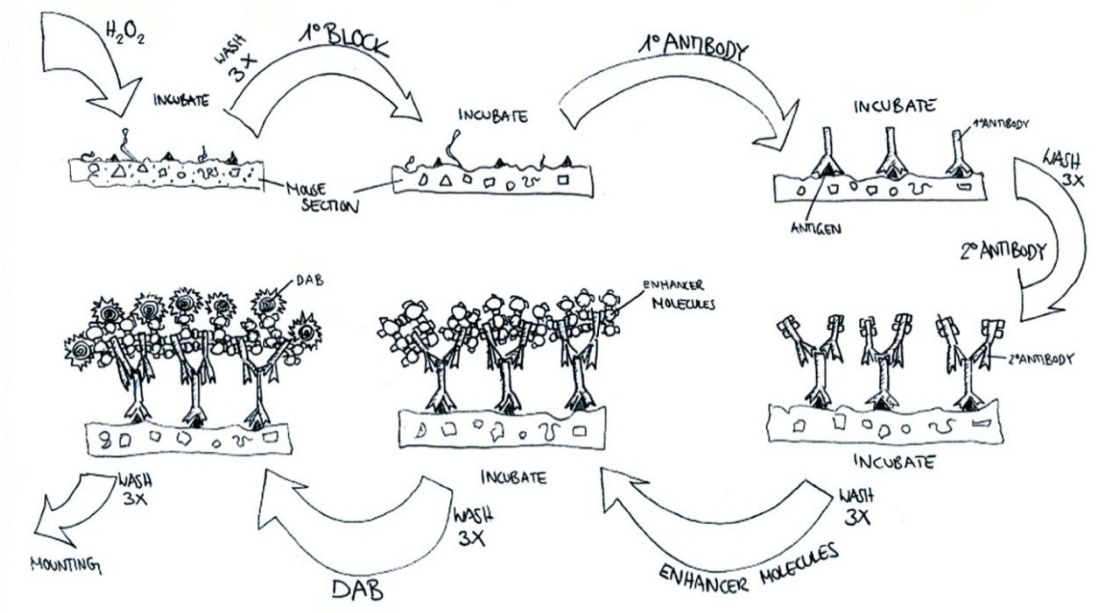

Figure 8. Schematic illustration of immunohistochemical procedure. After the initial quenching step (1% H_2O_2 in TBS) and the first block (15% normal serum), the first antibody is applied and the sections incubated overnight. Followed by enhancing the signal via application of secondary antibodies and avidin-biotin complex molecules, the procedure is finalised with a DAB development. Between each step all sections are washed three times with TBS and eventually mounted onto slides.

concentration of normal serum (30%) blocking solution was applied and secondly, an additional 2 hours blocking step in 30% normal serum in TBS-T was introduced before the application of the secondary antibody. These changes to the protocol ensured an unambiguous quantification of the CD4+ve and CD8+ve immune reactions, with a minimum of background staining.

2.4 Photomicroscopy

To document and provide an overview of the resulting immunohistochemical staining high-resolution, representative photomicrographs were taken with a x5, x10, x20, x40 or x63 objective on a Leica DMRB microscope (Leica Mikroskopie & Systeme GmbH, Wetzlar) with a Zeiss AxioCam HRc Rev 2 digital camera using the software AxioVision (version 4.7.2).

2.5 Nissl staining

To visualise neuronal cytoarchitechture and permit stereological analyses, a 1 in 6 series of 40µm sections from each brain was mounted onto gelatin-chrome alum coated Superfrost microscope slides (VWR) and air-dried overnight. All sections were then incubated for at least 45 min at 60°C in 0.05% cresyl fast violet and 0.05% acetic acid (VWR) (see **Figure 9**).

Subsequently, they were rinsed in distilled water and differentiated through a series of graded alcohols (70%, 80%, 90%, 95%, 100% I.M.S.) before clearing in 50:50 Xylene:I.M.S., followed by clearing in 100% Xylene and then finally coverslipped with DPX (VWR).

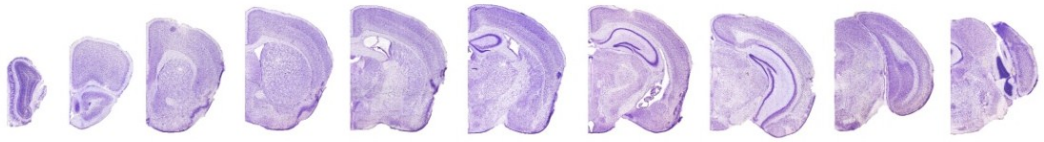

Figure 9. Representative Nissl sections. Coronal sections through the fore- and midbrain were cut at 40 μm and subsequently stained with the Nissl dye cresyl fast violet.

2.6 Stereology

To quantify differences between morphological and pathological phenotypes in the brains of the mice generated in this study, we used design-based stereology which enables us to estimate regional volumes, cell numbers, mean cellular volumes and length/thickness of biological structures (Schmitz and Hof, 2005). These methods are defined as design-based as the sampling scheme is 'designed' *a priori*, ensuring that the samples/probes become independent of size, shape spatial orientation and spatial distribution (West and Thomas Sutula, 2002). By considering the three-dimensional features of sections and spatial independence, systemic errors in calculations can be eliminated and data collection is more reliable than more biased qualitative sampling methods (Gundersen, 1988; West, 1993). As such, the design-based stereology methods enable unbiased comparisons between diseased, modified/treated or healthy brain phenotypes without prior assumptions about shape and size of brain structures as a result of disease.

While all stereological estimates are independent of specific brain structures, the accuracy of this estimation method does depend on reliable identification of structures being measured or counted. Therefore, the cytoarchitecture of each section was visualised by Nissl staining which enables identification of discrete boundaries between white and grey matter and different nuclei in each section. Each measurement was undertaken between clearly defined landmarks of rostral-caudal position. To assess the boundaries of each region/area of interest (ROI) the neuroanatomical landmarks described in '*The mouse brain in stereotactic co-coordinates*' (Paxinos and Franklin, 2001) were used. Furthermore, the delineation of different functional regions of the cortex was also defined with (Paxinos and Franklin, 2001).

Within this study, to characterise the impact of genetically removing immune-related cells, the entire brain volume, cortical volume, the thickness of the *primary somatosensory barrel field* (*S1BF*) of the cortex as well as neuronal counts of the *ventral posteromedial* and *posterolateral* (*VPM/VPL*) nuclei of the thalamus have been measured (see **Figure 10**). These parameters were chosen because their onset and progression have already been well-defined in *Ppt1* and *Cln3* deficient mice (Bible *et al.*, 2004; Pontikis *et al.*, 2004; Pontikis *et al.*, 2005; Kielar *et al.*, 2007), therefore providing neuropathological landmarks for assessing the impact of removing different subclasses of immune cells.

All stereological estimates were obtained using *StereoInvestigator* software (Microbrightfield Inc, Williston, VT) which enables semi-automated data collection. All measurements were performed on a Zeiss Axioskop 2 MOT (Zeiss, Germany) linked to a DAGE-MTI CCD-100 camera (Dage-MTI, Michigan City, IA) and were conducted blind to genotype and consistently across all diseased, double mutant and control brains.

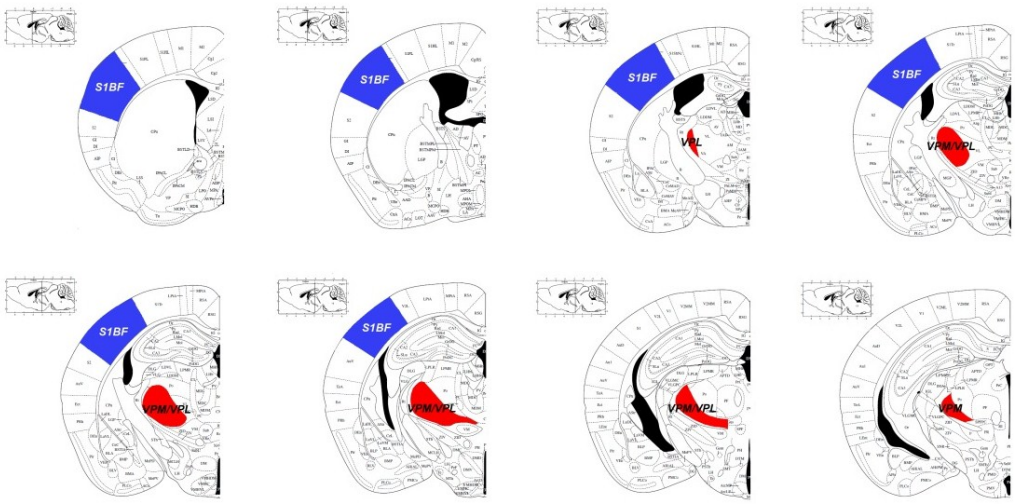

Figure 10. Schematic illustration of the somatosensory thalamocortical system. Boundaries of the *primary somatosensory barrel field* (*S1BF*) (blue) and the *ventral posteromedial* and *posterolateral* (*VPM/VPL*) nuclei of the thalamus (red) are highlighted in schematic illustrations of coronal sections of a mouse brain. A representative sub-sample of sections is depicted in rostrocaudal order (from top left to bottom right). Adapted from (Paxinos and Franklin, 2001).

a) Volume measurements

To estimate regional and total volumes without bias, volumes were calculated according to the Cavalieri principle (Cavalieri, 1665). Cavalieri realised that a series of sections through an object can be used to estimate its total volume. Conditions for a correct estimation are: The sections must be separated by a regular interval of a known distance, with the first section lying at a uniform random location within the section

interval. In this study all sections were cut with a thickness of 40μm and analysed as either 1 in 6, or 1 in 12 series of sections (depending on the area of interest). The volume of the object can be estimated by multiplying the total area (sum of all selected areas on each section) of the region of interest with the distance/interval between each section (Lucocq, 2007). By placing a grid with suitable point probes on top of each section and counting all points falling upon the region of interest, a precise estimate of volume can be calculated (see **Figure 11** for formula). Due to the inability to separate the top from bottom surfaces of a section and thus by measuring only the visible cross-sectional area of the object, volume estimations are vulnerable to over-projection (systematic overestimation of volume fraction). Therefore, all calculated volume estimations were corrected for over-projection (Gundersen *et al.*, 1999) and finally, the accuracy of the process assessed by coefficient errors (CE)/variance estimates (Cruz-Orive, 1999; Gundersen *et al.*, 1999). As long as there is sufficient point density - irrespective of the shape of the object - to estimate the area on the section, the Cavalieri method is a powerful tool which is applicable to many scientific questions and has therefore been regularly used in the past (Bahmer *et al.*, 1996; Roberts *et al.*, 1997; Bible *et al.*, 2004; Pontikis *et al.*, 2004; Bible *et al.*, 2005; Pontikis *et al.*, 2005; Kielar *et al.*, 2007; Sapara *et al.*, 2007; Trigylidas *et al.*, 2008; Acer *et al.*, 2011).

In this study, total brain volume, as well as regional volume of the cortex, were estimated in μm^3 with an appropriately spaced sampling grid (250μm for both: total brain volume and cortex) superimposed over Nissl stained sections. The size of the sampling grid for each region was determined so that the coefficient of error (CE) was always less than 0.1. As mentioned above, the number of points was counted using an x5 objective on a Zeiss Axioskop, using *StereoInvestigator* software.

b) Cortical thickness measurements

To determine whether differences in cortical atrophy were apparent between different genotypes and mouse populations, regional thickness measurements were performed on Nissl stained sections. The cortical *primary somatosensory barrel field* (*S1BF*) sub-region as defined in (Paxinos and Franklin, 2001) was measured in three consecutive sections by tracing 10 perpendicular, evenly spaced lines from the border of the white matter (corpus callosum) to the pial surface of the cortex. All measurements were undertaken blind to genotype and age. The results were expressed in μm as average length of all lines, respective of thickness of each cortical region as previously described (Bible *et al.*, 2004; Kielar *et al.*, 2007).

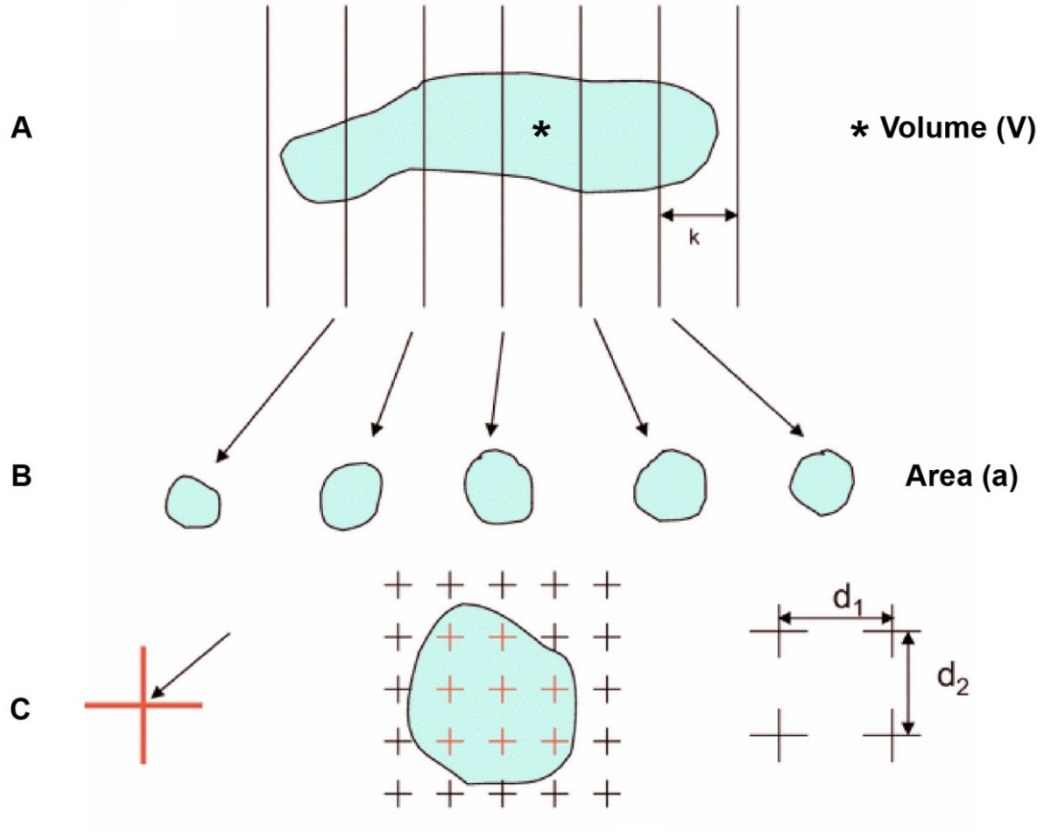

Figure 11. Diagrammatic representation of volume estimations using the Cavalieri method. (A) The Cavalieri method is applied onto any sectioned object/organelle/brain. Sections (of the brain) that are consistently in-between spaced (k) are randomly selected. (B) Investigator draws around the boundary of the region of interest in each section if it is present. (C) By superimposing a sampling grid with a known spacing distance (d_1 and d_2) onto each section, every cross/point falling into the region of interest gets counted (P). Strict counting rules are applied: Points are only counted if the intersection of the sampling crosses falls within the region (arrow). By multiplying the sum of all points counted within the region of interest on each section with the distance of points on the lattice results in the cross-sectional area per section (a). Taking all cross-sectional areas together, the total area (A) of the region of interest is then described with $A = \sum P \cdot d_1 \cdot d_2$. Thus, the overall volume can be estimated by multiplying the total cross-sectional area with the constant distance between the sections: $V = A \cdot k$. Adapted from (Lucocq, 2007).

c) Neuronal cell counts

Since it is often unfeasible to count all cells of a region of interest in histological tissue, the optical fractionator technique (West *et al.*, 1991) has been developed to count only a subsample of particles/objects and subsequently estimate the total number (see **Figure 12**). This method combines the two major developments in stereology: the optical dissector, a method to count neuronal nuclei in a three dimensional context and the fractionator, a systematic uniform sampling scheme (West, 1993). The optical dissector incorporates optical section planes by moving the focal plane up or down and estimates neuron numbers free of assumptions about their size or shape and is unaffected by lost caps (tissue alterations due to the histological sectioning process)

and over-projection (see above **section 2.6a**). This is important, because in diseased brains neurons often change size and could therefore be counted differently to healthy control neurons. The fractionator (Gundersen, 1986) overcomes this problem by applying systematic sampling to estimate the total number of neurons unaffected by shrinkage before, during, and after processing of the tissue (Schmitz and Hof, 2005).

To conduct unbiased design-based cell counts, the investigator first of all traces lines around, and thus, defines the boundaries of the brain region of interest. Secondly, a grid is superimposed and random dissector "counting frames" are applied onto the section according to the sampling grid size. Only cells within the frame are counted. Particular counting rules apply when only cells within - or cells touching - the green acceptance line are counted, while cells touching the red exclusion line are not included (see **Figure 12**). The overall numbers can be calculated/estimated, by taking into account the number of analysed sections *vs.* total number of sections ('section sampling fraction' = *ssf*), the area of the unbiased counting frames *vs.* the sampling area in each section ('area sampling fraction' = *asf*) and the unbiased height of the counting frame/space *vs.* the height/mean thickness of the whole section after histological processing ('height sampling fraction' = *hsf*) (Schmitz and Hof, 2005). Including the total number of cells counted (Q) this translates into following optical fractionator formula (West *et al.*, 1991; Howard and Reed, 1998):

$$\widehat{N} = Q \cdot \frac{1}{hsf} \cdot \frac{1}{asf} \cdot \frac{1}{ssf}$$

In this study all of these calculations were performed by *StereoInvestigator* (Microbrightfield Inc., Williston, VT) and the total estimate of neuronal numbers of all replicates of each genotype and age were presented as mean number of neurons.

To estimate the neuronal number in the *ventral posteromedial* and *posterolateral* (*VPM/VPL*) nuclei of the thalamus, the technique of the optical fractionator (Gundersen, 1986; West *et al.*, 1991) was used on Nissl stained sections as previously described (Bible *et al.*, 2004; Pontikis *et al.*, 2005; Kielar *et al.*, 2007). Nissl stains like cresyl violet stain all cells in the brain (neurons, astrocytes, microglia, oligodendrocytes etc.), and neurons have to be distinguished according to their cell morphology and staining characteristics (see **Figure 13**). To ensure the best possible visualisation of structures, all measurements were performed using an x100 oil-objective with a high numerical aperture of 1.4. Only healthy neurons with clearly identifiable nucleus, large

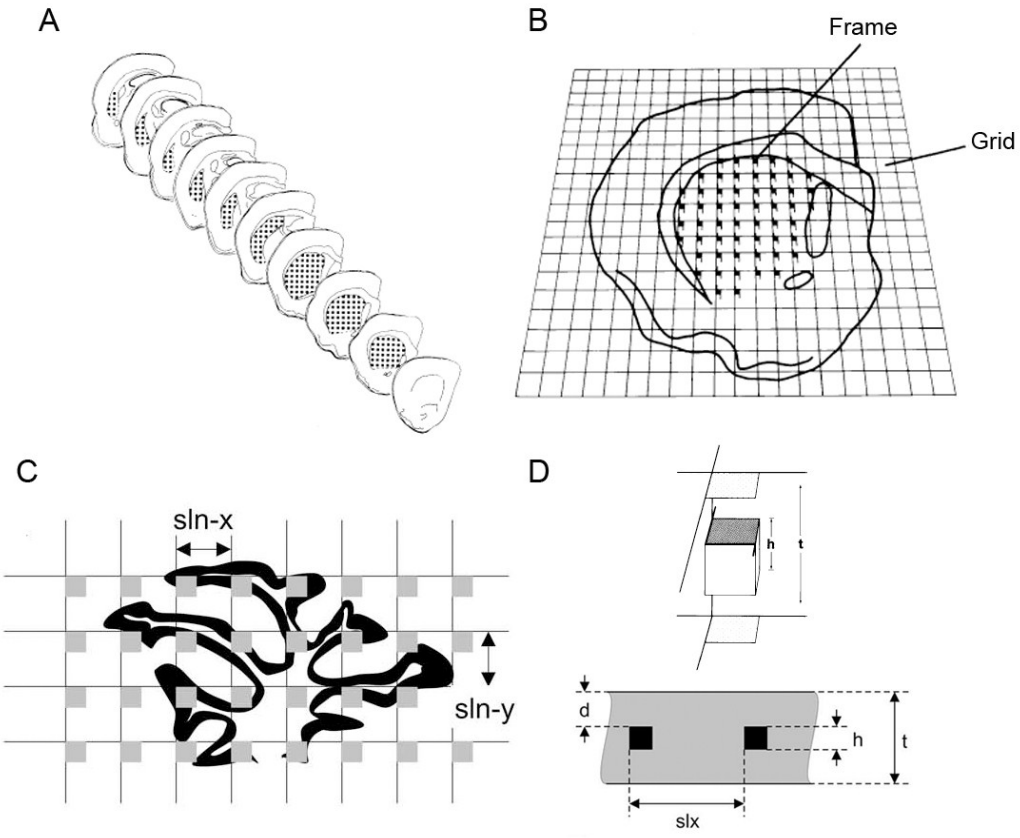

Figure 12. Schematic illustration of counting procedure using the optical fractionator calculation method. To estimate the total number of neurons in the regionn of interest, three parameters have to be considered: *ssf*, *asf* and *hsf*. (A) "*Section sampling fraction*": Every n[th] section containing the region of interest is selected at an equal interval after a random start to guarantee equal probabilities of being sampled. Thus, the selected sections constitute a known fraction of the sections in the series (*ssf*). (B) "*Area sampling fraction"*: Boundaries of region of interest are traced by an investigator and a grid superimposed over the sections. Objects/neurons are counted within a known fraction of the section area (*asf*). (C) This fraction corresponds to the combined area of each counting frame (*a(frame)*) (black boxes in (B) and gray boxes in (C)) and the profile area of the region of interest (*a(grid)*) (calculated from the grid size: *a(grid)* = $slnx \cdot slny$), in mathematical terms: $asf = a(frame)/a(grid)$. (D) Neurons are counted by focusing up and down the section within the height (h) of each counting frame (indicated as black box) which in relation to the section thickness (t) after histological processing results in "*height sampling fraction"* (*hsf*). After counting all neurons (Q) within this known (sub)fraction of the whole region of interest, the total number of neurons (N) can be calculated by applying the following formula: $\widehat{N} = Q \cdot 1/hsf \cdot 1/asf \cdot 1/ssf$. Adapted from (West, 2001; Schmitz and Hof, 2005).

cell body and clear (and light coloured) Nissl staining within their cytoplasm were counted. In contrast, astrocytes and microglia which are also visible in Nissl stained sections were not counted and could be distinguished by their small soma and darkly stained and granular cytoplasmic Nissl appearance. Obviously, this method is subject to the morphological identification skills of the investigator. Therefore, to minimise the mis-identification, strict criteria were used and only cells displaying all required characteristics and criteria were counted as neurons. Despite this potential limitation of Nissl staining, many researchers choose it in preference to immunohistochemical

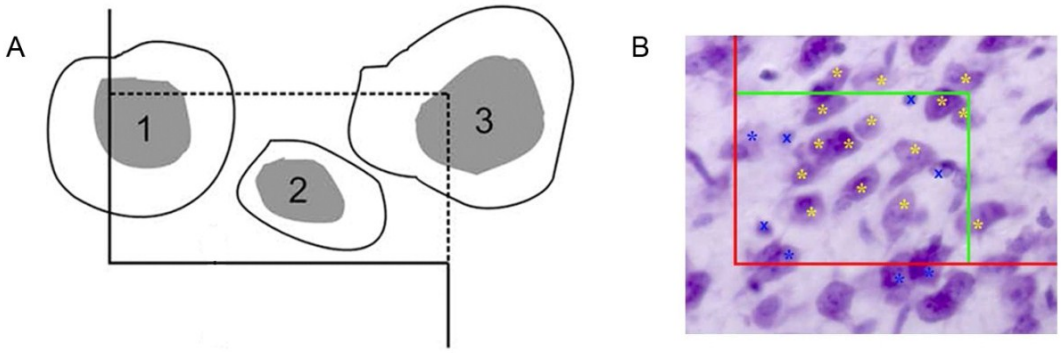

Figure 13. Counting frames explaining counting criteria for neurons. (A) Schematic and (B) real image of Nissl stained cells with superimposed counting frame. The investigator counts neurons applying strict criteria while focusing up and down the whole thickness of the section: 1) Morphological features: Only clearly distinguishable neurons (large cell body and clear nucleus and homogeneous Nissl staining within cytoplasm) are counted, while small cells (glia cells) with granular Nissl staining are neglected (marked blue x). 2) Only cells within counting frame (neuron no. 2 in (A) and yellow * in (B)) or cells touching the inclusion lines (dashed line in (A) and green lines in (B)) are counted, while cells hitting exclusion lines (solid lines in (A) and red lines in (B)) are not counted. Adapted from (Schmitz and Hof, 2005).

methods (McCormack *et al.*, 2002; Loos *et al.*, 2003; Dawodu and Thom, 2005; Payes *et al.*, 2008). This is because all such immostaining methods (e.g. the commonly used neuron marker NeuN) depend on visualising proteins that can be down-regulated below the threshold of immunohistochemical detection, leading to not counting unstained cells which are still present in the section. This is a risk in all pathological studies, since dying cells change their expression of many proteins, before they actually die (Andersson *et al.*, 2009; Kielar *et al.*, 2009). Therefore, in this study exclusively Nissl stained sections have been used to quantify neuronal numbers.

The neurons in the thalamic *VPM/VPL* nuclei have been counted in a 1 in 6 series of sections using a 175 x 175 μm grid and 74 x 42 μm counting frame and therefore ensuring a CE value of less than 0.1 to indicate sufficient sampling efficiency.

d) Lymphocyte counts

To characterise the extent and distribution of lymphocyte infiltration in *Ppt1*$^{-/-}$, *Cln3*$^{-/-}$ and wildtype brains, parallel 1 in 6 series of sections through each brain were stained for CD4 and CD8 following the immunohistochemical procedure described in **section 2.3** and mounted onto slides. Due to the sparse and arbitrary distribution of positively stained cells, stereological methods of quantification would prove inefficient. Instead, to determine the total number of lymphocytes in each brain, every mounted section (every sixth section through the brain) was manually counted by systematically scanning the section using a x20 objective on a Leica DMRB

microscope (Leica Mikroskopie & Systeme GmbH, Wetzlar). During all counts the investigator was blinded for age and genotype of the brains. Subsequently, the counts were multiplied by 6 to obtain the total number of lymphocytes per brain and the average number of lymphocytes per age and genotype calculated. Additionally, to provide more detailed information about the distribution of specific lymphocyte classes within the brain, each brain was divided rostral-caudally into 5 different brain regions (see **Figure 14** and **Table 6**). Last but not least, the lymphocyte counts were combined with brain volume measurements (of the total brain as well as of each of the 5 defined brain regions) using the Cavalieri method (see **section 2.6a**) and the cell density per brain volume (lymphocytes/mm^3) calculated. In this fashion, the total number of lymphocytes and a complete distribution map of CD4+ve and CD8+ve lymphocyte infiltration throughout the whole brain were obtained.

Table 6. Rostral-caudal breakdown of the mouse brain into five regions according to morphological landmarks. The cerebellum is not listed as it has been excluded from all measurements and analyses.

Brain region	Defining boundaries and content
I	Olfactoy bulb
II	Forebrain: Beginning of cortex until appearance of hippocampus
III	Forebrain with hippocampal structures
IV	Midbrain with superior colliculus
V	Midbrain with pons

2.7 Thresholding image analysis

To quantify and compare the relative levels of immune reactivity of GFAP+ve and CD68+ve staining between each genotype and age groups, we performed thresholding image analyses as described in earlier studies (Bible *et al.*, 2004; Pontikis *et al.*, 2004; Pontikis *et al.*, 2005; Kielar *et al.*, 2007). Blinded for genotype and treatment, 40 non-overlapping pictures were captured in 4 consecutive sections throughout the thalamus (*VPM/VPL* nuclei) and the cortical *S1BF* sub-region. All images were taken with a live video camera (JVC, 3CCD, KY-F55B), mounted onto a Zeiss Axioplan microscope using an x40 objective. Lamp intensity, video camera setup and microscope calibration have been kept constant during the entire analysis. Subsequently, using the *Image-Pro Plus 4.0* (Media Cybernetics) image analysis software, an appropriate threshold was chosen to distinguish between specific immunoreactivity

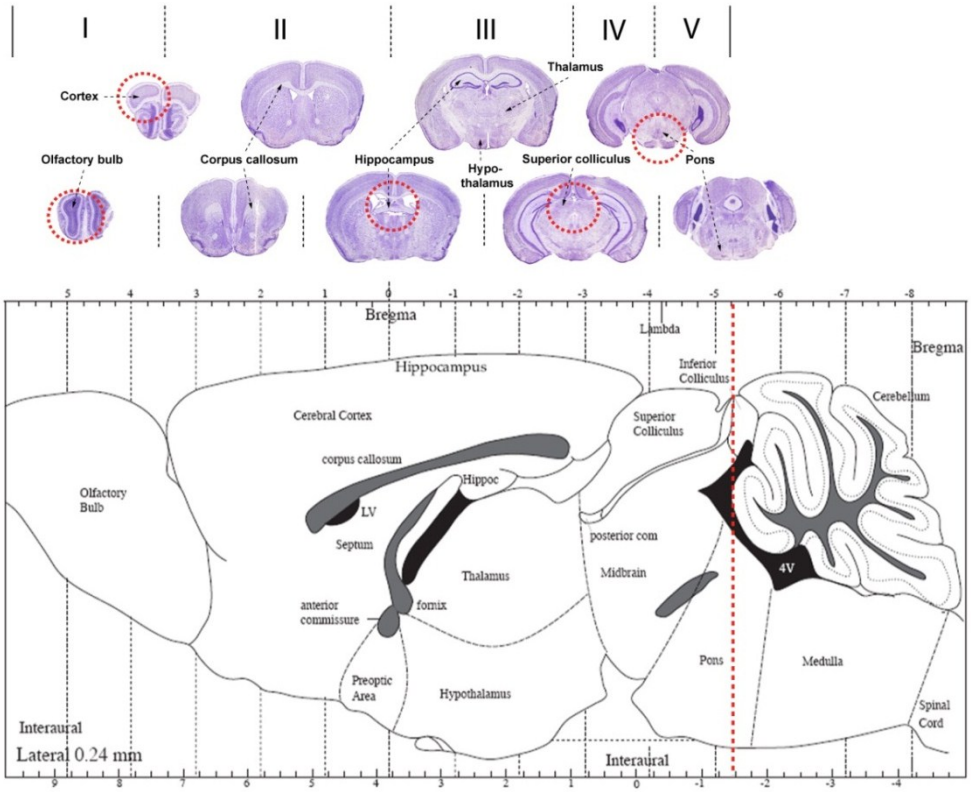

Figure 14. Illustration of regional breakdown of the mouse brain. Top: Representative Nissl stained sections, with brain regions of interest labelled and defining landmarks highlighted in red. Brain regions: I = Olfactory bulb, II = Forebrain from start of cortex (red) until hippocampus appears, III = Hippocampal (red) forebrain, IV = Midbrain with superior colliculus (red), V = Midbrain with pons (red). Bottom: Schematic lateral view of mouse brain with most important brain parts explained. The cerebellum is not considered as it has been excluded from all measurements and analyses. Adapted from (Paxinos and Franklin, 2001).

for each antigen and non-specific background. Once a suitable threshold has been defined, it was kept constant for all images analysed. Macros were setup and recorded to transfer the analysed data to an Excel spread sheet for further statistical analysis. The results of each region and antigen were presented as mean percentage area of immunoreactivity per (measured) field (± SEM).

2.8 Statistical analysis

To test for potential differences in quantitative data between genotypes and age groups two-way ANOVA's (with age and genotype as independent variables) or one-way ANOVA's (if only one age group was analysed) (*Graph Pad Prism 4.03*, Graph Pad software, Inc.) were conducted. In all cases, Bonferroni post hoc tests were performed and statistical significance considered at $p \leq 0.05$. The mean coefficient of error (CE) for all opticial fractionator and Cavalieri estimates were calculated according to the method of Gundersen and Jensen (Gundersen and Jensen, 1987) and was less than 0.1 in all samples (except for the late staged *Ppt1*$^{-/-}$ brains where the CE reached maximally 1.5-1.7 due to extreme neuron loss).

Chapter 3

Adaptive immune response in the NCL CNS

An inflammatory component to pathogenesis is not uncommon in neurodegenerative disorders (see **Chapter 1**), and has been described in Parkinson disease (Brochard *et al.*, 2009; Stone *et al.*, 2009), Alzheimer disease (McGeer and McGeer, 2003; Heneka and O'Banion, 2007), multiple sclerosis (Stadelmann *et al.*, 2011), amyotrophic lateral sclerosis (ALS) (Sta *et al.*, 2011) and other lysosomal storage disorders (LSDs) (Castaneda *et al.*, 2008) like Gaucher disease (Shoenfeld *et al.*, 1995; Mizukami *et al.*, 2002), GM1/2 gangliosidosis (Jeyakumar *et al.*, 2003), Krabbe disease (Wu *et al.*, 2000; Suzuki, 2003) and the mucopolysaccharidoses (MPSs) (Ohmi *et al.*, 2003; Ausseil *et al.*, 2008).

Similarly, immune reactions have also been described in the Infantile and Juvenile form of NCL (Pontikis *et al.*, 2004; Pontikis *et al.*, 2005; Kielar *et al.*, 2007; Lim *et al.*, 2007b; Macauley *et al.*, 2009; Weimer *et al.*, 2009). However, the main focus of this research has so far been on the increased innate immune responses in *Ppt1* and *Cln3* deficient mice (Pontikis *et al.*, 2004; Kielar *et al.*, 2007; Macauley *et al.*, 2009; Weimer *et al.*, 2009), with only recent appreciation of adaptive immune responses in these mice (Lim *et al.*, 2007b; Macauley *et al.*, 2011; Seehafer *et al.*, 2011). However, no extensive characterisation of adaptive immune cell responses in the brain of INCL and JNCL mice has been provided so far. To obtain this, a full series (n=5) of *Ppt1* and *Cln3* deficient and age-matched control brains at different stages of disease progression (*Ppt1*$^{-/-}$: 1, 3, 5 and 7 months of age/*Cln3*$^{-/-}$: 6.5, 12 and 21 months of age) were immunohistochemically stained for the general leukocyte marker (CD45) and the adaptive immune cell markers: cytotoxic T-cell (CD8) and T-helper cell (CD4).

In addition to surveying the distribution of cells immunoreactive for each marker and taking representative pictures, detailed cell counts of positively stained lymphocytes throughout the whole brain were complemented with total brain and regional volume measurements. Combining these measures allowed the calculation of relative lymphocyte density per region at each time point. Furthermore, by dividing the brain into defined rostrocaudal levels (see **Figure 14** and **Table 6** in **Chapter 2** for detail), we have obtained a detailed description of lymphocyte distribution throughout the brain and how it changes over time. This is the first time, the adaptive immune responses evident in Infantile and Juvenile NCL have been characterised in such detail.

3.1 Leukocytes in the CNS of Infantile and Juvenile NCL mice

To obtain a general overview of immune reactions occurring in NCL and control brains, a series of sections from each brain were stained for CD45, the '*general leukocyte marker*'. The CD45 molecule, also known as '*leukocyte common antigen*', describes the enzyme 'protein tyrosine phosphatase receptor type C' (PTPRC) and is a transmembrane protein found on all differentiated hematopoeic cells, except for erythrocytes (Thomas, 1989). As a member of the protein tyrosine phosophatase (PTP) family its function combines regulation of various cellular processes concerning cell cycle, growth and differentiation (Cool *et al.*, 1990; Denhertog *et al.*, 1993; Denu and Dixon, 1998; Paul and Lombroso, 2003). Additionally, it is an essential regulator in antigen presenting function of activated T- and B-cells (Brown *et al.*, 1994; Alexander, 2000; Huntington and Tarlinton, 2004), as well as being found on monocytes that serve as progenitors for macrophages and/or microglia (Patterson and Caldwell, 1992; Seta and Kuwana, 2007). Since various states of activation and morphologies of microglia and macrophages can be observed in the brain, and it not being possible to unambiguously distinguish between these cell types on the basis of a single marker, we will refer to 'microglia' as stained cells with elongated and/or branched processes in contrast to 'macrophages' with enlarged round, amoeboid-like cell bodies with no processes (see **Figure 15**). However, because microglia transform into brain macrophages during disease progression, several intermediate states of activation are often present in the brain, in which case cells will be described as the most morphologically appropriate cell type.

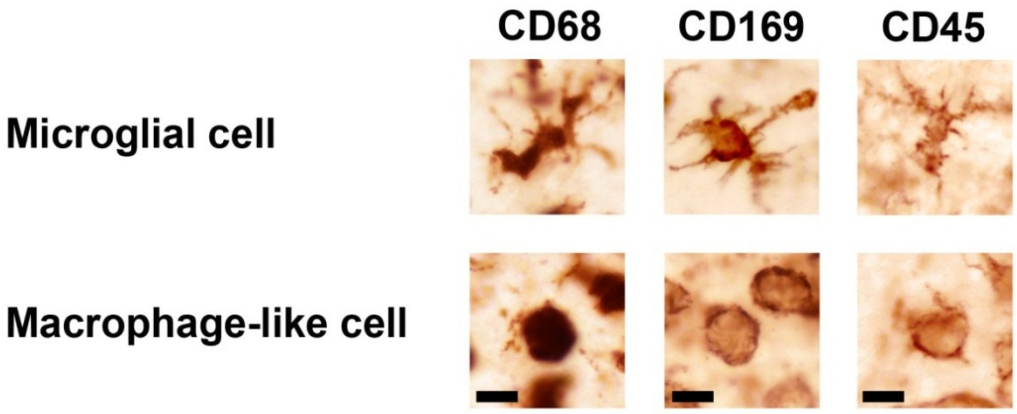

Figure 15. Distinction between microglial and macrophage morphology. Immunohistochemical staining for the microglial marker CD68, the macrophage marker CD169 and the leukocyte marker CD45 revealed both microglia and macrophage-like cells. Since these cell types cannot be unambiguously distinguished using these markers and because microglia transform into brain macrophages during disease progression, we will refer to 'microglia' as cells with distinct processes (top row) and 'macrophages' as cells with round cell bodies lacking processes (bottom row). Scale bar = 10 μm.

a) CD45 positive leukocytes in *Ppt1*$^{-/-}$ mice

Immunohistochemical staining for CD45 of the *Ppt1*$^{-/-}$ mouse model of INCL and age-matched wildtype mice at all four ages (1, 3, 5 and 7 months) revealed distinct CD45 immunoreactivity in the brain parenchyma of *Ppt1*$^{-/-}$ mice from 3 months onwards (see representative pictures of the thalamus in **Figure 16** and **Table 7** for a detailed summary of the distribution of CD45 immunoreactivity in *Ppt1*$^{-/-}$ mice over time). Almost no CD45+ve cells were detectable in either wildtype (at any age) or in 1 month old mutant mice. In wildtype mice CD45 stained cells could be seen only sporadically in the brain parenchyma, whereas most CD45+ve cells were present in the meninges, choroid plexus or at the edges of the ventricles (data not shown). Judged by their morphology, these CD45+ve cells in wildtype mice resembled either T-cells with round and small cell bodies, lacking any cell processes, or macrophages with elongated, crescent-shaped or amoeboid cell bodies. Generally comparing the staining of these two cell types, T-cells were often more intensely stained and clearer to detect than macrophages in wildtype and *Ppt1*$^{-/-}$ mice, which potentially could be explained by different levels of CD45 expression at the plasma membrane of each cell type.

i) 1 month old *Ppt1*$^{-/-}$ mice

In 1 month old mice, many CD45+ve cells could be detected within the olfactory bulb, and morphologically resembled T cells with round, small cell bodies and no processes (data not shown). In two of the five mutant mice at this age point there was a hint of microglial activation in the thalamus with faintly stained CD45 immunoreactive cells present in this brain region. As such, it could be speculated that the first signs of immune cell activation already occur at this time point, with T-cell like cells being the first detectable CD45+ve cells in the brain parenchyma (olfactory bulb).

ii) 3 month old *Ppt1*$^{-/-}$ mice

Between 1 and 3 months microglial and/or macrophage activation appears to begin in *Ppt1*$^{-/-}$ mice within the thalamus, showing first clear signs of immunological up-regulation at 3 months of age, as previously described (Kielar *et al.*, 2007). But in spite of intense CD45 staining, no single cell type could be identified in this region, with numerous different cellular morphologies evident (see **Figure 16**). These cells were mainly of a microglial appearance, but many shapes and sizes of cells including a few

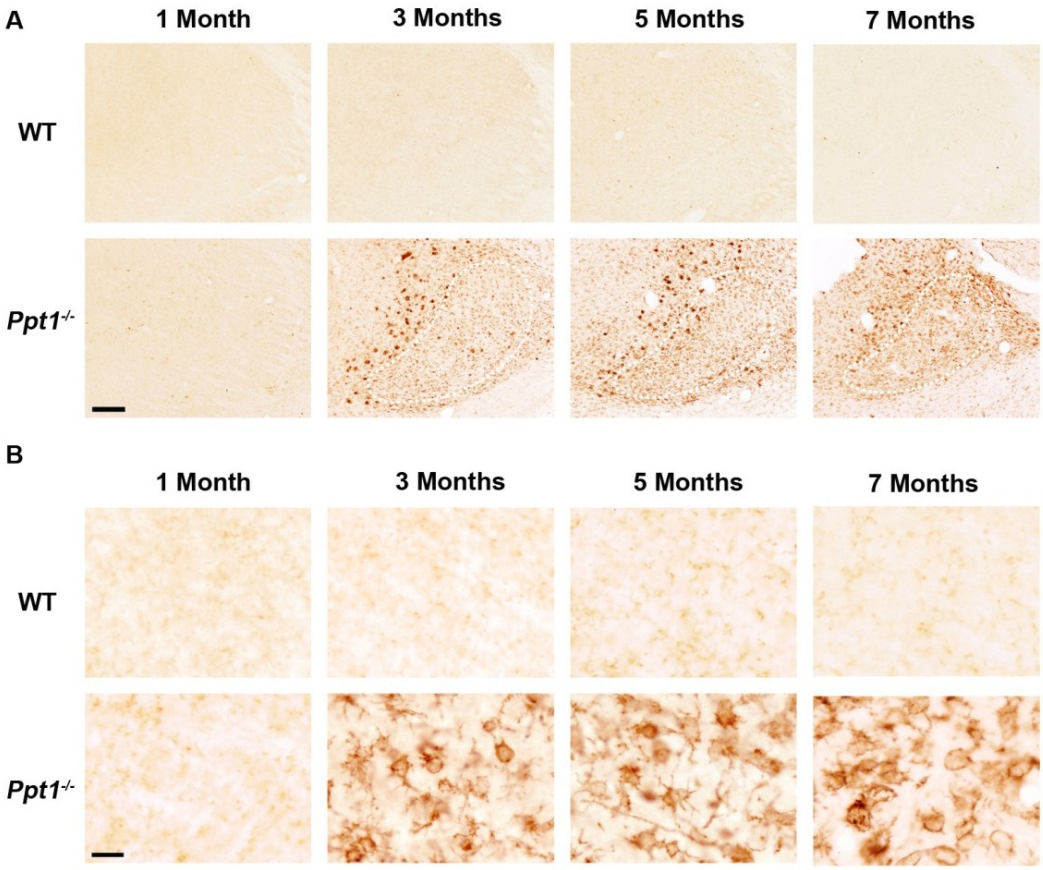

Figure 16. Progressive immune cell activation in *Ppt1*$^{-/-}$ mice. (A) Immunohistochemical staining for the general leukocyte marker CD45 in the thalamus of 1, 3, 5 and 7 month old *Ppt1*$^{-/-}$ and wildtype (WT) mice revealed widespread immune cell and lymphocyte activation within the ventral posterior nucleus (*VPM/VPL*) (---) in *Ppt1*$^{-/-}$ mice. From 3 months onwards, localised immune cell activation could be observed in the *VPM/VPL* nuclei of *Ppt1*$^{-/-}$ mice, which spread to involve the whole thalamus with increased age. In contrast, almost no CD45 immunoreactivity was seen at any age in the thalamus of WT brains. Scale bar = 200 μm. (B) Higher magnification pictures of CD45+ve cells in the thalamus of 1, 3, 5 and 7 month old *Ppt1*$^{-/-}$ mice and WT mice revealed various immune cells in mutant mice from 3 months onwards. Judged on their morphology, CD45+ve cells resembled macrophages and microglia, as well as lymphocytes. Whereas at 3 months of age microglia with elongated cell processes stained for CD45, with increased age and disease progression, more brain-macrophage like cells with round cell bodies and short (or no) processes displayed CD45 immunoreactivity (particularly at 7 months of age). Scale bar = 20 μm.

T-cells were present. Interestingly, morphologically distinct cell types were present within different thalamic regions. Whereas weaker CD45+ve macrophage-like cells were mainly located in the *ventral posteromedial* and *posterolateral nuclei* (*VPM/VPL*), darkly stained cells with brain macrophage-like morphology could be found in the *ventrolateral thalamic nucleus* (*VL*) and the *posterior thalamic nuclei* (*PO*), as defined by landmarks described in (Paxinos and Franklin, 2001). Additionally, the thalamic *medial geniculate nuclei* (*MG*) and the *dorsal lateral geniculate nucleus* (*LGNd*) showed intensely stained, brain macrophage-like CD45+ve cells scattered with sporadic T-cells.

Table 7. Detailed summary of the distribution of CD45 immunoreactivity in *Ppt1*$^{-/-}$ mice over time. Brains of 1, 3, 5 and 7 month old *Ppt1*$^{-/-}$ and wildtype mice were stained for CD45 and a list of brain nuclei showing CD45 immunoreactivity in *Ppt1*$^{-/-}$ mouse brains has been compiled. For each nucleus the extent of microglial (**Mic**), macrophage (**Mϕ**) and T-cell (**T**) activation have been recorded, whereby cells with distinct processes were classified as 'microglia'; round intensely immunoreactive cells without processes were defined as 'macrophages' (see also **Figure 15** for distinction) and small, round or oval shaped cell-bodies without any processes were specified as T-cells. Symbols: '**·**' = no immunoreactivity; for **Mic** and **Mϕ**: **(+)** = traces of cell-staining, **+** = faintly stained cells, **++** = pronounced cell-staining, **+++** = intense staining of activated cells; for **T**: **(+)** = sporadic T-cell found, **+** = several T-cells are present, **++** = increased T-cell infiltration, **+++** = most pronounced T-cell infiltration. Colour intensity reflects the activation status of each cell type (green = microglia, red = macrophages, blue = T-cells) to visualise the changes of CD45 immunoreactivity over time. I, II, III, IV, V or VI = lamina I-VI. Nuclei definition according to (Paxinos and Franklin, 2001).

Brain region/nucleus		1 Month				3 Months				5 Months				7 Months			
Thalamus		**Mic**	**Mϕ**	**T**	**Comments**	**Mic**	**Mϕ**	**T**	**Comments**	**Mic**	**Mϕ**	**T**	**Comments**	**Mic**	**Mϕ**	**T**	**Comments**
VPM/VPL	Ventral posteromedial and posterolateral thalamic nucleus	·	·	(+)		++	+	+		+++	++	+		·	+++	+	
VL	Ventrolateral thalamic nucleus	·	·	(+)		++	+++	+		++	+++	+		+++	++	+	
PO	Posterior thalamic nuclei	·	·	(+)		++	+++	+		++	+++	+		+++	++	+	
VM	Ventromedial thalamic nucleus	·	·	(+)		++	·	+		+++	·	+		++	+	+	
LGNd	Dorsal lateral geniculate nucleus	·	·	(+)		++	+	+		+++	++	+		+++	+++	+	
AM	Anteromedial thalamic nucleus	·	·	(+)		+	·	+		++	·	+		++	+	+	
AD	Anterodorsal thalamic nucleus	·	·	(+)		·	·	(+)		+	·	+		++	++	+	
AV	Anteroventral thalamic nucleus	·	·	(+)		+	·	+		++	·	+		+	++	+	
AVDM/VL	Anteroventral thalamic nucleus, dorsomedial/ventrolateral part	·	·	(+)		++	·	+		++	++	+		+++	++	+	
CM	Central medial thalamic nucleus	·	·	(+)		++	+	+		++	+	++		++	++	++	
LPLR/MR	lateral posterior thalamic nucleus, laterorostral/mediocaudal part	·	·	(+)		++	+	+		++	++	+		+++	++	+	
MD	Mediodorsal thalamic nucleus	·	·	·		+	·	+		++	·	+		++	+	+	
MDM/L	Mediodorsal thalamic nuclei, medial/lateral part	·	·	(+)		+	+	+		++	++	+		++	+++	+	
MGV/D/M	Medial geniculate nucleus, ventral/dorsal/medial part	·	·	(+)		++	+	+		++	++	+		++	+++	+	
Re	Reuniens thalamic nucleus	·	·	·		+	·	+		+	·	+		++	·	+	
Rh	Rhomboic thalamic nucleus	·	·	(+)		+	·	+		++	·	+		++	++	++	

Brain region/nucleus		1 Month				3 Months				5 Months				7 Months			
Thalamus		**Mic**	**Mϕ**	**T**	**Comments**	**Mic**	**Mϕ**	**T**	**Comments**	**Mic**	**Mϕ**	**T**	**Comments**	**Mic**	**Mϕ**	**T**	**Comments**
ZIV/D	Zona incerta	·	·	(+)		+	·	+		++	·	+		++	+	+	
Midbrain																	
RMC	Red nucleus, magnocellular part	·	·	·		++	·	+		++	·	+		+++	·	+	
RPC	Red nucleus, parvicellular part	·	·	·		+	·	+		+	·	+		+	·	+	
Hippocampus																	
CA1	Cornu Ammonis 1, subfield of hippocampus	·	·	(+)		·	·	+		++	+	+		+++	+	+	
CA2	Cornu Ammonis 2, subfield of hippocampus	·	·	(+)		·	·	+		·	·	+		·	·	+	
CA3	Cornu Ammonis 3, subfield of hippocampus	·	·	(+)		·	·	+		·	·	+		·	·	+	
DG	Dentate gyrus	(+)	·	(+)		+	·	+		++	·	+		+++	·	+	
S	Subiculum	·	·	(+)		+	·	+		++	+	+		+++	+	+	
Amygdala																	
AAD	Anterior amygdaloid area	·	·	(+)		+	·	+		++	+	++		+++	+	++	
AHipM	Amygdalohippocampal area	·	·	(+)		(+)	·	+		++	·	+		+	+	++	
APir	Amygdalopiriform transition area	·	·	(+)		+	·	+		+	+	+		++	+	++	
PMCo	Posteromedial cortical amygdaloid nucleus	·	·	(+)		·	·	(+)		+	·	+		+	·	+	
BLA	Basolateral amygdaloid nucleus	·	·	(+)		·	·	+		+	·	++		+	+	++	
CeC/M	Central amygdaloid nucleus, capsular part/medial division	·	·	(+)		·	·	+		+	·	++		+	·	++	
Basal ganglia																	
Cpu	Caudate putamen	·	·	+		++	+	++		++	+	+++		+++	+	+++	
LGP	Lateral globus pallidus	·	·	+		++	+	+		++	+	+		+++	+	+	
MGP	Medial globus pallidus	·	·	·		+	·	+		++	·	+		++	+	+	

Brain region/nucleus		1 Month				3 Months				5 Months				7 Months			
Basel ganglia		**Mic**	**Mϕ**	**T**	**Comments**	**Mic**	**Mϕ**	**T**	**Comments**	**Mic**	**Mϕ**	**T**	**Comments**	**Mic**	**Mϕ**	**T**	**Comments**
SN	Substantia nigra	·	·	·		++	·	+		+++	·	+		++	+	+	
VP	Ventral pallidum	·	·	(+)		+	·	+		++	·	++		+++	+	+++	
Cortex																	
Cortex	General pattern	·	·	(+)		++	·	++	(VI)	++	·	+++	(II/III/VI)	+	++	+++	(II/III/VI)
S1BF	Primary somatosensory barrel field	·	·	(+)		++	+	++	(VI, a bit II/III)	++	++	++	(VI, a bit II/III)	+	++	++	(VI & all layers)
S1HL/S1FL	Primary somatosensory cortex, hind-/forelimb region	·	·	(+)		+	+	++	(VI -II/III)	++	+	++	(VI & all layers)	+	++	+++	(VI & II/III)
S2	Secondary somatosensory cortex	·	·	(+)		+	+	++	(VI/II/III & all)	++	+	++	(VI/II/III & all)	+	++	++	(VI/II/III & all)
Au1/AuD/V	Auditory cortex (primary/secondary auditory cortex, dorsal/ventral)	·	·	(+)		++	·	++	(all laminae)	+++	+	+++	(all laminae)	+	++	+	(all laminae)
AID/V	Agranular insular cortex, dorsal/ventral	·	·	(+)		++	·	+	(all laminae)	+++	+	+++	(all laminae)	+	++	+	(VI/II & all)
V1	Visual cortex	·	·	(+)		+	·	+	(VI)	++	·	++	(VI/II/III & all)	++	++	+	(VI/II/III & all)
M1	Motor cortex 1	·	·	(+)		++	+	++	(II/III a bit VI/V)	++	+	++	(II/III/VI)	+	++	++	(VI/II/III & all bit)
M2	Motor cortex 2	·	·	(+)		++	+	+	(VI/V & all)	++	++	++	(all laminae)	+	++	++	(II/III & all)
RSA	The retrosplenial agranular cortex	·	·	(+)		+	+	+	(all laminae)	+	+	+	(II/III & all)	+	++	+	(II/III & all)
RSG	The retrosplenial granular cortex	·	·	(+)		++	+	+	(all laminae)	++	++	+	(II/III & all)	++	+++	+	(II/III & all)
Cig1/2	Cingulate cortex area 1/2	·	·	(+)		+	+	+	(II/III & VI & all a bit)	++	+	++	(II/III/VI & all)	+	++	+	(II/III & all)
Pir	Piriform cortex	·	·	(+)		+	+	+	(all laminae)	++	+	++	(II (Mϕ) & all)	+++	++	++	(II (Mϕ) & all)
VO/LO	Ventral/lateral orbital cortex	·	·	·		++	·	++	(VI/V & all a bit)	++	+	++	(all apart I)	+	++	+	(all laminae)
LEnt	Lateral entorhinal cortex	·	·	(+)		+	·	+		++	·	+		++	+	+	
DEn	Dorsal endopiriform nucleus	·	·	·		+	+	+		++	+	++		+	++	+	
VEn	Ventral endopiriform nucleus	·	·	·		·	·	+		·	·	+		·	·	+	

Brain region/nucleus		1 Month				3 Months				5 Months				7 Months			
Hypothalamus		**Mic**	**Mϕ**	**T**	**Comments**	**Mic**	**Mϕ**	**T**	**Comments**	**Mic**	**Mϕ**	**T**	**Comments**	**Mic**	**Mϕ**	**T**	**Comments**
IPACM/L	Interstitial nucleus of posterior limb of anterior commissure, med./lat. part	·	·	(+)		+	·	++		++	·	+++		++	·	+++	
MCPO	Magnocellular preoptic nucleus	·	·	·		+	+	+		++	+	++		+++	+	++	
HDB	Nucleus of horizontal limb of the diagonal band	·	·	·		+	+	+		++	+	++		+++	+	++	
Pons & Medulla																	
Pons	General pattern	·	·	(+)		+	·	+	(ventral)	++	·	++	(ventral)	++	(+)	++	throughout
Pr5	Principal sensory trigeminal nucleus	·	·	·		++	·	+		++	+	++		+++	+	++	
VLL	Ventral nucleus of lateral lemniscus	·	·	·		++	·	+		++	+	++		+++	·	++	
RtTg	Reticulotegmental nucleus of the pons	·	·	·		+	·	+		++	+	++		+++	+	++	
CIC	Central nucleus of the inferior colliculus	·	·	(+)		++	·	+		+++	·	+		+++	++	+	
ECIC	External cortex of the inferior colliculus	·	·	.		+	·	+		+	·	+		++	·	+	
Pn	Pontine nuclei	·	·	(+)		+	·	+		++	+	++		+++	+	++	
LDTg	Laterodorsal tegmental nucleus	·	·			+	·	+		+	·	+		++	·	+	
Mo5	Motor trigeminal nucleus	·	·	(+)		+	·	+		++	·	+		++	+	+	
Olfactory bulb																	
OB	Olfactory bulb – general pattern	(+)	·	+		+	·	++		++	+	+++		++	++	+++	
EPI	External plexiform layer of the olfactory bulb	·	·	(+)		+	+	++		++	+	+++		+++	++	+++	
GRO	Granular cell layer of the olfactory bulb	·	·	(+)		+	+	++		++	+	+++		+++	++	+++	
DTT	Dorsal tenia tecta	·	·	·		+	·	+		++	·	+		++	·	+	

In addition to the thalamus, other brain regions also showed the first signs of microglial activation at 3 months of age: in the cortex this activation was mainly in layer VI of several cortical regions immediately adjacent to the *corpus callosum,* but was most pronounced in the *somatosensory cortex* (mostly in *S1BF* and more scarcely in *S2*) and the *retrosplenial granular cortex* (*RSG*) - both of which connect to the thalamic nuclei. Whereas this microglial activation in the cortex appeared rather weak, other structures contained more intensely stained and presumably activated cells at this age. From rostral to caudal these included the *caudate putamen* (striatum) and *lateral globus pallidus* (*LGP*) which connect to the *substantia nigra* – all parts of the basal ganglia; *ventral nucleus of lemniscus* (*VLL*) which connect to the secondary sensory cortex, *subiculum* as the last part of the hippocampus, *external cortex of the inferior Colliculus* (*ECIC*) which receives projections from the somatosensory cortex and the thalamic *medial geniculate nuclei* (*MG*). Only in its rostral, but not in the caudal, parts did the *piriform cortex* show signs of microglial activation. Notably, no trace of immune cell up-regulation (in terms of CD45 immunoreactivity) could be seen in the hippocampus at 3 months, except for faintly stained microglia in the *dentate gyrus* (*DG*) and *subiculum*. In the most rostral part of the brain, the olfactory bulb was infiltrated by many CD45+ve T-cells (on the basis of their morphology) and also showed weakly stained microglia at this time point (data not shown).

Based on these morphological data a generalised weak immunological activation appears to occur at this 3 month time point, but this immune up-regulation always seemed to be confined to distinct regions, as seen for example in the rostral part of the cortex where microglial activation was observed, but not in the underlying *anterior olfactory nucleus* (Paxinos and Franklin, 2001).

iii) 5 month old *Ppt1*$^{-/-}$ mice

With increased age and disease progression, immune cell activation spread to other brain regions, with CD45 positive cells more widely present within the CNS. At 5 months of age, the cortex and most parts of the brain contained activated microglia and were also infiltrated by CD45+ve immune cells. In the olfactory bulb, besides morphologically identified T-cells, intensely stained activated microglia could be detected at 5 months of age. Furthermore, mostly microglia, macrophages, and occasionally T-cells, were positively stained for CD45 in the same nuclei of the thalamus (*VPM/VPL*, *LGNd*, *MG*) as seen at 3 months of age. As at 3 months of

age, the most activated macrophage-like cells could be found in *PO* and *VL* (see **Figure 16**). Within the cortex, immune cell activation was present in layer VI of most cortical regions. However, besides the generally higher overall activation of immune cells within the whole brain and especially in all those regions already described at 3 months of age, several additional brain regions also contained CD45+ve cells at 5 months of age: a distinct and intense microglial infiltration/activation was present in all layers of the *auditory cortex* (*Au1*, *AuV* and *AuD*), and to a lesser extent in the *secondary somatosensory cortex* (*S2*), along with an up-regulation of CD45 immunoreactivity in the rostral portions of the brain, namely the *cingulate cortex*. Additionally, faintly stained CD45+ve cells could be found in laminae II/III and sometimes also in lamina VI of the *motor cortex* (mainly M1, little M2). In the hippocampus an intensely stained band of CD45+ve activated microglia was present in the *CA1* subfield and to a lesser extent in the *dentate gyrus* (DG) (data not shown).

iv) 7 month old *Ppt1*$^{-/-}$ mice

At 7 months of age, intensely stained CD45+ve microglia, many with brain-macrophage morphology, together with T-cells were evident in most, if not all brain regions. Particularly intensely stained microglia could be seen, not just within thalamic nuclei (as most prominently seen in *VPM/VPL*, *LGNd*, *MG*, *PO* and *VL*) (see **Figure 16A**), but also in the *CA1* subfield and *dentate gyrus* of the hippocampus. Interestingly, the highly activated macrophage-like cells which were seen in *PO* and *VL* at the previous two ages, could not be detected at 7 months of age, but instead more brain-macrophages with round cell soma were present in these nuclei (see **Figure 16B**). Furthermore, CD45+ve cells were present in widespread cortical regions. This not only included staining in laminae II/III and VI of *M1/2* at this time point, but was also within most cortical layers of the *visual cortex* (*V1*) and also the *lateral entorhinal cortex* (*LEnt*), but most prominently in layer II/III of these cortical regions. Interestingly, at this age *S1BF* and *Au*, which had displayed intense CD45 staining at earlier ages, now displayed weaker immune/microglial activation at 7 months of age. Last but not least, pronounced macrophage/microglial activation could be detected in the *pons* and the *external cortex of the inferior Colliculus* (*ECIC*) of *Ppt1*$^{-/-}$ mice at 7 months of age (data not shown).

b) CD45 positive leukocytes in *Cln3*$^{-/-}$ mice

As conducted in *Ppt1*$^{-/-}$ mice, a series of sections from *Cln3*$^{-/-}$ brains, as murine model of Juvenile NCL, were also stained for CD45 at 3 age groups (6.5, 12 and 21 months). The first clear signs of CD45 immunoreactivity were apparent in *Cln3*$^{-/-}$ mice from 12 months onwards, and increased in intensity and abundance with disease progression (see **Figure 17** for representative pictures and **Table 8** for a detailed summary of the distribution of CD45 immunoreactivity in *Cln3*$^{-/-}$ mice over time). In wildtype (and 6.5 month old *Cln3*$^{-/-}$) mice CD45+ve cells (morphologically resembling T-cells and macrophages) could be detected mainly along the brain borders (in the meninges, choroid plexus or at the edges of the ventricles). In these mice, only sporadic CD45+ve cells (resembling T-cells) could be detected in the mid and forebrain parenchyma, whereas in the olfactory bulb many CD45 immunoreactive T-cells had accumulated (data not shown).

i) 6.5 month old *Cln3*$^{-/-}$ mice

As seen in wildtype mice at all ages, in 6.5 month old *Cln3*$^{-/-}$ mice CD45+ve cells could be mainly detected within the olfactory bulb or along the borders of the brain (namely in the meninges, the choroid plexus or along the ventricle walls). In the olfactory bulb, these CD45+ve cells morphologically resembled T cells with round, small cell bodies and no processes (data not shown), whereas a mixed population of T-cells and macrophages aligned along the brain borders. But T-cells showed more distinct CD45 immunoreactivity than macrophages, suggesting higher levels of CD45 expression on T-cells at this age (data not shown).

ii) 12 month old *Cln3*$^{-/-}$ mice

As at 6.5 months of age, CD45 immunoreactivity was also seen in the olfactory bulb of *Cln3*$^{-/-}$ mice at 12 months of age though many more CD45+ve cells were present. Besides most cells morphologically resembling lymphocytes, weak microglial staining could also be detected in the olfactory bulb. Yet, the clearest immune cell activation in the forebrain was observed in the *ventral posteromedial* and *posterolateral* (*VPM/VPL*) nuclei in *Cln3*$^{-/-}$ mice at this time point (see **Figure 17A**). A variety of cell shapes and morphologies were stained for CD45 in the *VPM/VPL* nuclei: cells resembling microglia with elongated processes, macrophages with short processes as well as some T-cells with darkly stained, very small cell bodies and no processes (see **Figure 17B**).

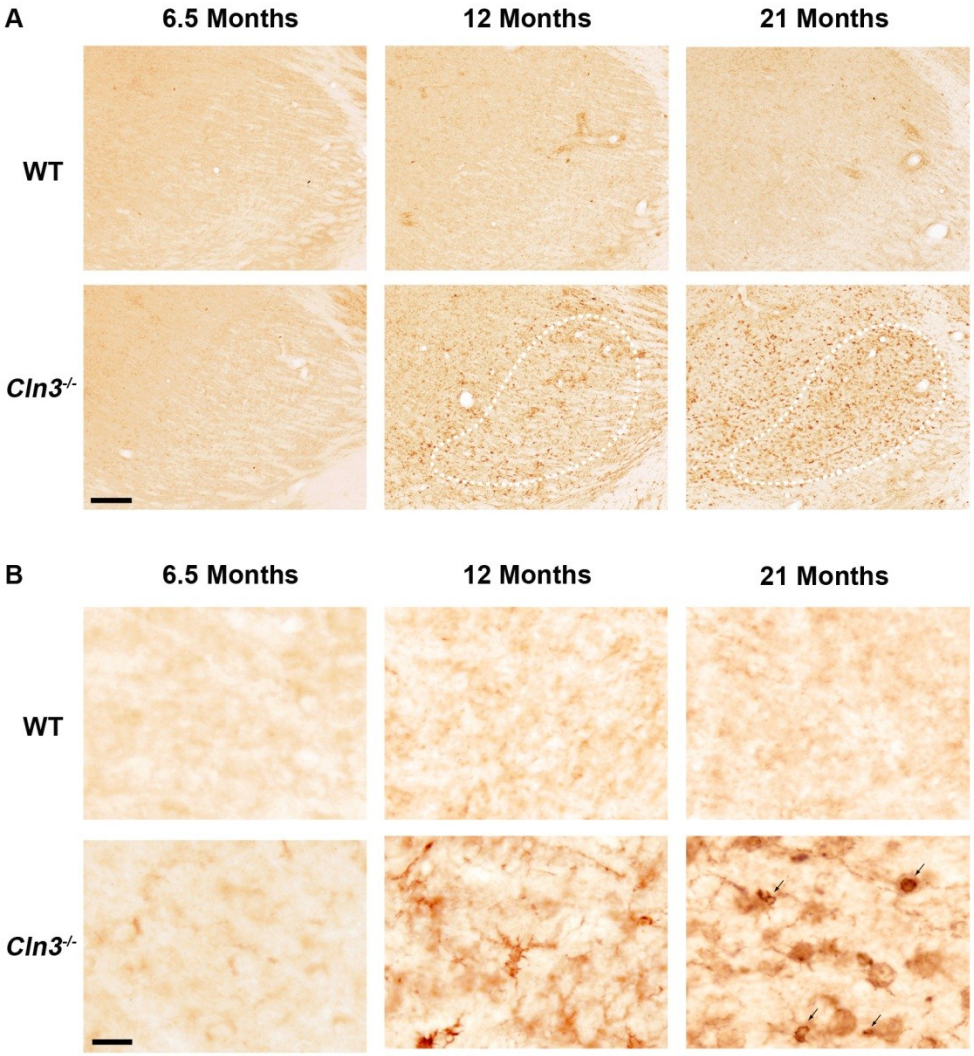

Figure 17. Progressive immune cell activation in *Cln3*$^{-/-}$ mice. (A) Immunohistochemical staining for the general leukocyte marker CD45 in the thalamus of 6.5, 12 and 21 month old *Cln3*$^{-/-}$ and wildtype (WT) mice revealed widespread immune cell and lymphocyte activation within the *ventral posterior nucleus* (*VPM/VPL*) (---) in *Cln3*$^{-/-}$ mice. From 12 months onwards, immune cell activation could be clearly observed in the *VPM/VPL* nuclei of *Cln3*$^{-/-}$ mice which increased in intensity and spread to involve the whole thalamus at 21 months of age. In contrast, almost no CD45 immunoreactivity was seen at any age in the thalamus of WT brains. Scale bar = 200 μm. (B) Higher magnification pictures of CD45+ve cells in the thalamus of 6.5, 12 and 21 month old *Cln3*$^{-/-}$ and WT mice revealed various types of immune cells in the mutant mice from 12 months onwards. Judged on their morphology, CD45+ve cells resembled macrophages, microglia as well as lymphocytes (arrows). Whereas at 12 months of age microglia with elongated cell processes stained for CD45 in *VPM/VPL* nuclei of *Cln3*$^{-/-}$ mice, mainly brain-macrophage like cells with round cell bodies and short (or no) processes displayed CD45 immunoreactivity at 21 months of age. Additionally, some CD45+ve cells resembling lymphocyte (arrows) with small round or oval shaped morphology without any cell processes could be detected in the thalamus of *Cln3*$^{-/-}$ mice. Scale bar = 20 μm.

According to landmarks in (Paxinos and Franklin, 2001), additional thalamic macrophage/microglial staining in the thalamus could be detected in the *mediodorsalthalamic nucleus* (*MD*) and the *posterior thalamic nuclei* (*PO*), but to a weaker extent than seen in *VPM/VPL*. Besides the thalamus, other brain regions also showed

weak microglial activation. These included the *caudate putamen* (striatum), the *parvicellular* and *magnocellular part* of the *red nucleus* (*RPC* and *RMC*), the *reticulotegmental nucleus of the pons* (*RtTg*) and much weaker palely stained microglial activation was seen in the *substantia nigra* and the caudal parts of the *subiculum* of the hippocampus (data not shown). In the cortex, faintly stained microglia were present in the two most ventral laminae VI and V, but a variety of sub-regions displayed more pronounced microglial activation, also mainly in the most ventral laminae (VI and V). From rostral to caudal, such microglial activation was seen in the *cingulate cortex* (*Cig1*, *Cig2*), the *motor cortex* (*M1* and *M2*), the *somatosensory cortex* (mainly in *S1HL*, *S1FL* and *S2*, but only marginal in *S1BF*), throughout all laminae of the *retrosplenial granular* and partly also in *the retrosplenial agranular cortex* (*RSG, RSA*) and the *primary* and *secondary auditory cortex* (*Au1*, *AuD* and *AuV*). Last but not least, distinct macrophage/microglial staining with CD45 could be observed along the lateral nuclei of the *piriform cortex* (*Pir*). Apart from these defined brain regions, some intensely stained macrophages or microglia with an enlarged cell body and many processes could be detected randomly scattered throughout the brain. Interestingly, many CD45+ve lymphocyte-like cells were seen in the olfactory bulb and were not as often found in more caudal parts of the brain of *Cln3*$^{-/-}$ mice at 12 months of age (data not shown).

iii) 21 month old *Cln3*$^{-/-}$ mice

As consequence of disease progression, in 21 month old *Cln3*$^{-/-}$ mice CD45 immunoreactivity was clearly increased with activated microglia present throughout the brain. However, certain brain regions demonstrated markedly more CD45 reactive macrophages/microglia, mostly with round and darkly stained cell soma (see example in **Figure 17B**). Generally speaking, the number of CD45+ve cells was not only increased, but staining of these cells was more intense in the same brain regions already described above at 12 months of age. However, several additional regions also showed macrophage/microglial staining in *Cln3*$^{-/-}$ mice at 21 months of age. From rostral to caudal, the following brain regions contained many CD45+ve cells. The olfactory bulb was particularly full of T-cells and contained clear macrophage and microglia staining at 21 months of age (data not shown). Cortical activations were seen in more ventral laminae (VI and V) of the cortex, with particularly intense CD45 staining in the *motor cortex* (*M1*, *M2*), *piriform cortex* (*Pir*) (with distinct microglial staining along its lateral nuclei, and especially pronounced T-cell infiltration), in the *agranular insular cortex* (*AID*, *AIV*), the *primary somatosensory cortex* (*S1 S1Tr* and *S1BF*), in the

Table 8. Detailed summary of the distribution of CD45 immunoreactivity in *Cln3*$^{-/-}$ mice over time. Brains of 6.5, 12 and 21 month old *Cln3*$^{-/-}$ and wildtype mice were stained for CD45 and a list of brain nuclei showing CD45 immunoreactivity in *Cln3*$^{-/-}$ mouse brains has been compiled. For each nucleus the extent of microglial (**Mic**), macrophage (**Mϕ**) and T-cell (**T**) activation have been recorded, whereby cells with distinct processes were classified as 'microglia'; round intensely immunoreactive cells without processes were defined as 'macrophages' (see also **Figure 15** for distinction) and small, round or oval shaped cell-bodies without any processes were specified as T-cells. Symbols: '·' = no immunoreactivity; for **Mic** and **Mϕ**: **(+)** = traces of cell-staining, **+** = faintly stained cells, **++** = pronounced cell-staining, **+++** = intense staining of activated cells; for **T**: **(+)** = sporadic T-cell found, **+** = several T-cells are present, **++** = increased T-cell infiltration, **+++** = most pronounced T-cell infiltration. Colour intensity reflects the activation status of each cell type (green = microglia, red = macrophages, blue = T-cells) to visualise the changes of CD45 immunoreactivity over time. I, II, III, IV, V or VI = lamina I-VI. Nuclei definition according to (Paxinos and Franklin, 2001).

Brain region/nucleus		6.5 Months				12 Months				21 Months			
Thalamus		**Mic**	**Mϕ**	**T**	**Comments**	**Mic**	**Mϕ**	**T**	**Comments**	**Mic**	**Mϕ**	**T**	**Comments**
VPM/VPL	Ventral posteromedial and posterolateral thalamic nucleus	·	·	(+)		+	++	+		+	+++	++	
VL	Ventrolateral thalamic nucleus	·	·	(+)		+	+	+		++	++	+	
PO	Posterior thalamic nuclei	·	·	(+)		+	+	+		++	++	+	
VM	Ventromedial thalamic nucleus	·	·	(+)		+	·	(+)		++	++	+	
LGNd	Dorsal lateral geniculate nucleus	.	·	(+)		+	·	(+)		++	+	+	
AM	Anteromedial thalamic nucleus	·	·	(+)		·	·	(+)		+	+	+	
AD	Anterodorsal thalamic nucleus	·	·	(+)		·	·	(+)		++	++	+	
AV	Anteroventral thalamic nucleus	·	·	(+)		·	·	(+)		++	++	+	
AVDM/VL	Anteroventral thalamic nucleus, dorsomedial/ventrolateral part	·	·	(+)		·	·	(+)		++	+++	+	
CM	Central medial thalamic nucleus	·	·	(+)		·	·	(+)		++	++	+	
LPLR/MR	lateral posterior thalamic nucleus, laterorostral/mediocaudal part	·	·	(+)		+	·	(+)		++	·	+	
MD	Mediodorsal thalamic nucleus	·	·	(+)		·	·	(+)		+	+	+	
MDM/L	Mediodorsal thalamic nuclei, medial/lateral part	·	·	(+)		+	+	(+)		++	++	+	
MGV/D/M	Medial geniculate nucleus, ventral/dorsal/medial part	·	·	(+)		·	·	(+)		+	+	+	
Re	Reuniens thalamic nucleus	·	·	(+)		·	·	(+)		·	·	(+)	
Rh	Rhomboic thalamic nucleus	·	·	·		(+)	·	(+)		+	+	+	

Brain region/nucleus		6.5 Months				12 Months				21 Months			
Thalamus		**Mic**	**Mϕ**	**T**	**Comments**	**Mic**	**Mϕ**	**T**	**Comments**	**Mic**	**Mϕ**	**T**	**Comments**
ZIV/D	Zona incerta	·	·	(+)		·	·	(+)		+	+	+	
Mid brain													
RMC	Red nucleus, magnocellular part	·	·	(+)		+	·	(+)		+	·	(+)	
RPC	Red nucleus, parvicellular part	·	·	(+)		+	·	(+)		++	·	(+)	
Hippocampus													
CA1	Cornu Ammonis 1, subfield of the hippocampus	·	·	(+)		·	·	+		.	·	+	
CA2	Cornu Ammonis 2, subfield of the hippocampus	·	·	(+)		·	·	+		.	·	+	
CA3	Cornu Ammonis 3, subfield of the hippocampus	·	·	(+)		·	·	+		·	·	+	
DG	Dentate gyrus	·	·	(+)		(+)	·	(+)		+	·	+	
S	Subiculum	·	·	·		(+)	·	(+)		++	·	+	
Amygdala													
AAD	Anterior amygdaloid area	·	·	(+)		·	·	(+)		+	·	+	
AHipM	Amygdalohippocampal area	·	·	(+)		·	·	(+)		·	·	(+)	
APir	Amygdalopiriform transition area	·	·	(+)		·	·	(+)		+	+	+	
PMCo	Posteromedial cortical amygdaloid nucleus	·	·	·		·	·	(+)		·	·	(+)	
BLA	Basolateral amygdaloid nucleus	·	·	(+)		(+)	·	(+)		(+)	·	(+)	
CeC/M	Central amygdaloid nucleus, capsular part/medial division	·	·	(+)		·	·	(+)		·	·	(+)	
Basal ganglia													
Cpu	Caudate putamen	·	·	+		+	·	+		+	(+)	++	
LGP	Lateral globus pallidus	·	·	(+)		+	·	+		++	(+)	+	
MGP	Medial globus pallidus	·	·	(+)		(+)	·	+		+	·	+	

Brain region/nucleus		6.5 Months				12 Months				21 Months			
Basel ganglia		**Mic**	**Mϕ**	**T**	**Comments**	**Mic**	**Mϕ**	**T**	**Comments**	**Mic**	**Mϕ**	**T**	**Comments**
SN	Substantia nigra	·	·	(+)		(+)	·	(+)		+	·	+	
VP	Ventral pallidum	·	·	(+)		·	·	+		+	·	+	
Cortex													
Cortex	General pattern	·	·	(+)	less than Ppt1	+	·	(+)	(V/VI)	++	+	+	(V/VI)
S1BF	Primary somatosensory barrel field	·	·	(+)		+	·	(+)	(V/VI)	+++	+	+	(V/VI)
S1HL/S1FL	Primary somatosensory cortex, hind-/forelimb region	·	·	(+)		+	·	(+)	(V/VI)	++	·	+	(V/VI)
S2	Secondary somatosensory cortex	·	·	(+)		+	·	(+)	(V/VI)	++	·	+	(V/VI)
Au1/AuD/V	Auditory cortex (primary/secondary auditory cortex, dorsal/ventral)	·	·	(+)		+	·	(+)	(V/VI)	++	·	+	(V/VI)
AID/V	Agranular insular cortex, dorsal/ventral	·	·	·		+	·	(+)	(V/VI)	++	·	+	(V/VI)
V1	Visual cortex	·	·	(+)		+	·	(+)	(V/VI)	++	·	+	(V/VI)
M1	Motor cortex 1	·	·	(+)		+	·	(+)	(V/VI)	++	·	+	(V/VI)
M2	Motor cortex 2	·	·	(+)		+	·	(+)	(V/VI)	+++	·	+	(V/VI)
RSA	The retrosplenial agranular cortex	·	·	(+)		+	·	(+)	(V/VI)	+	·	+	(V/VI)
RSG	The retrosplenial granular cortex	·	·	(+)		+	·	(+)	(V/VI)	++	·	+	(V/VI) (caudal)
Cig1/2	Cingulate cortex area 1/2	·	·	(+)		+	·	(+)	all layers	+	·	+	(VI - III)
Pir	Piriform cortex	·	·	(+)		+	+	+	(III & Mϕ in II)	++	+	++	(III & Mϕ in II)
VO/LO	Ventral/lateral orbital cortex	·	·	·		(+)	·	(+)		(+)	·	(+)	
LEnt	Lateral entorhinal cortex	·	·	(+)		+	·	+	all layers	++	++	+	(all layers, Mϕ in II)
DEn	Dorsal endopiriform nucleus	·	·	·		+	·	(+)		++	+	+	
VEn	Ventral endopiriform nucleus	·	·	(+)		+	·	(+)		+	·	+	

Brain region/nucleus		6.5 Months				12 Months				21 Months			
Hypothalamus		**Mic**	**Mϕ**	**T**	**Comments**	**Mic**	**Mϕ**	**T**	**Comments**	**Mic**	**Mϕ**	**T**	**Comments**
IPACM/L	Interstitial nucleus of posterior limb of anterior commissure, med./lat. part	·	·	+		·	·	+		+	·	+	
MCPO	Magnocellular preoptic nucleus	·	·	(+)		+	·	(+)		++	+	+	
HDB	Nucleus of horizontal limb of the diagonal band	·	·	(+)		+	·	(+)		++	+	+	
Pons and Medulla													
Pons	General pattern	·	·	(+)		+	·	+	(ventral)	++	(+)	+	(throughout)
Pr5	Principal sensory trigeminal nucleus	·	·	·		+	·	+		+	+	+	
VLL	Ventral nucleus of lateral lemniscus	·	·	·		+	+	+		++	++	+	
RtTg	Reticulotegmental nucleus of the pons	·	·	(+)		+	+	+		++	++	+	
ClC	Central nucleus of the inferior colliculus	·	·	·		(+)	·	+		++	·	+	
ECIC	External cortex of the inferior colliculus	·	·	(+)		·	·	(+)		+	·	+	
Pn	Pontine nuclei	·	·	(+)		+	·	+		++	++	+	
LDTg	Laterodorsal tegmental nucleus	·	·	(+)		·	·	(+)		·	·	+	
Mo5	Motor trigeminal nucleus	·	·	·		+	·	·		++	·	+	
Olfactory bulb													
OB	Olfactory bulb	·	·	+		+	+	++		++	++	+++	
EPI	External plexiform layer of the olfactory bulb	·	·	(+)		+	+	+		+	++	++	
GRO	Granular cell layer of the olfactory bulb	·	·	(+)		+	+	+		+	++	++	
DTT	Dorsal tenia tecta	·	·	(+)		++	·	(+)		·	++	+	(rostral)

caudal parts of the brain also in the *retrosplenial granular* cortex (*RSG*) and *lateral entorhinal cortex* (*LEnt*). Furthermore, the *dorsal endopiriform nucleus* (*DEn*) in the *piriform cortex* and the nearby *amygdalopiriform transition area* (*APir*) also displayed intensely stained brain-macrophages. Interestingly, only faint CD45 staining was detected in the *auditory cortex* (*Au1*, *AuD*) at this age (data not shown). In the more ventral parts of the forebrain, the thalamus represented the most prominent site of microglial activation in *Cln3*$^{-/-}$ mice, consistent with previous studies (Pontikis *et al.*, 2004; Pontikis *et al.*, 2005). Darkly stained CD45+ve cells were detected in several nuclei of the thalamus, including the *anteromedial* and *anteroventral thalamic nuclei* (*AM*, *AVDM*, *AVVL*), the *ventral posteromedial* and *posterolateral* (*VPM/VPL) nuclei* (see **Figure 17A**), the *ventromedial thalamic nucleus* (*VM*), the *dorsal lateral geniculate nucleus* (*LGNd*), the *medial geniculate nuclei* (*MG*) and *mediodorsal thalamic nucleus* (*MD*). Other brain regions with CD45 immunoreactive cells included the *caudate putamen* (striatum), the *lateral globus pallidus* (*LGP*), the *magnocellular preoptic nucleus* (MCPO), more caudally the *parvicellular part* of the *red nucleus* (*RPC*), the *subiculum* of the hippocampus and to a weaker extent the *substantia nigra*. Last but not least, wide-spread CD45+ve macrophage/microglial activation could be detected throughout the *pons*, but particularly intense staining was found in the *reticulotegmental nuclei of the pons* (*RtTg*) (data not shown). In all these brain regions, a mixed population of CD45 immunoreactive T-cells, macrophages and microglia was observed, with all three of these cell types consistently found in these regions. However, in contrast to earlier ages, lymphocyte-like CD45+ve cells were not restricted to the olfactory bulb and were now found throughout the brain parenchyma of *Cln3*$^{-/-}$ mice at 21 months of age.

Taken together, pronounced CD45 immunoreactivity was observed in the brains of both *Ppt1*$^{-/-}$ and *Cln3*$^{-/-}$ mice. In both mouse models, the earliest and most pronounced immune activation could be found in the *VPM/VPL* nuclei of the thalamus (see **Figure 16** and **Figure 17**), although other brain regions displayed similarly intense CD45 immunoreactivity at later stages of these diseases. However, in both mouse models, CD45 immunoreactivity was detected on cells morphologically resembling microglia, macrophages and T-cells. Therefore, these findings confirmed that both activated innate and adaptive immune cells are present and that pronounced inflammatory responses occur in INCL and JNCL mouse brains. Furthermore, this data provided an overview of where these different types of immune cells are distributed in *Ppt1*$^{-/-}$ and *Cln3*$^{-/-}$ brains, and how these relate to one another. Broadly

similar regions seem to be involved (i.e. contain or are infiltrated by CD45+ve cells) in both forms of NCL, but specific differences between *Ppt1*$^{-/-}$ and *Cln3*$^{-/-}$ mice could also be determined. This activation of immune cells in the brain started at different time points in *Ppt1* and *Cln3* deficient mice (3 months in *Ppt1*$^{-/-}$ and 12 months in *Cln3*$^{-/-}$ mice), which represent different stages of disease progression. Besides these temporal differences, regionally specific differences in where this activation occurred could be also observed between these mouse models. For example, in *Cln3*$^{-/-}$ mice no overt CD45 staining could be detected in the hippocampus (apart from the *subiculum* caudally), whereas *Ppt1*$^{-/-}$ mice displayed pronounced macrophage staining in the *CA1* and *dentate gyrus* of this brain region. Moreover, in the cortical regions, macrophage activation in *Cln3*$^{-/-}$ mice was mainly restricted to laminae VI and V, whereas in *Ppt1*$^{-/-}$ mice more dorsal laminae (II/III) also showed pronounced CD45 immunoreactivity. Likewise, the *visual cortex* (*V1*) showed no obvious microglial activation at later stages of the disease in *Cln3*$^{-/-}$ mice, in contrast to *Ppt1*$^{-/-}$ mice which displayed a pronounced CD45 activation in *V1* at 7 months of age (data not shown). However, *vice versa*, some brain regions only contained activated microglia in *Cln3*$^{-/-}$ mice, as for example the *parvicellular part* of the *red nucleus* (*RPC*) or the *magnocellular preoptic nucleus* (MCPO) which did not show any particular immune activation in *Ppt1*$^{-/-}$ mice at any time examined. Such comparisons between these mice are valid as both were bred on the same strain background. These differences are most likely explained by different rates of disease progression between INCL and JNCL, with *Ppt1*$^{-/-}$ mice, as the faster progressing form, displaying more widespread microglial activation. Equally, these findings also emphasise that these forms NCL are clearly different from one another (Cooper, 2010), even though they have been grouped into the same family of diseases.

3.2 Adaptive immune cells in the CNS of Infantile and Juvenile NCL

Having detected CD45 positive lymphocytes in the brains of both Infantile and Juvenile NCL mice, we wanted to characterise these cells in more detail by staining with specific markers of different classes of lymphocytes. Therefore, we stained a 1 in 6 series of sections of *Ppt1*$^{-/-}$ (1, 3, 5 and 7 month old), and *Cln3*$^{-/-}$ brains (6.5, 12 and 21 month old), and age-matched wildtype brains for CD8, the cytotoxic T-cell marker and CD4, the T-helper cell marker (see **Figure 18**, **Figure 19**, **Figure 25** and **Figure 26**). Subsequently, we performed detailed lymphocyte counts to characterise the total numbers of each of these subsets of lymphocytes in *Ppt1*$^{-/-}$and *Cln3*$^{-/-}$ mice, and

corresponding wildtype brains (see **Figure 21** and **Figure 27**). As a next step, we divided the analysed brain sections rostrocaudally into 5 different levels (see **Table 6** and **Figure 14** in **Chapter 2**) to define the distribution of each lymphocyte subset throughout the fore-and midbrain in more detail (see **Figure 22**, **Figure 23**, **Figure 28** and **Figure 29**). Last but not least, to determine the density of lymphocytes in each of these rostrocaudal levels, we obtained volume measurements of each (and the whole brain volume) (see **Appendix I** for results of the volume measurements), and calculated the density of lymphocytes per mm^3. Hence, by combining all of these measurements, we were able to characterise in detail the distribution pattern and density of cytotoxic T-cells and T-helper cells in the brains of Infantile and Juvenile NCL mice. Furthermore, since both NCL mouse models had been bred on the same background strain and the lymphocyte density data were corrected for brain volume, these lymphocyte data can be directly compared between these two mouse models.

a) T-cell infiltration in the brain of *Ppt1*$^{-/-}$ mice

As described in the **Chapter 1** (see **section 1.7a**), CD8 and CD4 are trans-membrane glycoproteins that act as co-receptors for the T-cell receptor (TCR) (Janeway, 1991). Whereas CD8 is found on cytotoxic T-cells to facilitate binding to major histocompatibility complex (MHC) molecule class I proteins and attached intracellular components (Engleman *et al.*, 1981; Meuer *et al.*, 1982; Norment and Littman, 1988; Connolly *et al.*, 1990; Abbas and Lichtman, 2011), CD4 is a characteristic molecule on T-helper cells which interacts with MHC II molecules and attached extracellular foreign peptides on the surface of antigen-presenting cells (Engleman *et al.*, 1981; Maddon *et al.*, 1985; Abbas and Lichtman, 2011).

Immunohistochemical staining for CD8 and CD4 markers revealed that both subsets of lymphocytes infiltrate the brain parenchyma of *Ppt1*$^{-/-}$ brains from 3 months onwards (see **Figure 18** and **Figure 19**). In contrast, only sporadic T-cells could be detected in the brains of wildtype mice, in which many T-cells could be found along brain margins, namely the ventricle walls, the meninges or choroid plexus. CD8+ve as well as CD4+ve T-cells characteristically displayed a small round cell soma without any processes, even though some T-cells also appeared with an oval or tapered cell morphology, as if they were fixed during the process of squeezing through vessels or between cells (see **Figure 18C** and **Figure 19C**).

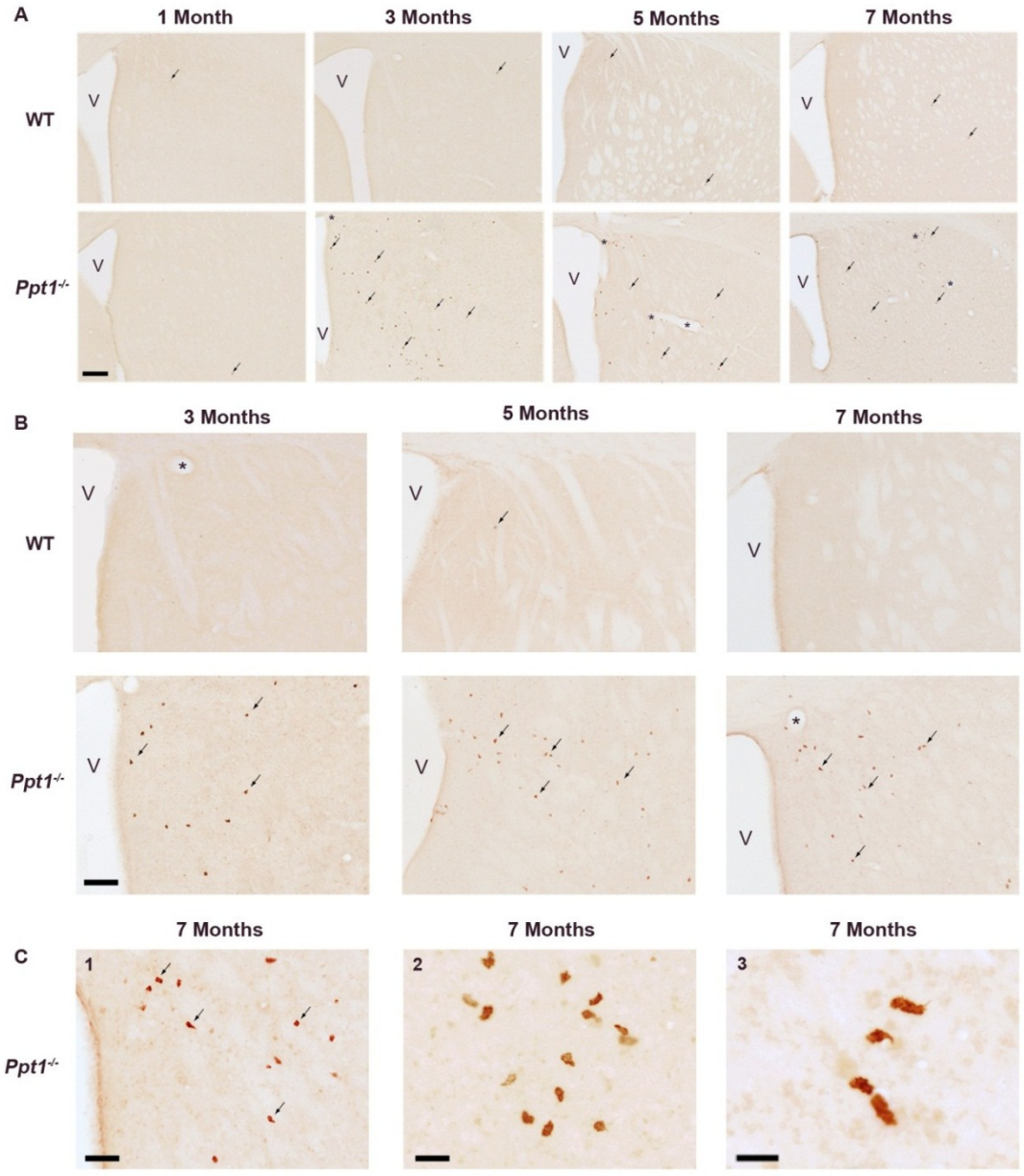

Figure 18. Progressive cytotoxic T-cell infiltration in *Ppt1*$^{-/-}$ mice. (A) Immunohistochemical staining for the cytotoxic T-cell marker CD8 in the striatum (*caudate putamen*) of 1, 3, 5 and 7 month old *Ppt1*$^{-/-}$ and wildtype (WT) mice revealed CD8+ve cells (arrows) in both genotypes. But many more CD8 immunoreactive cells were apparent in *Ppt1*$^{-/-}$ mouse brains from 3 months onwards compared to WT brains. In mutant mice, the numbers of CD8+ve T-cells increased with disease progression and evidence for lymphocyte clustering around ventricles (V) and occasionally blood vessels (*) could be suggested. Scale bar = 200 µm. (B, C) Higher magnification pictures of CD8+ve cytotoxic T-cells (B) in the striatum of 3, 5 and 7 month old WT and *Ppt1*$^{-/-}$ mice, (C1, C3) in striatum near ventricles and (C2) in the basal forebrain of 7 month old mutant mice. CD8 immunoreactive cells displayed characteristic T-cell morphology with small, round cell bodies and no processes. T-cells were prominently found in the olfactory bulb, near ventricles and/or white matter tracts. Scale bar in (B) = 100 µm, in (C1) = 50 µm, in (C2) = 25 µm and (C3) = 20 µm.

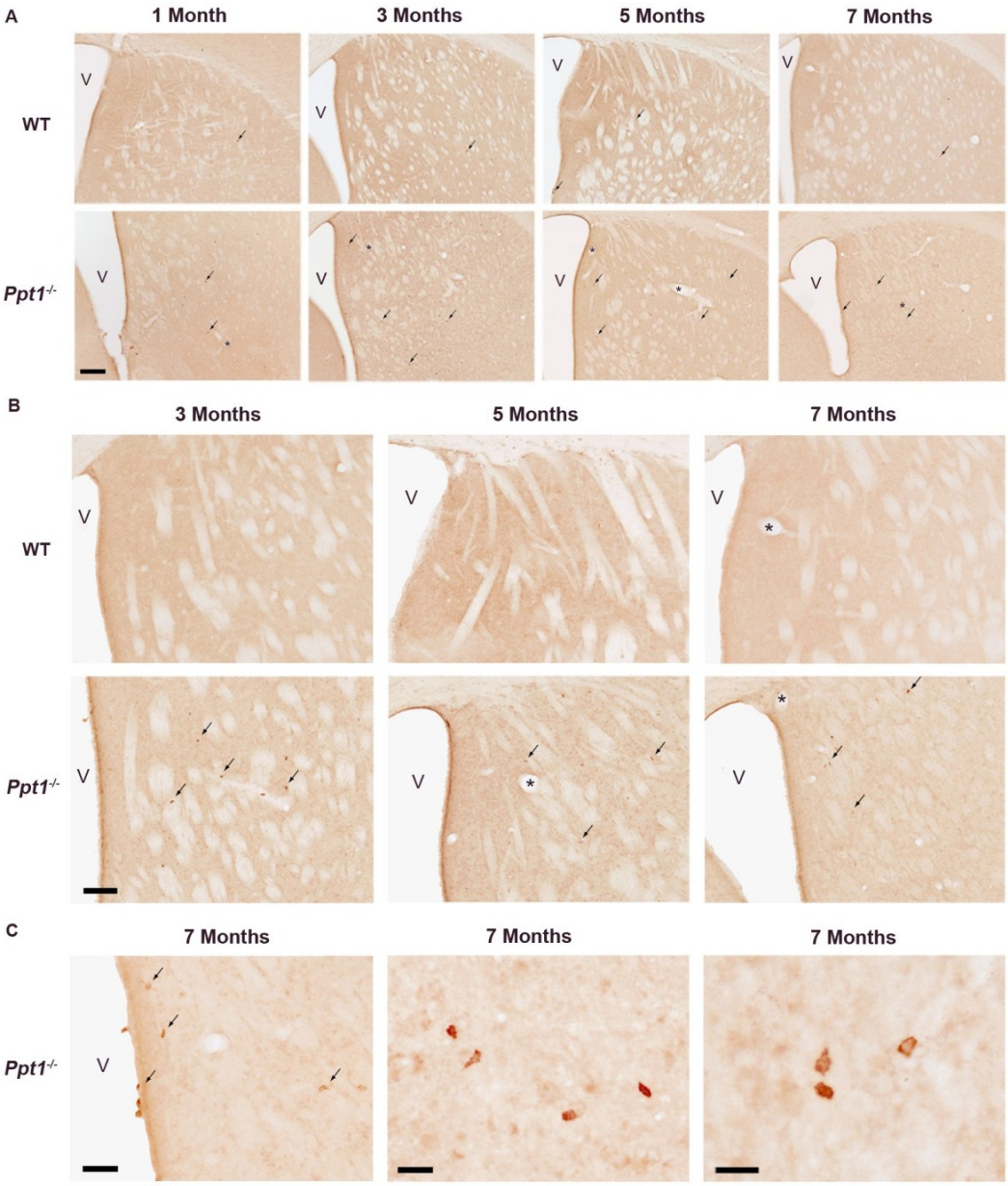

Figure 19. Progressive T-helper cell infiltration in *Ppt1*$^{-/-}$ mice. (A) Immunohistochemical staining for the T-helper cell marker CD4 in the striatum (*caudate putamen*) of 1, 3, 5 and 7 month old *Ppt1*$^{-/-}$ and wildtype (WT) mice revealed CD4+ve cells (arrows) in both genotypes. But many more CD4 immunoreactive cells were apparent in *Ppt1*$^{-/-}$ mouse brains from 3 months onwards compared to WT brains. In mutant mice, evidence for lymphocyte clustering around ventricles (V) and occasionally blood vessels (*) could be suggested. Scale bar = 200 μm. (B, C) Higher magnification pictures of CD4+ve T-helper cells (B) in the striatum of 3, 5 and 7 month old WT and *Ppt1*$^{-/-}$ mice, (C1) in the striatum near/along ventricles, (C2) in the *piriform cortex* and (C3) in the olfactory bulb of 7 month old mutant mice. CD4 immunoreactive cells displayed characteristic T-cell morphology with small, round cell bodies and no processes. T-cells were prominently found in the olfactory bulb, near ventricles and/or white matter tracts. Scale bar in (B) = 100 μm, in (C1) = 50 μm, in (C2) = 25 μm and (C3) = 20 μm.

Regarding their dispersion within the brain, CD8+ve and CD4+ve T-cells both showed similar distributions, but without any distinct pattern or obvious clustering around particular structures. Nevertheless, common themes could be discerned, with most T-cells found either in the rostral parts of the brain, in particular in the olfactory bulb, or in the proximity of ventricles. Furthermore, white matter tracts, in particular the *corpus callosum* or the *fimbria* of the hippocampus were preferential locations for lymphocytes, although this could equally be explained by the immediate proximity of these white matter tracts to the cerebral ventricles. Occasionally, some clustering of T-cells around blood vessels could be observed, even though this distribution was not frequently seen. According to these rather general patterns of T-cell distribution in the brain, CD8+ve and CD4+ve lymphocytes could be commonly found in following brain regions (in rostrocaudal order) (see **Figure 20**): olfactory bulb, *anterior olfactory*

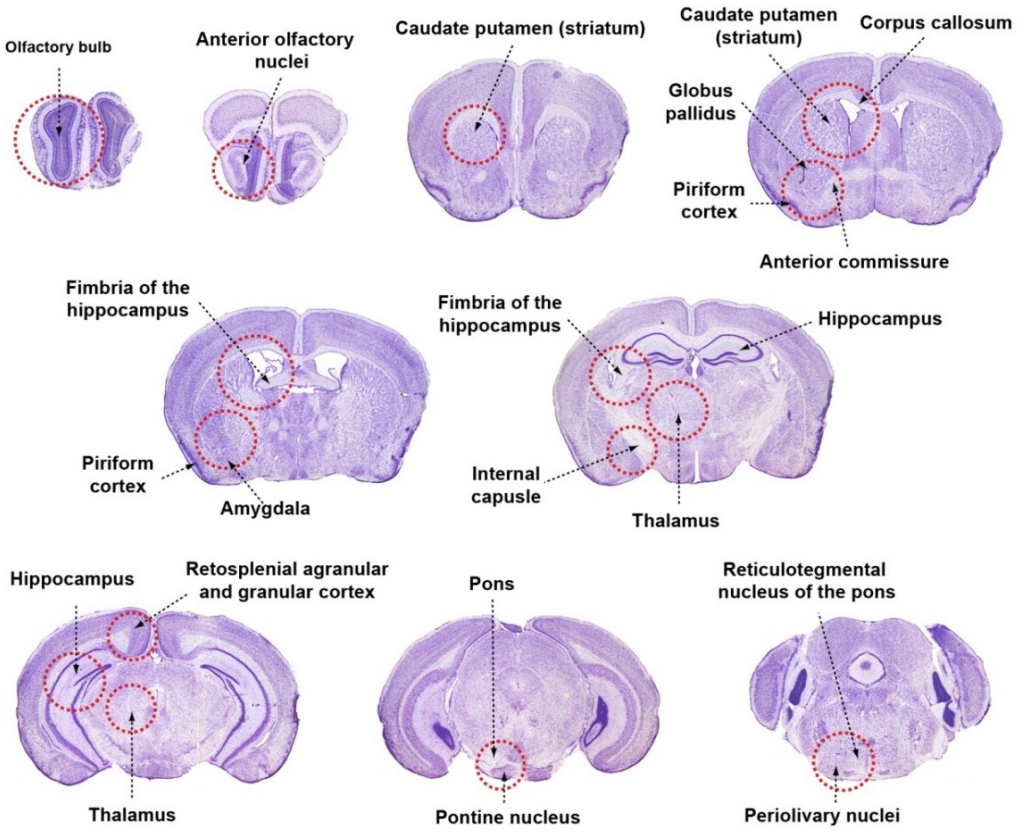

Figure 20. Lymphocyte distribution in the brain of *Ppt1*$^{-/-}$ and *Cln3*$^{-/-}$ mice. Qualitative assessment of lymphocyte distribution in the brain of *Ppt1*$^{-/-}$ and *Cln3*$^{-/-}$ mice revealed preferred T-cell accumulation (⋯) in the rostral parts of the brain and/or in the proximity of ventricles or white matter tracts. The following brain regions showed consistently increased lymphocyte infiltration in both NCL mice: olfactory bulb (where most T-cells were present), *anterior olfactory nuclei*, *caudate putamen* (striatum), *corpus callosum*, *globus pallidus*, *fimbria* of the hippocampus, *anterior commissure*, *piriform cortex*, *amygdala*, thalamus (throughout the thalamus, often seen in the *mediodorsal thalamic nuclei* but (particularly in *Cln3*$^{-/-}$ mice) also in the *ventral postero nuclei*), caudal parts of the *hippocampus*, *retrosplenial agranular and granular cortex* and the *pons* with the *pontine nucleus* and *periolivary nuclei*. Speculatively, this lymphocyte distribution could be explained by them being the easiest access routes for lymphocytes into the brain via the ventricles and olfactory bulb, or by migratory pathways along white matter tracts.

nuclei, *caudate putamen* (striatum), *globus pallidus*, *corpus callosum*, *fimbria* of the hippocampus, *piriform cortex*, area around the *anterior commissure,* several *amygdaloid nuclei*, throughout the thalamus including the *mediodorsal thalamic nuclei* and also seen in the thalamic *ventral posterior nuclei*, caudal parts of the *hippocampus*, *retrosplenial agranular and granular cortex* and the *pons* with the *pontine nucleus* and *periolivary nuclei*. The most likely explanation for this distribution of lymphocytes in the brain is probably found in the most favourable access routes, as for example the olfactory bulb or ventricles. Likewise, white matter tracts possibly serve as convenient migratory pathways in the brain. These possibilities will be discussed in more detail in **Chapter 7**.

To extend these qualitative findings of CD8+ve and CD4+ve T-cell distribution in the brain of *Ppt1*$^{-/-}$ mice, we performed detailed cell counts of each lymphocyte sub-population throughout the whole brain (1 in 6 series) of *Ppt1*$^{-/-}$ mice and corresponding wildtype mice. These total cell counts confirmed that CD8+ve cytotoxic T-cells infiltrate the *Ppt1*$^{-/-}$ CNS in significant numbers from 3 months onwards (see **Figure 21A**). By combining the total lymphocyte counts with whole brain volume (see **Appendix I: Figure 77**) and plotting them as the density of lymphocytes per mm^3, it could be shown that CD8+ve lymphocyte numbers constantly increase over time reaching a maximum at 7 months of age with around 280 cells/mm^3 (see **Figure 21A**).

In contrast, CD4+ve T-helper cells also infiltrate the *Ppt1*$^{-/-}$ CNS from 3 months onwards, but already reach their maximum level at this age with around 90 cells/mm^3, a density that does not increase further with disease progression (see **Figure 21B**). Comparing the relative infiltration of CD4+ve and CD8+ve cell types, there are three times as many CD8+ve cytotoxic T-cells present at the end stage of the disease, than CD4+ve T-helper cells (see **Figure 21C** and **Figure 21D**). However, the fact that CD4+ve cells already seem to reach their maximum density by 3 months of age, suggests that they are possibly more involved in pathogenesis at early stages compared to CD8+ve cells, which seem to become more prominent towards the end of the disease. This pattern would be consistent with the hypothesis that CD4+ve T-cells infiltrate the inflammation site at early stages of the disease to coordinate and recruit other immune cells, as for example CD8+ve T-cells (see **section 1.7a** in **Chapter 1**, (Germain, 1994; Zhu and Paul, 2008; Nakanishi *et al.*, 2009; Abbas and Lichtman, 2011)).

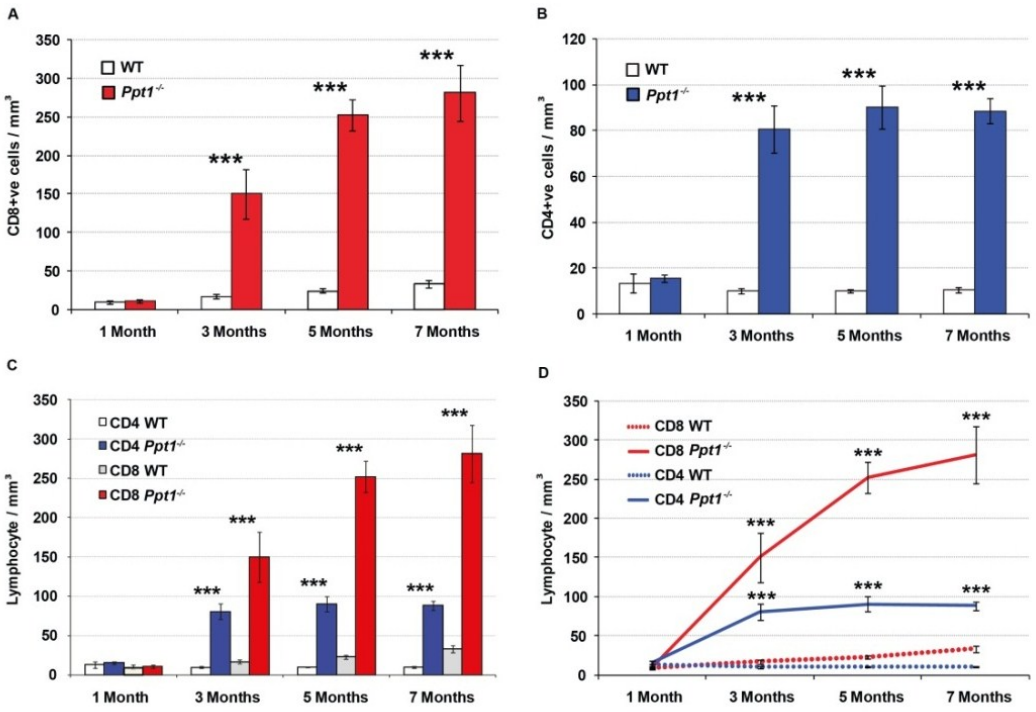

Figure 21. Progressive lymphocyte infiltration in *Ppt1*$^{-/-}$ mice. Systematically quantified counts of (A) CD8+ve cytotoxic T-cells and (B) CD4+ve T-helper cells in 1, 3, 5 and 7 month old *Ppt1*$^{-/-}$ and age-matched wildtype (WT) mice revealed significant lymphocyte infiltration from 3 months onwards in mutant mice. In contrast, only relatively few lymphocytes could be detected in WT mice. (C, D) Direct comparison of CD8+ve and CD4+ve immune cell infiltration demonstrated different dynamics and amounts of each T-cell subpopulation in *Ppt1*$^{-/-}$ (—) brains. Double to three times as many CD8+ve cytotoxic T-cells could be detected in mutant mice from 3 months onwards, compared to CD4+ve T-helper cells. Furthermore, the amount of CD8+ve T-cells steadily increased with disease progression in *Ppt1*$^{-/-}$ mice, whereas CD4+ve T-cells already reached a saturated level of infiltration by 3 months of age in these mice. Similarly, in WT (···) mice the amount of cytotoxic T-cells increased with age and more CD8+ve T-cells were found in healthy control mice, compared to CD4+ve T-cells. Values were calculated as density of lymphocytes/mm^3. The same data are presented as both histograms (A, B, C) and line graph (D). Statistics: Two-way ANOVA with Bonferroni post hoc test, ***$p<0.001$. Data shown as mean ± SEM, n = 5.

After dividing the brain into five rostrocaudal levels (see **Table 6** and **Figure 14** in **Chapter 2**) and measuring the volume of each of these defined brain regions (see **Appendix I: Figure 77**), the rostrocaudal distribution of all T-cell counts was quantified to determine any regional specificity of lymphocyte infiltration. Unsurprisingly, the timing of these regional changes mirror the patterns of the total numbers of both CD8+ve cytotoxic T-cells as well as CD4+ve T-helper cells, with infiltration of both cell types from 3 months onwards (see **Figure 22**). However, for both T-cell markers the highest numbers of cells and the first detectable lymphocyte infiltration occurred in level I/the olfactory bulb. The lymphocyte infiltration appears to start at this most rostral part of the brain at 1 month for CD8+ve and CD4+ve cells, and gradually spreads and increases over time to more caudal regions of the

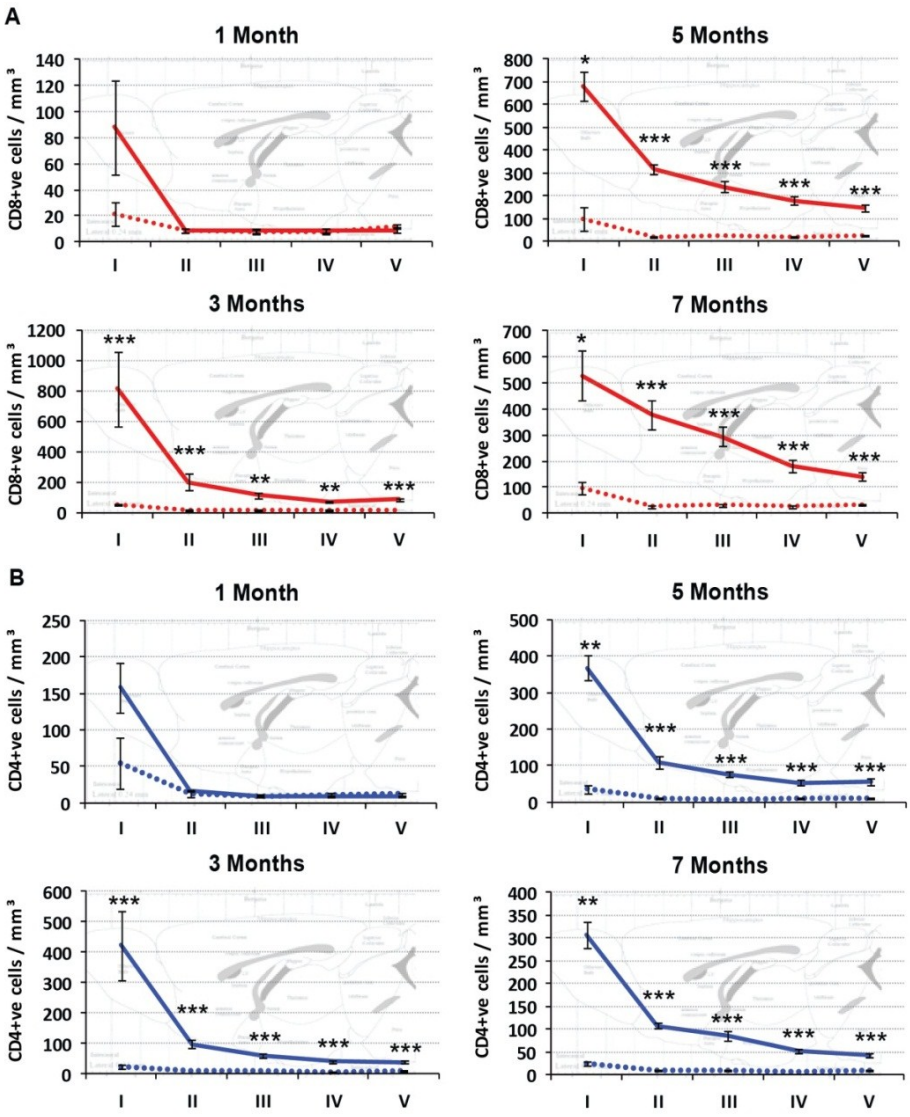

Figure 22. Regional distribution of lymphocytes in *Ppt1*$^{-/-}$ brains. Regional breakdown of total (A) CD8+ve and (B) CD4+ve lymphocyte counts (A) into five rostrocaudal brain levels at 1, 3, 5 and 7 months of age revealed similar infiltration patterns of both lymphocyte subpopulations. A significant increase in the number of CD8+ve cytotoxic T-cells and CD4+ve T-helper cells was detected from 3 months onwards in *Ppt1*$^{-/-}$(—) compared to wildtype (···) mice. In both mouse populations, the majority of T-cells were found in the olfactory bulb, suggesting it to be a common access route into the brain. In mutant mice, lymphocytes were distributed along a rostrocaudal gradient throughout the brain. Values were calculated as density of lymphocytes/mm^3. Brain levels: I = olfactory bulb, II = forebrain until hippocampus, III = hippocampal forebrain, IV = Midbrain with *superior colliculus*, V = midbrain with *pons*. Statistics: Two-way ANOVA with Bonferroni post hoc test, *p<0.05, **p<0.01, ***p<0.001. Data shown as mean ± SEM, n = 5.

brain. The olfactory bulb seems to offer a convenient access route for these lymphocytes to enter the brain, but no other regional selectivity for the lymphocyte infiltration could be detected.

Comparing both lymphocyte subsets, the amount of CD4+ve T-cells exceed that of CD8+ve T-cells at 1 month of age in the olfactory bulb, but become outnumbered at later stages (see **Figure 23**). This would strengthen the suggested early appearance

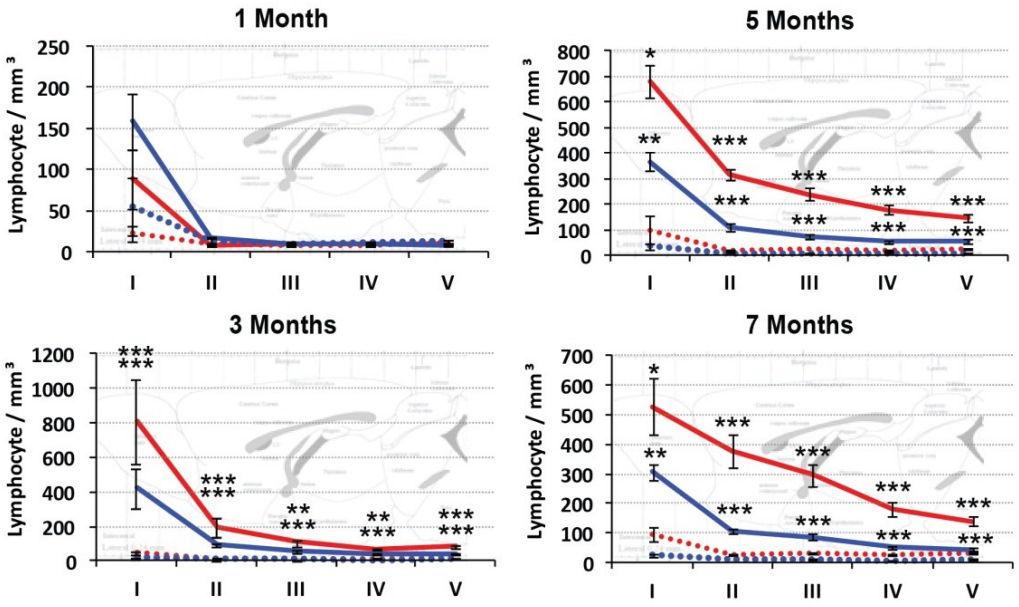

Figure 23. Direct comparison of regional distribution of CD8+ve and CD4+ve lymphocytes in *Ppt1*$^{-/-}$ mice. Regional breakdown of total lymphocyte counts into five rostrocaudal brain levels at 1, 3, 5 and 7 months of age in *Ppt1*$^{-/-}$ (—) and wildtype (···) mice revealed similar distribution patterns of CD8+ve (red) and CD4+ve T-cells (blue). Both subpopulations showed a significant increase from 3 months onwards in mutant mice compared to wildtype mice, whereas double to three times as many CD8+ve T-cells were present in the brain than CD4+ve T-cells. However, the distribution of both lymphocyte subpopulations followed a rostrocaudal gradient with most cells present in the olfactory bulb. Values were calculated as density of lymphocytes/mm^3. Brain levels: I = olfactory bulb, II = forebrain until hippocampus, III = hippocampal forebrain, IV = Midbrain with *superior colliculus*, V = midbrain with *pons*. Statistics: Two-way ANOVA with Bonferroni post hoc test, *p<0.05, **p<0.01, ***p<0.001. Data shown as mean ± SEM, n = 5.

and influence of CD4+ve T-helper cells in *Ppt1*$^{-/-}$ brains discussed above, whereas CD8+ve cytotoxic T-cells are apparently more numerous at later disease stages.

Calculating the ratio of CD8:CD4+ve cells in the whole brain of *Ppt1*$^{-/-}$ and wildtype mice revealed no significant difference between these genotypes. However, certain trends were apparent (see **Figure 24**). While at 1 month of age, more CD4+ve T-cells could be found in both genotypes, there were two to three times more CD8+ve cells than CD4+ve cells at subsequent ages. Indeed, mutant as well as control brains showed an age dependent increase of CD8+ve T-cell influx over time.

Taken together, our findings provide the first characterisation of adaptive immune cell infiltration in *Ppt1*$^{-/-}$ and wildtype mice. We not only demonstrated that increased numbers of T-cells are present in *Ppt1*$^{-/-}$ mice, but also defined in detail the spatial and temporal distribution of lymphocytes in the brains of these mice.

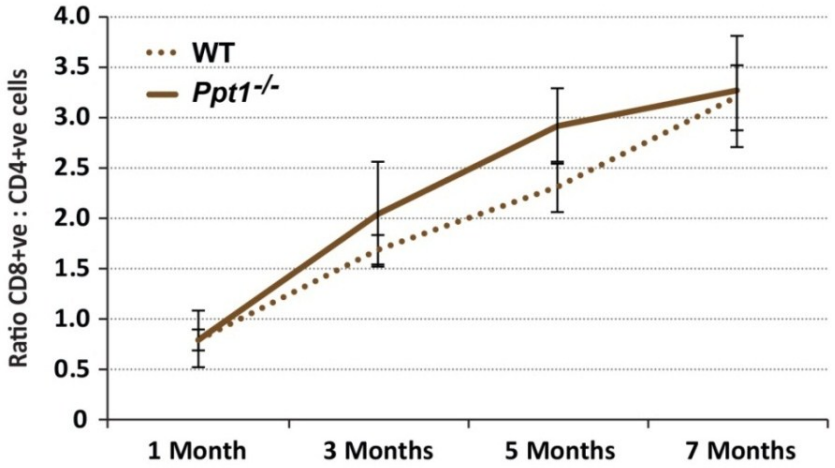

Figure 24. Unchanged CD8:CD4+ve T-cell ratios in *Ppt1*$^{-/-}$ mice. Calculation of the ratio between CD8+ve and CD4+ve T-cells revealed no significant difference between *Ppt1*$^{-/-}$(—) and wildtype (···) (WT) mice. Whereas at 1 month of age, more CD4+ve T-cells were present in the brains of both mouse populations, more CD8+ve lymphocytes could be detected from 3 months onwards compared to CD4+ve T-cells. Thus, an age-dependent increase of CD8+ve cells influx could be observed in mutant and wildtype brains over time. Statistics: Two-way ANOVA with Bonferroni post hoc test. Data shown as mean ± SEM, n = 5.

b) T-cell infiltration in *Cln3*$^{-/-}$ mice

Analogous to the analysis of *Ppt1*$^{-/-}$ brains (see **section 3.2a**), we assessed the extent and distribution of CD4+ve and CD8+ve lymphocytes within the brains of *Cln3*$^{-/-}$ mice and control mice at different stages of disease progression (6.5, 12 and 21 months). In addition to documenting data in representative pictures, lymphocyte counts were again made from the entire brain, as well as defined rostrocaudal levels. These were combined with regional volume measurements to provide lymphocyte density measurements and create an exact distribution map of lymphocyte infiltration in *Cln3*$^{-/-}$ brains over time. Furthermore, this is the first time such old (21 months) *Cln3* deficient mice have been analysed, with previous studies only extending to 14 or 19 months of age (Pontikis *et al.*, 2004; Herrmann *et al.*, 2008b).

Immunohistochemical staining of *Cln3*$^{-/-}$ and age-matched wildtype brains for CD8 and CD4 markers at all three ages (6.5, 12 and 21 months) revealed higher levels of lymphocyte infiltration in mutant mice. However, the degree of infiltration and its timing differed between these lymphocyte subsets. The first indication of increased numbers of lymphocytes of either type in *Cln3*$^{-/-}$ brains was seen at 12 months of age with more CD8+ve cytotoxic T-cells present in the olfactory bulb than in wildtype mice. However, widespread CD8+ve T-cell infiltration of the *Cln3*$^{-/-}$ brain only became apparent at 21 months of age (see **Figure 25**). In contrast, no evidence of an

increase in CD4+ve T-helper cells was seen until 21 months of age when many more infiltrated CD4+ve T-cells could be detected in *Cln3*$^{-/-}$ mice compared to wildtype mice (see **Figure 26**). The distribution of CD8+ve and CD4+ve lymphocytes in *Cln3*$^{-/-}$ brains resembled that seen in *Ppt1*$^{-/-}$ brains (see **Figure 20**). T-cells were predominantly found in the olfactory bulb, in proximity to ventricles and/or white matter tracts. Occasional clustering of lymphocytes around blood vessels was also observed in these *Cln3*$^{-/-}$ brains. Compared to *Ppt1*$^{-/-}$ mice, in *Cln3*$^{-/-}$ brains there appeared to be slightly more T-cells present in the *ventral posteromedial* and *posterolateral* (*VPM/VPL*) nuclei of the thalamus, a particular focus for pathology in NCL mice (Bible *et al.*, 2004; Pontikis *et al.*, 2004; Pontikis *et al.*, 2005; Cooper *et al.*, 2006; Kielar *et al.*, 2007; Partanen *et al.*, 2008; von Schantz *et al.*, 2009; Kuronen *et al.*, 2012; Schmiedt *et al.*, 2012; Thelen *et al.*, 2012), whereas no such accumulation of lymphocytes in these nuclei were observed in *Ppt1*$^{-/-}$ mice at any age. Furthermore, as already seen in younger control mice, only sporadic T-cells could be detected in the brains of aged wildtype mice, whereas most T-cells could be found along the brain margins, namely the ventricle walls, the meninges or choroid plexus of these mice.

To quantify these qualitative findings of the CD8 (see **Figure 25**) and CD4 (see **Figure 26**) staining across all ages, the total number of lymphocytes were counted and adjusted for whole brain volume (see **Appendix I: Figure 78**) to provide lymphocyte density measurements. In *Cln3*$^{-/-}$ brains, CD8+ve cytotoxic T-cells started to infiltrate at 12 months of age (seen as a trend) and reached significant levels at 21 months with ca. 250 lymphocytes/mm^3 (see **Figure 27A**). In contrast, CD4+ve T-helper cell numbers were only significantly increased at 21 months of age with ca. 55 cells/mm^3 in the brain of *Cln3*$^{-/-}$ mice (in **Figure 27B**), compared to age-matched wildtype mice. When directly comparing both lymphocyte subpopulations (see **Figure 27C** and **Figure 27D**), apart from the relative amount of cells (much fewer CD4+ve T-helper cells were present than CD8+ve cytotoxic T-cells), the sequence of infiltration was unexpected. CD4+ve T-helper infiltrate the brain only at later stages of the disease in *Cln3*$^{-/-}$ brains, in contrast to the T-cell infiltration pattern observed in *Ppt1*$^{-/-}$ mice. CD8+ve T-cell recruitment into the brain of *Cln3*$^{-/-}$ mice seems not to rely on the help of CD4+ve T-cells which traditionally are thought to orchestrate the immune response at the inflammation site (see **section 1.7a** in **Chapter 1**, (Germain, 1994; Zhu and Paul, 2008; Abbas and Lichtman, 2011; Phares *et al.*, 2012)).

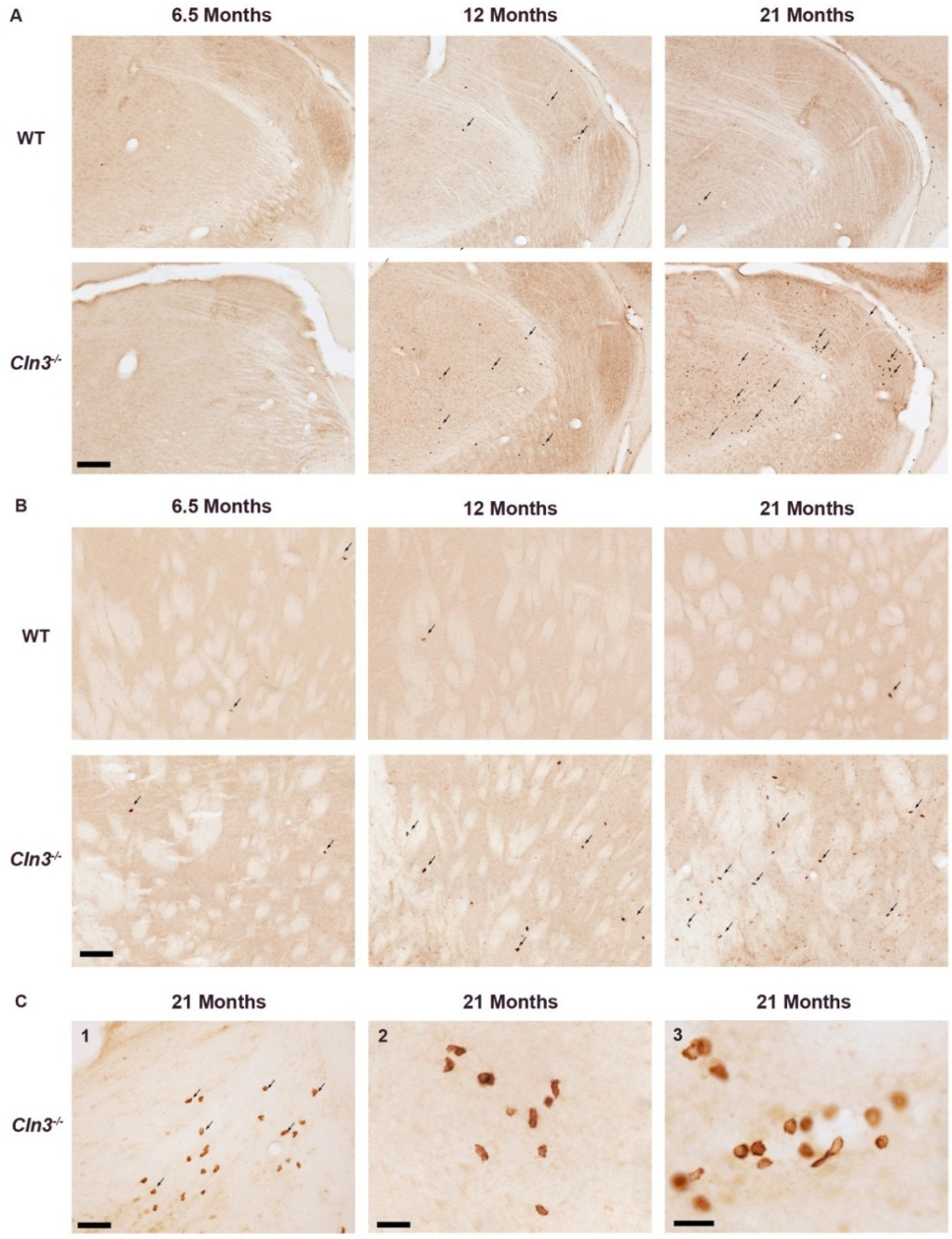

Figure 25. Progressive cytotoxic T-cell infiltration in *Cln3*$^{-/-}$ mice. (A) Immunohistochemical staining for the cytotoxic T-cell marker CD8 in the thalamus of 6.5, 12 and 21 month old *Cln3*$^{-/-}$ and wildtype (WT) mice revealed CD8+ve cells (arrows) in both genotypes. More CD8 immunoreactive cells were marginally apparent from 12 months onwards, but obviously so at 21 months in *Cln3*$^{-/-}$ mice compared to WT brains, in which only occasionally CD8+ve cells could be seen. Scale bar = 200 μm. (B, C) Higher magnification pictures of CD8+ve cytotoxic T-cells (B) in the striatum of 6.5, 12 and 21 month old WT and *Cln3*$^{-/-}$ mice, (C1) in white matter tracts near ventricles, (C2) in the thalamus and (C3) in the pons of 21 month old mutant mice. CD8 immunoreactive cells displayed characteristic T-cell morphology with small, round or oval cell bodies and no processes. T-cells were prominently found in the olfactory bulb, near ventricles and/or white matter tracts. Occasional clustering around blood vessels was also observed in mutant mice (see C3 as example). Scale bars in (B) = 100 μm, in (C1) = 50 μm, in (C2) = 25 μm and (C3) = 20 μm.

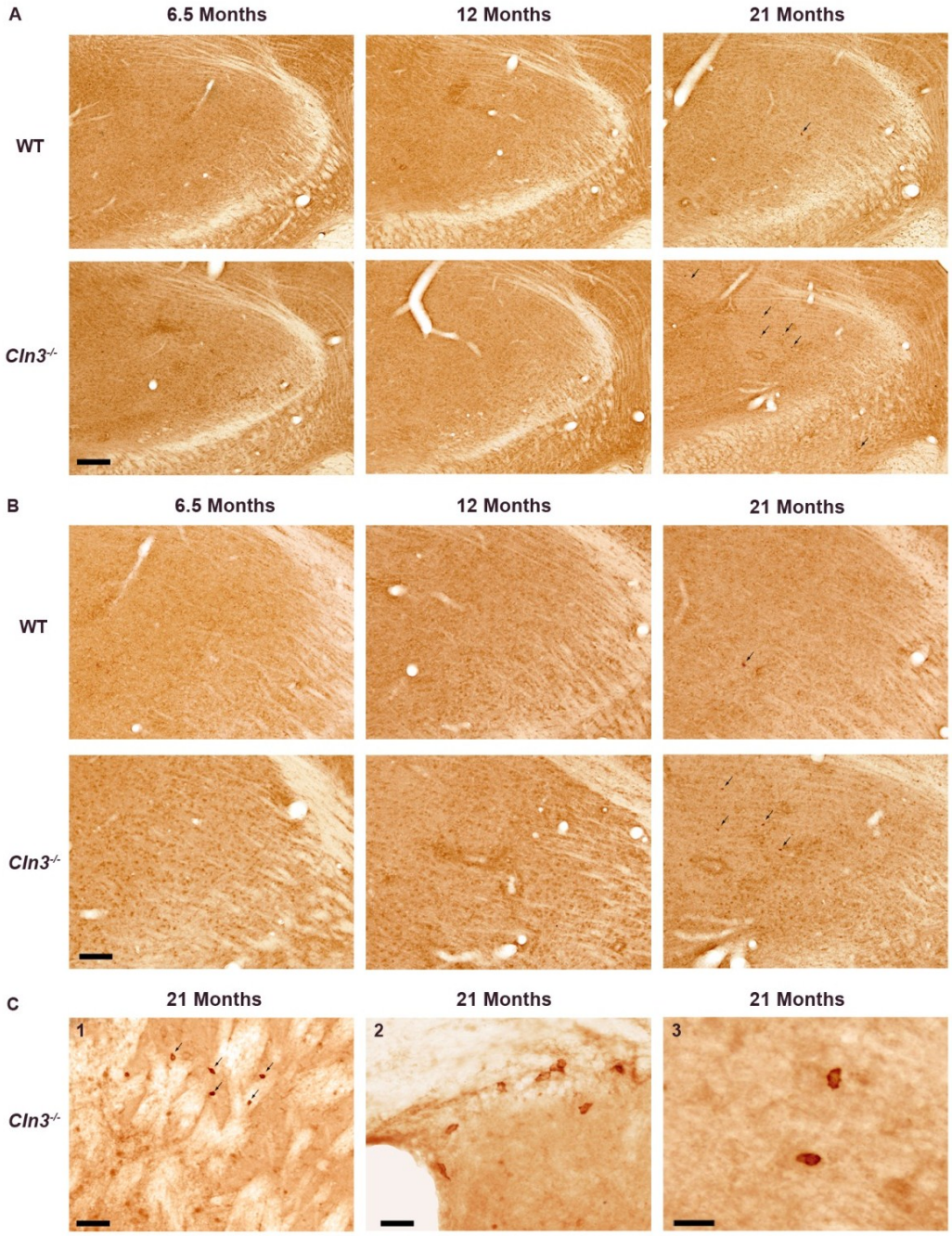

Figure 26. Progressive T-helper cell infiltration in *Cln3*$^{-/-}$ mice. (A) Immunohistochemical staining for the T-helper cell marker CD4 in the thalamus of 6.5, 12 and 21 month old *Cln3*$^{-/-}$ and wildtype (WT) mice revealed CD4+ve cells (arrows) in both genotypes. Many more CD4 immunoreactive cells were apparent at 21 months in *Cln3*$^{-/-}$ mice, compared to WT brains, in which very few CD4+ve cells could be seen. Scale bar = 200 μm. (B, C) Higher magnification pictures of CD4+ve T-helper cells (B) in the thalamus of 6.5, 12 and 21 month old WT and *Cln3*$^{-/-}$ mice, (C1) in the striatum, (C2) near ventricles and the *corpus callosum* and (C3) in the amygdala of 21 month old mutant mice. CD4 immunoreactive cells displayed characteristic T-cell morphology with small, round or oval cell bodies and no processes. T-cells were prominently found in the olfactory bulb, near ventricles and/or white matter tracts. Scale bars in (B) = 100 μm, in (C1) = 50 μm, in (C2) = 25 μm and (C3) = 20 μm.

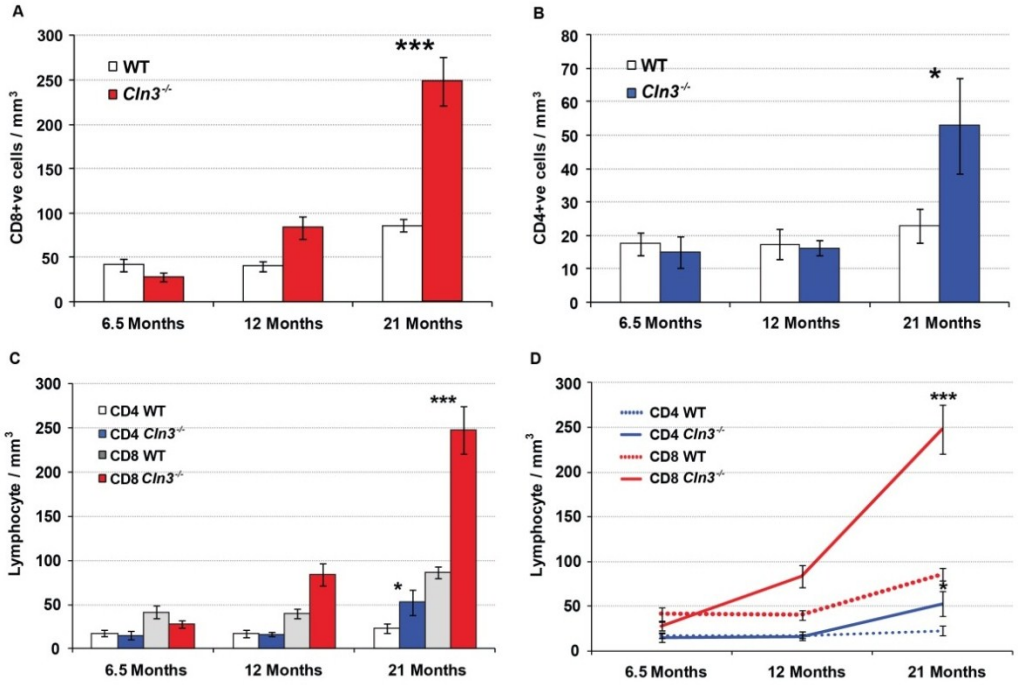

Figure 27. Progressive lymphocyte infiltration in *Cln3*$^{-/-}$ mice. Systematically quantified counts of (A) CD8+ve cytotoxic T-cells and (B) CD4+ve T-helper cells in 6.5, 12 and 21 month old *Cln3*$^{-/-}$ and age-matched wildtype (WT) mice revealed significant lymphocyte infiltration at 21 months of age in mutant mice. In contrast, only relatively few lymphocytes could be detected in WT mice. (C, D) Direct comparison of CD8+ve and CD4+ve immune cell infiltration demonstrated different dynamics and amounts of each T-cell subpopulation in *Cln3*$^{-/-}$ (—) brains. Significantly more CD8+ve T-cells were already evident from 12 months onwards compared to WT (···) mice, but this difference reached significant levels only at 21 months of age. In contrast, increased numbers of CD4+ve T-cell were only detected at 21 months of age in *Cln3*$^{-/-}$ mice, being significantly increased compared to WT mice. Furthermore, five times as many CD8+ve cytotoxic T-cells could be detected in mutant mice at 21 months of age, compared to CD4+ve T-helper cells. In WT mice, the amount of cytotoxic T-cells increased with age and more CD8+ve T-cells were found in healthy control mice at all ages, compared to CD4+ve T-cells. Values were calculated as density of lymphocytes/mm^3. The same data are presented as both histograms (A, B, C) and line graph (D). Statistics: Two-way ANOVA with Bonferroni post hoc test, *$p<0.05$, ***$p<0.001$. Data shown as mean ± SEM, n = 5.

Several explanations for this phenomenon shall be discussed below (see **section 3.3c**) and more extensively in **Chapter 7**.

By splitting the brain into five different rostrocaudal levels (see **Table 6** and **Figure 14** in **Chapter 2**) and combining regional volume measurements (see **Appendix I: Figure 78**) with all lymphocyte counts, it was possible to define the distribution of lymphocytes in *Cln3*$^{-/-}$ mice as a density of cells per mm^3 at each rostrocaudal level (see **Figure 28**). This analysis revealed similar patterns to total number of lymphocytes, with CD8+ve cytotoxic T-cells infiltrating from 12 months onwards, while only a moderate increase in the number of CD4+ve T-helper cells occurred at 21 months of age (see **Figure 27**).

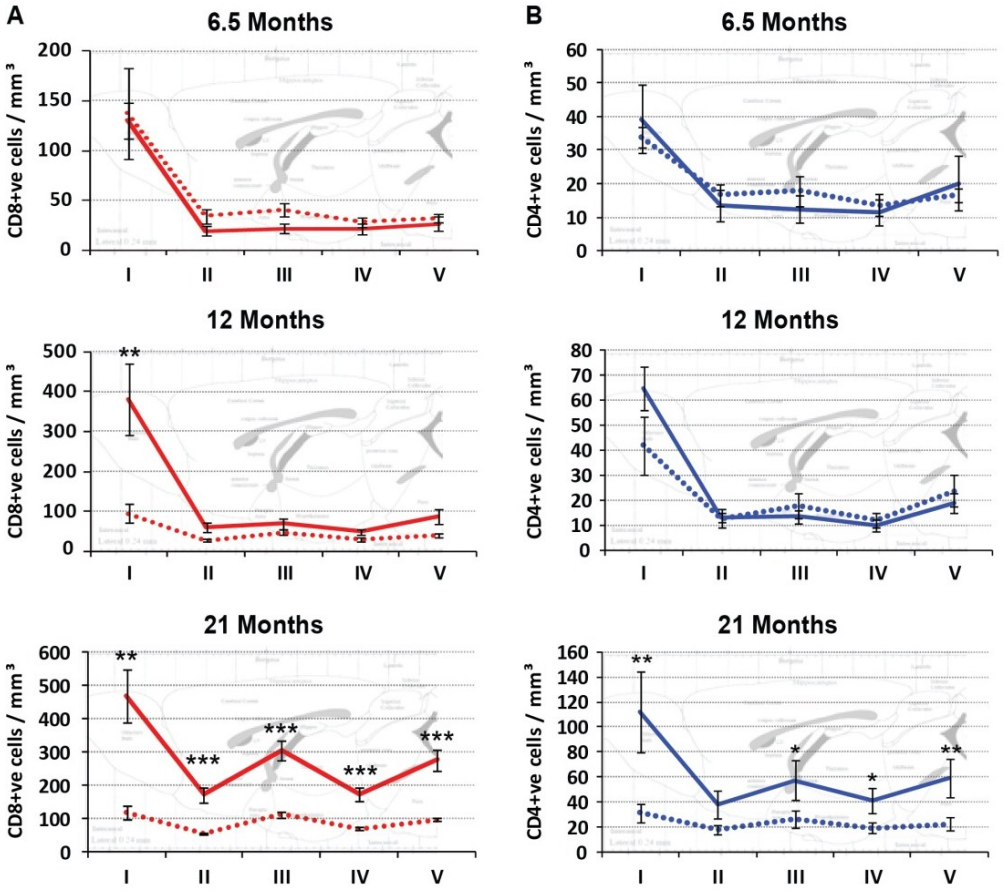

Figure 28. Regional distribution of lymphocytes in *Cln3*$^{-/-}$ brains. Regional breakdown of total (A) CD8+ve and (B) CD4+ve lymphocyte counts (A) into five rostrocaudal levels at 6.5, 12 and 21 months of age revealed different infiltration patterns between each lymphocyte subpopulation. A significant increase in the number of CD8+ve cytotoxic T-cells was first detected at 12 months of age in the olfactory bulb, but spread throughout the brain at 21 months of age in *Cln3*$^{-/-}$(—) compared to wildtype (···) mice. In contrast, significantly more CD4+ve T-helper cells were only seen at 21 months of age in mutant mice, compared to control mice. In both mouse populations, the majority of T-cells were found in the olfactory bulb, suggesting the olfactory bulb to be a common access route into the brain. In 21 month old mutant mice, lymphocytes were distributed in a region-specific manner with levels I, III and V showing more T-cell infiltration than levels II and IV. Values were calculated as density of lymphocytes/mm^3. Brain levels: I = olfactory bulb, II = forebrain until hippocampus, III = hippocampal forebrain, IV = Midbrain with *superior colliculus*, V = midbrain with *pons*. Statistics: Two-way ANOVA with Bonferroni post hoc test, *p<0.05, **p<0.01, ***p<0.001. Data shown as mean ± SEM, n = 5.

For both T-cell markers the highest numbers of cells, and the first detectable lymphocyte infiltration in *Cln3*$^{-/-}$ mice, occurred in level I/the olfactory bulb. This infiltration started at these most rostral levels of the brain at 12 months for CD8+ve, and 21 months for CD4+ve cells, and later spreads throughout the whole brain (see **Figure 28**). However, level III (thalamus and hippocampus, plus overlying cortex) was more highly infiltrated compared to levels II (rostral forebrain until appearance of hippocampus) or IV (midbrain before the pons including *superior colliculus*). This correlates well with the only significant effect on regional volume also occurring in level III of the mature *Cln3*$^{-/-}$ brain (see **Appendix I: Figure 78**).

Directly comparing both lymphocyte subsets, the amount of CD8+ve T-cells exceeded that of CD4+ve T-cells at every rostrocaudal level, irrespective of age (see **Figure 29**). Even though no difference in the degree of lymphocyte infiltration could be detected between wildtype and *Cln3*$^{-/-}$ mice at 6.5 months of age, in both genotypes roughly three times as many CD8+ve cells were already found in the olfactory bulb, compared to the number of CD4+ve T-cells at this time point. At 12 months of age, a disease related influx of CD8+ve T-cells occurred in the olfactory bulb of *Cln3*$^{-/-}$ mice, spreading more widely and finally resulting in five times as many cytotoxic T-cells throughout every brain region at 21 months of age compared to the number of CD4+ve T-helper cells.

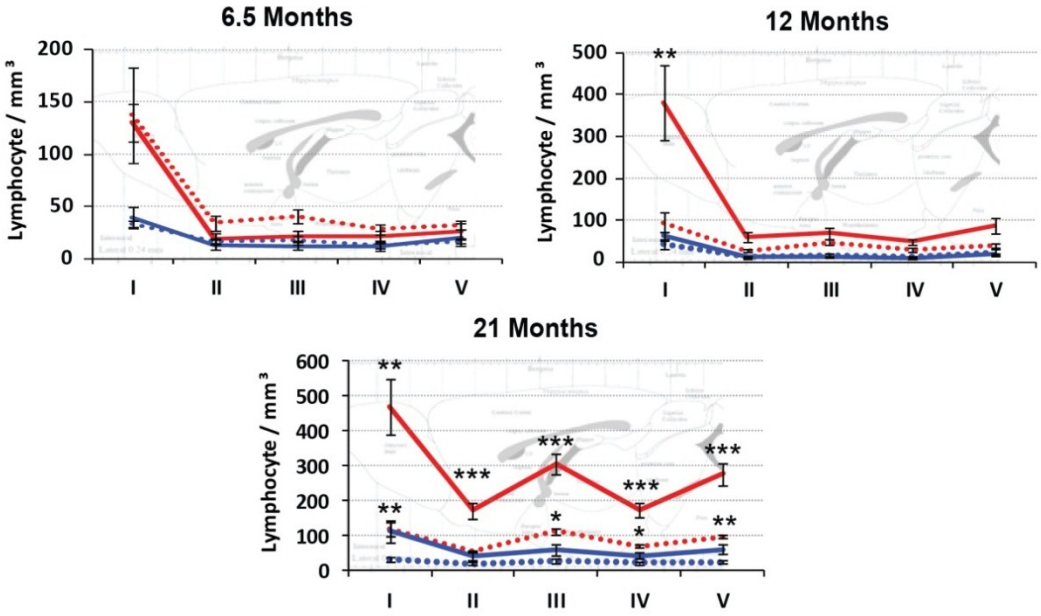

Figure 29. Direct comparison of regional distribution of CD8+ve and CD4+ve lymphocytes in *Cln3*$^{-/-}$ mice. Regional breakdown of total lymphocyte counts into five rostrocaudal brain levels at 6.5, 12 and 21 months of age in *Cln3*$^{-/-}$ (—) and wildtype (···) mice revealed different distributions of CD8+ve (red) and CD4+ve T-cells (blue). The first significant increase in the number of CD8+ve T-cells was seen in the olfactory bulb of *Cln3*$^{-/-}$ mice at 12 months of age compared to wildtype mice, but this significant difference could be detected in all brain regions of mutant mice at 21 months of age. In contrast, significantly increased numbers of CD4+ve T-cells were only seen at 21 months of age in *Cln3*$^{-/-}$ mice compared to control mice, but this difference was evident in every level of the brain except for level II in mutant mice. At 21 months of age, both subsets of lymphocytes were distributed in a region-specific manner with levels I, III and V showing more T-cell infiltration than levels II and IV, even though this pattern was more pronounced with CD8+ve T-cells. At this time point, about five times as many CD8+ve T-cells were found in every brain region compared to CD4+ve T-cells. Values were calculated as density of lymphocytes/mm^3. Brain levels: I = olfactory bulb, II = forebrain until hippocampus, III = hippocampal forebrain, IV = Midbrain with *superior colliculus*, V = midbrain with *pons*. Statistics: Two-way ANOVA with Bonferroni post hoc test, *p<0.05, **p<0.01, ***p<0.001. Data shown as mean ± SEM, n = 5.

Calculating the ratio of CD8:CD4+ve cells in the whole brain of *Cln3*$^{-/-}$ and wildtype mice at all ages confirmed the relative abundance of these two lymphocyte subsets (see **Figure 30**). In both genotypes at least two times, and up to five times as many CD8+ve cells than CD4+ve cells were present at all ages. In 12 month old *Cln3*$^{-/-}$ mice a disease-dependent influx of cytotoxic T-cells, combined with the absence of CD4+ve cell infiltration (see above) altered the ratio of lymphocyte sub-classes in mutant mice significantly from that seen in wildtype mice. Besides an age-dependent increase in the number of CD8+ve cells in both genotypes (as also seen in *Ppt1*$^{-/-}$ and their control mice), the CD8:CD4+ve ratio seems clearly affected by disease onset and manifestation at 12 months of age in *Cln3*$^{-/-}$ mice.

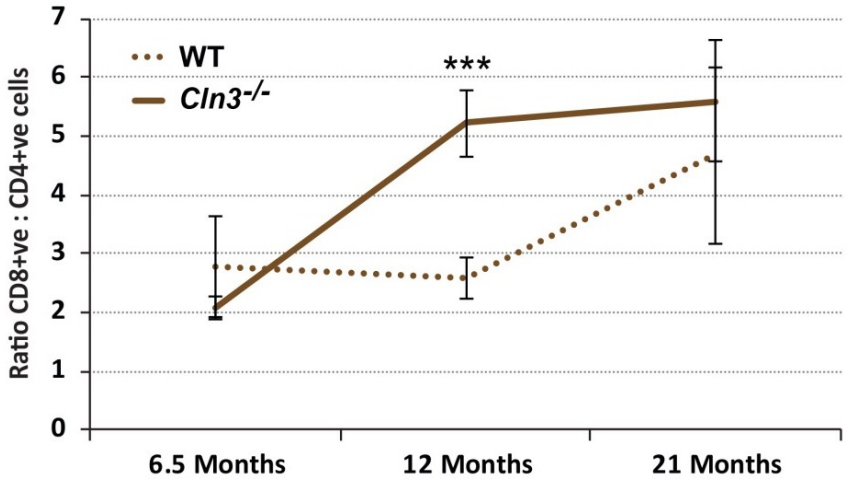

Figure 30. Increased CD8:CD4+ve T-cell ratio in *Cln3*$^{-/-}$ mice. Calculation of the ratios of CD8+ve and CD4+ve T-cells revealed a significant difference between *Cln3*$^{-/-}$(—) and wildtype (···) (WT) mice at 12 months of age. Besides an age-dependent increase of CD8+ve cells influx in mutant and WT mice, significantly more CD8+ve lymphocytes infiltrate the brain of mutant mice at 12 months of age, resulting in a *Cln3* deficiency dependent increase of CD8:CD4+ve T-cell ratio at this time point. However, at all ages more CD8+ve T-cells could be detected in both mouse populations, compared to CD4+ve T-cells. Statistics: Two-way ANOVA with Bonferroni post hoc test, ***$p<0.001$. Data shown as mean ± SEM, n = 5.

Thus, taken together, our data provide the first detailed characterisation of the temporal and spatial distribution of lymphocyte infiltration (for both markers CD4 and CD8) throughout the brains of *Cln3*$^{-/-}$ mice and their age matched controls.

3.3 Summary and discussion

In this chapter, we have for the first time assessed the distribution of the general leukocyte marker CD45 in both *Ppt1*$^{-/-}$ and *Cln3*$^{-/-}$ brains, and detailed how this changes over time, which illustrates simultaneously the innate and the adaptive immune responses in these brains. Secondly, and most importantly, we have provided

the first detailed characterisation of the adaptive immune response, in particular T-cells, in the brains of both mouse models. We have not only detailed the presence of T-cells in the brains of both forms of NCL, but also quantified the number of these T-cells, their regional distribution in the brain and how this changes during the course of the disease. Furthermore, making additional regional volume measurements enabled us to compare wildtype and NCL brains with a new rostral-caudal perspective. This regional atrophy data was incorporated with our T-cell counts to obtain the density of T-cells in each part of the brain. Last but not least, this study included 21 month old mice, the oldest *Cln3*$^{-/-}$ mice analysed to date, providing an important new perspective on the later stages of disease progression.

a) A wide range of immune cells is present in NCL brains

Characterising the immune responses in the NCL CNS highlighted that glial activation is a key feature of multiple forms of NCL (reviewed in (Cooper *et al.*, 2006; Jalanko and Braulke, 2009)). In both Infantile and Juvenile NCL localised glial activation has been described as starting within individual thalamic nuclei or specific cortical laminae in several studies (Bible *et al.*, 2004; Pontikis *et al.*, 2004; Pontikis *et al.*, 2005; Kielar *et al.*, 2007). However, to date, no direct comparison of innate and adaptive immune cells has been made in NCL brains. Using CD45, a marker which stains all types of immune cells ('*leukocytes*'), we were able to qualitatively survey the extent and distribution of each immunological cell type in the brains of *Ppt1*$^{-/-}$ and *Cln3*$^{-/-}$ mice at different stages of disease progression (see **Figure 16** and **Figure 17**). CD45 immunoreactive lymphocytes, microglia, and macrophages could be detected in widespread regions of *Ppt1*$^{-/-}$ brains from 3 months onwards, but only at much later stages of disease progression in *Cln3*$^{-/-}$ brains, at 12 and 21 months of age. The characteristic presence of microglia and macrophages could be identified in the thalamocortical regions of both *Ppt1*$^{-/-}$ and *Cln3*$^{-/-}$ brains, as has been described before (Bible *et al.*, 2004; Pontikis *et al.*, 2005; Kielar *et al.*, 2007), with scattered T-cell staining also present throughout the brain (see **Figure 16** and **Figure 17**). The majority of these CD45+ve T-cells were seen in the more rostral regions of the brain (especially in the olfactory bulb), but they were also consistently present in every brain region that displayed microglial activation. This pattern was particularly maintained in cortical regions, but was perhaps less obvious in the thalamic nuclei where the most intense CD45+ve glial activation occurred (see **Figure 16** and **Figure 17**). By comparing the appearance of microglial activation in the cortex between age groups, it could be

speculated that T-cells always seem to be present before, during and even after a wave of inflammatory microglial activation passed through a cortical region. These observations raised the question of what is the exact role of T-cells in the pathogenesis of these forms of NCL, which shall be addressed in the subsequent **Chapter 4**. To date, no T-cell or CD45 staining has been described in any detail in NCL brains, just being mentioned briefly in one study in 6 month old *Ppt1*$^{-/-}$ brains and one in 18 month old *Cln3*$^{-/-}$ mice, where CD45 staining was used as proof of the presence of T-cells (Lim *et al.*, 2007b; Macauley *et al.*, 2011). Taken together, our CD45 immunostaining data revealed evidence of pronounced microglial activation and T-cell infiltration in many brain regions of *Ppt1*$^{-/-}$ and *Cln3*$^{-/-}$ mice. This distribution of T-cells was widespread and exhibited a rostrocaudal gradient, mostly coinciding with, but not exclusively restricted to, the distribution of microglial activation.

b) Regional atrophy in NCL brains – a new rostral-caudal perspective

We measured the volume of the entire hemisphere and each of five rostral-caudally defined levels to provide a new way of looking at the progression of pathological changes in different brain regions (see **Appendix I: Figure 77** and **Appendix I: Figure 78** for detailed results). In *Ppt1*$^{-/-}$ mice, previously reported data of regional brain atrophy described only relatively late onset shrinkage of the cortex at 7 months of age ((Bible *et al.*, 2004) Kielar and Cooper, unpublished observations). Consistent with our data for an earlier onset of glial activation and neuron loss (see **Figure 32**, **Figure 36** and **Figure 40** in **Chapter 4**), this study revealed an earlier onset of regional brain atrophy in *Ppt1*$^{-/-}$ mice. Whole brain atrophy was already detected from 5 months onwards, whereas our rostral-caudal analysis revealed that some degree of atrophy was already evident at 3 and 5 months of age in the mid-levels of the forebrain, spreading to become a widespread atrophy at 7 months of age that included almost all rostrocaudal levels of the *Ppt1*$^{-/-}$ CNS. The only exception was level IV, which contains the midbrain, suggesting that this structure is affected to a lesser degree (see **Appendix I: Figure 77**). In *Cln3*$^{-/-}$ mice whole brain atrophy was only detected towards the disease end stage in 21 month old mice, with the mid-levels of the forebrain (level III, containing the thalamus and hippocampus) being the only rostral-caudal level to show a significantly reduced volume (see **Appendix I: Figure 78**). In previous studies of the two different JNCL mouse models, *Cln3*$^{\Delta ex7/8}$ knock-in mice displayed moderate atrophy in the thalamus at 12 months of age (Pontikis *et al.*, 2005), whereas no significant changes in regional volume were seen in early (5 months) and mid-staged (14 months) *Cln3*$^{-/-}$ mice (Pontikis *et al.*, 2004). Our study being the first investigation of progressive regional atrophy in *Cln3*$^{-/-}$ mice on a congenic

C57Bl/6 background, has extended these findings and demonstrated that cortical atrophy does indeed occur in 21 month old mice.

In summary, this part of this thesis has provided a novel rostral-caudal perspective on progressive brain atrophy in INCL and JNCL, revealing new and valuable information about when these changes first occur. Perhaps more importantly, these data were also crucial for being able to convert raw numbers of lymphocytes into cellular density measurements, taking into account these variations in regional atrophy.

c) Subtype-specific T-cell infiltration in NCL brains

As the main findings of this chapter, we provide for the first time a detailed characterisation of lymphocyte infiltration during disease progression in mouse models of both Infantile and Juvenile NCL. Indeed, our data revealed that significant lymphocyte infiltration occurs in both forms of NCL. Because both mouse models were bred onto the same congenic C57Bl/6 background, they could be directly compared for the first time. In mice with INCL an early T-cell infiltration could be described (from 3 months onwards), whereas in the mouse model of JNCL the same extent of lymphocyte infiltration was reached only at a late stage of disease progression (21 months) (see **Figure 21** and **Figure 27**). This is perhaps surprising in INCL, where lymphocyte involvement in pathogenesis has only recently been suspected at later stages of the disease (Macauley et al. 2011). In contrast in JNCL, which displays an autoimmune component and compromised BBB integrity (Chattopadhyay et al., 2003 a, 2003b; Lim et al., 2007), more pronounced lymphocyte infiltration might be expected. Interestingly, in *Ppt1*$^{-/-}$ mice both CD4+ve and CD8+ve cells were already present in the brain parenchyma at 3 months of age (see **Figure 18** and **Figure 19**). This is in contrast to the lymphocyte infiltration seen in *Cln3*$^{-/-}$ mice, in which only CD8+ve cytotoxic T-cells seem to infiltrate the brain, with the entry of CD4+ve T-helper cells delayed until the end stages of disease (see **Figure 25** and **Figure 26**). Qualitative assessment of the T-cell distribution in the brains of Infantile and Juvenile NCL mice revealed no obvious T-cell clustering in any brain region. The only discernible difference between the two NCL forms was that more T-cells were present in the *VPM/VPL* nuclei of *Cln3*$^{-/-}$ mice than in *Ppt1*$^{-/-}$ mice, at equivalent late stages of disease progression. This putative difference has not been quantified, but could speculatively be explained by specific T-cell attraction into neurodegenerative regions due to the autoimmune responses that occur in *Cln3*$^{-/-}$ mice (Lim *et al.*, 2007b), or perhaps the influence of astrocytes upon immune cell infiltration

(Voskuhl *et al.*, 2009), since *Cln3*$^{-/-}$ astrocytes show dysfunctional activation (Pontikis *et al.*, 2004; Tyynela *et al.*, 2004; Pontikis *et al.*, 2005; Parviainen, 2012). The other consistent trend in the distribution of lymphocytes that was evident in both *Ppt1*$^{-/-}$ and *Cln3*$^{-/-}$ mice was a tendency for T-cells to be present near ventricles and/or in white matter tracts. This observation is potentially linked to this being the most likely route of entry for T-cells into the brain, provided that favourable endothelial cell – lymphocyte interactions occur (Ransohoff et al. 2003; Wilson et al. 2010). All of these suggestions shall be discussed in more detail in **Chapter 7**.

Subsequent quantitative counts of lymphocytes in the brain demonstrated that in *Ppt1*$^{-/-}$ mice infiltrated CD4+ve T-cells already reached their maximal density at 3 months of age, whereas CD8+ve T-cells numbers gradually increased over time (see **Figure 21**). This resembles the typical function of each subset of T-cells (see **section 1.7a** in **Chapter 1**), with CD4+ve T-helper cells coordinating the inflammatory response and/or re-activating macrophages (see **section 1.7a** in **Chapter 1**, (Germain and Margulies, 1993; Zhu and Paul, 2008; Abbas and Lichtman, 2011)). Only a certain number of these cells are needed, whereas CD8+ve cytotoxic T-cells and their induction of apoptosis become more essential as the disease progresses (Townsend and Bodmer, 1989; Shresta *et al.*, 1998; Abbas and Lichtman, 2011)). The pattern of T-cell infiltration observed in *Cln3*$^{-/-}$ brains, with a delayed or absent CD4+ve T-helper cell infiltration, is not as straight forward (see **Figure 27**). As described in **Chapter 1** (see **section 1.7a**), the general consensus is that CD4+ve T-cells are not essential for successful CD8+ve T-cell activation and expansion (Castellino and Germain, 2006). However, the initial lack of CD4+ve T-cells, or the predominant infiltration of CD8+ve T-cells in the *Cln3* deficient brain could perhaps be linked to autoimmune processes (Lim et al. 2007), impaired cytokine expression by glial cells and altered inflammatory cues in the brain (Dihanich, 2010; Parviainen, 2012), or perhaps T-cell specific impairments caused by *Cln3* deficiency. Similar predominantly CD8+ve lymphocyte infiltration of the CNS has been described in Rasmussen's Encephalitis, an auto-immune disease in which cytotoxic T-cells have been identified as main contributors to neurodegeneration (Bauer *et al.*, 2002; Schwab *et al.*, 2009). Whether a comparable pathogenic role of CD8+ve T-cells exists in Juvenile NCL still has to be determined. Further explanations for the different sequences of lymphocyte infiltration in *Ppt1*$^{-/-}$ and *Cln3*$^{-/-}$ mice shall be discussed in **Chapter 7**.

By adding a rostrocaudal analysis of their distribution, the second part of the characterisation of lymphocyte infiltration also revealed distinct patterns between these two forms of NCL. Whereas most T-cells were found in the olfactory bulb in both forms of NCL, in *Ppt1*$^{-/-}$ mice both CD4 and CD8+ve T-cells spread caudally over long distances within the brain (see **Figure 22** and **Figure 23**). In contrast, in *Cln3*$^{-/-}$ mice CD8+ve T-cells were more restricted and appeared to accumulate predominantly in areas of the hippocampal forebrain (level III) and the midbrain with the pons (level V) (see **Figure 28** and **Figure 29**). The explanation for this region-specific distribution of lymphocytes in JNCL mice is unclear, but the thalamus and hippocampus are considered the primary pathological targets of the disease (Pontikis *et al.*, 2004; Pontikis *et al.*, 2005), which could potentially explain this pattern of lymphocyte infiltration. However, a similar rostrocaudal distribution of T-cells could be observed in 21 month old wildtype mice, suggesting that this pattern of lymphocyte infiltration may simply be an age-dependent phenotype that may be due to changes in protein expression on endothelial cells over time. In summary, analysis of CD8:CD4+ve cell ratios in both forms of the disease confirmed our data for each lymphocyte subtype. In murine INCL the T-cell ratio stays similar to that seen in wildtype mice at all ages, and therefore no disease-specific shift to one or the other type T-cell type appears to occur (see **Figure 24**). In contrast, in *Cln3*$^{-/-}$ mice a disease related shift to more CD8+ve (or, *vice versa*, to less CD4+ve cell types) could be detected at 12 months of age (**Figure 30**). This finding may reflect the sudden increase in CD8+ve cell infiltration at 12 months in *Cln3*$^{-/-}$ mice, combined with the simultaneous lack of CD4+ve cell infiltration (see **Figure 27**). Ratio analyses are useful tools to identify shifts towards T-cell specific inflammatory responses and elucidate potential key contributors to disease phenotypes (Zaffaroni *et al.*, 1991; Richartz-Salzburger *et al.*, 2007; Richards *et al.*, 2011). For example in the *substantia nigra* of Parkinson disease where 4:1 CD8:CD4 ratios can be found, these data identified CD8+ve T-cells as potentially being key players in disease pathogenesis (McGeer *et al.*, 1988; Brochard *et al.*, 2009). Thus, by quantifying the exact numbers, characterising lymphocyte subtype ratios, and the temporal and spatial distribution of both subpopulations of lymphocytes in Infantile and Juvenile NCL mouse brains, we were able to identify where and when each T-cell subset may contribute to disease progression in these mice.

d) Significance of findings

The studies in this chapter incorporate for the first time a description of the adaptive immune response into the documented pathogenesis of both INCL and JNCL (Pontikis *et al.*, 2005; Kielar *et al.*, 2007). Not only could we demonstrate that T-cells are present in the brains of both forms of NCL, but we also defined clear differences between the adaptive immune responses in INCL and JNCL. Encouraged by these findings, we undertook the immune deficient double knockout experiments described in the next chapter to investigate the contribution of T-cells to the pathogenesis of INCL. In this proof of principle study we have demonstrated that adaptive immune cells are a common feature in the brains of these two forms of NCL, and suggest that similar investigations of the adaptive immune responses should also be conducted in the other forms of Batten disease.

Chapter 4

Rag-1 deficient *Ppt1*$^{-/-}$ mice

After demonstrating in **Chapter 3** that T-cells infiltrate the brain of *Ppt1*$^{-/-}$ and *Cln3*$^{-/-}$ mice, we wanted to investigate the contribution of these adaptive immune cells to disease pathogenesis, focussing upon the murine model of INCL. Therefore, we crossed *Ppt1*$^{-/-}$ mice with mice deficient for Rag-1, an essential protein for the maturation process of T- and B-cells (see **section 1.11a** in **Chapter 1**), and therefore lack functioning T- and B-cells. Subsequently, we compared the resulting *Ppt1*$^{-/-}$/*Rag-1*$^{-/-}$ mice with single knockout *Ppt1* mice for well-described disease landmarks including glial activation, neuron loss and cortical atrophy (Bible *et al.*, 2004; Kielar *et al.*, 2007). Based on the findings by (Kielar *et al.*, 2007), we concentrated this analysis of *Ppt1*$^{-/-}$ and *Ppt1*$^{-/-}$/ *Rag-1*$^{-/-}$ mice on the thalamocortical system, specifically the thalamic *ventral posterior nuclei* (*VPM/VPL*) and the cortical *somatosensory barrier field* (*S1BF*), as interconnected brain regions that display particularly prominent pathology.

4.1 Increased hemisphere mass in *Ppt1*$^{-/-}$/*Rag-1*$^{-/-}$ mice

To get a first indication of the extent of neurodegeneration over time, the weight of one hemisphere from each brain was recorded after paraformaldehyde (PFA) fixation. Since our histological analysis focused on the forebrain, we actually recorded the mass of each hemisphere after separating of the cerebellum, but with olfactory bulb intact (see **section 2.2**, in **Chapter 2**). From 5 months onwards a significant decrease in hemisphere mass could be observed in *Ppt1*$^{-/-}$ mice, compared to age-matched wildtype mice (see **Figure 31**). At 5 months of age *Ppt1*$^{-/-}$ mice were 18.3% lighter and at 7 months of age were 25.45% lighter than age-matched wildtype mice.

Extending this analysis to include *Rag-1*$^{-/-}$ and *Ppt1*$^{-/-}$/*Rag-1*$^{-/-}$ double knockout mice, none of these genotypes showed any significant difference in hemisphere weight up to 3 months of age (see **Figure 31**). At 5 months of age, *Ppt1*$^{-/-}$/*Rag-1*$^{-/-}$ double knockouts lost 10.2% of hemisphere weight compared to the age-matched wildtype controls, but this still represents an 8.1% increase in mass compared to *Ppt1*$^{-/-}$ mice. From 3 months onwards, the hemispheres of double knockout mice were heavier than the ones of the corresponding *Ppt1* single knockouts. However, this amelioration of brain atrophy only reached significance at 5 months of age. This difference disappeared at 7 months of age when the hemisphere of *Ppt1*$^{-/-}$/*Rag-1*$^{-/-}$ double knockouts showed 5.8% less weight loss compared to *Ppt1*$^{-/-}$ mice, but were 19.6% lighter than wildtype mice.

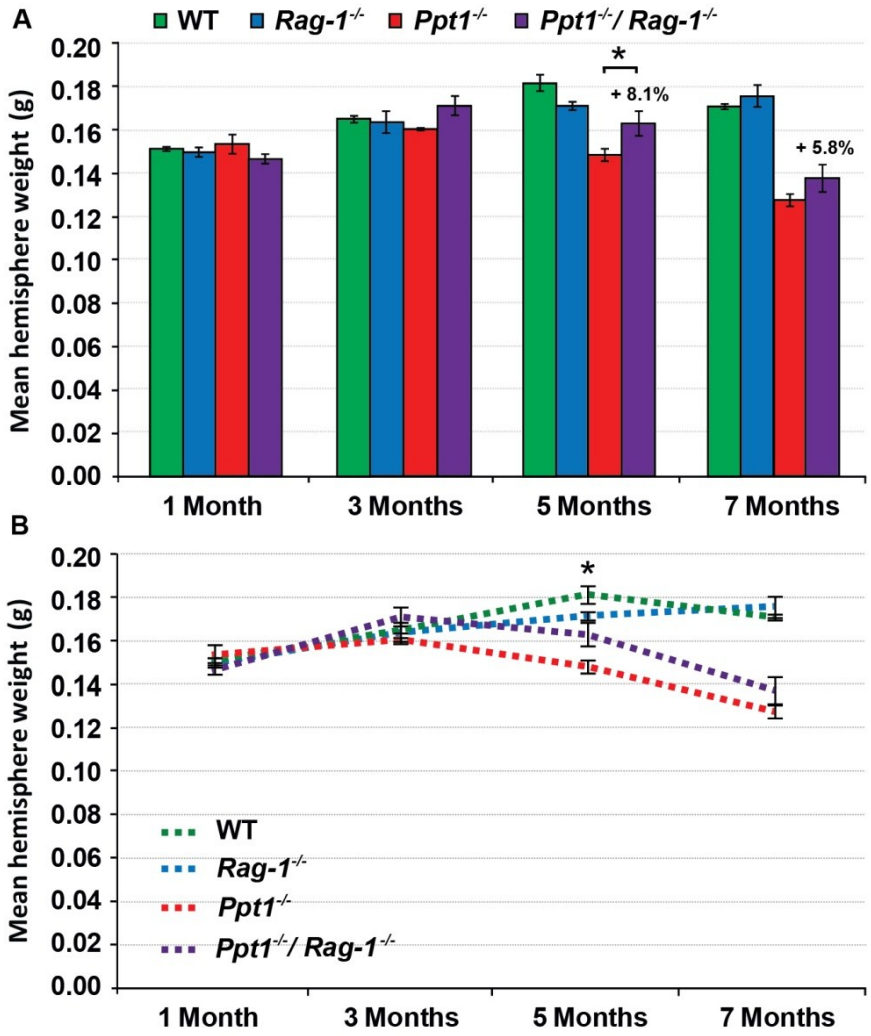

Figure 31. Progressive loss of brain mass in *Ppt1*$^{-/-}$ and *Ppt1*$^{-/-}$/*Rag-1*$^{-/-}$ mice. The weights of brain hemispheres from mice of each genotype (*Ppt1*$^{-/-}$, *Ppt1*$^{-/-}$/*Rag-1*$^{-/-}$, *Rag-1*$^{-/-}$ and wildtype) were measured after PFA fixation and removal of the cerebellum, but before further processing. From 5 months onwards there was a significant loss in hemisphere mass in *Ppt1*$^{-/-}$ mice, compared to age-matched wildtype mice (WT). Hemispheres from *Ppt1*$^{-/-}$/*Rag-1*$^{-/-}$ mice were significantly heavier than those from *Ppt1*$^{-/-}$ mice at 5 months of age, while at 7 months of age this difference was no longer significant. WT and *Rag-1*$^{-/-}$ controls showed no significant differences in hemisphere mass at any age. The same data are presented as both histogram (A) and line graph (B). Percentages indicate differences between *Ppt1*$^{-/-}$ and *Ppt1*$^{-/-}$/*Rag-1*$^{-/-}$ mice in comparison to age-matched WT mice. Statistics: Two-way ANOVA with Bonferroni post hoc test, *$p<0.05$. Data shown as mean ± SEM, n = 5.

These data give an indication of a transient phenotypic improvement of *Ppt1*$^{-/-}$/*Rag-1*$^{-/-}$ double knockouts compared to *Ppt1*$^{-/-}$ mice. However, such brain weight measurements have to be interpreted with caution as they are susceptible to many variable factors such as moisture content, weight differences due to injuries resulting from the harvesting of the brain or inconsistency of cerebellum removal. To minimize the effects of such variation in the measurements, the weighing procedure was performed in a strictly consistent manner by the same investigator.

4.2 Impact of *Rag-1* deficiency on reactive phenotypes in *Ppt1*$^{-/-}$ mice

Neuronal damage and dysfunction are classically accompanied by up-regulation of glial cell markers in the brain. The most prominent and abundant glial cells in the brain, astrocytes and microglia have been studied extensively and their activation has been identified as an early marker of on-going neuronal damage or dysfunction (Raivich *et al.*, 1999). An early glial activation can be also seen in the brains of NCL mice (see section **1.10** in **Chapter 1**, (Cooper *et al.*, 2006; Cooper, 2010) and demonstrates a characteristic feature of Infantile NCL and Juvenile NCL mice (Bible *et al.*, 2004; Pontikis *et al.*, 2004; Kielar *et al.*, 2007), but also for example in the South Hampshire sheep model of CLN6 disease (Oswald *et al.*, 2005; Kay *et al.*, 2006).

All of these studies describe a localised activation of astrocytes and/or microglia before overt neuron loss, and it has been proposed that this phenotype serves as the most accurate indicator of where this subsequent neuron loss will occur (Cooper, 2010). In order to characterise the onset and progression of this reactive phenotype in *Ppt1*$^{-/-}$/*Rag-1*$^{-/-}$ mice and to compare the findings directly to single *Ppt1*$^{-/-}$ mice, we stained a 1 in 6 series of sections from 5 mice of each genotype at 1, 3, 5 and 7 months of age for glial fibrillary acidic protein (GFAP) and the microglial marker CD68. Both glial markers can be analysed by thresholding image analysis, which measures the percentage and the intensity of stained areas in relevant brain regions (see **section 2.7** in **Chapter 2**). In comparison to the work of (Kielar *et al.*, 2007), we chose CD68 as a microglial marker instead of F4/80. The advantage of CD68 is that it results in a more distinct microglial cell labelling with lower background immunoreactivity that, if necessary, also can also be quantified by optical fractionator stereological counts, as we routinely do to assess neuron survival.

Based on the findings of (Kielar *et al.*, 2007), we concentrated the analysis of astrocytosis and microglial activation in *Ppt1*$^{-/-}$ and *Ppt1*$^{-/-}$/*Rag-1*$^{-/-}$ mice on the thalamocortical system: focusing on interconnected brain regions with particularly prominent pathology: the thalamic *ventral posterior nucleus* (*VPM/VPL*) and the cortical *somatosensory barrier field* (*S1BF*).

a) Attenuated astrocytosis in the thalamus of *Ppt1*$^{-/-}$/*Rag-1*$^{-/-}$ mice

Astrocytosis is a commonly used indicator of inflammation and is a precursor to neuron loss in Infantile NCL mice as described by (Kielar *et al.*, 2007), and other

forms of NCL (Oswald *et al.*, 2005; Pontikis *et al.*, 2005; Schmiedt *et al.*, 2012). As a baseline for comparison to *Ppt1*$^{-/-}$/*Rag-1*$^{-/-}$ mice we again stained sections from 1, 3, 5 and 7 month old wildtype and *Ppt1*$^{-/-}$ mice with the GFAP marker for activated astrocytes (see **Figure 32**) and subsequently performed thresholding image analyses to quantify the level of GFAP immunoreactivity in the thalamic *VPM/VPL* nuclei of all brains (see **Figure 33**).

This analysis confirmed and extended the previous report of astrocytosis in these mutant mice. The first traces of astrocytosis could already be detected in *Ppt1*$^{-/-}$ mice at 1 month of age, with scattered GFAP+ve astrocytes within *VPM/VPL*, but became much more obvious from 3 months onwards when many intensely stained GFAP+ve astrocytes were present in the *VPM/VPL* of *Ppt1*$^{-/-}$ mice (see **Figure 32A**). With further disease progression the intensity and distribution of GFAP staining increased at 5 months of age, and subsequently reached maximal intensity at the end stage of the disease (7 months of age). At the same time points, no overt astrocyte activation was seen in wildtype mice. Looking at these GFAP+ve astrocytes at higher magnification, hypertrophied cell soma with thickened cell processes upon an area-wide "carpet" of astrocytes could be detected from 3 months onwards in the *VPM/VPL* of *Ppt1*$^{-/-}$ mice (see **Figure 32B**). With disease progression the intensity and darkness of astrocyte cell staining increased, also manifesting itself as more intense staining of a dense meshwork of GFAP+ve astrocytes within the neuropil. In comparison, in 1 month old *Ppt1*$^{-/-}$ mice, and at all ages of wildtype mice, only sporadic faintly stained protoplasmic astrocytes with thin processes could be detected.

In *Ppt1*$^{-/-}$/*Rag-1*$^{-/-}$ double knockout mice the first evidence for astrocytosis was seen at 3 months of age and became more pronounced with disease progression (see **Figure 32A**), similar to that seen in *Ppt1*$^{-/-}$ mice. However, at every age studied *Ppt1*$^{-/-}$/*Rag-1*$^{-/-}$ double knockouts showed a reduced level of astrocytosis compared to single mutant INCL mice. This difference is clearly seen at higher magnification in *Ppt1*$^{-/-}$/*Rag-1*$^{-/-}$ double knockout mice at 3 and 5 months of age when GFAP+ve astrocytes displayed a much less pronounced hypertrophy and less intense staining of their processes (see **Figure 32B**). At these earlier time points the *VPM/VPL* was not completely filled with GFAP immunoreactive astrocytes in *Ppt1*$^{-/-}$/*Rag-1*$^{-/-}$ double knockouts, whereas at 7 months of age the astrocytosis extended throughout these nuclei.

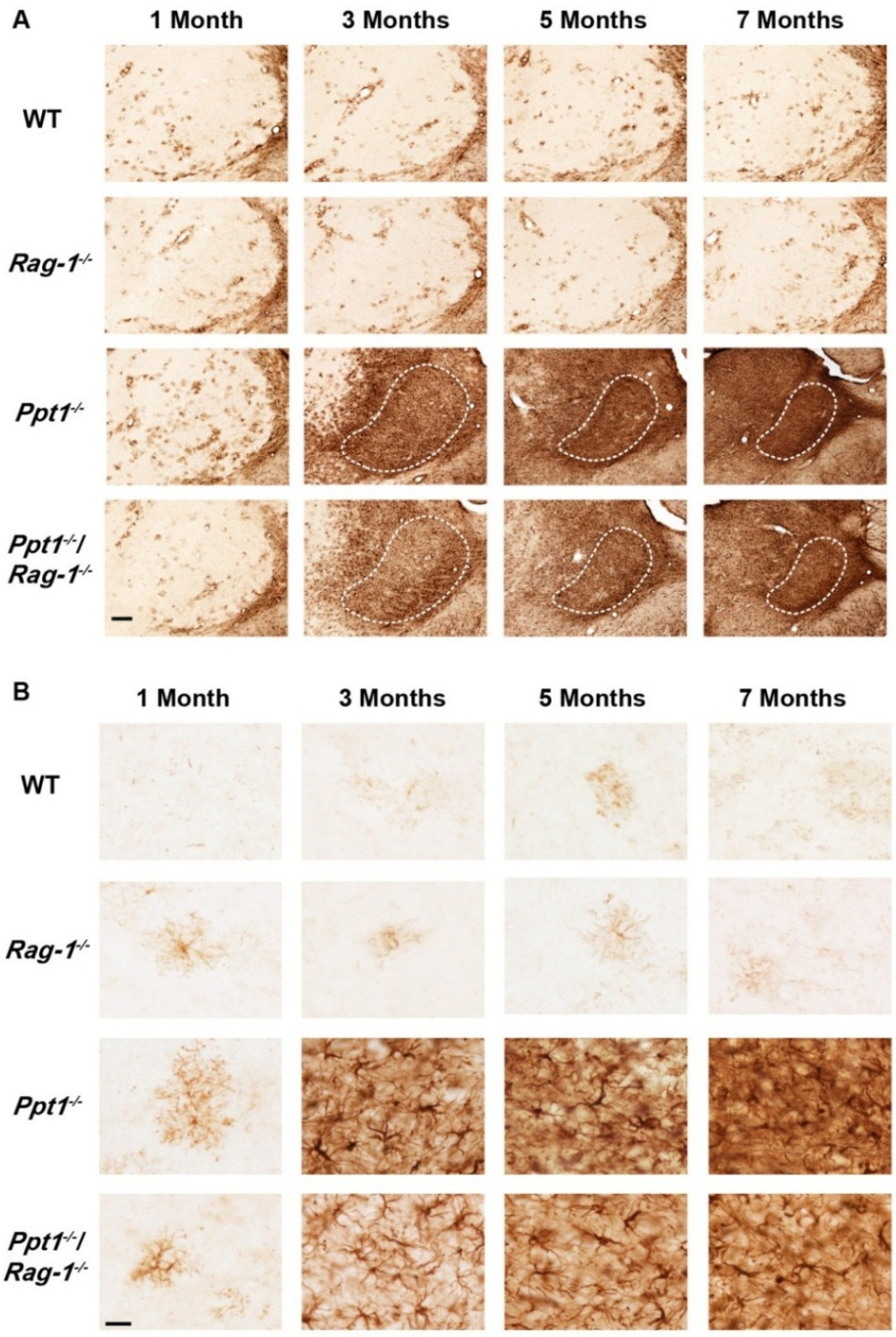

Figure 32. Progressive astrocytosis in the thalamus of *Ppt1*$^{-/-}$ and *Ppt1*$^{-/-}$*/Rag-1*$^{-/-}$ double knockout mice. (see figure caption on next page)

Figure 32. Progressive astrocytosis in the thalamus of *Ppt1*$^{-/-}$ and *Ppt1*$^{-/-}$/*Rag-1*$^{-/-}$ double knockout mice. (A) Immunohistochemical staining for the astrocyte marker glial fibrillary acidic protein (GFAP) in the thalamus of 1, 3, 5 and 7 month old mice revealed localised astrocytosis within the *ventral posterior nucleus* (*VPM/VPL*) (---) of INCL mice. At all ages, *Ppt1*$^{-/-}$/*Rag-1*$^{-/-}$ double knockout mice showed attenuated GFAP immunoreactivity compared to *Ppt1*$^{-/-}$ mice. From 3 months of age localised astrocytosis could be observed in the *VPM/VPL* of mutant mice, which spread to involve the whole thalamus with increased age. GFAP immunoreactivity was virtually absent in age-matched *Rag-1*$^{-/-}$ mice or wildtype (WT) mice. Scale bar = 200 μm (B) Higher magnification reveals the morphology of GFAP+ve astrocytes in the *VPM/VPL* of *Ppt1*$^{-/-}$ and *Ppt1*$^{-/-}$/*Rag-1*$^{-/-}$ mice at 1, 3, 5 and 7 month of age. Compared to the faintly immunoreactive protoplasmic astrocytes present in 1 month old mutant mice, many intensely stained fibrous astrocytes were present in *VPM/VPL* from 3 months onwards in both strains of mutant mice. These astrocytes displayed thickened processes and became more numerous with increased age until the thalamic neuropil was completely filled with GFAP+ve astrocytes and their processes by 7 months of age. In direct comparison between *Ppt1*$^{-/-}$ and *Ppt1*$^{-/-}$/*Rag-1*$^{-/-}$ mice, this astrocytosis was less pronounced in the double knockout mice at all ages. The *Ppt1*$^{-/-}$/*Rag-1*$^{-/-}$ mice displayed delayed and attenuated GFAP+ve cell staining with distinguishable single astrocytes at 3 months of age, and spatially inclusive and comprehensive astrocytosis only becoming apparent from 5 months onwards in these mice. In WT and *Rag-1*$^{-/-}$ mice only occasional faintly stained protoplasmic astrocytes with many long thin branched processes could be seen at all ages. Scale bar = 20 μm.

Quantification of GFAP immunoreactivity via thresholding image analysis confirmed these morphological observations (see **Figure 33**). GFAP immunnoreactivity was significantly increased in the thalamus of single as well as double *Ppt1* mutant mice from 3 months onwards and increased with disease progression. However, a similar reduction in GFAP immunoreactivity could be seen in *Ppt1*$^{-/-}$/*Rag-1*$^{-/-}$ double mutants at 3 and 5 months of age (15.7% at 3 months and 15.3% difference at 5 months). However, the level of GFAP immunoreactivity subsequently increased dramatically, almost reaching similar levels to those seen in *Ppt1*$^{-/-}$ single mutants at 7 months of age. Although a 7.8% mean reduction in GFAP immunoreactivity was measured in the immune deficient *Ppt1*$^{-/-}$/*Rag-1*$^{-/-}$ brains at this time point, this difference was not statistically significant mainly due to a higher variability in these data.

b) Attenuated astrocytosis in the cortex of *Ppt1*$^{-/-}$/*Rag-1*$^{-/-}$ mice

To complete our analysis of astrocytosis in the somatosensory thalamocortical system, we next analysed the relative level of GFAP+ve astrocytosis in the somatosensory cortical sub-region (*S1BF)* to which *VPM/VPL* projects, first comparing *Ppt1*$^{-/-}$ mice to age-matched wildtype animals. At 1 month of age *Ppt1*$^{-/-}$ mice already showed marginally increased GFAP immunoreactivity, with more darkly stained astrocytes throughout the *S1BF* cortex. But from 3 months onwards, clear widespread GFAP immunoreactivity could be observed throughout all laminae of *S1BF* (see **Figure 34A**) of *Ppt1*$^{-/-}$ mice, but most prominently in its deeper layers, in particular within lamina V.

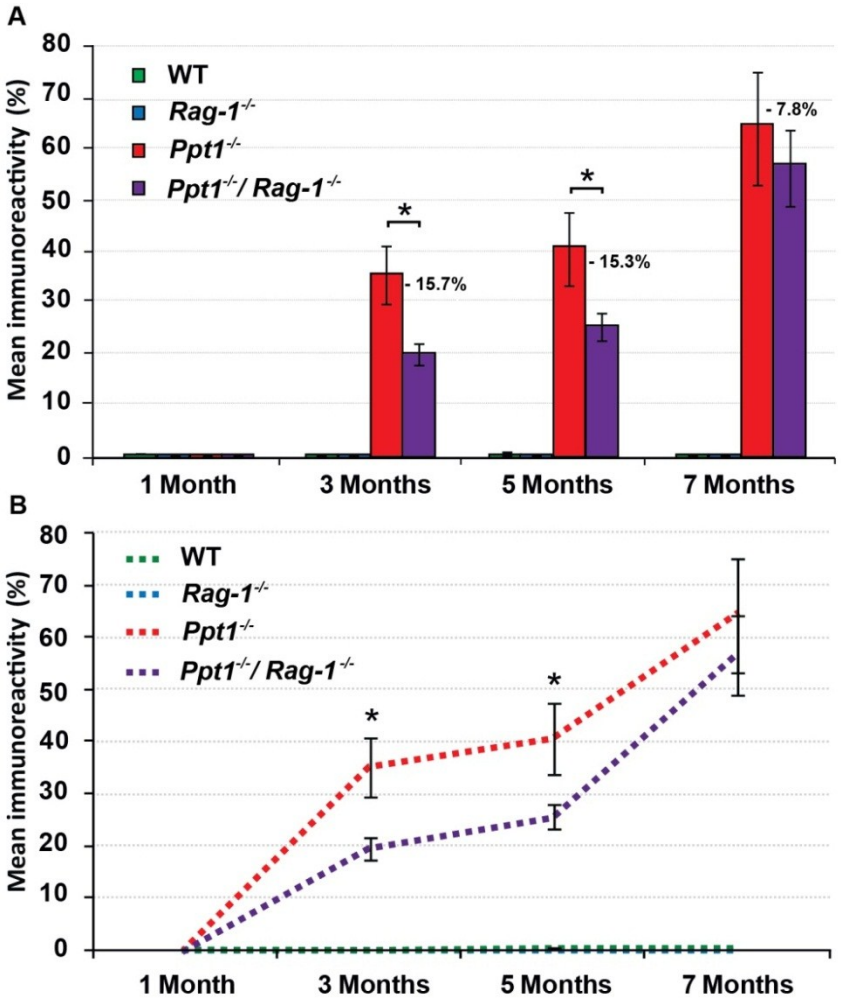

Figure 33. Reduced levels of astrocytosis in the thalamus (*VPM/VPL*) of *Ppt1*$^{-/-}$*/Rag-1*$^{-/-}$ double knockout mice. Thresholding image analysis revealed that the mean level of GFAP immunoreactivity in double knockout mice was significantly reduced at 3 and 5 months, compared to *Ppt1*$^{-/-}$ mice. In contrast, almost no GFAP immunoreactivity was detected in the thalamus of either *Rag-1*$^{-/-}$ or wildtype (WT) mice. Thus, *Ppt1*$^{-/-}$ and *Ppt1*$^{-/-}$*/Rag-1*$^{-/-}$ mice displayed significantly increased GFAP immunoreactivity from 3 months onwards compared to WT mice. The same data are presented as both histogram (A) and line graph (B). Percentages indicate differences between *Ppt1*$^{-/-}$ and *Ppt1*$^{-/-}$*/Rag-1*$^{-/-}$ mice. Statistics: Two-way ANOVA with Bonferroni post hoc test, *$p<0.05$. Data shown as mean ± SEM, n = 5.

The intensity of GFAP staining increased with age and spread to involve the upper layers of the cortex from 5 months onwards. At 7 months of age two distinct and darkly stained bands of activated astrocytes could be detected with darkest staining in laminae V and I (see **Figure 34A**).

In comparison to *Ppt1*$^{-/-}$ mice, the immune deficient *Ppt1*$^{-/-}$*/Rag-1*$^{-/-}$ double knockout mice showed a reduced astrocytosis in *S1BF* (see **Figure 34A**), similar to the effects seen in the thalamus of these mice (see **Figure 32**). Whereas at 3 months of age *Ppt1*$^{-/-}$ mice already showed wide-spread astrocytosis in *S1BF*, in immune deficient *Ppt1*$^{-/-}$*/Rag-1*$^{-/-}$ mice GFAP+ve astrocytes could only be found in lamina V at this age. Later in disease progression at 5 months of age this astrocytosis spread to be present in all

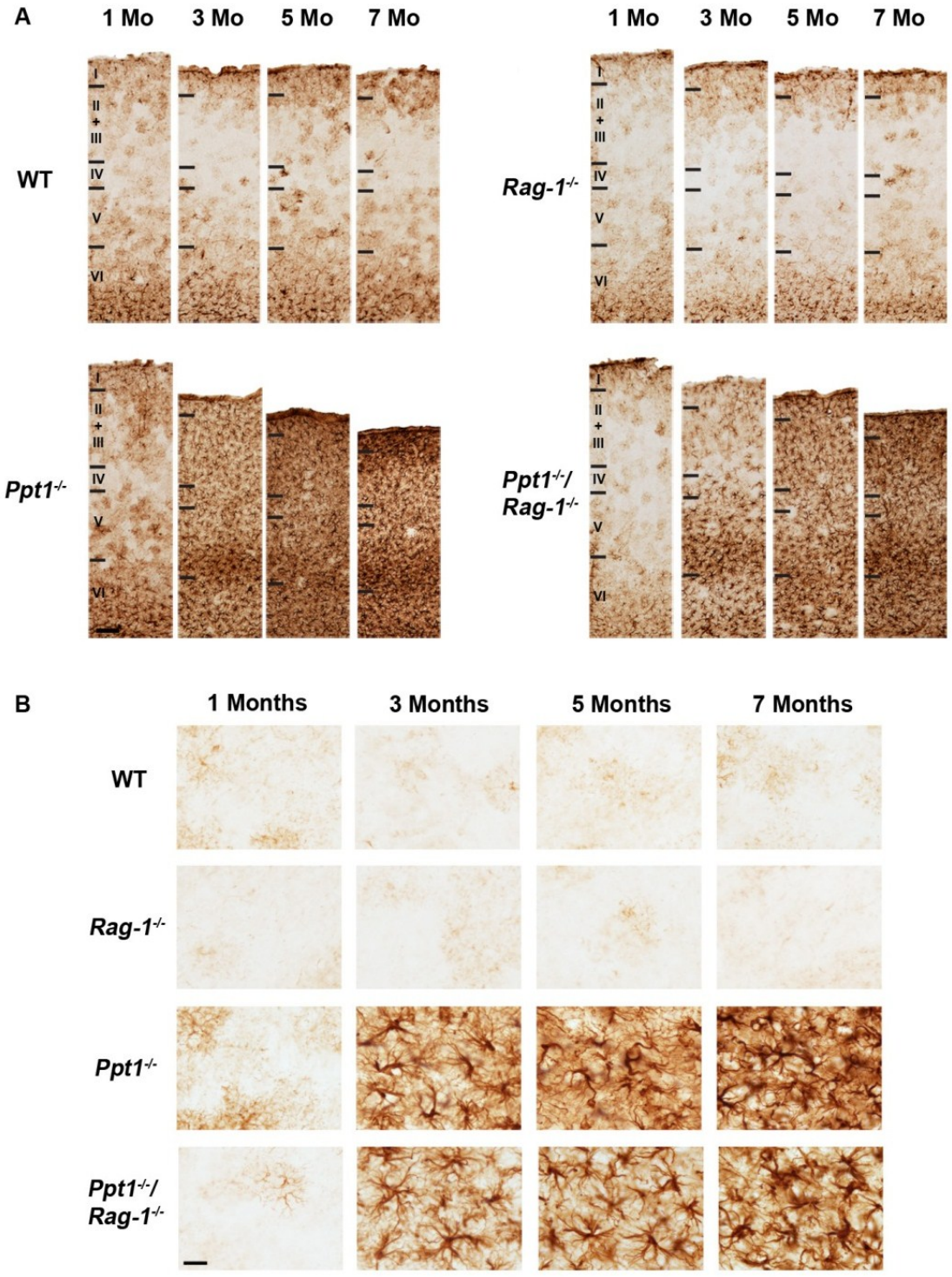

Figure 34. Progressive astrocytosis in the somatosensory barrel field (*S1BF*) cortex of *Ppt1*$^{-/-}$ and *Ppt1*$^{-/-}$*/Rag-1*$^{-/-}$ double knockout mice. (see figure caption on next page)

Figure 34. Progressive astrocytosis in the somatosensory barrel field (*S1BF*) cortex of *Ppt1*$^{-/-}$ and *Ppt1*$^{-/-}$/*Rag-1*$^{-/-}$ double knockout mice. (A) Immunohistochemical staining for the astrocyte marker glial fibrillary acidic protein (GFAP) in the *S1BF* of 1, 3, 5 and 7 month old mice revealed differences between *Ppt1*$^{-/-}$ and *Ppt1*$^{-/-}$/*Rag-1*$^{-/-}$ double knockout mice. *Ppt1*$^{-/-}$/*Rag-1*$^{-/-}$ double knockout mice showed a clearly delayed and reduced astrocytosis at 3 and 5 months of age, compared to *Ppt1*$^{-/-}$ mice. In single mutant *Ppt1*$^{-/-}$ mice widespread astrocytosis throughout all laminae of the cortex could be observed which increased in intensity with disease progression. Most prominent GFAP immunoreactivity was seen in deeper laminae (especially lamina V) from 3 months of age onwards, and in laminae I and II at 7 months of age. In contrast, in *Ppt1*$^{-/-}$/*Rag-1*$^{-/-}$ double knockout mice, at 3 months of age only lamina V of the cortex showed pronounced GFAP immunoreactivity and widespread astrocytosis throughout all layers was only apparent from 5 months of age onwards in these mice. At 7 months of age similar intensity and pattern of astrocytosis could be detected in *Ppt1*$^{-/-}$/*Rag-1*$^{-/-}$ mice as in *Ppt1*$^{-/-}$ mice. In WT and *Rag-1*$^{-/-}$ mice only occasional faintly stained protoplasmic astrocytes with many long thin branched processes could be seen at all ages. Scale bar = 100 μm. (B) Higher magnification of lamina V reveals the morphology of GFAP+ve astrocytes in the *S1BF* of *Ppt1*$^{-/-}$ and *Ppt1*$^{-/-}$/*Rag-1*$^{-/-}$ mice at 1, 3, 5 and 7 month of age. Compared to the faintly immunoreactive protoplasmic astrocytes present in 1 month old mutant mice, many intensely stained fibrous astrocytes were present in lamina V of the *S1BF* from 3 months onwards in both strains of mutant mice. These astrocytes displayed thickened processes and became more numerous with increased age. In direct comparison between *Ppt1*$^{-/-}$ and *Ppt1*$^{-/-}$/*Rag-1*$^{-/-}$ mice, this astrocytosis was less pronounced in the double knockout mice at all ages. Whereas in *Ppt1*$^{-/-}$ mice the majority of the neuropil of lamina V was spatially inclusively filled with GFAP+ve astrocytes and their processes from 3 months onwards, *Ppt1*$^{-/-}$/*Rag-1*$^{-/-}$ mice displayed delayed and attenuated GFAP+ve cell staining with distinguishable single astrocytes until 5 months of age. In WT and *Rag-1*$^{-/-}$ mice only occasional faintly stained protoplasmic astrocytes with many long thin branched processes were seen at all ages. Scale bar = 20 μm.

other laminae of *S1BF* in the double mutants, but to a much lesser extent than was seen in *Ppt1*$^{-/-}$ mice. Finally, as in the thalamus, at 7 months of age the distribution and intensity of GFAP immunoreactivity was seen at similar levels in *Ppt1*$^{-/-}$/*Rag-1*$^{-/-}$ mice and *Ppt1*$^{-/-}$ mice.

Similarly, higher magnification images of the astrocytosis in lamina V of the *S1BF* cortex confirmed the delayed and attenuated up-regulation of GFAP immunoreactivity in *Ppt1*$^{-/-}$/*Rag-1*$^{-/-}$ mice (see **Figure 34B**). Whereas in *Ppt1*$^{-/-}$/*Rag-1*$^{-/-}$ mice single astrocytes were distinguishable in lamina V until 5 months of age, astrocytes in *Ppt1*$^{-/-}$ mice displayed a more intense staining of their processes, leading to a more spatially inclusive astrocytosis already from 3 months onwards (see **Figure 34B**).

Quantifying this cortical GFAP staining via thresholding image analysis confirmed the significantly elevated astrocytosis in *S1BF* from 3 months onwards in *Ppt1*$^{-/-}$ mice, compared to wildtype animals, and this difference increased with age (see **Figure 35**). Although consistently lower levels of GFAP immunoreactivity were seen in the cortex of *Ppt1*$^{-/-}$/*Rag-1*$^{-/-}$ mice compared to *Ppt1*$^{-/-}$ mice, these changes did not reach statistical

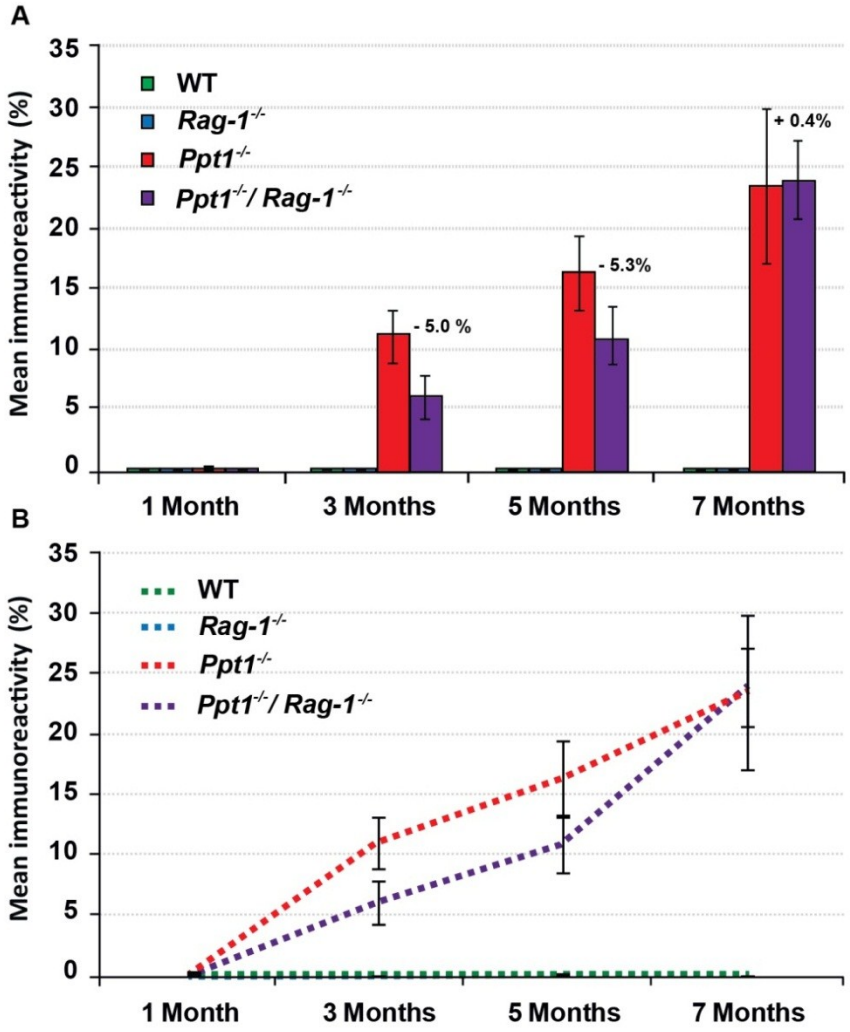

Figure 35. Marginally reduced levels of astrocytosis in the somatosensory barrel field (*S1BF*) cortex of *Ppt1*$^{-/-}$/*Rag-1*$^{-/-}$ double knockout mice. Thresholding image analysis reveals that the mean level of GFAP immunoreactivity in double knockout mice was marginally reduced at 3 and 5 months of age, compared to *Ppt1*$^{-/-}$ mice, but this difference was not significant. In contrast, almost no GFAP immunoreactivity was detected in the thalamus of either *Rag-1*$^{-/-}$ or wildtype (WT) mice. Thus, *Ppt1*$^{-/-}$ and *Ppt1*$^{-/-}$/*Rag-1*$^{-/-}$ mice displayed significantly increased GFAP immunoreactivity from 3 months onwards compared to WT mice. The same data are presented as both histogram (A) and line graph (B). Percentages indicate differences between *Ppt1*$^{-/-}$ and *Ppt1*$^{-/-}$/*Rag-1*$^{-/-}$ mice. Statistics: Two-way ANOVA with Bonferroni post hoc test. Data shown as mean ± SEM, n = 5.

significance. This is probably due to the generally lower intensity of GFAP staining in the cortex (compared to the thalamus) and the rather indistinct staining pattern of GFAP+ve astrocytes. During the earlier stages of the disease a reduction in GFAP immunoreactivity of 5.0% at 3 months and 5.3% at 5 months of age could be observed. However, at 7 months of age there was no detectable difference between the genotypes, as had been seen in the thalamus of these mice (see **Figure 33**). Astrocytosis in *S1BF* followed a similar time course to its afferent thalamic relay nuclei, but the relative level of astrocytosis was much lower in the cortex than in the thalamus. This is consistent with the observations described by (Kielar *et al.*, 2007),

who showed that astrocytosis in the cortex of *Ppt1*$^{-/-}$ mice can be seen from 3 months of age onwards, but lags behind thalamic astrocytosis.

c) Attenuated microglial activation in the thalamus of *Ppt1*$^{-/-}$/*Rag-1*$^{-/-}$ mice

Microglial activation has proved to be a sensitive indicator of neurological dysfunction and pathology (Raivich *et al.*, 1999; Streit *et al.*, 2004; Graeber and Streit, 2010). In *Ppt1*$^{-/-}$ mice the appearance of staining for the microglial marker F4/80 is a relatively late event, occurring at 5 months of age once neuron loss has already begun (Kielar *et al.*, 2007). To gain a more complete picture of microglial activation, we firstly stained tissue from *Ppt1*$^{-/-}$ mice at 1, 3, 5 and 7 months of age with CD68, a widely used and sensitive marker of microglial activation (Holness and Simmons, 1993; Ohmi *et al.*, 2003; Henkel *et al.*, 2004). This analysis revealed evidence for a much earlier microglial response within the thalamus of *Ppt1*$^{-/-}$ mice than had been seen via F4/80 staining (Kielar *et al.*, 2007). In wildtype mice of all ages CD68+ve microglia displayed a relative small cell soma and faint punctate staining of thin cellular processes (see **Figure 36**).

A very similar appearance was seen in 1 month old *Ppt1*$^{-/-}$ mice with CD68 staining that was perhaps slightly more intense than in age-matched wild type controls. However, from 3 months of age onwards intensely stained CD68+ve microglia were evident within the *VPM/VPL* of *Ppt1*$^{-/-}$ mice and displayed a range of morphologies see **Figure 36B**), many with swollen soma, but others with numerous thickened and branched processes and only some with an intensely stained cell soma. With disease progression many more darkly stained cells with swollen and intensely stained soma and shortened processes were evident within the *VPM/VPL* of *Ppt1*$^{-/-}$ mice. At 5 months of age, many more partially activated microglia were present, surrounded by a distinct halo of short processes around their cell soma. At 7 months of age the majority of microglial cells took on the characteristic highly activated morphology of brain macrophages. In the corresponding age-matched control brains, CD68 positive cells displayed the morphology of resident or resting microglia with small soma and long thin processes monitoring their direct proximity.

To identify the impact of knocking out *Rag-1* upon microglial activation in INCL mice, we also stained a complete series of immune deficient *Ppt1*$^{-/-}$/*Rag-1*$^{-/-}$ double knockout mice and *Rag-1*$^{-/-}$ single mutant mice for CD68 (see **Figure 36A**). At all ages examined, the *Ppt1*$^{-/-}$/*Rag-1*$^{-/-}$ double knockout mice showed reduced CD68+ve cell

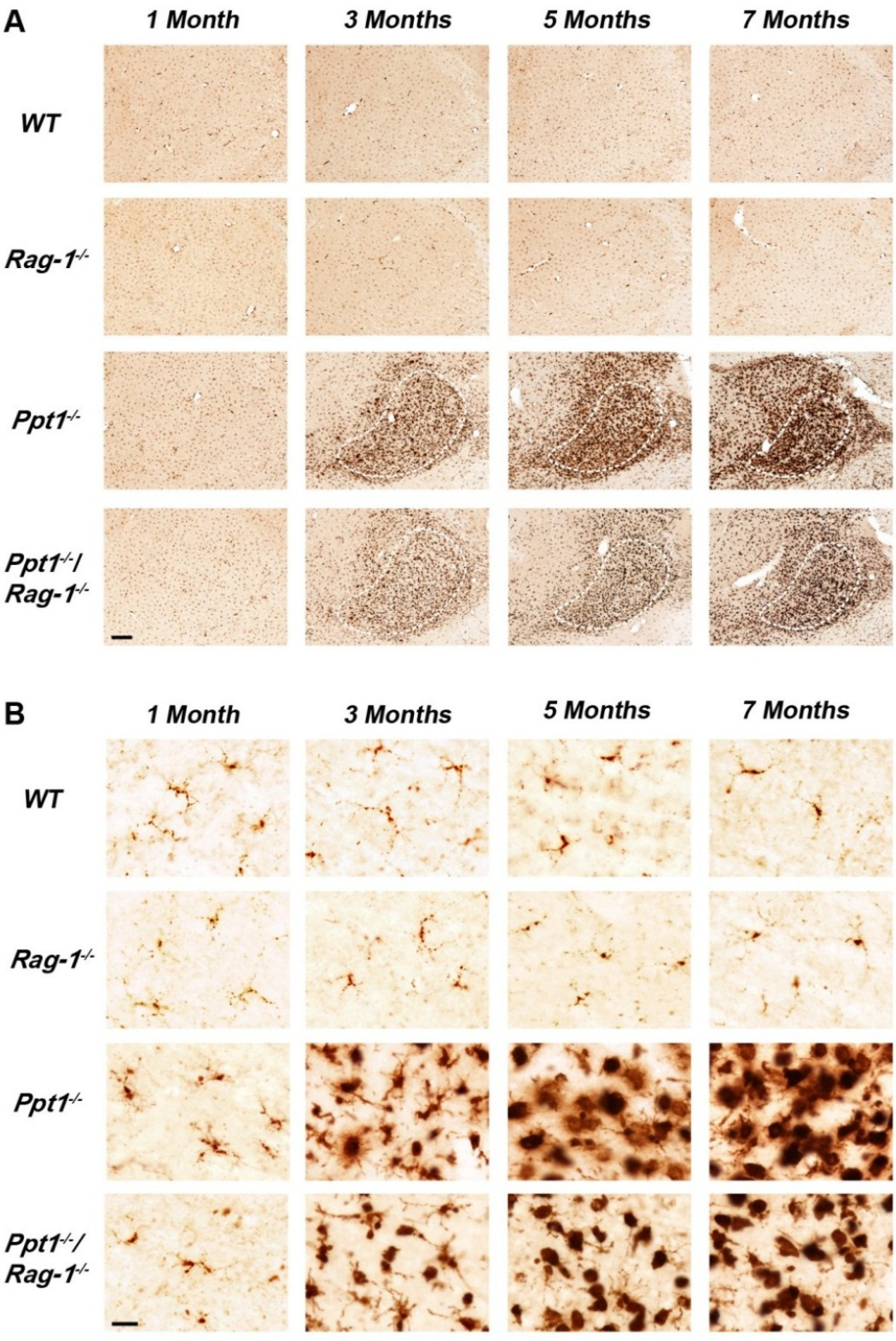

Figure 36. Progressive microglial activation in the thalamus (*VPM/VPL*) of *Ppt1*$^{-/-}$ and *Ppt1*$^{-/-}$*/Rag-1*$^{-/-}$ double knockout mice. (see Figure caption on next page)

Figure 36. Progressive microglial activation in the thalamus (*VPM/VPL*) of *Ppt1*$^{-/-}$ and *Ppt1*$^{-/-}$/*Rag-1*$^{-/-}$ double knockout mice. (A) Immunohistochemical staining for the microglial marker CD68 in the thalamus of 1, 3, 5 and 7 month old mice revealed localised microglial activation within the *ventral posterior nucleus* (*VPM/VPL*) (---) of INCL mice. At all ages, *Ppt1*$^{-/-}$/*Rag-1*$^{-/-}$ double knockout mice showed reduced CD68 immunoreactivity compared to *Ppt1*$^{-/-}$ mice. Microglial activation was observed in the *VPM/VPL* of INCL mice from 3 months onwards, which spread to involve the whole thalamus and gained in intensity with increased age. Similar microglial activation was absent in *Rag-1*$^{-/-}$ and wildtype (WT) mice, in which only faint staining of quiescent microglia could be detected. Scale bar = 200 μm. (B) Higher magnification pictures of CD68+ve microglia in the thalamus of 1, 3, 5 and 7 month old mice revealed differences in cell morphology and activation between immunodeficient double and single *Ppt1* mutant mice. *Ppt1*$^{-/-}$/*Rag-1*$^{-/-}$ double knockout mice showed reduced microglial activation in the thalamus at all ages in terms of cell size, staining intensity and transformation into brain macrophages. Microglia in *Ppt1*$^{-/-}$ mice were intensely CD68 immunoreactive with an enlarged and rounded cell soma from 3 months onwards, whereas microglia in *Ppt1*$^{-/-}$/*Rag-1*$^{-/-}$ double knockout mice remained relatively smaller at all ages, with elongated microglial processes present until 5 months of age. Only quiescent microglia could be detected in 1 month INCL mice and control animals (*Rag-1*$^{-/-}$ and WT). Scale bar = 20 μm.

staining, compared to single knockout *Ppt1*$^{-/-}$ mice. Microglial activation in *Ppt1*$^{-/-}$/*Rag-1*$^{-/-}$ double knockout mice, as judged by CD68 immunoreactivity, started at 3 months, increased over time and was most pronounced in the thalamic regions of these mice. CD68+ve cells in the double knockouts progressively showed the same age-associated increase in the appearance of microglia with an activated morphology, with swollen soma and thickened short processes, as had been seen in single *Ppt1*$^{-/-}$ mice, but with a relatively slower time-course. At 3 months of age, most CD68 positive microglia in *Ppt1*$^{-/-}$/*Rag-1*$^{-/-}$ mice possessed elongated thin processes, with only sporadic more intensely stained activated microglia, whereas in single knockout *Ppt1*$^{-/-}$ mice several macrophage like cell morphologies could already be found at this age (see third and fourth row of bottom panel in **Figure 36B**). At 5 months of age, the majority of CD68+ve cells in *Ppt1*$^{-/-}$/*Rag-1*$^{-/-}$ double knockout mice also morphologically resembled brain macrophages, but clearly showed weaker staining intensity than in age-matched *Ppt1*$^{-/-}$ mice. The same relative differences in CD68 staining between these genotypes could also be seen at 7 months of age, but with generally higher activation than at 5 months of age, with virtually all cells resembling highly activated and intensely stained macrophage-like cells. Interestingly, the halo of microglial cell processes around the soma of partially activated microglia seen in *Ppt1*$^{-/-}$ mice, could not be seen at all or only very weakly in *Ppt1*$^{-/-}$/*Rag-1*$^{-/-}$ double knockout mice at any age.

Quantifying these differences in CD68+ve microglial activation via thresholding image analysis confirmed the relative levels of staining in *Ppt1*$^{-/-}$ and *Ppt1*$^{-/-}$/*Rag-1*$^{-/-}$ double knockout mice (see **Figure 37**). In both single and double *Ppt1* mutant mice

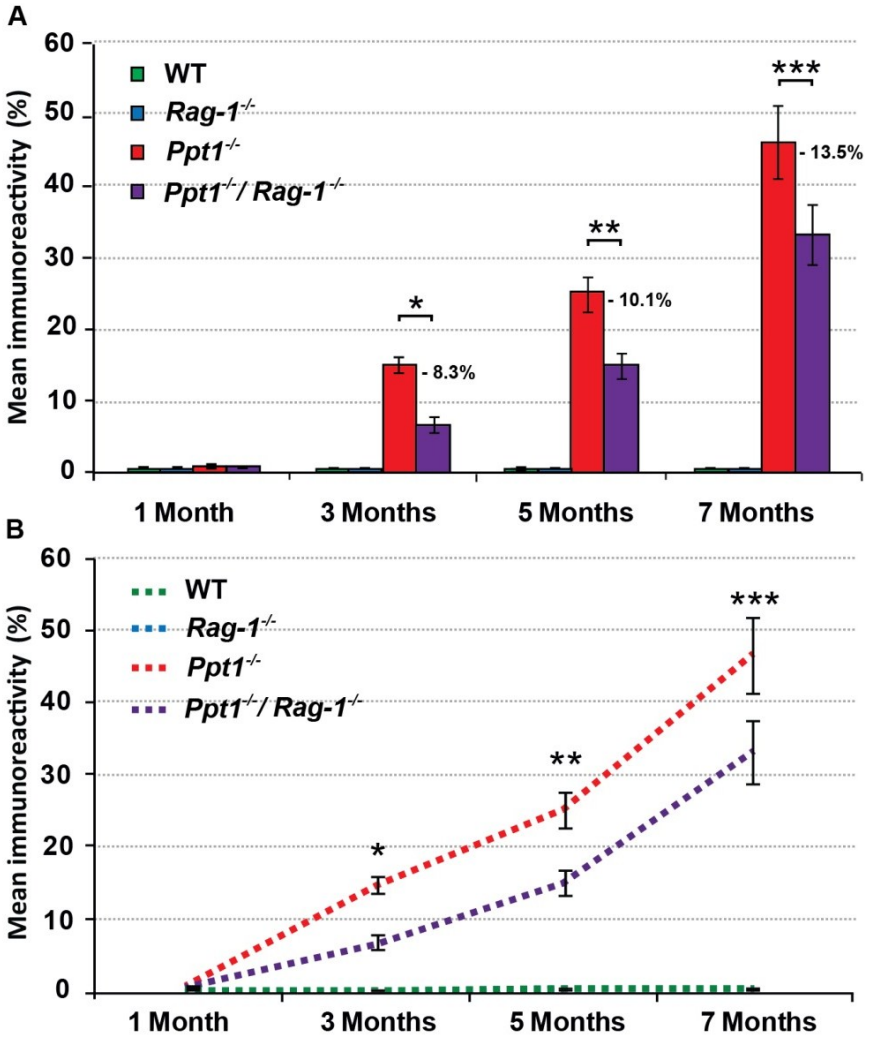

Figure 37. Reduced levels of microglial activation in the thalamus (*VPM/VPL*) of *Ppt1*$^{-/-}$*/Rag-1*$^{-/-}$ double knockout mice. Thresholding image analysis reveals that the mean level of CD68 immunoreactivity in double knockout mice was significantly reduced at 3, 5 and 7 months of age, compared to *Ppt1*$^{-/-}$ mice. In contrast, almost no CD68 immunoreactivity was detected in the thalamus of either *Rag-1*$^{-/-}$ or wildtype (WT) mice. Thus, *Ppt1*$^{-/-}$ and *Ppt1*$^{-/-}$*/Rag-1*$^{-/-}$ mice displayed significantly increased CD68 immunoreactivity from 3 months onwards compared to WT animals. The same data are presented as both histogram (A) and line graph (B). Percentages indicate differences between *Ppt1*$^{-/-}$ and *Ppt1*$^{-/-}$*/Rag-1*$^{-/-}$ mice. Statistics: Two-way ANOVA with Bonferroni post hoc test, *p<0.05, **p<0.01, ***p<0.001. Data shown as mean ± SEM, n = 5.

significantly increased levels of CD68 staining could be observed from 3 months onwards, compared to wildtype mice, which steadily increased in intensity with age and reached a maximum level at 7 months of age. From 3 months onwards significantly less CD68 immunoreactivity could be detected in the thalamus of *Ppt1*$^{-/-}$*/Rag-1*$^{-/-}$ double knockout mice, compared to single knockout *Ppt1*$^{-/-}$ mice. This difference became more pronounced with the progression of the disease, with 8.3% less immunoreactivity at 3 months, 10.1% less staining at 5 months and 13.5% less staining at 7 months of age in the double knockout mice. However, the shape of the curve of CD68 immunoreactivity over time, indicative of the rate of disease

progression, did not appear to change in these double knockout mice. These data suggest that microglial activation in the thalamus seemed to be weaker and delayed in the immune deficient *Ppt1*$^{-/-}$/*Rag-1*$^{-/-}$ mice, but followed the same general pattern over time as that seen in *Ppt1*$^{-/-}$ mice.

d) Attenuated microglia activation in the cortex of *Ppt1*$^{-/-}$/*Rag-1*$^{-/-}$ mice

In the somatosensory cortex (*S1BF*) of *Ppt1*$^{-/-}$ mice CD68+ve microglial activation could be observed from 3 months onwards (see **Figure 38**). At this time point in *Ppt1*$^{-/-}$ mice CD68 immunoreactivity was most pronounced in deeper layers, in particular within lamina VI, and subsequently microglial activation spread to involve the upper cortical layers of *S1BF* from 5 months of age onwards. At 7 months of age microglial activation could be detected throughout the entire somatosensory cortex of *Ppt1*$^{-/-}$ mice, with the most prominent bands of CD68+ve cells present in laminae II+III and VI (see **Figure 38A**).

At all ages examined, *Ppt1*$^{-/-}$/*Rag-1*$^{-/-}$ double knockout mice displayed delayed and reduced levels of microglial activation in *S1BF*, compared to single mutant *Ppt1*$^{-/-}$ mice (see **Figure 38A**). Whereas in *Ppt1*$^{-/-}$ mice significant microglial up-regulation of CD68 could be seen from 3 months onwards, in *Ppt1*$^{-/-}$/*Rag-1*$^{-/-}$ double knockout mice the first morphological indications of microglial activation could only just be detected at this time point. Similar to *Ppt1*$^{-/-}$ mice, this microglial activation started off in lamina VI of *S1BF* in *Ppt1*$^{-/-}$/*Rag-1*$^{-/-}$ double mutant mice and spread subsequently to involve more dorsal layers of the cortex. At 5 months of age only slightly elevated CD68 staining of microglia could be observed in these *Ppt1*$^{-/-}$/*Rag-1*$^{-/-}$ mice, compared to the markedly more pronounced staining evident in *Ppt1*$^{-/-}$ mice, indicative of a slowing of the innate immune response in these double mutant mice. However, at 7 months of age intense CD68+ve staining of microglia in *Ppt1*$^{-/-}$/*Rag-1*$^{-/-}$ double knockout mice had nearly reached the levels seen in *Ppt1*$^{-/-}$ mice. Many morphologically activated CD68+ve microglia were dispersed throughout the cortical mantle of double mutant mice at this time point, but in a much more homogenous and less laminar specific manner than was apparent in *Ppt1*$^{-/-}$ mice (see bottom right panel in **Figure 38A**). Direct comparison of the microglial morphology in lamina VI of the *S1BF* of both mutant mice (see **Figure 38B**), confirmed the delayed microglial activation of *Ppt1*$^{-/-}$/*Rag-1*$^{-/-}$ double knockout mice. Many intensely stained microglia with enlarged and round cell soma were seen in lamina VI of *Ppt1*$^{-/-}$ mice from 5 months onwards,

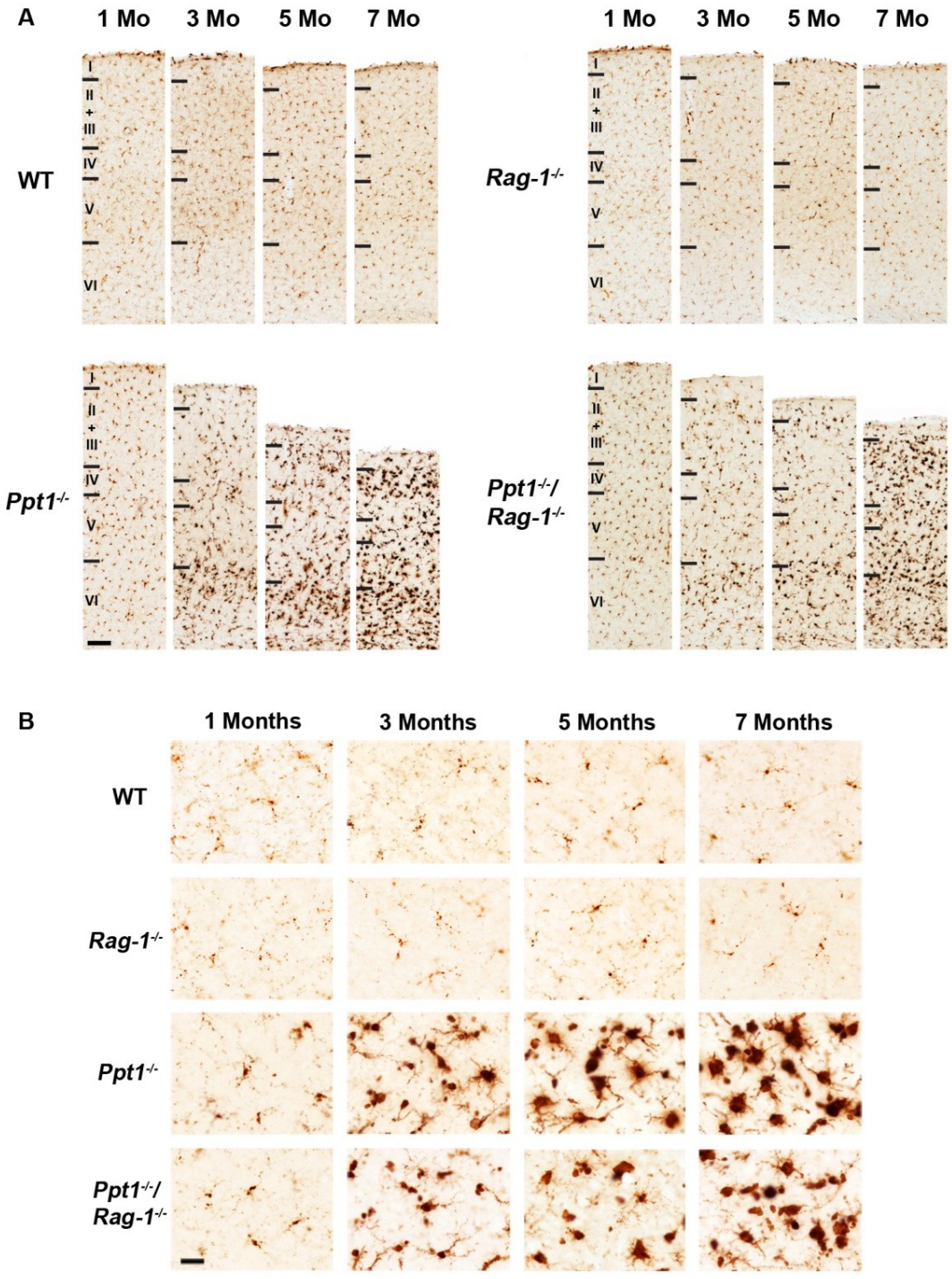

Figure 38. Progressive microglial activation in the somatosensory barrel field (*S1BF*) cortex of *Ppt1*$^{-/-}$ and *Ppt1*$^{-/-}$*/Rag-1*$^{-/-}$ double knockout mice. (see figure caption on next page)

Figure 38. Progressive microglial activation in the somatosensory barrel field (*S1BF*) cortex of *Ppt1*$^{-/-}$ and *Ppt1*$^{-/-}$/*Rag-1*$^{-/-}$ double knockout mice. (A) Immunohistochemical staining for the microglial marker CD68 in the *S1BF* of 1, 3, 5 and 7 month old mice revealed differences between *Ppt1*$^{-/-}$ and *Ppt1*$^{-/-}$/*Rag-1*$^{-/-}$ double knockout mice. *Ppt1*$^{-/-}$/*Rag-1*$^{-/-}$ double knockout mice clearly showed delayed and reduced microglial activation at all ages compared to *Ppt1*$^{-/-}$ mice. In *Ppt1*$^{-/-}$ mice intensely stained CD68 positive microglia were most prominent in deeper laminae (mainly layer VI) from 3 months of age onwards, but this microglial activation spread to upper layers and increased in intensity with disease progression. At 7 months of age widespread CD68 immunoreactivity was present throughout all layers, but most prominently in laminae II+III and VI. In contrast, in *Ppt1*$^{-/-}$/*Rag-1*$^{-/-}$ double knockout mice only weak microglial activation could be seen in lamina VI at 3 and 5 months of age, leading to microglial activation spread homogenously throughout all layers at 7 months of age. Similar activation was absent in control animals (*Rag-1*$^{-/-}$, wildtype (WT)) where only quiescent microglial staining could be detected. Scale bar = 100 μm. (B) Higher magnification pictures of CD68+ve microglia in lamina VI of the *S1BF* of 1, 3, 5 and 7 month old mice revealed differences in cell morphology and activation between immunodeficient double and single *Ppt1* mutant mice. *Ppt1*$^{-/-}$/*Rag-1*$^{-/-}$ double knockout mice showed reduced microglial activation in lamina VI of the *S1BF* at all ages in terms of numbers, cell size, staining intensity and transformation into brain macrophages. Intensely stained microglia with an enlarged and rounded cell soma were seen in *Ppt1*$^{-/-}$ mice from 5 months onwards, whereas microglia in *Ppt1*$^{-/-}$/*Rag-1*$^{-/-}$ double knockout mice remained relatively smaller at all ages, with elongated microglial processes present on most cells until 7 months of age. Only quiescent microglia could be detected in 1 month INCL mice and control animals (*Rag-1*$^{-/-}$ and WT). Scale bar = 20 μm

whereas microglia in *Ppt1*$^{-/-}$/*Rag-1*$^{-/-}$ mice remained smaller, were less darkly stained and displayed more elongated cell processes at all ages (see third and fourth row of **Figure 38B**).

Quantification of CD68 immunoreactivity via thresholding image analysis verified the qualitative observations described above. Microglial activation in *S1BF* of single and double *Ppt1* mutant mice followed a similar distribution and age-related increase with disease progression, as was seen in the thalamus. However, this CD68 immunoreactivity was always at much lower levels in the cortex (see **Figure 39**). In *Ppt1*$^{-/-}$ mice slightly elevated CD68 immunoreactivity could already be detected at 1 month of age compared to wildtype (WT) mice, but this difference did not reach statistical significance. The first significant microglial activation in the *S1BF* of *Ppt1*$^{-/-}$ mice was evident from 3 months onwards, compared to wildtype animals. This difference in CD68 staining became more pronounced with age, reaching a maximum at 7 months of age. In double mutant mice the introduction of *Rag1* deficiency also proved to have an effect upon microglial activation in the cortex of *Ppt1*$^{-/-}$ mice. At 1 month of age only marginally less (0.4%) CD68 immunoreactivity could be detected in *Ppt1*$^{-/-}$/*Rag-1*$^{-/-}$ mice compared to *Ppt1*$^{-/-}$ mice, whereas at 3 months of age a mean reduction of 1.3% and at 5 months of age of 2.4% CD68 immunoreactivity per analysed image were observed. However, it was only at 5 months of age that these differences reached significant levels. At 7 months of age, both genotypes showed

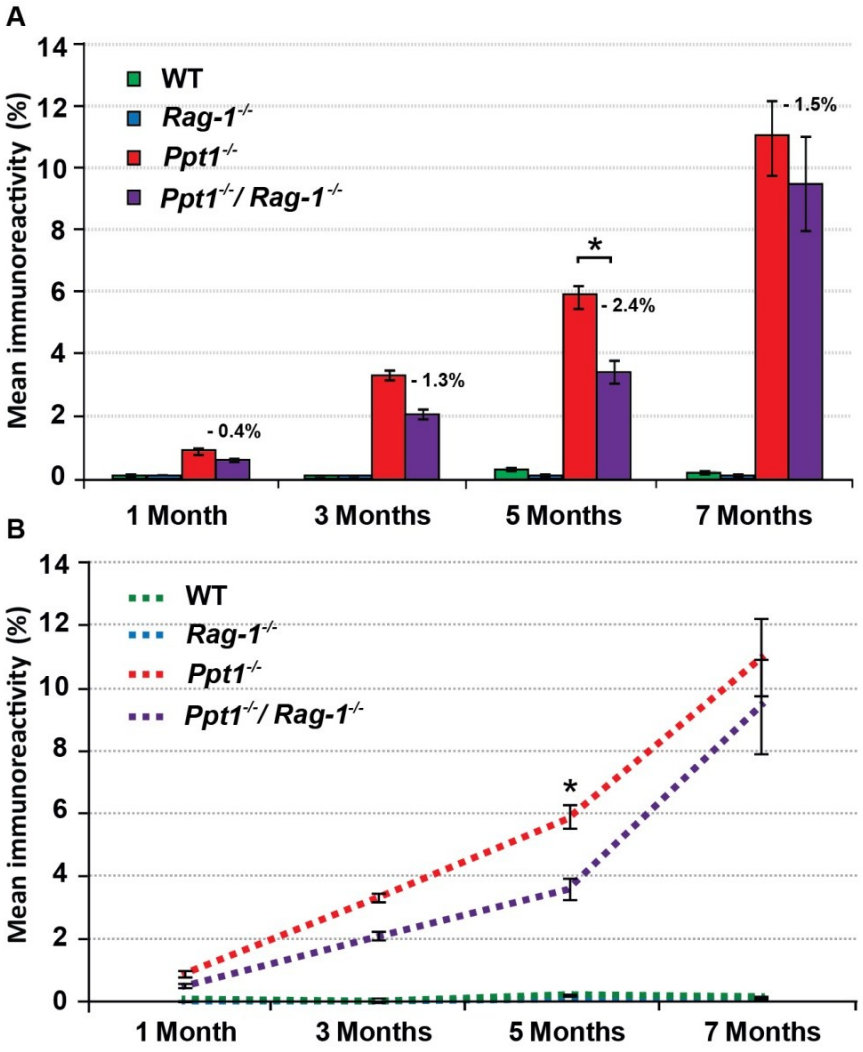

Figure 39. Reduced levels of microglial activation in the somatosensory barrel field (*S1BF*) cortex of *Ppt1*$^{-/-}$/*Rag-1*$^{-/-}$ double knockout mice. Thresholding image analysis reveals that the mean level of CD68 immunoreactivity in double knockout mice was marginally reduced at all ages, compared to *Ppt1*$^{-/-}$ mice, but these differences only reached significant levels at 5 months of age. In contrast, almost no CD68 immunoreactivity was detected in the thalamus of either *Rag-1*$^{-/-}$ or wildtype (WT) mice. As such, *Ppt1*$^{-/-}$ and *Ppt1*$^{-/-}$/*Rag-1*$^{-/-}$ mice displayed increased CD68 immunoreactivity from 1 month onwards compared to WT mice, but this difference only reached significant levels from 3 months onwards. The same data are presented as both histogram (A) and line graph (B). Percentages indicate differences between *Ppt1*$^{-/-}$ and *Ppt1*$^{-/-}$/*Rag-1*$^{-/-}$ mice. Statistics: Two-way ANOVA with Bonferroni post hoc test, *$p<0.05$. Data shown as mean ± SEM, n = 5.

similar levels of microglial activation with the reduction in CD68 immunoreactivity falling back to 1.5%. At this oldest time point, a higher variance prevented any statistical significance between the levels of CD68 staining between these genotypes.

Taken together, all our data of glial activation (see **Figure 33**, **Figure 35**, **Figure 37**, and **Figure 39**) revealed that microglial activation and astrocytosis become apparent in the thalamus as well as in the cortex at a similar early stage of disease progression, at 3 months of age. This coincides with the infiltration of lymphocytes (see **Figure 21** in

Chapter 3) and the first significant neuron loss (see **Figure 40**) in this brain region, highlighting its importance as a key stage in the pathogenesis of INCL. Furthermore, the absence of the adaptive immune system in the *Ppt1*$^{-/-}$/*Rag-1*$^{-/-}$ mice double knockout mice appeared to delay the microglial response in both regions to a relatively similar extent, but this effect is more evident in the thalamus, perhaps due to its higher levels of glial activation. Therefore, our data demonstrate that adaptive immune cells appear to have an enhancing effect on innate immune responses in the murine INCL brains.

4.3 Impact of *Rag-1* deficiency on neuron survival in *Ppt1*$^{-/-}$ mice

After establishing that the lack of adaptive immune cells attenuates the glial activation in *Ppt1*$^{-/-}$/*Rag-1*$^{-/-}$ double knockout mice, we next investigated if such differences in innate immune responses alter the previously described neurodegeneration in *Ppt1*$^{-/-}$ mice (Bible *et al.*, 2004; Kielar *et al.*, 2007).

a) Increased neuron survival in the thalamus of *Ppt1*$^{-/-}$/*Rag-1*$^{-/-}$ mice

Pronounced neuron loss in *VPM/VPL* could first be detected from 3 months onwards in *Ppt1*$^{-/-}$ mice, compared to age-matched wildtype mice (see **Figure 40**). At this time point, 57.6% less neurons were present in *Ppt1* deficient mice, compared to age-matched wildtype controls. At 5 months of age over 79 % of neurons were lost in these single mutant mice, while at 7 months of age only 5.2% of *VPM/VPL* relay neurons remain alive in this nucleus of the thalamus compared to age-matched controls. In addition to revealing the progressive loss of *VPM/VPL* neurons these data reveal that the greatest loss of these neurons occurs between 1 and 3 months of age, but at the later stages neuron loss continues at a much slower rate. These data stand in contrast to previous findings in INCL mice (Kielar *et al.*, 2007), in which neuron loss in the thalamic *VPM/VPL* nuclei have only been detected from 5 months onwards. This discrepancy is most likely explained by the usage of a different cohort of (putatively more affected) mice and in the different counting criteria that may be employed by individual investigators.

Knocking out the adaptive immune system in *Ppt1*$^{-/-}$ mice significantly improved the survival of *VPM/VPL* thalamic relay neurons in *Ppt1*$^{-/-}$/*Rag-1*$^{-/-}$ double knockout mice at 3 months of age, with 19.8% more neurons present than in *Ppt1*$^{-/-}$ mice (see **Figure 40**), a 62.1% survival rate compared to age-matched wildtype mice. However, this

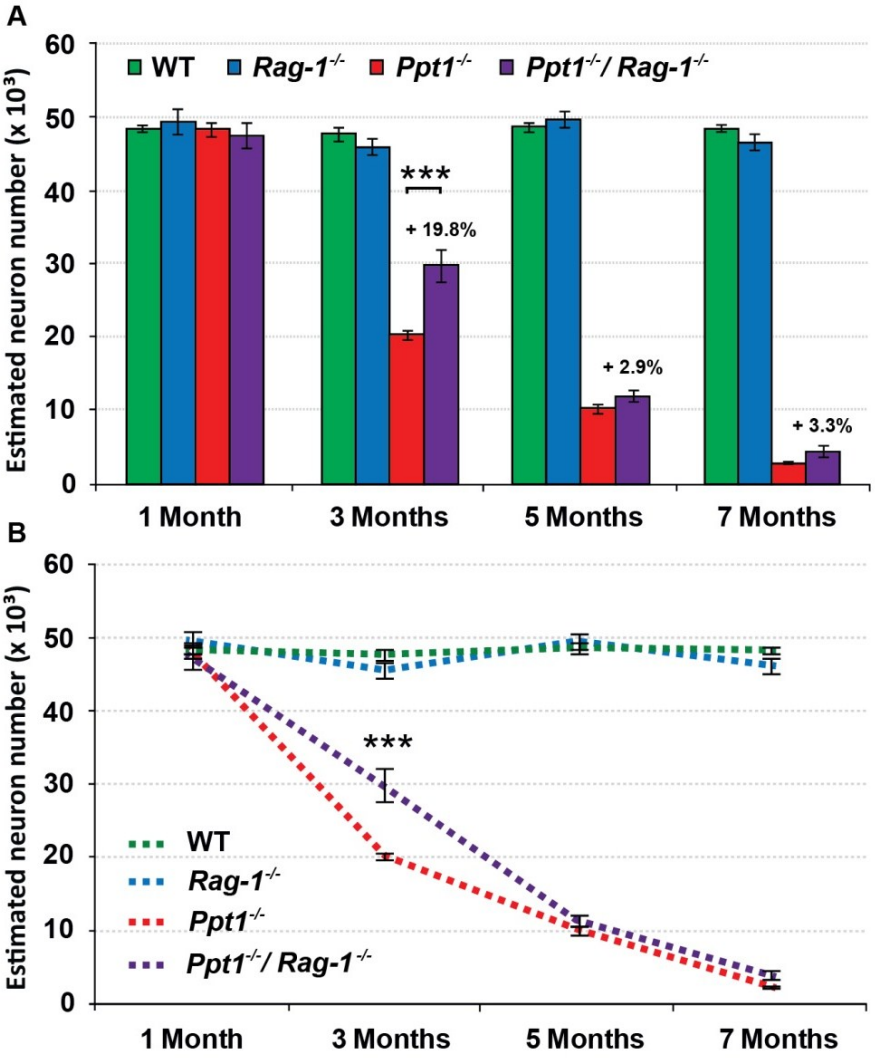

Figure 40. Progressive loss of thalamic (*VPM/VPL*) neurons in *Ppt1*$^{-/-}$ and *Ppt1*$^{-/-}$*/Rag-1*$^{-/-}$ mice. Unbiased optical fractionator estimates of number of Nissl stained thalamic relay neurons in the *ventral posterior nucleus* (*VPM/VPL*) of *Ppt1*$^{-/-}$, *Ppt1*$^{-/-}$*/Rag-1*$^{-/-}$, *Rag-1*$^{-/-}$ and age-matched wildtype (WT) control mice at different stages of disease progression. Significantly fewer *VPM/VPL* neurons were present in both single and double *Ppt1* mutant mice from 3 months onwards compared to WT mice, and continued to decline in number with increased age. Nonetheless, neuron loss was significantly slowed down in *Ppt1*$^{-/-}$*/Rag-1*$^{-/-}$ mice. Significantly more neurons were present in *Ppt1*$^{-/-}$*/Rag-1*$^{-/-}$ mice at 3 months compared to *Ppt1*$^{-/-}$ mice, but *VPM/VPL* neuron number in *Ppt1*$^{-/-}$*/Rag-1*$^{-/-}$ mice decreased to similar levels at later stages of the disease. *Rag-1*$^{-/-}$ and WT mice showed no significant difference in neuron numbers at any age. The same data are presented as both histogram (A) and line graph (B). Percentages indicate differences between *Ppt1*$^{-/-}$ and *Ppt1*$^{-/-}$*/Rag-1*$^{-/-}$ mice compared to age-matched WT mice. Statistics: Two-way ANOVA with Bonferroni post hoc test, ***$p<0.001$. Data shown as mean ± SEM, n = 5.

effect almost completely vanished at later stages of the disease with no significant difference being found subsequently between *Ppt1*$^{-/-}$ and *Ppt1*$^{-/-}$*/Rag-1*$^{-/-}$ mice. Indeed, only a minimal improvement in *VPM/VPL* neuron survival could be detected with only 2.9% more neurons at 5 months and 3.3% more neurons at 7 months of age in these double knockouts. Compared to age-matched wildtype mice this represents the survival of just 23.9% of these neurons at 5 months, and just 8.5% of *VPM/VPL*

neurons surviving at 7 months of age in *Ppt1*$^{-/-}$/*Rag-1*$^{-/-}$ double knockouts. In contrast, *VPM/VPL* neuron numbers in *Rag-1*$^{-/-}$ control mice did not significantly differ from wildtype animals at any age examined.

In summary, a lack of mature T- and B-cells, as a result of *Rag-1* deficiency, delays and slows down disease progression during its early stages in the somatosensory thalamus, one of the most affected brain structures in *Ppt1*$^{-/-}$ mice (Kielar *et al.*, 2007). However, this apparent slowing down of disease progression is abolished from 5 months onwards, when other pathologic driving forces appear to become more relevant. It appears that once a certain threshold of pathologic events is reached, the loss of *VPM/VPL* neurons is inevitable and rapidly catches up with the extent of neuron loss seen in *Ppt1* deficient mice (see **Figure 40**; (Kielar *et al.*, 2007)). Nevertheless, the adaptive immune system appears to accelerate the final outcome and blocking these responses may still have a beneficial effect in slowing disease progression. However, because the thalamus is the most and earliest affected region in the INCL brain, perhaps a more sustainable protective effect may be seen in less affected regions of the brain.

b) Increased neuron survival in the cortex of *Ppt1*$^{-/-}$/*Rag-1*$^{-/-}$ mice

VPM/VPL neurons relay somatosensory information to the barrel field cortex (*S1BF*), which also shows progressive neuron loss in *Ppt1*$^{-/-}$ mice, subsequent to events within the thalamus (Kielar *et al.*, 2007). Although originally omitted in this thesis due to time restrictions, similar optical fractionator counts have now been performed in the somatosensory cortex (*S1BF*) of 3, 5 and 7 month old mice of all genotypes by Steven Duckett, a MSc student in the PSDL. He demonstrated a significant improvement in the survival of lamina V *S1BF* neurons in *Ppt1*$^{-/-}$/*Rag-1*$^{-/-}$ mice at 5 months of age compared to single *Ppt1*$^{-/-}$ mice (see **Appendix II: Figure 79**). However, this difference was no longer apparent at 7 months of age. Therefore, the genetic removal of adaptive immune cells also reduced neuron loss in the cortical *S1BF* sub-region, but in a delayed manner compared to events in the thalamus. However, as a prelude to performing more detailed counts of neuron survival in the cortex of *Ppt1*$^{-/-}$/*Rag-1*$^{-/-}$ double knockout mice, we also obtained cortical volume measurements and thickness measurements in the *S1BF* region (see next **section 4.4** below).

4.4 Impact of *Rag-1* deficiency on cortical atrophy in *Ppt1*$^{-/-}$ mice

In human INCL marked cortical atrophy has already been reported (Haltia *et al.*, 1973a), and in mice this happens in a regionally selective manner, being more pronounced in sensory than motor cortex and occurring at different times (Bible *et al.*, 2004; Kielar *et al.*, 2007). To determine the relative extent of cortical atrophy in immune deficient *Ppt1*$^{-/-}$/*Rag-1*$^{-/-}$ double knockout mice, we measured the entire cortical volume of all genotypes at all four ages in Nissl stained sections using the unbiased Cavalieri method (see **Figure 41**). Firstly, comparing *Ppt1*$^{-/-}$ mice to age-matched wildtype animals, there was a progressive reduction in overall cortical volume

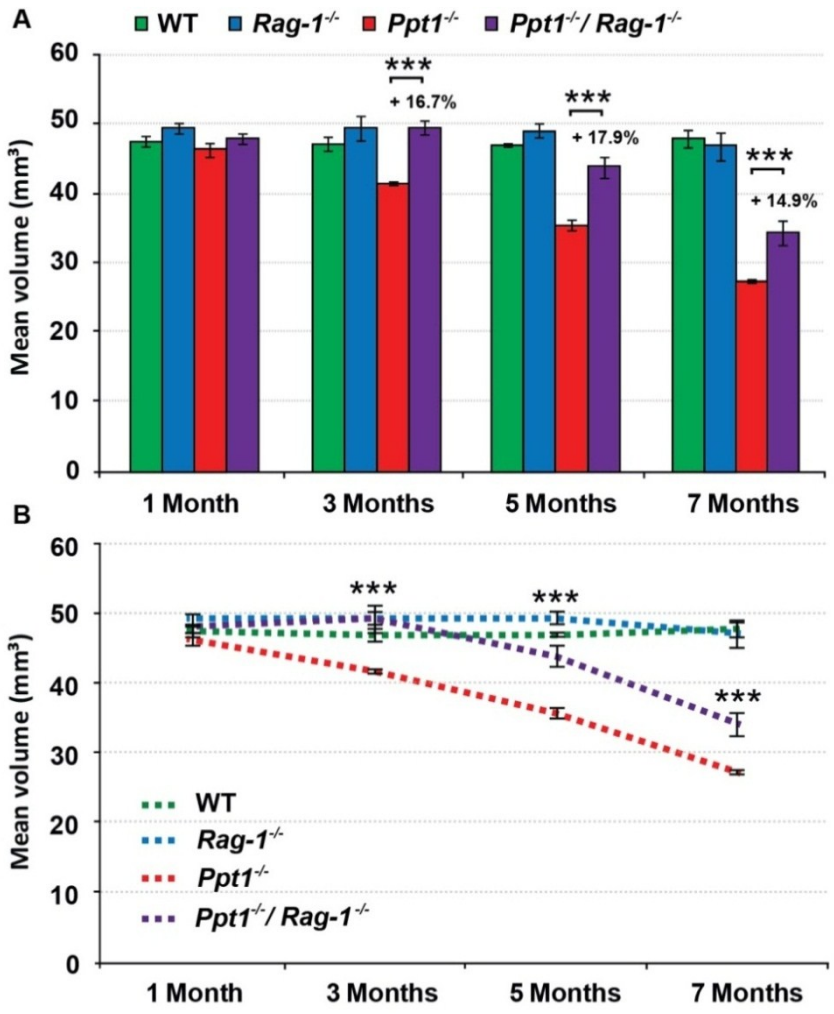

Figure 41. Cortical atrophy in *Ppt1*$^{-/-}$ and *Ppt1*$^{-/-}$/*Rag-1*$^{-/-}$ mice. Unbiased Cavalieri estimates of cortical volume of *Ppt1*$^{-/-}$, *Ppt1*$^{-/-}$/*Rag-1*$^{-/-}$, *Rag-1*$^{-/-}$ and age-matched wildtype (WT) control animals at different stages of disease progression. Cortical atrophy was significantly less pronounced in *Ppt1*$^{-/-}$/*Rag-1*$^{-/-}$ mice from 3 months onwards, compared to *Ppt1*$^{-/-}$ mice. Compared to WT mice, *Ppt1*$^{-/-}$ mice displayed cortical atrophy from 3 months onwards, whereas cortical volume in *Ppt1*$^{-/-}$/*Rag-1*$^{-/-}$ mice resembled that of WT mice until 5 months of age, and only showed significant atrophy at 7 months of age. *Rag-1*$^{-/-}$ and WT mice showed no significant difference in cortical volume at any age. The same data are presented as both histogram (A) and line graph (B). Percentages indicate differences between *Ppt1*$^{-/-}$ and *Ppt1*$^{-/-}$/*Rag-1*$^{-/-}$ mice compared to age-matched WT mice. Statistics: Two-way ANOVA with Bonferroni post hoc test, ***$p<0.001$. Data shown as mean ± SEM, n = 5.

in these mutant mice. From 3 months of age onwards the cortical volume was significantly reduced in *Ppt1*$^{-/-}$ mice with an 11.4% reduction at 3 months, a 23.8% reduction at 5 months and a 43.2% (almost half) reduction at 7 months of age. Disabling active T- and B-cells, lead to a significant improvement in cortical volume in *Ppt1*$^{-/-}$/*Rag-1*$^{-/-}$ double knockout mice from 3 months onwards. At 3 and 5 months of age no significant difference between wildtype and double knockout mice could be detected, which reflects a 16.7% and a 17.9% improvement in cortical volume compared to single *Ppt1*$^{-/-}$ knockout mice. Yet, at 7 months the cortical volume of these immune deficient *Ppt1*$^{-/-}$/*Rag-1*$^{-/-}$ double knockout mice was significantly reduced by 28.3% compared to age-matched WT control animals. However, even at this advanced time point these mice still exhibited a significantly (14.9%) larger cortex than age-matched *Ppt1*$^{-/-}$ mice.

To further investigate these findings of cortical atrophy we additionally measured the cortical thickness in *S1BF* (see **Figure 34** and **Figure 38** for representative pictures of *S1BF* thickness). From 3 months onwards significant cortical thinning in *S1BF* could be observed in INCL mice (see **Figure 42**). Starting off with a rather subtle, but significant 6.1% reduction in *S1BF* thickness in *Ppt1*$^{-/-}$ mice at 3 months of age, this significant difference increased to 11.5% thinning at 5 months, and to 19.7% thinning at 7 months of age compared to age-matched wildtype mice. These data suggest that the cortical thinning in the somatosensory cortex actually occurs earlier than was previously suggested in these mice (Kielar *et al.*, 2007).

Extending these measurements to *Ppt1*$^{-/-}$/*Rag-1*$^{-/-}$ double knockout and *Rag-1*$^{-/-}$ mice, we found that up to 5 months of age no significant cortical thinning could be detected in *Ppt1*$^{-/-}$/*Rag-1*$^{-/-}$ double knockouts compared to wildtype mice (see **Figure 34A** and **Figure 38A** for representative pictures, and quantification in **Figure 42**). Significant cortical atrophy only appeared at 7 months of age with 8.4% cortical thinning in *Ppt1*$^{-/-}$/*Rag-1*$^{-/-}$ mice compared to wildtype animals. In comparison to *Ppt1*$^{-/-}$ mice, the immune deficient *Ppt1*$^{-/-}$/*Rag-1*$^{-/-}$ mice showed significantly less cortical thinning from 3 months onwards with a mean difference of cortical thickness between these two mouse population of 7.2% at 3 months, 8.7% at 5 months and of 11.3% at 7 months of age compared to age-matched wildtype control values. These data suggest a significant improvement in the extent of thinning of *S1BF* by blocking the adaptive immune system.

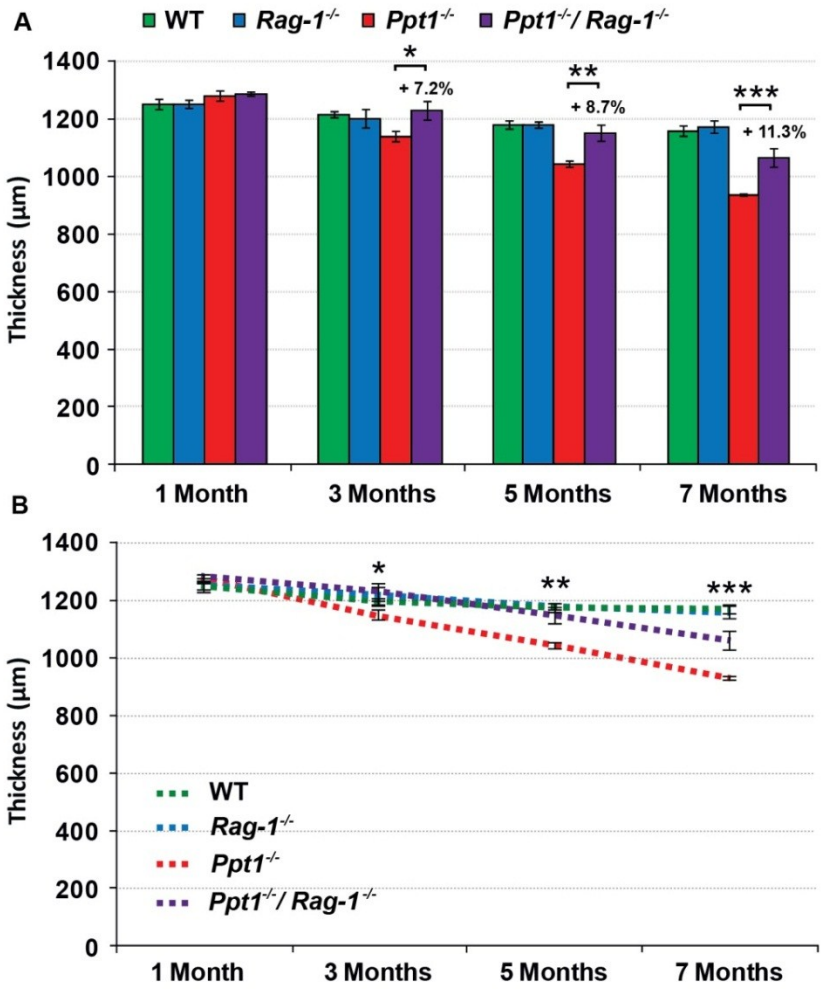

Figure 42. Progressive thinning of the somatosensory barrel field (*S1BF*) cortex in *Ppt1*$^{-/-}$ and *Ppt1*$^{-/-}$*/Rag-1*$^{-/-}$ mice. Cortical thickness measurements of *Ppt1*$^{-/-}$, *Ppt1*$^{-/-}$*/Rag-1*$^{-/-}$, *Rag-1*$^{-/-}$ and age-matched wildtype (WT) control mice at different stages of disease progression revealed progressive thinning of *S1BF*. Thinning of the cortical mantle of *S1BF* was significantly reduced in *Ppt1*$^{-/-}$*/Rag-1*$^{-/-}$ mice from 3 months onwards. Compared to WT mice, *Ppt1*$^{-/-}$ mice displayed significant cortical thinning in *S1BF* from 3 months onwards, whereas *S1BF* thickness in *Ppt1*$^{-/-}$*/Rag-1*$^{-/-}$ mice was not significantly different from that in WT mice until 7 months of age. *Rag-1*$^{-/-}$ and WT mice showed no significant difference in cortical volume at any age. The same data are presented as both histogram (A) and line graph (B). Percentages indicate differences between *Ppt1*$^{-/-}$ and *Ppt1*$^{-/-}$*/Rag-1*$^{-/-}$ mice compared to age-matched WT mice. Statistics: Two-way ANOVA with Bonferroni post hoc, *$p<0.05$, **$p<0.01$, ***$p<0.001$. Data shown as mean ± SEM, n = 5.

Taken together, these data suggest that blocking the adaptive immune system in *Ppt1*$^{-/-}$*/Rag-1*$^{-/-}$ mice results in a significant improvement of the overall cortical atrophy and particularly the cortical thinning in *S1BF* compared to single *Ppt1*$^{-/-}$ mice. Furthermore, it could be speculated that the adaptive inflammatory components make a greater contribution to pathogenesis in less affected regions like the cortex compared to the thalamus. However, alternatively, this apparently greater improvement on disease pathogenesis in the cortex could also simply be a result of the less pronounced

influence of Ppt1 deficiency upon cortical regions. These different possibilities shall be discussed in more detail in **Chapter 7**.

4.5 Increased lifespan in *Ppt1*$^{-/-}$/*Rag-1*$^{-/-}$ mice

Lastly, to determine the influence of *Rag-1* deficiency upon the lifespan of *Ppt1*$^{-/-}$ mice our collaborators in Würzburg, Germany, compared the lifespan of *Ppt1*$^{-/-}$ mice and *Ppt1*$^{-/-}$/*Rag-1*$^{-/-}$ mice. This analysis revealed that *Ppt1*$^{-/-}$/*Rag-1*$^{-/-}$ double knockout mice had a prolonged life span living 265 days, which is approximately 8% longer than *Ppt1*$^{-/-}$ mice that have an average lifespan of 245 days (unpublished data, J Groh, University of Würzburg, Germany). These findings, together with the improvement in pathological phenotypes in the brain of the *Ppt1*$^{-/-}$/*Rag-1*$^{-/-}$ double knockout mice suggest that removing the adaptive immune response has beneficial effects in this murine model of INCL.

4.6 Summary and discussion

The data presented in this chapter not only reveal new information about the nature and extent of glial activation in *Ppt1*$^{-/-}$ mice, but also provide evidence that cells of the adaptive immune system actively contribute to the pathogenesis of INCL (see also **Table 9**, **Table 10** and **Figure 43** for a summary overview).

Table 9. Summary of the comparison between *Ppt1*$^{-/-}$ and WT mice. Table was based on all experiments described in **Chapter 4**. In the left column: "type of analysis", across the top: "age of mice". Symbols: = no difference, ↑ significant increase, ↓ significant decrease, = (↑) increasing trend without significance, = (↓) decreasing trend without significance.

		1 Month	3 Months	5 Months	7 Months
Brain weight		=	=	↓	↓
Astrocytosis	***Thalamus***	=	↑	↑	↑
	S1BF	=	↑	↑	↑
Microglial activation	***Thalamus***	=	↑	↑	↑
	S1BF	= (↓)	↑	↑	↑
Neuronal survival		=	↓	↓	↓
Cortical thickness	***S1BF***	=	↓	↓	↓
Cortical volume		=	↓	↓	↓

Table 10. Summary of the comparison between *Ppt1*$^{-/-}$ and *Ppt1*$^{-/-}$*/Rag-1*$^{-/-}$ mice. Table was based on all experiments described in **Chapter 4**. In the left column: "type of analysis", across the top: "age of mice". Symbols: **=** no difference, ↑ significant increase, ↓ significant decrease, = (↑) increasing trend without significance, = (↓) decreasing trend without significance.

		1 Month	3 Months	5 Months	7 Months
Brain weight		=	=	↑	= (↑)
Astrocytosis	***Thalamus***	=	↓	↓	= (↓)
	S1BF	=	= (↓)	= (↓)	=
Microglial activation	***Thalamus***	=	↓	↓	↓
	S1BF	= (↓)	= (↓)	↓	= (↓)
Neuronal survival		=	↑	=	=
Cortical thickness	***S1BF***	=	↑	↑	↑
Cortical volume		=	↑	↑	↑

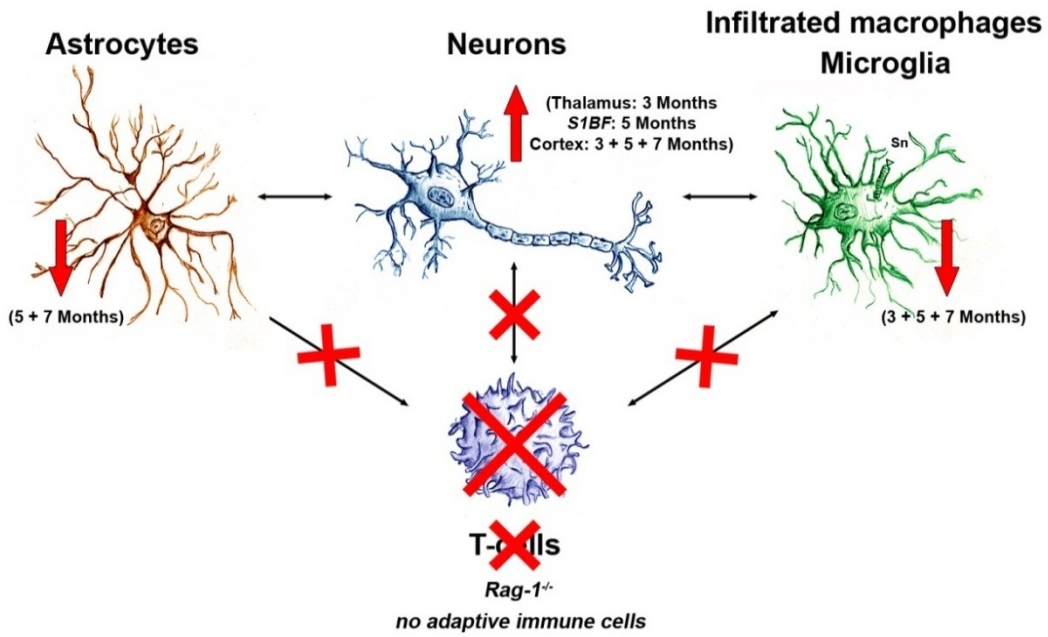

Figure 43. Schematic summary of altered phenotypes in the brain of *Ppt1*$^{-/-}$*/Rag-1*$^{-/-}$ mice. We characterised astrocytosis (illustrated as 'astrocytes'), microglial activation (illustrated as 'infiltrated macrophages, microglia') and neuron survival (illustrated as 'neurons') in *Ppt1*$^{-/-}$*/Rag-1*$^{-/-}$ mice. As a consequence of the *Rag-1* deficiency, no adaptive immune cells (T- and B-cells) were in the body and thus no interactions between T-cells and other cell types in the brain can occur in *Ppt1*$^{-/-}$*/Rag-1*$^{-/-}$ mice (B-cells are not depicted since they have not yet been described in *Ppt1*$^{-/-}$ mouse brains). Their absence results in decreased microglial activation at 3, 5 and 7 months of age; decreased astrocytosis at 5 and 7 months of age; and increased neuron survival at 3 months in the thalamus and at 5 months in the primary somatosensory barrel field (*S1BF*) cortex (summarised as 'cortex'). Additionally, cortical volume and *S1BF* cortical thickness are increased at 3, 5 and 7 months of age. Overall, the lack of adaptive immune cells delays disease progression in *Ppt1*$^{-/-}$*/Rag-1*$^{-/-}$ mice.

a) Early pathology in *Ppt1*$^{-/-}$ mice

Astrocytosis and microglial activation are characteristic features in the neuropathology of Infantile NCL mice (Bible *et al.*, 2004; Kielar *et al.*, 2007; Macauley *et al.*, 2009). We have confirmed and extended the previous descriptions of glial activation from these mice (Bible *et al.*, 2004; Kielar *et al.*, 2007), by identifying an earlier onset of glial activation and neuronal loss that is already underway at 3 months of age.

In contrast to our previous studies, which were restricted to using F4/80 as a microglial marker (Bible *et al.*, 2004; Kielar *et al.*, 2007), our data using CD68 immunostaining revealed an earlier and more pronounced microglial activation in the brains of *Ppt1*$^{-/-}$ mice than had previously been described at 5 months of age (Kielar *et al.*, 2007). Indeed, we could demonstrate that marked microglial activation in the thalamus was already present at 3 months of age, together with the first evidence of laminar specific microglial activation in *S1BF* at this age (see **Figure 36, Figure 37** and **Figure 38**). Remarkably in this cortical region there was a suggestion of microglial activation having already begun at 1 month of age, (see **Figure 38B** and **Figure 39**). This striking difference between the apparent onset of microglial activation in *Ppt1*$^{-/-}$ mice, simply by using a different marker, highlights the importance of using more than one antigen to investigate such reactive changes. The consequence is that we have to consider that microglia may play a role at much earlier time points in INCL pathogenesis than had been assumed previously. It was thought that microglia only became activated in *Ppt1*$^{-/-}$ mice once neuron loss was already underway (Kielar *et al.*, 2007), but our new data raise the possibility of an earlier involvement in disease progression and it will be important to determine whether this is a positive or negative contribution to pathogenesis. Regarding astrocytosis, similar to microglial activation, first indications of elevated GFAP immunoreactivity could be detected as early as 1 month of age in the thalamus and in *S1BF* of *Ppt1*$^{-/-}$ mice (see **Figure 32** and **Figure 34**), but significant astrocytosis was only detected from 3 months onwards in the present study (see **Figure 33** and **Figure 35**). These findings are consistent with previous studies that demonstrated GFAP+ve up-regulation in *Ppt1*$^{-/-}$ mice from the same time point (3 months) onwards (Kielar *et al.*, 2007; Macauley *et al.*, 2011). Taken together, our new data from *Ppt1*$^{-/-}$ mice reveal that both astrocytosis and microglial activation appear to start in the thalamus and in *S1BF* at 3 months of age, highlighting this as a key stage in disease progression.

Another key finding of this study is that neuron loss in the thalamus of *Ppt1*$^{-/-}$ mice isalready underway at 3 months of age and that this loss becomes more pronounced with disease progression (see **Figure 40**). These data are again different to previous reports of thalamic neuron loss in these mice (Kielar *et al.*, 2007), in which significant neuron loss in *VPM/VPL* was only found from 5 months of age onwards. There are two main reasons to potentially explain this difference. Firstly, these counts were made by different observers who may apply different criteria when making stereological cell counts from Nissl stained sections. For instance, two different investigators are likely to apply different criteria for what will be counted as a neuron during sampling, for which reason it is of uppermost importance that each analysis is performed by only one investigator. Secondly, and more importantly, natural variation in the rate of disease progression between different cohorts of mice could account for these observed differences. Being kept in a different animal facility, the mice used in this study may have been affected earlier than those in the (Kielar *et al.*, 2007) study due to different food regimes, litter conditions which may potentially influence their phenotypes. Such potential differences are exaggerated further by small sampling sizes. In our study, the n of 5 as a sampling size of the entire population may be sufficient for statistical comparisons, but in reality reflects a relatively small sample size. However, such compromises are often necessary due to high animal costs and time taken to perform these studies.

Our new data also shed further light on the relative timing of neuron loss and glial activation, suggesting that these events actually occur at the same time (see **Figure 33**, **Figure 35**, **Figure 37**, **Figure 39** and **Figure 40**). These data suggest there is no prior activation of the innate immune response before neuron loss occurs in these mice, leaving the unanswered question of which is the primary effect. Does neuron loss cause glial up-regulation and T-cell infiltration or do the glial cells and/or T-cells cause neuronal death subsequently or are they independent events that are triggered by an (as yet) unidentified pathological trigger? Recently it has been shown that synaptic changes and altered cytokine expression occur before 3 months of age in *Ppt1*$^{-/-}$ mice (Kielar *et al.*, 2009). These data suggest that sometime between 1 and 3 months of age a switch, or a threshold, must be reached to initiate immune reactions or/and neuronal loss at the same time. Speculatively, *Ppt1* deficiency seems to be tolerated at early stages of the disease, but eventually manifests itself firstly in neurons by axonal and synaptic rearrangements which in turn activate microglia and astrocytes, as repair

mechanisms of the brain (Graeber and Streit, 2010; Sofroniew and Vinters, 2010). However, because the disturbance caused by *Ppt1* deficiency persists, a self-enhancing cycle of immune activation is set in motion leading to chronic neurodegeneration (Gao and Hong, 2008). These immune activations incorporate on the one hand astrocytosis and microglial activation, but on the other hand, as demonstrated in **Chapter 3**, also include adaptive immune cell infiltration.

b) Adaptive immune cells accelerate pathogenesis of *Ppt1*$^{-/-}$ mice

The most significant finding presented in this chapter is that the adaptive part of the immune system appears to have an enhancing effect on astrocytosis and microglial activation and to accelerate neuron loss. By genetically removing functioning T- and B-cells, we could reduce the degree of innate immune activation, as well as delay neuronal loss in INCL mice, and even prolong the life span of *Ppt1*$^{-/-}$ mice.

Our data revealed that the timing of reactive changes was altered in *Ppt1*$^{-/-}$/*Rag-1*$^{-/-}$ double knockouts, with astrocytosis and microglial activation both being relatively reduced in the thalamus of these mice from 3 months onwards (see **Figure 33** and **Figure 37**). Nevertheless, by end stage of the disease, at 7 months, the astrocyte response appeared to have caught up and reached similar levels to that seen in *Ppt1*$^{-/-}$ mice, whereas microglial activation remained at lower levels throughout all age groups. Comparing the relative effects on astrocytosis and microglial activation in *Ppt1*$^{-/-}$/*Rag-1*$^{-/-}$ mice, the adaptive immune response (T- and B-cells) appears to have a greater and more consistent influence on microglial activation (see **Figure 33** and **Figure 37**). This is particularly obvious when considering the cortical *S1BF* region. CD68+ve up-regulation was reduced at all ages in the *S1BF* cortex of *Ppt1*$^{-/-}$/*Rag-1*$^{-/-}$ mice (see **Figure 39**). The reduction in astrocytosis in *S1BF* was less pronounced and did not reach any significance in *Ppt1*$^{-/-}$/*Rag-1*$^{-/-}$ mice (see **Figure 35**), but nevertheless followed the same patterns and temporal sequences as in the thalamus (see **Figure 33**).

Thus, it appears that the lack of T- (and B-) cells did not reverse or stop the neuronal death, but instead slowed it down (see **Figure 40**). This improved phenotype of immune deficient *Ppt1*$^{-/-}$ mice is consistent with similar findings of other studies using the *Rag-1* deficiency in myelin-degenerative disease models (Ip *et al.*, 2006; Kroner *et al.*, 2010), which are also caused by a single genetic mutation and lead to chronic neurodegenerative phenotypes similar to the NCLs. These studies demonstrated that

secondary adaptive immune reactions (particularly CD8+ve T-cells) can be of clear pathological significance. However, in the present study this improvement vanished at 5 and 7 months of age, indicating that other driving forces must be responsible for the neurodegeneration seen in *Ppt1*$^{-/-}$/*Rag-1*$^{-/-}$ mice at these time points. These forces may include the continued Ppt1 deficiency, innate immune reactions or other (yet) unidentified mechanisms. It could be speculated that the thalamic *VPM/VPL* nuclei are too severely affected to be capable of being rescued at the later stages of the disease. Although most of the neurons in the thalamus are dead at this point, it may be possible to produce a greater improvement in other less affected brain regions, for example the cortex. Additional data of cortical neuron counts (S Duckett MSc student in PSDL, see **Appendix II: Figure 79**) in *Ppt1*$^{-/-}$/*Rag-1*$^{-/-}$ mice confirmed this suggestion showing an improved survival of *S1BF* neurons in these mice at 5 months of age. These recent findings confirmed our previous expectations based on the cortical thickness and volume measurements that adaptive immune cells (most likely the T-cell infiltration from 3 months onwards) also play a significant role in disease deterioration in the cortex. Not only did we observe increased *S1BF* thickness, but also less overall cortical atrophy in *Ppt1*$^{-/-}$/*Rag-1*$^{-/-}$ double knockouts (see **Figure 41** and **Figure 42**). As a side note, the extent and impact of infiltrating macrophages has not been quantified in our *Ppt1*$^{-/-}$/*Rag-1*$^{-/-}$ mice, although they (being undistinguishable from activated CD68+ve microglia) may also influence the attenuation of disease phenotypes in the brain. This issue shall be examined in more detail in **Chapter 5**.

c) Significance of findings

The studies in this chapter have demonstrated that neuroinflammation, and in particular the adaptive immune responses, is a key feature of Infantile NCL. Genetic removal of the adaptive immune cells slowed down disease progression, but did not stop it. These data indicate that besides the adaptive immune cells, other disease driving forces must be in place. These may include innate immune reactions with exaggerated microglial activation or astrocytosis, other infiltrated immune cells like macrophages, other (yet) unidentified events in the periphery and brain or simply the persistent *Ppt1* deficiency of every cell type in the brain and body. However, since the adaptive immune responses do clearly exert a negative influence upon disease progression, we are confident that our findings may pave the way for disease attenuating therapeutic approaches in the future. This suggestion is supported by the moderately improved life span of immune deficient *Ppt1*$^{-/-}$ mice reported by our

collaborators (J Groh, University of Würzburg, unpublished data and personal communication). Because the basis for successful therapeutic interventions will depend upon a better understanding of inflammatory events and their relevance to disease progression, our data, as proof of principle studies, form the basis for potential immunosuppressive therapies.

Chapter 5

Sialoadhesin deficient *Ppt1*$^{-/-}$ mice

In the previous chapter we demonstrated the influence of the adaptive immune response upon the neurodegenerative processes that occur in murine Infantile NCL. At the same time, we obtained more detail about the nature of the innate immune response that occurs in the early stages of this disease. Besides astrocytosis and microglial activation, other innate immune cells are also recruited to inflammatory sites within the brain (Andersson *et al.*, 1992; Ousman and David, 2000; Hendriks *et al.*, 2005). These may include dendritic cells or neutrophils (although their infiltration may vary depending on CNS injury and/or BBB integrity (Perry *et al.*, 1995; Schnell *et al.*, 1999; Campbell *et al.*, 2008; Sayed *et al.*, 2010) but, in particular peripheral macrophages infiltrate the brain parenchyma (Andersson *et al.*, 1992; Greter *et al.*, 2005; Hendriks *et al.*, 2005; King *et al.*, 2009; Mildner *et al.*, 2009; Prinz *et al.*, 2011). These immune cells interact with other cells in the brain and influence the inflammatory response (Stoll and Jander, 1999; Hendriks *et al.*, 2005; Carson *et al.*, 2006a). Therefore, we hypothesised that altering the binding ability of infiltrated macrophages may have an impact on disease outcome and progression. The binding protein sialoadhesin (Sn) is a potential candidate to be important in such cell-cell communication. Indeed, in proteolipid protein (PLP) overexpressing mouse models of myelin-neurodegenerative conditions the lack of Sn can have an (attenuating) impact on brain and nerve pathology (Kobsar *et al.*, 2006; Ip *et al.*, 2007). As described in **Chapter 1** (see **section 1.11b**), Sn, as a cell adhesion molecule, is found on the surface of macrophages in lymphoid tissues (particularly in spleen, lymph nodes) and the adrenal gland, but is absent in the brain parenchyma under healthy conditions (Dijkstra *et al.*, 1985; Crocker and Gordon, 1986; Perry *et al.*, 1992; van den Berg *et al.*, 2001). However, in the case of inflammation, injury or a BBB breach of any sort, Sn is expressed on infiltrating macrophages, as well as nearby microglia in the brain parenchyma (Perry *et al.*, 1992). The exact role of Sn is still under debate, but this protein may function as a positive regulator of adaptive immune responses (Crocker and Redelinghuys, 2008) by interacting with CD4+ve T-regulatory cells (Wu *et al.*, 2009), and CD8+ve T-cells (Muerkoster *et al.*, 1999; Ip *et al.*, 2007) or, as most recently suggested, it may represent a general inflammatory and autoimmunity regulatory molecule via recognition of self and non-self (see **section 1.11b** in **Chapter 1** and (Klaas and Crocker, 2012)).

This chapter aims to elucidate the importance of the crosstalk between macrophages and other immune cells in the brain, in particular during inflammatory or

neurodegenerative events. After knocking out the macrophage binding protein Sn in Infantile NCL mice, we compared *Ppt1*$^{-/-}$/*Sn*$^{-/-}$ mice with regular *Ppt1*$^{-/-}$ mice. Consequently, the same analyses, as described in the previous chapter for *Ppt1*$^{-/-}$/*Rag-1*$^{-/-}$ mice, have also been performed in *Ppt1*$^{-/-}$/*Sn*$^{-/-}$ mice. Besides brain weight measurements, astrocytosis, microglial activation, neuron survival and cortical atrophy were measured in the somatosensory thalamus (*VPM/VPL*) and cortex (*S1BF*), which have been shown to be the most affected brain regions in *Ppt1*$^{-/-}$ mice (Kielar *et al.*, 2007). By performing these analyses at 1, 3, 5 and 7 months of age we could compare the progressive phenotypes of *Ppt1*$^{-/-}$/*Sn*$^{-/-}$ mice with *Ppt1*$^{-/-}$ and the corresponding *Sn*$^{-/-}$ and wildtype control mice.

5.1 Sialoadhesin positive cells in the CNS of *Ppt1*$^{-/-}$ mice

Firstly, to investigate where and when Sn is expressed in *Ppt1*$^{-/-}$ and healthy control brains, we stained sections from these mice at all ages (n=2) for Sn, which is also referred to as CD169. Because Sn is only expressed in the brain on infiltrating macrophages, and microglia in vicinity of their infiltration or at inflammatory sites (Perry *et al.*, 1992; Klaas and Crocker, 2012), we would hypothesise that CD169 can be used as a distinctive marker for identifying region-specific inflammation sites in the brain.

CD169 immunostaining revealed very few immunoreactive cells in 1 month old mutant or wildtype brains. An exception was in the basal forebrain of 1 month old wildtype mice, where scattered Sn+ve microglia with ramified processes were present along the anterior commissure, the ventral parts of the globus pallidus and its rostral extension towards the bed nucleus of the stria terminalis (data not shown). Otherwise, in wildtype mice CD169 immunoreactive cells were mainly found in the meninges and in the choroid plexus lining the wall of the ventricles, which is consistent with previous observations (Perry *et al.*, 1992) (see **Figure 44E**). However, elongated CD169+ve cells could be detected in the brain parenchyma along many brain vessels, indicating that Sn+ve macrophages are also present in the perivascular space of healthy control mice (see **Figure 44E**).

In *Ppt1*$^{-/-}$ mice, many CD169+ve cells could be detected from 3 months onwards in various brain regions, which were characterised according to (Paxinos and Franklin, 2001) (see next paragraphs below and **Table 11** for a detailed summary of the

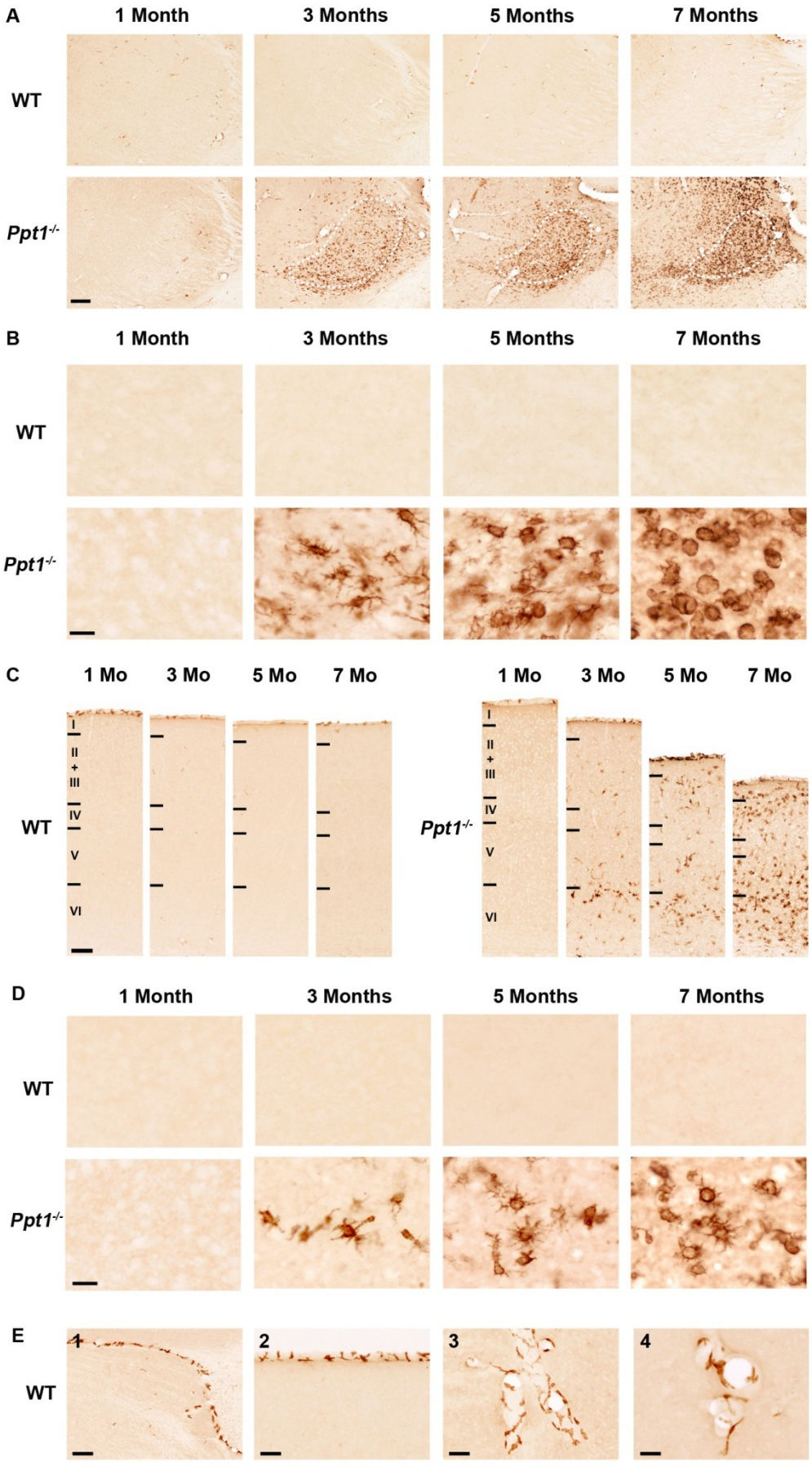

Figure 44. Progressive expression of sialoadhesin positive cells in the thalamus and the somatosensory barrel field (*S1BF*) cortex of *Ppt1*$^{-/-}$ mice. (see figure caption on next page)

Figure 44. Progressive expression of sialoadhesin positive cells in the thalamus and the somatosensory barrel field (*S1BF*) cortex of *Ppt1*$^{-/-}$ mice. (A) Immunohistochemical staining for the peripheral macrophage/microglial marker CD169 (sialoadhesin) in the thalamus of 1, 3, 5 and 7 month old mice revealed localised CD169 expression within the *ventral posterior nucleus* (*VPM/VPL*) (---) of *Ppt1*$^{-/-}$ mice. Distinct macrophage-like cell staining could be observed in mutant mice, whereas similar staining was absent in wildtype (WT) mice. Scale bar = 200 μm. (B) Higher magnification pictures of the thalamus of *Ppt1*$^{-/-}$ and WT mice at 1, 3, 5 and 7 months of age demonstrated morphological changes of CD169+ve cells with disease progression. Whereas at 3 months of age, CD169+ve cells display small cell soma with elongated processes resembling partially activated microglia, at 5 and 7 months of age predominantly macrophage-like cells with round cell bodies, and short or absent processes were detected. Scale bar = 20 μm. (C) Immunohistochemical staining for CD169 in the somatosensory cortex *S1BF* of 1, 3, 5 and 7 month old *Ppt1*$^{-/-}$ and WT mice revealed CD169 positive cells in *Ppt1*$^{-/-}$ mice most prominent in deeper laminae (mainly layer VI) from 3 months of age onwards. CD169 immunoreactive microglia/macrophages spread to more dorsal layers and increased in intensity with disease progression. At 7 months of age widespread CD169 immunoreactivity was present throughout all layers, but most prominently in laminae II+III and VI. Similar staining was absent in WT animals where only CD169+ve macrophages in the meninges could be detected. Scale bar = 100 μm. (D) Higher magnification pictures of lamina VI of the *S1BF* of *Ppt1*$^{-/-}$ and WT mice at 1, 3, 5 and 7 months of age revealed CD169+ve cells in mutant mice from 3 months onwards. CD169+ve cells with darkly stained, small cell bodies resembling both microglia with and macrophage-like cells without elongated processes were seen in lamina VI at 3 months of age. With disease progression, the proportion of macrophage-like cells with round, darkly stained cell soma and no, or only short, processes increased at 5 months of age, eventually representing the predominant cell morphology at 7 months of age. Scale bar = 20 μm. (E) Examples of CD169+ve cell staining in WT mice. CD169+ve macrophages were found in the choroid plexus along the ventricle walls (along the fimbria of the hippocampus and the *dorsal lateral geniculate nucleus* (*LGNd*) in E1), in the meninges (E2), but also surrounding parenchymal blood vessel as perivascular macrophages (E3 and E4). Scale bars in (E1, E2) = 50 μm, in (E3, E4) = 25 μm.

distribution of CD169 immunoreactivity in *Ppt1*$^{-/-}$ mice over time). Generally, the quantity and intensity of CD169 immunoreactivity increased with disease progression and reached its maximal level at 7 months of age (see **Figure 44**). At each time point, cells with various morphologies stained for CD169, resembling microglia with ramified cell processes, as well as macrophages without any cell processes (see examples in **Figure 44B** and **Figure 44D**). Since via CD169 staining alone these two cell types cannot be distinguished, we subsequently will refer to cells with elongated and ramified processes as 'microglia' and round cells without any or only short processes as 'macrophages' (see **Figure 15** in **Chapter 3** for the morphological criteria used to distinguish between these cell types).

a) CD169 expression in 1 month old *Ppt1*$^{-/-}$ brains

Similar to wildtype mice, the majority of CD169+ve cells were found at the borders of the brain parenchyma (meninges, choroid plexus, ventricle walls) and in the perivascular space around the blood vessels of 1 month old *Ppt1*$^{-/-}$ mice. These CD169+ve cells displayed macrophage-like cell morphology with either round, amoeboid or crescent-shaped soma along the meninges or vermicular, elongated cells

Table 11. Detailed summary of the distribution of CD169 immunoreactivity in *Ppt1*$^{-/-}$ mice over time. Brains of 1, 3, 5 and 7 month old *Ppt1*$^{-/-}$ and wildtype mice were stained for CD169 and a list of brain nuclei showing CD169 immunoreactivity in *Ppt1*$^{-/-}$ mouse brains has been compiled. For each nucleus the extent of microglial (**Mic**) and macrophage (**Mϕ**) activation have been recorded, whereby cells with distinct processes were classified as 'microglia'; round intensely immunoreactive cells without processes were defined as 'macrophages' (see also **Figure 15** for distinction). Symbols: '·' = no immunoreactivity, **(+)** = traces of cell-staining, **+** = faintly stained cells, **++** = pronounced cell-staining, **+++** = intense staining of activated cells. Colour intensity reflects the activation status of each cell type (green = microglia, red = macrophages) to visualise the changes of CD169 immunoreactivity over time. I, II, III, IV, V or VI = lamina I-VI. Nuclei definition according to (Paxinos and Franklin, 2001).

Brain region/nucleus		1 Month			3 Months			5 Months			7 Months		
Thalamus		**Mic**	**Mϕ**	**Comments**	**Mic**	**Mϕ**	**Comments**	**Mic**	**Mϕ**	**Comments**	**Mic**	**Mϕ**	**Comments**
VPM/VPL	Ventral posteromedial and posterolateral thalamic nucleus	·	·		++	+		++	++		·	+++	
VL	Ventrolateral thalamic nucleus	·	·		+	+		+	++		+++	++	
PO	Posterior thalamic nuclei	·	·		+	+		+	++		+++	++	
VM	Ventromedial thalamic nucleus	·	·		·	·		(+)	·		++	+	
LGNd	Dorsal lateral geniculate nucleus	·	·		++	·		++	+		·	+++	
AM	Anteromedial thalamic nucleus	·	·		·	·		+	+		·	+++	
AD	Anterodorsal thalamic nucleus	·	·		·	·		++	·		+++	++	
AV	Anteroventral thalamic nucleus	·	·		(+)	·		++	+		++	+++	
AVDM/VL	Anteroventral thalamic nucleus, dorsomedial/ventrolateral part	·	·		+	·		++	++		·	+++	
CM	Central medial thalamic nucleus	·	·		+	+		++	+		++	++	
LPLR/MR	lateral posterior thalamic nucleus, laterorostral/mediocaudal part	·	·		++	·		++	+		·	+++	
MD	Mediodorsal thalamic nucleus	·	·		·	·		+	·		++	·	
MDM/L	Mediodorsal thalamic nuclei, medial/lateral part	·	·		+	·		++	+		+++	++	
MGV/D/M	Medial geniculate nucleus, ventral/dorsal/medial part	·	·		++	+		+	++		·	+++	
Re	Reuniens thalamic nucleus	·	·		·	·		++	·		+++	++	
Rh	Rhomboic thalamic nucleus	·	·		·	·		+	+		+	+++	
ZIV/D	Zona incerta	·	·		·	·		++	·		+++	+	

Brain region/nucleus		1 Month			3 Months			5 Months			7 Months		
Mid brain		**Mic**	**Mϕ**	**Comments**	**Mic**	**Mϕ**	**Comments**	**Mic**	**Mϕ**	**Comments**	**Mic**	**Mϕ**	**Comments**
RMC	Red nucleus, magnocellular part	·	·		·	·		+	·		+	+	
RPC	Red nucleus, parvicellular part	·	·		(+)	·		+	·		++	+	
Hippocampus													
CA1	Cornu Ammonis 1, subfield of hippocampus	·	·		·	·		+	+		+++	++	
CA2	Cornu Ammonis 2, subfield of hippocampus	·	·		·	·		·	·		+	+	
CA3	Cornu Ammonis 3, subfield of hippocampus	·	·		·	·		·	·		+	+	
DG	Dentate gyrus	·	·		·	·		·	·		++	+	
S	Subiculum	·	·		·	·		·	·		+	+	
Amygdala													
AAD	Anterior amygdaloid area	·	·		+	·		+	·		+++	·	
AHipM	Amygdalohippocampal area	·	·		(+)	·		+	·		+	+	
APir	Amygdalopiriform transition area	·	·		·	·		+	·		+	+	
PMCo	Posteromedial cortical amygdaloid nucleus	·	·		·	·		(+)	·		+		
BLA	Basolateral amygdaloid nucleus	·	·		(+)	·		(+)	·		+	+	
CeC/M	Central amygdaloid nucleus, capsular part/medial division	+	·		++	·		+++	·		+++	+	
Basal ganglia													
Cpu	Caudate putamen	(+)	·	(near amygdala)	+	+		++	+		+++	+	
LGP	Lateral globus pallidus	·	·		+	·		++	·		++	+	
MGP	Medial globus pallidus	·	·		(+)	·		+	·		++	+	

Brain region/nucleus		1 Month			3 Months			5 Months			7 Months		
Basel ganglia		**Mic**	**Mϕ**	**Comments**	**Mic**	**Mϕ**	**Comments**	**Mic**	**Mϕ**	**Comments**	**Mic**	**Mϕ**	**Comments**
SN	Substantia nigra	·	·		+	·		++	·		++	+	
VP	Ventral pallidum	+	·		++	·		++	·		+++	+	
Cortex													
Cortex	General pattern	·	·		+	·	(VI)	+	+	(VI & II/III) more II than III	++	+++	(VI & V & II/III)
S1BF	Primary somatosensory barrel field	·	·		+	+	(VI)	++	+	(VI)	++	++	(mainly VI & all)
S1HL/S1FL	Primary somatosensory cortex, hind-/forelimb region	·	·		+	+	(VI)	++	+	(VI/II/III)	+++	++	(II/III & VI)
S2	Secondary somatosensory cortex	·	·		+	+	(VI)	++	+	(VI & a bit in II/III)	++	++	(II & VI)
Au1/AuD/V	Auditory cortex (primary/secondary auditory cortex, dorsal/ventral)	·	·		+	·	(VI)	++	+	(VI & II/III)	++	++	(II/III & VI a bit)
AID/V	Agranular insular cortex, dorsal/ventral	·	·		(+)	·		++	+	(VI & a bit in II/III)	++	++	(VI & II/III)
V1	Visual cortex	·	·		+	·	all a bit	++	+	(mainly II & all)	+++	++	(II/III & VI a bit)
M1	Motor cortex 1	·	·		+	+	(VI & all a bit)	++	+	(VI & II)	++	++	(VI & II/III)
M2	Motor cortex 2	·	·		+	+	(VI & all a bit)	++	+	(VI & II & all)	+++	++	(VI & II/III)
RSA	The retrosplenial agranular cortex	·	·		+	+	(V & a bit VI)	++	++	(II/III & V & all a bit)	·	+++	(II/III & all) caudally more activated
RSG	The retrosplenial granular cortex	·	·		++	+	(V & a bit VI)	+++	++	(II/III & V & all a bit)	·	+++	(II/III & all) caudally more activated
Cig1/2	Cingulate cortex area 1/2	·	·		++	·	(V)	++	+	(VI/II/III)	+++	+++	(mainly II/III & all)
Pir	Piriform cortex	·	·		(+)	·	(III)	++	+	(mainly II/a bit III)	++	++	(mainly II (Mϕ) & lll)
VO/LO	Ventral/lateral orbital cortex	·	·		(+)	·		+	++		++	++	
LEnt	Lateral entorhinal cortex	·	·		·	·		+	+	(VI & V)	++	+	(all layers)
DEn	Dorsal endopiriform nucleus	·	·		(+)	·		+	+		++	++	
VEn	Ventral endopiriform nucleus	·	·		·	·		(+)	·		+	+	

Brain region/nucleus		1 Month			3 Months			5 Months			7 Months		
Hypothalamus		**Mic**	**Mϕ**	**Comments**	**Mic**	**Mϕ**	**Comments**	**Mic**	**Mϕ**	**Comments**	**Mic**	**Mϕ**	**Comments**
IPACM/L	Interstitial nucleus of posterior limb of anterior commissure, med./lat. part	+	·		++	·		++	·		+++	·	
MCPO	Magnocellular preoptic nucleus	(+)	·		+	·		++	·		+++	+	
HDB	Nucleus of horizontal limb of the diagonal band	(+)	·		+	·		++	·		+++	+	
Pons & Medulla													
Pons	General pattern	·	·		+	·	(ventral)	++	+	(ventral)	+++	+	(middle/ventral)
Pr5	Principal sensory trigeminal nucleus	·	·		++	·		+++	+		+++	++	
VLL	Ventral nucleus of lateral lemniscus	·	·		+	·		++	·		++	++	
RtTg	Reticulotegmental nucleus of the pons	·	·		++	·		++	+		+++	++	
CIC	Central nucleus of the inferior colliculus	·	·		+	·		++	+		+++	++	
ECIC	External cortex of the inferior colliculus	·	·		+	·		++	·		++	+	
Pn	Pontine nuclei	·	·		·	·		+	·		++	++	
LDTg	Laterodorsal tegmental nucleus	·	·		+	·		+	+		+	++	
Mo5	Motor trigeminal nucleus	·	·		+	·		+	·		+++	.	
Olfactory bulb													
OB	Olfactory bulb	·	·		+	+		++	++		+++	++	
EPI	External plexiform layer of the olfactory bulb	·	·		+	+		++	++		+++	++	
GRO	Granular cell layer of the olfactory bulb	·	·		+	+		++	++		+++	++	
DTT	Dorsal tenia tecta	·	·		·	·		++	+		++	++	

wrapping themselves around blood vessels in the parenchyma (as seen in **Figure 44E** in WT mice). In addition, faintly stained CD169+ve microglia were present in the basal forebrain and in the ventral parts of the *caudate putamen* (striatum) (data not shown). The distribution of these CD169 immunoreactive cells extended over several nuclei, being present in parts of the *interstitial nucleus of the posterior limb of the anterior commissure* (*IPACL* and *IPACM*), within the ventral parts of the *caudate putamen* (striatum) and *globus pallidus* (*GP*) and the *central amygdaloid nucleus* (*CeM* and *CeC*). The distribution of these cells was in relatively close proximity to the *anterior commissure* and did not extend into the caudal parts of the *amygdala*. These findings suggest an early inflammatory reaction that is already underway at 1 month of age in these brain regions of *Ppt1*$^{-/-}$ mice, but since CD169+ve cells were found in similar locations in 1 month old wildtype mice, an unknown stimulus specific to this brain region could also be a possible explanation.

b) CD169 expression in 3 month old *Ppt1*$^{-/-}$ mice

At 3 months of age, distinct CD169 immunoreactivity could be detected on macrophage and/or microglial cells in several regions of the brain parenchyma of *Ppt1*$^{-/-}$ mice. Most prominently the thalamic *ventral posteromedial* and *posterolateral nuclei* (*VPM/VPL*, but most activated in *VPL*) displayed CD169+ve cells which resembled activated microglia with long and ramified processes, but also scattered round brain-macrophage-like cells (see **Figure 44A** and **Figure 44B**). CD169+ve macrophage/microglial activation was also seen in other nuclei of the thalamus, namely in the *medial geniculate nucleus* (MGV and MGD) and the *dorsal lateral geniculate nucleus* (*LGNd*), albeit to a lower extent than in *VPM/VPL*. Interestingly, in the same basal forebrain regions which showed first signs of CD169 up-regulation in 1 month old *Ppt1*$^{-/-}$ mice, more pronounced microglial activation could now be detected at 3 months of age. These CD169+ve cells were mostly microglia with ramified and elongated processes, besides some scattered cells with more brain-macrophage like morphology. As at 1 month of age, the distribution of this activation was not confined to one nucleus and its spread into caudal brain regions correlated with the presence of the *anterior commissure* (*AC*) or the *interstitial nucleus of the posterior limb of the anterior commissure* (IPAC). Compared to 1 month old *Ppt1*$^{-/-}$ mice, besides in the *central amygdaloid nucleus* (*CeC*), CD169 immunoreactivity additionally spread to the *basolateral amygdaloid nucleus* (*BLA*) and the *anterior amygdaloid area* (*AAD*) (data not shown). However, CD169 immunoreactivity could be also detected in more rostral parts of the

brain. In the olfactory bulb the first traces of microglial activation were noticeable, and the *caudate putamen* (striatum) was scattered with isolated CD169+ve macrophages/microglia. Likewise, weak CD169 immunoreactivity was also detected in the caudal parts of the brain, particularly in the *substantia nigra*, *laterodorsal tegmental nucleus* (*LDTg*) (which sends cholinergic projections to the thalamus, *substantia nigra* and hippocampus), but also the *reticulotegmental nucleus of the pons* (*RtTg*) showed CD169+ve macrophage/microglial staining (data not shown). In the cortex, CD169+ve cells could generally be seen in lamina VI of most sub-regions, but particular pronounced staining was observed in the *motor cortex* (*M1* and *M2*), *cingulate cortex* (*Cg1* and *Cg2*), *somatosensory cortex* (*S1BF*, *S1Fl*, *S1HL* and *S2*) (see **Figure 44C** and **Figure 44D**) and the *retrosplenial granular cortex* (*RSG*). In the cortical *M1*, *M2* and *RSG* sub-regions CD169+ve cell staining could sometimes be detected in more dorsal laminae of the cortex. Additionally, occasional CD169+ve microglia were also found in the *auditory cortex* (*Au1* and *AuD*) and the *lateral orbital cortex* (*LO*) of 3 month old *Ppt1*$^{-/-}$ mice.

c) CD169 expression in 5 month old *Ppt1*$^{-/-}$ mice

As a consequence of disease progression, CD169 immunoreactivity intensified in those brain regions that were stained at earlier ages, but also spread to additional brain regions of 5 month old *Ppt1*$^{-/-}$ mice. At this stage of disease progression CD169+ve cells were widely present throughout the brain and took on a more activated and round macrophage-like morphology, with short or absent processes (see **Figure 44B** and **Figure 44D**). This was particularly obvious in the *VPM/VPL* nuclei of the thalamus, which contained many intensely stained cells with this morphology (see **Figure 44D**). Nevertheless, a series of specific brain regions also displayed intense CD169 immunoreactivity. Starting rostrally, the olfactory bulb was full of CD169+ve brain-macrophage-like cells, and macrophage/microglial CD169 immunoreactivity was seen throughout all sub-regions of the cortex with obvious brain-macrophage staining in lamina VI and II/III. This CD169+ve cell staining pattern was particularly pronounced in the *motor cortex* (M1 and M2), the *cingulate cortex* (*Cg1* and *Cg2*), the *primary somatosensory cortex* (*S1BF*, *S1HL*, *S1*) (see **Figure 44C** and **Figure 44D**), the *agranular insular cortex* (*AID* and *AIV*), the *retrosplenial granular cortex* (RSG), the *visual cortex* (*V1* and *V2*) and the *auditory cortex* (*Au1* and *AuD*). Interestingly, in the *piriform cortex* (*Pir*) almost no CD169+ve cell staining could be seen, apart from mainly macrophage-like (and occasional microglial) CD169 immunoreactivity in the *dorsal endopiriform nucleus* (*DEn*). In subcortical structures CD169 immunoreactive

microglial/macrophage-like cells were present in the *caudate putamen* (striatum), in many nuclei of the thalamus, namely the *anterodorsal* and *anteroventral thalamic nuclei* (*AV* and *AD*), the *ventral posterior nucleus* (*VPM/VPL*) (see **Figure 44A** and **Figure 44B**), with activation spreading into the *posterior thalamic nuclear group* (*PO*) and the *ventrolateral thalamic nucleus* (*VL*), the *mediodorsal thalamic nuclei* (MDM and MDL), the *central medial thalamic nucleus* (*CM*), the *dorsal lateral geniculate nucleus* (*LGNd*) as well as the *medial geniculate nucleus* (*MGM*) which all showed intensely stained CD169+ve brain-macrophages with round cell bodies. Besides these thalamic regions, for the first time CD169+ve brain-macrophages could also be detected in the hippocampus at this time point. However, their distribution was restricted to the *CA1* sub-field, with no cell staining evident in *CA2* to *CA4* (data not shown). Moreover, intensely CD169+ve microglial staining (with sporadically present macrophage-like cells) was also seen in the ventral parts of the striatum around the *interstitial nucleus of the posterior limb of the anterior commissure* (*IPACL* and *IPACM*) which mirrored the location of CD169+ve immunoreactivity already detected in 1 and 3 month old *Ppt1*$^{-/-}$ mice. More caudally, the *amygdalohippocampal area* (*AHipM*) and the *posteromedial cortical amygdaloid nucleus* (*PMCo*) all displayed microglial/macrophage-like cell staining (data not shown). Additionally, CD169+ve microglia/macrophages were present throughout the ventral parts of the pons, with particularly intensely stained brain-macrophage cells present in the *reticulotegmental nucleus of the pons* (*RtTg*) and macrophage/microglial cells in the *principal sensory trigeminal nucleus* (*Pr5VL*). Last but not least, in contrast to weakly stained microglial cells that were seen in the *substantia nigra*, the *external cortex of the inferior colliculus* (*ECIC*) and the *central nucleus of the inferior colliculus* (*CIC*) showed many activated CD169+ve brain-macrophages (data not shown).

d) CD169 expression in 7 month old *Ppt1*$^{-/-}$ brains

With a life expectancy of about 8 months (Gupta *et al.*, 2001), immune reactions in *Ppt1*$^{-/-}$ mice are actively progressing at 7 months of age. Correspondingly, high CD169 immunoreactivity was observed in most brain regions of *Ppt1*$^{-/-}$ mice at this age. In those brain regions like the *VPM/VPL* nuclei of the thalamus that had shown highest CD169 staining at earlier ages, there were many darkly stained brain-macrophages (see **Figure 44A** and **Figure 44B**), whereas in brain regions that displayed CD169 staining for the first time at this age there were many macrophage/microglial cells in various states of activation. However, besides an overall higher activation of cells compared to previous ages, CD169 immunoreactivity followed a region-specific distribution with

the following nuclei and brain regions displaying distinctive CD169+ve cell activation/infiltration. Most prominently highly activated brain-macrophages were observed in various nuclei of the thalamus. These included, similar to the CD169+ve expression in 5 month old *Ppt1*$^{-/-}$ mice, the *anterodorsal* and *anteroventral thalamic nuclei* (*AV* and *AD*), the *ventral posterior nuclei* (*VPM/VPL*) (see **Figure 44A**) with adjacent parts of the *posterior thalamic nuclear group* (*PO*) and the *ventrolateral thalamic nucleus* (*VL*), the *mediodorsal thalamic nuclei* (MDM and MDL), the *central medial thalamic nucleus* (*CM*), the *dorsal lateral geniculate nucleus* (*LGNd*) as well as the *medial geniculate nucleus* (*MGM*). In addition, intensely stained round CD169+ve macrophages could be found in the *reuniens thalamic nucleus* (*Re*), the *lateral posterior thalamic nucleus* (*LPLR*) and the *zona incerta* (ZIV) of 7 month old *Ppt1*$^{-/-}$ mice (data not shown). As already seen at 5 months of age, intensely stained CD169+ve brain-macrophages were present along the *CA1* sub-field of the hippocampus at 7 months of age, but these cells were more numerous and more intensely stained than in 5 month old *Ppt1*$^{-/-}$ mice (data not shown). The pronounced accumulation of macrophages /microglia in *CA1* is consistent with previous findings on pyramidal neuron and interneuron loss in this region of the hippocampus of 7 month old *Ppt1*$^{-/-}$ mice (Bible *et al.*, 2004; Mitchison *et al.*, 2004). Furthermore, the cortex of these mice displayed marked CD169+ve cell activation throughout many sub-regions with intensely stained brain-macrophages and some microglial cells found predominantly in laminae II/III and VI. This pattern of staining was clearly seen in the *motor cortex* (*M1* and *M2*), *cingulate cortex* (*Cg1* and *Cg2*), the *auditory cortex* (*Au1* and *AuV*) and the *visual cortex* (*V1*) in which laminae II/III showed the most intense staining. Interestingly, the *somatosensory cortex* presented a mixed picture with lamina VI most prominently (and only to a moderate extent laminae II/III) showing CD169 staining within *S1BF* (see **Figure 44C** and **Figure 44D**), whereas *S1HF*, *S1FL* and *S2* displayed the most pronounced CD169+ve brain-macrophage activation in laminae II/III, or to a similar extent in laminae VI and II/III. Similarly, the *piriform cortex* showed CD169 immunoreactivity mainly in the *dorsal and ventral endopiriform nuclei* (*DEn* and *VEn*) near the corpus callosum. In the olfactory bulb, the entire parenchyma was scattered with CD169+ve activated microglial cells, but intensely stained CD169+ve brain-macrophages filled the *mitral cell layer of the olfactory bulb* (*MI*) (data not shown). Furthermore, in the midbrain and pons there were many intensely stained CD169+ve brain-macrophages, as at previous ages, in the *reticulotegmental nucleus of the pons* (*RtTg*), *substantia nigra*, the *external cortex of the*

inferior colliculus (*ECIC*) and the *central nucleus of the inferior colliculus* (*CIC*). Additionally, besides a widespread CD169+ve microglial/macrophage activation in the ventral parts of the pons, the *magnocellular* and *parvicellular* part of the *red nucleus* (*RMC* and *RPC*), the *motor trigeminal nucleus* (*Mo5*) and dorsal parts of the *subiculum* of the hippocampus also displayed intensely CD169 stained round brain-macrophage-like cells (data not shown). In addition to widespread microglial/macrophage CD169 immunoreactivity in the *caudate putamen* (striatum), a specific accumulation of CD169+ve brain-macrophages could be detected in lateral parts of the striatum, ventral to the *S2* cortex and the *corpus callosum*, but only at the mid-levels of the forebrain. Last but not least, as detected throughout all age groups in *Ppt1*$^{-/-}$ mice, marked microglial/macrophage-like CD169 immunoreactivity was seen in the basal forebrain of 7 month old *Ppt1*$^{-/-}$ mice with CD169+ve cells in the *ventral pallidum* (*VP*), the *magnocellular preoptic nucleus* (*MCPO*) and the *nucleus of the horizontal limb of the diagonal band* (*HDB*), spreading dorsally around the *anterior commissure* into the *globus pallidus* (*GP*) and the *caudate putamen* (striatum) (data not shown).

In summary, this qualitative survey of CD169 expression in *Ppt1*$^{-/-}$ mice demonstrated that increasingly more Sn+ve macrophages and microglia are present in the brain parenchyma with on-going disease progression (see **Figure 44**). This is in contrast to wildtype mice in which CD169 immunoreactivity is restricted to macrophages at the brain margins and in the perivascular spaces (see **Figure 44E**). As a side note, similar Sn+ve cell staining (along the meninges and in the perivascular spaces) was also detectable in *Ppt1*$^{-/-}$ mice at all ages, in addition to the CD169 immunoreactivity in various brain nuclei, described above. However, the morphology of Sn+ve cells within the parenchyma changed according to disease progression. At 3 months of age Sn+ve cells displayed various morphologies with long and ramified processes, at 5 months of age Sn+ve cells take on a more activated and round macrophage-like morphology; resulting in round and darkly stained cells with almost no cell processes present at 7 months of age (see **Figure 44B** and **Figure 44D**). However, because it is impossible to distinguish between microglia and infiltrated macrophages with this CD169 marker, we must assume that at all ages a mix of macrophages and microglia are present in the thalamus. Nonetheless, according to their morphology, we can speculate that at earlier stages microglia with elongated processes and a subset of infiltrated macrophages are stained by this marker, but that predominately macrophages and brain macrophage-

like microglia were visible at the end stages of the disease (see also discussion in **Chapter 7**).

Taken together, our data confirmed that Sn is expressed by infiltrated macrophages and microglia in the vicinity of on-going inflammation in *Ppt1*$^{-/-}$ mice, consistent with sites observed previously in other models (Perry *et al.*, 1992; Klaas and Crocker, 2012).

To investigate the importance of these cell types to INCL pathogenesis and their interaction with other immune cells in the brain, we subsequently created Infantile NCL mice with Sn deficiency by crossing *Ppt1*$^{-/-}$ mice with *Sn*$^{-/-}$ mice (see **Chapter 2**). In the following parts of this chapter, these *Ppt1*$^{-/-}$/*Sn*$^{-/-}$ double knockouts will be compared to single mutant *Ppt1*$^{-/-}$ mice using the characteristic neuropathological landmarks of murine INCL (Bible *et al.*, 2004; Kielar *et al.*, 2007).

5.2 Reduced hemisphere mass of *Ppt1*$^{-/-}$ and *Ppt1*$^{-/-}$/*Sn*$^{-/-}$ mice

As a general indicator of mouse condition and potential pathological changes we measured the weight of each hemisphere, as we had performed in our analysis of *Ppt1*$^{-/-}$/*Rag-1*$^{-/-}$ double knockouts in **Chapter 4**, after paraformaldehyde fixation and including the olfactory bulb, but after removal of the cerebellum (see section **section 2.2** in **Chapter 2**). Although the comparison of average hemisphere weights is rather a crude measurement, the ongoing effects of neurodegeneration already became evident in *Ppt1*$^{-/-}$ and *Ppt1*$^{-/-}$/*Sn*$^{-/-}$ mice from 3 months onwards (see **Figure 45**). However, significant loss of hemisphere mass could only be detected from 5 months onwards. *Ppt1*$^{-/-}$/*Sn*$^{-/-}$ double knockouts lost 12.8% of hemisphere mass, compared to age-matched wildtype controls at 5 months of age, which represented a 5.5 % improvement in hemisphere mass *vs.* *Ppt1*$^{-/-}$ mice (although this difference was not significant). The double knockout hemispheres remained heavier than the corresponding *Ppt1* single knockout brain hemispheres from this time point onwards. At 7 months of age *Ppt1*$^{-/-}$/*Sn*$^{-/-}$ double knockout hemispheres showed 6.3% less weight loss compared to *Ppt1*$^{-/-}$ hemispheres, but were 19.1% lighter than those from wildtype mice. In summary, additionally knocking out Sn in *Ppt1*$^{-/-}$ mice marginally impacted hemisphere mass from 5 months onwards, but this improvement did not reach significant levels at any time point.

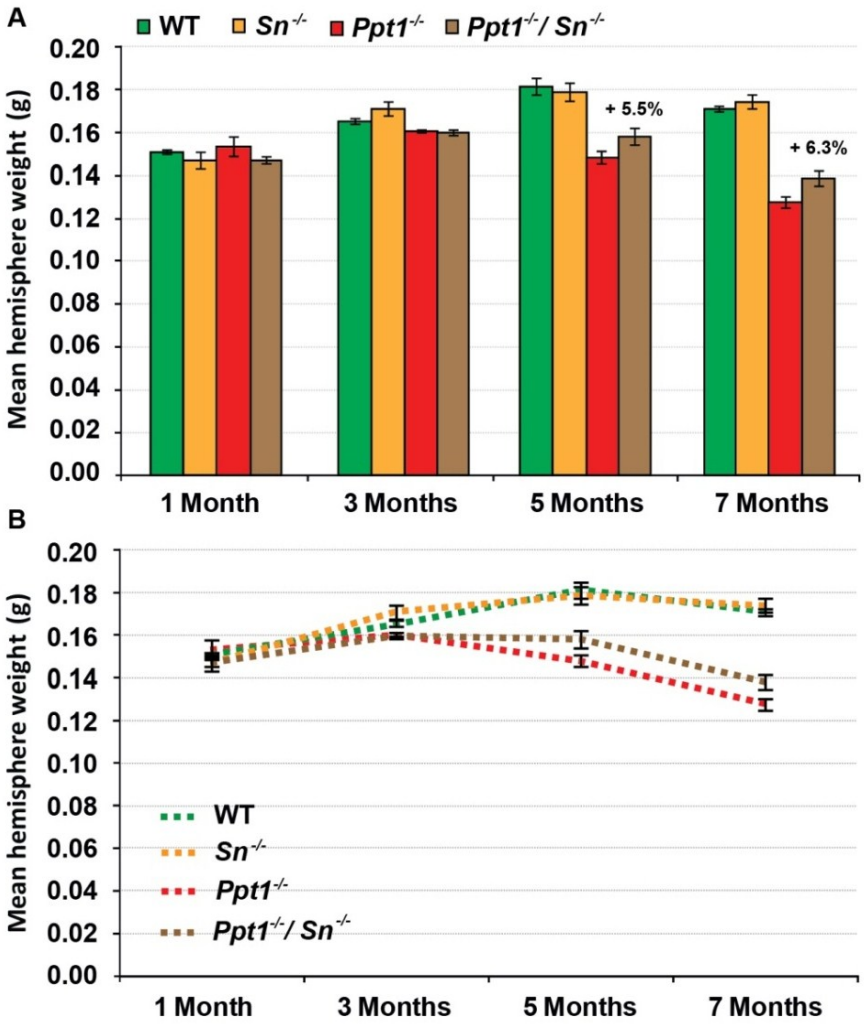

Figure 45. Marginally reduced loss of brain mass in *Ppt1*$^{-/-}$/*Sn*$^{-/-}$ mice. The weights of brain hemispheres from mice of each genotype (*Ppt1*$^{-/-}$, *Ppt1*$^{-/-}$/*Sn*$^{-/-}$, *Sn*$^{-/-}$ and wildtype) were measured after PFA fixation and removal of the cerebellum, but before further processing. From 5 months onwards there was a significant loss in hemisphere mass in *Ppt1*$^{-/-}$ and *Ppt1*$^{-/-}$/*Sn*$^{-/-}$ mice, compared to age-matched wildtype (WT) mice. Hemispheres from *Ppt1*$^{-/-}$/*Sn*$^{-/-}$ mice were marginally heavier than those from *Ppt1*$^{-/-}$ mice at 5 and 7 months of age, but these differences were not significant. WT and *Sn*$^{-/-}$ controls showed no significant differences in hemisphere mass at any age. The same data are presented as both histogram (A) and line graph (B). Percentages indicate differences between *Ppt1*$^{-/-}$ and *Ppt1*$^{-/-}$/*Sn*$^{-/-}$ mice in comparison to age-matched WT mice. Statistics: Two-way ANOVA with Bonferroni post hoc test. Data shown as mean ± SEM, n = 5.

5.3 Impact of *Sn* deficiency on reactive phenotypes in *Ppt1*$^{-/-}$ mice

As described in **Chapter 4** for *Ppt1*$^{-/-}$/ *Rag-1*$^{-/-}$ mice, we stained sections from *Ppt1*$^{-/-}$/*Sn*$^{-/-}$ mice, *Ppt1*$^{-/-}$, *Sn*$^{-/-}$ and wildtype control mice (n=5) at 1, 3, 5 and 7 months of age for the glial fibrillary acidic protein (GFAP) and the microglial marker CD68. Subsequently, we quantified the intensity of staining for these markers via thresholding image analysis. Based on the findings of (Kielar *et al.* 2007) we focused our analysis upon two severely affected components of the thalamocortical system: the thalamic *ventral posterior nucleus* (*VPM/VPL*) and the cortical *somatosensory barrier field* (*S1BF*) (see **Figure 10** in **Chapter 2**).

a) Enhanced astrocytosis in the thalamus of *Ppt1*$^{-/-}$/*Sn*$^{-/-}$ mice

As described in the previous **Chapter 4** (see **section 4.2a**), astrocytosis becomes clearly apparent in the thalamus of *Ppt1*$^{-/-}$ mice from 3 months onwards. A similar onset of astrocytosis was seen in *Ppt1*$^{-/-}$/*Sn*$^{-/-}$ mice (see **Figure 46A**). Although the first traces of astrocytosis could be detected at 1 month of age in *Ppt1*$^{-/-}$ mice, no appreciable activation of astrocytes was detected in *Ppt1*$^{-/-}$/*Sn*$^{-/-}$ mice at this time point. However, from 3 months onwards intensely GFAP immunoreactive astrocytes could be observed in the thalamus of both INCL mice. This astrocytosis continued to increase in intensity with disease progression. Interestingly, the astrocytes in the macrophage/microglia deficient *Ppt1*$^{-/-}$/*Sn*$^{-/-}$ mice appeared to be slightly more darkly stained at 3 and 5 months of age, and clearly showed more intense GFAP immunoreactivity at 7 months of age than that seen in age-matched *Ppt1*$^{-/-}$ mice (see **Figure 46**).

Higher magnification pictures demonstrated this phenotype of more pronounced astrocytosis in *Ppt1*$^{-/-}$/*Sn*$^{-/-}$ more clearly (see **Figure 46B**). The darkness and intensity of GFAP staining of astrocytes in the double knockout mice exceeded that in the single *Ppt1*$^{-/-}$ mice. Whereas at 3 months of age individual astrocytes with thickened processes could be distinguished, a continuous "carpet" of stained astrocytes could be seen by the end stage of the disease. This transition to a staining pattern that filled the entire thalamus was evident to a similar extent in both double and single knockout mice, but the density and intensity of GFAP staining was clearly greater in the *Ppt1*$^{-/-}$/*Sn*$^{-/-}$ mice.

Quantifying the intensity of GFAP immunoreactivity by thresholding image analysis defined the extent of this difference in astrocytosis between *Ppt1*$^{-/-}$/*Sn*$^{-/-}$ and *Ppt1*$^{-/-}$ mice (see **Figure 47**). Already at 3 months of age, a mean increase of 13.3% in GFAP+ve staining intensity in these double knockout mice could be observed, but this was not statistically significant due to the high variation between individual mice. A similar picture could be seen at 5 months of age, with a 3.4% increase in GFAP immunoreactivity in the double knockout mice, which again was not statistically significant. This is in contrast to the markedly increased level of astrocytosis in *Ppt1*$^{-/-}$/*Sn*$^{-/-}$ mice seen at 7 months of age, when the thalamus of these double knockout mice was completely filled with intensely stained astrocytes (see **Figure 46**), with more than 1.5 times or 30.6% more GFAP immunoreactivity than in *Ppt1*$^{-/-}$ mice. At this

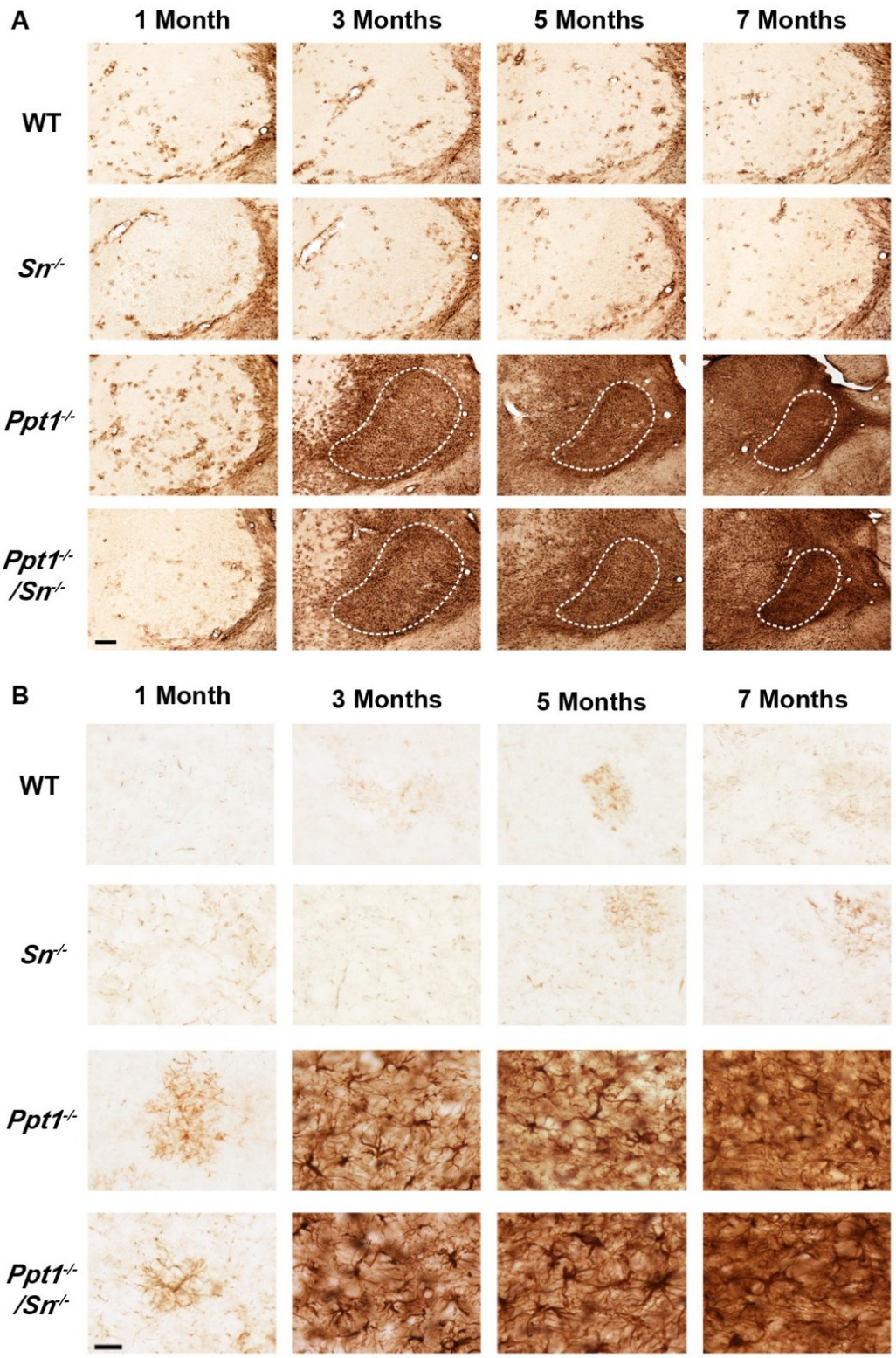

Figure 46. Progressive astrocytosis in the thalamus of *Ppt1*$^{-/-}$ and *Ppt1*$^{-/-}$/*Sn*$^{-/-}$ double knockout mice. (see figure caption on next page)

Figure 46. Progressive astrocytosis in the thalamus of *Ppt1*$^{-/-}$ and *Ppt1*$^{-/-}$/*Sn*$^{-/-}$ double knockout mice. (A) Immunohistochemical staining for the astrocyte marker glial fibrillary acidic protein (GFAP) in the thalamus of 1, 3, 5 and 7 month old mice revealed localised astrocytosis within the *ventral posterior nucleus* (*VPM/VPL*) (---) of INCL mice. At all ages, *Ppt1*$^{-/-}$/*Sn*$^{-/-}$ double knockout mice showed enhanced GFAP immunoreactivity compared to *Ppt1*$^{-/-}$ mice. From 3 months of age localised astrocytosis was observed in the *VPM/VPL* of mutant mice which spread to involve the whole thalamus with increased age. GFAP immunoreactivity was virtually absent in age-matched *Rag-1*$^{-/-}$ mice or wildtype (WT) mice. Scale bar = 200 μm (B) Higher magnification reveals the morphology of GFAP+ve astrocytes in the *VPM/VPL* of *Ppt1*$^{-/-}$ and *Ppt1*$^{-/-}$/*Sn*$^{-/-}$ mice at 1, 3, 5 and 7 month of age. Compared to the faintly immunoreactive protoplasmic astrocytes present in 1 month old mutant mice, many intensely stained fibrous astrocytes were present in the *VPM/VPL* from 3 months onwards in both strains of INCL mice. These astrocytes displayed thickened processes and became more numerous with increased age until the thalamic neuropil was completely filled with GFAP+ve astrocytes and their processes by 7 months of age. A direct comparison between *Ppt1*$^{-/-}$ and *Ppt1*$^{-/-}$/*Sn*$^{-/-}$ mice revealed that the astrocytosis was more pronounced in the double knockout mice at all ages. These *Ppt1*$^{-/-}$/*Sn*$^{-/-}$ mice displayed astrocytes with more intensely stained cell bodies and thicker processes resulting in overall darker GFAP+ve staining than in *Ppt1*$^{-/-}$ mice at all ages. In WT and *Sn*$^{-/-}$ mice only occasional faintly stained protoplasmic astrocytes with many long thin branched processes could be seen at all ages. Scale bar = 20 μm.

time point the double knockout mice displayed 84.4% higher levels of GFAP staining than age-matched wildtype mice (see **Figure 47**), and exhibited many more intensely activated astrocytes than *Ppt1*$^{-/-}$ mice.

The astrocytosis present in *Ppt1*$^{-/-}$/*Sn*$^{-/-}$ mice seemed to increase in a stepwise manner over time. The first wave of activation occurred at 3 months, which stayed constant at 5 months of age, until some unknown factors triggered an even higher level of activation at 7 months of age. In comparison, the astrocytosis that occurred in *Ppt1*$^{-/-}$ mice steadily increased with disease progression. It seemed that as soon as a certain pathological threshold was reached in the double knockout mice, astrocytosis became uncontrolled. These data suggest that Sn+ve microglia may directly, or indirectly, influence astrocytosis in the INCL brain. The presence of a functioning sialoadhesin adhesion molecule on macrophages/microglia must in some fashion tame or restrain the activation of astrocytes either via direct cell to cell contact, or perhaps indirectly via the activation or down-regulation of other cells. Whether this hyper-activation of astrocytes has benign or negative consequences for neuron survival will be discussed in **Chapter 7**.

b) Enhanced astrocytosis in the cortex of *Ppt1*$^{-/-}$/*Sn*$^{-/-}$ mice

Consistent with the astrocytosis seen in the thalamus, the activation of astrocytes in the somatosensory cortex (*S1BF*) of *Sn* deficient *Ppt1* double mutants exhibited a similar pattern during disease progression (see **Figure 48**). From 3 months onwards a widespread astrocytosis could be detected throughout *S1BF*. Nevertheless, certain

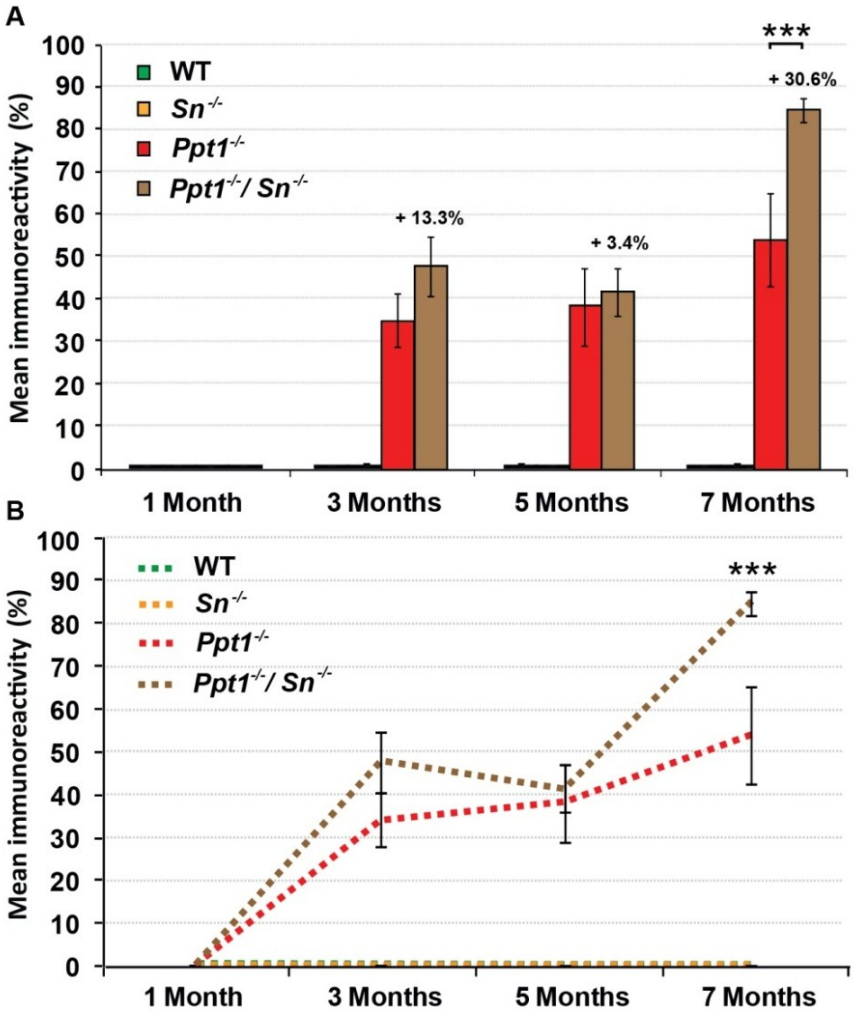

Figure 47. Increased levels of astrocytosis in the thalamus (*VPM/VPL*) of *Ppt1*$^{-/-}$/*Sn*$^{-/-}$ double knockout mice. Thresholding image analysis revealed that the mean level of GFAP immunoreactivity in double knockout mice was marginally enhanced at 3 and 5 months, but significantly at 7 months of age compared to *Ppt1*$^{-/-}$ mice. In contrast, almost no GFAP immunoreactivity was detected in the thalamus of either *Sn*$^{-/-}$ or wildtype (WT) mice. Both *Ppt1*$^{-/-}$ and *Ppt1*$^{-/-}$/*Sn*$^{-/-}$ mice displayed significantly increased GFAP immunoreactivity from 3 months onwards compared to WT mice. The same data are presented as both histogram (A) and line graph (B). Percentages indicate differences between *Ppt1*$^{-/-}$and *Ppt1*$^{-/-}$/*Sn*$^{-/-}$ mice. Statistics: Two-way ANOVA with Bonferroni post hoc test, ***$p<0.001$. Data shown as mean ± SEM, n = 5.

laminae, including lamina V from 3 months, and laminae I and II from 5 months onwards, contained more prominent astrocytosis in *Ppt1*$^{-/-}$/*Sn*$^{-/-}$ double knockout mice. In comparison to single mutant *Ppt1*$^{-/-}$ mice, the overall intensity of astrocytosis was enhanced in the double knockout mice. In *Ppt1*$^{-/-}$ mice astrocytosis followed a laminar-specific pattern, with deeper layers containing more darkly stained astrocytes at early ages. In contrast, *Ppt1*$^{-/-}$/*Sn*$^{-/-}$ double knockout mice already displayed a more or less homogenous pattern of astrocytosis at 3 months of age, which only later lead to more subtle laminar-specificity (see **Figure 48A**).

In summary, similar patterns of astrocytosis seemed to occur in *Ppt1*$^{-/-}$/*Sn*$^{-/-}$ double

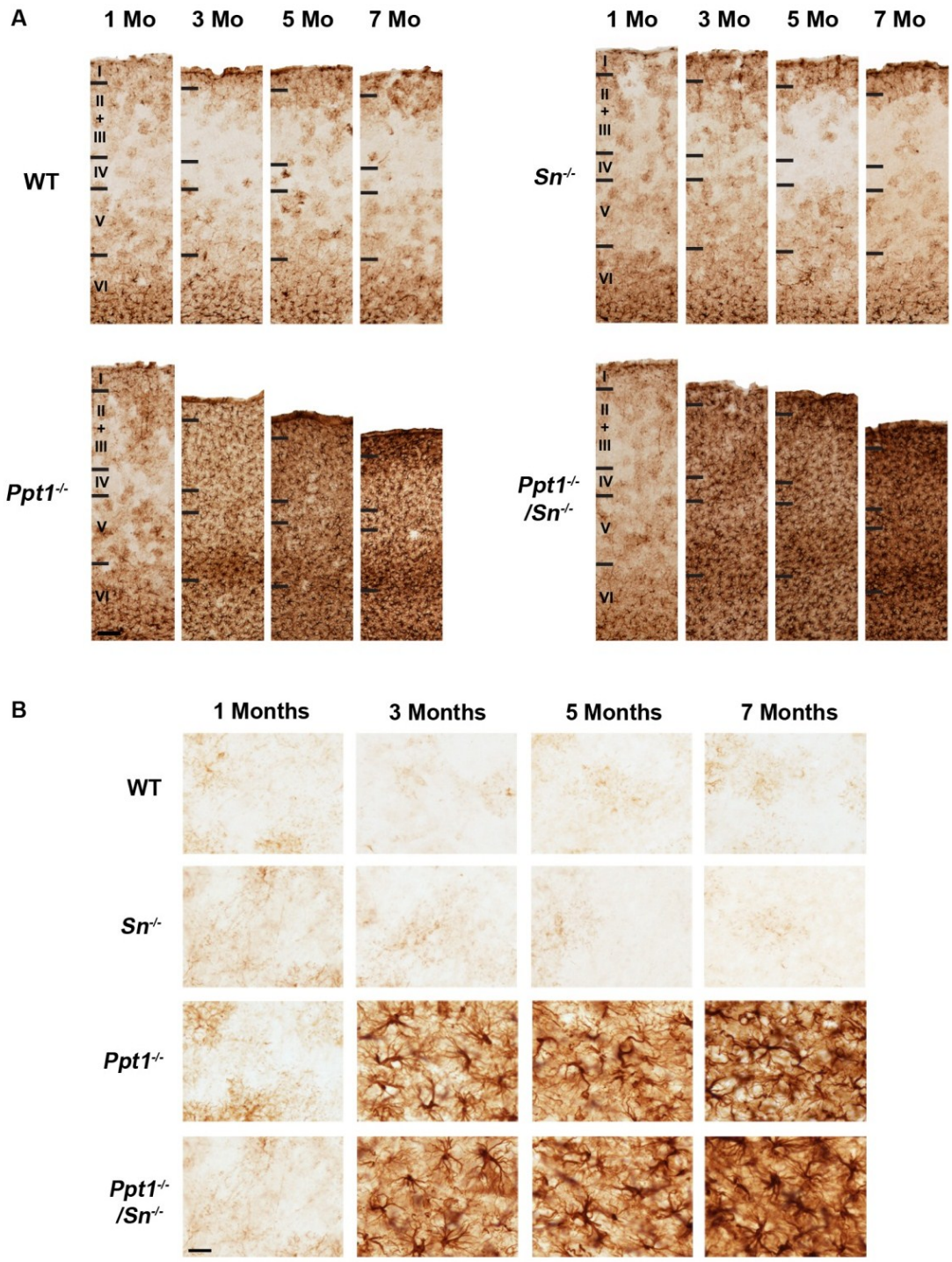

Figure 48. Progressive astrocytosis in the somatosensory barrel field (*S1BF*) cortex of *Ppt1*$^{-/-}$ and *Ppt1*$^{-/-}$/*Sn*$^{-/-}$ double knockout mice. (see figure caption on next page)

Figure 48. Progressive astrocytosis in the somatosensory barrel field (*S1BF*) cortex of *Ppt1*$^{-/-}$ and *Ppt1*$^{-/-}$/*Sn*$^{-/-}$ double knockout mice. Immunohistochemical staining for the astrocyte marker glial fibrillary acidic protein (GFAP) in the *S1BF* of 1, 3, 5 and 7 month old mice revealed differences between *Ppt1*$^{-/-}$ and *Ppt1*$^{-/-}$/*Sn*$^{-/-}$ double knockout mice. *Ppt1*$^{-/-}$/*Sn*$^{-/-}$ double knockout mice showed a clearly enhanced astrocytosis at all ages, but particularly at 7 months of age compared to *Ppt1*$^{-/-}$ mice. In single mutant *Ppt1*$^{-/-}$ mice widespread astrocytosis was present throughout all lamina of the cortex, which increased in intensity with disease progression. Most prominent GFAP immunoreactivity was seen in deeper laminae (especially lamina V) from 3 months of age onwards and lamina I (and II) at 7 months of age. In contrast, in *Ppt1*$^{-/-}$/*Sn*$^{-/-}$ double knockout mice more homogenous widespread astrocytosis throughout all layers was apparent from 3 months onwards compared to *Ppt1*$^{-/-}$ mice. But at 7 months of age the most prominent GFAP immunoreactivity was present in laminae V and I (and II) in *Ppt1*$^{-/-}$/*Sn*$^{-/-}$ mice, as was seen in *Ppt1*$^{-/-}$ mice at this time point. In WT and *Sn*$^{-/-}$ mice only occasional faintly stained protoplasmic astrocytes with many long thin processes could be seen at all ages. Scale bar = 100 μm. (B) Higher magnification revealed the morphology of GFAP+ve astrocytes in lamina V of the *S1BF* cortex of *Ppt1*$^{-/-}$ and *Ppt1*$^{-/-}$/*Sn*$^{-/-}$ mice at 1, 3, 5 and 7 month of age. Compared to the faintly immunoreactive protoplasmic astrocytes present in 1 month old mutant mice, many intensely stained fibrous astrocytes were present in the *S1BF* from 3 months onwards in both strains of mutant mice. These astrocytes displayed thickened processes and became more numerous with increased age until the cortical neuropil of lamina V was completely filled with GFAP+ve astrocytes and their processes by 7 months of age. A direct comparison between *Ppt1*$^{-/-}$ and *Ppt1*$^{-/-}$/*Sn*$^{-/-}$ mice revealed that the astrocytosis was more pronounced in the double knockout mice at all ages. These *Ppt1*$^{-/-}$/*Sn*$^{-/-}$ mice displayed astrocytes with more intensely stained cell bodies and thicker processes resulting in overall darker GFAP+ve staining than in *Ppt1*$^{-/-}$ mice at all ages. In WT and *Sn*$^{-/-}$ mice only occasional faintly stained protoplasmic astrocytes with many long thin branched processes could be seen at all ages. Scale bar = 20 μm.

knockout mice as seen in *Ppt1*$^{-/-}$ mice, but in general astrocytosis was more pronounced in these double mutant mice. Higher magnification pictures of lamina V of the *S1BF* cortex confirmed this phenotype of more pronounced astrocytosis in *Ppt1*$^{-/-}$/*Sn*$^{-/-}$ (see **Figure 48B**). Both *Ppt1*$^{-/-}$ and *Ppt1*$^{-/-}$/*Sn*$^{-/-}$ mice showed hypertrophic astrocyte staining with darkly stained processes from 3 months onwards in lamina V. But the intensity of GFAP immunoreactivity on cell bodies and processes was more pronounced in *Ppt1*$^{-/-}$/*Sn*$^{-/-}$ mice compared to *Ppt1*$^{-/-}$ mice. This difference was marginally seen at 3 and 5 months of age, but clearly at 7 months of age when the neuropil of lamina V was completely filled with GFAP+ve astrocytes and their processes in *Ppt1*$^{-/-}$/*Sn*$^{-/-}$ mice (see **Figure 48B**).

Quantification of GFAP immunoreactivity via thresholding image analysis revealed that cortical astrocytosis in the double knockout mice was increased at all ages compared to single mutant *Ppt1* mice: at 3 months by 7.5%, at 5 months by 3.5% and at 7 months by 22.5%, reaching significant levels at 3 and 7 months of age (see **Figure 49**). Although lower levels of astrocytosis could be seen in the cortex, compared to the thalamus, the smaller variance in the *Ppt1*$^{-/-}$/*Sn*$^{-/-}$ mice resulted in a more significant difference in astrocytosis in the somatosensory cortex (*S1BF*). As in the thalamus, the same stepwise manner of activation could be observed in the double mutant mice.

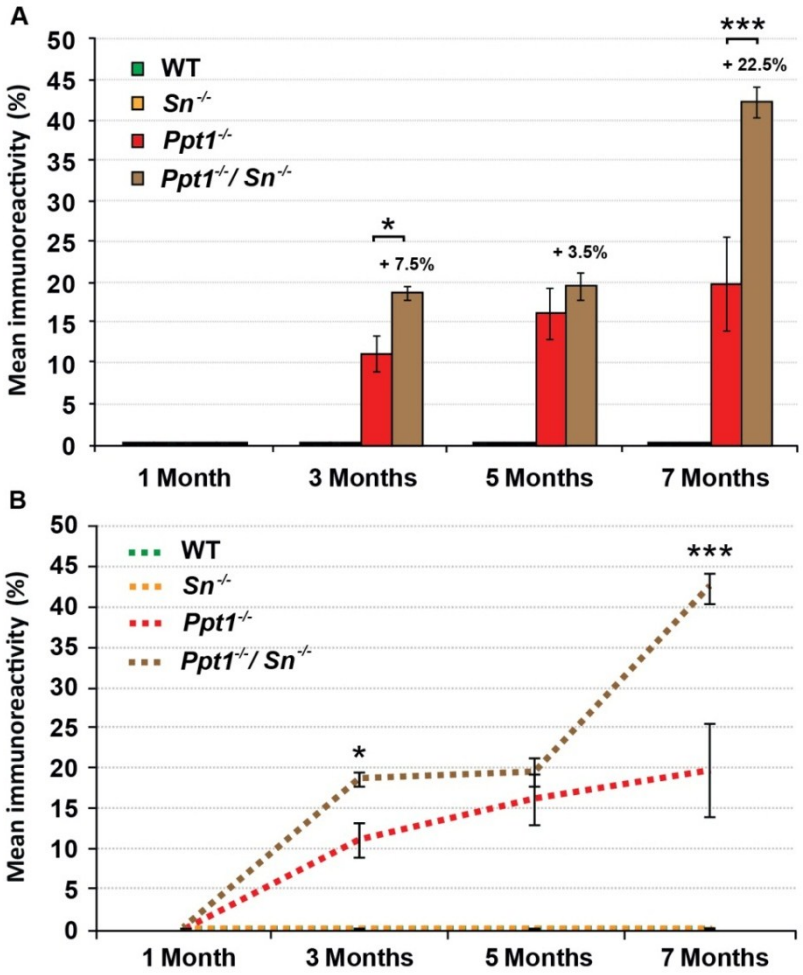

Figure 49. Increased levels of astrocytosis in the somatosensory barrel field (*S1BF*) cortex of *Ppt1*$^{-/-}$/*Sn*$^{-/-}$ double knockout mice. Thresholding image analysis reveals that the mean level of GFAP immunoreactivity in double knockout mice was increased at all ages and reached significant levels at 3 and 7 months of age, compared to *Ppt1*$^{-/-}$ mice. In contrast, almost no GFAP immunoreactivity was detected in the thalamus of either *Sn*$^{-/-}$ or wildtype (WT) animals. Both *Ppt1*$^{-/-}$ and *Ppt1*$^{-/-}$/*Sn*$^{-/-}$ mice displayed significantly increased GFAP immunoreactivity from 3 months onwards compared to WT animals. The same data are presented as both histogram (A) and line graph (B). Percentages indicate differences between *Ppt1*$^{-/-}$ and *Ppt1*$^{-/-}$/*Sn*$^{-/-}$ mice. Statistics: Two-way ANOVA with Bonferroni post hoc test, *p<0.05, ***p<0.001. Data shown as mean ± SEM, n = 5.

This data potentially revealed an unexpected link between macrophage/microglia crosstalk and astrocytosis, and enforces the importance of studying and understanding how each cell type in the brain may be involved in pathogenesis.

c) Attenuated microglial activation in the thalamus of *Ppt1*$^{-/-}$/*Sn*$^{-/-}$ mice

To reveal the extent of microglial activity in the brains of the different genotypes of mice, we stained *Ppt1*$^{-/-}$/*Sn*$^{-/-}$, *Ppt1*$^{-/-}$, *Sn*$^{-/-}$ and WT control brains for CD68, which stains monocytes, macrophages and also microglia (Lee *et al.*, 1992; Holness *et al.*, 1993; Holness and Simmons, 1993). We stained brains from mice of these genotypes (n=5) at all four ages groups (1, 3, 5 and 7 months) and quantified potential differences in CD68 staining intensity by thresholding image analysis.

In *Sn*$^{-/-}$ and WT mice palely stained CD68+ve microglia were present in the thalamic *VPM/VPL* nuclei and throughout the brain, displaying the morphology of quiescent microglia with a small cell soma and thin ramified processes (see **Figure 50B**). However, in *Ppt1*$^{-/-}$ mice, evidence for microglial activation could be detected in the *VPM/VPL* nuclei from 3 months onwards, with an increased intensity of CD68 immunoreactivity and the first signs of morphologically transformed microglia (see **Figure 50**). This process increased steadily over the course of the disease, as described in more detail in **Chapter 4** (see **section 4.2c** in **Chapter 4**). In comparison, *Ppt1*$^{-/-}$/*Sn*$^{-/-}$double mutant mice showed a very similar microglial phenotype (see **Figure 50**). From 3 months onwards the first signs of microglial activation could be detected, which appeared similar or perhaps slightly less intense than that seen in *Ppt1*$^{-/-}$ single mutant mice. Although this microglial activation also increased in intensity with disease progression in *Ppt1*$^{-/-}$/*Sn*$^{-/-}$ double mutant mice, the extent of this activation was reduced in Sn deficient double knockout mice as judged by the intensity of CD68+ve staining (see **Figure 50**), suggesting a role for Sn in the process of microglial activation. This difference in the relative level of microglial activation (as judged morphologically) was even clearer in higher magnification pictures (see **Figure 50B**). Whereas at 3 months of age similar patterns and shapes of CD68+ve cells were detected in *Ppt1*$^{-/-}$/*Sn*$^{-/-}$double mutant mice, from 5 months onwards microglia in these mice showed clear morphological evidence for reduced levels of activation. A mix of microglial morphologies could be seen in *Ppt1*$^{-/-}$/*Sn*$^{-/-}$ mice at 5 months of age with some microglia still possessing elongated processes, while others showed the typical darkly stained, swollen soma with a halo of shortened processes. Indeed, at this 5 month time point the difference in microglial morphology in *Ppt1*$^{-/-}$/*Sn*$^{-/-}$ and *Ppt1*$^{-/-}$ mice was more subtle, whereas at 7 months of age, all microglia in *Ppt1*$^{-/-}$/*Sn*$^{-/-}$double mutant mice seemed to be smaller and less intensely stained than those in *Ppt1*$^{-/-}$ mice. Most strikingly, the microglia in the double knockout mice lacked the intensely stained halo of short processes around their soma as was apparent in age-matched *Ppt1*$^{-/-}$ mice (see **Figure 50B**). Since these short processes serve as the sensing devices by which microglia interact with their immediate vicinity and other cell types, it is possible that these processes may particularly be affected by inactivation of Sn in *Ppt1*$^{-/-}$/*Sn*$^{-/-}$ mice. Nevertheless, this awaits experimental verification by detailed characterisation of *Sn*$^{-/-}$ and *Ppt1*$^{-/-}$/*Sn*$^{-/-}$ microglia in cell culture systems. Based on this interpretation, the altered microglial phenotype in *Ppt1*$^{-/-}$/*Sn*$^{-/-}$ mice would corroborate the role of Sn in cell-cell communication.

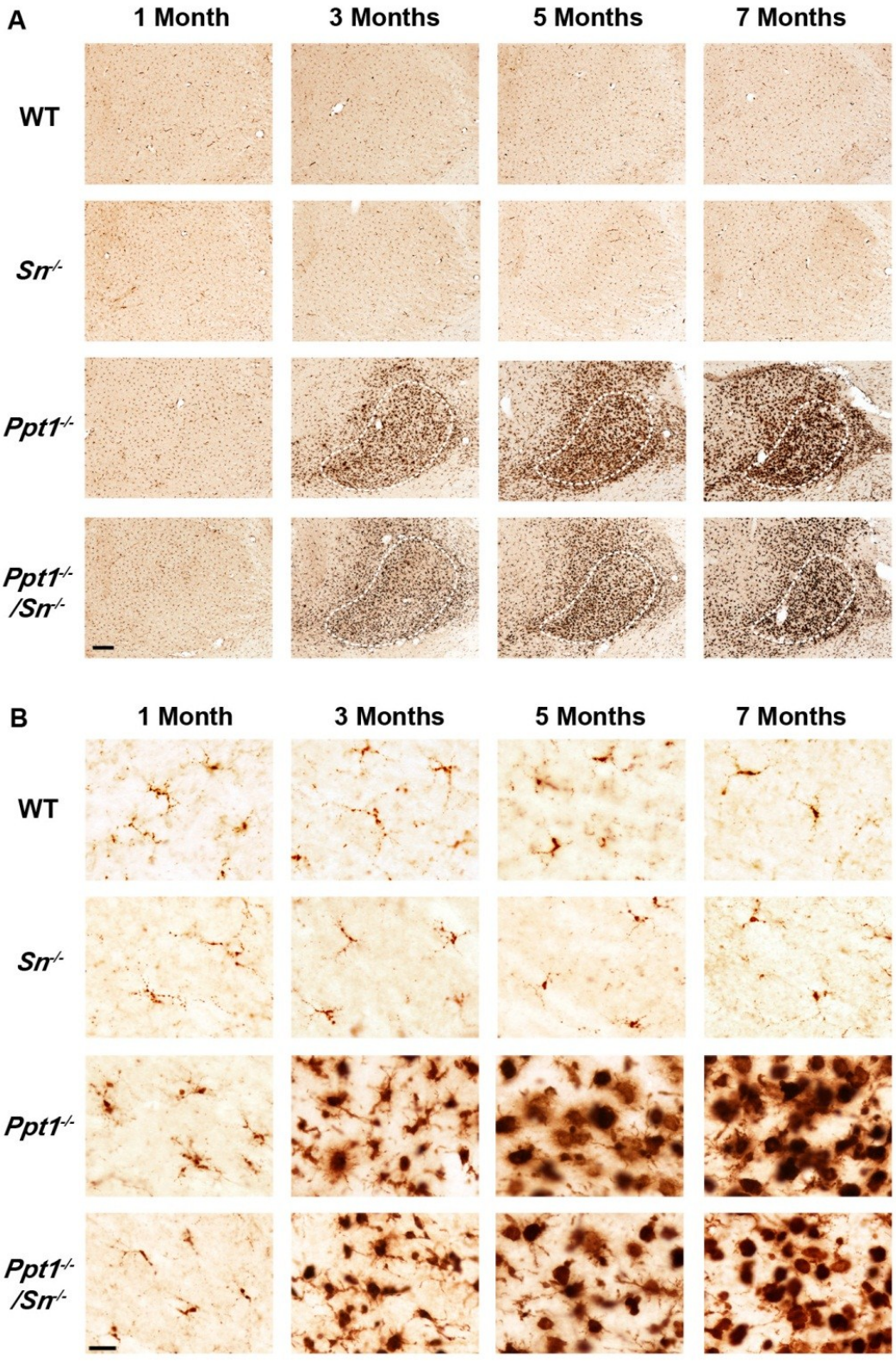

Figure 50. Progressive microglial activation in the thalamus (*VPM/VPL*) of *Ppt1*$^{-/-}$ and *Ppt1*$^{-/-}$*/Sn*$^{-/-}$ double knockout mice. (see figure caption on next page)

Figure 50. Progressive microglial activation in the thalamus (*VPM/VPL*) of *Ppt1*$^{-/-}$ and *Ppt1*$^{-/-}$/*Sn*$^{-/-}$ double knockout mice. (A) Immunohistochemical staining for the microglial marker CD68 in the thalamus of 1, 3, 5 and 7 month old mice revealed localised microglial activation within the *ventral posterior nucleus* (*VPM/VPL*) (---) of INCL mice. *Ppt1*$^{-/-}$/*Sn*$^{-/-}$ double knockout mice showed reduced CD68 immunoreactivity at all ages, but more clearly seen from 5 months onwards compared to *Ppt1*$^{-/-}$ mice. Microglial activation was observed in the *VPM/VPL* of INCL mice from 3 months onwards, which spread to involve the whole thalamus and gained in activation levels with increased age. Similar microglial activation was absent in *Sn*$^{-/-}$ and wildtype (WT) mice in which only quiescent microglia were stained. Scale bar = 200 μm. (B) Higher magnification pictures of CD68+ve microglia in the thalamus of 1, 3, 5 and 7 month old mice revealed differences in cell morphology and activation between Sn deficient double and single *Ppt1* mutant mice. *Ppt1*$^{-/-}$/*Sn*$^{-/-}$ double knockout mice showed clearly reduced microglial activation in the thalamus from 5 months onwards in terms of cell size, staining intensity and transformation into brain macrophages. Microglia in *Ppt1*$^{-/-}$ mice were intensely CD68 immunoreactive with an enlarged and rounded cell soma from 3 months onwards, whereas microglia in *Ppt1*$^{-/-}$/*Sn*$^{-/-}$ double knockout mice remained relatively smaller at all ages, with fewer short processes surrounding the microglial cell soma at 5 and 7 months of age. Only quiescent microglia could be detected in 1 month INCL mice, *Sn*$^{-/-}$ and WT control mice. Scale bar = 20 μm.

Quantification of CD68 immunoreactivity via thresholding image analysis defined more clearly the differences in the extent of microglial activation in the *VPM/VPL*, between *Ppt1*$^{-/-}$/*Sn*$^{-/-}$ and single mutant *Ppt1* mice (see **Figure 51**). At 3 months of age, both mouse populations showed significantly elevated CD68 immunoreactivity in the thalamus compared to control mice, but no overt difference could be observed in this response between the two INCL mouse strains. In contrast, from 5 months onwards a significant decrease in CD68 staining was apparent in *Ppt1*$^{-/-}$/*Sn*$^{-/-}$ mice compared to *Ppt1*$^{-/-}$ mice, with 7.5% less CD68 immunoreactivity seen at 5 months of age and a similar reduction of 6.2% at 7 months of age in the double knockout mice. However, at these time points *Ppt1*$^{-/-}$/*Sn*$^{-/-}$ mice still show highly activated microglial and macrophage staining and infiltration compared to control mice (see **Figure 51**). The additional lack of Sn did not appear to reverse the process of microglial activation in the brain, but delayed and diminished its extent. This delay seemed to occur at 5 months of age when the microglial activation is in full swing. Speculatively, this reduction could be due to the recruitment of peripheral monocytes/macrophages to the thalamic *VPM/VPL* nuclei between 3 and 5 months of age. Since *Ppt1*$^{-/-}$/*Sn*$^{-/-}$ microglia seem to be initially able to become activated normally until 3 months of age, even without Sn, the subsequent differences in their morphology may reflect altered crosstalk between microglia and infiltrating immune cells/macrophages.

d) Similar microglial activation in the cortex of *Ppt1*$^{-/-}$/*Sn*$^{-/-}$ mice

To investigate whether Sn deficiency also results in similar effects in the cortex of INCL mice, the same analyses performed in the thalamus were undertaken in the

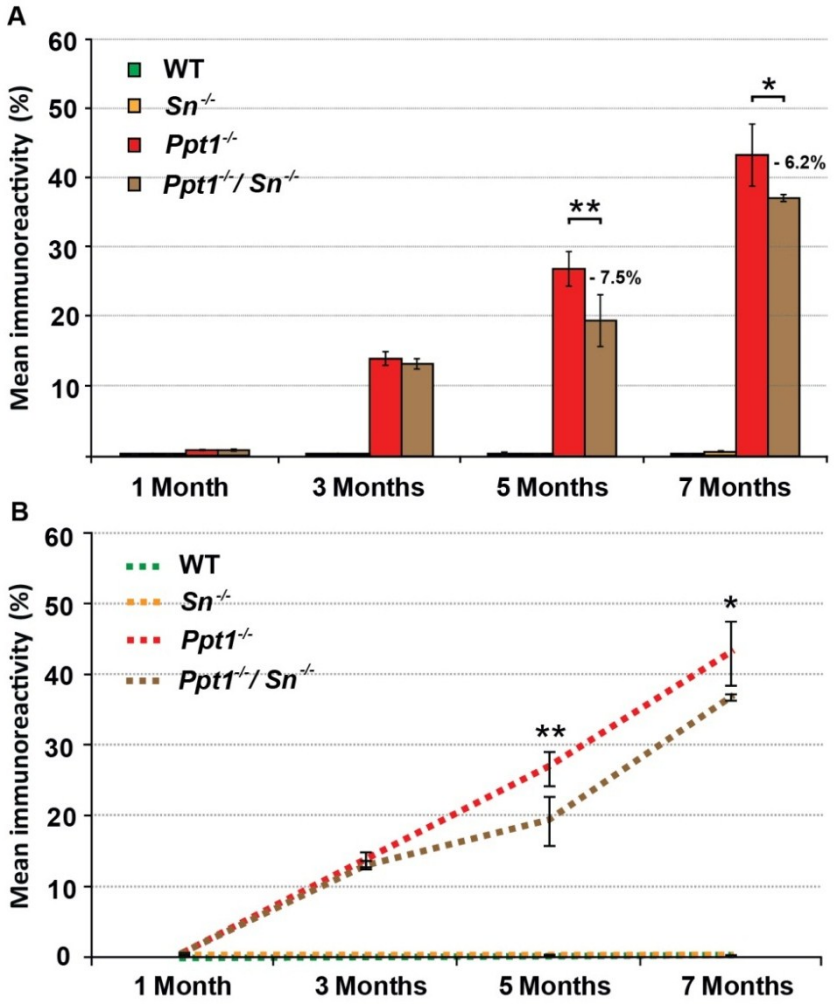

Figure 51. Reduced levels of microglial activation in the thalamus (*VPM/VPL*) of *Ppt1*$^{-/-}$/*Sn*$^{-/-}$ double knockout mice. Thresholding image analysis revealed that the mean level of CD68 immunoreactivity in double knockout mice was significantly reduced at 5 and 7 months of age, compared to *Ppt1*$^{-/-}$ mice. In contrast, almost no CD68 immunoreactivity was detected in the thalamus of either *Sn*$^{-/-}$ or wildtype (WT) animals. Both *Ppt1*$^{-/-}$ and *Ppt1*$^{-/-}$/*Sn*$^{-/-}$ mice displayed significantly increased CD68 immunoreactivity from 3 months onwards compared to WT animals. The same data are presented as both histogram (A) and line graph (B). Percentages indicate differences between *Ppt1*$^{-/-}$ and *Ppt1*$^{-/-}$/*Sn*$^{-/-}$ mice. Statistics: Two-way ANOVA with Bonferroni post hoc test, *$p<0.05$, **$p<0.01$. Data shown as mean ± SEM, n = 5.

somatosensory cortex (*S1BF*). As described in **Chapter 4** (see **section 4.2d**), the relative level of CD68 imunoreactivity in *Ppt1*$^{-/-}$ mice was much lower in the cortex than in the thalamus. In addition to layer specific differences, there were also fewer activated microglia in the cortex. However, over the course of the disease this microglial activation became more pronounced and reached its maximum at 7 months of age (see **Figure 52**).

In terms of CD68 staining, microglial activation appeared to occur to similar extents at all ages in the *S1BF* of *Ppt1*$^{-/-}$ mice and *Ppt1*$^{-/-}$/*Sn*$^{-/-}$ double knockout mice (see **Figure 52A**). Only a slight reduction could be suggested at 3 and 5 months of age. At these

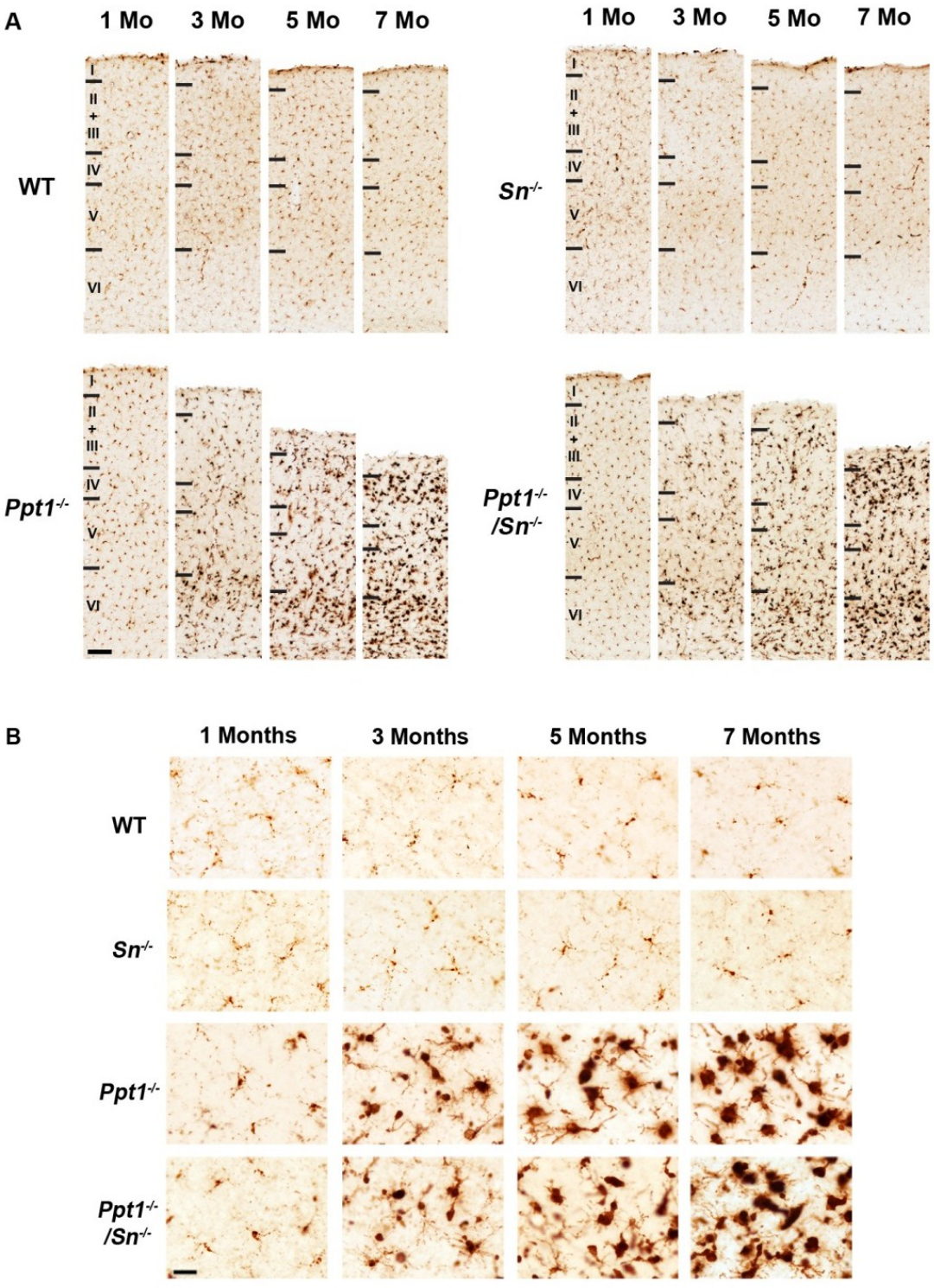

Figure 52. Progressive microglial activation in the somatosensory barrel field (*S1BF*) cortex of *Ppt1*$^{-/-}$ and *Ppt1*$^{-/-}$/*Sn*$^{-/-}$ double knockout mice. (see figure caption on next page)

Figure 52. Progressive microglial activation in the somatosensory barrel field (*S1BF*) cortex of *Ppt1*$^{-/-}$ and *Ppt1*$^{-/-}$/*Sn*$^{-/-}$ double knockout mice. Immunohistochemical staining for the microglial marker CD68 in the *S1BF* of 1, 3, 5 and 7 month old mice revealed only marginal differences between *Ppt1*$^{-/-}$ and *Ppt1*$^{-/-}$/*Sn*$^{-/-}$ double knockout mice. *Ppt1*$^{-/-}$/*Sn*$^{-/-}$ double knockout mice showed slightly reduced microglial activation at 3 and 5 months of age, compared to *Ppt1*$^{-/-}$ mice. In *Ppt1*$^{-/-}$ mice intensely stained CD68 positive microglia were most prominent in deeper laminae (mainly layer VI) from 3 months of age onwards, but this microglial activation spread to upper layers and increased in intensity with disease progression. At 7 months of age widespread CD68 immunoreactivity was present throughout all layers, but most prominently in laminae II+III and VI. In *Ppt1*$^{-/-}$/*Sn*$^{-/-}$ double knockout mice slightly weaker microglial activation could be seen in lamina VI at 3 and 5 months of age, leading to similar levels and distribution of microglial activation at 7 months of age, as that seen in *Ppt1*$^{-/-}$ mice. Similar activation was absent in *Sn*$^{-/-}$ and wildtype (WT) control animals where only quiescent microglial staining could be detected. Scale bar = 100 μm. (B) Higher magnification pictures of CD68+ve microglia in lamina VI of the *S1BF* of 1, 3, 5 and 7 month old mice revealed marginal differences in cell morphology and activation between *Sn* deficient double and single *Ppt1* mutant mice. CD68+ve microglia in *Ppt1*$^{-/-}$/*Sn*$^{-/-}$ double knockout mice showed marginally reduced microglial activation in terms of cell size and staining intensity at 3 and 5 months of age. Intensely stained microglia with an enlarged and rounded cell soma were seen in *Ppt1*$^{-/-}$ mice from 5 months onwards, whereas in *Ppt1*$^{-/-}$/*Sn*$^{-/-}$ double knockout mice microglia of similar size and activation were only seen at 7 months of age. At this last time point no clear difference between the genotypes could be detected. Only quiescent microglia were observed in 1 month INCL mice and control animals (*Sn*$^{-/-}$ and WT). Scale bar = 20 μm.

time points the pattern of CD68 staining in *Ppt1*$^{-/-}$/*Sn*$^{-/-}$ mice seemed a little more diffuse and less laminar specific than in *Ppt1*$^{-/-}$ mice. Whilst *Ppt1*$^{-/-}$ mice showed pronounced microglial activation in lamina VI at 3 and 5 months of age, the double mutants displayed the same general pattern of activation, but less prominently in lamina VI. Looking at the morphology of microglia at these time points (see **Figure 52B**): At 3 months of age, both mouse genotypes displayed microglia of similar morphology with occasional CD68+ve cells with slightly swollen cell soma and elongated processes. At 5 months of age CD68+ve microglia in *Ppt1*$^{-/-}$ mice showed halo-like short processes around many cells in lamina VI. These short processes were absent in *Ppt1*$^{-/-}$/*Sn*$^{-/-}$ double knockout mice at the same age, reflecting the similar microglial morphologies seen in the thalamus of these mice. However, at 7 months of age no qualitative differences in microglial morphology could be detected between *Ppt1*$^{-/-}$/*Sn*$^{-/-}$ and *Ppt1*$^{-/-}$ mice (see **Figure 52B**).

Quantifying CD68+ve immunoreactivity in the somatosensory cortex by thresholding image analysis showed no significant difference between *Ppt1*$^{-/-}$/*Sn*$^{-/-}$ and *Ppt1*$^{-/-}$ mice at any time point (see **Figure 53**). Only at 5 months of age was there a small reduction in CD68 staining, but the high variance in the double knockout group at this time point precluded any statistical significance. As such, additionally knocking out Sn seemed to have relatively little effect on microglial activation in the *S1BF* region of the cortex. This strengthens the hypothesis that microglia themselves do not require Sn to

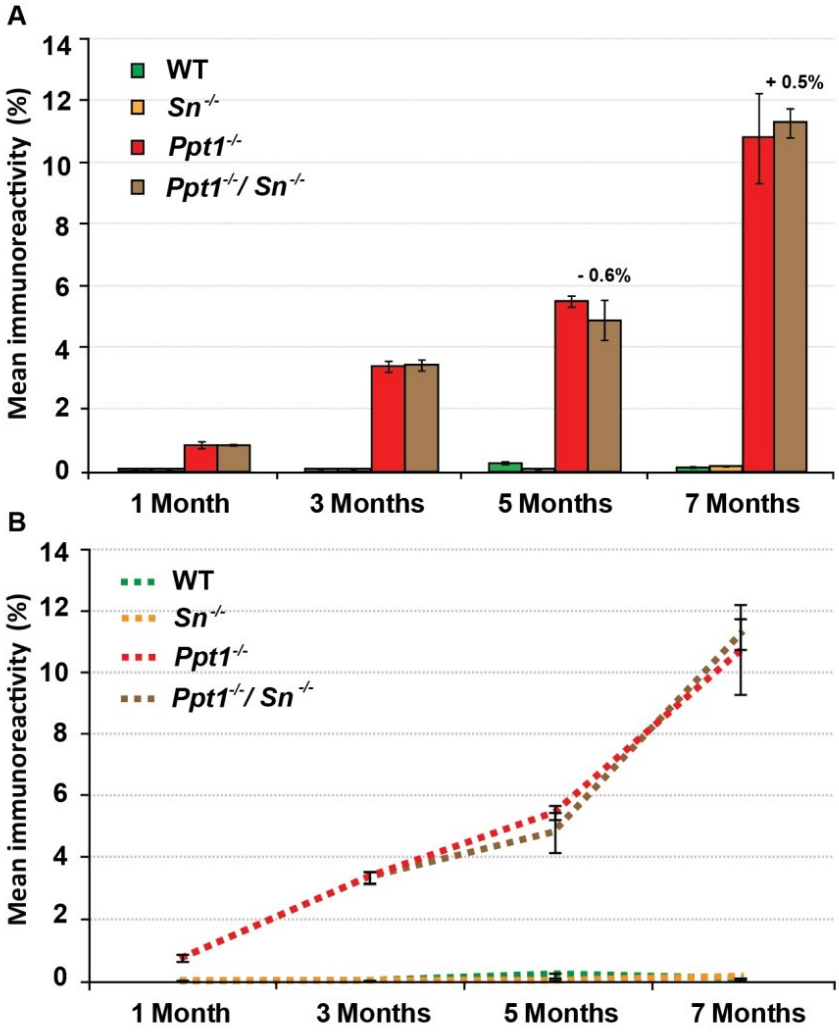

Figure 53. Similar levels of microglial activation in the somatosensory barrel field (*S1BF*) cortex of *Ppt1*$^{-/-}$/*Sn*$^{-/-}$ double knockout mice. Thresholding image analysis revealed that the mean level of CD68 immunoreactivity in double knockout mice was similar to that seen in *Ppt1*$^{-/-}$ mice at all ages. Almost no CD68 immunoreactivity was detected in the thalamus of either *Sn*$^{-/-}$ or wildtype (WT) animals. Both *Ppt1*$^{-/-}$ and *Ppt1*$^{-/-}$/*Sn*$^{-/-}$ mice displayed increased CD68 immunoreactivity from 1 month onwards compared to WT animals, but this difference only reached significant levels from 3 months onwards. The same data are presented as both histogram (A) and line graph (B). Percentages indicate differences between *Ppt1*$^{-/-}$and *Ppt1*$^{-/-}$/*Sn*$^{-/-}$ mice. Statistics: Two-way ANOVA with Bonferroni post hoc test. Data shown as mean ± SEM, n = 5.

become activated initially, nor to maintain or increase activation among themselves. This suggests that Sn dependent crosstalk may not be as important in cortical regions. Alternatively, perhaps fewer other immune cells are present in, or recruited to, the cortex to enhance the on-going immune reaction via Sn, as appears to happen in the thalamus. Perhaps this external recruitment only occurs after a certain threshold of activation is reached. It is possible that the level of microglial activation in *S1BF* in INCL is too low to see any effect, and other brain regions would show a difference (as we have shown in the thalamus).

5.4 Impact of *Sn* deficiency on neuron survival in *Ppt1*$^{-/-}$ mice

After detecting differences in the time course and extent of astrocytosis and microglial activation in *Ppt1*$^{-/-}$/*Sn*$^{-/-}$ double knockout mice, we next asked if this change in innate immune responses has any effect upon somatosensory relay neuron survival in *VPM/VPL*.

a) Increased neuron survival in the thalamus of *Ppt1*$^{-/-}$/*Sn*$^{-/-}$ mice

As described in **Chapter 4** (see **section 4.3**), in mice deficient for *Ppt1* alone a dramatic loss in neuronal *VPM/VPL* neuron number could be seen from 3 months onwards. Performing unbiased optical fractionator counts in Nissl stained sections from age-matched *Ppt1*$^{-/-}$/*Sn*$^{-/-}$, *Ppt1*$^{-/-}$, *Sn*$^{-/-}$ and wildtype mice revealed the following results (see **Figure 54**): The first detectable significant loss of *VPM/VPL* neurons could be seen in *Ppt1*$^{-/-}$/*Sn*$^{-/-}$ mice at 3 months of age, compared to wildtype mice. At this time point neuron survival was increased in *Sn* deficient double mutant mice by 10.2% *vs.* *Ppt1*$^{-/-}$ mice, in comparison with age-matched control mice values. However, neuron survival was not significantly improved at later stages, even though a slight trend towards increased *VPM/VPL* neuron numbers was seen at 5 months, with 6.9% more neurons, and subsequently 4.5% more *VPM/VPL* neurons in these double mutant mice at 7 months of age. Indeed, at 5 months of age, the mean survival of *VPM/VPL* neurons was at 27.9% of wildtype values in *Ppt1*$^{-/-}$/*Sn*$^{-/-}$ mice, but the high variability between individual mice precluded any significant difference between these genotypes. This is in comparison to 7 month old mice in which only 9.7% of wildtype neuron numbers were present in the double knockout mice. At this time point the difference between *Ppt1*$^{-/-}$/*Sn*$^{-/-}$ and *Ppt1*$^{-/-}$ mice was of such low magnitude that it was not statistically significant (see **Figure 54**). In summary, the extent of *VPM/VPL* thalamic neuron loss in *Ppt1*$^{-/-}$/*Sn*$^{-/-}$ mice was consistently reduced *vs.* *Ppt1*$^{-/-}$ mice at all ages, but reached significant levels only in the earlier stages of the disease. Nevertheless, the *VPM/VPL* neurons in the thalamus of *Sn* deficient INCL mice still undergo a pronounced loss, indicating that other influences may be responsible for their death. Possible mechanisms and interpretations of these results shall be discussed in **Chapter 7**. However, most likely the *VPM/VPL* relay neurons in the thalamus represent a population of cells that are most vulnerable to the effects of Ppt1 deficiency. As such, it could be speculated that in other brain regions where microglial activation is less pronounced a greater effect of Sn inactivation may be seen.

This hypothesis could be tested by counting the neurons of other brain regions, for example in the cortex.

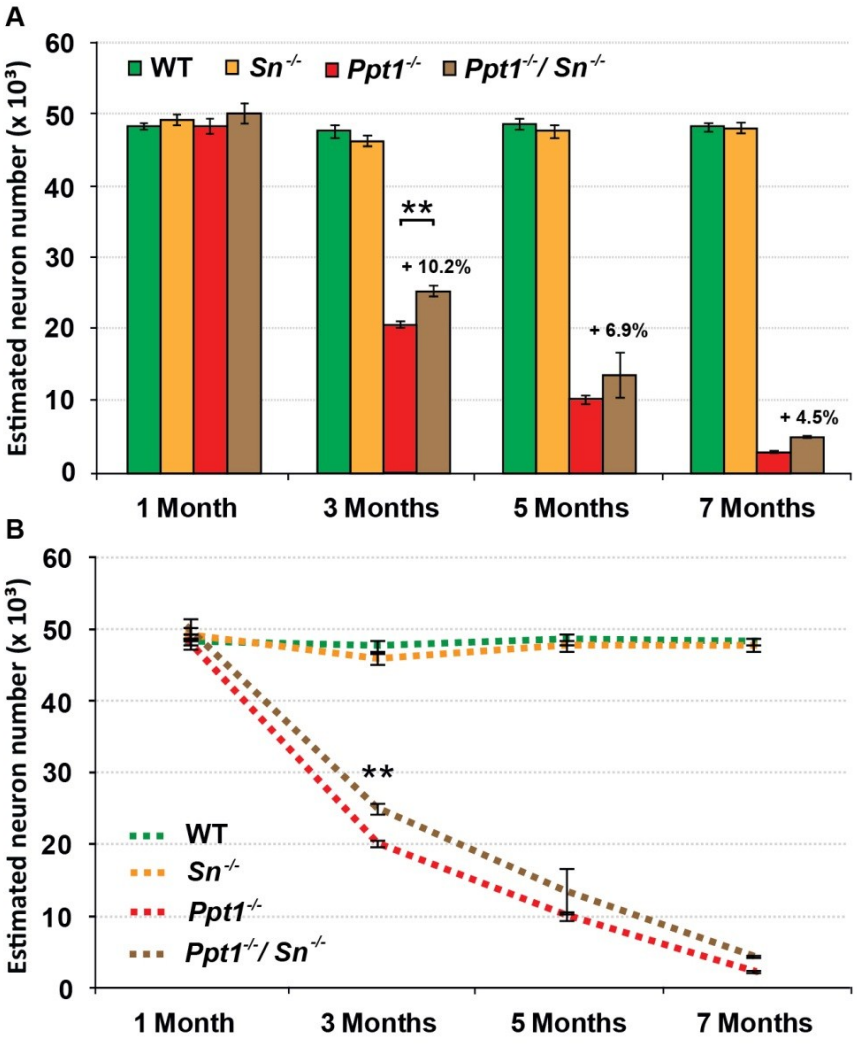

Figure 54. Progressive loss of thalamic (*VPM/VPL*) neurons in *Ppt1*$^{-/-}$ and *Ppt1*$^{-/-}$/*Sn*$^{-/-}$ mice. Unbiased optical fractionator estimates of number of Nissl stained thalamic relay neurons in the *ventral posterior nucleus* (*VPM/VPL*) of *Ppt1*$^{-/-}$, *Ppt1*$^{-/-}$/*Sn*$^{-/-}$, *Sn*$^{-/-}$ and age-matched wildtype (WT) control mice at different stages of disease progression. Significantly fewer *VPM/VPL* neurons were present in both single and double *Ppt1* mutant mice from 3 months onwards compared to WT animals, and continued to decline in number with increased age. Nonetheless, neuron loss was significantly slowed down in *Ppt1*$^{-/-}$/*Sn*$^{-/-}$ mice. Significantly more neurons were present in *Ppt1*$^{-/-}$/*Sn*$^{-/-}$ mice at 3 months compared to *Ppt1*$^{-/-}$ mice. Marginally elevated *VPM/VPL* neuron numbers were also detected in *Ppt1*$^{-/-}$/*Sn*$^{-/-}$ mice at later stages of the disease, but these differences did not reach statistical significance. *Sn*$^{-/-}$ and WT mice showed no significant difference in neuron numbers at any age.The same data are presented as both histogram (A) and line graph (B). Percentages indicate differences between *Ppt1*$^{-/-}$and *Ppt1*$^{-/-}$/*Sn*$^{-/-}$ mice compared to age-matched WT mice. Statistics: Two-way ANOVA with Bonferroni post hoc test, **p<0.01. Data shown as mean ± SEM, n = 5.

b) Neuron survival in the cortex of *Ppt1*$^{-/-}$/*Sn*$^{-/-}$ mice

As described by (Kielar *et al.*, 2007) the entire thalamocortical system is affected in *Ppt1*$^{-/-}$ mice. Relay neurons from the thalamus are lost before neuron loss occurs in

the target regions to which they project. Therefore, we planned to investigate the impact of Sn deficiency in the cortex of *Ppt1*$^{-/-}$ mice. Ideally, counts of neuron number within laminae IV, V and VI would have been performed, the laminae which receive projections from the thalamus or which project back to it. However, due to time constraints this full analysis could not be undertaken. Instead, to obtain a general overview of how Sn deficiency impacts the cortex in *Ppt1*$^{-/-}$ mice, two key cortical phenotypes were measured: namely total cortical volume and the cortical thickness of *S1BF*. These two factors are good indicators of disease progression and often coincide with neuron loss (Bible *et al.*, 2004; Kielar *et al.*, 2007).

5.5 Impact of *Sn* deficiency on cortical atrophy in *Ppt1*$^{-/-}$ mice

As in **Chapter 4** (see **section 4.4**), we measured the total cortical volume and the thickness of the somatosensory cortex *S1BF* in the brains of *Ppt1*$^{-/-}$/*Sn*$^{-/-}$ double knockout mice, *Ppt1*$^{-/-}$, *Sn*$^{-/-}$ and WT control mice. These analyses of the total cortical volume and a vulnerable cortical sub-region (*S1BF*) should give sufficient indication of the extent and timing of degeneration in the cortex of *Ppt1*$^{-/-}$/*Sn*$^{-/-}$ double knockout mice.

a) Increased cortical volume of *Ppt1*$^{-/-}$/*Sn*$^{-/-}$ mice

As in the previous **Chapter 4** (see **section 4.4**), we measured the volume of the cortical mantle in each mouse population at all four age groups (1, 3, 5 and 7 months of age) (see **Figure 55**). Compared to *Ppt1*$^{-/-}$ mice, which *vs.* wildtype mice demonstrated a significant loss of cortical volume from 3 months onwards, *Ppt1*$^{-/-}$/*Sn*$^{-/-}$ double knockout mice showed a slight improvement in cortical volume from 3 months onwards. Whereas the mean difference of 2.5% (calculated *vs.* age-matched wildtype mice) between *Ppt1*$^{-/-}$/*Sn*$^{-/-}$ and *Ppt1*$^{-/-}$ mice did not reach significance at 3 months of age; at 5 months of age a significant improvement of 12.5% in cortical volume was evident in *Ppt1*$^{-/-}$/*Sn*$^{-/-}$ mice. However, this amelioration of cortical atrophy was reduced to 3.9% at the end of the disease and was no longer significant. At this time point of 7 months of age, the *Ppt1*$^{-/-}$/*Sn*$^{-/-}$ double knockout mice also showed a significant cortical atrophy of 39.3% compared to age-matched wildtype mice. Cortical volume in *Sn*$^{-/-}$ mice did not differ from that in wildtype mice at any age point. Considered together, these data reveal that the cortical atrophy observed in the single *Ppt1*$^{-/-}$ mutant mice, was also seen in *Ppt1*$^{-/-}$/*Sn*$^{-/-}$ double knockout mice.

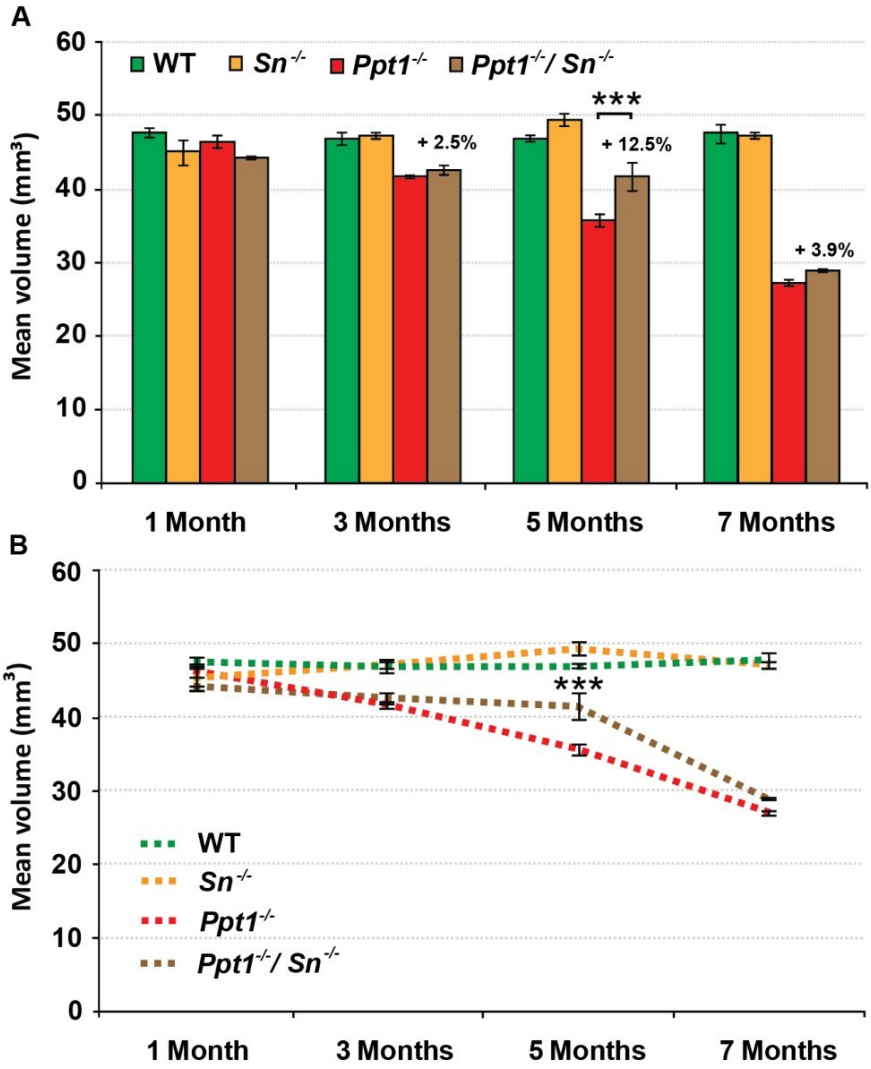

Figure 55. Reduced cortical atrophy in *Ppt1*$^{-/-}$/*Sn*$^{-/-}$ mice. Unbiased Cavalieri estimates of cortical volume in *Ppt1*$^{-/-}$, *Ppt1*$^{-/-}$/*Sn*$^{-/-}$, *Sn*$^{-/-}$ and age-matched wildtype (WT) control animals at different stages of disease progression. Cortical atrophy was significantly less pronounced in *Ppt1*$^{-/-}$/*Sn*$^{-/-}$ mice at 5 months of age, compared to *Ppt1*$^{-/-}$ mice. A marginal improvement in cortical volume was also detected at 3 and 7 months of age in the double knockouts, compared to single *Ppt1*$^{-/-}$ mice, but these differences did not reach significant levels. Compared to WT mice, both *Ppt1*$^{-/-}$ and *Ppt1*$^{-/-}$/*Sn*$^{-/-}$ mice displayed significant cortical atrophy from 3 months onwards. *Sn*$^{-/-}$ and WT mice showed no significant difference in cortical volume at any age. The same data are presented as both histogram (A) and line graph (B). Percentages indicate differences between *Ppt1*$^{-/-}$and *Ppt1*$^{-/-}$/*Sn*$^{-/-}$ mice compared to age-matched WT mice. Statistics: Two-way ANOVA with Bonferroni post hoc test, ***$p<0.001$. Data shown as mean ± SEM, n = 5.

b) Increased cortical thickness of *Ppt1*$^{-/-}$/*Sn*$^{-/-}$ mice

As a second disease-related cortical phenotype, *Ppt1*$^{-/-}$ mice display the first significant cortical thinning of 6.1% in *S1BF* from 3 months onwards compared to age-matched wildtype mice (see **Figure 56**). This thinning increased with disease progression and reached its maximum extent in severely affected 7 month old *Ppt1*$^{-/-}$ mice with a 19.7% reduction in *S1BF* thickness. In contrast, *S1BF* thickness measurements in *Ppt1*$^{-/-}$/*Sn*$^{-/-}$ double knockout mice revealed that these mice not only showed an improved *S1BF*

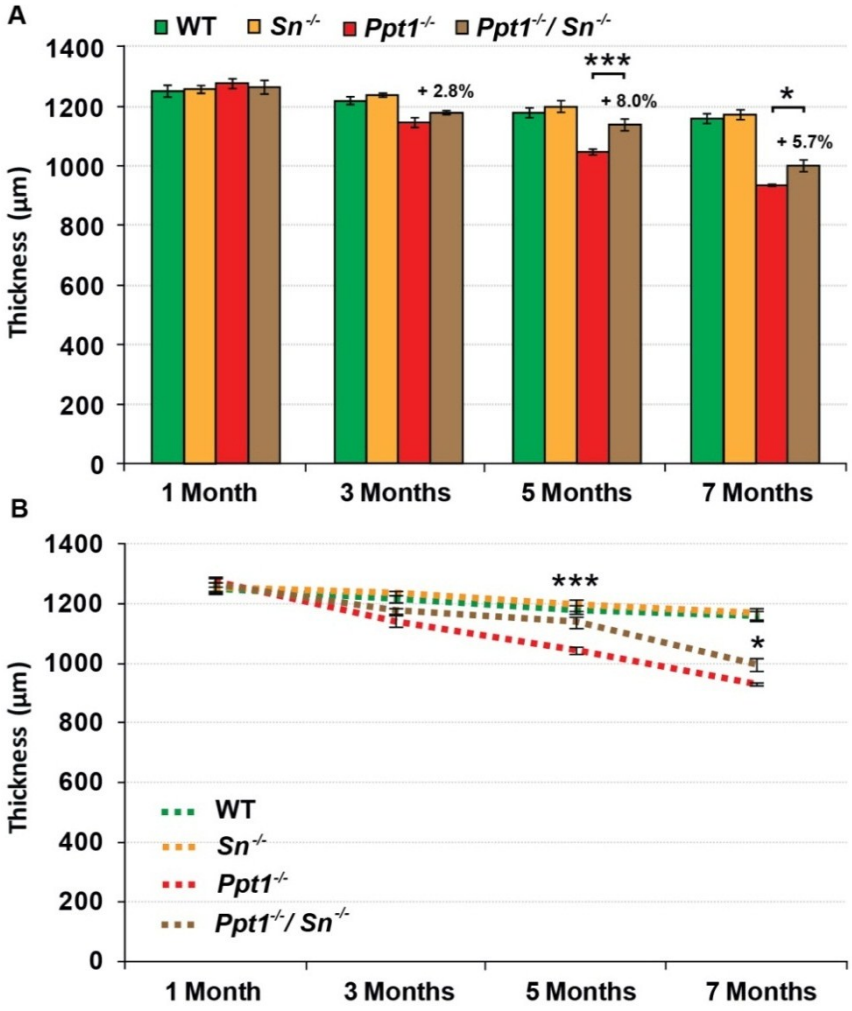

Figure 56. Reduced cortical thinning of the somatosensory barrel field (*S1BF*) cortex in *Ppt1*$^{-/-}$/*Sn*$^{-/-}$ mice. Cortical thickness measurements in *Ppt1*$^{-/-}$, *Ppt1*$^{-/-}$/*Sn*$^{-/-}$, *Sn*$^{-/-}$ and age-matched wildtype (WT) controls at different stages of disease progression. Thinning of the cortical mantle of *S1BF* was significantly reduced in *Ppt1*$^{-/-}$/*Sn*$^{-/-}$ mice from 5 months onwards. Compared to WT mice, *Ppt1*$^{-/-}$ mice displayed significant cortical thinning in *S1BF* from 3 months onwards, whereas *S1BF* thickness in *Ppt1*$^{-/-}$/*Sn*$^{-/-}$ mice was not significantly different from that in WT mice until 7 months of age. *Sn*$^{-/-}$ and WT mice showed no significant difference in cortical thickness at any age. The same data are presented as both histogram (A) and line graph (B). Percentages indicate differences between *Ppt1*$^{-/-}$and *Ppt1*$^{-/-}$/*Sn*$^{-/-}$ mice compared to age-matched WT mice. Statistics: Two-way ANOVA with Bonferroni post hoc test, *p<0.05, ***p<0.001. Data shown as mean ± SEM, n = 5.

thickness from 3 months onwards, but that they also resembled wildtype mice until 5 months of age (see **Figure 48A** and **Figure 52A** for representative pictures, see **Figure 56** for quantification). The only significant reduction in these double mutant mice could be seen at 7 months of age, compared to wildtype mice. Increases of 2.8%, 8.0% and 5.7% in *S1BF* thickness were apparent in *Ppt1*$^{-/-}$/*Sn*$^{-/-}$ double knockout mice at 3, 5 and 7 months of age respectively compared to single *Ppt1*$^{-/-}$ mice (calculated *vs.* age-matched wildtype mice). These differences in *S1BF* thickness did not reach significant levels at 3 months, but were proved to be statistically robust at 5 and 7

months of age. *S1BF* thickness in *Sn*$^{-/-}$ mice did not differ from wildtype controls at any age point. In summary, the additional absence of Sn did not reverse, but instead delayed the progression of cortical thinning in *Ppt1*$^{-/-}$ mice. Only at 7 months of age could the effects of disease progression be detected in the somatosensory cortex of *Ppt1*$^{-/-}$/*Sn*$^{-/-}$ double knockout mice.

Our data for both disease-associated cortical phenotypes indicated that the influence of Sn upon disease progression not only occurs in the thalamus, but also extends to the cortex. Comparing these effects upon these two regions (see **Figure 54**, **Figure 55** and **Figure 56**), the alteration of immune responses seemed to have a greater and longer lasting impact upon the cortex, a brain region that exhibits less pronounced glial activation. The mechanisms that could underlie this amelioration of cortical pathology shall be discussed below (see **section 5.6b**). However, whether these improvements can actually be linked to reduced cortical neuron loss is only speculation at this point in time.

5.6 Increased lifespan in *Ppt1*$^{-/-}$/*Sn*$^{-/-}$ mice

Last, but not least, our collaborators in Würzburg, Germany, performed life span/survival rate experiments of *Ppt1*$^{-/-}$ mice and *Ppt1*$^{-/-}$/*Sn*$^{-/-}$ mice. These experiments formed the link between the characterisation of the *Sn* deficient *Ppt1*$^{-/-}$ mice described above. They demonstrated that *Ppt1*$^{-/-}$/*Sn*$^{-/-}$ double knockout mice showed a prolonged life span and lived roughly 10% longer, until 271 days, whereas normal *Ppt1*$^{-/-}$ mice had an average lifespan of 245 days (unpublished data Janos Groh, University of Würzburg, Germany). These findings confirmed the improved pathological features in the brain described above.

5.7 Summary and discussion

In this chapter we have shown that that the deletion of Sn, a binding protein normally present on macrophages, has an ameliorating impact upon disease progression in INCL mice. After characterising Sn expressing cells and their distribution in the brain of *Ppt1*$^{-/-}$ mice, the absence of Sn resulted in cell type-specific alterations in *Ppt1*$^{-/-}$/*Sn*$^{-/-}$ mice: Whereas microglial activation and neuronal loss were reduced, a surprising enhancement of astrocytosis could be observed (see also **Table 12**, **13** and **Figure 57** for a summary overview) together with a moderately prolonged lifespan in *Ppt1*$^{-/-}$/*Sn*$^{-/-}$ mice.

Table 12. Summary of the comparison between *Ppt1*$^{-/-}$ and WT mice. Table was based on the same analyses conducted in **Chapters 4** and **5**. In the left column: "type of analysis", across the top row: "age of mice". Symbols: = no difference, ↑ significant increase, ↓ significant decrease, = (↑) increasing trend without significance, = (↓) decreasing trend without significance.

		1 Month	3 Months	5 Months	7 Months
Brain weight		=	=	↓	↓
Sialoadhesin	***Thalamus***	=	↑	↑	↑
	S1BF	=	↑	↑	↑
Astrocytosis	***Thalamus***	=	↑	↑	↑
	S1BF	=	↑	↑	↑
Microglial activation	***Thalamus***	=	↑	↑	↑
	S1BF	= (↓)	↑	↑	↑
Neuronal survival		=	↓	↓	↓
Cortical thickness	***S1BF***	=	↓	↓	↓
Cortical volume		=	↓	↓	↓

Table 13. Summary of the comparison between *Ppt1*$^{-/-}$ and *Ppt1*$^{-/-}$*/Sn*$^{-/-}$ mice. Table was based on the same analyses conducted in **Chapter 5**. In the left column: "type of analysis", across the top row: "age of mice". Symbols: = no difference, ↑ significant increase, ↓ significant decrease, = (↑) increasing trend without significance, = (↓) decreasing trend without significance.

		1 Month	3 Months	5 Months	7 Months
Brain weight		=	=	= (↑)	= (↑)
Astrocytosis	***Thalamus***	=	= (↑)	= (↑)	↑
	S1BF	=	↑	= (↑)	↑
Microglial activation	***Thalamus***	=	=	↓	↓
	S1BF	=	=	= (↓)	=
Neuronal survival		=	↑	= (↑)	= (↑)
Cortical thickness	***S1BF***	=	= (↑)	↑	↑
Cortical volume		=	=	↑	= (↑)

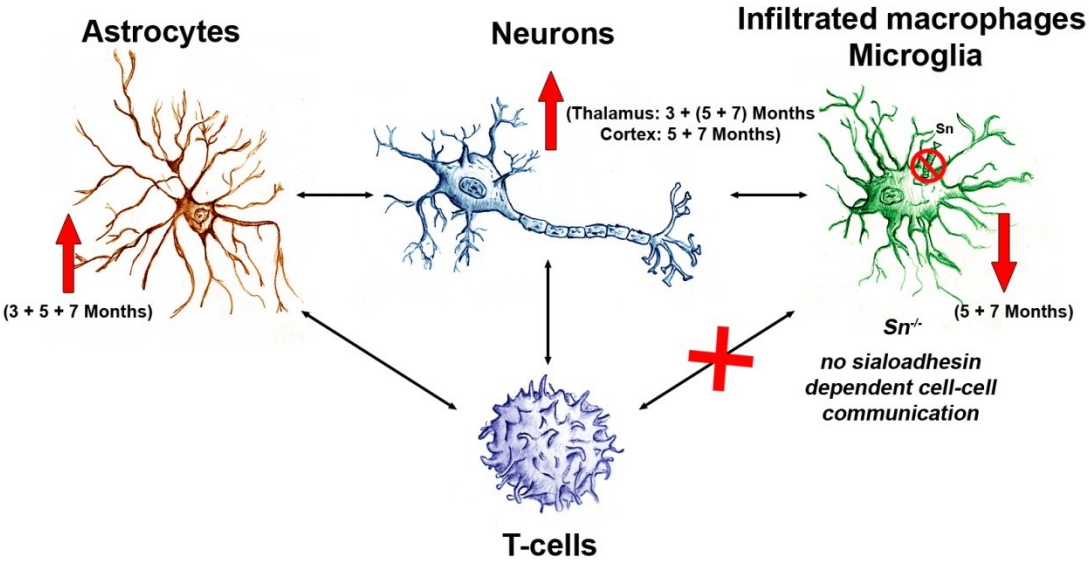

Figure 57. Schematic summary of altered phenotypes in the brain of *Ppt1*$^{-/-}$/*Sn*$^{-/-}$ mice. We characterised astrocytosis (illustrated as 'astrocytes'); microglial activation (illustrated as 'infiltrated macrophages, microglia'); and neuron survival (illustrated as 'neurons') in *Ppt1*$^{-/-}$/*Sn*$^{-/-}$ mice. As a consequence of sialoadhesin (Sn) deficiency, no Sn dependent cell-cell communication occurs between macrophages and T-cells (respectively B-cells) in the body and in the brain of *Ppt1*$^{-/-}$/*Sn*$^{-/-}$ mice (B-cells are not depicted, since they have not yet been described in *Ppt1*$^{-/-}$ mouse brains). The absence of Sn results in decreased microglial activation at 5 and 7 months of age; increased astrocytosis at 3, 5 and 7 months of age; and increased neuron survival at 3 months and marginally also at 5 and 7 months in the thalamus. Additionally, cortical volume and the thickness of the primary somatosensory barrel field (*S1BF*) cortex (abbreviated as 'cortex') are increased at 5 and 7 months of age. Overall, the lack of Sn delays disease progression in *Ppt1*$^{-/-}$/*Sn*$^{-/-}$ mice.

a) Sialoadhesin expressing cells in the *Ppt1*$^{-/-}$ CNS

This study is the first to document Sn expression in *Ppt1*$^{-/-}$ mice. Although, a few Sn expressing cells were already seen at 1 month of age in the basal forebrain of *Ppt1*$^{-/-}$ mice, the first overt presence of Sn+ve macrophage-like cells occurred in the thalamus and *S1BF* cortex of *Ppt1*$^{-/-}$ mice from 3 months onwards (see **Figure 44**). The intensity of Sn immunoreactivity, as well as the number of stained cells increased with disease progression and reached their maximum at 7 months of age. In wildtype mice Sn+ve macrophages could generally, be found either in the meninges, in the choroid plexus lining the walls of the ventricles or in the perivascular spaces around parenchymal blood vessels (see **Figure 44E**), even though a weak up-regulation of Sn+ve microglial cells was also observed in the basal forebrain of 1 month old wildtype mice. In general, our observations were consistent with previous findings that demonstrated Sn brain expression on meningeal macrophages and inflammatory macrophages and/or microglia (Perry *et al.*, 1992; Klaas and Crocker, 2012). Such ambiguity is a common feature of most macrophage/microglial markers. It is not possible to unambiguously distinguish Sn+ve infiltrated macrophages from Sn+ve

microglia, and as such the stained cells in our experiments could be either cell type (see discussion in **Chapter 7**).

However, looking at their morphology in the thalamus at higher magnification (see **Figure 44B** and **Figure 44D**), we speculate that at 3 months of age mainly microglia with long and thin processes stain for Sn, with scattered infiltrated macrophages or microglia derived brain macrophages with amoeboid cell bodies and small processes. This morphological pattern of Sn+ve cells gradually shifts towards more cells resembling macrophages with short processes at 5 months of age. The morphology of Sn+ve cells was clearly further altered at 7 months of age, with predominantly round, brain-macrophage-like cells observed. A similar sequence of events occurred in the *S1BF* cortex, with an increased number and staining intensity of Sn+ve cells at 7 months of age in both regions suggesting that a turning point in disease progression occurs between 5 and 7 months, in respect of Sn+ve expression and morphological activation of microglia, and the possible infiltration of peripheral macrophages in *Ppt1*$^{-/-}$ mice.

Nevertheless, the distribution of Sn+ve staining in *Ppt1*$^{-/-}$ mice resembled that of other macrophage/microglial markers like F4/80, CD68 and CD45 in INCL mice (see **Figure 50** and **Figure 52**; **Figure 16** and **section 3.1a** in **Chapter 3**; (Kielar *et al.*, 2007)). All of these markers demonstrate distinctive and most pronounced cell staining in the thalamus of *Ppt1*$^{-/-}$ mice, with subsequent up-regulation in other cortical and midbrain regions during the course of the disease, leading to similar levels of highly activated brain-macrophages in most brain regions of the *Ppt1*$^{-/-}$ mice by the end of the disease (see for example **Figure 44B** and **Figure 44D**; **Figure 50B** and **Figure 52B**). However, comparing the distribution of Sn+ve staining specifically with that of CD68+ve microglia (see **Figure 44A** and **Figure 44C**; **Figure 50A** and **Figure 52A**), there were clearly many less cells expressing Sn than CD68 in the thalamus and cortex of *Ppt1*$^{-/-}$ mice, suggesting that Sn is only expressed in a subset of microglia in the brain. Furthermore, the Sn immunoreactivity observed in the basal forebrain near the *amygdala* and nuclei of the *anterior commissure* of 1 month old *Ppt1*$^{-/-}$ mice represented another striking difference between these two markers. Speculatively, this Sn+ve staining reflects a hitherto unknown, early vulnerability of certain neurons of the basal forebrain. This hypothesis is strengthened by the fact that the same brain region displayed enhanced Sn and CD68 immunoreactivity at subsequent ages.

However, since similar staining was also detected in 1 month old (but not in older) wildtype mice, this pattern could also be a relic of putative developmental expression of Sn in certain brain regions. Perhaps even more speculatively, this Sn expression pattern possibly could be caused by an altered BBB permeability and 'leakage' of Sn stimulating factors in this brain region at 1 month of age.

However, since the qualitative assessment of Sn expression in *Ppt1*$^{-/-}$ brains was so far only restricted to 2 replicates, these findings have to be confirmed and extended to unambiguously explain these differences between the markers. Nevertheless, these observations strengthen our initial suggestion and hypothesis, that CD169 could be used as a distinctive marker for identifying region-specific sites of inflammation in the brain. Depending on the scientific question being asked, CD169 could even prove to be more sensitive than commonly used CD68 or F4/80 markers, since it is not expressed on every microglia/macrophage.

b) Cell specific alterations slow down disease progression in *Ppt1*$^{-/-}$/*Sn*$^{-/-}$ mice

By genetically removing Sn we demonstrated a series of specific cellular alterations that are accompanied by delayed neuronal loss (see **Figure 54**), and eventually result in a moderately prolonged lifespan of *Ppt1*$^{-/-}$/*Sn*$^{-/-}$ mice. The lack of Sn resulted in reduced microglial activation, but only at the later stages of the disease in the thalamus and not within the cortex (see **Figure 51** and **Figure 53**). The initial stages of microglial activation in *Ppt1*$^{-/-}$ mice therefore do not appear to be directly linked to Sn expressing macrophages. Instead, Sn seems important for the maintenance and further activation of microglia in the thalamus during the progression of INCL. Furthermore, the reduction in microglial activation in *Ppt1*$^{-/-}$/*Sn*$^{-/-}$ mice is probably not linked to direct macrophage-microglia interactions themselves, as previous work demonstrated Sn to be a T- and B-cell specific binding protein with a rather low binding affinity to other macrophages (van den Berg *et al.*, 1992). More likely, CNS microglia interact in a Sn dependent manner with adaptive immune cells (with CD8+ve T-effector cell functions (Muerkoster *et al.*, 1999) or with CD4+ve T-regulatory cells (Wu *et al.*, 2009)), which as a consequence could speculatively re-activate and change the brain environment via the increased (or altered) expression of cytokines and inflammatory molecules in *Ppt1*$^{-/-}$ mice. Whatever the underlying mechanism, it clearly occurs in a regionally specific fashion, with no reduction in microglial activation evident in the *S1BF* cortex of *Ppt1*$^{-/-}$/*Sn*$^{-/-}$ mice (see **Figure 53**). However, in this brain region of

these double knockout mice, microglial activation did display less pronounced laminar specificity (see **Figure 52A**), suggesting more subtle effects upon cortical microglial activation. Therefore, our data suggests that Sn+ve cells may indeed have a brain region-specific impact on microglial activation, and it would be important to understand the underlying cues and signals. These data also highlight the fact that in each brain region a different microclimate of cytokines and molecular signals may prevail, as a result of the complex crosstalk between cell types, although this awaits experimental verification.

As a second key landmark in INCL disease progression, astrocytosis in the thalamus and *S1BF* cortex were also analyzed in *Ppt1*$^{-/-}$/*Sn*$^{-/-}$ double knockout mice. To our initial surprise, this astrocytosis was increased in both brain regions (see **Figure 47** and **Figure 49**). This finding hints at a previously unsuspected functional link between Sn+ve macrophages/microglia and astrocytes. To our knowledge no other study has yet described the nature of astrocytosis in *Sn*$^{-/-}$ mice under either healthy or diseased conditions. Indeed, until now, *Sn*$^{-/-}$ mice have mainly been considered with respect to autoimmune diseases or myelin deficiencies where astrocytosis is present (Williams *et al.*, 2007), but the nature and extent of this astrocyte response has not been looked at in any detail (Kobsar *et al.*, 2006; Ip *et al.*, 2007; Wu *et al.*, 2009). As such, this study on Infantile INCL in which widespread astrocytosis is a characteristic feature (Bible *et al.*, 2004; Kielar *et al.*, 2007), provides an ideal first platform to investigate the possibility of Sn dependent effects on astrocytes. So far we can only speculate about the link between Sn+ve macrophages and astrocytes: possible changes of cytokine levels, altered properties of the BBB or Sn dependent events in the body periphery are all putative explanations for the Sn dependent interlinking of these two cell types. These possibilities shall be discussed in more detail in **Chapter 7**. Future investigations will hopefully clarify the exact link between Sn+ve macrophages/microglia and astrocytes.

In addition to these effects upon reactive changes, neuron survival was also improved in the thalamus of *Ppt1*$^{-/-}$/*Sn*$^{-/-}$ double knockout mice at 3 months of age, and a slightly increased survival was even sustained until the end of the disease, although it did not reach statistically significant levels at 5 and 7 months of age (see **Figure 54**). Compared to *Ppt1*$^{-/-}$ mice, neuron loss occurred at a similar rate in the double knockout mice, just to a lower extent. The most likely explanation for this increased neuronal survival could be due to a reduction in the levels of CD8+ve T-cells in these

mice, due to the lack of activation stimuli from infiltrated Sn+ve macrophages. Although, the detailed negative and positive control measurements of T-cell infiltration in *Sn*$^{-/-}$ and *Ppt1*$^{-/-}$/*Sn*$^{-/-}$ mice have not been conducted, we assume that T-cell maturation and function in *Sn*$^{-/-}$ mice is not altered. We feel this assumption is justified by the previous characterisation of steady-state *Sn*$^{-/-}$ mice, which showed only a small increase in CD8+ve T-cell number in the spleen and lymph nodes, but no changes in T-cell development (Oetke *et al.*, 2006). However, we would also surmise that due to compromised macrophage stimulation less T-cells may infiltrate the brain of *Ppt1*$^{-/-}$/*Sn*$^{-/-}$ mice compared to *Ppt1*$^{-/-}$ mice. This hypothesis is coherent with previous studies in other neurodegenerative disease models that demonstrated a reduction of CD8+ve in diseased *Sn*$^{-/-}$ mice (Kobsar *et al.*, 2006; Ip *et al.*, 2007). Speculatively, the generation of a slightly more neuroprotective environment, via cytokines secreted by astrocytes, could explain the slightly improved neuronal survival in *Ppt1*$^{-/-}$/*Sn*$^{-/-}$ double knockout mice over all ages, but particularly at the end of the disease (5 and 7 months of age). This would be consistent with the suggested neuroprotective role of astrocytes in the pathogenesis of INCL (Macauley *et al.*, 2011). Nevertheless, the unexpected dramatic increase in astrocytosis in *Ppt1*$^{-/-}$/*Sn*$^{-/-}$ mice at 7 months of age was not reflected by an increase in neuronal numbers in the thalamus, suggesting that there may not necessarily be a direct link between these events in all brain regions.

In the cortex, as a representative example of a less severely affected region in murine INCL, the additional deficiency of Sn had an impact that occurred later, but was also longer lasting, upon disease phenotypes (see **Figure 55** and **Figure 56**). The gradual course of cortical atrophy in *Ppt1*$^{-/-}$ mice is clearly altered in *Ppt1*$^{-/-}$/*Sn*$^{-/-}$ mice, with an initial delay and subsequent alteration in the rate of disease progression at 5 months of age, which then succumbs to other disease accelerating mechanisms at the later stage of the disease (as was also seen for astrocytosis in these mice). The net result of these events is an only slightly improved phenotype at 7 months of age. However, it is tempting to think that these improved cortical phenotypes occur via similar mechanisms to those seen in the thalamus, but it cannot be assumed that this is the case.

c) Significance of findings

Sn has drawn increasing attention to itself in recent years as an emerging immune regulatory protein involved in the crosstalk between the innate and adaptive immune system (Martinez-Pomares and Gordon 2012). In the context of INCL, we have shown that Sn appears to enhance disease manifestations in *Ppt1*$^{-/-}$ mice via accelerating neuron loss and cortical atrophy, and enhancing microglial activation, but also attenuating astrocytosis. This study is the first demonstration of a potential link between Sn and astrocyte activation. The mechanisms through which these interactions occur, either directly or indirectly would be an interesting area for future research. In the absence of Sn, *Ppt1*$^{-/-}$ mice have a moderately increased life expectancy, which might pave the way for testing whether drugs may have similar therapeutic effects via specifically blocking Sn activity. Nevertheless our data suggest that disease progression is only partially dependent on Sn expression and any therapeutic efforts in this direction are likely to be partial at the best, and would probably be most promising if used in combination with other therapeutic approaches.

Furthermore, this part of our study again emphasizes how complex the crosstalk is likely to be between the different cellular components of the brain. Even the slightest change in binding properties of macrophages/microglia appears to have an influence on many other cell types. As demonstrated in this chapter, this can potentially be used to manipulate the balance of immune reactions in a neuroprotective direction. If this is to become a reality, it will be essential to understand the exact role of each cell type and how this changes over the course of the disease. This study has provided some clues about the importance of macrophage infiltration in INCL, and at the same time provides more insights into the inflammatory interactions of glial and immune cells in the brain. Considered collectively, this new information may ultimately lead to more targeted and specific therapeutic interventions against INCL that have maximal efficiency and the fewest possible side effects.

Chapter 6

Sialoadhesin deficient *Cln3*$^{-/-}$ mice

After demonstrating a moderate delaying effect of sialoadhesin (Sn) deficiency upon disease progression in *Ppt1*$^{-/-}$ mice in the previous chapter, we next investigated whether Sn played a similar role in another major form of NCL. Juvenile NCL (JNCL) is caused by mutations in the *CLN3* gene, and *Cln3* deficient mice (*Cln3*$^{-/-}$) mice have been widely used as a model for JNCL (see **section 1.2c** and **Table 2** in **Chapter 1**). These mice also display a characteristic early activation of astrocytes and microglia (Pontikis *et al.*, 2004; Pontikis *et al.*, 2005). Therefore, we wanted to determine whether impairing macrophage/microglial cell communication by inactivating Sn in *Cln3*$^{-/-}$ mice would have any impact on their well-characterised neuropathological phenotype.

To achieve this we crossed *Cln3*$^{-/-}$ mice with *Sn*$^{-/-}$ mutant mice and created *Cln3*$^{-/-}$/*Sn*$^{-/-}$ double knockout mice. Since *Cln3*$^{-/-}$ mice display a much later onset and disease progression, these mice had to be aged for a much longer time than *Ppt1*$^{-/-}$/*Sn*$^{-/-}$ mice to reach an equivalent stage of disease progression. As a consequence, the results shown here represent a pilot study to obtain an indication of potential phenotypic changes in *Ppt1*$^{-/-}$/*Sn*$^{-/-}$ mice. We analysed a small number of mice (n = 4 for JNCL forms and n = 2 of control mice) and restricted the analysis to one age group (18 months). In case of interesting findings, the intention is to continue these studies with other age groups and higher n numbers. All mice were analysed for the same phenotypes explored in **Chapters 4** and **Chapter 5**, including brain hemisphere weight, astrocytosis, microglial activation, neuronal number, cortical thickness and cortical volume.

6.1 Sialoadhesin positive cells in the CNS of *Cln3*$^{-/-}$ mice

As in the previous chapter, we first wanted to define where Sn is expressed in *Cln3*$^{-/-}$ and WT control brains. To do this we stained sections from 18 month old mice of each genotype (n=2) for Sn or CD169. Since CD169 is only expressed by infiltrated macrophages and microglia in their vicinity (Perry *et al.*, 1992; Klaas and Crocker, 2012), this protein can be useful to identify region specific activation sites of inflammation in the brain (see **Figure 44** in **Chapter 5**). However, since CD169 is expressed on both infiltrated systemic macrophages and CNS resident microglia, it is not possible to unambiguously distinguish them from each other simply by CD169 staining. As such, we based any classification of Sn positive cells solely on morphological appearance. As in **Chapter 5**, we refer to microglia as cells with elongated ramified processes and (brain-) macrophages with round cells with only

short or no processes (see **Figure 15** in **Chapter 3** for the morphological criteria used to make this distinction). However, both cell morphologies could frequently be found in affected brain regions of *Cln3*$^{-/-}$ mice.

In 18 month old wildtype mice CD169+ve macrophage-like cells were only found at the margins of the brain parenchyma (meninges and choroid plexus lining the walls of the ventricles), but also on macrophages in the perivascular spaces surrounding many cerebral blood vessels (see example in **Figure 44** in **Chapter 5**). The Sn+ve cells in the meninges resembled macrophages of various morphologies (from round, crescent-shaped over to amoeboid), whereas the Sn+ve cells around the blood vessels appeared elongated and wormlike.

In 18 month old *Cln3*$^{-/-}$ mice CD169 staining could be detected in several regions of the brain parenchyma (see **Table 14** for a detailed summary of the distribution of CD169 immunoreactivity in 18 month old *Cln3*$^{-/-}$ mice). Whereas no staining could be detected in the olfactory bulb, weak Sn+ve macrophage/microglial staining was spread throughout the entire cortex in laminae VI and V. Such Sn+ve expression was most prominently seen in the *motor cortex* (mainly in lamina VI of *M2* and laminae VI and V of *M1*), the *agranular insular cortex* (AID and AIV), the *somatosensory cortex* (*S1BF*, *S1FL* and pronounced in caudal parts of *S2*) (see **Figure 58B1**), the *auditory cortex* (*AuV*, *AuD* and *Au1* particularly pronounced in caudal parts) and the *visual cortex* (*V1*) to a lesser degree. Strikingly, the *piriform cortex* from mid-levels of the forebrain towards more caudal parts of the brain, displayed a variety of intensely stained CD169+ve macrophage/microglial cells (data not shown). In particular, the *dorsal endopiriform nucleus* (*DEn*) seemed to preferentially contain such cells. Similar CD169 expression levels were also seen on microglia/macrophage-like cells in the *lateral entorhinal cortex* (*LEnt*) in more caudal parts of the brain (data not shown). However, in contrast to the rather scattered CD169+ve cell distribution in the cortex, the thalamus contained most pronounced CD169+ve cell staining. Intensely stained brain-macrophage-like cells expressing CD169 were detected in the *anterodorsal* and *anteroventral thalamic nuclei* (*AV* and *AD*), the *ventromedial* and *ventrolateral thalamic nucleus* (*VM* and *VL*), the *central medial thalamic nucleus* (*CM*), the *mediodorsal thalamic nuclei* (*MDM*), the *dorsal lateral geniculate nucleus* (*LGNd*), the *medial geniculate nucleus* (*MGM*), the *lateral posterior thalamic nuclei* (*LPMC and LPMR*), and characteristically the *ventral posterior nucleus* (*VPM/VPL*) (see **Figure 58A1**) and some adjacent parts of the *posterior*

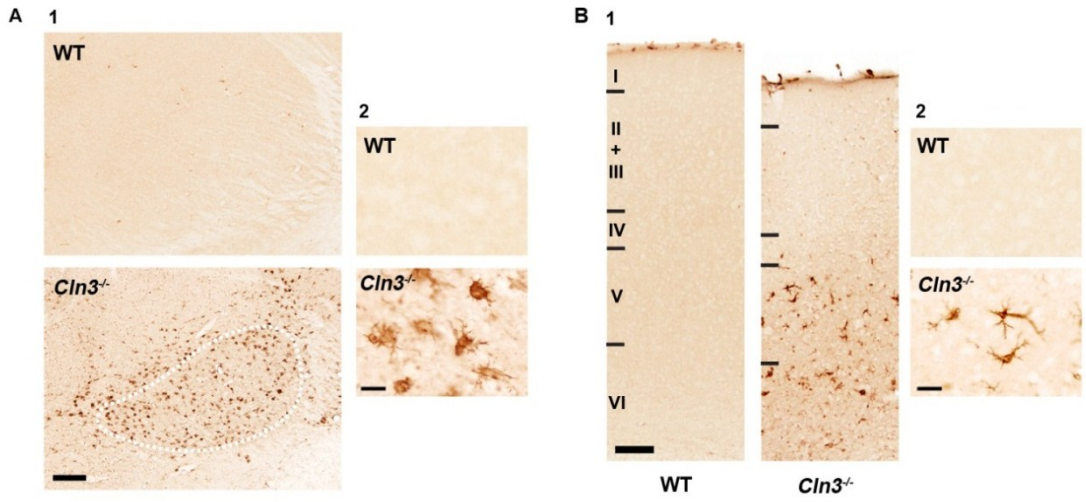

Figure 58. Sialoadhesin positive cells in the thalamus and the somatosensory barrel field (*S1BF*) cortex of *Cln3*$^{-/-}$ mice. (A1) Immunohistochemical staining for the peripheral macrophage/microglial marker CD169 (sialoadhesin) in the thalamus of 18 month old mice revealed localised CD169 expression within the *ventral posterior nucleus* (*VPM/VPL*) (---) of *Cln3*$^{-/-}$ mice. Distinct macrophage-like cell staining could be observed in mutant mice, whereas similar staining was absent in wildtype (WT) mice. Scale bar = 200 μm. (A2) Higher magnification confirmed the morphology of CD169+ve cells in the thalamus of *Cln3*$^{-/-}$ mice as brain-macrophages with short or no cell processes. Scale bar = 20 μm. (B) Immunohistochemical staining for CD169 in the somatosensory cortex *S1BF* revealed CD169 positive cells in the deeper laminae (mainly V, partly VI) which resemble intermediately activated microglia with elongated processes and some macrophage-like cells with small cell bodies without processes. Similar activation was absent in WT mice in which only macrophages in the meninges could be detected. Scale bar = 100 μm. (B2) Higher magnification of CD169+ve cells in lamina V of the *S1BF* demonstrated that mainly activated microglia-like cells with elongated cell processes stained for CD169 in *Cln3*$^{-/-}$ mice. Scale bar = 20 μm.

thalamic nuclear group (PO). Other brain regions that contained CD169+ve macrophages/microglia included the ventral parts of the *subiculum* of the hippocampus, the *pontine nuclei* (*Pn*), the *reticulotegmental nucleus of the pons* (*RtTg*), the *magnocellular* part of the *red nucleus* (*RMC*) and less intense microglial staining in the *principal sensory trigeminal nucleus* (*Pr5VL*) (data not shown).

Out of all these brain regions that contained Sn+ve macrophages in 18 month old *Cln3*$^{-/-}$ mice, we focused our attention on the thalamus and the somatosensory cortex (*S1BF*) (see **Figure 10** in **Chapter 2**), since the thalamocortical system is, similar to other NCL forms, a particular focus for JNCL pathology (Pontikis *et al.*, 2005; Weimer *et al.*, 2006).

As described above, there was a particularly pronounced concentration of Sn+ve cells in the somatosensory thalamus of 18 month old *Cln3*$^{-/-}$ mice (see **Figure 58A1)**. Macrophage-like cells of variable morphology could be detected particularly in the *VPM/VPL* nuclei of the thalamus, ranging from weakly stained cells with amoeboid

Table 14. Detailed summary of the distribution of CD169 immunoreactivity in *Cln3*$^{-/-}$ mice. Brains of 18 month old *Cln3*$^{-/-}$ and wildtype mice were stained for CD169 and a list of brain nuclei showing CD169 immunoreactivity in *Cln3*$^{-/-}$ mouse brains has been compiled. For each nucleus the extent of microglial (**Mic**) and macrophage (**Mϕ**) activation have been recorded, whereby cells with distinct processes were classified as 'microglia'; round intensely immunoreactive cells without processes were defined as 'macrophages' (see also **Figure 15** for distinction). Symbols: '·' = no immunoreactivity, **(+)** = traces of cell-staining, **+** = faintly stained cells, **++** = pronounced cell-staining, **+++** = intense staining of activated cells. Colour intensity reflects the activation status of each cell type (green = microglia, red = macrophages) to visualise the differences of CD169 immunoreactivity between nuclei. I, II, III, IV, V or VI = lamina I-VI. Nuclei definition according to (Paxinos and Franklin, 2001).

Brain region/nucleus		18 Months		
Thalamus		**Mic**	**Mϕ**	**Comments**
VPM/VPL	Ventral posteromedial and posterolateral thalamic nucleus	++	+	
VL	Ventrolateral thalamic nucleus	++	++	
PO	Posterior thalamic nuclei	++	++	
VM	Ventromedial thalamic nucleus	·	·	
LGNd	Dorsal lateral geniculate nucleus	+	+	
AM	Anteromedial thalamic nucleus	+	+	
AD	Anterodorsal thalamic nucleus	++	·	
AV	Anteroventral thalamic nucleus	++	++	
AVDM/VL	Anteroventral thalamic nucleus, dorsomedial/ventrolateral part	++	++	
CM	Central medial thalamic nucleus	++	++	
LPLR/MR	lateral posterior thalamic nucleus, laterorostral/mediocaudal part	++	+	
MD	Mediodorsal thalamic nucleus	·	·	
MDM/L	Mediodorsal thalamic nuclei, medial/lateral part	++	++	
MGV/D/M	Medial geniculate nucleus, ventral /dorsal /medial part	(+)	·	
Re	Reuniens thalamic nucleus	·	·	
ZIV/D	Zona incerta	++	++	
Rh	Rhomboic thalamic nucleus	++	++	
Midbrain				
RMC	Red nucleus, magnocellular part	(+)	·	
RPC	Red nucleus, parvicellular part	+	+	
Hippocampus				
CA1	Cornu Ammonis 1, subfield of hippocampus	·	·	
CA2	Cornu Ammonis 2, subfield of hippocampus	·	·	
CA3	Cornu Ammonis 3, subfield of hippocampus	·	·	
DG	Dentate gyrus	·	·	
S	Subiculum	+	+	(ventral)
Amygdala				
AAD	Anterior amygdaloid area	(+)	·	
AHipM	Amygdalohippocampal area	·	·	
APir	Amygdalopiriform transition area	+	+	
PMCo	Posteromedial cortical amygdaloid nucleus	·	·	
BLA	Basolateral amygdaloid nucleus	·	·	
CeC/M	Central amygdaloid nucleus, capsular part/medial division	·	·	

Brain region/nucleus		18 Months		
Basal ganglia		**Mic**	**Mϕ**	**Comments**
Cpu	Caudate putamen	(+)	·	
LGP	Lateral globus pallidus	(+)	·	
MGP	Medial globus pallidus	(+)	·	
SN	Substantia nigra	·	·	
VP	Ventral pallidum	(+)	·	
Cortex				
Cortex	General pattern	+	+	(VI/V)
S1BF	Primary somatosensory barrel field	+	+	(VI/V)
S1HL/S1FL	Primary somatosensory cortex, hind-/forelimb region	+	+	(VI/V)
S2	Secondary somatosensory cortex	+	+	(VI/V)
Au1/AuD/V	Auditory cortex (primary/secondary auditory cortex, dorsal/ventral)	++	+	(VI/V)
AID/V	Agranular insular cortex, dorsal/ventral	+	+	(VI/V)
V1	Visual cortex	+	+	(VI/V)
M1	Motor cortex 1	+	+	(VI/V)
M2	Motor cortex 2	+	+	(VI/V)
RSA	The retrosplenial agranular cortex	·	·	
RSG	The retrosplenial granular cortex	(+)	·	(V)
Cig1/2	Cingulate cortex area 1/2	·	·	
Pir	Piriform cortex	++	+	(III & Mϕ in II)
VO/LO	Ventral/lateral orbital cortex	·	·	
LEnt	Lateral entorhinal cortex	++	+	(all laminae) (VI: Mϕ)
DEn	Dorsal endopiriform nucleus	+	++	
VEn	Ventral endopiriform nucleus	+	+	
Hypothalamus				
IPACM/L	Interstitial nucleus of posterior limb of anterior commissure, med./lat. part	·	·	
MCPO	Magnocellular preoptic nucleus	+	·	
HDB	Nucleus of horizontal limb of the diagonal band	+	·	
Pons & Medulla				
Pons	General pattern	+	·	(apart from specific nuclei)
Pr5	Principal sensory trigeminal nucleus	++	+	
VLL	Ventral nucleus of lateral lemniscus	+	+	
RtTg	Reticulotegmental nucleus of the pons	++	++	
CIC	Central nucleus of the inferior colliculus	·	·	
ECIC	External cortex of the inferior colliculus	·	·	
Pn	Pontine nuclei	++	++	
LDTg	Laterodorsal tegmental nucleus	·	·	
Mo5	Motor trigeminal nucleus	(+)	·	
Olfactory bulb				
OB	Olfactory bulb	+	+	
EPI	External plexiform layer of the olfactory bulb	+	+	
GRO	Granular cell layer of the olfactory bulb	+	+	
DTT	Dorsal tenia tecta	+	++	

cell soma and short processes to more intensely stained cells with round soma and no processes (see **Figure 58A2**). Similarly, in the somatosensory cortex (*S1BF)* of *Cln3*$^{-/-}$ mice macrophage-like Sn+ve cells could be detected in the deeper layers (see **Figure 58B1**), in particular within laminae V and VI. These contained many Sn-expressing cells which resembled partly activated microglia with enlarged cell soma and elongated branched processes, but some appearing like activated macrophages with very few processes (see **Figure 58B2**).

Collectively, these data demonstrate that Sn+ve cells are not only present in severely affected *Cln3*$^{-/-}$ mice, but are concentrated in regions where pathological changes are on-going.

6.2 Reduced hemisphere mass of *Cln3*$^{-/-}$ and *Cln3*$^{-/-}$/*Sn*$^{-/-}$ mice

As a general indicator of neurodegeneration, the weights of all brain hemispheres were measured after paraformaldehyde fixation and removal of the cerebellum (see **Figure 59**). Both *Cln3*$^{-/-}$ and *Cln3*$^{-/-}$/*Sn*$^{-/-}$ mice showed a significant reduction in hemisphere mass compared to WT controls at 18 months of age. Brain hemispheres from *Cln3*$^{-/-}$ mice were 19.9% lighter than those from WT controls, whereas *Cln3*$^{-/-}$/*Sn*$^{-/-}$ double knockout mice displayed only a 14.2% reduction in hemisphere mass compared to wildtype mice. Indeed, *Cln3*$^{-/-}$/*Sn*$^{-/-}$ double knockout hemispheres were 5.8% heavier than *Cln3*$^{-/-}$ single mutant mouse hemispheres in relation to wildtype mice. However, this difference between *Cln3*$^{-/-}$ and *Cln3*$^{-/-}$/*Sn*$^{-/-}$ mice was not statistically significant.

Although such weight measurements may be subject to many variable factors like moisture content, cerebellum separation or damage to the brain during harvesting, these data gave us the first indications of possible differences between *Cln3*$^{-/-}$ and *Cln3*$^{-/-}$/*Sn*$^{-/-}$ double knockout mice and prompted us to perform further analyses of these brains.

6.3 Impact of *Sn* deficiency on reactive phenotypes in *Cln3*$^{-/-}$ mice

Because Sn is expressed on the surface of brain macrophages (Perry *et al.*, 1992; Ip *et al.*, 2007), it would be of great interest to determine the extent to which the absence of Sn affects innate immune responses in *Cln3*$^{-/-}$ mice. Therefore, we stained tissue from 18 month old *Cln3*$^{-/-}$ and WT control mice for the astrocyte marker GFAP and the microglial marker CD68. We focused our analysis on the two most affected regions in

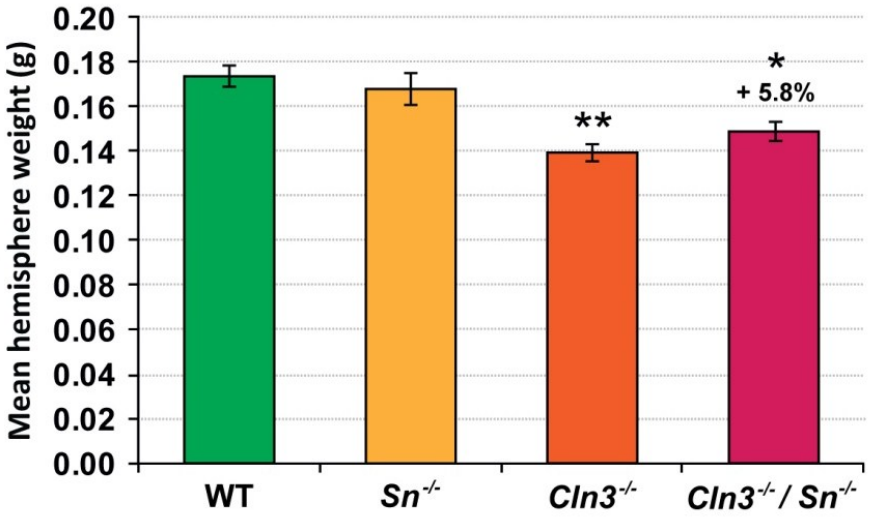

Figure 59. Loss of brain mass in *Cln3*$^{-/-}$ and *Cln3*$^{-/-}$/*Sn*$^{-/-}$ mice. The weights of 18 month old brain hemispheres from mice of each genotype (*Cln3*$^{-/-}$, *Cln3*$^{-/-}$/*Sn*$^{-/-}$, *Sn*$^{-/-}$ and wildtype) were measured after PFA fixation and removal of the cerebellum, but before further processing. A significant loss in hemisphere mass was observed in *Cln3*$^{-/-}$ and *Cln3*$^{-/-}$/*Sn*$^{-/-}$ mice, compared to age-matched wildtype (WT) mice. Hemispheres from *Cln3*$^{-/-}$/*Sn*$^{-/-}$ mice were marginally heavier than *Cln3*$^{-/-}$ mice, but this difference was not significant. Percentage indicates difference between *Cln3*$^{-/-}$ and *Cln3*$^{-/-}$/*Sn*$^{-/-}$ mice in comparison to WT mice. Statistics: One-way ANOVA with Bonferroni post hoc test, *p<0.05, **p<0.01. Data shown as mean ± SEM, n = 2 (WT and *Sn*$^{-/-}$) or n = 4 (*Cln3*$^{-/-}$ and *Cln3*$^{-/-}$/*Sn*$^{-/-}$).

Cln3$^{-/-}$ mice: the thalamic *ventral posterior nucleus* (*VPM/VPL*) and the cortical *somatosensory barrel field* (*S1BF)* according to (Pontikis *et al.*, 2004; Pontikis *et al.*, 2005) (see **Figure 10** in **Chapter 2**). Immunohistochemical staining and subsequent quantification via thresholding image analysis were performed for both regions in all brains.

a) Astrocytosis in the thalamus of *Cln3*$^{-/-}$ and *Cln3*$^{-/-}$/*Sn*$^{-/-}$ mice

Whereas no staining, or only very occasional faintly stained protoplasmic astrocytes could be detected in *Sn*$^{-/-}$ as well as wildtype mice, both *Cln3*$^{-/-}$ and *Cln3*$^{-/-}$/*Sn*$^{-/-}$ mice displayed a pronounced astrocytosis in the thalamus (see **Figure 60A**). Here, the presence of many intensely stained and hypertrophied GFAP+ve astrocytes with thickened processes that formed a dense meshwork was observed within the neuropil of 18 month old *Cln3*$^{-/-}$ mice. This staining was most pronounced, but not confined to *VPM/VPL*, spreading into adjacent thalamic nuclei. A similar distribution of GFAP immunoreactivity was evident in *Cln3*$^{-/-}$/*Sn*$^{-/-}$ double knockout mice, but its intensity appeared to be slightly reduced compared to single mutant *Cln3*$^{-/-}$ mice, which was more apparent at higher power (see **Figure 60B**).

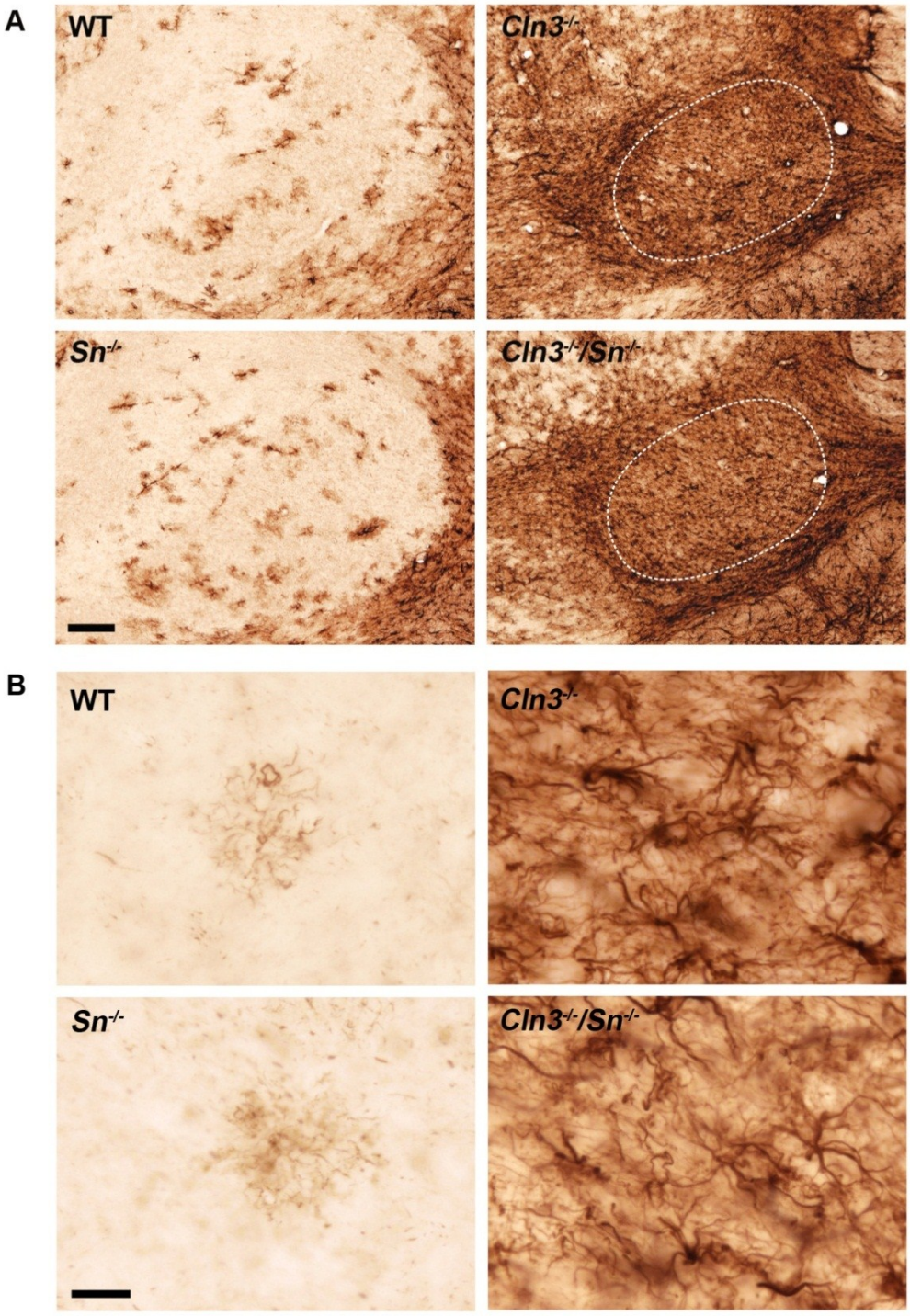

Figure 60. Similar astrocytosis in the thalamus of *Cln3*$^{-/-}$ and *Cln3*$^{-/-}$/*Sn*$^{-/-}$ double knockout mice. (see figure caption on next page)

Figure 60. Similar astrocytosis in the thalamus of *Cln3*$^{-/-}$ and *Cln3*$^{-/-}$/*Sn*$^{-/-}$ double knockout mice. (A) Immunohistochemical staining for the astrocyte marker glial fibrillary acidic protein (GFAP) in the thalamus of 18 month old mice revealed localised astrocytosis within the *ventral posterior nucleus* (*VPM/VPL*) (---) of JNCL mice. *Cln3*$^{-/-}$/*Sn*$^{-/-}$ double knockout mice showed similar levels of GFAP immunoreactivity compared to *Cln3*$^{-/-}$ mice. GFAP immunoreactivity was virtually absent in age-matched *Sn*$^{-/-}$ mice or wildtype (WT) mice. Scale bar = 200 μm (B) Higher magnification revealed similar morphology and density of GFAP+ve astrocytes in the *VPM/VPL* of *Cln3*$^{-/-}$ and *Cln3*$^{-/-}$/*Sn*$^{-/-}$ mice at 18 months of age. Marginally reduced intensity of GFAP immunoreactivity was apparent in *Cln3*$^{-/-}$/*Sn*$^{-/-}$ mice, but many intensely stained fibrous astrocytes were present in *VPM/VPL* of single as well as double *Cln3* mutant mice. These astrocytes displayed thickened processes and filled the thalamic neuropil completely with GFAP+ve astrocytes and their processes. In WT and *Sn*$^{-/-}$ mice only occasional faintly stained protoplasmic astrocytes with many long thin processes could be seen. Scale bar = 20 μm.

Subsequent thresholding image analysis revealed there was a mean 6.0% reduction of GFAP+ve staining intensity in the double knockout mice compared to *Cln3*$^{-/-}$ mice (see **Figure 61**). However, due to a high variation between individual mice, this difference did not reach a statistically significant level. However, the astrocytosis in the thalamus of both *Cln3*$^{-/-}$ and *Cln3*$^{-/-}$/*Sn*$^{-/-}$ mice was significantly elevated compared to control WT or *Sn*$^{-/-}$ brains. These findings are consistent with data published in knock-in mice at 12 months of age (Pontikis *et al.*, 2005), in which a pronounced astrocytosis could be detected in the *VPM/VPL* nuclei of the thalamus.

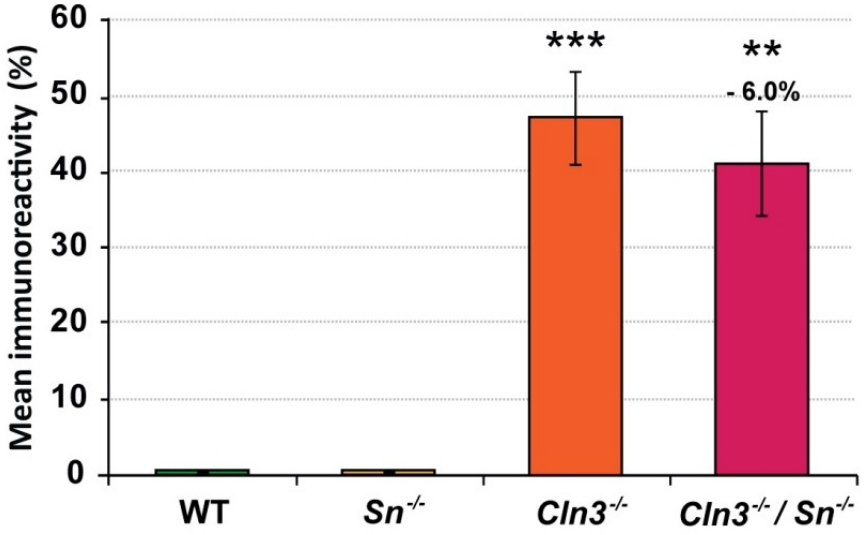

Figure 61. Marginally reduced levels of astrocytosis in the thalamus (*VPM/VPL*) of *Cln3*$^{-/-}$/*Sn*$^{-/-}$ double knockout mice. Thresholding image analysis revealed that the mean level of GFAP immunoreactivity in double knockout mice was marginally reduced in *Cln3*$^{-/-}$/*Sn*$^{-/-}$ mice, compared to *Cln3*$^{-/-}$ mice, but this difference was not significant. Single as well as double *Cln3* mutant mice showed significant astrocytosis compared to WT mice. In contrast, almost no GFAP immunoreactivity was detected in the thalamus of either *Sn*$^{-/-}$ or wildtype (WT) mice. Percentage indicates difference between *Cln3*$^{-/-}$ and *Cln3*$^{-/-}$/*Sn*$^{-/-}$ mice. Statistics: Two-way ANOVA with Bonferroni post hoc test, **p<0.01, ***p<0.001. Data shown as mean ± SEM, n = 2 (WT and *Sn*$^{-/-}$) or n = 4 (*Cln3*$^{-/-}$ and *Cln3*$^{-/-}$/*Sn*$^{-/-}$).

b) Astrocytosis in the cortex of *Cln3*$^{-/-}$ and *Cln3*$^{-/-}$/*Sn*$^{-/-}$ mice

In contrast to the widespread astrocytosis in the thalamus of *Cln3*$^{-/-}$ and *Cln3*$^{-/-}$/*Sn*$^{-/-}$ mice, the *S1BF* region displayed more localised GFAP staining. A laminar-specific pattern of astrocytosis was evident in both of these strains of mutant mice, with the most intense staining largely confined to the deeper laminae (V and VI) of this cortical sub-region (see **Figure 62A**). This pattern was not restricted to *S1BF* and was seen in other regions of the cortex, but to a lesser extent. This pattern of astrocytosis within the more ventral layers of *S1BF* was similar in both lines of *Cln3* deficient mice, but with additional scattered astrocytes present in the more dorsal layers in *Cln3*$^{-/-}$/*Sn*$^{-/-}$ double knockout mice that were more intensely stained than those in *Cln3*$^{-/-}$ mice. Similarly, higher magnification pictures of lamina VI of the *S1BF* cortex also revealed no overt differences between the two genotypes (see **Figure 62B**). In both mouse populations intensely stained fibrous astrocytes with hypertrophic cell bodies and thickened processes were present in lamina VI. As only putative difference it could be suggested that the astrocytes in *Cln3*$^{-/-}$/*Sn*$^{-/-}$ double knockout mice displayed marginally less ramified and less intensely stained cell processes (see **Figure 62B**). In contrast, astrocytosis in *Sn*$^{-/-}$ and wildtype control mice was largely confined to the most ventral parts of lamina VI, adjacent to the corpus callosum and the occasional GFAP positive astrocyte in laminae I and II (see **Figure 62A**).

These findings are consistent with data published in *Cln3* knock-in mice at 12 months of age (Pontikis *et al.*, 2005), in which astrocytosis could be detected in the deeper, but also in the most superficial layers of *S1BF*. In our mice, the astrocytosis was present in both laminae VI and V, whereas in (Pontikis *et al.*, 2005) the GFAP+ve activation in knock-in mice could only be found in laminae VI and I. This may reflect the slightly different targeting strategies employed in these two commonly used models of JNCL.

Quantification of GFAP immunoreactivity in the *S1BF* region via thresholding image analysis revealed a 1.9% reduction in staining intensity in *Cln3*$^{-/-}$/*Sn*$^{-/-}$ mice compared to single mutant mice (see **Figure 63**), but this difference between *Cln3*$^{-/-}$ and *Cln3*$^{-/-}$/*Sn*$^{-/-}$ mice was not significant. Nevertheless, this level of astrocytosis present in *S1BF* of both *Cln3*$^{-/-}$ and *Cln3*$^{-/-}$/*Sn*$^{-/-}$ mice was significantly higher than that seen in WT control and *Sn*$^{-/-}$ brains.

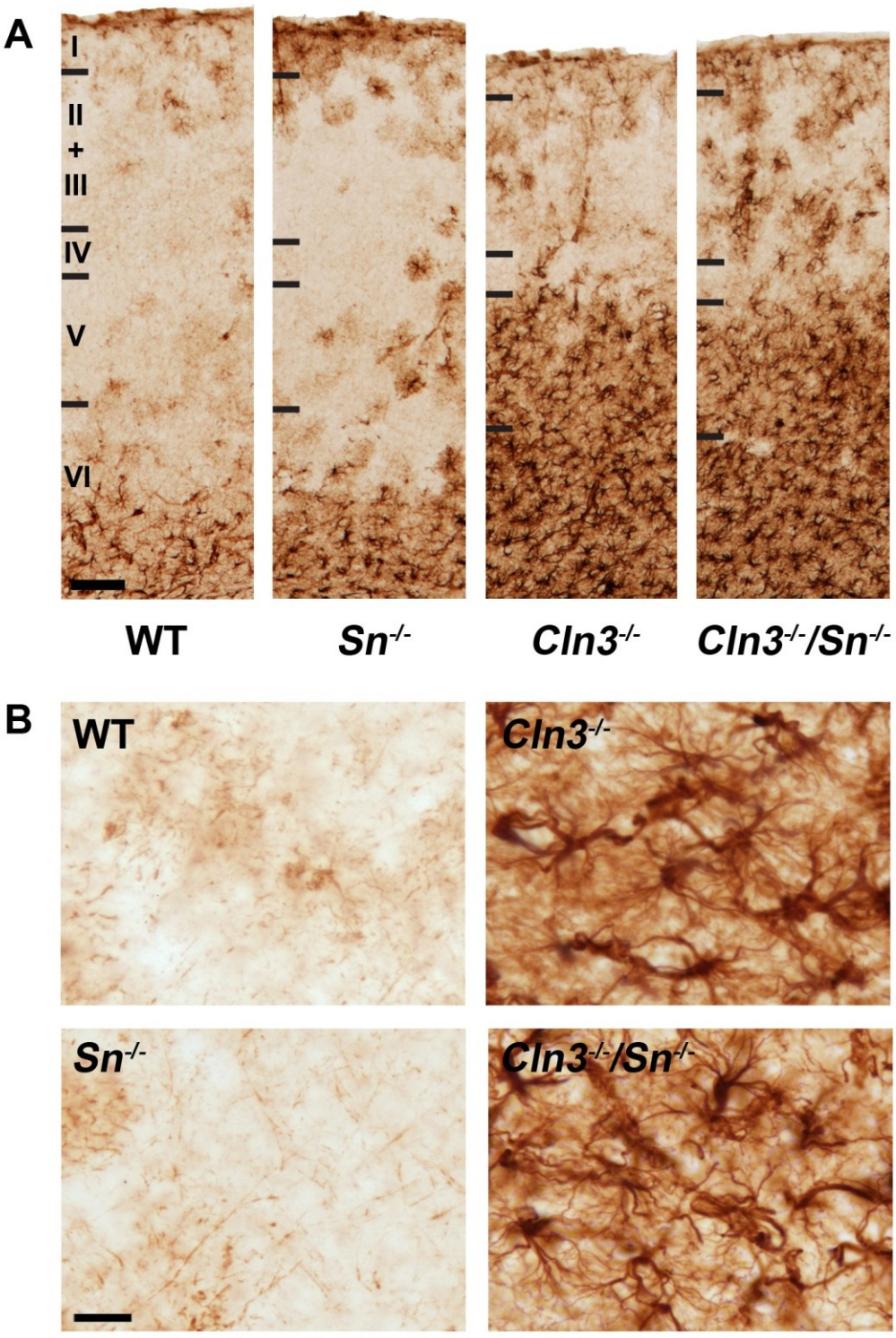

Figure 62. Similar astrocytosis in the somatosensory barrel field (*S1BF*) cortex of *Cln3*$^{-/-}$ and *Cln3*$^{-/-}$/*Sn*$^{-/-}$ mice. (see figure caption on next page)

Figure 62. Similar astrocytosis in the somatosensory barrel field (*S1BF*) cortex of *Cln3*$^{-/-}$ and *Cln3*$^{-/-}$/*Sn*$^{-/-}$ mice. (A) Immunohistochemical staining for astrocyte marker glial fibrillary acidic protein (GFAP) in the *S1BF* of 18 month old mice revealed no overt difference in astrocytosis between *Cln3*$^{-/-}$ and *Cln3*$^{-/-}$/*Sn*$^{-/-}$ double knockout mice. In both single and double *Cln3* mutant mice GFAP immunoreactivity was prominently seen in deeper laminae (mainly V and VI) of the cortex with some faintly stained protoplasmic astrocytes in more dorsal laminae. Only marginally, if at all, reduced, intensity of GFAP immunoreactivity was evident in *Cln3*$^{-/-}$/*Sn*$^{-/-}$ mice. In control mice (*Sn*$^{-/-}$ and wildtype (WT)) astrocytosis was mainly confined to the most ventral parts of lamina VI, with occasional faintly stained protoplasmic astrocytes with many long thin branched processes in more dorsal layers. Scale bar = 100 μm. (B) Higher magnification pictures of lamina VI of the *S1BF* revealed similar morphology and density of GFAP+ve astrocytes in *Cln3*$^{-/-}$ and *Cln3*$^{-/-}$/*Sn*$^{-/-}$ mice at 18 months of age. Many intensely stained fibrous astrocytes with hypertrophic cell soma and thickened processes were present in the *S1BF* of single as well as double *Cln3* mutant mice. Marginally less intensely stained and less ramified processes could be suggested in *Cln3*$^{-/-}$/*Sn*$^{-/-}$ mice, compared to single *Cln3*$^{-/-}$ mice. In WT and *Sn*$^{-/-}$ mice only occasional faintly stained protoplasmic astrocytes with many long thin processes could be seen. Scale bar = 20 μm.

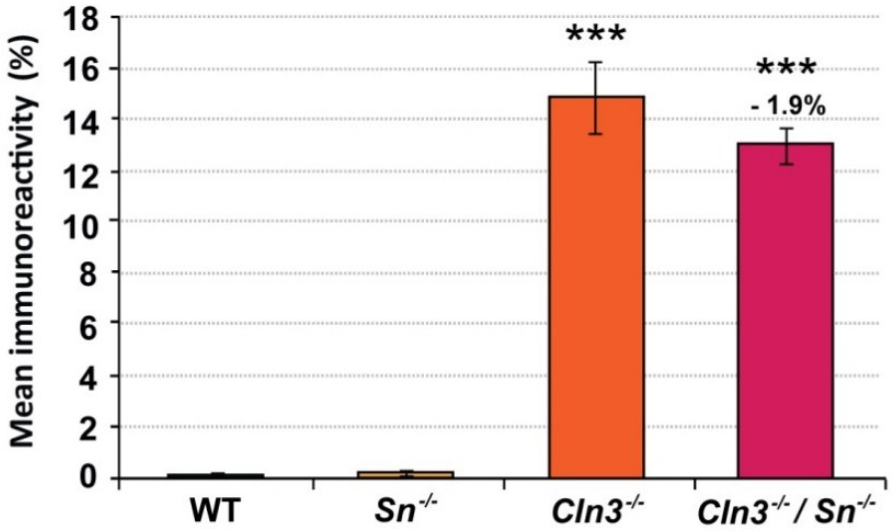

Figure 63. Marginally reduced levels of astrocytosis in the somatosensory barrel field (*S1BF*) cortex of 18 month *Cln3*$^{-/-}$/*Sn*$^{-/-}$ double knockout mice. Thresholding image analysis revealed that the mean level of GFAP immunoreactivity in *Cln3*$^{-/-}$/*Sn*$^{-/-}$ double knockout mice was marginally reduced compared to *Cln3*$^{-/-}$ mice, but this difference was not significant. Nevertheless, both single and double *Cln3* mutant mice showed significantly increased GFAP immunoreactivity compared to wildtype (WT) mice. Almost no GFAP immunoreactivity was detected in the thalamus of either *Sn*$^{-/-}$ or wildtype (WT) mice. Percentages indicate differences between *Cln3*$^{-/-}$ and *Cln3*$^{-/-}$/*Sn*$^{-/-}$ mice. Statistics: One-way ANOVA with Bonferroni post hoc test, ***$p<0.001$. Data shown as mean ± SEM, n = 2 (WT and *Sn*$^{-/-}$) or n = 4 (*Cln3*$^{-/-}$ and *Cln3*$^{-/-}$/*Sn*$^{-/-}$).

Taken together, these data demonstrate that in 18 month old *Cln3*$^{-/-}$ mice pronounced astrocytosis is present in the thalamus as well as in *S1BF,* and that the lack of Sn results in a marginal, but not significant attenuation of GFAP immunoreactivity in both brain regions of *Cln3*$^{-/-}$/*Sn*$^{-/-}$ mice.

c) Microglial activation in the thalamus of *Cln3*$^{-/-}$ and *Cln3*$^{-/-}$/*Sn*$^{-/-}$ mice

To determine the impact of *Sn* deficiency upon microglial activation in *Cln3*$^{-/-}$ mice all brains were immunostained for CD68, an analysis that has not been conducted previously in 18 month old *Cln3*$^{-/-}$ mice. Pronounced activation of microglia could be detected with many intensely stained CD68+ve cells present in the thalamic *VPM/VPL* nuclei in 18 month old JNCL mice, similar to the distribution observed in INCL mice (see **Figure 64A** and compare **Figure 37A** in **Chapters 4** and **Figure 50A** in **Chapter 5**). These CD68+ve cells displayed a range of morphologies, suggesting multiple stages of microglial activation were apparent. These morphologies ranged from more palely stained microglia with long ramified processes (mostly seen outside the *VPM/VPL* nuclei), to intermediately activated cells with a mixture of shorter ramified processes, to highly activated microglia with a brain macrophage-like appearance as darkly stained round cells with short stubby processes (see **Figure 64B**). These most highly activated microglial cells were seen mostly just within the orders of the *VPM/VPL*, especially in its ventral portion. In contrast, CD68 staining was virtually absent in *Sn*$^{-/-}$ and wildtype control mice, revealing only quiescent microglia with small cell bodies and thin long ramified processes.

Inactivating Sn, an important binding protein on brain macrophages (Perry *et al.*, 1992; Ip *et al.*, 2007) appeared to have only a slight alleviating effect on microglial activation in the thalamus of *Cln3*$^{-/-}$ mice. Morphologically some microglia could be interpreted as being in a less activated state, particularly in the *VPL* nuclei of the thalamus, as was evident at higher magnification (see **Figure 64B**). However, these effects were not very pronounced and there was no clear qualitative difference in microglial activation between *Cln3*$^{-/-}$ and *Cln3*$^{-/-}$/*Sn*$^{-/-}$ mice.

Quantification via thresholding image analysis confirmed the significant difference in the level of microglial activation between both *Cln3* deficient mouse populations, and either *Sn*$^{-/-}$ or WT controls, both of which showed minimal CD68 immunoreactivity (see **Figure 65**). A mean reduction in staining intensity of 2.0% was detected in *Cln3*$^{-/-}$/*Sn*$^{-/-}$ mice compared to single *Cln3* mutant mice, but due to the high variation in mice of both genotypes, no significant difference could be detected. Compared to *Ppt1*$^{-/-}$ mice, the staining intensity of 18 month old *Cln3*$^{-/-}$ mice was equivalent to the level of microglial activation seen in 3 month old *Ppt1*$^{-/-}$ mice, confirming that a weaker and much delayed inflammatory response can be observed in *Cln3*$^{-/-}$ mice.

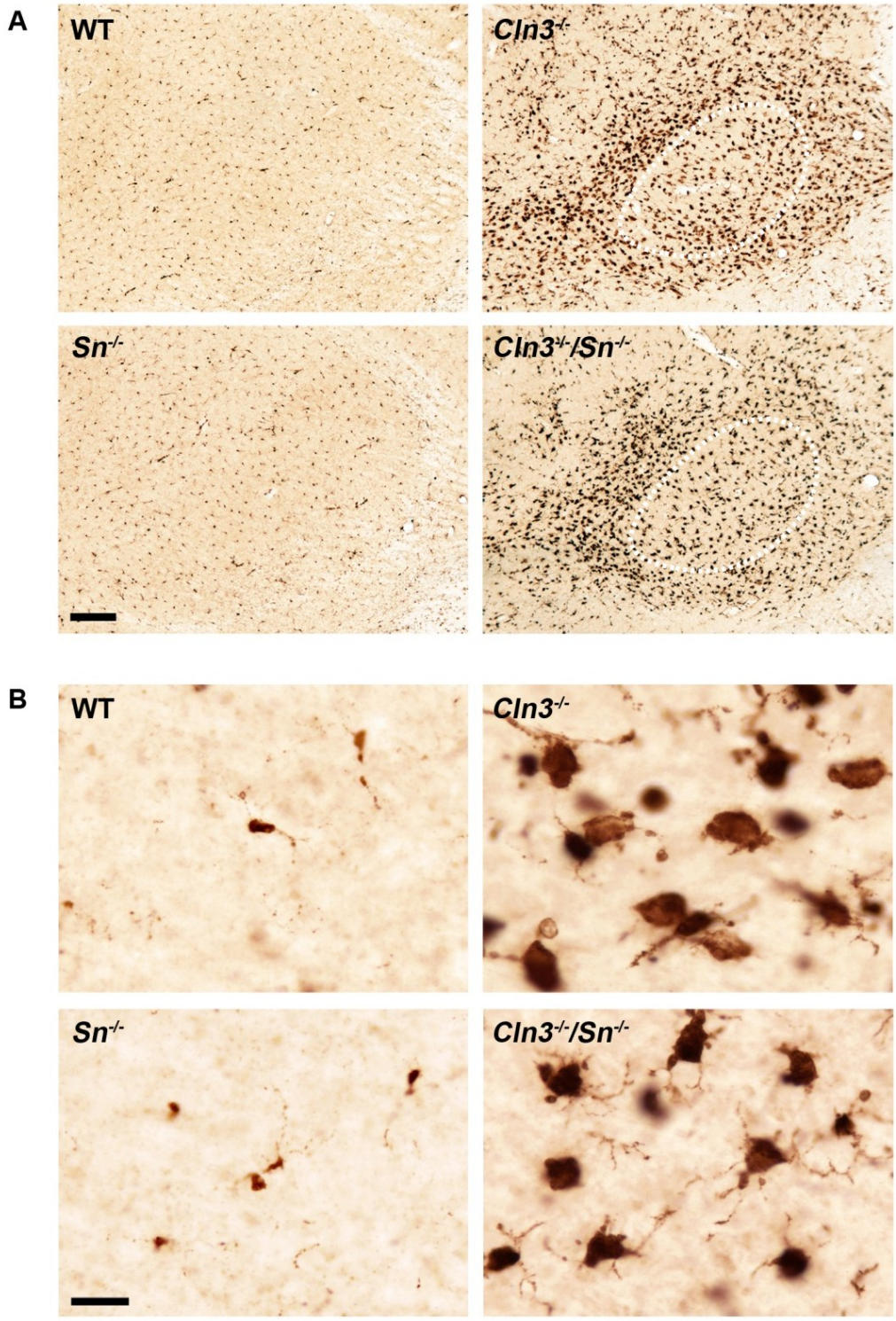

Figure 64. Marginally reduced microglial activation in the thalamus (*VPM/VPL*) of *Cln3*$^{-/-}$ and *Cln3*$^{-/-}$/*Sn*$^{-/-}$ double knockout mice. (see figure caption on next page)

Figure 64. Marginally reduced microglial activation in the thalamus (*VPM/VPL*) of *Cln3*$^{-/-}$ and *Cln3*$^{-/-}$/*Sn*$^{-/-}$ double knockout mice. (A) Immunohistochemical staining for the microglial marker CD68 in the thalamus of 18 month old mice revealed localised microglial activation within the *ventral posterior nucleus* (*VPM/VPL*) (---) of both *Cln3* mutant mice. *Cln3*$^{-/-}$/*Sn*$^{-/-}$ double knockout mice showed marginally reduced CD68 immunoreactivity compared to *Cln3*$^{-/-}$ mice. Similar microglial activation was absent in *Sn*$^{-/-}$ and wildtype (WT) mice in which only quiescent stained microglia could be detected. Scale bar = 200 μm. (B) Higher magnification pictures of CD68+ve microglia in the thalamus of 18 month old mice revealed marginal differences in cell morphology and activation between double and single *Cln3* mutant mice. It could be suggested that *Cln3*$^{-/-}$/*Sn*$^{-/-}$ double knockout mice showed slightly reduced microglial activation in the thalamus in terms of cell size and processes. Microglia in *Cln3*$^{-/-}$ mice were intensely CD68 immunoreactive with an enlarged and rounded cell soma and small processes, whereas microglia in *Cln3*$^{-/-}$/*Sn*$^{-/-}$ double knockout mice seemed little bit smaller with more elongated microglial processes. Only quiescent microglia were detected in control mice (*Sn*$^{-/-}$ and WT). Scale bar = 20 μm.

However, such comparisons should be interpreted with caution given the different mixed strain background of the *Cln3*$^{-/-}$ mice used, rather than the congenic C57Bl/6 background of all other mice in this thesis. However, it is possible to get a qualitative impression of the relative extent of microglial activation in *Cln3*$^{-/-}$ and *Ppt1*$^{-/-}$ mice, which is consistent with unpublished observations comparing the reactive phenotypes of these mice on the same C57Bl/6 background (JD Cooper, personal communication).

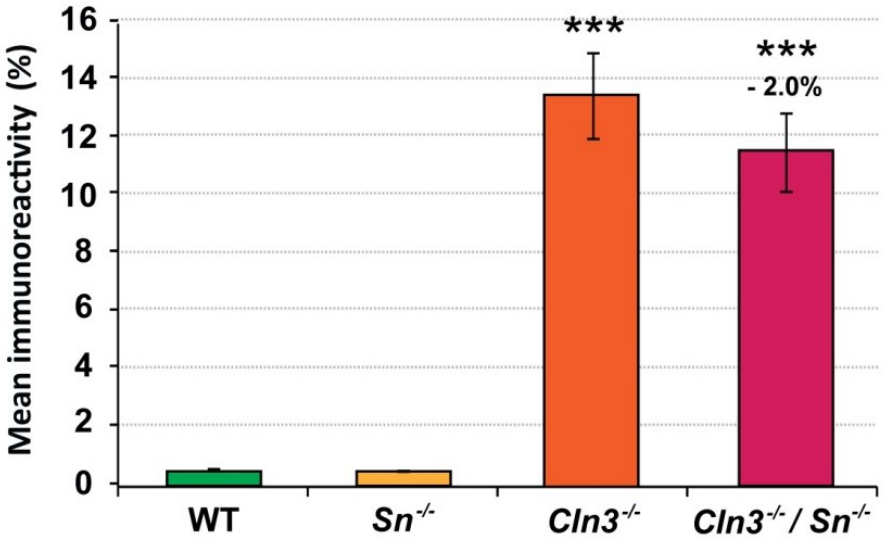

Figure 65. Marginally reduced levels of microglial activation in the thalamus (*VPM/VPL*) of *Cln3*$^{-/-}$/*Sn*$^{-/-}$ double knockout mice. Thresholding image analysis revealed that the mean level of CD68 immunoreactivity in double knockout mice was only marginally reduced compared to *Cln3*$^{-/-}$ mice. However, this difference did not reach statistical significance. Nevertheless, both single and double *Cln3* mutant mice showed significantly increased CD68 immunoreactivity compared to wildtype (WT) mice. Almost no CD68 immunoreactivity was detected in the thalamus of either *Rag-1*$^{-/-}$ or wildtype (WT) mice. Percentage indicates differences between *Cln3*$^{-/-}$ and *Cln3*$^{-/-}$/*Sn*$^{-/-}$ mice. Statistics: One-way ANOVA with Bonferroni post hoc test, ***$p<0.001$. Data shown as mean ± SEM, n = 2 (WT and *Sn*$^{-/-}$) or n = 4 (*Cln3*$^{-/-}$ and *Cln3*$^{-/-}$/*Sn*$^{-/-}$).

d) Microglial activation in the cortex of *Cln3*$^{-/-}$ and *Cln3*$^{-/-}$/*Sn*$^{-/-}$ mice

Similar to astrocytosis in the *S1BF* cortex (see **Figure 62A**), CD68+ve cell staining was detected in a layer specific manner in *Cln3* mutant mice (see **Figure 66A**). In the deeper cortical laminae (VI and V) of *S1BF*, intensely stained CD68+ve brain macrophages could be identified with round, darkly stained cell bodies and short processes. In the other laminae less intensely stained microglia with a smaller cell body were present. This evidence for laminar-specific microglial activation is in contrast to previous F4/80 data (Pontikis *et al.*, 2005), suggesting that CD68 provides a more sensitive marker of these events than F4/80. However, no overt differences in cell distribution, cell morphology or staining intensity could be seen between *Cln3*$^{-/-}$/*Sn*$^{-/-}$ mice and single mutant *Cln3*$^{-/-}$ mice (see **Figure 66**). Higher magnification pictures of lamina VI of the *S1BF* revealed microglia with intensely stained cell soma and short processes resembling brain-macrophages, as well as less activated microglia with elongated processes to a similar extent in both *Cln3*$^{-/-}$ mutant mouse strains (see **Figure 66B**). Compared to the relative paucity of Sn (CD169) staining (see **Figure 58B**) many more CD68+ve microglia were present in the cortex of *Cln3*$^{-/-}$ mice than CD169+ve macrophages. The difference between these two markers suggests on the one hand that Sn+ve cells in *S1BF* are predominantly not microglia, but perhaps infiltrated macrophages, or alternatively that Sn is only expressed and up-regulated on a subset of microglia. The mechanisms that trigger Sn expression in the brain are so far unknown, but Sn expression seems to coincide with sites of active neurodegeneration or inflammation in the brain. These issues shall be further discussed in **Chapter 7**.

Thresholding image analysis of CD68+ve immunoreactivity in the *S1BF* of all 18 month old brains revealed significantly more staining in both *Cln3*$^{-/-}$ mice and *Cln3*$^{-/-}$/*Sn*$^{-/-}$ mice than in either *Sn*$^{-/-}$ or WT control mice. There was, however, no significant difference between CD68 immunoreactivity in *Cln3*$^{-/-}$ mice and *Cln3*$^{-/-}$/*Sn*$^{-/-}$ mice (see **Figure 67**). Only 0.2% less mean staining intensity could be detected in the double knockout mice compared to the single *Cln3*$^{-/-}$ mice. The only obvious difference could be seen in the variation in these data, with *Cln3*$^{-/-}$/*Sn*$^{-/-}$ mice showing a much smaller variability in CD68 immunoreactivity than *Cln3*$^{-/-}$ mice.

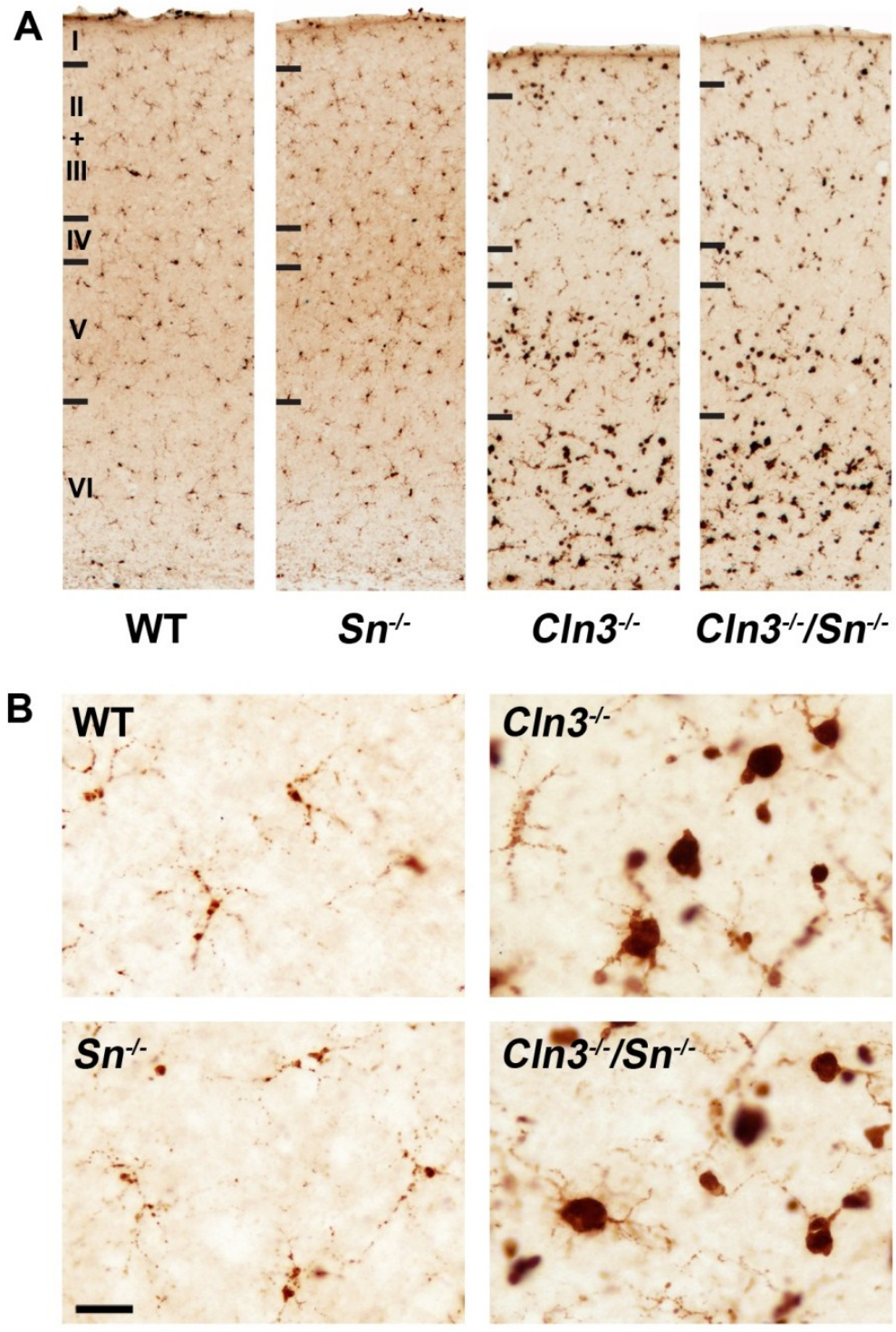

Figure 66. Similar microglial activation in the somatosensory barrel field (*S1BF*) cortex of *Cln3*$^{-/-}$ and *Cln3*$^{-/-}$/*Sn*$^{-/-}$ double knockout mice. (see figure caption on next page)

Figure 66. Similar microglial activation in the somatosensory barrel field (*S1BF*) cortex of *Cln3*$^{-/-}$ and *Cln3*$^{-/-}$/*Sn*$^{-/-}$ double knockout mice. Immunohistochemical staining for the microglial marker CD68 in the *S1BF* of 18 month old mice revealed no overt differences between *Cln3*$^{-/-}$ and *Cln3*$^{-/-}$/*Sn*$^{-/-}$ double knockout mice. In both single and double *Cln3* mutant mice, intensely stained CD68 positive microglia were most prominent in laminae VI and V of the *S1BF* with only isolated activated microglia in more dorsal laminae. Similar activation was absent in control mice (*Sn*$^{-/-}$ wildtype (WT)) in which only quiescent microglial staining could be detected. Scale bar = 100 μm. (B) Higher magnification pictures of CD68+ve microglia in lamina VI of the *S1BF* cortex of 18 month old mice revealed no differences in cell morphology and activation between double and single *Cln3* mutant mice. Both genotypes displayed intensely CD68 immunoreactive microglia of various activation states, resembling either brain macrophages with an enlarged cell soma and small processes, or intermediately activated microglia with elongated processes. Only quiescent microglia were detected in control mice (*Sn*$^{-/-}$ and WT). Scale bar = 20 μm.

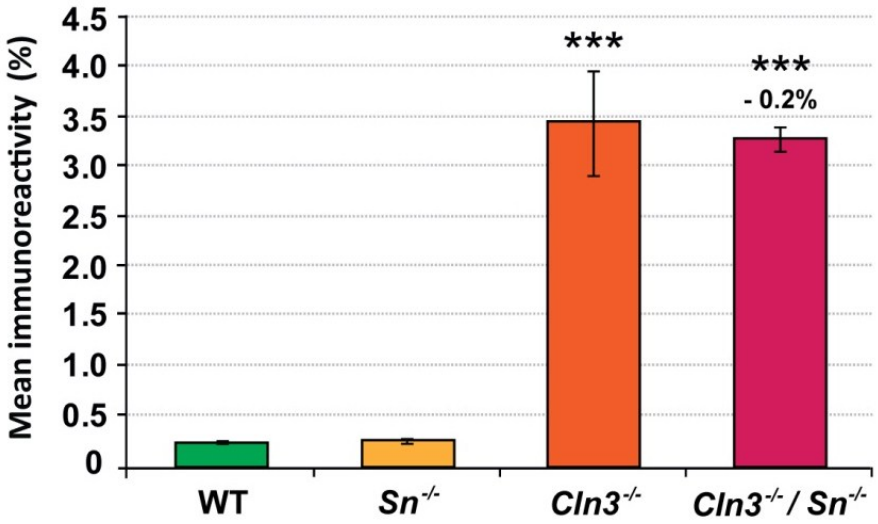

Figure 67. Unchanged levels of microglial activation in the somatosensory barrel field (*S1BF*) cortex of *Cln3*$^{-/-}$/*Sn*$^{-/-}$ double knockout mice. Thresholding image analysis revealed that the mean level of CD68 immunoreactivity did not differ between *Cln3*$^{-/-}$/*Sn*$^{-/-}$ double knockout and *Cln3*$^{-/-}$ mice in *S1BF*. Nevertheless, both single and double *Cln3* mutant mice showed significantly increased CD68 immunoreactivity compared to wildtype (WT) mice. Almost no CD68 immunoreactivity was detected in *S1BF* of either *Sn*$^{-/-}$ or wildtype (WT) mice. Percentage indicates difference between *Cln3*$^{-/-}$ and *Cln3*$^{-/-}$/*Sn*$^{-/-}$ mice. Statistics: One-way ANOVA with Bonferroni post hoc test, ***$p<0.001$. Data shown as mean ± SEM, n = 2 (WT and *Sn*$^{-/-}$) or n = 4 (*Cln3*$^{-/-}$ and *Cln3*$^{-/-}$/*Sn*$^{-/-}$).

6.4 Impact of *Sn* deficiency on neuron survival in *Cln3*$^{-/-}$ mice

Having defined the impact of Sn deficiency upon the innate immune responses in the thalamus and *S1BF* of *Cln3*$^{-/-}$ mice, we next investigated whether these changes in astrocytosis and microglial activation correlated with any effects upon neuronal survival.

a) Neuron survival in the thalamus of *Cln3*$^{-/-}$ and *Cln3*$^{-/-}$/*Sn*$^{-/-}$ mice

Unbiased estimates of the number of Nissl stained *VPM/VPL* neurons were obtained

from mice of all genotypes using the optical fractionator method, with this analysis performed blind to genotype. This analysis revealed a significant loss of *VPM/VPL* neurons in both *Cln3*$^{-/-}$/*Sn*$^{-/-}$ and *Cln3*$^{-/-}$ mice compared to WT controls or *Sn*$^{-/-}$ mice, but these occurred to different extents (see **Figure 68**). Compared to WT controls 52% of *VPM/VPL* neurons were lost in 18 month old *Cln3*$^{-/-}$ mice, whereas *Cln3*$^{-/-}$/*Sn*$^{-/-}$ mice showed less neuron loss with only 33.1% loss of *VPM/VPL* neurons. This represented a significant 18.9% improvement in *VPM/VPL* neuron survival by inactivating Sn in *Cln3*$^{-/-}$ mice. These findings suggest that Sn may contribute to neuron loss in the thalamus of JNCL mice.

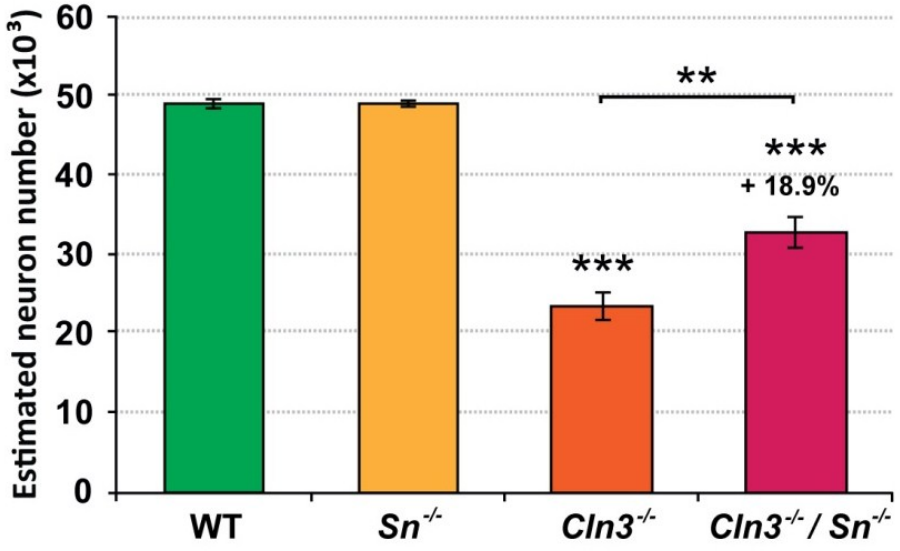

Figure 68. Increased survival of thalamic (*VPM/VPL*) neurons in *Cln3*$^{-/-}$/*Sn*$^{-/-}$ mice. Unbiased optical fractionator estimates of number of Nissl stained thalamic relay neurons in the ventral posterior nucleus (*VPM/VPL*) of 18 month old *Cln3*$^{-/-}$, *Cln3*$^{-/-}$/*Sn*$^{-/-}$ and controls (*Sn*$^{-/-}$ and wildtype (WT)) revealed that significantly more *VPM/VPL* neurons were present in *Cln3*$^{-/-}$/*Sn*$^{-/-}$ double knockout mice than in *Cln3*$^{-/-}$ mice. However, both single and double *Cln3* mutant mice displayed significantly fewer neurons compared to WT mice. Percentage indicates difference between *Cln3*$^{-/-}$and *Cln3*$^{-/-}$/*Sn*$^{-/-}$ mice compared to age-matched WT mice. Statistics: One-way ANOVA with Bonferroni post hoc test, **p<0.01, ***p<0.001. Data shown as mean ± SEM, n = 2 (WT and *Sn*$^{-/-}$) or n = 4 (*Cln3*$^{-/-}$ and *Cln3*$^{-/-}$/*Sn*$^{-/-}$).

b) Neuron survival in the cortex of *Cln3*$^{-/-}$ and *Cln3*$^{-/-}$/*Sn*$^{-/-}$ mice

Due to time constraints counts of neuron number in the *S1BF* cortex had to be omitted. Instead, as described in the previous chapters, cortical thickness and cortical volume measurements were performed to provide a first indication of pathogenesis in cortical regions.

6.5 Impact of *Sn* deficiency on cortical atrophy in *Cln3*$^{-/-}$ mice

Having defined the extent of neuron loss in the somatosensory thalamus of *Sn* deficient *Cln3*$^{-/-}$ mice we next examined its target cortical region, *S1BF*, by measuring its thickness and taking measurements of total cortical volume. This is the first time that *Cln3*$^{-/-}$ mice as old as 18 months have been analysed for these parameters.

a) Cortical volume of *Cln3*$^{-/-}$ and *Cln3*$^{-/-}$/*Sn*$^{-/-}$ mice

First of all, the total cortical volume of all 18 month old brains was measured and compared. Both JNCL mouse populations showed a significant reduction in cortical volume compared to the *Sn*$^{-/-}$ or WT controls (see **Figure 69**). *Cln3*$^{-/-}$ mice displayed a cortical atrophy of 22.5% compared to wildtype mice, but this was partially ameliorated in *Cln3*$^{-/-}$/*Sn*$^{-/-}$ double knockout mice which showed only a 16.6% reduction in cortical volume compared to the wildtype mice, although this difference was not statistically significant.

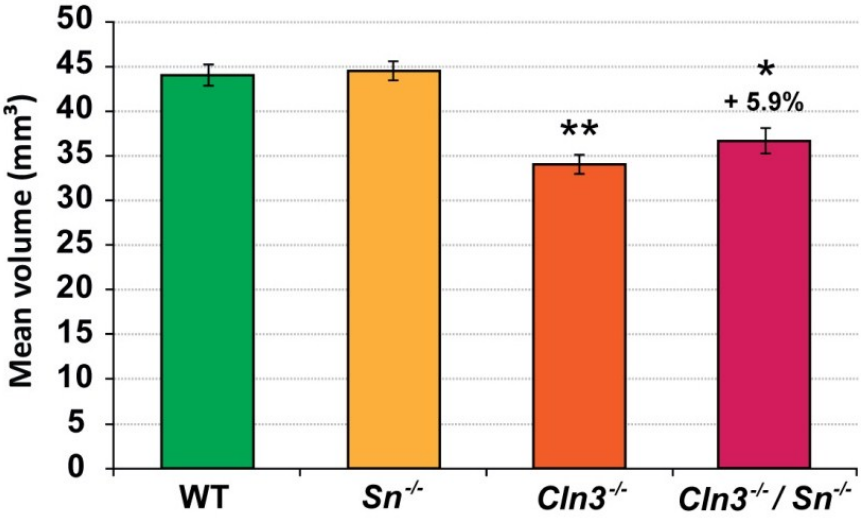

Figure 69. Marginally reduced cortical atrophy in *Cln3*$^{-/-}$/*Sn*$^{-/-}$ mice. Unbiased Cavalieri estimates of cortical volume of 18 month old *Cln3*$^{-/-}$, *Cln3*$^{-/-}$/*Sn*$^{-/-}$ and control mice (*Sn*$^{-/-}$ and wildtype (WT)) revealed a marginally reduced cortical atrophy in *Cln3*$^{-/-}$/*Sn*$^{-/-}$ mice compared to *Cln3*$^{-/-}$ mice. However, this difference did not reach statistical significance. In contrast, both single and double *Cln3* mutant mice demonstrated significantly reduced cortical volumes compared to WT mice. Percentage indicates difference between *Cln3*$^{-/-}$ and *Cln3*$^{-/-}$/*Sn*$^{-/-}$ mice compared to age-matched WT mice. Statistics: One-way ANOVA with Bonferroni post hoc test, *$p<0.05$, **$p<0.01$. Data shown as mean ± SEM, n = 2 (WT and *Sn*$^{-/-}$) or n = 4 (*Cln3*$^{-/-}$ and *Cln3*$^{-/-}$/*Sn*$^{-/-}$).

b) Cortical thickness of *Cln3*$^{-/-}$ and *Cln3*$^{-/-}$/*Sn*$^{-/-}$ mice

Cortical thickness measurements provide an overview of how severely a cortical region is affected. Our analysis focused on the somatosensory cortical region *S1BF*,

which is the target of relay neurons in *VPM/VPL* and is atrophied in *Cln3* deficient mice (Pontikis *et al.*, 2005).

Single mutant *Cln3*$^{-/-}$ mice showed a 7.5% reduction in thickness of *S1BF* compared to wildtype mice at 18 months of age (see **Figure 62A** and **Figure 66A** for representative pictures, see **Figure 70** for quantification), but this difference was not statistically significant. *Cln3*$^{-/-}$/*Sn*$^{-/-}$ double knockout mice showed a similar reduction in *S1BF* thickness. These mice displayed a 6.2% cortical thinning compared to wildtype mice, a very moderate 1.2% improvement compared to single knockout *Cln3*$^{-/-}$ mice. Although Sn may potentially have some effect on neuronal survival in the cortex, the cortical thinning in *Cln3*$^{-/-}$ mice is so marginal at this age that it is unlikely to be a very pronounced effect. Nevertheless, it will be important to explore this possibility by obtaining counts of *S1BF* neuron number.

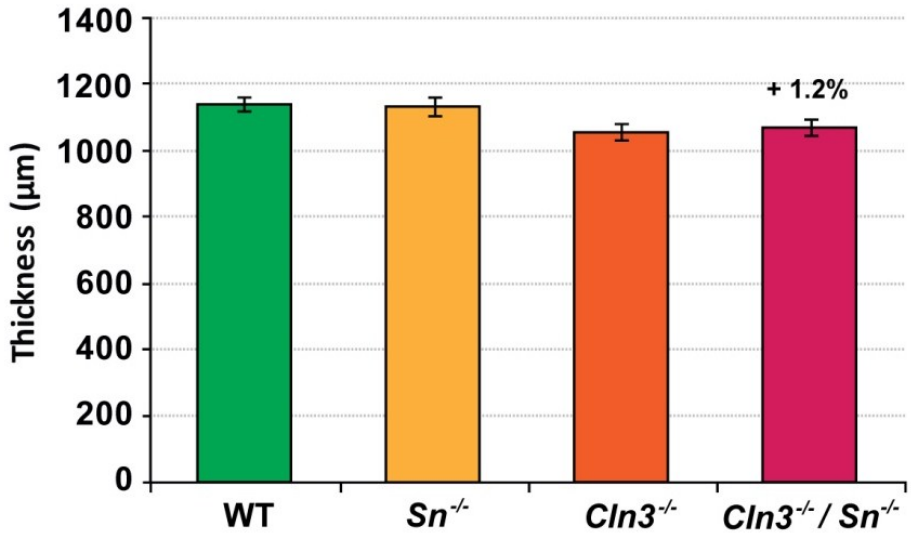

Figure 70. Similar thickness of the somatosensory barrel field (*S1BF*) cortex in *Cln3*$^{-/-}$ and *Cln3*$^{-/-}$/*Sn*$^{-/-}$ mice. Cortical thickness measurements of 18 month old *Cln3*$^{-/-}$, *Cln3*$^{-/-}$/*Sn*$^{-/-}$ and control mice (*Sn*$^{-/-}$ and wildtype (WT)) revealed no significant difference between the genotypes. Compared to WT mice, marginal cortical thinning of *S1BF* could be suggested in *Cln3*$^{-/-}$ and *Cln3*$^{-/-}$/*Sn*$^{-/-}$ mice, whereupon *Cln3*$^{-/-}$/*Sn*$^{-/-}$ mice showed less thinning of the two. Percentage indicates difference between *Cln3*$^{-/-}$and *Cln3*$^{-/-}$/*Sn*$^{-/-}$ mice compared to WT mice. Statistics: One-way ANOVA with Bonferroni post hoc test. Data shown as mean ± SEM, n = 2 (WT and *Sn*$^{-/-}$) or n = 4 (*Cln3*$^{-/-}$ and *Cln3*$^{-/-}$/*Sn*$^{-/-}$).

In summary, cortical atrophy does not seem to be strongly affected by the lack of Sn in *Cln3*$^{-/-}$ mice. It is likely that there are other mechanisms that have a greater influence upon pathological events in the cortical mantle. Nevertheless, the macrophage expressed binding protein sialoadhesin seemed to contribute at least partially to these events within the cortex.

c) Lifespan in *Cln3*$^{-/-}$/*Sn*$^{-/-}$ mice

Unfortunately, no lifespan experiments have yet been performed on *Cln3*$^{-/-}$/*Sn*$^{-/-}$ mice. As this work was only a pilot study investigating the potential effect of Sn deficiency on *Cln3*$^{-/-}$ mice, hopefully future work will add the factor time to the equation by looking at mice at different (earlier) time points and also by defining the average life expectancy of *Cln3*$^{-/-}$/*Sn*$^{-/-}$ double knockout mice.

6.6 Summary and discussion

In this chapter, we have described three main findings: First of all, we successfully characterised for the first time the disease manifestations in the thalamocortical system of 18 month old *Cln3*$^{-/-}$ mice. Secondly, we have demonstrated that Sn+ve cells can be found in inflammatory regions of the *Cln3*$^{-/-}$ brain. Thirdly, and most importantly, we have shown that Sn actively contributes to the neurodegenerative process in JNCL mice (see also **Table 15** and **Figure 71** for a summary overview).

Table 15. Summary of the comparisons between *Cln3*$^{-/-}$ and WT (middle column), plus *Cln3*$^{-/-}$ and *Cln3*$^{-/-}$/*Sn*$^{-/-}$ mice (right column). Table was based on the same analyses conducted in **Chapter 6**. Please note that *Cln3*$^{-/-}$ were congenic on a 129Sv, *Cln3*$^{-/-}$/*Sn*$^{-/-}$ mice on a mixed 129Sv and C57BL/6 and WT mice congenic on a C57BL/6 strain background. In the left column: "type of analysis", across the top rows: "genotype comparison" and "age of mice". Symbols: = no difference, ↑ significant increase, ↓ significant decrease, = (↑) increasing trend without significance, = (↓) decreasing trend without significan

		***Cln3*$^{-/-}$ *vs.* WT**	***Cln3*$^{-/-}$ *vs. Cln3*$^{-/-}$/*Sn*$^{-/-}$**
		18 Months	**18 Months**
Sialoadhesin	***Thalamus***	↑	.
	S1BF	↑	.
Brain weight		↓	= (↑)
Astrocytosis	***Thalamus***	↑	= (↓)
	S1BF	↑	= (↓)
Microglial activation	***Thalamus***	↑	= (↓)
	S1BF	↑	=
Neuronal survival		↓	↑
Cortical thickness	***S1BF***	= (↓)	=
Cortical volume		↓	= (↑)

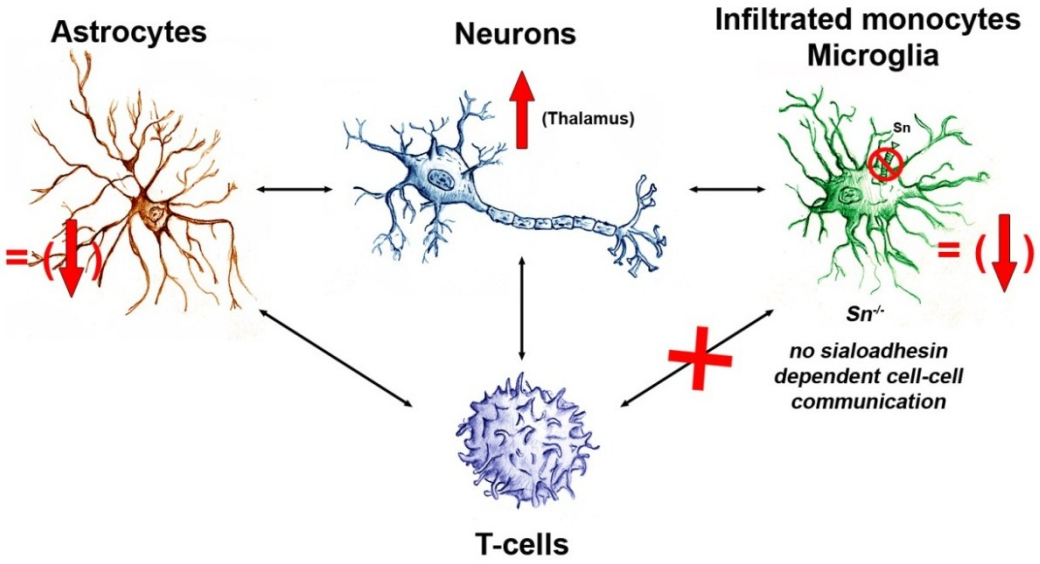

Figure 71. Schematic summary of altered phenotypes in the brain of 18 month old *Cln3*$^{-/-}$/*Sn*$^{-/-}$ mice. We characterised astrocytosis (illustrated as 'astrocytes'); microglial activation (illustrated as 'infiltrated macrophages, microglia'); and neuron survival (illustrated as 'neurons') in *Cln3*$^{-/-}$/*Sn*$^{-/-}$ mice. As a consequence of the sialoadhesin (Sn) deficiency, no Sn dependent cell-cell communication occurs between macrophages and T-cells (respectively B-cells) in the body and in the brain of *Cln3*$^{-/-}$/*Sn*$^{-/-}$ mice (B-cells are not depicted, because only few or no significantly elevated B-cells levels have been detected in *Cln3*$^{-/-}$ mouse brains compared to wildtype animals (Lim *et al.*, 2007a)). The absence of Sn results in no significant change in microglial activation or astrocytosis (decreasing trend indicated in brackets), but does lead to increased neuron survival in the thalamus. Additionally, the cortical volume and the thickness of the primary somatosensory barrel field (*S1BF*) cortex did not show any change (not shown). Overall, the lack of Sn only partially rescues the neurodegeneration in *Cln3*$^{-/-}$/*Sn*$^{-/-}$ mice.

a) Pathological characterisation of 18 month old *Cln3*$^{-/-}$ mice

We have successfully performed the first complete analysis of glial activation, neuronal survival and cortical atrophy in 18 month old *Cln3*$^{-/-}$ mice. Compared to previous published studies in JNCL mice (Pontikis *et al.*, 2004; Pontikis *et al.*, 2005; Herrmann *et al.*, 2008b), these were the oldest *Cln3*$^{-/-}$ mice analysed so far for glial activation and neuron survival. Other characterisations of glial responses in similarly aged *Cln3* deficient mice have so far only been performed in 14 month old *Cln3*$^{-/-}$ mice (Pontikis *et al.*, 2004), or in 12 and 19 month old *Cln3* knock-in mice (Pontikis *et al.*, 2005; Herrmann *et al.*, 2008b) and see **section 1.10** in **Chapter 1**). In *Cln3*$^{-/-}$ mice early developmental changes have been reported in the cerebellum already at one week post-natal (Weimer *et al.*, 2009), followed by optic nerve pathology and storage material accumulation occurring from 5-6 months onwards (Sappington *et al.*, 2003). The first neuron loss to occur in these mice has been described in the *dorsal lateral geniculate* (*LGNd*) nuclei at 6 months of age. However, major neurological deficits and

symptoms can only be seen from 16 months onwards leaving the mice with a survival age of just over 20 months (Mitchison *et al.*, 1999; Cooper *et al.*, 2006). Therefore, 18 month old mice can be considered fairly severely affected, but are not in their terminal stages, leaving some room for potential improvements by a suitable therapeutic intervention.

In terms of the innate immune responses, we could observe GFAP+ve astrocytosis and CD68+ve microglial activation in the thalamus and *S1BF* of 18 month old *Cln3*$^{-/-}$ mice (see **Figure 60**, **Figure 62**, **Figure 64** and **Figure 66**). The distribution of astrocytosis in the thalamus was similar to that described in 12 month old *Cln3* knock-in mice (Pontikis *et al.*, 2005). GFAP+ve astrocytosis in *S1BF* showed a more extensive spread into dorsal laminae (besides VI, V also partly IV) in 18 month old *Cln3*$^{-/-}$ mice (see **Figure 62A**, compared to 12 month old *Cln3* knock-in mice (Pontikis *et al.*, 2005); JD Cooper, personal communication). This discrepancy is possibly due to the difference in genetic backgrounds between these mice, but is more likely due to the age difference in these cohorts of mice.

Our microglial staining with CD68 also stands in contrast to the so far described F4/80+ve microglial activation in 5, 12 or 14 month old JNCL mice and the CD11b+ve microglial activation in 19 month old JNCL mice (Pontikis *et al.*, 2004; Pontikis *et al.*, 2005; Herrmann *et al.*, 2008b). Only a moderate or slight activation of microglial cells could be detected in these previous studies, whereas pronounced thalamic *VPM/VPL* and *S1BF* specific microglial activation was evident in 18 month old *Cln3*$^{-/-}$ mice (see **Figure 64A** and **Figure 66A**). As in our studies in *Ppt1*$^{-/-}$ mice (see **Figure 36** and **Figure 38** in **Chapter 4**) this discrepancy between earlier studies and the present study can probably be explained by the use of CD68 as a different microglial marker. This antigen appears to be more sensitive as a marker of microglial activation than either F4/80 or CD11b, and is now routinely used for this purpose in both mouse and human NCL tissue.

In contrast to glial activation, which has been shown to already occur at one week postnatally in the cerebellum of *Cln3*$^{-/-}$ mice (Weimer *et al.*, 2009) and from 3 months of age onwards in *Cln3* knock-in mice (Herrmann *et al.*, 2008b), neurodegenerative changes have been demonstrated at the earliest at 6 months of age in the *dorsal lateral geniculate* (*LGNd*) and *VPM/VPL* thalamic nuclei (Weimer *et al.*, 2006); JD Cooper, personal communication), and of Purkinje cerebellar neurons in *Cln3*$^{-/-}$ mice (Weimer

et al., 2009). Further, neurodegeneration was described in 10 month old *Cln3* knock-in mice in the retina (Cotman *et al.*, 2002), and at 12 months of age in the thalamocortical system of the forebrain, including the *VPM/VPL* nuclei of the thalamus and the *S1BF* cortex of *Cln3*$^{-/-}$ mice (Pontikis *et al.*, 2005). As such, it was no surprise to also find neuron loss in the thalamus of 18 month old *Cln3*$^{-/-}$ mice in this study (see **Figure 68**), even if these were on a mixed and therefore different strain background to the studies mentioned above. These data highlight the robust nature of this phenotype, and emphasise the pathological targeting of the thalamus in multiple different strains of *Cln3* deficient mice.

Finally, we could not detect any reduction in the thickness of *S1BF* of 18 month old *Cln3*$^{-/-}$ mice (see **Figure 70**), but did find a small, but significant degree of overall cortical atrophy instead (see **Figure 69**). This first observation is at odds with data from 12 month old *Cln3* knock-in mice in which thinning of *S1BF* was observed (Pontikis *et al.*, 2005), although the usual caveats of strain background and the different targeting constructs used to generate these models must be borne in mind. Previous studies in *Cln3* deficient mice (Pontikis *et al.*, 2004; Pontikis *et al.*, 2005) did not find any atrophy of the cortex up to 15 months of age. As such our new data from 18 month old *Cln3*$^{-/-}$ mice suggest that cortical atrophy in these mice seems to have a relatively late onset, as it does in mouse models of other forms of NCL (reviewed in (Cooper *et al.*, 2006; Cooper, 2010)).

b) Sialoadhesin expressing cells in *Cln3*$^{-/-}$ brains

This study is the first to describe the distribution of Sn immunoreactivity in *Cln3* deficient mice. Besides several other brain regions, we could identify many intensely stained Sn+ve cells in the thalamus and in the *S1BF* cortex of 18 month old *Cln3*$^{-/-}$ mice (see **Figure 58**), compared to an absence of cell staining in the brain parenchyma or only perivascular and meningeal Sn+ve macrophage-like cells in age-matched wildtype mice, as previously described in other wildtype mice (see **Figure 44E** in **Chapter 5**; (Perry et al. 1992)). To our knowledge, this study is the first extensive characterisation of Sn+ve cells in a form of NCL. In general, very few studies have so far investigated the Sn expression in the brain at all (Perry *et al.*, 1992; Ip *et al.*, 2007), with most of them focusing on Sn+ve macrophages in the body periphery (Crocker *et al.*, 1991; Muerkoster *et al.*, 1999; Miyake *et al.*, 2007; Phan *et al.*, 2009; Revilla *et al.*, 2009; Asano *et al.*, 2011; McGaha *et al.*, 2011). In our study, the Sn+ve stained cells

were a mixed population of typical macrophage-like cells with amoeboid cell bodies and small short processes, together with microglial cells with elongated and ramified processes. Even though it is impossible to unambiguously distinguish whether Sn+ve cells are either peripheral infiltrated macrophages or resident microglial cells in the inflammatory brain (see discussion in **Chapter 7**), these Sn+ve cells were only located in the same areas of the brain where acute CD68+ve microglial activation could be detected (see **Figure 64** and **Figure 66**). Qualitatively judged, fewer Sn+ve cells than CD68+ve microglia were seen in such regions, indicating that Sn is probably only expressed in a subset of microglia/macrophages (compare **Figure 58** with **Figure 64** and **Figure 66**). Nevertheless, the location of Sn+ve cells clearly overlaps with sites of innate immune activation in the *Cln3*$^{-/-}$ brain, suggesting that Sn+ve cells could potentially be involved in these inflammatory responses and neurodegeneration. Subsequently, this hypothesis has been tested by the characterisation of *Cln3*$^{-/-}$/*Sn*$^{-/-}$ double knockout mice, as was presented in this chapter.

c) Sialoadhesin enhances neurodegeneration

To address the role of Sn in JNCL pathogenesis we generated *Cln3*$^{-/-}$/*Sn*$^{-/-}$ double knockout mice, which lacked this macrophage-expressed binding protein, and analysed their neuropathological phenotype at 18 months of age. This analysis revealed that the additional deficiency of Sn only marginally attenuated glial activation in the thalamus, and relatively to a similar extent also in the cortex, of *Cln3*$^{-/-}$/*Sn*$^{-/-}$ mice (see **Figure 60**, **Figure 62**, **Figure 64** and **Figure 66**). Indeed, no significant difference could be detected for any measurement of glial response in these mice (see **Figure 61**, **Figure 63**, **Figure 65** and **Figure 67**). This was the case, even though Sn is abundantly expressed on macrophage-like cells in both the thalamus and the cortex of *Cln3*$^{-/-}$ mice (see **Figure 58**). As such, the impact of Sn expressing macrophages upon glia in 18 month old *Cln3*$^{-/-}$ mice appears to be limited. This is most likely explained by the relatively late onset of adaptive immune responses (see **Figure 27** in **Chapter 3**) upon which Sn can act as an immune regulatory binding protein between macrophages and other (adaptive) immune cells in *Cln3*$^{-/-}$ brains.

Furthermore, similar to *Cln3*$^{-/-}$ mice, no significant improvement in the thinning of *S1BF* was apparent in *Cln3*$^{-/-}$/*Sn*$^{-/-}$ mice, but there was a slight reduction in overall cortical atrophy compared to these single mutant mice (see **Figure 69** and **Figure 70**). These data suggest that Sn and/or Sn+ve cells potentially play a pathological role in

disease progression in the cortex, but it will be important to perform counts of neuron number in the cortex of *Cln3*$^{-/-}$/*Sn*$^{-/-}$ mice to determine whether this is the case.

Finally, the loss of thalamic relay neurons was significantly reduced in *Cln3*$^{-/-}$/*Sn*$^{-/-}$ double knockout mice compared to *Cln3*$^{-/-}$ mice (see **Figure 68**). Therefore, it appears that Sn-mediated interactions have a direct impact on neurodegeneration, since when they are abolished neuron survival is improved. Plausibly, these interactions could be between adaptive immune cells (T-cells and B-cells) and Sn+ve macrophages (Muerkoster *et al.*, 1999; van den Berg *et al.*, 2001; Ip *et al.*, 2007; Wu *et al.*, 2009), or putative microglia and Sn+ve macrophages (van den Berg *et al.*, 1992; Schadee-Eestermans *et al.*, 2000). Despite not quantifying the extent of T-cell infiltration in *Cln3*$^{-/-}$/*Sn*$^{-/-}$ double knockout mice, we would speculate that less T-cells are likely to infiltrate the brains of these double mutant mice compared to *Cln3*$^{-/-}$ mice; mainly due to an expected lower level of activation of T-cells by macrophages. However, since the role of T-cells themselves in *Cln3*$^{-/-}$ mice (for example via creation and characterisation of *Cln3*$^{-/-}$/*Rag-1*$^{-/-}$ mice) is yet to be investigated, and T-cells only appear to enter the brain at late stages of the disease (see **Figure 27** in **Chapter 3**), the impact of T-cell infiltration on neuron survival in *Cln3*$^{-/-}$/*Sn*$^{-/-}$ mouse brains remains speculative, but not unlikely. However, we did not see any obvious differences in glial activation in the thalamus of these *Cln3*$^{-/-}$/*Sn*$^{-/-}$ mice where less neurodegeneration was observed, meaning, that other (as yet unidentified) events may be responsible. These may lie outside the CNS, with the systemic autoimmune response that occurs in *Cln3* deficient mice perhaps contributing an influence (Chattopadhyay *et al.*, 2002a; Lim *et al.*, 2007b). Indeed, there could be several alternative explanations which will be discussed in more detail in **Chapter 7**. Firstly, Sn deficiency may have a direct impact on antigen presentation to B-cells, and reduce the amount of autoantibodies targeting brain antigens. Secondly, the lack of interactions between Sn and adaptive immune cells, which are essential for immune cell activation, may result in a less pronounced autoimmune response. Thirdly, the lack of Sn may enhance the abnormal signaling of immune cells in *Cln3*$^{-/-}$ mice, which are already compromised due to *Cln3* deficiency (Dihanich, 2010; Parviainen, 2012). Taken together, this could lead to a less inflammatory micro-environment in the brain of *Cln3*$^{-/-}$/*Sn*$^{-/-}$ double knockout mice, a slightly reduced glial activation and consequently better neuronal survival.

d) Significance of findings

This study has investigated the role of Sn in JNCL and the part that a, so far overlooked, Sn+ve macrophage cell population plays in this disorder. By knocking out this binding protein on the surface of macrophages we were able partially to slow down the neurodegenerative process that occurs in Juvenile NCL. As an underlying hypothesis, we speculate that Sn attenuates the neuroinflammation and in particular the autoimmune responses in JNCL mice, which leads to a slowing down of disease progression. However, since we could not completely reverse these disease phenotypes, other detrimental forces must be present in the brain. Nevertheless, Sn may be an attractive target for immunosuppressive interventions in Juvenile NCL. Because there is still no effective treatment for this devastating disease, even slowing down disease progression could be beneficial. Furthermore, the specific blockade of Sn alone, or in combination with other treatment strategies, could potentially produce fewer side effects than a generalised immune suppression. Whatever the implications, our findings will hopefully pave the way for the development of future treatment strategies.

Chapter 7

General discussion

The main objectives of these studies were to investigate the possible pathogenic role of neuroinflammation in the brain of two forms of NCL, and to determine whether the adaptive immune cell response, in particular, is a primary or secondary cause of neurodegeneration. Via two different genetic manipulations of the immune system we have demonstrated that neuroinflammation appears to accelerate disease progression in Infantile and Juvenile NCL.

Firstly, we identified that adaptive immune cells (T-cells) are widely present in the brain of both Infantile and Juvenile NCL mice, which is in stark contrast to their virtual absence in healthy wildtype mice. Subsequently, we crossbred *Ppt1*$^{-/-}$ mice with immune deficient *Rag-1*$^{-/-}$ mice (without T- and B-cells). Our findings suggest that the resulting lack of adaptive immune cells attenuates innate immune responses and delays neurodegenerative events in *Ppt1*$^{-/-}$/*Rag-1*$^{-/-}$ mice.

In a second set of experiments, we wanted to clarify to which extent a simple deficiency of sialoadhesin (Sn), an adaptive immune regulatory binding protein normally present on macrophages could affect disease progression in Infantile and Juvenile NCL mice. This protein was mainly chosen for three reasons. Firstly, our collaborators had previously demonstrated that Sn deficiency in a mouse model of a slowly progressing demyelinating CNS disorder leads to reduced CD8+ve T-cell infiltration and disease amelioration (Ip *et al.*, 2007). Secondly, having demonstrated the presence and pathogenic nature of adaptive immune cells in the brain of Infantile (and Juvenile) NCL (see **Chapter 3** and **Chapter 4**), as an adaptive immune cell regulatory protein Sn represented an interesting and promising therapeutic target. Thirdly, the role of infiltrating peripheral macrophages in the brain of INCL and JNCL has not yet been well characterised and investigating the effect of Sn deficiency would elucidate their pathological relevance in these two NCL forms in more detail. For all these reasons, we crossbred *Ppt1*$^{-/-}$ and *Cln3*$^{-/-}$ mice with *Sn*$^{-/-}$ mice to create double knockouts lacking the macrophage marker Sn, but having the appropriate form of NCL. Our results demonstrated distinct impacts of Sn deficiency between INCL and JNCL. Contrasting effects upon different types of glia were seen in *Ppt1*$^{-/-}$/*Sn*$^{-/-}$ double knockout mice, whereas both microglial activation and neurodegeneration were decreased, astrocytosis was surprisingly elevated. In contrast, *Cln3*$^{-/-}$/*Sn*$^{-/-}$ double knockout mice displayed only a marginal attenuation of innate immune responses (glial activation), but a significant reduction in neuron loss. Thus, we could prove that

Sn may play an accelerating role in neurodegenerative events in both INCL and JNCL.

Taking a genetic approach rather than administering an immunosuppressive drug, as done in other studies (Seehafer *et al.*, 2011), we could define the effect of adaptive immune cells and Sn on other CNS cell types, and upon disease progression. These 'proof of principle' studies have demonstrated that immune cells do indeed have a pathogenic impact in Infantile and Juvenile NCL mice. Therefore our findings may prove to be valuable for future immunosuppressive therapeutic approaches with the aim of improving life expectancy and/or life quality of Infantile and Juvenile NCL patients.

7.1 Adaptive immune cell infiltration in NCL brains

In **Chapter 3** we have supplied the first detailed characterisation of the extent, nature and distribution of T-cell infiltration, revealing both differences and similarities between the Infantile and Juvenile forms of NCL. Although our data demonstrated the presence of CD8+ve, as well as CD4+ve, T-cells in the brains of both forms of NCL, our findings also raised a number of unanswered questions.

a) Sequence of T-cell infiltration

Our lymphocyte data in **Chapter 3** revealed contrasting sequences of T-cell infiltration in *Cln3*$^{-/-}$ and *Ppt1*$^{-/-}$ mice. In contrast to a simultaneous infiltration of CD8+ve and CD4+ve T-cells in *Ppt1*$^{-/-}$ mice at 3 months of age (see **Figure 21** in **Chapter 3**), CD4+ve T-cells appeared to infiltrate the JNCL mouse brain only at the later stage of the disease and certainly following CD8+ve T-cell infiltration (see **Figure 27** in **Chapter 3**). Although CD4+ve cells generally (but not invariably) facilitate the activation and expansion of CD8+ve T-cells in the secondary lymphoid organs (as described in **section 1.7a** in **Chapter 1**), the timing of infiltration of each T-cell sub-population into the inflammation site (brain, in our case) can vary as a consequence of different stimuli that trigger or maintain the immune activation (Taub and Oppenheim, 1994; Carson *et al.*, 1999; Penna *et al.*, 2002; Brisebois *et al.*, 2006; Abbas and Lichtman, 2011). Furthermore, in comparison to the activation process in lymphoid tissue, the cooperation of T-cell subsets at the inflammation site varies between immune reactions and is less well understood (Bevan, 2004; Nakanishi *et al.*, 2009; Phares *et al.*, 2012; Wiesel and Oxenius, 2012). However, both T-cell subsets would classically be expected to infiltrate the inflammation site (at least to some

extent) ((Andersson *et al.*, 1992; Seder and Ahmed, 2003; Abbas and Lichtman, 2011; Phares *et al.*, 2012; Wiesel and Oxenius, 2012); MJ Lim, personal communication). Therefore, our data revealed that *Cln3*$^{-/-}$ mice unexpectedly show an initial absence or "delayed" arrival of CD4+ve T-cells in the brain (see **Figure 27** in **Chapter 3**), which raises questions about why this should be the case. However, a similar sequence of T-cell infiltration to that we observed in *Cln3*$^{-/-}$ mice has been seen, for example, in Theiler's virus or Sindbis virus (SINV) infected mice in which virus specific CD8+ve T-cells infiltrate the brain initially and CD4+ve T-cell arrival could only be documented much later in the brains of these mice, which eventually leads to a demyelinating auto-immune disease (Katz-Levy *et al.* 2000; Begolka *et al.* 2001; Mendez-Fernandez *et al.* 2003; Metcalf and Griffin 2011). In the body periphery, T-effector cell recruitment to an inflammation site is thought to generally be antigen-independent and solely rely upon adhesion molecules and chemokines, whereas subsequent preferential proliferation and retention of antigen-specific T cells within inflamed tissues ensures a successful immune response (Wakim *et al.*, 2008; Ghani *et al.*, 2009; Abbas and Lichtman, 2011). Similar recruitment processes occurring in the supposedly 'immune privileged' brain have not been definitively established, as most studies suggest antigen-independent crossing of the BBB into the perivascular space, but antigen-specific entry into the brain parenchyma (Ransohoff *et al.*, 2003; Galea *et al.*, 2007b; Melzer *et al.*, 2009); yet, some researchers also favour the possibility of naïve T-cells entering the brain (Brabb *et al.*, 2000; Greter *et al.*, 2005; McMahon *et al.*, 2005). However, the different timing of T-cell infiltration seen in Infantile and Juvenile NCL clearly demonstrate that disease subtype specific immune responses occur (see **Figure 21** and **Figure 27** in **Chapter 3**). In the following sections we will discuss which mechanisms could account for these differences in T-cell infiltration between these NCL subtypes and in particular, for the delayed arrival of CD4+ve T-cell infiltration in *Cln3*$^{-/-}$ mice.

Firstly, *Cln3*$^{-/-}$ astrocytes and microglia show alterations in the secretion of a range of cytokines (Dihanich, 2010; Kielian, 2012; Parviainen, 2012). Cell culture experiments on *Cln3*$^{-/-}$ microglia after ceramide or glutamate stimulation revealed increased levels of cytokines, for example interleukin 1-β (IL-1β), compared to stimulated wildtype microglia (Kielian, 2012); JD Cooper, personal communication). IL-1β is thought to act as a pro-inflammatory cytokine recruiting T-cells to inflammation sites (Gery *et al.*, 1972; Lidington *et al.*, 1998). Likewise, the microglial expression of other cytokines

may also speculatively be altered in the *Cln3*$^{-/-}$ brain (e.g. IL-12) which could enhance Th_1 directed cell immunity, increase CD8+ve T-cell cytotoxic activity and overall favour CD8+ve T-cell infiltration. However, other microglial cell culture experiments studying cytokine expression after lipopolysaccharides (LPS) stimulation (50ng/ml) showed reduced levels of microglial cytokine secretion, including for example RANTES, compared to wildtype microglia ((Dihanich, 2010); BP Williams, personal communication). These latter results resembled studies conducted on cultured *Cln3*$^{-/-}$ astrocytes stimulated with LPS plus interferon gamma (LPS: 1μg/ml and IFN-γ: 100U/ml), which also demonstrated a significant reduction in the secreted levels of several cytokines and chemokines compared to stimulated wildtype astrocytes (Parviainen, 2012). Amongst many others, but of particular interest in this context, are the significantly reduced secretion of RANTES and Interleukin-4 (IL-4) from *Cln3*$^{-/-}$ astrocytes (Parviainen, 2012). Whereas, on the one hand, RANTES is a chemo-attractant for T-cells and plays an active role in recruiting leukocytes into inflammatory sites (Schall *et al.*, 1988; Miller and Krangel, 1992), on the other hand it also selectively supports the migration of monocytes and CD4+ve T-cells across the endothelial wall by increasing the adherence of CD4+ve lymphocytes to endothelial cells (Schall *et al.*, 1990). In contrast, IL-4 induces Th_2 cell differentiation and humoral immune responses as an antagonist of IL-12 (Jansen *et al.*, 1990; Trinchieri, 1995; Asselin *et al.*, 1997). Thus, reduced expression of both cytokines in *Cln3*$^{-/-}$ astrocytes could speculatively alter or hinder CD4+ve T-helper cell recruitment and infiltration into the JNCL brain. Interestingly, whereas mainly a reduction in cytokine secretion could be detected in *Cln3*$^{-/-}$astrocytes, *Cln3*$^{-/-}$ microglia showed an up-regulated or reduced expression of cytokines compared to wildtype glial cells, depending on experimental setup (Dihanich, 2010; Kielian, 2012; Parviainen, 2012). These contrasting results are most likely explained by the different stimulation methods used, but it will be important to define which scenario reflects the *in vivo* situation. In any case, all experiments indicated an alteration in the cytokine secretion profile of both astrocytes and microglia due to *Cln3* deficiency. Such altered profiles may favour CD8+ve T-cell infiltration and plausibly delay the recruitment and/or infiltration of CD4+ve T-cells into *Cln3*$^{-/-}$ brains. Different chemokines can alter the expression of selectin and integrin cell binding molecules on endothelial cells (Hickey, 1999), and/or the interactions of lymphocytes with the glia limitans (Ransohoff *et al.*, 2003; Farina *et al.*, 2007). This may result in one lymphocyte subset being more favoured to cross the

BBB than the other (see **section 1.7b** in **Chapter 1**). However, these interpretations are purely speculative at present and have to be interpreted with caution, especially, as the above experiments have been conducted in cell culture and thus, these observations need to be translated into *in vivo* situations.

Other than the dysfunction of *Cln3*$^{-/-}$ glia, another possible explanation for the observed T-cell recruitment in *Cln3*$^{-/-}$ brains is the altered BBB integrity that has been reported in *Cln3*$^{-/-}$ mice (Lim *et al.*, 2007b). This higher permeability of the BBB may suggest easier access via the glia limitans, but may also reflect a higher activation status or binding tendency of vascular endothelial cells at the BBB, each of which may have an influence upon the infiltration of different classes of lymphocytes into the JNCL CNS. Although the precise nature of the deficit of BBB integrity remains unknown, the secretion profiling of *Cln3*$^{-/-}$ astrocyte cultures mentioned above also revealed significantly decreased levels of the (soluble) vascular cell adhesion molecule 1 (VCAM-1) and of CD40 which are likely to influence the capacity of endothelial cells to recruit leukocytes. VCAM-1 is an essential surface protein on brain endothelial cells, which is involved in the tethering and rolling of T-cells along vascular walls before their extravasation (Johnson-Leger *et al.*, 2000; Matheny *et al.*, 2000), but can also be expressed by astrocytes or as in a soluble form in acute brain inflammation/injuries (Hurwitz *et al.*, 1992; Eddleston and Mucke, 1993; Blann *et al.*, 1999). VCAM-1 has been shown to be crucial for T-cell entry into the CNS parenchyma when expressed on astrocytes (Gimenez *et al.*, 2004). CD40, on the other hand, is a co-stimulatory molecule mainly found on APCs and B-cells, which interacts with CD40-ligand on CD4+ve T-cells (reviewed in (Munroe, 2009)), but it also has been shown to be expressed by brain endothelial cells where it could potentially mediate CD4+ve T-cell migration across the BBB (Omari and Dorovini-Zis, 2003; Urban *et al.*, 2011). The expression of CD40 on astrocytes is still controversial (reviewed in (Dong and Benveniste, 2001)), but it is also active in secreted soluble form (Fanslow *et al.*, 1992; Mocali *et al.*, 2004; Scalabrino, 2009). Thus, reduced expression levels of these two or similar proteins on astrocytes, or in the vicinity of astrocytes is likely to have an influence upon how lymphocytes, especially CD4+ve T-cells, interact with different cellular components of the brain vasculature of *Cln3*$^{-/-}$ mice. Nevertheless, this is again only speculation and highlights the need to explore these issues experimentally.

Thirdly, different brain entry mechanisms of CD4+ve compared to CD8+ve T-cells could potentially be a factor. CD4+ve T-cell brain infiltration is thought to be dependent upon perivascular antigen presenting cells (APCs) to re-activate lymphocytes and enable brain parenchyma entry (Ransohoff *et al.*, 2003; Becher *et al.*, 2006). In contrast, antigen-specific CD8+ve T-cell infiltration is not dependent on perivascular APCs, but via the luminal expression of MHC I molecules by cerebral endothelial cells (Galea *et al.*, 2007b; Melzer *et al.*, 2009). Furthermore, it has been speculated that T-cell brain infiltration might be less restrictive for CD8+ve T-cells than for CD4+ve T-cells (Cabarrocas *et al.*, 2003). This hypothesis is based on studies demonstrating higher numbers and recruitment of CD8+ve T-cells compared to CD4+ve T-cells in mouse brains after injection of previously primed antigen presenting dendritic cells (DCs) (Carson *et al.*, 1999), or in healthy wildtype mice (Brabb *et al.*, 2000). Likewise, another study assessing T-cell infiltration in healthy and injured spinal cords showed similar results with higher CD8+ve T-cell infiltration compared to CD4+ve lymphocytes (Bradl *et al.*, 2005). Such easier access of CD8+ve T-cells to the CNS could be explained by different entry mechanisms (Ransohoff *et al.*, 2003; Galea *et al.*, 2007b), or perhaps better by their different responses to chemokines, as both subpopulations of T-cells show distinct chemokine receptors (i.e. CCR9 is only found on CD8+ve T-cells) which can result in altered interactions of lymphocytes with vascular endothelial cells or the glia limitans (Carramolino *et al.*, 2001; Svensson *et al.*, 2002). Additionally, several chemokines preferentially recruit only one subset of T-cells (e.g. MIP-1 α recruits CD8+ve T-cells) (Serody *et al.*, 2000). All of these mechanisms could explain the predominant CD8+ve T-cell infiltration in *Cln3*$^{-/-}$ mice. However, alternatively, it could also be possible that the resident brain APCs are dysfunctional in *Cln3*$^{-/-}$ brains, specifically impairing and delaying the CD4+ve T-cell infiltration, but this issue is yet to be investigated. For example, future culture experiments on isolated *Cln3*$^{-/-}$ APCs could clarify to what extent these cells are dysfunctional and whether their interaction with CD4+ve T-cells is impaired. Additionally, specific APC knockout or correction experiments in *Cln3*$^{-/-}$ mice could determine whether a selective APC dependent T-cell entry mechanism actually occurs in JNCL mice. Nevertheless, since recent studies also describe lymphocyte entry into the brain without previous T-cell activation or APC re-activation, these explanations may not be sufficient (Greter *et al.*, 2005; McMahon *et al.*, 2005).

Next, the delayed infiltration of CD4+ve T-cells may speculatively result from the lack

of CD4+ve T-cell activation in the first place. As discussed in **Chapter 1** (see **section 1.7a**), a high level of antigen may trigger a CD8+ve T-cell activation without CD4+ve T-cell involvement, as long as the APCs become sufficiently primed (Bachmann *et al.*, 1998; Bevan, 2004). Or alternatively, the inflammatory stimuli in the brain may simply not require the typical CD4+ve T-cell immune properties of activating macrophages (and B-cells), but instead depend predominantly upon CD8+ve T-cell immune functions of apoptosis induction. Nevertheless, because JNCL has recently been shown to be (at least partly) an autoimmune disease (Lim *et al.*, 2007b; Seehafer *et al.*, 2011), an irregular and unbalanced immune response could be predicted which possibly could reflect itself in distorted CD8+ve or CD4+ve T-cell activation and frequencies. Maybe auto-antibodies themselves react with GAD65 (Chattopadhyay *et al.*, 2002a; Chattopadhyay *et al.*, 2002b; Lim *et al.*, 2006) or α-fetoprotein (Castaneda and Pearce, 2008), or other unknown early auto-reactive antigens, to cause CD8+ve T-cells to become activated in peripheral or cervical lymph nodes and initiate the inflammatory process without CD4+ve T-helper cells. This hypothesis is strengthened by previous findings of increased amounts of CD8+ve cells in the cervical lymph nodes and spleen (but not in the peripheral lymph nodes) of 2 month old *Cln3*$^{-/-}$ mice compared to wildtype animals (Lim *et al.*, 2007b). Furthermore, decreased CD4/CD8 ratios could be detected in the same mutant mice, indicating a localized immune irregularity in the draining lymph nodes of the brain as early as at 2 months of age (Lim *et al.*, 2007b).

Finally, *Cln3* deficiency may directly, or indirectly, impair the immunological functions of CD4+ve T-cells themselves. Autophagy has been shown to be crucial for T-cell survival (Stephenson *et al.*, 2009), and as dysfunctional autophagy already has been documented in JNCL (Cao *et al.*, 2006; Cotman and Staropoli, 2012), reduced T-cell survival could be also expected in *Cln3*$^{-/-}$ mice. Indeed, reduced T-cell populations and CD4/CD8 ratios have been described in the blood of 4 month old *Cln3* knock-in mice and, as mentioned above, in the cervical lymph nodes and spleen of 2 month old *Cln3*$^{-/-}$ mice (Lim *et al.*, 2007b; Staropoli *et al.*, 2012), although no direct correlation or explanation has been experimentally linked to these phenomena so far. Furthermore, endosomal/lysosomal pathways are essential for many immune functions, including antigen presentation via the loading of MHC I and MHC II molecules and cytotoxic T-cell functions, as described extensively in **Chapter 1** (see **section 1.9** and reviewed in (Castaneda *et al.*, 2008)). Therefore, a functional deficit in immune cells or CD4+ve

T-cells themselves could be suspected in *Cln3*$^{-/-}$ mice. These findings go hand in hand with the appearance of vacuolated lymphocytes in JNCL patients, which is used as a clinical diagnostic tool for Juvenile NCL (Anderson *et al.*, 2005), even though a direct link between vacuolisation and T-cell function has not yet been elucidated.

Taken together, whatever the underlying mechanism, the contrasting sequence of adaptive immune cell infiltrations in Juvenile and Infantile NCL mice support the fact that these two forms of NCL, even though belonging to the same family of disorders, are clearly distinct disease entities which may display independent inflammatory and neurodegenerative mechanisms (Cooper, 2010).

b) Relative frequencies of T-cell subsets

More CD8+ve T-cells than CD4+ve T-cells could be detected in the brains of both *Ppt1*$^{-/-}$ and *Cln3*$^{-/-}$ mice (see **Figure 21** and **Figure 27** in **Chapter 3**). Furthermore, CD4+ve T-cell reached a saturation level of infiltration in *Ppt1*$^{-/-}$ mice (at 3 months of age), whereas CD8+ve T-cells steadily increased in quantity throughout disease progression in *Ppt1*$^{-/-}$ and *Cln3*$^{-/-}$ mice (see **Figure 21** and **Figure 27** in **Chapter 3**). These patterns are most likely explained by the function of each T-cell subtype. Since CD4+ve T-helper cells are traditionally thought to regulate and control the adaptive immune responses (Zhu and Paul, 2008; Zhu and Paul, 2010; Abbas and Lichtman, 2011), a certain saturation of infiltrating T-cells at the inflammation site could be expected due to a putative trade-off between required cell numbers and regulatory effector functions. Similarly, the other CD4+ve T-cell effector function of enhancing macrophage (and B-cell) activation (see **section 1.7a** in **Chapter 1**, (Stout, 1993; Zhu and Paul, 2008; Abbas and Lichtman, 2011)) is likely to be restricted to the amount of macrophages in the brain/inflammation site. In contrast, due to the cytotoxic effector function of CD8+ve T-cells in inducing apoptosis of infected or malfunctioning cells (Nagata, 1996; Shresta *et al.*, 1998; Abbas and Lichtman, 2011), CD8+ve T-cell infiltration would be predicted to steadily increase until complete clearance of the pathogenic stimuli (e.g. virus) is accomplished. Furthermore, the frequencies of each T-cell subset could be simply explained by different proliferation capacities which have been shown to be greater for CD8+ve T-cells (Homann *et al.*, 2001), or by different antigen recognition efficiency due to the presence of more MHC I molecules than MHC II at the inflammation site (Seder and Ahmed, 2003). However, in chronic neurodegenerative disorders the mechanisms that trigger the immune system are

constantly maintained or even amplified (Gao and Hong, 2008), and no saturation of CD8+ve T-cell infiltration can be reached (as seen **Figure 21** and **Figure 27** in **Chapter 3**). Accordingly, CD8+ve T-cells often outnumber CD4+ve T-cells in chronic neurodegenerative disorders ((Neumann *et al.*, 2002; Melzer *et al.*, 2009); MJ Lim, personal communication), as seen for example in lesions of multiple sclerosis (Booss *et al.*, 1983; Lassmann *et al.*, 2001; Friese and Fugger, 2009), the *substantia nigra* of Parkinson disease (Baba *et al.*, 2005; Brochard *et al.*, 2009), in ALS (Holmoy, 2008), or in Alzheimer disease brains (Togo *et al.*, 2002). This consistent increase in the number of CD8+ve T-cells in the chronically inflamed CNS may simply reflect the unchecked cytotoxic T-cell effector function described above, but speculatively could also suggest that similar stimuli or cues (like neuronal death or other hitherto unknown components) are present in neurodegenerative CNS disorders which favour a CD8+ve T-cell immune response. But even if such common stimuli exist, the pathogenic, regulatory or even neuroprotective role of CD8+ve T-cells in the CNS is likely to vary between diseases (Nicholson *et al.*, 1999; Klein *et al.*, 2005b; Schwartz and Kipnis, 2005; Chiu *et al.*, 2008; Ip *et al.*, 2012). However, taken together, the relative frequency of CD8+ve T-cells in *Ppt1*$^{-/-}$ and *Cln3*$^{-/-}$ mice reflects a consistent and common pattern, in contrast to the speculatively low frequencies of CD4+ve T-cell in *Cln3*$^{-/-}$ mouse brains (as discussed in **section 7.1a** above).

c) Entry point of T-cells

This is the first study to detail the distribution of T-cells in *Ppt1*$^{-/-}$ and *Cln3*$^{-/-}$ mice. Our findings suggest the preferential entrance of T-cells to the brain through the olfactory route, since the highest accumulation of T-cells was observed in the rostral part of both the *Ppt1*$^{-/-}$ and *Cln3*$^{-/-}$ brains, but, interestingly a similar distribution was also seen in wildtype brains (see **Figure 22**, **Figure 23**, **Figure 28** and **Figure 29** in **Chapter 3**). According to the literature, T-cells preferably enter the CSF/brain through the choroid plexus of the ventricles, or meninges via blood and the perivascular space (see **Figure 3** in **Chapter 1** (Ransohoff *et al.*, 2003; Wilson *et al.*, 2010)). However, neither of these routes can fully explain the distribution of T-cells we observed in our NCL mouse models and speculatively, other anatomical features have to be considered too.

In the rodent brain the subarachnoid space, including the CSF, directly interconnects with the nasal sub mucosa through the cribriform plate of the ethmoid bone alongside

the olfactory nerves (Kida *et al.*, 1993; Walter *et al.*, 2006). The CSF produced in the choroid plexus flows through the ventricle into the subarachnoid space, where it circulates forwards inferior to the olfactory bulb and drains through the cribriform plate into the nasal lymphatics, and eventually the deep cervical lymph nodes (Kida *et al.*, 1993; Walter *et al.*, 2006). Through this pathway putative antigens from the CNS can reach cervical lymph nodes for subsequent T-cell activation (Cserr *et al.*, 1992; Hickey, 2001). Likewise, T-cell and dendritic cell exit from the CNS along with the CSF via the cribriform plate and into the cervical lymph nodes has been also demonstrated (Carson *et al.*, 1999; Karman *et al.*, 2004; Goldmann *et al.*, 2006; Hatterer *et al.*, 2006). But whether this cellular migration is an actively directed or rather passive process along the CSF flow has not been determined in these studies. Nevertheless, comparing our data with these findings, it would be tempting to speculate that T-cells coming from the cervical lymph nodes may potentially use the same route to enter the brain parenchyma of NCL mice, but such pathways have not been documented so far and therefore seem rather unlikely. Likewise, particle passage (or in our case T-cell transport) from the parenchyma via the drainage of interstitial fluid out of the brain along perivascular space, vessels or cranial nerves is not thought to occur (Zhang *et al.*, 1992; Carare *et al.*, 2008). Accordingly, the transport of particles or cells in the opposite direction from the periphery along cranial nerves directly into the perivascular space seems an unlikely entry mechanism for lymphocytes into the brain, and indeed has not been described, even under inflammatory conditions and higher permeability of the BBB (Carrithers *et al.*, 2000; Engelhardt and Ransohoff, 2005). Therefore, such anatomical explanations, as tempting they may seem to explain our data, are not sufficient to account for the increased T-cell distribution in the olfactory bulb.

The best described entry route of T-cells into the brain is via the blood stream (Ransohoff *et al.*, 2003; Wilson *et al.*, 2010). Thus, as another explanation for the distribution of T-cells observed in our study, we could speculate that the vascular endothelial cells are more activated and express molecules more favourable for cell adhesion in the olfactory bulb than in other parts of the brain guaranteeing easier access to leukocytes. Indeed, BBB permeability has been described to be higher in the olfactory bulb of mice (Ueno *et al.*, 1996; Ueno *et al.*, 1998; Deckner, 2001). Furthermore, it has been shown that the permeability of the BBB increases with age and can vary between brain regions (Vorbrodt *et al.*, 1995; Ueno *et al.*, 1997). In

particular, capillaries of the olfactory bulb develop ultra-structural changes (like increased laminar cavitation) with increasing age (Hinds and McNelly, 1982). Speculatively, such enhanced permeability features of the olfactory bulb could lead to increased T-cell infiltration. Since increased BBB permeability, as is seen under inflammatory or irradiated conditions, is often associated with increased leukocyte adhesion to the brain vasculature (Petty and Lo, 2002; Yuan *et al.*, 2003; Persidsky *et al.*, 2006; Gavins *et al.*, 2007), this hypothesis seems plausible. Therefore this feature could potentially not only explain the highest accumulation of T-cells in the rostral parts of the brain, but also the increasing T-cell infiltration observed in wildtype mice over time (see **Figure 22**, **Figure 23**, **Figure 28** and **Figure 29** in **Chapter 3**), and could possibly even explain the region specific T-cell distribution in 21 month old *Cln3*$^{-/-}$ mice, which shall be discussed in the next section (see **Figure 28** and **Figure 29** in **Chapter 3**).

Taken together, our findings are consistent with the proposed entry of T-cells into the CNS via the blood stream in the choroid plexus or the meninges similar to the lymphocyte infiltration seen in humans, but in rodents, the olfactory bulb seems the preferred route of T-cell infiltration into the brain. This may be due to higher permeability of the BBB and perhaps altered adhesion properties of the vascular endothelial cells in the olfactory bulb, but also could be explained by other unknown mechanisms like increased accumulation of perivascular APCs in the olfactory bulb or a more tightly arranged brain microvasculature. However, we cannot completely rule out that other routes of T-cell entry exist in rodents, as for example from the cervical lymph nodes along the pathways of the CSF via the cribriform plate. All in all, our study represents a classical example for how pivotal it is to consider species-dependent differences between animals and humans when interpreting data.

d) T-cell distribution within brain parenchyma

Interpreting the cellular distribution of both subsets of T-cells in the *Ppt1*$^{-/-}$, or *Cln3*$^{-/-}$, CNS is less straight forward. Besides the specific T-cell accumulation in mid-levels of the forebrain of 21 month old *Cln3*$^{-/-}$ mice (see **Figure 28** and **Figure 29** in **Chapter 3**), the distribution of T-cells in *Ppt1*$^{-/-}$ and younger *Cln3*$^{-/-}$ mice generally followed a rostrocaudal gradient within the brain, with most of the cells being found in the olfactory bulb (see **Figure 22**, **Figure 23**, **Figure 28** and **Figure 29** in **Chapter 3**). Furthermore, while counting these T-cells we noticed that both T-cell subsets were

often detected near cerebral ventricles and/or in white matter tracts, but only occasionally were lymphocytes observed in the proximity of blood vessels (as putative entry point), suggesting that the blood vessels in the brain parenchyma of the fore- and midbrain are not the primary route for T-cells to infiltrate the brain (see **section 7.1c** above). However, because only large cross-sectional capillaries were apparent in our brain sections, we did not directly investigate the interactions between lymphocytes and blood vessels (including small capillaries and venules) in the brain parenchyma, the possibility of lymphocyte entry via postcapillary venules into the brain cannot be ruled out and is likely to occur (see **section 1.7b** in **Chapter 1** and (Owens *et al.*, 2008). Future co-localisation studies of CD4+ve or CD8+ve T-cell staining with brain vasculature markers will hopefully shed further light on this matter in *Ppt1*$^{-/-}$ and *Cln3*$^{-/-}$ brains. Nevertheless, explanations for the distribution of T-cells could be many and varied.

First of all, the ventricles, being in direct communication with the choroid plexus (that have fenestrated endothelial cells) may provide a general easy access route for T-cells (see **section 7.1c** above and (Wilson *et al.*, 2010)). In contrast, white matter tracts possibly serve as easy passageways for lymphocytes to travel within the brain. The migration of T-cells through the brain parenchyma has been described as random search behaviour (Mrass *et al.*, 2006; Melzer *et al.*, 2009; Wilson *et al.*, 2010), although a guided T-cell movement within the parenchyma has also been suggested (Mrass *et al.*, 2006; Wilson *et al.*, 2009). This may be via conduits formed by follicular dendritic cells, fibroblastic reticular or stromal cells, as has been seen in peripheral lymph nodes (Bajenoff *et al.*, 2006). Nevertheless, since other mechanisms of directed T-cell migration through the parenchyma via chemokines and cytokines remain controversial (Kawakami *et al.*, 2005; Schaeffer *et al.*, 2009), there have so far been no reports of a direct preference of white matter over gray matter for the passage of T-cells.

As another explanation for the observed rostrocaudal distribution of T-cells, it has been suggested that T-cells may 'hijack' the rostral migratory stream, which consists of new-born neurons travelling from the subventricular zone to the olfactory bulb (Maria B, 1993; Lois and Alvarezbuylla, 1994). Remarkably, the sites of lymphocyte infiltration we observed in *Ppt1*$^{-/-}$ and *Cln3*$^{-/-}$ brains (see **Figure 20** in **Chapter 3**) closely resembled that of brain dendritic cells (bDC) expressing CD11b in embryonic and adult mouse brains (Bulloch *et al.*, 2008). These CD11b+ve bDCs were distributed

in the circumventricular organs (subfornical organ, posterior pituitary, pineal gland, subcommisural organ etc.) (Bulloch *et al.*, 2008). These areas, due to an incomplete BBB, are known to allow direct access of pathogens or chemicals from the CSF and blood into the parenchyma (Ganong, 2000). Furthermore, the dendritic cells (and possibly also T-cells) were aligned along and around two extracellular pathways, the peripheral olfactory system connection between the nose and rostral brain, as well as along the pathways associated with the peripheral trigeminal system (Thorne *et al.*, 2004), which also connects the nasal passages with the brainstem and spinal cord regions (Liu *et al.*, 2001). Both of these routes are used as a sensory and humoral input to transport molecular signals such as pheromones into the brain (McClintock *et al.*, 2001), but may potentially also serve as an easily accessible portal to the brain for T-cells. In support of this hypothesis, a recent study in experimental autoimmune encephalomyelitis (EAE), the animal model for multiple sclerosis, demonstrated increased CD45+ve staining and inflammatory responses in the circumventricular organs (Schulz and Engelhardt, 2005). Additionally, inflammatory protein deposits have been found in the circumventricular organs of rat brains after systemic inflammations (Peress *et al.*, 1989; Schroder and Linke, 1999), indicating this to be a potential portal of inflammatory cells to the brain (Siso *et al.*, 2010).

In summary, the observed distribution of CD8+ve and CD4+ve T-cells in both forms of NCL appears to be mainly defined by the different entrance routes these cells may possibly take (olfactory bulb, circumventricular organs and ventricles) which in turn depends on the immune subtype, the condition of migrating immune cells, the activation state of the neural parenchyma and the endothelial cells in the vicinity of each entry point (Hickey, 1999). However, the explanation for T-cell accumulation in the mid-levels of the forebrain of 21 month old *Cln3*$^{-/-}$ mice (see **Figure 28** and **Figure 29** in **Chapter 3**) is less clear, but is likely to reflect changes in one, or more, of the above mentioned parameters. Therefore, this T-cell distribution pattern could be linked to a leaky BBB barrier in *Cln3*$^{-/-}$ mice (Lim *et al.*, 2007b), which is often associated with altered vascular endothelial cell activation/adhesion molecule expression, as has seen in other conditions (Yuan *et al.*, 2003; Gavins *et al.*, 2007; Comim *et al.*, 2011), and subsequently allow T-cells easier access in, for example, ventricular regions of the brain. This hypothesis is strengthened by the suggestions of an age-dependent and region specific increase of the BBB permeability (see **section 7.1c** above (Vorbrodt *et al.*, 1995; Ueno *et al.*, 1997).

Alternatively, altered cytokine expression by glial cells in *Cln3*$^{-/-}$ mice could plausibly attract T-cells to certain brain regions where glial activation is most pronounced (Kielian, 2012; Parviainen, 2012); JD Cooper personal communication). Whereas cytokine expression by *Cln3*$^{-/-}$ astrocytes is generally reduced in cell culture (Parviainen, 2012), *Cln3*$^{-/-}$ microglia displayed increased levels of cytokines and possibly represent the more relevant glial cells in this context of T-cell attraction (Kielian, 2012); JD Cooper, personal communication). This hypothesis is consistent with findings suggesting that astrocytes can restrict T-cell trafficking and infiltration into damaged or inflamed brain regions (John *et al.*, 2005; Voskuhl *et al.*, 2009), which shall be discussed further below in more detail (see **section 7.3a**). But then again, such restrictions could be compromised in *Cln3*$^{-/-}$ astrocytes due to their altered biology and protein secretion (Parviainen, 2012) and in turn, could speculatively lead to more T-cell accumulation in *Cln3*$^{-/-}$ mice.

Thus, neurodegenerative processes (like oxidative stress (Weimer *et al.*, 2007), disturbances in autophagy (Cao *et al.*, 2006) or calcium homeostasis (Chang *et al.*, 2007) resulting in synaptic dysfunctions (Luiro *et al.*, 2006; Tuxworth *et al.*, 2009), which are likely to lead to axonal rearrangements and synaptic changes as seen in other NCL mice (Kim *et al.*, 2008; Kielar *et al.*, 2009)), could also stimulate (micro)glial activation and speculatively T-cell attractant cytokine release in affected thalamocortical brain regions of *Cln3*$^{-/-}$ brains (Pontikis *et al.*, 2004; Pontikis *et al.*, 2005). Such mechanisms could potentially explain the observed pattern of increased T-cell accumulation in the mid-levels of the forebrain of *Cln3*$^{-/-}$ mice at 21 month of age. This hypothesis is strengthened by the qualitative observation of a putative accumulation of CD8+ve T-cells in the thalamic *VPM/VPL* nuclei of 21 month old *Cln3*$^{-/-}$ mice, whereas no similar distribution could be observed in *Ppt1*$^{-/-}$ mice (see **section 3.2b** in **Chapter 3**). Speculatively, such patterns could reflect a JNCL specific (auto-) immune response via CD8+ve T-cells which potentially are drawn to regions with increased neurodegeneration (Pontikis *et al.*, 2004; Pontikis *et al.*, 2005). Furthermore, this hypothesis could also explain the predominant CD8+ve T-cell infiltration in comparison to a delayed and moderate CD4+ve T-helper cells infiltration in *Cln3*$^{-/-}$ mice (see **Figure 27** in **Chapter 3** and **section 7.1a** above). However, more pragmatically, the accumulation of T-cells in the mid-levels of the forebrain could be a solely age-dependent phenotype since a similar rostrocaudal distribution of T-cells (but to a much lower extent) also was observed in 21 month old wildtype mice.

Therefore, we would favour an anatomical explanation for the increased T-cell accumulation in the mid-levels of the forebrain due to age-dependent alterations of the BBB around the ventricles, but would also not completely reject the possibility of CD8+ve T-cell specific accumulation in brain regions where neurodegeneration is more pronounced. Hopefully, BBB permeability and leukocyte-endothelial adhesion molecule expression analyses in 21 month old *Cln3*$^{-/-}$ and wildtype mice would clarify this issue. However, it will be just as important to conduct adaptive immune cell double knockout experiments on *Cln3*$^{-/-}$ mice (similar to the ones conducted in **Chapter 4** for INCL mice with *Ppt1*$^{-/-}$/*Rag-1*$^{-/-}$) to investigate whether CD8+ve T-cells accumulate in the *Cln3*$^{-/-}$ brain as a secondary reaction due to on-going neurodegeneration, or if CD8+ve T-cells as an auto-immune reaction putatively cause neurodegeneration in the first place.

e) T-cell surveillance

It is well documented that T-cells are also present in the brain parenchyma of healthy mice and patients and carry out constant surveillance of the micro-environment of the brain (see **section 1.7b** in **Chapter 1**, (Hickey, 2001; Wilson *et al.*, 2010)). Indeed, previously activated T-cells have the ability, by expressing the required molecules on their cell surface, to cross the BBB and enter the parenchyma even under non-inflammatory conditions (Hickey *et al.*, 1991; Carrithers *et al.*, 2000). However, there is still disagreement about the exact molecular phenotype of these monitoring T-cells. It is most commonly believed that predominately CD4+ve memory T-cells, which have been previously activated, monitor the healthy CNS (Wekerle *et al.*, 1987; Hickey *et al.*, 1991; Engelhardt and Ransohoff, 2005; Wilson *et al.*, 2010). However, it has been suggested that CD8+ve T-cells are also capable of surveillance in the CNS, and may even be the dominant cell type for this process (Cabarrocas *et al.*, 2003; Loeffler *et al.*, 2011). In our experiments we detected only small amounts of CD4+ve cells, just predominantly CD8+ve cells in the brain of wildtype mice (see **Figure 21** and **Figure 27** in **Chapter 3**). However, looking at the regional distribution of both T-cell subtypes in wildtype mice, the main accumulation of T-cells was observed in the olfactory bulb (as was also seen in both NCL mouse models). But from 5 months onwards, two to three times as many CD8+ve cells were found in the olfactory bulb of wildtype mice compared to CD4+ve cells (see **Figure 23** and **Figure 29** in **Chapter 3**). As such, these data suggest that the olfactory bulb is most likely an easy access portal for these T-cells (see **section 7.1c** above). Indeed, T-cells, in particular

CD8+ve T-cells are able to access the rostral brain parenchyma in wildtype mice, even in the absence of inflammation (see **Figure 22**, **Figure 23**, **Figure 28** and **Figure 29** in **Chapter 3**). The relatively large numbers of CD8+ve cells, in comparison to CD4+ve cells, could potentially be explained by less restricted or different means of brain infiltration by CD8+ve *vs.* CD4+ve T-cells (see **section 7.1a** and **7.1c** above, (Cabarrocas *et al.*, 2003; Galea *et al.*, 2007b; Melzer *et al.*, 2009), or by the high turnover of olfactory neurons exposed to an ever-changing environment (Astic and Saucier, 2001; Cowan and Roskams, 2002). However, it appeared that T-cells were unable to spread to more caudal regions of wildtype brains, probably due to the lack of sustaining antigen presenting cells and cytokines. Taken together, our data supply further evidence for a more prominent role of CD8+ve T-cells as the CNS monitoring cell type (Loeffler *et al.*, 2011) and argue against CD4+ve memory T-cells being the predominant cellular mediator of surveillance in healthy wildtype brains (Hickey, 2001; Engelhardt and Ransohoff, 2005).

Although the mechanisms that underlie T-cell infiltration in NCL mice remain speculative and need further investigation, to our knowledge our study is the first to characterise the lymphocyte infiltration in murine models of NCL in such detail. For example, future tracing and live imaging of T-cell trafficking into the brain as recently performed for dendritic cells or T-cells (Flugel *et al.*, 1999; John *et al.*, 2011; Odoardi *et al.*, 2012) in combination with fluorescence-activated cell sorting (FACS), co-localisation studies and more region specific immunohistochemical analyses of different brain parts (i.e. spinal cord, olfactory bulb, cranial nerve and cervical lymph nodes) could potentially clarify in more detail which T-cell subsets are present, exactly where in the brain they are, and with which cells they interact. Furthermore, brain region specific BBB analyses for putative trafficking determinants, as much as various knockout or tissue-specific induction experiments of, for example, cell endothelial molecules or APCs would give additional insights into the mechanisms involved in T-cell entry into the brain. However, with our data we were able to directly compare the Infantile and Juvenile NCL forms (which was eligible as both mouse models were kept on the same strain background). We identified similarities, as well as discrepancies between these forms of NCL. For example, very similar CD8+ve T-cell density could be found at the end stages of both forms of NCL, even though completely different progression rates and mechanisms were evident in each disease subtype. Such paradoxes highlight the importance of understanding the role of the adaptive immune

cells in the pathogenesis of each form of NCL, which will hopefully become clearer in the future with increasing knowledge about the underlying mechanisms of these diseases.

7.2 Sialoadhesin expression in NCL brains

a) Macrophage *vs.* microglia

As described in the **Chapter 1** (see **section 1.11b**), Sn is only expressed on the meninges and choroid plexus of healthy brains, but under inflammatory conditions Sn is also evident in the brain parenchyma on infiltrated macrophages and nearby microglia (Perry *et al.*, 1992). Therefore, it is not possible to directly distinguish between Sn+ve macrophages and microglia in the brain, and only co-localisation studies with Sn and additional macrophage markers can resolve this issue. Our collaborators demonstrated via such co-localisation that about 90% of CD11b+ve cells in the optic nerve also expressed Sn in proteolipid protein (PLP) overexpressing mice, a mouse model of a chronic myelin inflammatory disease (Ip *et al.*, 2007). As it seems unlikely that all of these Sn+ve cells integrated in the optic nerve, our collaborators hypothesised that it is not only infiltrated macrophages that may express Sn, but rather that resident microglia can also do this in a slowly progressive chronic disease. Considering the fact that microglia can take on neuroprotective or neurotoxic roles in the brain (see **section 1.6b** in **Chapter 1**; (Ekdahl *et al.*, 2009; Graeber and Streit, 2010)), our collaborators provocatively hypothesised that the expression of Sn on microglial cells could be predictive for the pathological versus protective role of these cells (Ip *et al.*, 2007). Even though we did not perform co-localisation experiments ourselves, our data clearly demonstrated that less than 90% of CD68+ve microglia cells expressed Sn in the thalamus, and much fewer in the cortex of *Ppt1*$^{-/-}$ and *Cln3*$^{-/-}$ mice (see **Figure 44**, **Figure 50**, **Figure 52** in **Chapter 5** and **Figure 58**, **Figure 64**, **Figure 66** in **Chapter 6**). However, since an undetermined, but considerable percentage of macrophage-like cells still express Sn in the thalamus of both models of NCL, it could be possible that we are not only looking at infiltrated macrophages, but also an expression pattern of Sn that indicates a more reactive (and neurotoxic) stage of microglial up-regulation. This hypothesis is supported by the sudden increase observed in Sn+ve cell numbers and change in morphology (amoeboid, round cells with no processes instead of cells with several processes) at 7 months of age in *Ppt1*$^{-/-}$ brains (see **Figure 44B** and **Figure 44D** in **Chapter 5**).

However, this expression pattern could, of course, be simply explained as being a consequence of normal disease progression or a sudden influx of infiltrating macrophages in affected brain regions.

Generally speaking, judged by their morphology, in most brain regions we predominantly observed a mix of Sn+ve microglia with ramified processes and Sn+ve brain-macrophages without any, or only short processes, in both types of NCL brains. Three possible scenarios may result in such a staining pattern in the brain. First of all, certain unknown cues (as for example on-going neurodegeneration) could trigger Sn expression in the brain on resident microglia, which during disease progression transform into Sn+ve brain-macrophages. Various degrees of on-going neurodegeneration and/or neuron vulnerability between brain regions would produce a mixed macrophage/microglial phenotype in each region. Secondly, Sn+ve macrophages could possibly infiltrate the brain parenchyma from the systemic circulation, attracted by on-going neurodegeneration and chemokines released by other glial or immune cells. Subsequently, resident microglia could up-regulate Sn in response to the infiltration of Sn+ve systemic macrophages in their vicinity. Or thirdly, cytokines or activation factors (for example IFN-α which has been shown to trigger up-regulation of Sn in many species (van den Berg *et al.*, 1996; Delputte *et al.*, 2007; Rempel *et al.*, 2008; Klaas and Crocker, 2012) in the blood serum could 'leak' or diffuse into inflammatory brain regions and induce Sn expression by microglia. Depending on their state of activation, Sn+ve microglia subsequently phenotypically resemble either microglia with ramified processes or brain-macrophages. Any of these scenarios are possible in INCL and JNCL brains, and since these mechanisms are not mutually exclusive, it is likely that a combination of these events could occur in the NCL brains, either simultaneously or variably during the course of the disease. Furthermore, due to differences in the integrity of the BBB between *Ppt1*$^{-/-}$ and *Cln3*$^{-/-}$ mice (Lim *et al.*, 2007b; Saha *et al.*, 2012), different events may occur in each of the two forms of NCL. However, our data does not allow us to unambiguously disentangle the true mechanism behind the up-regulation of Sn expression in the brain. We would speculate that in early disease stages, neurodegenerative cues in the brain, in combination with sporadic macrophage infiltration, induce Sn expression by brain resident microglia. However, with disease progression and the accompanying enhancement of inflammatory responses, vascular endothelial cell adhesion molecules could be up-regulated and the permeability of the glia limitans and the BBB increased

(Persidsky *et al.*, 2006), with more macrophages and putatively cytokines from the blood entering the brain, while more microglia transform into brain-macrophages. Taken together, such events could then result in the mixed phenotypes of Sn+ve macrophages/microglia that we observed in our experiments at all ages (see **Figure 44** in **Chapter 5** and **Figure 58** in **Chapter 6**). Future studies will be needed to clarify which of these processes are occurring in *Ppt1*$^{-/-}$ and *Cln3*$^{-/-}$ mice. Bone-marrow transplantation of GFP-labelled macrophages, or the specific depletion of systemic macrophages by liposome uptake, as performed previously (Bauer *et al.*, 1995; Tran *et al.*, 1998; Tanaka *et al.*, 2003; Chinnery *et al.*, 2010), could investigate to which extent peripheral macrophages infiltrate the brain in INCL and JNCL mice. Furthermore, as previously performed in *Cln3*$^{-/-}$ mice (Lim *et al.*, 2007b), peripheral injections of dextran or serum with subsequent immunohistochemical analysis of marker/serum proteins (e.g. albumin or immunoglobulins) in the brain could clarify the extent to which BBB integrity is compromised in *Ppt1*$^{-/-}$ mice; an issue which remains controversial.

b) INCL *vs.* JNCL

In both *Ppt1*$^{-/-}$ and *Cln3*$^{-/-}$ mice similar distributions of Sn+ve expression were observed, with the main site of activation being in the thalamic *VPM/VPL* nuclei where glial activation is also predominantly seen in NCL mice (Bible *et al.*, 2004; Pontikis *et al.*, 2004; Pontikis *et al.*, 2005; Kielar *et al.*, 2007; Partanen *et al.*, 2008; von Schantz *et al.*, 2009; Kuronen *et al.*, 2012; Schmiedt *et al.*, 2012; Thelen *et al.*, 2012). Nevertheless, clear differences in Sn+ve activation patterns between these forms of NCL were also identified. Specific brain regions and nuclei including the *retrosplenial granular cortex* (*RSG*), *CA1* of the hippocampus, the nuclei around *the anterior commissure* (*IPAC/IPAM*) together with the *ventral pallidum* (VP and the *amygdaloid nuclei (Bal, CeC, CeM),* the *substantia nigra*, the *external cortex of the inferior colliculus* (*ECIC*) or the *central nucleus of the inferior colliculus* (*CIC*) only showed Sn staining in *Ppt1*$^{-/-}$ mice. In contrast, Sn+ve macrophages in the dorsal parts of the *lateral posterior thalamic nuclei* (*LPMC and LPMR*) were only found in *Cln3*$^{-/-}$ mice. Furthermore, the distribution of Sn immunoreactivity in the *S1BF* region of the cortex was clearly different between these two disease forms. Whereas *Cln3*$^{-/-}$ mice showed only restricted Sn+ve staining of the deeper laminae (V and VI), in *Ppt1*$^{-/-}$ mice Sn+ve cells were mainly found in lamina VI, but sporadically also in the upper layers of the cortex (apart from 7 month old animals where all laminae showed Sn+ve cells in *Ppt1*$^{-/-}$ mice) (see **Figure 44C** in

Chapter 5 and **Figure 58B** in **Chapter 6**). In both types of NCL, Sn+ve macrophages were present in the same laminae of *S1BF* and the same thalamic nuclei where most glial activation could also be observed (see **Figure 44**, **Figure 46**, **Figure 48**, **Figure 50**, **Figure 52** in **Chapter 5** and **Figure 58**, **Figure 60**, **Figure 62**, **Figure 64**, **Figure 66** in **Chapter 6**, (Pontikis *et al.*, 2005; Kielar *et al.*, 2007)). Therefore, Sn may be a suitable marker or indicator for subsequent neuron loss in NCL brains, just as GFAP or CD68 haven proved to be in previous studies (Bible *et al.*, 2004; Pontikis *et al.*, 2004; Pontikis *et al.*, 2005; Kielar *et al.*, 2007). Even better, due to the fact that Sn is exclusively expressed on infiltrated macrophages and microglia in the most affected brain regions, Sn could potentially be used as indicator of the most acutely affected brain regions at any point in disease progression. In support of this suggestion, neuron loss has already been demonstrated in most regions of highest Sn expression: in the thalamic *VPM/VPL* nuclei in *Ppt1*$^{-/-}$, as well as *Cln3*$^{-/-}$ mice (see **Figure 44A** in **Chapter 5** and **Figure 58B** in **Chapter 6**, (Pontikis *et al.*, 2005; Kielar *et al.*, 2007)) and in lamina V of *S1BF* in *Ppt1*$^{-/-}$ mice (see **Appendix II: Figure 79** by S Duckett, MSc project; JD Cooper, personal communication). Furthermore, in direct comparison of activation status, Sn+ve cells (judged by staining intensity and cell morphology) in 18 month old *Cln3*$^{-/-}$ mice resembled 3 month old Sn+ve cells in *Ppt1*$^{-/-}$ mice. At these time points, the Sn+ve cells of both genotypes showed a mix of activated microglial cell staining with elongated processes and brain macrophage-like cells with amoeboid, round cell bodies without cell processes (see **Figure 44B** and **Figure 44D** in **Chapter 5** and **Figure 58A2** and **Figure 58B2** in **Chapter 6**). These comparisons are not exactly accurate as these mice have been bred on different backgrounds, but nevertheless it demonstrates the delayed and slower disease progression in JNCL mice compared to INCL mice. Taken together, clear differences in Sn+ve cell activation sites and morphologies were seen between the INCL and JNCL mouse models. These discrepancies are most simply explained by different rates of disease progression. Nevertheless, at the same time, these findings could suggest that Sn and Sn+ve macrophages/microglia play different roles in these two diseases. In any case, such differences strengthen the hypothesis that these NCL forms represent separate diseases (Cooper, 2010), even though they have been grouped into the same family of disorders.

7.3 Interactions between adaptive immune cells and glial cells (INCL)

a) Direct or indirect interactions

As demonstrated in **Chapter 4**, the absence of functioning T- and B-cells had an attenuating effect on astrocytosis as well as microglial activation in the brains of *Ppt1*$^{-/-}$/*Rag-1*$^{-/-}$ mice (see **Figure 33**, **Figure 35**, **Figure 37** and **Figure 39** in **Chapter 4**). In other words, the adaptive immune response must have an accelerating and enhancing effect on glial activation in murine INCL. This may be explained by a direct interaction between glial cells and adaptive immune cells, or indirectly by an increased inflammatory brain environment created by adaptive immune cells in the brain (Benveniste, 1998; Schroeter and Jander, 2005). The pronounced reduction in microglial activation in the absence of adaptive immune cells in *Ppt1*$^{-/-}$/*Rag-1*$^{-/-}$ mice confirmed that direct interactions between microglia and T-cells may also occur in the infantile form of NCL. At the same time, this finding may speculatively suggest that the number of Sn+ve macrophages (disguised by microglial activation) could be reduced in *Ppt1*$^{-/-}$/*Rag-1*$^{-/-}$ mice due to a less inflammatory brain environment, created by the absence of T-cells. However, since the relative abundance of (Sn+ve) infiltrated macrophages has not yet been determined in *Ppt1*$^{-/-}$/*Rag-1*$^{-/-}$ mice (via CD169+ve staining), the precise interactions that may occur between T-cells and infiltrated macrophages remain open to debate. Nevertheless, combined with the data from *Ppt1*$^{-/-}$/*Sn*$^{-/-}$ mice (see **Chapter 5**) we would speculate that Sn+ve macrophages and T-cells reciprocally activate or attenuate themselves. This issue is of course further complicated by the difficulty in distinguishing immunohistochemically between infiltrated macrophages and microglia (see **section 7.2** above).

In contrast to infiltrated macrophages, in a resting state microglia are poor antigen presenting cells (Matyszak *et al.*, 1999; Lynch and Mills, 2011), but as soon as transformed into brain macrophage-like cells, they are very competent enhancers of the inflammatory response via the presentation of MHC II to CD4+ve T-cells as well as via MHC I cross-presentation to CD8+ve T-cells (Hickey and Kimura, 1988; Kreutzberg, 1996). These interactions between T-cells and glia cells are further influenced by a wide range of cytokines expressed by both cell types (Issazadeh *et al.*, 1995; Aloisi *et al.*, 2000b). In contrast, astrocytosis did not seem to be as greatly reduced in *Ppt1*$^{-/-}$/*Rag-1*$^{-/-}$ mice, as were the effects upon microglial activation (see **Figure 33**, **Figure 35**, **Figure 37** and **Figure 39** in **Chapter 4**), suggesting a less

direct link between astrocytes and T-cells. Astrocytes have also been proven to express MHC I/II molecules (Wong *et al.*, 1984; Lavi *et al.*, 1988), but are generally believed to be rather weak antigen presenting cells (reviewed in (Aloisi *et al.*, 2000b; Dong and Benveniste, 2001)). Furthermore, astrocytes have been shown to play important roles in the regulation of leukocyte trafficking in the CNS under inflammatory conditions (John *et al.*, 2005). After stroke or injury, astrocytic scars formed around damaged areas of the CNS have been shown to limit the spread of inflammatory cells from these damaged areas into neighbouring healthy tissue (Bush *et al.*, 1999; Sofroniew, 2005; Herrmann *et al.*, 2008a). Conversely, a recent study directly demonstrated that astrocytosis restricts T-cell infiltration into damaged CNS parenchyma (Voskuhl *et al.*, 2009). This study is supported by work experimentally inhibiting or diminishing astrocytosis which leads to exacerbated immune cell infiltration (Liedtke *et al.*, 1998; Bush *et al.*, 1999; Macauley *et al.*, 2011; Toft-Hansen *et al.*, 2011). This property of astrocytes possibly explains why we did not observe any specific focal T-cell accumulation in the thalamic *VPM/VPL* nuclei of *Ppt1*$^{-/-}$ mice, even though widespread T-cell infiltration was observed in these mice (see **Figure 16** in **Chapter 3**). At the same time, the speculatively suggested accumulation of CD8+ve T-cells in the thalamic *VPM/VPL* nuclei of *Cln3*$^{-/-}$ mice (see **Figure 17** and **section 3.2b** in **Chapter 3**), potentially argues against this hypothesis. However, since *Cln3*$^{-/-}$ astrocytes have been shown to display dysfunctions in morphological activation and cytokine secretion (Parviainen, 2012), the T-cell restrictive properties of *Cln3*$^{-/-}$ astrocytes are likely to be also compromised, and therefore the astrocytosis in *Cln3*$^{-/-}$ mice possibly does not display the typical restrictive features mentioned above. Moreover, the same restrictive influence of astrocytes upon T-cells may also explain the lack of any positive influence upon neuron survival in the thalamus at later stages of the disease in *Ppt1*$^{-/-}$/*Rag1*$^{-/-}$ double knockouts (see **Figure 40** in **Chapter 4**). Perhaps the intense and localized astrocytosis in this nucleus obliterates the accelerating influence of T-cells in the thalamus of these mice. Consequently, in regions with less astrocytosis, like the cortex, the absence of T-cells would possibly favour longer lasting neuronal survival, as has recently been demonstrated (see **Appendix II: Figure 79** by S Duckett, MSc project). In summary, we are confronted with a complex symphony of activation processes and cell-cell interactions, which most likely vary between brain regions and at different stages of disease progression. Nevertheless, we have proven in our *Ppt1*$^{-/-}$/*Rag-1*$^{-/-}$ studies that adaptive immune cells do have a direct effect on glial cells in the brain.

b) What comes first?

By including different time points in our studies, we could address key "chicken or egg" questions – which immune response (astrocytes, microglia or T-cells) is activated first? This was of utmost importance, in order to potentially identify the main initiator of pathology in *Ppt1*$^{-/-}$ mice (see overview of events in **Figure 72**). However, from our data, significant T-cell infiltration, astrocytosis, microglial activation and Sn+ve macrophage up-regulation (suggesting Sn+ve monocyte infiltration) all occurred at the same time (3 months of age) of disease progression of *Ppt1*$^{-/-}$ mice. Speculatively, the morphology of CD68+ve microglia in the thalamus of *Ppt1*$^{-/-}$ mice suggested these cells were already in the early stages of activation at 1 month of age, although this difference was not significant via thresholding image analysis at this age (see **Figure 36**, **Figure 37**, **Figure 38** and **Figure 39** in **Chapter 4**). Likewise, judging by the qualitative observations, astrocytes in 1 month old *Ppt1*$^{-/-}$ mice already appear slightly more activated compared to wildtype mice, although this difference was not significant via thresholding image analysis, due to the patchy and heterogeneous nature of this GFAP staining (see **Figure 31**, **Figure 32**, **Figure 33** and **Figure 34**). Additionally, as reported in **Chapter 3**, there are already many more CD8+ve and CD4+ve T-cells in the olfactory bulb of *Ppt1*$^{-/-}$ mice at 1 month of age (again not reaching significance) (see **Figure 22** and **Figure 23** in **Chapter 3**), which does not rule out the possibility of earlier immune-related changes occurring in the INCL brain. In support of this idea, another study demonstrated that significantly altered cytokine expression is detectable as early as 1 month of age in the brains of *Ppt1*$^{-/-}$ mice (Kielar *et al.*, 2009). As described in **Chapter 1** (see **section 1.10**) early glial up-regulation has been also described in other NCL forms, for example, prenatally (40 to 20 days before birth) in *Cln6*$^{-/-}$ sheep (Kay *et al.*, 2006), or in the cerebellum of 1 week old *Cln3*$^{-/-}$ mice (Weimer *et al.*, 2009). Nevertheless, since in our study we did not focus upon such early changes, such suggestions of earlier disease phenotypes remain speculative.

What exactly triggers such glial responses and why these should be apparently "delayed" (being first seen at 3 months and not at 1 month of age), are crucial questions to be addressed in the future. Yet, an early developmental glial activation, which subsides temporarily to only reappear again at later stages of the disease, as seen for example in *Cln6*$^{-/-}$ sheep (Oswald *et al.*, 2005; Kay *et al.*, 2006), cannot be ruled out completely, since our study did not include early developmental stages. Nevertheless, one possible explanation for the 'delayed' glial response in *Ppt1*$^{-/-}$ mice

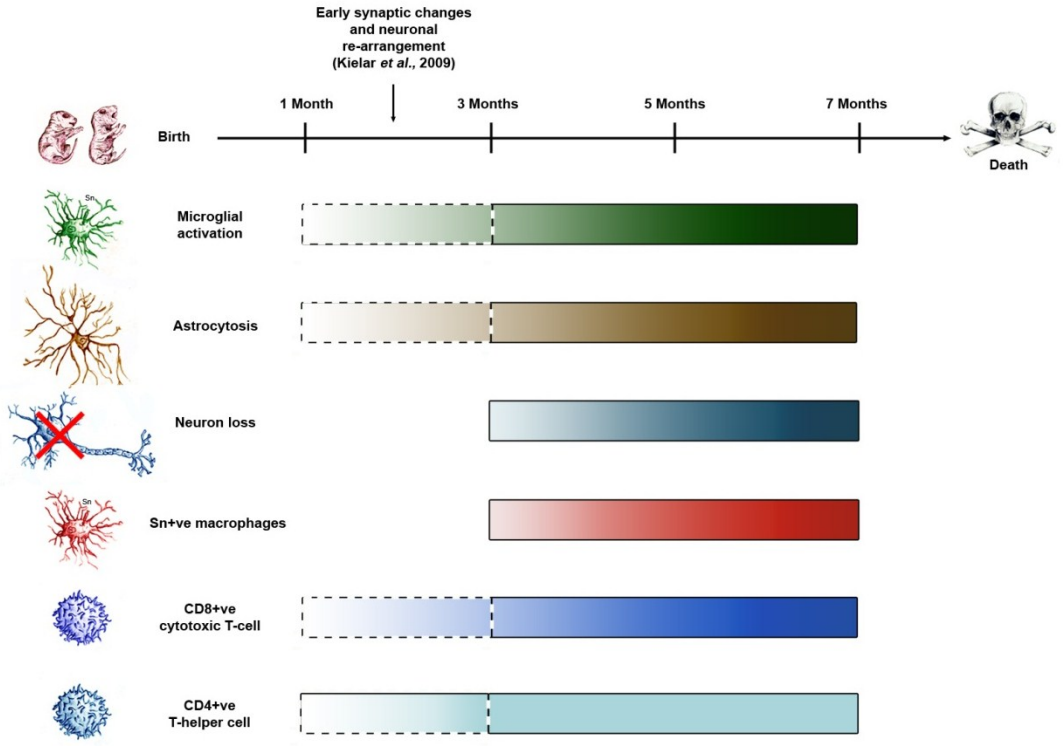

Figure 72. Schematic overview of temporal sequence of pathological events in the forebrain and midbrain of *Ppt1*$^{-/-}$ mice. With a life expectancy of 7-8 months of age (top row), we analysed *Ppt1*$^{-/-}$ mouse brains at four time points (1, 3, 5 and 7 months) for innate (microglial activation (CD68), astrocytosis (GFAP), Sn+ve macrophage activation (CD169)) and adaptive immune responses (cytotoxic T-cells (CD8), T-helper cells (CD4) infiltration) in relation to neurodegeneration (counts of Nissl stained neuron number). From 3 months onwards all of these parameters were significantly elevated in *Ppt1*$^{-/-}$ mice, compared to wildtype mice (solid line boxes). Each immune reaction became more pronounced with disease progression, except for CD4+ve T-helper cell infiltration, which already reached its saturation point by 3 months of age in *Ppt1*$^{-/-}$ mice. Earlier signs of immune reactivity could be suggested (dashed line boxes), on the basis of morphology and increased immunoreactivity, with CD68+ve microglial activation and GFAP+ve astrocytosis appearing marginally elevated at 1 month in *Ppt1*$^{-/-}$ mice. Likewise, elevated numbers of T-cells were detected in the olfactory bulb of *Ppt1*$^{-/-}$ compared to wildtype mice. But in all cases, when quantified, these differences did not reach statistical significance. In addition, early synaptic changes and neuronal re-arrangements have previously been reported before 3 months of age (Kielar *et al.*, 2009).

could be a neuronal modulation of glial cells by suppressing the inflammatory responses of microglia and astrocytes via the secretion of neuroprotective substances and/or direct cell-cell interactions, as described in **Chapter 1** (see **section 1.8**). Alternatively, preliminary data suggests that the biology of INCL astrocytes is also impaired, albeit differently to the defects seen in JNCL astrocytes (JD Cooper and BP Williams, personal communication). Whereas *Cln3*$^{-/-}$ astrocytes show an attenuated response to stimulation, by failing to morphologically transform from a flat polyglonal morphology to cells with small bodies and many processes (Parviainen, 2012), *Ppt1*$^{-/-}$ astrocytes under basal conditions morphologically appear to be already partially stimulated and subsequently only respond incompletely to further stimulation in culture by extending their processes, but not reducing their somal size (Milà, 2012).

Furthermore, both types of astrocytes display defects in their secretion of a range of mitogen, chemokines and pro- and anti-inflammatory cytokines, but in different ways: *Ppt1*$^{-/-}$ astrocytes generally secreted more and *Cln3*$^{-/-}$ astrocytes less of a wide (but not the same) range of secretory molecules compared to wildtype astrocytes (Milà, 2012; Parviainen, 2012). Such glial dysfunction is likely to influence disease progression in *Ppt1*$^{-/-}$ and *Cln3*$^{-/-}$ mice and it will be important to determine the underlying mechanisms.

Nevertheless, we were definitively able to demonstrate in our *Ppt1*$^{-/-}$/*Rag-1*$^{-/-}$ double knockout mice that the adaptive immune cell response is clearly not the cause of glial activation, since astrocytosis and microglial activation have not been completely abolished in the absence of adaptive immune cells. It is unclear whether the adaptive immune cell response would be completely suppressed if the innate immune response was abolished, and is not addressed by the studies we have performed. Previous studies suggested that astrocytes trigger T-cell infiltration into the brain via chemokine release (Glabinski *et al.*, 1997; Ransohoff and Tani, 1998). However, it is possible that glial activation and T-cell responses are also independently triggered by another mechanism, for example the onset of neurodegeneration, or perhaps the primary or secondary downstream consequences of lipid storage in brain cells.

All in all, with our studies we were not able to disentangle the exact sequence of all these events in the pathogenesis of *Ppt1*$^{-/-}$ mice. However, based on the above reasoning, we would speculate that microglial activation is the earliest type of glial activation to occur, which subsequently leads to GFAP+ve up-regulation in astrocytes sometime between 1 and 3 months of age, with these events leading eventually to T-cell infiltration in *Ppt1*$^{-/-}$ mouse brains. Thus, studying an intermediate early time point of 2 months of age could possibly clarify these speculations in future studies of *Ppt1*$^{-/-}$ mice.

In comparison to the analyses we performed in *Ppt1*$^{-/-}$ mice, we only investigated the glial activation and innate immune responses in detail at one time point (18 months) in *Cln3*$^{-/-}$ mice, and therefore cannot draw any conclusions about the progression of pathological events in these mice (see **Figure 73** for overview). However, our data reveal that adaptive immune cell infiltration (see **Figure 27** in **Chapter 3**) into the forebrain and midbrain of *Cln3*$^{-/-}$ mice occurred from 12 months onwards, whereas

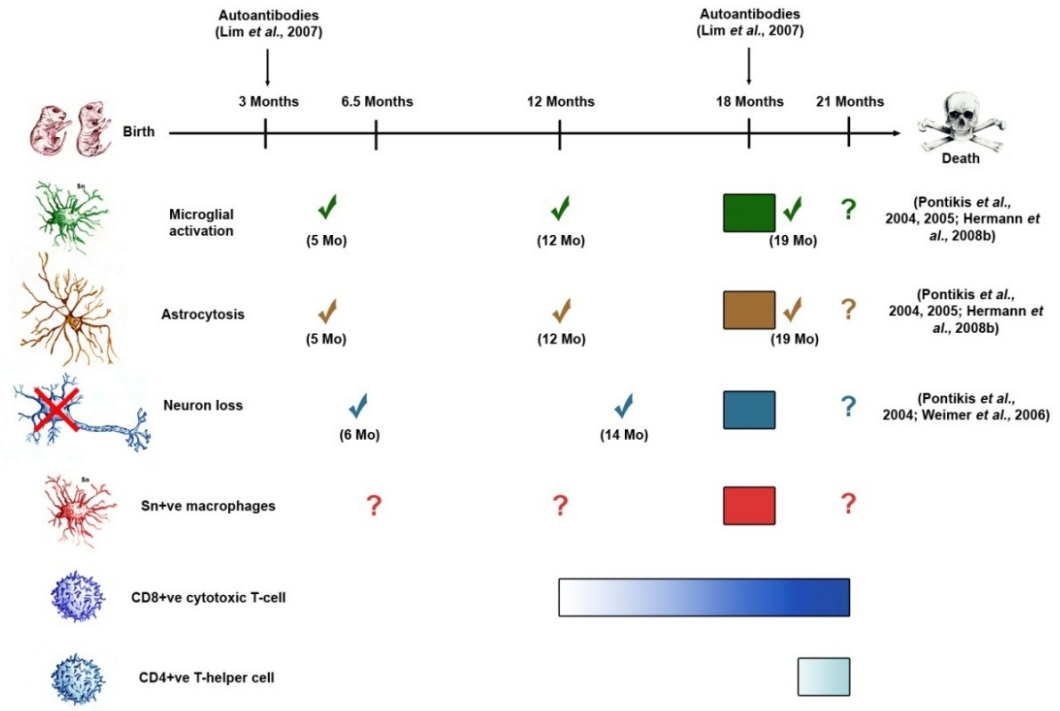

Figure 73. Schematic overview of temporal appearance of pathological events in the forebrain and midbrains of *Cln3*$^{-/-}$ mice. With a life expectancy of 21-22 months of age (top row), we analysed *Cln3*$^{-/-}$ mouse brains at four time points (6.5, 12 and 21 months) for adaptive immune responses (cytotoxic T-cells (CD8), T-helper cells (CD4) infiltration), and at one time point (18 months) for innate immune responses (microglial activation (CD68), astrocytosis (GFAP), Sn+ve macrophage activation (CD169)) in relation to neurodegeneration (Nissl stained neuron number). From 12 months onwards significantly increased numbers of CD8+ve cytotoxic T-cells were detected, whereas significantly more CD4+ve T-helper cells were only observed at 21 months of age in *Cln3*$^{-/-}$ mice (solid line boxes). At 18 months of age, all innate immune responses and neurodegeneration were significantly increased in *Cln3*$^{-/-}$ mice compared to wildtype mice. These data are consistent with our previous studies showing elevated glial activation at 5, 12 and 19 months of age and neurodegeneration at 6 and 14 months of age in the forebrain of *Cln3* deficient mice (Pontikis *et al.*, 2004, 2005; Weimer *et al.*, 2006; Hermann *et al.*, 2008b). Additionally, autoantibodies have been described in 3 (western plot analysis) and in 18 (immunohistochemical analysis) month old *Cln3*$^{-/-}$ mice (Lim *et al.*, 2007). Question marks indicate unknown parameters, because experiments have not yet been conducted. Please note that this overview includes data from *Cln3* deficient mice on C57BL/6 (this study; Hermann *et al.,* 2008b), 129Sv (this study; Pontikis *et al.*, 2004; Weimer *et al.*, 2006) and mixed 129Sv/CD1 (Pontikis *et al.*, 2005) strain backgrounds. It also includes both knock-in (Pontikis *et al.*, 2005; Hermann *et al.,* 2008b) and knockout (this study; Pontikis *et al.*, 2004; Weimer *et al.*, 2006; Lim *et al.* 2007) mice. This comparison is made based on there being no overt differences in disease phenotypes between different mutant mice on each background strain (JD Cooper, personal communication).

glial activation has previously been reported to occur as early as 5 months of age in the forebrain (Pontikis *et al.*, 2004), or even 1 week after birth in the cerebellum (Weimer *et al.*, 2009) of *Cln3*$^{-/-}$ mice. It is important to note that both of these earlier studies and our analysis of glial, Sn+ve macrophage and neurodegenerative responses (see **Chapter 6**) used mice bred on a 129/Sv strain background, in contrast to the C57Bl/6 congenic *Cln3*$^{-/-}$ mice used in this study to characterised T-cell responses (see **Chapter 3**), which means such comparisons may not be entirely valid (see **Figure 73** for

overview). Therefore, the infiltration of (CD8+ve) T-cells may seem to occur later in disease progression than innate immune responses, but this speculation needs to be confirmed with the analysis of glial activation and neurodegeneration at earlier time points in C57Bl/6 congenic *Cln3*$^{-/-}$ mice, which will hopefully clarify the sequence of pathological events in *Cln3*$^{-/-}$ mice.

7.4 Adaptive immune responses and neurodegeneration

As one of the main focuses of this PhD thesis, we examined the impact of adaptive immune cells upon neuron survival in *Ppt1*$^{-/-}$ mice. Consequently, we demonstrated that the lack of adaptive immune cells has a delaying effect on neuron loss in the thalamic *VPM/VPL* nuclei of *Ppt1*$^{-/-}$/*Rag-1*$^{-/-}$ mice at 3 months of age (see **Figure 40** in **Chapter 4**). Therefore, our data clearly suggests an influence of adaptive immune cells upon neurodegeneration in *Ppt1*$^{-/-}$ mice (see **Figure 74** for summary overview of proposed events in *Ppt1*$^{-/-}$/*Rag-1*$^{-/-}$ mice). These findings are consistent with studies in other diseases such as multiple sclerosis (Delgado and Sheremata, 2006; Stadelmann *et al.*, 2011), leukodystrophies (Wu *et al.*, 2000; Kovács *et al.*, 2005; Ip *et al.*, 2006) or Parkinson disease (Brochard *et al.*, 2009), in which adaptive immune cells have been associated with neuron loss. Adaptive immune cells have been shown to act on neuron survival in either direct or indirect ways. They can damage axons which eventually leads to retrograde neurodegeneration (Stadelmann *et al.*, 2011; Ip *et al.*, 2012), but may also directly induce apoptosis in the cell soma of neurons (Giuliani *et al.*, 2003; Vogt *et al.*, 2009).

In each disease different adaptive immune cell-mediated mechanisms can cause neurodegeneration. Whereas B-cells can produce (auto-) antibodies against neuronal antigens, as for example neurofascin in multiple sclerosis (Mathey *et al.*, 2007), T-cell activation can indirectly result in neuron loss via pro-inflammatory cytokine release and subsequent microglial activation, which in turn can harm neurons via non-specific immune mediators like nitric oxide (NO), proteases or other reactive oxygen species (Le *et al.*, 2001; Dutta and Trapp, 2007; Lull and Block, 2010; Zhang *et al.*, 2011). Such reactive oxygen species are thought to impair mitochondrial function in neurons, resulting in cellular energy failure and subsequent neuronal or axonal damage (Dutta *et al.*, 2006; Di Filippo *et al.*, 2010; Lassmann, 2011). Furthermore, T-cells may launch immune reactions directly against neuronal antigens, for example neurofilament,

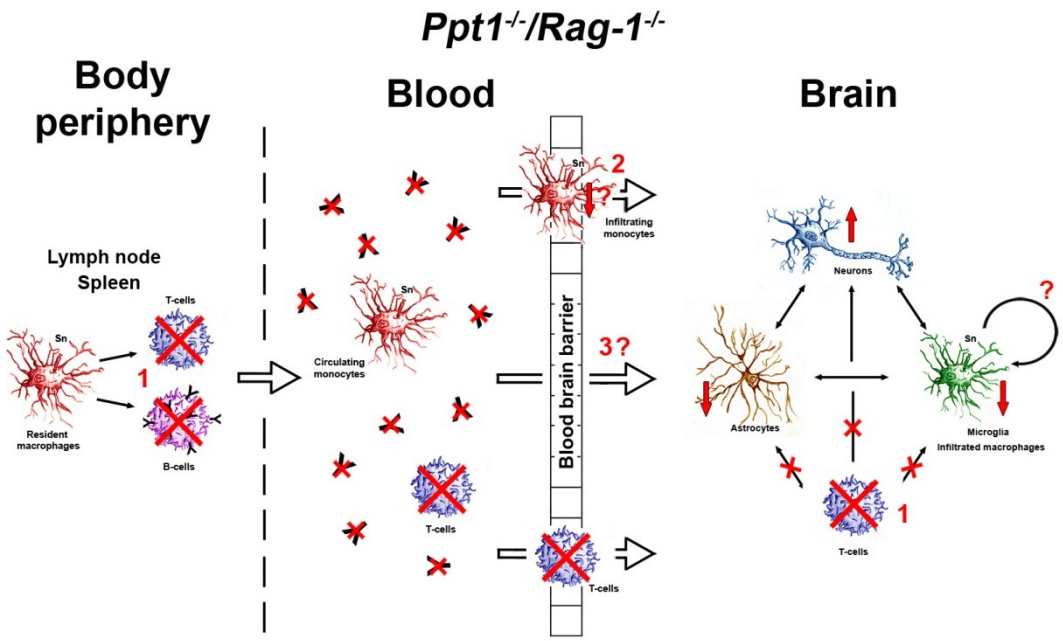

Figure 74. Proposed summary of events that occur in *Ppt1*$^{-/-}$*/Rag-1*$^{-/-}$ mice. The effects of Rag-1 deficiency appear to be exerted at multiple levels (body periphery, blood and brain) in *Ppt1*$^{-/-}$*/Rag-1*$^{-/-}$ mice. In the body periphery of these mice (particularly in the lymph nodes and spleen) no functional T- and B-cells are present (1). Consequently, therefore no antibodies or T-cells can be found in the blood. However, (Sn+ve) circulating monocytes are normally transported to the blood brain barrier (BBB) via the systemic circulation, where they can cross into the brain after interactions with endothelial cells and astrocytes. In the brain, infiltrated macrophages reach the site of inflammation (only investigated in *Ppt1*$^{-/-}$ mouse brains, but assumed to be similar in *Ppt1*$^{-/-}$*/Rag-1*$^{-/-}$ brains) where they are morphologically indistinguishable from microglia that have transformed into brain-macrophages. The amount of infiltrating Sn+ve monocytes has not yet been determined in *Ppt1*$^{-/-}$*/Rag-1*$^{-/-}$ brains, but speculatively their numbers are reduced due to less inflammatory conditions in the brain (indicated by ↓?) (2). The extent of self-activation/interaction between microglia and infiltrated macrophages is unknown (indicated by circled arrow and ?). However, the absence of T-cells led to a significant reduction (indicated by ↓) in microglial activation (represented as 'microglia' and 'infiltrated macrophages') and astrocytosis (represented as 'astrocytes'). As another consequence, neuron survival (represented as 'neurons') was transiently increased (indicated by ↑) in *Ppt1*$^{-/-}$*/Rag-1*$^{-/-}$ mice (at early disease stages). Speculatively, these changes have most likely been caused by less inflammatory conditions in the brain (1, 2) and/or other unmeasured cells or changes in the brain (3).

contactin-2 or beta-synuclein (Mor *et al.*, 2003; Derfuss *et al.*, 2009; Krishnamoorthy *et al.*, 2009). Additionally, the direct induction of neuronal death via the secretion of T-cell cytokines like tumour necrosis factor-α (TNF-α) itself has also been suggested, even though this hypothesis remains controversial (Rousselet *et al.*, 2002; Gaur and Aggarwal, 2003; Ferger *et al.*, 2004; Sriram *et al.*, 2006). Furthermore, CD8+ve cytotoxic T-cells classically can induce apoptosis in neurons after MHC-I antigen recognition via Fas-FasL interactions or granzymes and perforin release at the 'immunological synapse' (see **section 1.7a** in **Chapter 1**, (Rensing-Ehl *et al.*, 1996; Medana *et al.*, 2000; Abbas and Lichtman, 2011)). Moreover, during this induction of apoptosis, the leakage of effector molecules can cause collateral damage to bystander

neurons (Isaaz *et al.*, 1995; Wiedemann *et al.*, 2006), and additionally are suggested to disturb electrical excitability and signalling of neurons, leading to further neuronal death (reviewed in (Melzer *et al.*, 2009)). However, both T-cell subsets (CD4+ve and CD8+ve) are also capable of inducing apoptosis in neurons in an antigen- and MHC-independent manner via direct cell-cell contact mediated by FasL, Lymphocyte function-associated antigen 1 (LFA-1) or CD40 molecules (Giuliani *et al.*, 2003). However, these latter experiments were conducted in human cells and may not be directly translatable to mice. Last but not least, CD4+ve Th17 cells have been shown to express granzyme B and directly induce neuronal cell death (Kebir *et al.*, 2007). Thus, taken together, adaptive immune cells display various mechanisms to potentially induce neurodegeneration and have a pathogenic impact on disease progression (reviewed in (Amor *et al.*, 2009; Goverman, 2009).

Several studies utilising *Rag-1*$^{-/-}$ mice in models of various CNS disorders have similarly reported improved phenotypes, in mostly (autoimmune) myelin/axonal disorders (Sun *et al.*, 2001; Ip *et al.*, 2006; Pirko *et al.*, 2012). Depending on the disease, the main contribution to neuronal damage has been allocated either to the CD4 and/or CD8+ve T-cell subsets (Neumann *et al.*, 2002; Huang *et al.*, 2009). As typical examples, in Rasmussen Encephalitis or X-linked adrenoleukodystrophy CD8+ve T-cell subsets are mainly linked to neurodegeneration (Ito *et al.*, 2001; Bauer *et al.*, 2002), whereas CD4+ve T-cells have been classically linked to multiple sclerosis (Delgado and Sheremata, 2006), although there is also emerging evidence of pathological CD8+ve T-cell involvement in this disorder (Friese and Fugger, 2009). By reconstituting *Ppt1*$^{-/-}$/*Rag-1*$^{-/-}$ mice with bone marrow transplants of CD4$^{-/-}$ or CD8$^{-/-}$ mice, using a well-established protocol (Ip *et al.*, 2006), our collaborators have identified that it is CD8+ve T-cells that are the main mediator of disease pathology in the optic nerve of *Ppt1*$^{-/-}$ mice (unpublished data, J Groh and R Martini, University of Würzburg). It cannot be assumed that the same is also true for the pathology in the brain of INCL mice, but this is likely to be the case. As described above, CD8+ve T-cells may act directly on neurons in *Ppt1*$^{-/-}$ brains via Fas-FasL contact or granzymes and perforin release to induce apoptotic cascades in neurons (Mullereberhard, 1988; Cherin *et al.*, 1996; Nagata, 1996). Additionally, or independently, cytotoxic T-cells can indirectly activate microglia and macrophages in *Ppt1*$^{-/-}$ brains via pro-inflammatory cytokine release, which can subsequently cause neurodegenerative processes by additional nitric oxide and reactive oxygen release (Brookes *et al.*, 2003; Gurlo and von

Grafenstein, 2003; Hendriks *et al.*, 2005). Our findings of a pronounced reduction in microglial activation in *Ppt1*$^{-/-}$/*Rag-1*$^{-/-}$ mice favours the validity of this second hypothesis with microglia contributing to neuron loss in *Ppt1*$^{-/-}$ mice. Furthermore, our findings from Sn deficient double knockout experiments in INCL (as well as JNCL) mice (see **Chapter 5** and **Chapter 6**) also indirectly demonstrated the pathogenic influence of macrophages upon neuronal survival. Most likely a combination of direct apoptotic, as well as indirect effects of CD8+ve T-cells, results in the observed neuron loss in *Ppt1*$^{-/-}$ mice (see **Figure 40** in **Chapter 4**). Nevertheless, divergent roles of adaptive immune cells upon neurons have also been suggested. As mentioned in **Chapter 1** (see **section 7.1a**), adaptive immune cells may exhibit neuroprotective (Moalem *et al.*, 2000; Bieber *et al.*, 2003; Serpe *et al.*, 2003; Jones *et al.*, 2005) or neurodegenerative effects (Medana *et al.*, 2001; Bien *et al.*, 2002; Neumann *et al.*, 2002). Indeed, this may vary between disorders or even within the progression of a specific disease (Kerschensteiner *et al.*, 2003). Therefore, it seems likely that the role of adaptive immune cells also varies between different forms of NCL. In particular, in *Cln3*$^{-/-}$ mice where T-cells infiltrate in a completely different manner than is seen in *Ppt1*$^{-/-}$ mice (see **Figure 21** and **Figure 27** in **Chapter 3**), other cues and effector functions of adaptive immune cells may also be present. Based on the auto-immune responses in *Cln3*$^{-/-}$ mice (Chattopadhyay *et al.*, 2002a; Lim *et al.*, 2007b), so far only B-cell deficient *Cln3*$^{-/-}$/*μMT*$^{-/-}$ mice have been investigated (Seehafer *et al.*, 2011). Even though increased neuron survival (alongside with reduced neuroinflammation and improved rotarod performances) has been demonstrated in *Cln3*$^{-/-}$/*μMT*$^{-/-}$ mice (Seehafer *et al.*, 2011), we would speculate, based on our (CD8+ve) T-cell infiltration data in *Cln3*$^{-/-}$ mice (see **Figure 27** in **Chapter 3**), that possibly an even greater improvement could be achieved by knocking out T-cells (in particular CD8+ve T-cells). Hopefully future studies will investigate the exact impact of T-cells in mouse models of Juvenile and other forms of NCL.

7.5 Glial cells and neurodegeneration

As detailed in the **Chapter 1** (see **section 1.10**), a characteristic feature of the NCLs is glial activation that characteristically precedes neuron loss, and is especially pronounced in the thalamocortical system (Bible *et al.*, 2004; Pontikis *et al.*, 2004; Pontikis *et al.*, 2005; Cooper *et al.*, 2006; Kielar *et al.*, 2007; Partanen *et al.*, 2008; von Schantz *et al.*, 2009; Kuronen *et al.*, 2012; Schmiedt *et al.*, 2012; Thelen *et al.*, 2012).

Consistent with these observations, in all the experiments performed in this thesis glial activation was evidently detected in both *Ppt1*$^{-/-}$ and *Cln3*$^{-/-}$ mouse brains (see **Figure 32**, **Figure 34**, **Figure 36**, **Figure 38** in **Chapter 4** and **Figure 60**, **Figure 62**, **Figure 64**, **Figure 66** in **Chapter 6**), and was used as one of the outcome measures of disease progression in our studies. However, it is still not definitively known whether astrocytes and microglia take on neuroprotective or harmful roles in INCL and JNCL (see **section 1.6** and **1.10** in **Chapter 1**). Although our focus in this thesis was on adaptive immune responses and infiltrating macrophages, our experiments in immune deficient *Ppt1*$^{-/-}$ and *Cln3*$^{-/-}$ double knockout mice also revealed some clues towards answering this question. Firstly, in all our double knockout experiments we determined that the absence of adaptive immune cells, or of Sn expression, cannot completely reverse neuron loss in the NCL brain (see **Figure 40** in **Chapter 4**, **Figure 54** in **Chapter 5** and **Figure 68** in **Chapter 6**). However, at the same time, glial activation was always still apparent in these double knockout brains suggesting that astrocytes and/or microglia are probably greater contributors to neurodegenerative processes. In *Ppt1*$^{-/-}$ mice, this is particularly likely in the later stages of the disease when the influence of adaptive immune or Sn+ve macrophages on neuronal survival vanished, but glial activation and neuron loss both continued (see **Figure 40** in **Chapter 4**, **Figure 54** in **Chapter 5**). In contrast, in *Ppt1*$^{-/-}$/*Sn*$^{-/-}$ double knockouts the slightly improved neuron survival at all ages could potentially be linked to the increased astrocytosis in these mice (see **Figure 47** and **Figure 49** in **Chapter 5**).

Speculatively, astrocytes might generate a more neuroprotective environment via anti-inflammatory cytokine release or formation of a glial scar around areas of neuron loss, which either could attenuate the effector functions of other immune cells or result in reduced immune cell infiltration via putatively altered BBB permeability in *Ppt1*$^{-/-}$/*Sn*$^{-/-}$ mice. However, our study design did not allow us to disentangle the role of each glial cell type in INCL or JNCL and thus, any interpretation remains speculative. One approach to address this issue was undertaken in a recent study crossbreeding *Ppt1*$^{-/-}$ mice with a strain of mutant mice that are deficient in both of the astrocyte intermediate filament proteins GFAP and Vimentin (Vim), and therefore have dysfunctional astrocytes (Macauley *et al.*, 2011). In this study, *Ppt1*$^{-/-}$/*GFAP*$^{-/-}$/*Vim*$^{-/-}$ triple mutant mice displayed an accelerated INCL disease phenotype and died significantly earlier than *Ppt1*$^{-/-}$ mice. Furthermore, these authors identified increased cytokine levels and accelerated immune cell (T-cell and monocyte) responses, but no

impaired BBB integrity in the brain of the triple knockout mice. These data suggested that astrocytes play a neuroprotective role in *Ppt1*$^{-/-}$ mice. The authors hypothesized that impaired astrocytes influence inflammatory cytokine levels in the brain and lead to an augmentation of microglial activation and immune cell infiltration, which accelerates disease progression. This interpretation is consistent with our findings in **Chapter 4** where we linked adaptive immune cells with disease deterioration. However, direct effects of astrocytes upon neuron survival cannot be ruled out in *Ppt1*$^{-/-}$/*GFAP*$^{-/-}$/*Vim*$^{-/-}$ triple mutant mice. Similar data from other disease or lesion models including experimental autoimmune encephalomyelitis (EAE) (Voskuhl *et al.*, 2009), brain trauma (Wilhelmsson *et al.*, 2004; Myer *et al.*, 2006) or spinal cord injuries (Faulkner *et al.*, 2004) provided further examples that manipulation or ablation of astrocyte function leads to increased neurodegeneration, increased tissue damage and neuroinflammation. All of these studies provide valid examples for a neuroprotective role of astrocytes in neurodegenerative disorders, and this also appears to be the case in INCL (Macauley *et al.*, 2011).

To our knowledge, no similar approach has yet been applied to microglial cells in the context of any form of NCL. However, the possibility of a changing role for astrocytes and microglia over the course of disease progression should not be neglected (Gao and Hong, 2008; Appel *et al.*, 2011). Depending on the extent and stage of disease progression, astrocytes or microglia may initially be neuroprotective by initiating repair mechanisms and glial scar formation (Glezer *et al.*, 2007; Muzio *et al.*, 2007; Li *et al.*, 2008; Hines *et al.*, 2009), but subsequently exert a negative effect on neuron survival if the neuroinflammation persists (Gao and Hong, 2008; Brambilla *et al.*, 2009; Graeber *et al.*, 2011). This is particularly true in the context of chronic neurodegenerative diseases like the NCLs, because the *Ppt1* and *Cln3* deficiency in our mice is persistent and cannot be eliminated or repaired by inflammatory responses, in contrast to other immune up-regulations like viral infections, which eventually can be eliminated (Gao and Hong, 2008; Griffin and Metcalf, 2011; Khatami, 2011). Furthermore, as described in **Chapter 1** (see **section 1.8**), direct modulation of glial responses by neurons may also play a role in defining neuroprotective or neurotoxic effects of glial cells by attenuating or enhancing inflammatory responses (Biber *et al.*, 2007; Levite, 2008; Tian *et al.*, 2009).

Another approach to identify the exact effect of glial cells on neurodegeneration would be to create cell type-specific, so called "conditional knockout" mice

(Orban *et al.*, 1992). Based for example on the most commonly used Cre/Lox system (Hoess *et al.*, 1982; Sauer and Henderson, 1988) specific genes can be manipulated/knocked out in targeted organs or cell types, such as within the brain. Such a cell type-specific strategy is currently underway for JNCL, with mice bearing a floxed *Cln3* allele now generated in readiness for crossing to appropriate cell-type specific *cre* driver lines (JD Cooper, personal communication). However, in INCL with a deficiency in a soluble enzyme (Ppt1), such an approach is complicated since healthy and deficient cells can cross-correct one another (see **section 1.3a** in **Chapter 1**, (Sands and Davidson, 2006)). One possibility would be to link the cell specific NCL mutation with a deficiency in mannose-6-phosphate receptor on which cross-correction is dependent, or alternatively to breed mice with a membrane tethered form of Ppt1 to conduct these experiments with. Alternatively, one could manipulate an essential function of each specific glial cell type in the context of complete *Ppt1* deficiency, which would remove the complication of cross-correction. This approach would resemble our double knockout experiments, but restricting deficiency (for example Sn) to certain cells and/or tissues. Furthermore, there is also the possibility of producing stage-specific inducible knockouts of targeted genes, for example via tetracycline (tet/off or tet/on) (Gossen and Bujard, 1992; Gossen *et al.*, 1995) or tamoxifen induction (Metzger *et al.*, 1995). Therefore, any desired cell deficiency would be able to be induced in a flexible spatiotemporal manner (for review see (Zhang *et al.*, 2012)). On this basis, we are confident that in the near future new studies will come closer to elucidating the exact relationship between glia and neurodegeneration in the NCLs.

7.6 Interactions between sialoadhesin and glial cells

a) Microglia

Reviewing our data from *Ppt1*$^{-/-}$/*Sn*$^{-/-}$ (**Chapter 5**) and *Cln3*$^{-/-}$/*Sn*$^{-/-}$ (**Chapter 6**) double knockout mice, we conclude that Sn has an enhancing effect on microglial activation, but only at the later stages of the disease in *Ppt1*$^{-/-}$ mice and only minimally in *Cln3*$^{-/-}$ mice. The observed reduction in microglial activation in both double knockout mice is consistent with other studies carried out by our collaborators in Würzburg, in which they showed reduced numbers of CD11b+ve cells in *Sn*$^{-/-}$ PLP overexpressing or heterozygous *P0* deficient mice (Kobsar *et al.*, 2006; Ip *et al.*, 2007). In contrast, another study demonstrated increased microglial activation during prion pathogenesis

in *Sn*$^{-/-}$ mice (Bradford *et al.*, 2012). Therefore, the exact role of Sn in the brain, and its effect on microglia is still elusive. However, we would speculate that the most likely explanation for the observed discrepancy between (Bradford *et al.*, 2012) and other studies (including ours) is found in the extent of T-cell involvement in disease progression. Sn has been demonstrated in cell based studies to bind favourably to granulocytes (neutrophils), other myeloid cells and lymphocytes (Crocker *et al.*, 1995; Hartnell *et al.*, 2001). However, in the spleen or lymph nodes Sn was characterised as a lymphocyte-specific protein with rather low binding affinity for other macrophages (van den Berg *et al.*, 1992; Schadee-Eestermans *et al.*, 2000). In support of these findings, recent studies suggested a prominent involvement of Sn in adaptive immune response regulation (see **section 1.11b** in **Chapter 1**, (Crocker and Redelinghuys, 2008)) and for Sn interacting directly with T-cells (Muerkoster *et al.*, 1999; Ip *et al.*, 2007; Wu *et al.*, 2009). Therefore, we would speculate that the significant reduction in microglial activation in *Ppt1*$^{-/-}$/*Sn*$^{-/-}$ mice (see **Figure 51** in **Chapter 5**) and also minimally seen in *Cln3*$^{-/-}$/*Sn*$^{-/-}$ (see **Figure 64** in **Chapter 6**) is probably not linked to direct macrophage-microglial interactions, but indirectly results from diminished T-cell activation. Our findings of early Sn+ve expression (from 3 months) in *Ppt1*$^{-/-}$ brains (see **Figure 44** of **Chapter 5**) support this hypothesis. If direct macrophage-microglial interactions would stimulate each other, reduced microglial activation would be expected to be seen already at 3 months of age in *Ppt1*$^{-/-}$/*Sn*$^{-/-}$ mice. Instead, an indirect interaction via T-cells could explain the delayed change in the phenotype of these mice. However, the discrepancy between the detection of Sn+ve cells in *Ppt1*$^{-/-}$ mice at 3 months of age (see **Figure 44** of **Chapter 5**) and microglial reduction in *Ppt1*$^{-/-}$/*Sn*$^{-/-}$ mice (see **Figure 51** in **Chapter 5**) could also be explained simply by an up-regulation of Sn on microglia at 3 months of age, and actual peripheral macrophage infiltration occurring only at 5 months of age. This hypothesis is consistent with previous findings of initial microglial activation with a delayed macrophage infiltration from the body periphery during CNS inflammation (Andersson *et al.*, 1992). Furthermore, this interpretation is strengthened by the morphological appearance of Sn+ve cells at these two time points, with the majority of Sn+ve cells resembling brain-macrophages at 5 months of age whereas mainly microglia-like Sn+ve cells with cell processes can be detected at 3 months of age (see **Figure 44B** and **Figure 44D** in **Chapter 5**). This whole topic is of course made even more complicated by the difficulties of unambiguously distinguishing Sn+ve

macrophages and Sn+ve microglia (see **section 7.2a** above). Nevertheless, it cannot be ruled out that crosstalk may occur between microglia, or with infiltrated macrophages. This may cause these cells to enhance each other's activation in a Sn dependent manner, since similar Sn dependent macrophage-macrophage interactions have been reported in the spleen (Schadee-Eestermans *et al.*, 2000). Future studies will hopefully elucidate the potential role of direct interactions between microglia and Sn in more detail. Last but not least, this reduction in microglial activation could hypothetically also be explained by less efficient and compromised infiltration of Sn+ve monocytes from the blood stream into the brain. Theoretically, a lack of Sn-dependent mechanisms to cross the BBB would lead to less infiltration of monocytes into the brain, and eventually to a less inflammatory brain environment. This could be the case in *Ppt1*$^{-/-}$/*Sn*$^{-/-}$ mice, but may also play a role in the attenuated phenotype of *Cln3*$^{-/-}$/*Sn*$^{-/-}$ mice. Future co-culture studies of Sn+ve macrophages/monocytes and endothelial cells could elucidate such potential mechanisms, and the roles of astrocytes at the BBB should not be neglected.

b) Astrocytes

In our Sn deficient double knockout studies contrasting effects upon astrocytosis could be observed between *Ppt1*$^{-/-}$/*Sn*$^{-/-}$ and *Cln3*$^{-/-}$/*Sn*$^{-/-}$ mice. Whereas in *Cln3*$^{-/-}$/*Sn*$^{-/-}$ mice only a marginal reduction in astrocytosis could be detected (see **Figure 61** and **Figure 63** in **Chapter 6**), to our initial surprise an enhanced astrocytosis was evident in *Ppt1*$^{-/-}$/*Sn*$^{-/-}$ mice at all ages, but particularly at 7 months of age (see **Figure 47** and **Figure 49** in **Chapter 5**). To our knowledge, these studies represent the first demonstration of an, as yet, undescribed link between Sn and astrocytosis. Because in *Ppt1*$^{-/-}$/*Sn*$^{-/-}$ mice none of the parameters showed changes similar to that seen for astrocytosis as consequence of Sn deficiency, it is important to consider what possible mechanisms could lead to such a phenotype.

Each cell in the brain cell (glia, neuron and immune cell) is surrounded by, and reacts to, a wide range of cytokines and chemokines (Quan and Herkenham, 2002; Guyon *et al.*, 2008). As such, the increased level of astrocytosis in *Ppt1*$^{-/-}$/*Sn*$^{-/-}$ mice could simply reflect a Sn-dependent alteration in cytokine expression in the brain, a possibility which should certainly be investigated in future studies. Such cytokine alterations may be created, for example by a distorted CD8:CD4 balance in the brain. Consistent with previous findings of a reduction of CD8+ve T-cells and an up-regulation of CD4+ve

T-regulatory cells in *Sn* deficient mice (Kobsar *et al.*, 2006; Ip *et al.*, 2007; Wu *et al.*, 2009), a decreased inflammatory brain environment may be present in *Ppt1*$^{-/-}$/*Sn*$^{-/-}$ mice. However, confronted with ongoing neurodegeneration, T-cells in the brain may simultaneously enhance the neuroprotective properties of astrocytes (Garg *et al.*, 2008; Macauley *et al.*, 2011), leading to enhanced astrocytosis in *Ppt1*$^{-/-}$/*Sn*$^{-/-}$ mice. A complete absence of T-cells, as in the *Ppt1*$^{-/-}$/*Rag-1*$^{-/-}$ mice, would not evoke such events and therefore represents a possible underlying mechanism. However, a possible flaw in this hypothesis is that immune down-regulation via CD4+ve T-regulatory cells may also decrease astrocyte responses, as observed for example in HIV studies (Liu *et al.*, 2009). However in such viral systems no genetically caused, persistent neurodegenerative processes can be found as in *Ppt1*$^{-/-}$/*Sn*$^{-/-}$ mice and therefore other inflammatory mechanisms are likely to be involved.

As an alternative, but very speculative explanation, it could be suggested that increased factors like cytokines, hormones or growth factors (Morrison *et al.*, 1985; Polikov *et al.*, 2010) in the serum as a consequence of Sn depletion in the body, or the entry of other systemic cells via the BBB, which have not been measured in our experiments, could possibly cause further astrocytosis in *Ppt1*$^{-/-}$/*Sn*$^{-/-}$ mice. Since astrocytes help maintain the integrity and are a key part of the BBB (Bradbury, 1984), they are likely to be affected by such processes. Indeed, comparable events have recently been described in *Ppt1*$^{-/-}$ mice (Saha *et al.*, 2012). It was shown that the up-regulation of CD4+ Th17 effector cells and their production of IL-17R in the periphery (more precisely the spleen) and in the brain initiated endothelial cells to release matrix metalloproteinases (MMPs), which in turn degraded tight junction proteins (Saha *et al.*, 2012). Increased levels of MMPs would then also further trigger the production of MMPs by astrocytes, which was postulated to lead to BBB leakage and most likely also enhance astrocytosis. Following up such ideas regarding the BBB, perhaps under inflammatory conditions infiltrating Sn+ve macrophages form specific Sn-dependent cell-cell interactions with endothelial cells or astrocytes while crossing the BBB into the brain (Dosquet *et al.*, 1992; Ransohoff *et al.*, 2003; Reijerkerk *et al.*, 2012). Consequently, the lack of Sn may trigger further astrocytosis, but it is unclear how this happens. Taking this idea further, if Sn+ve macrophages themselves are the main cause for the enhanced astrocytosis in *Ppt1*$^{-/-}$/*Sn*$^{-/-}$ mice, and assuming that astrocytes take over a neuroprotective role (Macauley *et al.*, 2011), this would then confirm that Sn+ve macrophages may indirectly cause harm to neurons by attenuating astrocytosis in

Ppt1$^{-/-}$ mice. Furthermore, as mentioned in **Chapter 1** (see **section 1.10a**), recent studies on *Ppt1*$^{-/-}$ astrocytes in cell culture suggested they are functionally compromised (Milà, 2012), and *Sn* deficiency may amplify such astrocyte deficits in *Ppt1*$^{-/-}$/*Sn*$^{-/-}$ mice. These changes could also potentially have direct effects on astrocytosis and events at the BBB in these mice, although this would need to be investigated directly.

Last but not least, systemic events may also be responsible for the enhanced astrocytosis in *Ppt1*$^{-/-}$/*Sn*$^{-/-}$ double knockout mice. As already mentioned in **Chapter 1** (see **section 1.11c**), Sn+ve macrophages in the spleen have been suggested to be involved in the recognition and discrimination of self and non-self of apoptotic cell associated antigens (Klaas and Crocker, 2012). In other studies, depletion of Sn+ve macrophages resulted in a breach of self-tolerance by non-recognition of apoptotic cell debris via Sn+ve macrophages in the spleen (Miyake *et al.*, 2007). Consequently, the lack of Sn+ve macrophages accelerated disease progression by enhanced T-cell activation and cytokine production towards self-antigens (Miyake *et al.*, 2007; McGaha *et al.*, 2011). Because Sn may play a putative role in phagocytosis, antigen intake and presentation, and the recognition of apoptotic cells (Jones *et al.*, 2003; Revilla *et al.*, 2009; Delputte *et al.*, 2011; Klaas and Crocker, 2012), Sn deficiency could speculatively result in similar phenotypes and stimulate autoimmune responses in *Sn*$^{-/-}$ mice. Therefore, similar events may take place systemically in *Ppt1*$^{-/-}$/*Sn*$^{-/-}$ double knockout mice, which would potentially increase auto-immune responses and cytokines in the blood and therefore possibly could have a direct impact on astrocytosis. Alternatively, and even more speculatively, it is possible that Sn+ve macrophages in the brain normally facilitate the suppression of apoptotic cell (auto) antigens. As such, Sn deficiency could lead to an increased auto-immune reaction in the brain resulting in an enhanced pro-inflammatory environment, which could eventually be reflected in increased astrocytosis in *Ppt1*$^{-/-}$/*Sn*$^{-/-}$ double knockout mice. Because neurons die in *Ppt1*$^{-/-}$ mice from 3 months onwards (see **Figure 54** in **Chapter 5**), the increased astrocytosis in *Ppt1*$^{-/-}$/*Sn*$^{-/-}$ mice from the same time point onwards could potentially be explained by the breach of self-tolerance which is normally regulated by Sn+ve macrophages. Furthermore, the rapid explosion of GFAP+ve up-regulation /astrocytosis at 7 months of age may then be explained by a sudden increase in cell death in these affected regions. However, such explanations remain pure speculation so far and the putative link between apoptotic cell debris and Sn+ve macrophages in

the brain still requires future investigation. Unambiguous proof of the involvement of Sn in phagocytosis, antigen presentation in general, but specifically also in the recognition of apoptotic cells (reviewed in (Klaas and Crocker, 2012)), would have to be obtained. This could be achieved, for example, by exposing pure cultures of Sn+ve and *Sn*$^{-/-}$ macrophages to cell debris or by setting up neuron and *Sn*$^{-/-}$ macrophages co-cultures systems. In addition, the injection and tracing of labelled self-antigens into healthy and *Sn*$^{-/-}$ mouse brains could help to verify the putative role of Sn+ve macrophages in the uptake and recognition of apoptotic cell debris in the CNS.

c) INCL *vs.* JNCL

Finally in this context, it is important to address the question of how to explain the opposing effects of Sn deficiency upon astrocytosis in *Ppt1*$^{-/-}$/*Sn*$^{-/-}$ and *Cln3*$^{-/-}$/*Sn*$^{-/-}$ mice. In contrast to *Ppt1*$^{-/-}$ mice, the lack of Sn in *Cln3*$^{-/-}$ brains seems to marginally reduce astrocytosis, which could speculatively be explained by the 'conventional' CD8+ve T-cell and microglial down regulation as seen in other studies (Kobsar *et al.*, 2006; Ip *et al.*, 2007). However, we have not quantified the T-cell infiltration in *Ppt1*$^{-/-}$/*Sn*$^{-/-}$ mice so far and therefore, cannot be completely certain that such processes are actually occurring. Another explanation for the overt difference in astrocyte response between these mice could be the discrepancies in BBB integrity between these two forms of NCL. The BBB of *Cln3*$^{-/-}$ mice is already compromised at an early time point, namely from 3 months onwards (Lim *et al.*, 2007b). Therefore, in 18 month old *Cln3*$^{-/-}$ mice the BBB is perhaps already sufficiently leaky that the Sn deficiency, or any Sn related systemic impact, does not increase astrocytosis in the brain any further. In contrast, in *Ppt1*$^{-/-}$ mice the integrity of the BBB is still a controversial topic as some studies have not detected any impairments ((Macauley *et al.*, 2011); MS Sands, personal communication), but others have demonstrated BBB leakage late in the disease (see paragraph above) (Saha *et al.*, 2012). The autoimmune component of *Cln3*$^{-/-}$ mice is also likely to alter the effect of Sn deficiency upon disease manifestations including astrocytosis in *Cln3*$^{-/-}$/*Sn*$^{-/-}$ mice (see **section 1.10** in **Chapter 1**, (Lim *et al.*, 2007b)), whereas no autoimmune component has so far been described in INCL mice. Ultimately, in *Cln3*$^{-/-}$ mice both astrocytes and (Sn+ve) macrophages may be dysfunctional (Pontikis *et al.*, 2004; Getty *et al.*, 2011; Parviainen, 2012) and the lack of Sn may have a different effect, or no effect, on astrocytosis in *Cln3*$^{-/-}$/*Sn*$^{-/-}$ mice as a consequence of *Cln3* deficiency. However, until any clear connection between astrocytes and Sn+ve macrophages can be established, it will

remain unresolved which effect upon astrocytes in *Sn* deficient NCL mice represents the normal pathological influence of Sn. We surmise that the reactions in Juvenile NCL, with a clearly defined autoimmune influence in pathogenesis and transformational glial deficits, may possibly represent an abnormal pattern. This is in comparison to the pathogenesis of Infantile NCL, which displays no overt autoimmune effects and no dramatic glial abnormalities documented so far.

Considering all these data together, in both *Sn*$^{-/-}$ NCL double knockout mice we are probably observing a mix of several consequences of Sn deficiency. We would hypothesise that on one hand, microglial activation and T-effector cell reactions are reduced due to the lack of interactions between Sn+ve macrophages and T-cells. On the other hand, other mechanisms may be enhanced such as T-regulatory cell type stimulation, Sn-dependent changes at the BBB barrier, increased susceptibility to auto-antigens of apoptotic cell debris or unknown systemic effects. Even though these interpretations remain speculative, the sum of all these putative interactions, and the different disease mechanisms, does give rise to elevated astrocytosis in *Ppt1*$^{-/-}$/*Sn*$^{-/-}$ mice, whereas the opposite is seen in *Cln3*$^{-/-}$/*Sn*$^{-/-}$ double knockout mice. Therefore, these differences indicate diverse roles and implications for Sn and Sn+ve macrophages in these two forms of NCL, which would be interesting to follow up with future studies comparing for example *Ppt1*$^{-/-}$/*Sn*$^{-/-}$ and *Cln3*$^{-/-}$/*Sn*$^{-/-}$ macrophages in cell culture systems or Sn+ve macrophages in the spleen and lymph nodes of *Ppt1*$^{-/-}$ and *Cln3*$^{-/-}$ mice.

7.7 Sialoadhesin and neurodegeneration

We have demonstrated in this thesis that Sn has a direct influence on neurodegeneration in both Infantile (see **Figure 54** in **Chapter 5**) and Juvenile NCL (see **Figure 68** in **Chapter 6**), since the lack of Sn had an ameliorating effect on neuron survival in both forms of NCL. However, it is likely that Sn affects neurodegeneration by different mechanisms in these forms of NCL, since Cln3 and Ppt1 proteins exhibit contrasting functions and properties (see **section 1.2b** and **1.2c** in **Chapter 1**), and their deficiency results in different disease manifestations (reviewed in (Jalanko and Braulke, 2009; Cooper, 2010)) for example, disease specific glial dysfunction or autoimmune responses in *Cln3*$^{-/-}$ mice (Ramirez-Montealegre and Pearce, 2005; Lim *et al.*, 2006; Castaneda and Pearce, 2008; Parviainen, 2012). Based on all the measurements we have undertaken in *Ppt1*$^{-/-}$/*Sn*$^{-/-}$ mice, and other *Sn*

deficient studies (Kobsar *et al.*, 2006; Ip *et al.*, 2007), we would speculate that in *Ppt1*$^{-/-}$/*Sn*$^{-/-}$ mice the reduction of CD8+ve T-cell and/or Sn-dependent enhancement of astrocytosis (see **section 7.6b** above) act as the main neuroprotective force (see **Figure 75** for an overview of proposed events in *Ppt1*$^{-/-}$/*Sn*$^{-/-}$ mice). Quantifying T-cell infiltration in *Ppt1*$^{-/-}$/*Sn*$^{-/-}$ mice could potentially validate this hypothesis by detecting reduced amounts of (CD8+ve) T-cells in the brains of these mice. Furthermore, assessing Sn+ve monocyte infiltration, respectively Sn+ve macrophage activation in *Ppt1*$^{-/-}$/*Rag-1*$^{-/-}$ mice may also indirectly shed light upon the potential interaction of T-cells with Sn+ve macrophages.

In contrast, in Juvenile NCL, apart from the increase in neuron number, none of the parameters we measured in *Cln3*$^{-/-}$/*Sn*$^{-/-}$ mice showed any real difference, leaving unanswered questions about the reasons for the observed amelioration of disease in these mice.

Firstly, as suggested for *Ppt1*$^{-/-}$/*Sn*$^{-/-}$ mice, a reduced inflammatory environment within the CNS could have a significant impact on neuronal survival via CD8+ve T-cell attenuation or CD4+ve T-cell proliferation (Kobsar *et al.*, 2006; Ip *et al.*, 2007; Wu *et al.*, 2009). However, T-cells in *Cln3*$^{-/-}$ mice are only apparent at a later stage of the disease, with significant lymphocyte infiltration only evident at 21 months of age (see **Figure 27** in **Chapter 3**), the impact on neuron survival and the brain environment may not be as substantial as that suggested for *Ppt1*$^{-/-}$ mice. Alternatively, the previous identification of autoimmune responses in *Cln3*$^{-/-}$ mice (Lim *et al.*, 2007a; Castaneda and Pearce, 2008) may highlight that adaptive immune cells (including T-cells) could play a more prominent role in *Cln3*$^{-/-}$ mice than in *Ppt1*$^{-/-}$ mice. Indeed, even a late occurring (CD8+ve) T-cell infiltration in *Cln3*$^{-/-}$ mice could putatively have substantial impact on neurodegeneration. Therefore, the reduction of T-cell numbers in *Cln3*$^{-/-}$/*Sn*$^{-/-}$ mice is a valid hypothesis for increased neuron survival, and counting the number of these cells in the brains of *Cln3*$^{-/-}$/*Sn*$^{-/-}$ mice will hopefully clarify this issue.

Similarly, as already mentioned for *Ppt1*$^{-/-}$/*Sn*$^{-/-}$ mice, Sn deficiency could also theoretically compromise the infiltration of monocytes into the brain. If Sn is indeed necessary for monocytes to interact with endothelial cells and cross the BBB, then the lack of Sn would lead to a reduced infiltration of monocytes into *Cln3*$^{-/-}$/*Sn*$^{-/-}$ mouse brains. This in turn could increase neuron survival, either directly via a reduced release

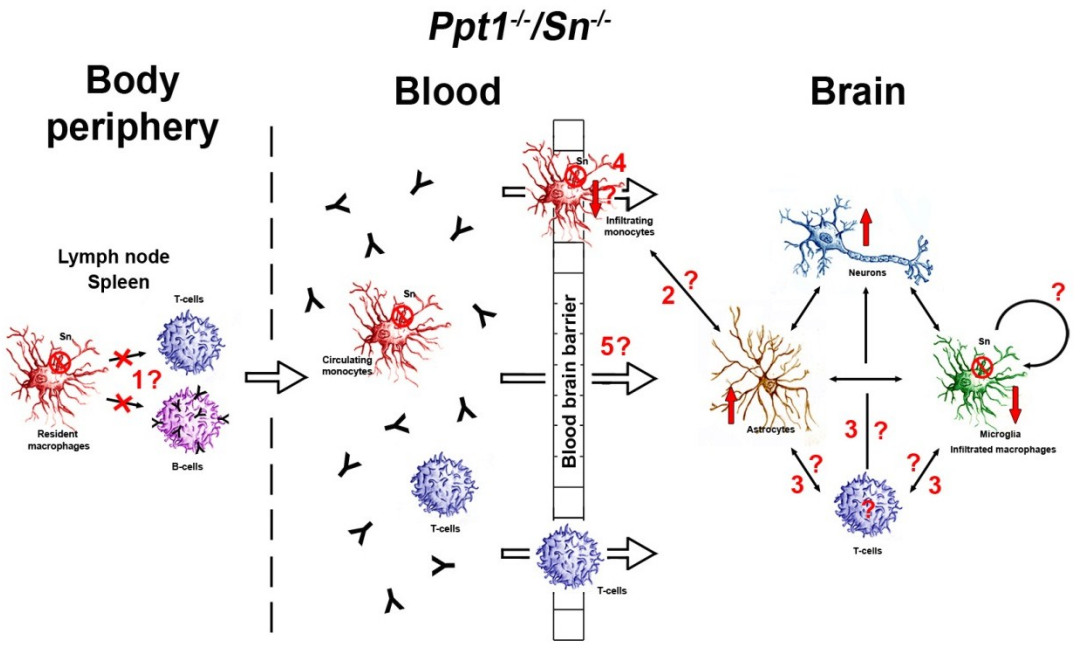

Figure 75. Proposed summary of events that occur in *Ppt1*$^{-/-}$/*Sn*$^{-/-}$ mice. Sialoadhesin (Sn) deficiency may impact at multiple levels (body periphery, blood and brain) in *Ppt1*$^{-/-}$/*Sn*$^{-/-}$ mice. In the lymph nodes and spleen, resident macrophages lack Sn-dependent interactions and putatively alter T- and B-cell activation (1). Antibodies, T-cells and Sn-deficient circulating monocytes are transported to the blood brain barrier (BBB) via the systemic circulation. However, deposition of IgGs has not yet been reported in brains of *Ppt1*$^{-/-}$ mice. Sn deficiency may also influence monocytes crossing the BBB via altering the interactions with endothelial cell and astrocytes in the brain (2). Speculatively, such changes could lead to enhanced (indicated as ↑) astrocytosis (represented as 'astrocytes'). Similarly, T-cells are likely to cross the BBB and interact with brain cells (neurons, astrocytes and microglia) (oligodendrocytes not being a focus of this study are not depicted) (3), but the extent of T-cell infiltration and its influence in the brains of *Ppt1*$^{-/-}$/*Sn*$^{-/-}$ mice has not yet been investigated. However, Sn deficiency led to a significant reduction (indicated by ↓) in microglial activation (represented as 'microglia' and 'infiltrated macrophages'), and significant enhancement of astrocytosis (represented as 'astrocytes'). The former could be a result of less (efficient) infiltration of circulating monocytes at the BBB due to their Sn deficiency (indicated by ↓?) (4). The extent of Sn dependent self-activation/interaction between microglia and infiltrated macrophages is unknown (indicated by circled arrow and ?). In contrast, neuron survival (represented as 'neurons') was increased (indicated as ↑) in *Ppt1*$^{-/-}$/*Sn*$^{-/-}$ mice (at early disease stages). Speculatively, these changes may be caused by reduced T-cell activation (1), less inflammatory conditions in the brain (2, 3, 4) and/or other unmeasured cells or changes in the brain (5).

of nitric oxide (NO), proteases or other reactive oxygen species (Le *et al.*, 2001; Dutta and Trapp, 2007; Lull and Block, 2010; Zhang *et al.*, 2011), or indirectly via lessinflammatory conditions in the brains of *Cln3*$^{-/-}$/*Sn*$^{-/-}$ mice. However, if this would be the case, a more pronounced reduction of microglial activation would have been expected in *Cln3*$^{-/-}$/*Sn*$^{-/-}$ mice. Nevertheless, Sn-dependent BBB interactions have not been described so far, but co-cultures of Sn+ve monocytes/macrophages and endothelial cells may help to elucidate such mechanisms.

As a third explanation for increased neuron survival in *Cln3*$^{-/-}$/*Sn*$^{-/-}$ mice, systemic effects of Sn+ve macrophages may occur. As described in **Chapter 1** (see **section**

1.11c), Sn+ve macrophages have been shown to present antigen to (and activate) B-cells in the spleen and lymph nodes (Carrasco and Batista, 2007; Junt *et al.*, 2007; Pape *et al.*, 2007; Gonzalez *et al.*, 2011). Thus speculatively, Sn deficiency could have a direct impact on B-cell activation and antibody production, although a direct role of Sn in antigen presentation and phagocytosis (as well as endocytosis) has yet to be proven unambiguously ((Revilla *et al.*, 2009) and reviewed in (Klaas and Crocker, 2012)). In the context of reported autoimmune responses in *Cln3*$^{-/-}$ mice (see **section 1.10** in **Chapter 1**, (Chattopadhyay *et al.*, 2002a; Lim *et al.*, 2007b; Castaneda and Pearce, 2008)), Sn deficiency could lead to a reduced production of antibodies against self-antigens and consequently increased neuron survival. In support of this hypothesis, the lack of detectable B-cells in the brain of *Cln3*$^{-/-}$ brains confirmed that auto-antibody production most likely occurs systemically rather than in the CNS (Lim *et al.*, 2007b). Likewise, IgG deposition has been found in human JNCL, as well as *Cln3*$^{-/-}$ mice and has been linked to complement activation (Lim *et al.*, 2007b). Even though IgG deposition has been proposed to be only a regular immunosurveillance function of IgGs in removing non-viable neurons (Stein *et al.*, 2002), in other diseases neuropathological and apoptotic features of IgGs in the brain have already been demonstrated (D'Andrea, 2003; Jernigan *et al.*, 2003). Sn deficiency could consequently also reduce IgG production in *Cln3*$^{-/-}$/*Sn*$^{-/-}$ mice and increase neuronal survival, but this is yet to be verified experimentally. This potential reduction in auto-antibodies in the brain would also account for the slightly lower glial activation in *Cln3*$^{-/-}$/*Sn*$^{-/-}$ double knockout mice, and therefore indirectly contribute to a less inflammatory environment in the brain and again enhance neuron survival. As such, it will be important to make measurements of auto-antibody concentration and IgG deposition in *Cln3*$^{-/-}$/*Sn*$^{-/-}$ double knockout mice to test these hypotheses.

In this context, as a potential confounder of our study, it should be noted that besides a small increase in CD8+ve T-cells, *Sn*$^{-/-}$ mice also show a small decrease in B220+ B-cells in the spleen and lymph nodes (Oetke *et al.*, 2006). As a consequence of this reduction, slightly reduced immunoglobulin M (IgM) levels were also detected, whereas no differences in IgG antibodies were seen in *Sn*$^{-/-}$ mice (Oetke *et al.*, 2006). Even though the same measurements were not made in either *Sn*$^{-/-}$ mice, or in the *Sn*$^{-/-}$ NCL mice used in this study, we are confident that due to the magnitude of increased neuron survival in *Cln3*$^{-/-}$/*Sn*$^{-/-}$ mice and of the disease attenuation in *Ppt1*$^{-/-}$/*Sn*$^{-/-}$ mice,

these differences in neuron numbers and disease progression are not founded on these minor deviations of *Sn*$^{-/-}$ mice from wildtype mice.

Furthermore, as already mentioned above in the context of *Ppt1*$^{-/-}$/*Sn*$^{-/-}$ mice, other studies depleting Sn+ve macrophages in the spleen of various disease models have demonstrated enhanced autoimmune responses due to a breach of self-tolerance via non-recognition of apoptotic cell debris (Miyake *et al.*, 2007; McGaha *et al.*, 2011). Such events led to accelerated disease progression by activating CD8+ve T-cells, dendritic cells and cytokine production towards self-antigens (Miyake *et al.*, 2007; McGaha *et al.*, 2011). Although the lack of Sn may hypothetically lead to similar results in *Cln3*$^{-/-}$/*Sn*$^{-/-}$ mice, we observed the opposite phenotype with attenuated neurodegeneration in the double mutants compared to *Cln3*$^{-/-}$ mice (see **Figure 68** in **Chapter 6**). This, once more, suggests that the driving force of the autoimmune response reported in *Cln3*$^{-/-}$ mice is most likely found neither in apoptotic neurons and cell debris in the CNS nor in T-cell activation. Instead, B-cells (including interactions with Sn) and their production of autoantibodies are probably more crucial to disease pathology in *Cln3*$^{-/-}$ mice. Last but not least, whereas *Cln3* deficiency in immune cells themselves possibly already lead to a marked autoimmune response in JNCL mice (Lim *et al.*, 2007b), Sn deficiency may disturb or enhance existing immune cell dysfunction in *Cln3*$^{-/-}$/*Sn*$^{-/-}$ mice. Alternatively, this could explain the less pronounced inflammatory response and increased neuron survival in these mice (see **Figure 76** for proposed summary of events in *Cln3*$^{-/-}$/*Sn*$^{-/-}$ mice).

In summary, although we showed that Sn has an accelerating effect on neurodegeneration, with the parameters we measured it is not possible to identify unambiguously how Sn deficiency results in the ameliorated phenotypes of both NCL double knockout mice. Whereas we would hypothesize that Sn+ve macrophage-T-cell interactions are predominantly responsible for accelerating neurodegeneration in *Ppt1*$^{-/-}$ mice, Sn+ve macrophage-B-cell interactions are more likely to be important in *Cln3*$^{-/-}$ mice. Whether these interactions occur in the brain and/or in secondary lymphoid organs alone remains to be seen. However, our results further suggest that systemic events may play a more important role in both forms of NCL than has previously been anticipated.

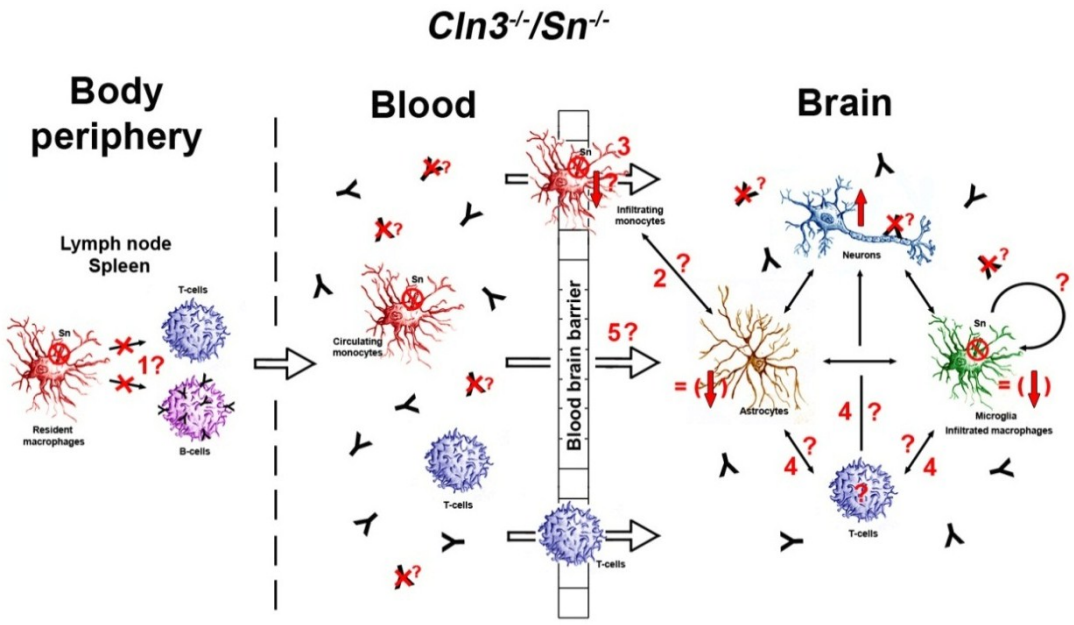

Figure 76. Proposed summary of events that occur in *Cln3*$^{-/-}$/*Sn*$^{-/-}$ mice. Sialoadhesin (Sn) deficiency may exert its influence at multiple levels (body periphery, blood and brain) in *Cln3*$^{-/-}$/*Sn*$^{-/-}$ mice. In the lymph nodes and spleen, resident macrophages lack Sn-dependent interactions and this may putatively alter T- and B-cells activation. This could lead to either reduced or enhanced T-cell activation, and perhaps also reduced (auto-)antibody production (1). As a consequence less (auto-) antibodies may be present in the blood and in the brain (indicated as X?), which has been previously described in *Cln3*$^{-/-}$ mice due to BBB leakage (Lim *et al.*, 2007). Besides antibodies, T-cells and circulating monocytes are also transported to the blood brain barrier (BBB) via the systemic circulation. Furthermore, Sn deficiency may also influence monocytes crossing the BBB via altered interactions between endothelial cells and astrocytes in the brain (2). Speculatively, less infiltrating monocytes (indicated by ↓?) could lead to slightly attenuated neuroinflammation and neuron loss (3). Likewise, T-cells are likely to cross the BBB and interact with brain cells (neurons, astrocytes and microglia) (oligodendrocytes not being a focus of this study are not depicted) (4), but the extent of T-cell infiltration and its influence in the brain of *Cln3*$^{-/-}$/*Sn*$^{-/-}$ mice has not yet been investigated. However, Sn deficiency led to a marginal reduction (indicated by = (↓)) in microglial activation (represented as 'microglia' and 'infiltrated macrophages') and astrocytosis (represented as 'astrocytes'). The extent of Sn dependent self-activation/interaction between microglia and infiltrated macrophages is unknown (indicated by circled arrow and ?). In contrast, neuron survival (represented as 'neurons') was increased in 18 month old *Cln3*$^{-/-}$/*Sn*$^{-/-}$ mice. Speculatively, this may be caused by reduced (auto-)antibody levels (1), less inflammatory conditions in the brain (2, 3, 4) and/or other unmeasured cells or changes in the brain (5).

7.8 Therapeutic implications of our findings

In our studies we looked at two different immune modifications: The effect of Rag-1 and Sn deficiencies were both investigated in *Ppt1*$^{-/-}$ mice, and the latter also investigated in *Cln3*$^{-/-}$ mice. The overall objective of our studies was to test the potential of these two immune modulations as therapeutic interventions in INCL and JNCL. The following paragraphs discuss the potential benefits of our studies and compare them to existing immune therapies.

a) Rag-1 *vs.* Sn

Since we conducted both Rag-1 and Sn deficient experiments in *Ppt1*$^{-/-}$ mice we were able to directly compare the effect of these genetic manipulations of the immune system upon neurodegeneration and most importantly upon lifespan. In immune deficient *Ppt1*$^{-/-}$/*Rag-1*$^{-/-}$ mice we saw an overall reduction in inflammatory responses in the brain (see **Figure 33**, **Figure 35**, **Figure 37** and **Figure 39** in **Chapter 4**), combined with reduced neuron loss at early stages of the disease (see **Figure 40** in **Chapter 4**) and an increase of lifespan to 265 days (unpublished data, J Groh, University of Würzburg). In contrast, the lack of Sn resulted in a weaker, but longer lasting improvement in neuron survival (see **Figure 54** in **Chapter 5**) and mixed effects upon glial activation in *Ppt1*$^{-/-}$/*Sn*$^{-/-}$ mice (see **Figure 47**, **Figure 49**, **Figure 51** and **Figure 53** in **Chapter 5**), together with a similar or even slightly greater impact upon lifespan (271 days) (unpublished data, J Groh, University of Würzburg). These findings revealed that a minor modulation of the adaptive immune response in *Ppt1*$^{-/-}$/*Sn*$^{-/-}$ mice can have a similar effect on lifespan as a complete eradication of adaptive immune cells in *Ppt1*$^{-/-}$/*Rag-1*$^{-/-}$ mice. Likewise, a subtle alteration of the immune system showed a significant improvement in neurodegeneration in *Cln3*$^{-/-}$/*Sn*$^{-/-}$ mice. Unfortunately, a directly comparable complete depletion of adaptive immune cells via Rag-1 deficiency is yet to be attempted in *Cln3*$^{-/-}$ mice. Nevertheless the question remains, which of the two immune modifications is 'better' or has a more significant impact? Or in other words, are the adaptive immune cells or Sn+ve macrophages more detrimental to disease outcome? The flaw in these questions is that, in our opinion, there is no oversimplified 'good' or 'bad' guy in inflammatory neurodegenerative CNS diseases. Indeed, because neuroinflammation is a dynamic process (Gao and Hong, 2008; Harry and Kraft, 2008; Frank-Cannon *et al.*, 2009; Rivest, 2009), the cost-benefit ratio of each manipulation of the immune system may vary in different contexts. We agree with other authors that it is most likely that dynamic immune interventions will be the way forward in the future (Wyss-Coray and Mucke, 2002; Schwartz and Kipnis, 2005; Zipp and Aktas, 2006; Gao and Hong, 2008). When inflammatory reactions are beneficial, boosting of the immune response should be considered, but when inflammation appears to be destructive, attenuation of the responsible immune cells, or their conversion into a beneficial role should be strived for. In summary, a more detailed understanding of the factors that contribute to disease progression will be essential for ultimately devising effective therapeutic

approaches. However, as long as there is a basic lack of knowledge about the underlying disease mechanisms in the NCLs (e.g. the function of deficient proteins, precise cellular involvements etc.), any improvement at all of neurodegeneration and lifespan is more than favourable in these disorders. Therefore we postulate that both Rag-1 as well as Sn could be considered as promising therapeutic targets. However, specific blockade of Sn (Halkes *et al.*, 2003) could potentially produce fewer side effects than a generalised immune suppression.

b) Other immune therapies

Immune modulatory therapies have mainly focused on the Juvenile form of NCL, because in the other NCL forms no overt auto-immune involvement has been demonstrated so far. The identification of auto-immune responses in both human and murine Juvenile NCL (Chattopadhyay *et al.*, 2002a; Chattopadhyay *et al.*, 2002b; Lim *et al.*, 2006; Lim *et al.*, 2007b; Castaneda and Pearce, 2008) sparked off investigations into potential immune suppressive therapies in CLN3 deficient patients. Recently improvements in motor function and neuron survival have been reported after immune suppressive interventions in *Cln3*$^{-/-}$ mice (Seehafer *et al.*, 2011), and initiated a Phase I clinical trial with the pharmacological drug *CellCept* on Juvenile NCL patients (*http://clinicaltrials.gov/ct2/show/NCT01399047*). Another previous study administered the steroid prednisolone to JNCL patients, which reduced the level of GAD65 auto-antibodies, but did not significantly change the course of disease (Aberg *et al.*, 2008). In this context, our studies examining Sn deficiency in *Cln3*$^{-/-}$ mice add another possible means to modulate of the immune system via Sn targeted therapy.

In *Ppt1*$^{-/-}$ mice the therapeutic focus has so far been on methods to deliver the missing enzyme (via either direct enzyme replacement, gene therapy or stem cell grafts), plus some largely unsuccessful small molecule based therapies (Griffey *et al.*, 2006; Tamaki *et al.*, 2009; Dawson *et al.*, 2010; Hu *et al.*, 2012). Only in a recent study from Prof. M Sands' laboratory did researchers administer an immune modulating drug called *Minozac* to *Ppt1*$^{-/-}$ mice (Shyng, 2012). This treatment was part of a combination therapeutic approach together with gene therapy (see **section 7.8c** below for more detailed discussion). *Minozac* can readily cross the BBB and inhibits pro-inflammatory cytokines production by activated glia in the brain (Lloyd *et al.*, 2008; Hu *et al.*, 2012). Despite moderately increased cortical thickness measurements the treatment with *Minozac* alone provided little or no benefit upon motor function or lifespan in *Ppt1*$^{-/-}$

mice. Compared to our data for lifespan extensions following Sn or Rag-1 deficient interventions, we would speculate that drugs modulating the adaptive immune system and/or Sn as putative therapeutic target will most likely have a greater impact on disease progression than *Minozac* did in this study.

c) Combination therapies

Although moderate improvements in lifespan, or at least key disease phenotypes, have been observed in all our double knockout mice, these genetic interventions did not completely reverse the neurodegenerative outcome of either *Ppt1*$^{-/-}$ or *Cln3*$^{-/-}$ mice. Nevertheless, we would predict that immune modulations in combination with other treatment strategies may improve their efficacy. Such combination therapies have been attempted in several LSD mice including MPSVII (Sands *et al.*, 1997), Sandhoff disease (Jeyakumar *et al.*, 2001; Lee *et al.*, 2007b) or Krabbe disease (Biswas and LeVine, 2002; Lin *et al.*, 2007). The success of these approaches has been variable, but some promising results were produced in a mouse model of Krabbe disease with almost 2.5 times extended lifespan (Lin *et al.*, 2007).

In recent years combination therapies have also been tested on NCL mice. A recent combination of CNS directed AAV2/5 mediated gene therapy with the immunosuppressant drug *Minozac* on *Ppt1*$^{-/-}$ mice (Shyng, 2012). The mice treated with both therapies showed significantly improved motor function and a lifespan extension of about 12 weeks (median survival of 47 weeks = 11.75 months or 329 days), compared to untreated *Ppt1*$^{-/-}$ mice (median survival of 35 weeks = 8.75 months or 245 days). As already mentioned above, *Minozac* alone did not extend lifespan, but gene therapy alone resulted in a 10 week improvement in lifespan (median survival of 45 weeks = 11.25 months or 315 days). Nevertheless, this study revealed for the first time that immune modulation may enhance the efficacy of other therapeutic approaches. However, recently the field of experimental therapies for Infantile NCL was revolutionized by the combination of BMT and CNS-directed gene therapy in *Ppt1*$^{-/-}$ mice (Macauley *et al.*, 2012). In this study, AAV treatment alone resulted in an increase in lifespan of about 4.5 months (median survival of 54 weeks = 13.5 months or 378 days). This increase in lifespan is by far the most successful single therapeutic intervention for INCL mice up to date which is most likely explained by the usage of a new AAV2/5 vector that has a higher capacity for transducing neurons. BMT therapy alone produced no such improvement on lifespan, even resulting in a worse outcome

with increased glial activation in the CNS compared to untreated *Ppt1*$^{-/-}$ mice. However, the combination of both therapies more than doubled the lifespan of the treated *Ppt1*$^{-/-}$ mice to a median survival of 74 weeks or 18.5 months (= 518 days). These results are astonishing, particularly because BMT itself did not result in any improvement at all in either behavioural or pathological outcome measures. The authors hypothesized that two main reasons could account for these observed improvements. On the one hand, the combination treatment not only targeted the brain via gene therapy, but simultaneously treated the systemic effects of disease via the BMT. Indeed, INCL and all other NCLs are primarily thought of as neurodegenerative disorders, but since every cell in the body is affected by the same genetic defect the concept of systemic and visceral pathology is now emerging as being important (Galvin *et al.*, 2008; Hu *et al.*, 2012). On the other hand, the presumed reduction of neuroinflammatory processes via BMT, suggests that these mechanisms may play an, up to now, under-appreciated role in pathogenesis (Macauley *et al.*, 2012). Interestingly, we could draw similar conclusions from our studies. We demonstrated that neuroinflammation (in particular adaptive immune cells) has an impact in the brains of INCL mice, but we also could speculate based on our findings of increased astrocytosis in *Ppt1*$^{-/-}$/*Sn*$^{-/-}$ mice, that systemic effects (modulated by Sn+ve macrophages) in the body periphery could potentially account for changes in the brain.

All in all, these recent therapeutic advances in mouse models are promising. In direct comparison to these effects upon lifespan, the improvements we observed in our *Ppt1*$^{-/-}$/*Rag-1*$^{-/-}$ and *Ppt1*$^{-/-}$/*Sn*$^{-/-}$ mice were rather moderate with 265, and 271 days respectively, compared to the expected 245 day lifespan of untreated *Ppt1*$^{-/-}$ mice (unpublished data, J Groh, University of Würzburg). Nevertheless, as a 'proof of principle' study we believe that our approach with similar combination therapies may have a greater impact than BMT – as we have already observed a more pronounced improvement in our studies on lifespan of *Ppt1* deficient mice than seen after BMT treatment alone (Macauley *et al.*, 2012). Therefore, in the future it would be of great interest to combine a blockade of Sn (Halkes *et al.*, 2003; Magesh *et al.*, 2011) or adaptive immune cells with other promising therapies like CNS-directed gene therapy.

Interestingly, no such combination therapy approach has been attempted so far in Juvenile NCL. This is largely due to the lack of efficient therapies in the first place.

Minor successes in treatment have been seen in small molecule therapies such as glutamate receptor antagonist or immune suppressive drug administration (see **section 7.8b** above, (Aberg *et al.*, 2008; Seehafer *et al.*, 2011)). But the first combinatory study for JNCL is now in preparation, which will investigate the treatment of *CellCept* in combination with other anti-inflammatory drugs in *Cln3*$^{-/-}$ mice (JD Cooper, personal communication). However, the lack of any real understanding of the CLN3 protein's function and the mechanistic causes of the disease has limited the scope for successful therapeutic interventions. Nevertheless, based on the data of our Sn deficient studies, this may represent another contribution in moving towards a therapeutic strategy. Encouraged by the positive findings resulting from using combination therapies in Infantile NCL mice it is to be hoped that similar advances will one day be realized for Juvenile NCL.

Chapter 8

Conclusions

Our study has revealed that immune cells play a pathogenic role in both Infantile and Juvenile forms of NCL. We have demonstrated for the first time the extent and nature of T-cell infiltration in both forms of NCL. Furthermore, we could ameliorate neuroinflammation and increase neuronal survival in *Ppt1*$^{-/-}$ mice by genetically removing adaptive immune system components, providing proof of the pathogenic role of adaptive immune cells in Infantile NCL. It will be important to perform similar genetic manipulation studies in *Cln3*$^{-/-}$ mice to identify the exact role of T- and B-cells in Juvenile NCL.

As a second goal of this study we wanted to characterise the role of sialoadhesin (Sn) expressing cells in the context of Infantile and Juvenile NCL. As a regulatory protein and functional link between innate and adaptive immune responses, a role for Sn could be predicted in disease progression. Indeed, in Infantile as well as Juvenile NCL, the lack of Sn increased neuron survival and attenuated disease progression, validating a pathogenic role for Sn in these forms of NCL. Furthermore, we demonstrated an unexpected link between macrophage-expressed Sn and astrocytosis in *Ppt1*$^{-/-}$ brains. These findings highlight the importance of understanding the role of each cell type in disease progression and how even the smallest irregularity in one cell type can affect the other cellular components of the brain. Furthermore, our data raised the possibility that peripheral immune cells and/or other systemic events may contribute to the neurodegenerative process in INCL and JNCL.

In summary, we have demonstrated how two different immune modulatory approaches can have similar effects in ameliorating disease in two forms of NCL. Adaptive immune cells and Sn, which is essential for the proper function of infiltrated peripheral macrophages and microglia in the brain, could be promising targets for therapeutic strategies in the currently incurable Infantile and Juvenile forms of Batten disease.

'The heights by great men reached and kept,

Were not attained by sudden flight,

But they, while their companions slept,

Were toiling upward in the night.'

Henry Wadsworth Longfellow

'In the end, it's not the years in your life that count. It's the life in your years.'

Abraham Lincoln

References

Abbas AK and Lichtman AH (2011). Basic Immunology: Functions and Disorders of the Immune System *Philadelphia, PA*, Saunders, Elsevier Inc.

Abbott NJ (2005). "Dynamics of CNS barriers: evolution, differentiation, and modulation." *Cell Mol Neurobiol* **25**(1): 5-23.

Abbott NJ, Patabendige AA, Dolman DE, Yusof SR and Begley DJ (2010). "Structure and function of the blood-brain barrier." *Neurobiol Dis* **37**(1): 13-25.

Abbott NJ, Ronnback L and Hansson E (2006). "Astrocyte-endothelial interactions at the blood-brain barrier." *Nat Rev Neurosci* **7**(1): 41-53.

Aberg L, Talling M, Harkonen T, Lonnqvist T, Knip M, Alen R, Rantala H and Tyynela J (2008). "Intermittent prednisolone and autoantibodies to GAD65 in juvenile neuronal ceroid lipofuscinosis." *Neurology* **70**(14): 1218-1220.

Acer N, Demir M, Ucar T, Pekmez H and Goktas A (2011). "Estimation of the Eyeball and Orbital Volume Using the Cavalieri Principle on Computed Tomography Images." *Balkan Medical Journal* **28**(2): 184-188.

Achord DT, Brot FE, Bell CE and Sly WS (1978). "Human beta-glucuronidase: in vivo clearance and in vitro uptake by a glycoprotein recognition system on reticuloendothelial cells." *Cell* **15**(1): 269-278.

Adams HR, Beck CA, Levy E, Jordan R, Kwon JM, Marshall FJ, Vierhile A, Augustine EF, de Blieck EA, Pearce DA and Mink JW (2010). "Genotype does not predict severity of behavioural phenotype in juvenile neuronal ceroid lipofuscinosis (Batten disease)." *Dev Med Child Neurol* **52**(7): 637-643.

Ahtiainen L, Kolikova J, Mutka AL, Luiro K, Gentile M, Ikonen E, Khiroug L, Jalanko A and Kopra O (2007). "Palmitoyl protein thioesterase 1 (Ppt1)-deficient mouse neurons show alterations in cholesterol metabolism and calcium homeostasis prior to synaptic dysfunction." *Neurobiol Dis* **28**(1): 52-64.

Ahtiainen L, Luiro K, Kauppi M, Tyynela J, Kopra O and Jalanko A (2006). "Palmitoyl protein thioesterase 1 (PPT1) deficiency causes endocytic defects connected to abnormal saposin processing." *Exp Cell Res* **312**(9): 1540-1553.

Ahtiainen L, Van Diggelen OP, Jalanko A and Kopra O (2003). "Palmitoyl protein thioesterase 1 is targeted to the axons in neurons." *J Comp Neurol* **455**(3): 368-377.

Aktas O, Ullrich O, Infante-Duarte C, Nitsch R and Zipp F (2007). "Neuronal damage in brain inflammation." *Arch Neurol* **64**(2): 185-189.

Alexander DR (2000). "The CD45 tyrosine phosphatase: a positive and negative regulator of immune cell function." *Seminars in Immunology* **12**(4): 349-359.

Allen MJ, Myer BJ, Khokher AM, Rushton N and Cox TM (1997). "Pro-inflammatory cytokines and the pathogenesis of Gaucher's disease: increased release of interleukin-6 and interleukin-10." *QJM* **90**(1): 19-25.

Aloisi F, Ria F and Adorini L (2000a). "Regulation of T-cell responses by CNS antigen-presenting cells: different roles for microglia and astrocytes." *Immunology Today* **21**(3): 141-147.

Aloisi F, Serafini B and Adorini L (2000b). "Glia-T cell dialogue." *J Neuroimmunol* **107**(2): 111-117.

Ambrosini E and Aloisi F (2004). "Chemokines and glial cells: a complex network in the central nervous system." *Neurochem Res* **29**(5): 1017-1038.

Amigorena S and Savina A (2010). "Intracellular mechanisms of antigen cross presentation in dendritic cells." *Current Opinion in Immunology* **22**(1): 109-117.

Amor S, Puentes F, Baker D and van der Valk P (2009). "Inflammation in neurodegenerative diseases." *Immunology* **129**(2): 154-169.

An Haack K, Narayan SB, Li H, Warnock A, Tan L and Bennett MJ (2011). "Screening for calcium channel modulators in CLN3 siRNA knock down SH-SY5Y neuroblastoma cells reveals a significant decrease of intracellular calcium levels by selected L-type calcium channel blockers." *Biochimica et biophysica acta* **1810**(2): 186-191.

Anderson G, Smith VV, Malone M and Sebire NJ (2005). "Blood film examination for vacuolated lymphocytes in the diagnosis of metabolic disorders; retrospective experience of more than 2,500 cases from a single centre." *J Clin Pathol* **58**(12): 1305-1310.

Andersson AM, Dihanich S, Williams BP, Mitchison HM, Rezaie P and Cooper JD (2009). "Evidence for altered microglial responses in juvenile Batten disease." *Neuropathology and Applied Neurobiology* **35**: 38-38.

Andersson PB, Perry VH and Gordon S (1992). "The acute inflammatory response to lipopolysaccharide in CNS parenchyma differs from that in other body tissues." *Neuroscience* **48**(1): 169-186.

Angata T and Brinkman-Van der Linden E (2002). "I-type lectins." *Biochim Biophys Acta* **1572**(2-3): 294-316.

Appay V (2004). "The physiological role of cytotoxic CD4(+) T-cells: the holy grail?" *Clin Exp Immunol* **138**(1): 10-13.

Appel SH, Zhao W, Beers DR and Henkel JS (2011). "The microglial-motoneuron dialogue in ALS." *Acta myologica : myopathies and cardiomyopathies : official journal of the Mediterranean Society of Myology / edited by the Gaetano Conte Academy for the study of striated muscle diseases* **30**(1): 4-8.

Arantes RM and Andrews NW (2006). "A role for synaptotagmin VII-regulated exocytosis of lysosomes in neurite outgrowth from primary sympathetic neurons." *J Neurosci* **26**(17): 4630-4637.

Argaw AT, Gurfein BT, Zhang Y, Zameer A and John GR (2009). "VEGF-mediated disruption of endothelial CLN-5 promotes blood-brain barrier breakdown." *Proc Natl Acad Sci U S A* **106**(6): 1977-1982.

Asano K, Nabeyama A, Miyake Y, Qiu CH, Kurita A, Tomura M, Kanagawa O, Fujii S and Tanaka M (2011). "CD169-positive macrophages dominate antitumor immunity by crosspresenting dead cell-associated antigens." *Immunity* **34**(1): 85-95.

Ascano M, Bodmer D and Kurovilla R (2012). "Endocytic trafficking of neurotrophins in neural development." *Trends Cell Biol* **22**(5): 266-273.

Asselin S, Breban M and Fradelizi D (1997). "Action of cytokines IL-12 and IL-4 on T helper cells - Cellular immunity or humoral immunity?" *Presse Medicale* **26**(6): 278-283.

Astic L and Saucier D (2001). "Neuronal plasticity and regeneration in the olfactory system of mammals: morphological and functional recovery following olfactory bulb deafferentation." *Cellular and Molecular Life Sciences* **58**(4): 538-545.

Aula P, Rapola J and Andersson LC (1975). "Distribution of cytoplasmic vacuoles in blood T and B lymphocytes in two lysosomal disorders." *Virchows Arch B Cell Pathol* **18**(4): 263-271.

Ausseil J, Desmaris N, Bigou S, Attali R, Corbineau S, Vitry S, Parent M, Cheillan D, Fuller M, Maire I, Vanier MT and Heard JM (2008). "Early Neurodegeneration Progresses Independently of Microglial Activation by Heparan Sulfate in the Brain of Mucopolysaccharidosis IIIB Mice." *Plos One* **3**(5): 11.

Azzi G, Bernaudin JF, Bouchaud C, Bellon B and Fleury-Feith J (1990). "Permeability of the normal rat brain, spinal cord and dorsal root ganglia microcirculations to immunoglobulins G." *Biol Cell* **68**(1): 31-36.

Baba Y, Kuroiwa A, Uitti RJ, Wszolek ZK and Yamada T (2005). "Alterations of T-lymphocyte populations in Parkinson disease." *Parkinsonism Relat Disord* **11**(8): 493-498.

Bach FH, Grillot-Courvalin C, Kuperman OJ, Sollinger HW, Hayes C, Sondel PM, Alter BJ and Bach ML (1977). "Antigenic requirements for triggering of cytotoxic T lymphocytes." *Immunol Rev* **35**: 76-96.

Bach G, Chen CS and Pagano RE (1999). "Elevated lysosomal pH in Mucolipidosis type IV cells." *Clin Chim Acta* **280**(1-2): 173-179.

Bachmann MF, Zinkernagel RM and Oxenius A (1998). "Immune responses in the absence of costimulation: viruses know the trick." *J Immunol* **161**(11): 5791-5794.

Backer R, Schwandt T, Greuter M, Oosting M, Jungerkes F, Tuting T, Boon L, O'Toole T, Kraal G, Limmer A and den Haan JM (2010). "Effective collaboration between marginal metallophilic macrophages and CD8+ dendritic cells in the generation of cytotoxic T cells." *Proc Natl Acad Sci U S A* **107**(1): 216-221.

Badwey JA and Karnovsky ML (1980). "Active oxygen species and the functions of phagocytic leukocytes." *Annual Review of Biochemistry* **49**: 695-726.

Bahmer FA, Hantirah S and Baum HP (1996). "Rapid and unbiased estimation of the volume of cutaneous malignant melanoma using Cavalieri's principle." *American Journal of Dermatopathology* **18**(2): 159-164.

Bailey SL, Schreiner B, McMahon EJ and Miller SD (2007). "CNS myeloid DCs presenting endogenous myelin peptides 'preferentially' polarize CD4(+) T-H-17 cells in relapsing EAE." *Nature Immunology* **8**(2): 172-180.

Bajenoff M, Egen JG, Koo LY, Laugier JP, Brau F, Glaichenhaus N and Germain RN (2006). "Stromal cell networks regulate lymphocyte entry, migration, and territoriality in lymph nodes." *Immunity* **25**(6): 989-1001.

Ballabh P, Braun A and Nedergaard M (2004). "The blood-brain barrier: an overview: structure, regulation, and clinical implications." *Neurobiol Dis* **16**(1): 1-13.

Balreira A, Lacerda L, Miranda CS and Arosa FA (2005). "Evidence for a link between sphingolipid metabolism and expression of CD1d and MHC-class II: monocytes from Gaucher disease patients as a model." *Br J Haematol* **129**(5): 667-676.

Barral P, Polzella P, Bruckbauer A, van Rooijen N, Besra GS, Cerundolo V and Batista FD (2010). "CD169(+) macrophages present lipid antigens to mediate early activation of iNKT cells in lymph nodes." *Nat Immunol* **11**(4): 303-312.

Barres BA (2008). "The mystery and magic of glia: a perspective on their roles in health and disease." *Neuron* **60**(3): 430-440.

Barton NW, Brady RO, Dambrosia JM, Di Bisceglie AM, Doppelt SH, Hill SC, Mankin HJ, Murray GJ, Parker RI, Argoff CE and et al. (1991). "Replacement therapy for inherited enzyme deficiency--macrophage-targeted glucocerebrosidase for Gaucher's disease." *N Engl J Med* **324**(21): 1464-1470.

Bassing CH, Swat W and Alt FW (2002). "The mechanism and regulation of chromosomal V(D)J recombination." *Cell* **109 Suppl**: S45-55.

Batlevi Y and La Spada AR (2011). "Mitochondrial autophagy in neural function, neurodegenerative disease, neuron cell death, and aging." *Neurobiology of Disease* **43**(1): 46-51.

Bauer J, Bien CG and Lassmann H (2002). "Rasmussen's encephalitis: a role for autoimmune cytotoxic T lymphocytes." *Curr Opin Neurol* **15**(2): 197-200.

Bauer J, Bradl M, Hickey WF, Forss-Petter S, Breitschopf H, Linington C, Wekerle H and Lassmann H (1998). "T-cell apoptosis in inflammatory brain lesions - Destruction of T cells does not depend on antigen recognition." *American Journal of Pathology* **153**(3): 715-724.

Bauer J, Huitinga I, Zhao W, Lassmann H, Hickey WF and Dijkstra CD (1995). "The role of macrophages, perivascular cells, and microglial cells in the pathogenesis of experimental autoimmune encephalomyelitis." *Glia* **15**(4): 437-446.

Becher B, Bechmann I and Greter M (2006). "Antigen presentation in autoimmunity and CNS inflammation: how T lymphocytes recognize the brain." *Journal of Molecular Medicine* **84**(7): 532-543.

Becher B, Prat A and Antel JP (2000). "Brain-immune connection: Immune-regulatory properties of CNS-resident cells." *Glia* **29**(4): 293-304.

Bechmann I, Galea I and Perry VH (2007). "What is the blood brain barrier (not)?" *Trends in Immunology* **28**(1): 5-11.

Bechmann I, Kwidzinski E, Kovac AD, Simburger E, Horvath T, Gimsa U, Dirnagl U, Priller J and Nitsch R (2001). "Turnover of rat brain perivascular cells." *Experimental Neurology* **168**(2): 242-249.

Bechmann I, Mor G, Nilsen J, Eliza M, Nitsch R and Naftolin F (1999). "FasL (CD95L, Apo1L) is expressed in the normal rat and human brain: evidence for the existence of an immunological brain barrier." *Glia* **27**(1): 62-74.

Beck DW, Vinters HV, Hart MN and Cancilla PA (1984). "Glial cells influence polarity of the blood-brain barrier." *J Neuropathol Exp Neurol* **43**(3): 219-224.

Beck M (2001). "Variable clinical presentation in lysosomal storage disorders." *J Inherit Metab Dis* **24 Suppl 2**: 47-51; discussion 45-46.

Ben-Hur T (2008). "Immunomodulation by neural stem cells." *J Neurol Sci* **265**(1-2): 102-104.

Benitez BA, Alvarado D, Cai YF, Mayo K, Chakraverty S, Norton J, Morris JC, Sands MS, Goate A and Cruchaga C (2011). "Exome-Sequencing Confirms DNAJC5 Mutations as Cause of Adult Neuronal Ceroid-Lipofuscinosis." *Plos One* **6**(11).

Bennett MJ, Gayton AR, Rittey CD and Hosking GP (1994). "Juvenile neuronal ceroid-lipofuscinosis: developmental progress after supplementation with polyunsaturated fatty acids." *Dev Med Child Neurol* **36**(7): 630-638.

Benveniste EN (1998). "Cytokine actions in the central nervous system." *Cytokine & Growth Factor Reviews* **9**(3-4): 259-275.

Berghoff M, Samsam M, Müller M, Kobsar I, Toyka KV, Kiefer R, Mäurer M and Martini R (2005). "Neuroprotective effect of the immune system in a mouse model of severe dysmyelinating hereditary neuropathy: enhanced axonal degeneration following disruption of the RAG-1 gene." *Molecular and Cellular Neuroscience* **28**(1): 118-127.

Bernard A and Boumsell L (1984a). "The Clusters of Differentiation (CD) defined by the 1st International workshop on human-leukocyte differentiation antigens." *Human Immunology* **11**(1): 1-10.

Bernard A and Boumsell L (1984b). "Differentiation human-leukocyte antigens - a proposed nomenclature." *Immunology Today* **5**(6): 158-159.

Bessis A, Bechade C, Bernard D and Roumier A (2007). "Microglial control of neuronal death and synaptic properties." *Glia* **55**(3): 233-238.

Beutler E, Kay A, Saven A, Garver P, Thurston D, Dawson A and Rosenbloom B (1991). "Enzyme replacement therapy for Gaucher disease." *Blood* **78**(5): 1183-1189.

Bevan MJ (2004). "Helping the CD8(+) T-cell response." *Nat Rev Immunol* **4**(8): 595-602.

Biber K, Neumann H, Inoue K and Boddeke HW (2007). "Neuronal 'On' and 'Off' signals control microglia." *Trends Neurosci* **30**(11): 596-602.

Bible E, Griffey M, Wozniak D, Wong M, Rothman S, Wentz A, Cooper JD and Sands MS (2005). "Adeno-associated virus 2-mediated gene therapy improves neuropathology and behavioural performance in a mouse model of infantile

neuronal ceroid lipofuscinosis (INCL)." *Neuropathology and Applied Neurobiology* **31**(2): 227-227.

Bible E, Gupta P, Hofmann SL and Cooper JD (2004). "Regional and cellular neuropathology in the palmitoyl protein thioesterase-1 null mutant mouse model of infantile neuronal ceroid lipofuscinosis." *Neurobiology of Disease* **16**(2): 346-359.

Bieber AJ, Kerr S and Rodriguez M (2003). "Efficient central nervous system remyelination requires T cells." *Annals of Neurology* **53**(5): 680-684.

Bien CG, Bauer J, Deckwerth TL, Wiendl H, Deckert M, Wiestler OD, Schramm J, Elger CE and Lassmann H (2002). "Destruction of neurons by cytotoxic T cells: A new pathogenic mechanism in Rasmussen's encephalitis." *Annals of Neurology* **51**(3): 311-318.

Bier E (2005). "Drosophila, the golden bug, emerges as a tool for human genetics." *Nat Rev Genet* **6**(1): 9-23.

Biffi A, De Palma M, Quattrini A, Del Carro U, Amadio S, Visigalli I, Sessa M, Fasano S, Brambilla R, Marchesini S, Bordignon C and Naldini L (2004). "Correction of metachromatic leukodystrophy in the mouse model by transplantation of genetically modified hematopoietic stem cells." *J Clin Invest* **113**(8): 1118-1129.

Biswas S and LeVine SM (2002). "Substrate-reduction therapy enhances the benefits of bone marrow transplantation in young mice with globoid cell leukodystrophy." *Pediatr Res* **51**(1): 40-47.

Blann A, Kumar P, Krupinski J, McCollum C, Beevers DG and Lip GY (1999). "Soluble intercelluar adhesion molecule-1, E-selectin, vascular cell adhesion molecule-1 and von Willebrand factor in stroke." *Blood Coagul Fibrinolysis* **10**(5): 277-284.

Blond D, Campbell SJ, Butchart AG, Perry VH and Anthony DC (2002). "Differential induction of interleukin-1beta and tumour necrosis factor-alpha may account for specific patterns of leukocyte recruitment in the brain." *Brain Res* **958**(1): 89-99.

Boehm T, Hess I and Swann JB (2012). "Evolution of lymphoid tissues." *Trends Immunol* **33**(6): 315-321.

Booss J, Esiri MM, Tourtellotte WW and Mason DY (1983). "Immunohistological analysis of T lymphocyte subsets in the central nervous system in chronic progressive multiple sclerosis." *Journal of the Neurological Sciences* **62**(1-3): 219-232.

Bosma GC, Custer RP and Bosma MJ (1983). "A severe combined immunodeficiency mutation in the mouse." *Nature* **301**(5900): 527-530.

Bosma GC, Fried M, Custer RP, Carroll A, Gibson DM and Bosma MJ (1988). "Evidence of functional lymphocytes in some (leaky) SCID mice." *Journal of Experimental Medicine* **167**(3): 1016-1033.

Bosma MJ and Carroll AM (1991). "The SCID mouse mutant - definition, characterization, and potential uses." *Annual Review of Immunology* **9**: 323-350.

Boudinot P, Marriotti-Ferrandiz ME, Pasquier LD, Benmansour A, Cazenave PA and Six A (2008). "New perspectives for large-scale repertoire analysis of immune receptors." *Mol Immunol* **45**(9): 2437-2445.

Braak H and Goebel HH (1978). "Loss of pigment-laden stellate cells: a severe alteration of the isocortex in juvenile neuronal ceroid-lipofuscinosis." *Acta Neuropathol* **42**(1): 53-57.

Braak H and Goebel HH (1979). "Pigmentoarchitectonic pathology of the isocortex in juvenile neuronal ceroid-lipofuscinosis: axonal enlargements in layer IIIab and cell loss in layer V." *Acta Neuropathol* **46**(1-2): 79-83.

Braakman I and Bulleid NJ (2011). "Protein folding and modification in the mammalian endoplasmic reticulum." *Annu Rev Biochem* **80**: 71-99.

Brabb T, von Dassow P, Ordonez N, Schnabel B, Duke B and Goverman J (2000). "In situ tolerance within the central nervous system as a mechanism for preventing autoimmunity." *J Exp Med* **192**(6): 871-880.

Bradbury MWB (1984). "The structure and function of the blood-brain-barrier." *Federation Proceedings* **43**(2): 186-190.

Bradford B, Crocker P and Mabbott N (2012). "Knockout of sialoadhesin enhances microglial accumulation during prion pathogenesis." *Prion* **6**: 49-49.

Bradl M, Bauer J, Flugel A, Wekerle H and Lassmann H (2005). "Complementary contribution of CD4 and CD8 T lymphocytes to T-cell infiltration of the intact and the degenerative spinal cord." *Am J Pathol* **166**(5): 1441-1450.

Brambilla R, Persaud T, Hu X, Karmally S, Shestopalov VI, Dvoriantchikova G, Ivanov D, Nathanson L, Barnum SR and Bethea JR (2009). "Transgenic inhibition of astroglial NF-kappa B improves functional outcome in experimental autoimmune encephalomyelitis by suppressing chronic central nervous system inflammation." *J Immunol* **182**(5): 2628-2640.

Braulke T and Bonifacino JS (2009). "Sorting of lysosomal proteins." *Biochim Biophys Acta* **1793**(4): 605-614.

Brean A (2004). "An account of a strange instance of disease--Stengel-Batten-Spielmayer-Vogt disease." *Tidsskr Nor Laegeforen* **124**(7): 970-971.

Brigl M and Brenner MB (2004). "CD1: antigen presentation and T cell function." *Annu Rev Immunol* **22**: 817-890.

Brisebois M, Zehntner SP, Estrada J, Owens T and Fournier S (2006). "A pathogenic role for CD8+ T cells in a spontaneous model of demyelinating disease." *J Immunol* **177**(4): 2403-2411.

Brochard V, Combadiere B, Prigent A, Laouar Y, Perrin A, Beray-Berthat V, Bonduelle O, Alvarez-Fischer D, Callebert J, Launay JM, Duyckaerts C, Flavell RA, Hirsch EC and Hunot S (2009). "Infiltration of CD4(+) lymphocytes into the brain contributes to neurodegeneration in a mouse model of Parkinson disease." *Journal of Clinical Investigation* **119**(1): 182-192.

Bromley SK, Burack WR, Johnson KG, Somersalo K, Sims TN, Sumen C, Davis MM, Shaw AS, Allen PM and Dustin ML (2001). "The immunological synapse." *Annual Review of Immunology* **19**: 375-396.

Brookes RH, Pathan AA, McShane H, Hensmann M, Price DA and Hill AV (2003). "CD8+ T cell-mediated suppression of intracellular Mycobacterium tuberculosis growth in activated human macrophages." *Eur J Immunol* **33**(12): 3293-3302.

Brossart P and Bevan MJ (1997). "Presentation of exogenous protein antigens on major histocompatibility complex class I molecules by dendritic cells: pathway of presentation and regulation by cytokines." *Blood* **90**(4): 1594-1599.

Brown AM, Baltan Tekkok S and Ransom BR (2004). "Energy transfer from astrocytes to axons: the role of CNS glycogen." *Neurochem Int* **45**(4): 529-536.

Brown AM and Ransom BR (2007). "Astrocyte glycogen and brain energy metabolism." *Glia* **55**(12): 1263-1271.

Brown DM (2010). "Cytolytic CD4 cells: Direct mediators in infectious disease and malignancy." *Cell Immunol* **262**(2): 89-95.

Brown VK, Ogle EW, Burkhardt AL, Rowley RB, Bolen JB and Justement LB (1994). "Multiple components of the B-cell antigen receptor complex associate with the protein tyrosine-phosphatase, CD45." *Journal of Biological Chemistry* **269**(25): 17238-17244.

Bruck W, Goebel HH and Dienes P (1991). "B and T lymphocytes are affected in lysosomal disorders--an immunoelectron microscopic study." *Neuropathol Appl Neurobiol* **17**(3): 219-222.

Bsibsi M, Ravid R, Gveric D and van Noort JM (2002). "Broad expression of Toll-like receptors in the human central nervous system." *J Neuropathol Exp Neurol* **61**(11): 1013-1021.

Bulloch K, Miller MM, Gal-Toth J, Milner TA, Gottfried-Blackmore A, Waters EM, Kaunzner UW, Liu K, Lindquist R, Nussenzweig MC, Steinman RM and McEwen BS (2008). "CD11c/EYFP transgene illuminates a discrete network of dendritic cells within the embryonic, neonatal, adult, and injured mouse brain." *Journal of Comparative Neurology* **508**(5): 687-710.

Bush TG, Puvanachandra N, Horner CH, Polito A, Ostenfeld T, Svendsen CN, Mucke L, Johnson MH and Sofroniew MV (1999). "Leukocyte infiltration, neuronal degeneration, and neurite outgrowth after ablation of scar-forming, reactive astrocytes in adult transgenic mice." *Neuron* **23**(2): 297-308.

Butcher EC (1991). "Leukocyte-endothelial cell recognition: three (or more) steps to specificity and diversity." *Cell* **67**(6): 1033-1036.

Cabarrocas J, Bauer J, Piaggio E, Liblau R and Lassmann H (2003). "Effective and selective immune surveillance of the brain by MHC class I-restricted cytotoxic T lymphocytes." *Eur J Immunol* **33**(5): 1174-1182.

Cahoy JD, Emery B, Kaushal A, Foo LC, Zamanian JL, Christopherson KS, Xing Y, Lubischer JL, Krieg PA, Krupenko SA, Thompson WJ and Barres BA (2008). "A transcriptome database for astrocytes, neurons, and oligodendrocytes: a new resource for understanding brain development and function." *J Neurosci* **28**(1): 264-278.

Camp LA and Hofmann SL (1993). "Purification and properties of a palmitoyl-protein thioesterase that cleaves palmitate from H-Ras." *J Biol Chem* **268**(30): 22566-22574.

Camp LA, Verkruyse LA, Afendis SJ, Slaughter CA and Hofmann SL (1994). "Molecular cloning and expression of palmitoyl-protein thioesterase." *J Biol Chem* **269**(37): 23212-23219.

Campbell JJ, Hedrick J, Zlotnik A, Siani MA, Thompson DA and Butcher EC (1998). "Chemokines and the arrest of lymphocytes rolling under flow conditions." *Science* **279**(5349): 381-384.

Campbell JJ, Qin S, Bacon KB, Mackay CR and Butcher EC (1996). "Biology of chemokine and classical chemoattractant receptors: differential requirements for adhesion-triggering versus chemotactic responses in lymphoid cells." *J Cell Biol* **134**(1): 255-266.

Campbell SJ, Anthony DC, Oakley F, Carlsen H, Elsharkawy AM, Blomhoff R and Mann DA (2008). "Hepatic nuclear factor kappa B regulates neutrophil recruitment to the injured brain." *Journal of Neuropathology and Experimental Neurology* **67**(3): 223-230.

Cao Y, Espinola JA, Fossale E, Massey AC, Cuervo AM, MacDonald ME and Cotman SL (2006). "Autophagy is disrupted in a knock-in mouse model of juvenile neuronal ceroid lipofuscinosis." *Journal of Biological Chemistry* **281**(29): 20483-20493.

Carare RO, Bernardes-Silva M, Newman TA, Page AM, Nicoll JAR, Perry VH and Weller RO (2008). "Solutes, but not cells, drain from the brain parenchyma along basement membranes of capillaries and arteries: significance for cerebral amyloid angiopathy and neuroimmunology." *Neuropathology and Applied Neurobiology* **34**(2): 131-144.

Carlos TM and Harlan JM (1994). "Leukocyte-endothelial adhesion molecules." *Blood* **84**(7): 2068-2101.

Carpentier JL, Fehlmann M, Van Obberghen E, Gorden P and Orci L (1985). "Insulin receptor internalization and recycling: mechanism and significance." *Biochimie* **67**(10-11): 1143-1145.

Carramolino L, Zaballos A, Kremer L, Villares R, Martin P, Ardavin C, Martinez AC and Marquez G (2001). "Expression of CCR9 beta-chemokine receptor is modulated in thymocyte differentiation and is selectively maintained in CD8(+) T cells from secondary lymphoid organs." *Blood* **97**(4): 850-857.

Carrasco YR and Batista FD (2007). "B cells acquire particulate antigen in a macrophage-rich area at the boundary between the follicle and the subcapsular sinus of the lymph node." *Immunity* **27**(1): 160-171.

Carrithers MD, Visintin I, Kang SJ and Janeway CA (2000). "Differential adhesion molecule requirements for immune surveillance and inflammatory recruitment." *Brain* **123**: 1092-1101.

Carrithers MD, Visintin I, Viret C and Janeway Jr CA (2002). "Role of genetic background in P selectin-dependent immune surveillance of the central nervous system." *Journal of Neuroimmunology* **129**(1-2): 51-57.

Carson MJ, Doose JM, Melchior B, Schmid CD and Ploix CC (2006a). "CNS immune privilege: hiding in plain sight." *Immunol Rev* **213**: 48-65.

Carson MJ, Reilly CR, Sutcliffe JG and Lo D (1999). "Disproportionate recruitment of CD8+ T cells into the central nervous system by professional antigen-presenting cells." *Am J Pathol* **154**(2): 481-494.

Carson MJ, Thrash JC and Walter B (2006b). "The cellular response in neuroinflammation: The role of leukocytes, microglia and astrocytes in neuronal death and survival." *Clin Neurosci Res* **6**(5): 237-245.

Castaneda JA, Lim MJ, Cooper JD and Pearce DA (2008). "Immune system irregularities in lysosomal storage disorders." *Acta Neuropathologica* **115**(2): 159-174.

Castaneda JA and Pearce DA (2008). "Identification of alpha-fetoprotein as an autoantigen in juvenile Batten disease." *Neurobiol Dis* **29**(1): 92-102.

Castellino F and Germain RN (2006). "Cooperation between CD4+ and CD8+ T cells: when, where, and how." *Annu Rev Immunol* **24**: 519-540.

Cavalieri B (1665). Geometrica indivisibilibus continuorum *Bononiae* Typis Clementis Ferronij (reprinted 1966 as Geometria Degli Indivisibili. Torino: Unione Tipografico-Editrice Torinese).

Chang JW, Choi H, Cotman SL and Jung YK (2011). "Lithium rescues the impaired autophagy process in CbCln3(Deltaex7/8/Deltaex7/8) cerebellar cells and reduces neuronal vulnerability to cell death via IMPase inhibition." *J Neurochem* **116**(4): 659-668.

Chang JW, Choi H, Kim HJ, Jo DG, Jeon YJ, Noh JY, Park WJ and Jung YK (2007). "Neuronal vulnerability of CLN3 deletion to calcium-induced cytotoxicity is mediated by calsenilin." *Human Molecular Genetics* **16**(3): 317-326.

Chang RC, Hudson P, Wilson B, Haddon L and Hong JS (2000). "Influence of neurons on lipopolysaccharide-stimulated production of nitric oxide and tumor necrosis factor-alpha by cultured glia." *Brain Res* **853**(2): 236-244.

Chang TY, Chang CC, Ohgami N and Yamauchi Y (2006). "Cholesterol sensing, trafficking, and esterification." *Annu Rev Cell Dev Biol* **22**: 129-157.

Charles AC, Merrill JE, Dirksen ER and Sanderson MJ (1991). "Intercellular signaling in glial cells: calcium waves and oscillations in response to mechanical stimulation and glutamate." *Neuron* **6**(6): 983-992.

Chattopadhyay S, Ito M, Cooper JD, Brooks AI, Curran TM, Powers JM and Pearce DA (2002a). "An autoantibody inhibitory to glutamic acid decarboxylase in the neurodegenerative disorder Batten disease." *Human Molecular Genetics* **11**(12): 1421-1431.

Chattopadhyay S, Kriscenski-Perry E, Wenger DA and Pearce DA (2002b). "An autoantibody to GAD65 in sera of patients with juvenile neuronal ceroid lipofuscinoses." *Neurology* **59**(11): 1816-1817.

Chen YH, Chang M and Davidson BL (2009). "Molecular signatures of disease brain endothelia provide new sites for CNS-directed enzyme therapy." *Nat Med* **15**(10): 1215-1218.

Cherin P, Herson S, Crevon MC, Hauw JJ, Cervera P, Galanaud P and Emilie D (1996). "Mechanisms of lysis by activated cytotoxic cells expressing perforin and granzyme-B genes and the protein TIA-1 in muscle biopsies of myositis." *Journal of Rheumatology* **23**(7): 1135-1142.

Chinnery HR, Ruitenberg MJ and McMenamin PG (2010). "Novel Characterization of Monocyte-Derived Cell Populations in the Meninges and Choroid Plexus and Their Rates of Replenishment in Bone Marrow Chimeric Mice." *Journal of Neuropathology and Experimental Neurology* **69**(9): 896-909.

Chiu IM, Chen A, Zheng Y, Kosaras B, Tsiftsoglou SA, Vartanian TK, Brown RH, Jr. and Carroll MC (2008). "T lymphocytes potentiate endogenous neuroprotective inflammation in a mouse model of ALS." *Proc Natl Acad Sci U S A* **105**(46): 17913-17918.

Cho S and Dawson G (2000). "Palmitoyl protein thioesterase 1 protects against apoptosis mediated by Ras-Akt-caspase pathway in neuroblastoma cells." *J Neurochem* **74**(4): 1478-1488.

Choi C and Benveniste EN (2004). "Fas ligand/Fas system in the brain: regulator of immune and apoptotic responses." *Brain Res Brain Res Rev* **44**(1): 65-81.

Choi HK, Ryu HJ, Kim JE, Jo SM, Choi HC, Song HK and Kang TC (2012). "The roles of P2X7 receptor in regional-specific microglial responses in the rat brain following status epilepticus." *Neurol Sci* **33**(3): 515-525.

Christopherson KS, Ullian EM, Stokes CC, Mullowney CE, Hell JW, Agah A, Lawler J, Mosher DF, Bornstein P and Barres BA (2005). "Thrombospondins are astrocyte-secreted proteins that promote CNS synaptogenesis." *Cell* **120**(3): 421-433.

Cialone J, Augustine EF, Newhouse N, Adams H, Vierhile A, Marshall FJ, de Blieck EA, Kwon J, Rothberg PG and Mink JW (2011). "Parent-reported benefits of flupirtine in juvenile neuronal ceroid lipofuscinosis (Batten disease; CLN3) are not supported by quantitative data." *J Inherit Metab Dis* **34**(5): 1075-1081.

Ciubotariu R, Colovai AI, Pennesi G, Liu Z, Smith D, Berlocco P, Cortesini R and Suciu-Foca N (1998). "Specific Suppression of Human CD4+ Th Cell Responses to Pig MHC Antigens by CD8+CD28- Regulatory T Cells." *The Journal of Immunology* **161**(10): 5193-5202.

Codlin S and Mole SE (2009). "S. pombe btn1, the orthologue of the Batten disease gene CLN3, is required for vacuole protein sorting of Cpy1p and Golgi exit of Vps10p." *J Cell Sci* **122**(Pt 8): 1163-1173.

Cohen JJ, Duke RC, Fadok VA and Sellins KS (1992). "Apoptosis and programmed cell-death in immunity." *Annual Review of Immunology* **10**: 267-293.

Collison LW, Workman CJ, Kuo TT, Boyd K, Wang Y, Vignali KM, Cross R, Sehy D, Blumberg RS and Vignali DA (2007). "The inhibitory cytokine IL-35 contributes to regulatory T-cell function." *Nature* **450**(7169): 566-569.

Colton CA and Wilcock DM (2010). "Assessing activation states in microglia." *CNS Neurol Disord Drug Targets* **9**(2): 174-191.

Comim CM, Vilela MC, Constantino LS, Petronilho F, Vuolo F, Lacerda-Queiroz N, Rodrigues DH, da Rocha JL, Teixeira AL, Quevedo J and Dal-Pizzol F (2011). "Traffic of leukocytes and cytokine up-regulation in the central nervous system in sepsis." *Intensive Care Med* **37**(4): 711-718.

Connolly JM, Hansen TH, Ingold AL and Potter TA (1990). "Recognition by CD8 on Cytotoxic T Lymphocytes is Ablated by Several Substitutions in the Class I α 3 Domain: CD8 and the T-Cell Receptor Recognize the Same Class I Molecule." *Proceedings of the National Academy of Sciences of the United States of America* **87**(6): 2137-2141.

Constantin G (2008). "Chemokine signaling and integrin activation in lymphocyte migration into the inflamed brain." *J Neuroimmunol* **198**(1-2): 20-26.

Cool DE, Tonks NK, Zander N, Lorenzen J, Andreasson P, Margolis RL, Krebs EG and Fischer EH (1990). Protein tyrosine phosphatases in cell cycle and signal transduction. Dumont, J. E., J. Nunez and R. J. B. King**:** 37-44.

Cooper JD (1990). Neuronal ceroid lipofuscinosis. Encyclopedia of Movement Disorders. K. Kompoliti and L. Verhagen Metman. Oxford, Academic Press. **2:** 291-295.

Cooper JD (2003). "Progress towards understanding the neurobiology of Batten disease or neuronal ceroid lipofuscinosis." *Curr Opin Neurol* **16**(2): 121-128.

Cooper JD (2010). "The neuronal ceroid lipofuscinoses: the same, but different?" *Biochem Soc Trans* **38**: 1448-1452.

Cooper JD, Messer A, Feng AK, Chua-Couzens J and Mobley WC (1999). "Apparent loss and hypertrophy of interneurons in a mouse model of neuronal ceroid lipofuscinosis: evidence for partial response to insulin-like growth factor-1 treatment." *J Neurosci* **19**(7): 2556-2567.

Cooper JD, Russell C and Mitchison HM (2006). "Progress towards understanding disease mechanisms in small vertebrate models of neuronal ceroid lipofuscinosis." *Biochimica et Biophysica Acta (BBA) - Molecular Basis of Disease* **1762**(10): 873-889.

Cope A, Le Friec G, Cardone J and Kemper C (2011). "The Th1 life cycle: molecular control of IFN-gamma to IL-10 switching." *Trends in Immunology* **32**(6): 278-286.

Cornell-Bell AH, Finkbeiner SM, Cooper MS and Smith SJ (1990). "Glutamate induces calcium waves in cultured astrocytes: long-range glial signaling." *Science* **247**(4941): 470-473.

Cotman SL and Staropoli JF (2012). "The juvenile Batten disease protein, CLN3, and its role in regulating anterograde and retrograde post-Golgi trafficking." *Clinical Lipidology* **7**(1): 79-91.

Cotman SL, Vrbanac V, Lebel LA, Lee RL, Johnson KA, Donahue LR, Teed AM, Antonellis K, Bronson RT, Lerner TJ and MacDonald ME (2002). "Cln3(Deltaex7/8) knock-in mice with the common JNCL mutation exhibit progressive neurologic disease that begins before birth." *Hum Mol Genet* **11**(22): 2709-2721.

Coutinho MF, Prata MJ and Alves S (2012). "Mannose-6-phosphate pathway: A review on its role in lysosomal function and dysfunction." *Molecular Genetics and Metabolism* **105**(4): 542-550.

Cowan CM and Roskams AJ (2002). "Apoptosis in the mature and developing olfactory neuroepithelium." *Microscopy Research and Technique* **58**(3): 204-215.

Crawley JN (2007). What's Wrong With My Mouse: Behavioral Phenotyping of Transgenic and Knockout Mice. *Hoboken, New Jersey*, John Wiley & Sons Inc.

Crivellato E, Vacca A and Ribatti D (2004). "Setting the stage: an anatomist's view of the immune system." *Trends Immunol* **25**(4): 210-217.

Crocker PR (2002). "Siglecs: sialic-acid-binding immunoglobulin-like lectins in cell-cell interactions and signalling." *Curr Opin Struct Biol* **12**(5): 609-615.

Crocker PR, Clark EA, Filbin M, Gordon S, Jones Y, Kehrl JH, Kelm S, Le Douarin N, Powell L, Roder J, Schnaar RL, Sgroi DC, Stamenkovic K, Schauer R, Schachner M, van den Berg TK, van der Merwe PA, Watt SM and Varki A (1998). "Siglecs: a family of sialic-acid binding lectins." *Glycobiology* **8**(2): v.

Crocker PR, Freeman S, Gordon S and Kelm S (1995). "Sialoadhesin binds preferentially to cells of the granulocytic lineage." *J Clin Invest* **95**(2): 635-643.

Crocker PR and Gordon S (1985). "Isolation and characterization of resident stromal macrophages and hematopoietic cell clusters from mouse bone marrow." *J Exp Med* **162**(3): 993-1014.

Crocker PR and Gordon S (1986). "Properties and distribution of a lectin-like hemagglutinin differentially expressed by murine stromal tissue macrophages." *J Exp Med* **164**(6): 1862-1875.

Crocker PR and Gordon S (1989). "Mouse macrophage hemagglutinin (sheep erythrocyte receptor) with specificity for sialylated glycoconjugates characterized by a monoclonal antibody." *J Exp Med* **169**(4): 1333-1346.

Crocker PR, Kelm S, Dubois C, Martin B, McWilliam AS, Shotton DM, Paulson JC and Gordon S (1991). "Purification and properties of sialoadhesin, a sialic acid-binding receptor of murine tissue macrophages." *EMBO J* **10**(7): 1661-1669.

Crocker PR, Mucklow S, Bouckson V, McWilliam A, Willis AC, Gordon S, Milon G, Kelm S and Bradfield P (1994). "Sialoadhesin, a macrophage sialic acid binding receptor for haemopoietic cells with 17 immunoglobulin-like domains." *EMBO J* **13**(19): 4490-4503.

Crocker PR, Paulson JC and Varki A (2007). "Siglecs and their roles in the immune system." *Nat Rev Immunol* **7**(4): 255-266.

Crocker PR and Redelinghuys P (2008). "Siglecs as positive and negative regulators of the immune system." *Biochem Soc Trans* **36**(Pt 6): 1467-1471.

Crocker PR and Varki A (2001). "Siglecs, sialic acids and innate immunity." *Trends in Immunology* **22**(6): 337-342.

Croisier E and Graeber MB (2006). "Glial degeneration and reactive gliosis in alpha-synucleinopathies: the emerging concept of primary gliodegeneration." *Acta Neuropathol* **112**(5): 517-530.

Cruz-Orive LM (1999). "Precision of Cavalieri sections and slices with local errors." *Journal of Microscopy* **193**(3): 182-198.

Cserr HF, Harlingberg CJ and Knopf PM (1992). "Drainage of brain extracellular fluid into blood and deep cervical lymph and its immunological significance." *Brain Pathology* **2**(4): 269-276.

Czirr E and Wyss-Coray T (2012). "The immunology of neurodegeneration." *Journal of Clinical Investigation* **122**(4): 1156-1163.

D'Andrea MR (2003). "Evidence linking neuronal cell death to autoimmunity in Alzheimer's disease." *Brain Res* **982**(1): 19-30.

Daginakatte GC, Gadzinski A, Emnett RJ, Stark JL, Gonzales ER, Yan P, Lee JM, Cross AH and Gutmann DH (2008). "Expression profiling identifies a molecular signature of reactive astrocytes stimulated by cyclic AMP or proinflammatory cytokines." *Exp Neurol* **210**(1): 261-267.

Dahlen SE, Bjork J, Hedqvist P, Arfors KE, Hammarstrom S, Lindgren JA and Samuelsson B (1981). "Leukotrienes promote plasma leakage and leukocyte adhesion in post-capillary venules - in vivo effects with relevance to the acute inflammtory response." *Proceedings of the National Academy of Sciences of the United States of America-Biological Sciences* **78**(6): 3887-3891.

Dai J, Vrensen GF and Schlingemann RO (2002). "Blood-brain barrier integrity is unaltered in human brain cortex with diabetes mellitus." *Brain Res* **954**(2): 311-316.

Daly TM, Lorenz RG and Sands MS (2000). "Abnormal immune function in vivo in a murine model of lysosomal storage disease." *Pediatr Res* **47**(6): 757-762.

Das AK, Becerra CH, Yi W, Lu JY, Siakotos AN, Wisniewski KE and Hofmann SL (1998). "Molecular genetics of palmitoyl-protein thioesterase deficiency in the U.S." *J Clin Invest* **102**(2): 361-370.

Das AM, von Harlem R, Feist M, Lucke T and Kohlschutter A (2001). "Altered levels of high-energy phosphate compounds in fibroblasts from different forms of neuronal ceroid lipofuscinoses: further evidence for mitochondrial involvement." *Eur J Paediatr Neurol* **5 Suppl A**: 143-146.

Davidson B (2012). AAV-TPP1 Transduction of Brain Ependyma in TPP1-null Dogs Results in Widespread CNS Distribution of TPP1 Enzyme and improves NCL Disease Phenotypes. 13th International Conference on Neuronal Ceroid Lipofuscinoses (Batten Disease) (NCL 2012). *Rolay Holloway College, London, UK*, Oral presentation 47**:** Oral presentation 47.

Davis MM, Boniface JJ, Reich Z, Lyons D, Hampl J, Arden B and Chien Y (1998). "Ligand recognition by alpha beta T cell receptors." *Annu Rev Immunol* **16**: 523-544.

Dawodu S and Thom M (2005). "Quantitative neuropathology of the entorhinal cortex region in patients with hippocampal sclerosis and temporal lobe epilepsy." *Epilepsia* **46**(1): 23-30.

Dawson G, Schroeder C and Dawson PE (2010). "Palmitoyl:protein thioesterase (PPT1) inhibitors can act as pharmacological chaperones in infantile Batten disease." *Biochem Biophys Res Commun* **395**(1): 66-69.

De Baere MI, Van Gorp H, Nauwynck HJ and Delputte PL (2011). "Antibody binding to porcine sialoadhesin reduces phagocytic capacity without affecting other macrophage effector functions." *Cell Immunol* **271**(2): 462-473.

De Duve C (1963). "The lysosome." *Scientific American* **208**: 64-72.

De Duve C, Pressman BC, Gianetto R, Wattiaux R and Appelmans F (1955). "Tissue fractionation studies. 6. Intracellular distribution patterns of enzymes in rat-liver tissue." *Biochem J* **60**(4): 604-617.

de la Hoz CL, Oliveira AL, Queiroz Lde S and Langone F (2003). "Wallerian degeneration in C57BL/6J and A/J mice: differences in time course of neurofilament and myelin breakdown, macrophage recruitment and iNOS expression." *J Anat* **203**(6): 567-578.

de Voer G, van der Bent P, Rodrigues AJ, van Ommen GJ, Peters DJ and Taschner PE (2005). "Deletion of the Caenorhabditis elegans homologues of the CLN3 gene, involved in human juvenile neuronal ceroid lipofuscinosis, causes a mild progeric phenotype." *J Inherit Metab Dis* **28**(6): 1065-1080.

Deckner ML (2001). "The olfactory nerve layer is exposed to blood-borne molecules." *Society for Neuroscience Abstracts* **27**(2): 1637.

Deganuto M, Pittis MG, Pines A, Dominissini S, Kelley MR, Garcia R, Quadrifoglio F, Bembi B and Tell G (2007). "Altered intracellular redox status in Gaucher disease fibroblasts and impairment of adaptive response against oxidative stress." *J Cell Physiol* **212**(1): 223-235.

DeLegge MH and Smoke A (2008). "Neurodegeneration and inflammation." *Nutrition in Clinical Practice* **23**(1): 35-41.

Delgado S and Sheremata WA (2006). "The role of CD4+ T-cells in the development of MS." *Neurol Res* **28**(3): 245-249.

Dell'Angelica EC and Payne GS (2001). "Intracellular cycling of lysosomal enzyme receptors: cytoplasmic tails' tales." *Cell* **106**(4): 395-398.

Delputte PL, Van Breedam W, Barbe F, Van Reeth K and Nauwynck HJ (2007). "IFN-alpha treatment enhances porcine Arterivirus infection of monocytes via upregulation of the porcine Arterivirus receptor sialoadhesin." *J Interferon Cytokine Res* **27**(9): 757-766.

Delputte PL, Van Gorp H, Favoreel HW, Hoebeke I, Delrue I, Dewerchin H, Verdonck F, Verhasselt B, Cox E and Nauwynck HJ (2011). "Porcine sialoadhesin (CD169/Siglec-1) is an endocytic receptor that allows targeted delivery of toxins and antigens to macrophages." *Plos One* **6**(2): e16827.

Denhertog J, Pals C, Peppelenbosch MP, Tertoolen LGJ, Delaat SW and Kruijer W (1993). "Receptor protein-tyrosine phosphatase-alpha activates PP60(C-SRC) and is involved in neuronal differentiation." *Embo Journal* **12**(10): 3789-3798.

Denu JM and Dixon JE (1998). "Protein tyrosine phosphatases: mechanisms of catalysis and regulation." *Current Opinion in Chemical Biology* **2**(5): 633-641.

Derfuss T, Parikh K, Velhin S, Braun M, Mathey E, Krumbholz M, Kumpfel T, Moldenhauer A, Rader C, Sonderegger P, Pollmann W, Tiefenthaller C, Bauer J, Lassmann H, Wekerle H, Karagogeos D, Hohlfeld R, Linington C and Meinl E (2009). "Contactin-2/TAG-1-directed autoimmunity is identified in multiple sclerosis patients and mediates gray matter pathology in animals." *Proc Natl Acad Sci U S A* **106**(20): 8302-8307.

Desnick RJ, Astrin KH and Bishop DF (1989). "Fabry disease: molecular genetics of the inherited nephropathy." *Adv Nephrol Necker Hosp* **18**: 113-127.

Desnick RJ, Thorpe SR and Fiddler MB (1976). "Toward enzyme therapy for lysosomal storage diseases." *Physiol Rev* **56**(1): 57-99.

Dhar S, Bitting RL, Rylova SN, Jansen PJ, Lockhart E, Koeberl DD, Amalfitano A and Boustany RM (2002). "Flupirtine blocks apoptosis in batten patient lymphoblasts and in human postmitotic CLN3- and CLN2-deficient neurons." *Ann Neurol* **51**(4): 448-466.

Di Filippo M, Chiasserini D, Tozzi A, Picconi B and Calabresi P (2010). "Mitochondria and the link between neuroinflammation and neurodegeneration." *J Alzheimers Dis* **20 Suppl 2**: S369-379.

Dickson DW, Mattiace LA, Kure K, Hutchins K, Lyman WD and Brosnan CF (1991). "Microglia in human disease, with an emphasis on acquired immune deficiency syndrome." *Lab Invest* **64**(2): 135-156.

Dihanich S (2010). Endogenous Brain Repair Mechanisms in Batten Disease. PhD thesis, King's College London.

Dijkstra CD, Dopp EA, Joling P and Kraal G (1985). "The heterogeneity of mononuclear phagocytes in lymphoid organs: distinct macrophage subpopulations in the rat recognized by monoclonal antibodies ED1, ED2 and ED3." *Immunology* **54**(3): 589-599.

Dimayuga PC, Chyu KY, Kirzner J, Yano J, Zhao XN, Zhou JC, Shah PK and Cercek B (2011). "Enhanced Neointima Formation Following Arterial Injury in Immune Deficient Rag-1-/- Mice Is Attenuated by Adoptive Transfer of CD8(+) T cells." *Plos One* **6**(5).

Dittel BN (2008). "CD4 T cells: Balancing the coming and going of autoimmune-mediated inflammation in the CNS." *Brain Behav Immun* **22**(4): 421-430.

Doherty GJ and McMahon HT (2009). Mechanisms of Endocytosis. Annual Review of Biochemistry. Palo Alto, Annual Reviews. **78:** 857-902.

Dolman CL, McLeod PM and Chang EC (1980). "Lymphocytes and urine in ceroid lipofuscinosis." *Arch Pathol Lab Med* **104**(9): 487-490.

Dong C and Flavell RA (2001). "Th1 and Th2 cells." *Current Opinion in Hematology* **8**(1): 47-51.

Dong Y and Benveniste EN (2001). "Immune function of astrocytes." *Glia* **36**(2): 180-190.

Dorf ME, Berman MA, Tanabe S, Heesen M and Luo Y (2000). "Astrocytes express functional chemokine receptors." *J Neuroimmunol* **111**(1-2): 109-121.

Dosquet C, Weill D and Wautier JL (1992). "Molecular mechanism of blood monocyte adhesion to vascular endothelial cells." *Nouv Rev Fr Hematol* **34 Suppl**: S55-59.

Dringen R (2000). "Metabolism and functions of glutathione in brain." *Progress in Neurobiology* **62**(6): 649-671.

Drogemuller K, Helmuth U, Brunn A, Sakowicz-Burkiewicz M, Gutmann DH, Mueller W, Deckert M and Schluter D (2008). "Astrocyte gp130 expression is critical for the control of Toxoplasma encephalitis." *J Immunol* **181**(4): 2683-2693.

Drozina G, Kohoutek J, Jabrane-Ferrat N and Peterlin BM (2005). "Expression of MHC II genes." *Curr Top Microbiol Immunol* **290**: 147-170.

Ducreux J, Tyteca D, Ucakar B, Medts T, Crocker PR, Courtoy PJ and Vanbever R (2009). "PEGylation of anti-sialoadhesin monoclonal antibodies enhances their inhibitory potencies without impairing endocytosis in mouse peritoneal macrophages." *Bioconjug Chem* **20**(2): 295-303.

Dunina-Barkovskaya AY (2004). "Phagocytosis - Three in one: Endocytosis, exocytosis, adhesion." *Biologicheskie Membrany* **21**(4): 243-270.

Dustin ML (2008). "T-cell activation through immunological synapses and kinapses." *Immunological Reviews* **221**: 77-89.

Dutta R, McDonough J, Yin X, Peterson J, Chang A, Torres T, Gudz T, Macklin WB, Lewis DA, Fox RJ, Rudick R, Mirnics K and Trapp BD (2006). "Mitochondrial dysfunction as a cause of axonal degeneration in multiple sclerosis patients." *Ann Neurol* **59**(3): 478-489.

Dutta R and Trapp BD (2007). "Pathogenesis of axonal and neuronal damage in multiple sclerosis." *Neurology* **68**(22 Suppl 3): S22-31; discussion S43-54.

Eddleston M and Mucke L (1993). "Molecular profile of reactive astrocytes--implications for their role in neurologic disease." *Neuroscience* **54**(1): 15-36.

Ekdahl CT, Kokaia Z and Lindvall O (2009). "Brain inflammation and adult neurogenesis: The dual role of microglia." *Neuroscience* **158**(3): 1021-1029.

Eliason SL, Stein CS, Mao Q, Tecedor L, Ding SL, Gaines DM and Davidson BL (2007). "A knock-in reporter model of Batten disease." *J Neurosci* **27**(37): 9826-9834.

Elkabes S, DiCicco-Bloom EM and Black IB (1996). "Brain microglia/macrophages express neurotrophins that selectively regulate microglial proliferation and function." *J Neurosci* **16**(8): 2508-2521.

Elward K and Gasque P (2003). ""Eat me" and "don't eat me" signals govern the innate immune response and tissue repair in the CNS: emphasis on the critical role of the complement system." *Mol Immunol* **40**(2-4): 85-94.

Eng CM, Guffon N, Wilcox WR, Germain DP, Lee P, Waldek S, Caplan L, Linthorst GE, Desnick RJ and International Collaborative Fabry Disease Study G (2001). "Safety and efficacy of recombinant human alpha-galactosidase A--replacement therapy in Fabry's disease." *N Engl J Med* **345**(1): 9-16.

Eng LF, Vanderhaeghen JJ, Bignami A and Gerstl B (1971). "An acidic protein isolated from fibrous astrocytes." *Brain Res* **28**(2): 351-354.

Engelhardt B (2008). "The blood-central nervous system barriers actively control immune cell entry into the central nervous system." *Current Pharmaceutical Design* **14**(16): 1555-1565.

Engelhardt B and Ransohoff RM (2005). "The ins and outs of T-lymphocyte trafficking to the CNS: anatomical sites and molecular mechanisms." *Trends in Immunology* **26**(9): 485-495.

Engelhardt B and Wolburg H (2004). "Mini-review: Transendothelial migration of leukocytes: through the front door or around the side of the house?" *European Journal of Immunology* **34**(11): 2955-2963.

Engleman EG, Benike CJ, Grumet FC and Evans RL (1981). "Activation of human lymphocyte-T subsets - helper and suppressor-cytotoxic T-cells recognize and respond to distinct histocompatibilty antigens." *Journal of Immunology* **127**(5): 2124-2129.

Fabbri M, Bianchi E, Fumagalli L and Pardi R (1999). "Regulation of lymphocyte traffic by adhesion molecules." *Inflammation Research* **48**(5): 239-246.

Fan JQ, Ishii S, Asano N and Suzuki Y (1999). "Accelerated transport and maturation of lysosomal alpha-galactosidase A in Fabry lymphoblasts by an enzyme inhibitor." *Nat Med* **5**(1): 112-115.

Fanslow WC, Anderson DM, Grabstein KH, Clark EA, Cosman D and Armitage RJ (1992). "Soluble forms of CD40 inhibit biologic responses of human B-cells." *Journal of Immunology* **149**(2): 655-660.

Farina C, Aloisi F and Meinl E (2007). "Astrocytes are active players in cerebral innate immunity." *Trends Immunol* **28**(3): 138-145.

Farina C, Krumbholz M, Giese T, Hartmann G, Aloisi F and Meinl E (2005). "Preferential expression and function of Toll-like receptor 3 in human astrocytes." *J Neuroimmunol* **159**(1-2): 12-19.

Faulkner JR, Herrmann JE, Woo MJ, Tansey KE, Doan NB and Sofroniew MV (2004). "Reactive astrocytes protect tissue and preserve function after spinal cord injury." *J Neurosci* **24**(9): 2143-2155.

Felger JC, Abe T, Kaunzner UW, Gottfried-Blackmore A, Gal-Toth J, McEwen BS, Iadecola C and Bulloch K (2010). "Brain dendritic cells in ischemic stroke: Time course, activation state, and origin." *Brain, Behavior, and Immunity* **24**(5): 724-737.

Fendrick SE, Xue QS and Streit WJ (2007). "Formation of multinucleated giant cells and microglial degeneration in rats expressing a mutant Cu/Zn superoxide dismutase gene." *J Neuroinflammation* **4**: 9.

Feng D, Nagy JA, Pyne K, Dvorak HF and Dvorak AM (1998). "Neutrophils emigrate from venules by a transendothelial cell pathway in response to FMLP." *J Exp Med* **187**(6): 903-915.

Ferger B, Leng A, Mura A, Hengerer B and Feldon J (2004). "Genetic ablation of tumor necrosis factor-alpha (TNF-alpha) and pharmacological inhibition of TNF-synthesis attenuates MPTP toxicity in mouse striatum." *J Neurochem* **89**(4): 822-833.

Fernandez-Fernandez S, Almeida A and Bolanos JP (2012). "Antioxidant and bioenergetic coupling between neurons and astrocytes." *Biochem J* **443**(1): 3-11.

Filaci G, Fravega M, Negrini S, Procopio F, Fenoglio D, Rizzi M, Brenci S, Contini P, Olive D, Ghio M, Setti M, Accolla RS, Puppo F and Indiveri F (2004). "Nonantigen specific CD8(+) T suppressor lymphocytes originate from CD8(+)CD28(-) T cells and inhibit both T-cell proliferation and CTL function." *Human Immunology* **65**(2): 142-156.

Filimonenko M, Stuffers S, Raiborg C, Yamamoto A, Malerod L, Fisher EM, Isaacs A, Brech A, Stenmark H and Simonsen A (2007). "Functional multivesicular bodies are required for autophagic clearance of protein aggregates associated with neurodegenerative disease." *J Cell Biol* **179**(3): 485-500.

Finn R, Kovacs AD and Pearce DA (2010). "Altered Sensitivity to Excitotoxic Cell Death and Glutamate Receptor Expression Between Two Commonly Studied Mouse Strains." *Journal of Neuroscience Research* **88**(12): 2648-2660.

Finn R, Kovacs AD and Pearce DA (2011). "Altered sensitivity of cerebellar granule cells to glutamate receptor overactivation in the Cln3 Delta ex7/8-knock-in mouse model of juvenile neuronal ceroid lipofuscinosis." *Neurochemistry International* **58**(6): 648-655.

Finn R, Kovacs AD and Pearce DA (2012). "Altered Glutamate Receptor Function in the Cerebellum of the Ppt1(-/-) Mouse, a Murine Model of Infantile Neuronal Ceroid Lipofuscinosis." *Journal of Neuroscience Research* **90**(2): 367-375.

Finsen B and Owens T (2011). "Innate immune responses in central nervous system inflammation." *FEBS Lett* **585**(23): 3806-3812.

Fischer H-G and Reichmann G (2001). "Brain Dendritic Cells and Macrophages/Microglia in Central Nervous System Inflammation." *The Journal of Immunology* **166**(4): 2717-2726.

Flannagan RS, Jaumouille V and Grinstein S (2012). The Cell Biology of Phagocytosis. Annual Review of Pathology: Mechanisms of Disease, Vol 7. A. K. Abbas, S. J. Galli and P. M. Howley. Palo Alto, Annual Reviews. **7:** 61-98.

Flugel A, Willem M, Berkowicz T and Wekerle H (1999). "Gene transfer into CD4+ T lymphocytes: green fluorescent protein-engineered, encephalitogenic T cells illuminate brain autoimmune responses." *Nat Med* **5**(7): 843-847.

Fossale E, Wolf P, Espinola JA, Lubicz-Nawrocka T, Teed AM, Gao H, Rigamonti D, Cattaneo E, MacDonald ME and Cotman SL (2004). "Membrane trafficking and mitochondrial abnormalities precede subunit c deposition in a cerebellar cell model of juvenile neuronal ceroid lipofuscinosis." *BMC Neurosci* **5**: 57.

Fraldi A, Annunziata F, Lombardi A, Kaiser HJ, Medina DL, Spampanato C, Fedele AO, Polishchuk R, Sorrentino NC, Simons K and Ballabio A (2010). "Lysosomal fusion and SNARE function are impaired by cholesterol accumulation in lysosomal storage disorders." *Embo Journal* **29**(21): 3607-3620.

Frank-Cannon TC, Alto LT, McAlpine FE and Tansey MG (2009). "Does neuroinflammation fan the flame in neurodegenerative diseases?" *Molecular Neurodegeneration* **4**.

Fratantoni JC, Hall CW and Neufeld EF (1968). "Hurler and Hunter syndromes: mutual correction of the defect in cultured fibroblasts." *Science* **162**(3853): 570-572.

Friese MA and Fugger L (2009). "Pathogenic CD8(+) T cells in multiple sclerosis." *Ann Neurol* **66**(2): 132-141.

Futerman AH and van Meer G (2004). "The cell biology of lysosomal storage disorders." *Nat Rev Mol Cell Biol* **5**(7): 554-565.

Gadola SD, Silk JD, Jeans A, Illarionov PA, Salio M, Besra GS, Dwek R, Butters TD, Platt FM and Cerundolo V (2006). "Impaired selection of invariant natural killer T cells in diverse mouse models of glycosphingolipid lysosomal storage diseases." *J Exp Med* **203**(10): 2293-2303.

Galea I, Bechmann I and Perry VH (2007a). "What is immune privilege (not)?" *Trends in Immunology* **28**(1): 12-18.

Galea I, Bernardes-Silva M, Forse PA, van Rooijen N, Liblau RS and Perry VH (2007b). "An antigen-specific pathway for CD8 T cells across the blood-brain barrier." *Journal of Experimental Medicine* **204**(9): 2023-2030.

Galvin N, Vogler C, Levy B, Kovacs A, Griffey M and Sands MS (2008). "A murine model of infantile neuronal ceroid lipofuscinosis-ultrastructural evaluation of storage in the central nervous system and viscera." *Pediatr Dev Pathol* **11**(3): 185-192.

Ganong WF (2000). "Circumventricular organs: Definition and role in the regulation of endocrine and autonomic function." *Clinical and Experimental Pharmacology and Physiology* **27**(5-6): 422-427.

Gao HM and Hong JS (2008). "Why neurodegenerative diseases are progressive: uncontrolled inflammation drives disease progression." *Trends Immunol* **29**(8): 357-365.

Garden GA and Moller T (2006). "Microglia biology in health and disease." *J Neuroimmune Pharmacol* **1**(2): 127-137.

Garg SK, Banerjee R and Kipnis J (2008). "Neuroprotective immunity: T cell-derived glutamate endows astrocytes with a neuroprotective phenotype." *J Immunol* **180**(6): 3866-3873.

Gasque P, Dean YD, McGreal EP, VanBeek J and Morgan BP (2000). "Complement components of the innate immune system in health and disease in the CNS." *Immunopharmacology* **49**(1-2): 171-186.

Gaur U and Aggarwal BB (2003). "Regulation of proliferation, survival and apoptosis by members of the TNF superfamily." *Biochem Pharmacol* **66**(8): 1403-1408.

Gavins F, Yilmaz G and Granger DN (2007). "The evolving paradigm for blood cell-endothelial cell interactions in the cerebral microcirculation." *Microcirculation* **14**(7): 667-681.

Germain RN (1994). "MHC-dependent antigen processing and peptide presentation: providing ligands for T lymphocyte activation." *Cell* **76**(2): 287-299.

Germain RN and Margulies DH (1993). "The biochemistry and cell biology of antigen processing and presentation." *Annu Rev Immunol* **11**: 403-450.

German DC, Liang CL, Song T, Yazdani U, Xie C and Dietschy JM (2002). "Neurodegeneration in the Niemann-Pick C mouse: glial involvement." *Neuroscience* **109**(3): 437-450.

Gery I, Gershon RK and Waksman BH (1972). "Potentiation of the T-lymphocyte response to mitogens. I. The responding cell." *J Exp Med* **136**(1): 128-142.

Gething MJ and Sambrook J (1992). "Protein folding in the cell." *Nature* **355**(6355): 33-45.

Getty AL, Benedict JW and Pearce DA (2011). "A novel interaction of CLN3 with nonmuscle myosin-IIB and defects in cell motility of Cln3(-/-) cells." *Exp Cell Res* **317**(1): 51-69.

Ghani S, Feuerer M, Doebis C, Lauer U, Loddenkemper C, Huehn J, Hamann A and Syrbe U (2009). "T cells as pioneers: antigen-specific T cells condition inflamed sites for high-rate antigen-non-specific effector cell recruitment." *Immunology* **128**(1 Suppl): e870-880.

Gimenez MA, Sim JE and Russell JH (2004). "TNFR1-dependent VCAM-1 expression by astrocytes exposes the CNS to destructive inflammation." *J Neuroimmunol* **151**(1-2): 116-125.

Giuliani F, Goodyer CG, Antel JP and Yong VW (2003). "Vulnerability of human neurons to T cell-mediated cytotoxicity." *J Immunol* **171**(1): 368-379.

Glabinski AR, Tani M, Strieter RM, Tuohy VK and Ransohoff RM (1997). "Synchronous synthesis of alpha- and beta-chemokines by cells of diverse lineage in the central nervous system of mice with relapses of chronic experimental autoimmune encephalomyelitis." *Am J Pathol* **150**(2): 617-630.

Glezer I, Simard AR and Rivest S (2007). "Neuroprotective role of the innate immune system by microglia." *Neuroscience* **147**(4): 867-883.

Godfrey DI, McConville MJ and Pellicci DG (2006). "Chewing the fat on natural killer T cell development." *J Exp Med* **203**(10): 2229-2232.

Goebel HH (1995). "The neuronal ceroid-lipofuscinoses." *J Child Neurol* **10**(6): 424-437.

Goebel HH, Mole SE and Lake BD (1999). The neuronal ceroid lipofuscinoses (Batten disease). *Amsterdam*, IOS Press.

Goebel HH and Wisniewski KE (2004). "Current state of clinical and morphological features in human NCL." *Brain Pathol* **14**(1): 61-69.

Goldmann J, Kwidzinski E, Brandt C, Mahlo J, Richter D and Bechmann I (2006). "T cells traffic from brain to cervical lymph nodes via the cribroid plate and the nasal mucosa." *Journal of Leukocyte Biology* **80**(4): 797-801.

Goldstein JL, Brown MS, Anderson RG, Russell DW and Schneider WJ (1985). "Receptor-mediated endocytosis: concepts emerging from the LDL receptor system." *Annu Rev Cell Biol* **1**: 1-39.

Gonzalez-Scarano F and Baltuch G (1999). "Microglia as mediators of inflammatory and degenerative diseases." *Annu Rev Neurosci* **22**: 219-240.

Gonzalez SF, Degn SE, Pitcher LA, Woodruff M, Heesters BA and Carroll MC (2011). "Trafficking of B cell antigen in lymph nodes." *Annu Rev Immunol* **29**: 215-233.

Gordon GR, Mulligan SJ and MacVicar BA (2007). "Astrocyte control of the cerebrovasculature." *Glia* **55**(12): 1214-1221.

Gordon S (2003). "Alternative activation of macrophages." *Nat Rev Immunol* **3**(1): 23-35.

Gordon S, Clarke S, Greaves D and Doyle A (1995). "Molecular immunobiology of macrophages: recent progress." *Curr Opin Immunol* **7**(1): 24-33.

Gordon S and Taylor PR (2005). "Monocyte and macrophage heterogeneity." *Nature Reviews Immunology* **5**(12): 953-964.

Gossen M and Bujard H (1992). "Tight control of gene expression in mammalian cells by tetracycline-responsive promoters." *Proc Natl Acad Sci U S A* **89**(12): 5547-5551.

Gossen M, Freundlieb S, Bender G, Muller G, Hillen W and Bujard H (1995). "Transcriptional activation by tetracyclines in mammalian cells." *Science* **268**(5218): 1766-1769.

Gottfried-Blackmore A, Kaunzner UW, Idoyaga J, Felger JC, McEwen BS and Bulloch K (2009). "Acute in vivo exposure to interferon-Î³ enables resident brain dendritic cells to become effective antigen presenting cells." *Proceedings of the National Academy of Sciences* **106**(49): 20918-20923.

Goverman J (2009). "Autoimmune T cell responses in the central nervous system." *Nature Reviews Immunology* **9**(6): 393-407.

Gowing G, Philips T, Van Wijmeersch B, Audet JN, Dewil M, Van Den Bosch L, Billiau AD, Robberecht W and Julien JP (2008). "Ablation of proliferating microglia does not affect motor neuron degeneration in amyotrophic lateral sclerosis caused by mutant superoxide dismutase." *J Neurosci* **28**(41): 10234-10244.

Graeber MB and Kreutzberg GW (1986). "Astrocytes increase in glial fibrillary acidic protein during retrograde changes of facial motor neurons." *J Neurocytol* **15**(3): 363-373.

Graeber MB, Li W and Rodriguez ML (2011). "Role of microglia in CNS inflammation." *Febs Letters* **585**(23): 3798-3805.

Graeber MB and Moran LB (2002). "Mechanisms of cell death in neurodegenerative diseases: fashion, fiction, and facts." *Brain Pathol* **12**(3): 385-390.

Graeber MB and Streit WJ (1990). "Microglia: immune network in the CNS." *Brain Pathol* **1**(1): 2-5.

Graeber MB and Streit WJ (2010). "Microglia: biology and pathology." *Acta Neuropathologica* **119**(1): 89-105.

Greenwood J, Etienne-Manneville S, Adamson P and Couraud PO (2002). "Lymphocyte migration into the central nervous system: Implication of ICAM-1 signalling at them blood-brain barrier." *Vascular Pharmacology* **38**(6): 315-322.

Greter M, Heppner FL, Lemos MP, Odermatt BM, Goebels N, Laufer T, Noelle RJ and Becher B (2005). "Dendritic cells permit immune invasion of the CNS in an animal model of multiple sclerosis." *Nat Med* **11**(3): 328-334.

Griffey M, Bible E, Vogler C, Levy B, Gupta P, Cooper J and Sands MS (2004). "Adeno-associated virus 2-mediated gene therapy decreases autofluorescent storage material and increases brain mass in a murine model of infantile neuronal ceroid lipofuscinosis." *Neurobiology of Disease* **16**(2): 360-369.

Griffey M, Macauley SL, Ogilvie JM and Sands MS (2005). "AAV2-Mediated ocular gene therapy for infantile neuronal ceroid lipofuscinosis." *Molecular Therapy* **12**(3): 413-421.

Griffey MA, Wozniak D, Wong M, Bible E, Johnson K, Rothman SM, Wentz AE, Cooper JD and Sands MS (2006). "CNS-directed AAV2-mediated gene therapy ameliorates functional deficits in a murine model of infantile neuronal ceroid lipofuscinosis." *Molecular Therapy* **13**(3): 538-547.

Griffin DE and Metcalf T (2011). "Clearance of virus infection from the CNS." *Curr Opin Virol* **1**(3): 216-221.

Grundemann C, Bauer M, Schweier O, von Oppen N, Lassing U, Saudan P, Becker KF, Karp K, Hanke T, Bachmann MF and Pircher H (2006). "Cutting edge: identification of E-cadherin as a ligand for the murine killer cell lectin-like receptor G1." *J Immunol* **176**(3): 1311-1315.

Guerder S and Matzinger P (1989). "Activation versus tolerance: a decision made by T helper cells." *Cold Spring Harb Symp Quant Biol* **54 Pt 2**: 799-805.

Guicciardi ME, Leist M and Gores GJ (2004). "Lysosomes in cell death." *Oncogene* **23**(16): 2881-2890.

Gundersen HJG (1986). "Stereology of arbitrary particles - a review of unbiased number and size estimators and the presentation of some new ones, in memory of Thompson, William, R." *Journal of Microscopy-Oxford* **143**: 3-45.

Gundersen HJG (1988). "The nucleator." *Journal of Microscopy-Oxford* **151**: 3-21.

Gundersen HJG and Jensen EB (1987). "The efficiency of systematic-sampling in stereology and its prediction." *Journal of Microscopy-Oxford* **147**: 229-263.

Gundersen HJG, Jensen EBV, Kieu K and Nielsen J (1999). "The efficiency of systematic sampling in stereology-reconsidered." *Journal of Microscopy-Oxford* **193**: 199-211.

Gupta P, Soyombo AA, Atashband A, Wisniewski KE, Shelton JM, Richardson JA, Hammer RE and Hofmann SL (2001). "Disruption of PPT1 or PPT2 causes neuronal ceroid lipofuscinosis in knockout mice." *Proceedings of the National Academy of Sciences of the United States of America* **98**(24): 13566-13571.

Gurlo T and von Grafenstein H (2003). "Antigen-independent cross-talk between macrophages and CD8+ T cells facilitates their cooperation during target destruction." *Int Immunol* **15**(9): 1063-1071.

Guyon A, Massa F, Rovere C and Nahon JL (2008). "How cytokines can influence the brain: A role for chemokines?" *Journal of Neuroimmunology* **198**(1-2): 46-55.

Hahn S, Gehri R and Erb P (1995). "Mechanism and biological significance of CD4-mediated cytotoxicity." *Immunol Rev* **146**: 57-79.

Hailer NP, Heppner FL, Haas D and Nitsch R (1997). "Fluorescent dye prelabelled microglial cells migrate into organotypic hippocampal slice cultures and ramify." *Eur J Neurosci* **9**(4): 863-866.

Halassa MM, Fellin T and Haydon PG (2007a). "The tripartite synapse: roles for gliotransmission in health and disease." *Trends Mol Med* **13**(2): 54-63.

Halassa MM, Fellin T, Takano H, Dong JH and Haydon PG (2007b). "Synaptic islands defined by the territory of a single astrocyte." *J Neurosci* **27**(24): 6473-6477.

Halkes KM, St Hilaire PM, Crocker PR and Meldal M (2003). "Glycopeptides as oligosaccharide mimics: high affinity sialopeptide ligands for sialoadhesin from combinatorial libraries." *J Comb Chem* **5**(1): 18-27.

Haltia M (2003). "The neuronal ceroid-lipofuscinoses." *J Neuropathol Exp Neurol* **62**(1): 1-13.

Haltia M (2006). "The neuronal ceroid-lipofuscinoses: from past to present." *Biochim Biophys Acta* **1762**(10): 850-856.

Haltia M, Rapola J and Santavuori P (1973a). "Infantile type of so-called neuronal ceroid-lipofuscinosis. Histological and electron microscopic studies." *Acta Neuropathol* **26**(2): 157-170.

Haltia M, Rapola J, Santavuori P and Keranen A (1973b). "Infantile type of so-called neuronal ceroid-lipofuscinosis. 2. Morphological and biochemical studies." *J Neurol Sci* **18**(3): 269-285.

Hanisch UK (2002). "Microglia as a source and target of cytokines." *Glia* **40**(2): 140-155.

Hanisch UK and Kettenmann H (2007). "Microglia: active sensor and versatile effector cells in the normal and pathologic brain." *Nat Neurosci* **10**(11): 1387-1394.

Hanke ML and Kielian T (2011). "Toll-like receptors in health and disease in the brain: mechanisms and therapeutic potential." *Clin Sci (Lond)* **121**(9): 367-387.

Hardy RR, Li YS, Allman D, Asano M, Gui M and Hayakawa K (2000). "B-cell commitment, development and selection." *Immunol Rev* **175**: 23-32.

Harmatz P, Whitley CB, Waber L, Pais R, Steiner R, Plecko B, Kaplan P, Simon J, Butensky E and Hopwood JJ (2004). "Enzyme replacement therapy in mucopolysaccharidosis VI (Maroteaux-Lamy syndrome)." *J Pediatr* **144**(5): 574-580.

Harrington LE, Hatton RD, Mangan PR, Turner H, Murphy TL, Murphy KM and Weaver CT (2005). "Interleukin 17-producing CD4+ effector T cells develop via a lineage distinct from the T helper type 1 and 2 lineages." *Nat Immunol* **6**(11): 1123-1132.

Harry GJ and Kraft AD (2008). "Neuroinflammation and microglia: considerations and approaches for neurotoxicity assessment." *Expert Opinion on Drug Metabolism & Toxicology* **4**(10): 1265-1277.

Harshyne LA, Watkins SC, Gambotto A and Barratt-Boyes SM (2001). "Dendritic cells acquire antigens from live cells for cross-presentation to CTL." *Journal of Immunology* **166**(6): 3717-3723.

Hartnell A, Steel J, Turley H, Jones M, Jackson DG and Crocker PR (2001). "Characterization of human sialoadhesin, a sialic acid binding receptor expressed by resident and inflammatory macrophage populations." *Blood* **97**(1): 288-296.

Haseloff RF, Blasig IE, Bauer HC and Bauer H (2005). "In search of the astrocytic factor(s) modulating blood-brain barrier functions in brain capillary endothelial cells in vitro." *Cell Mol Neurobiol* **25**(1): 25-39.

Haskell RE, Carr CJ, Pearce DA, Bennett MJ and Davidson BL (2000). "Batten disease: evaluation of CLN3 mutations on protein localization and function." *Hum Mol Genet* **9**(5): 735-744.

Hatterer E, Davoust N, Didier-Bazes M, Vuaillat C, Malcus C, Belin M-Fo and Nataf S (2006). "How to drain without lymphatics? Dendritic cells migrate from the cerebrospinal fluid to the B-cell follicles of cervical lymph nodes." *Blood* **107**(2): 806-812.

Hawkes C and Kar S (2004). "The insulin-like growth factor-II/mannose-6-phosphate receptor: structure, distribution and function in the central nervous system." *Brain Res Brain Res Rev* **44**(2-3): 117-140.

Heikema AP, Bergman MP, Richards H, Crocker PR, Gilbert M, Samsom JN, van Wamel WJ, Endtz HP and van Belkum A (2010). "Characterization of the specific interaction between sialoadhesin and sialylated Campylobacter jejuni lipooligosaccharides." *Infect Immun* **78**(7): 3237-3246.

Heinonen O, Kyttala A, Lehmus E, Paunio T, Peltonen L and Jalanko A (2000). "Expression of palmitoyl protein thioesterase in neurons." *Mol Genet Metab* **69**(2): 123-129.

Helenius A and Aebi M (2001). "Intracellular functions of N-linked glycans." *Science* **291**(5512): 2364-2369.

Hellsten E, Vesa J, Olkkonen VM, Jalanko A and Peltonen L (1996). "Human palmitoyl protein thioesterase: evidence for lysosomal targeting of the enzyme and disturbed cellular routing in infantile neuronal ceroid lipofuscinosis." *EMBO J* **15**(19): 5240-5245.

Hendriks JJ, Teunissen CE, de Vries HE and Dijkstra CD (2005). "Macrophages and neurodegeneration." *Brain Res Brain Res Rev* **48**(2): 185-195.

Heneka MT and O'Banion MK (2007). "Inflammatory processes in Alzheimer's disease." *Journal of Neuroimmunology* **184**(1-2): 69-91.

Henkel JS, Engelhardt JI, Siklos L, Simpson EP, Kim SH, Pan TH, Goodman JC, Siddique T, Beers DR and Appel SH (2004). "Presence of dendritic cells, MCP-1, and activated microglia/macrophages in amyotrophic lateral sclerosis spinal cord tissue." *Annals of Neurology* **55**(2): 221-235.

Herrmann JE, Imura T, Song B, Qi J, Ao Y, Nguyen TK, Korsak RA, Takeda K, Akira S and Sofroniew MV (2008a). "STAT3 is a critical regulator of astrogliosis and scar formation after spinal cord injury." *J Neurosci* **28**(28): 7231-7243.

Herrmann P, Druckrey-Fiskaaen C, Kouznetsova E, Heinitz K, Bigl M, Cotman SL and Schliebs R (2008b). "Developmental impairments of select neurotransmitter systems in brains of Cln3(Deltaex7/8) knock-in mice, an animal model of juvenile neuronal ceroid lipofuscinosis." *J Neurosci Res* **86**(8): 1857-1870.

Hers HG (1965). "Inborn lysosomal diseases." *Gastroenterology* **48**(5): 625-&.

Hers HG (1972). "Role of lysosomes in pathogenicity of storage disease " *Biochimie* **54**(5-6): 753-&.

Hewett JA (2009). "Determinants of regional and local diversity within the astroglial lineage of the normal central nervous system." *J Neurochem* **110**(6): 1717-1736.

Hickey WF (1999). "Leukocyte traffic in the central nervous system: the participants and their roles." *Seminars in Immunology* **11**(2): 125-137.

Hickey WF (2001). "Basic principles of immunological surveillance of the normal central nervous system." *Glia* **36**(2): 118-124.

Hickey WF, Hsu BL and Kimura H (1991). "Lymphocyte-T entry into the Central-Nervous-System." *Journal of Neuroscience Research* **28**(2): 254-260.

Hickey WF and Kimura H (1988). "Perivascular microglial cells of the CNS are bone marrow-derived and present antigen in vivo." *Science* **239**(4837): 290-292.

Hinds JW and McNelly NA (1982). "Capillaries in aging rat olfactory bulb: A quantitative light and electron microscopic analysis." *Neurobiology of Aging* **3**(3): 197-207.

Hines DJ, Hines RM, Mulligan SJ and Macvicar BA (2009). "Microglia processes block the spread of damage in the brain and require functional chloride channels." *Glia* **57**(15): 1610-1618.

Hirawat S, Welch EM, Elfring GL, Northcutt VJ, Paushkin S, Hwang S, Leonard EM, Almstead NG, Ju W, Peltz SW and Miller LL (2007). "Safety, tolerability, and pharmacokinetics of PTC124, a nonaminoglycoside nonsense mutation

suppressor, following single- and multiple-dose administration to healthy male and female adult volunteers." *J Clin Pharmacol* **47**(4): 430-444.

Hirota K, Duarte JH, Veldhoen M, Hornsby E, Li Y, Cua DJ, Ahlfors H, Wilhelm C, Tolaini M, Menzel U, Garefalaki A, Potocnik AJ and Stockinger B (2011). "Fate mapping of IL-17-producing T cells in inflammatory responses." *Nat Immunol* **12**(3): 255-263.

Hoess RH, Ziese M and Sternberg N (1982). "P1 site-specific recombination: nucleotide sequence of the recombining sites." *Proc Natl Acad Sci U S A* **79**(11): 3398-3402.

Hofmann SL, Das AK, Yi W, Lu JY and Wisniewski KE (1999). "Genotype-phenotype correlations in neuronal ceroid lipofuscinosis due to palmitoyl-protein thioesterase deficiency." *Mol Genet Metab* **66**(4): 234-239.

Holmes C, Cunningham C, Zotova E, Woolford J, Dean C, Kerr S, Culliford D and Perry VH (2009). "Systemic inflammation and disease progression in Alzheimer disease." *Neurology* **73**(10): 768-774.

Holmoy T (2008). "T cells in amyotrophic lateral sclerosis." *European Journal of Neurology* **15**(4): 360-366.

Holness CL, Dasilva RP, Fawcett J, Gordon S and Simmons DL (1993). "Macrosalin, a mouse macrophage-restricted glycoprotein, is a member of the LAMP/LGP family." *Journal of Biological Chemistry* **268**(13): 9661-9666.

Holness CL and Simmons DL (1993). "Molecular cloning of CD68, a human macrophage marker related to lysosomal glycoproteins." *Blood* **81**(6): 1607-1613.

Homann D, Teyton L and Oldstone MB (2001). "Differential regulation of antiviral T-cell immunity results in stable CD8+ but declining CD4+ T-cell memory." *Nat Med* **7**(8): 913-919.

Hopwood JJ, Bunge S, Morris CP, Wilson PJ, Steglich C, Beck M, Schwinger E and Gal A (1993a). "Molecular basis of mucopolysaccharidosis type II: mutations in the iduronate-2-sulphatase gene." *Human mutation* **2**(6): 435-442.

Hopwood JJ, Vellodi A, Scott HS, Morris CP, Litjens T, Clements PR, Brooks DA, Cooper A and Wraith JE (1993b). "Long-term clinical progress in bone marrow transplanted mucopolysaccharidosis type I patients with a defined genotype." *J Inherit Metab Dis* **16**(6): 1024-1033.

Howard CV and Reed MG (1998). Microscopy Handbooks; Unbiased stereology: Three dimensional measurement in microscopy. Microscopy Handbooks; Unbiased stereology: Three dimensional measurement in microscopy, BIOS Scientific Publishers Ltd., St. Thomas House, Becket Street, Oxford OX1 ISJ, England; BIOS Scientific Publishers, P. O. Box 605, Herndon, Virginia 20172-0605. **41:** xvii+246p.

Howe CL, Valletta JS, Rusnak AS and Mobley WC (2001). "NGF signaling from clathrin-coated vesicles: evidence that signaling endosomes serve as a platform for the Ras-MAPK pathway." *Neuron* **32**(5): 801-814.

Hsing LC and Rudensky AY (2005). "The lysosomal cysteine proteases in MHC class II antigen presentation." *Immunol Rev* **207**: 229-241.

Hu J, Lu JY, Wong AM, Hynan LS, Birnbaum SG, Yilmaz DS, Streit BM, Lenartowicz EM, Thompson TC, Cooper JD and Hofmann SL (2012). "Intravenous high-dose enzyme replacement therapy with recombinant palmitoyl-protein thioesterase reduces visceral lysosomal storage and modestly prolongs survival in a preclinical mouse model of infantile neuronal ceroid lipofuscinosis." *Mol Genet Metab.*

Huang P, Westmoreland SV, Jain RK and Fukumura D (2011). "Spontaneous nonthymic tumors in SCID mice." *Comp Med* **61**(3): 227-234.

Huang XY, Reynolds AD, Mosley RL and Gendelman HE (2009). "CD 4+T cells in the pathobiology of neurodegenerative disorders." *Journal of Neuroimmunology* **211**(1-2): 3-15.

Huntington ND and Tarlinton DM (2004). "CD45: direct and indirect government of immune regulation." *Immunology Letters* **94**(3): 167-174.

Hunziker W and Geuze HJ (1996). "Intracellular trafficking of lysosomal membrane proteins." *Bioessays* **18**(5): 379-389.

Hurwitz AA, Lyman WD, Guida MP, Calderon TM and Berman JW (1992). "Tumor necrosis factor alpha induces adhesion molecule expression on human fetal astrocytes." *J Exp Med* **176**(6): 1631-1636.

Husemann J and Silverstein SC (2001). "Expression of scavenger receptor class B, type I, by astrocytes and vascular smooth muscle cells in normal adult mouse and human brain and in Alzheimer's disease brain." *Am J Pathol* **158**(3): 825-832.

Iadecola C and Nedergaard M (2007). "Glial regulation of the cerebral microvasculature." *Nat Neurosci* **10**(11): 1369-1376.

Ikeda K, Goebel HH, Burck U and Kohlschutter A (1982). "Ultrastructural pathology of human lymphocytes in lysosomal disorders: a contribution to their morphological diagnosis." *Eur J Pediatr* **138**(2): 179-185.

Infante-Duarte C, Waiczies S, Wuerfel J and Zipp F (2008). "New developments in understanding and treating neuroinflammation." *J Mol Med (Berl)* **86**(9): 975-985.

Ingersoll MA, Platt AM, Potteaux S and Randolph GJ (2011). "Monocyte trafficking in acute and chronic inflammation." *Trends Immunol* **32**(10): 470-477.

Ip CW, Kroner A, Bendszus M, Leder C, Kobsar I, Fischer S, Wiendl H, Nave KA and Martini R (2006). "Immune cells contribute to myelin degeneration and axonopathic changes in mice overexpressing proteolipid protein in oligodendrocytes." *Journal of Neuroscience* **26**(31): 8206-8216.

Ip CW, Kroner A, Crocker PR, Nave K-A and Martini R (2007). "Sialoadhesin deficiency ameliorates myelin degeneration and axonopathic changes in the CNS of PLP overexpressing mice." *Neurobiology of Disease* **25**(1): 105-111.

Ip CW, Kroner A, Groh J, Huber M, Klein D, Spahn I, Diem R, Williams SK, Nave KA, Edgar JM and Martini R (2012). "Neuroinflammation by cytotoxic T-lymphocytes impairs retrograde axonal transport in an oligodendrocyte mutant mouse." *Plos One* **7**(8): e42554.

Isaaz S, Baetz K, Olsen K, Podack E and Griffiths GM (1995). "Serial killing by cytotoxic T lymphocytes: T cell receptor triggers degranulation, re-filling of the lytic granules and secretion of lytic proteins via a non-granule pathway." *Eur J Immunol* **25**(4): 1071-1079.

Isosomppi J, Heinonen O, Hiltunen JO, Greene ND, Vesa J, Uusitalo A, Mitchison HM, Saarma M, Jalanko A and Peltonen L (1999). "Developmental expression of palmitoyl protein thioesterase in normal mice." *Brain Res Dev Brain Res* **118**(1-2): 1-11.

Issazadeh S, Ljungdahl A, Hojeberg B, Mustafa M and Olsson T (1995). "Cytokine production in the central nervous system of Lewis rats with experimental autoimmune encephalomyelitis: dynamics of mRNA expression for interleukin-10, interleukin-12, cytolysin, tumor necrosis factor alpha and tumor necrosis factor beta." *J Neuroimmunol* **61**(2): 205-212.

Itagaki S, McGeer PL and Akiyama H (1988). "Presence of T-cytotoxic suppressor and leukocyte common antigen positive cells in Alzheimers-disease brain-tissue." *Neuroscience Letters* **91**(3): 259-264.

Ito M, Blumberg BM, Mock DJ, Goodman AD, Moser AB, Moser HW, Smith KD and Powers JM (2001). "Potential environmental and host participants in the early white matter lesion of adreno-leukodystrophy: morphologic evidence for CD8 cytotoxic T cells, cytolysis of oligodendrocytes, and CD1-mediated lipid antigen presentation." *J Neuropathol Exp Neurol* **60**(10): 1004-1019.

Ito M, Maruyama T, Saito N, Koganei S, Yamamoto K and Matsumoto N (2006). "Killer cell lectin-like receptor G1 binds three members of the classical cadherin family to inhibit NK cell cytotoxicity." *J Exp Med* **203**(2): 289-295.

Ivy GO, Schottler F, Wenzel J, Baudry M and Lynch G (1984). "Inhibitors of lysosomal enzymes: accumulation of lipofuscin-like dense bodies in the brain." *Science* **226**(4677): 985-987.

Iwasaki A and Medzhitov R (2010). "Regulation of Adaptive Immunity by the Innate Immune System." *Science* **327**(5963): 291-295.

Jain P, Coisne C, Enzmann G, Rottapel R and Engelhardt B (2010). "alpha beta Integrin Mediates the Recruitment of Immature Dendritic Cells across the Blood-Brain Barrier during Experimental Autoimmune Encephalomyelitis." *The Journal of Immunology* **184**(12): 7196-7206.

Jalanko A and Braulke T (2009). "Neuronal ceroid lipofuscinoses." *Biochim Biophys Acta* **1793**(4): 697-709.

Jalanko A, Vesa J, Manninen T, von Schantz C, Minye H, Fabritius AL, Salonen T, Rapola J, Gentile M, Kopra O and Peltonen L (2005). "Mice with Ppt1Deltaex4 mutation replicate the INCL phenotype and show an inflammation-associated loss of interneurons." *Neurobiol Dis* **18**(1): 226-241.

Janes RW, Munroe PB, Mitchison HM, Gardiner RM, Mole SE and Wallace BA (1996). "A model for Batten disease protein CLN3: functional implications from homology and mutations." *FEBS Lett* **399**(1-2): 75-77.

Janeway CA, Jr. (1989). "Approaching the asymptote? Evolution and revolution in immunology." *Cold Spring Harb Symp Quant Biol* **54 Pt 1**: 1-13.

Janeway CA, Jr. (1991). "The co-receptor function of CD4." *Seminars in Immunology* **3**(3): 153-160.

Jansen JH, Fibbe WE, Willemze R and Kluinnelemans JC (1990). "Interleukin-4 - a regulatory protein." *Blut* **60**(5): 269-274.

Janssen EM, Lemmens EE, Wolfe T, Christen U, von Herrath MG and Schoenberger SP (2003). "CD4+ T cells are required for secondary expansion and memory in CD8+ T lymphocytes." *Nature* **421**(6925): 852-856.

Jernigan M, Morcos Y, Lee SM, Dohan FC, Jr., Raine C and Levin MC (2003). "IgG in brain correlates with clinicopathological damage in HTLV-1 associated neurologic disease." *Neurology* **60**(8): 1320-1327.

Jeyakumar M, Norflus F, Tifft CJ, Cortina-Borja M, Butters TD, Proia RL, Perry VH, Dwek RA and Platt FM (2001). "Enhanced survival in Sandhoff disease mice receiving a combination of substrate deprivation therapy and bone marrow transplantation." *Blood* **97**(1): 327-329.

Jeyakumar M, Thomas R, Elliotâ€□ Smith E, Smith DA, van der Spoel AC, dâ€™Azzo A, Hugh Perry V, Butters TD, Dwek RA and Platt FM (2003). "Central nervous system inflammation is a hallmark of pathogenesis in mouse models of GM1 and GM2 gangliosidosis." *Brain* **126**(4): 974-987.

Jhunjhunwala S, van Zelm MC, Peak MM and Murre C (2009). "Chromatin architecture and the generation of antigen receptor diversity." *Cell* **138**(3): 435-448.

Jiang HR, Hwenda L, Makinen K, Oetke C, Crocker PR and Forrester JV (2006). "Sialoadhesin promotes the inflammatory response in experimental autoimmune uveoretinitis." *J Immunol* **177**(4): 2258-2264.

Joffre OP, Segura E, Savina A and Amigorena S (2012). "Cross-presentation by dendritic cells." *Nature Reviews Immunology* **12**(8): 557-569.

Johanson CE, Duncan JA, 3rd, Klinge PM, Brinker T, Stopa EG and Silverberg GD (2008). "Multiplicity of cerebrospinal fluid functions: New challenges in health and disease." *Cerebrospinal Fluid Res* **5**: 10.

John B, Ricart B, Tait Wojno ED, Harris TH, Randall LM, Christian DA, Gregg B, De Almeida DM, Weninger W, Hammer DA and Hunter CA (2011). "Analysis of behavior and trafficking of dendritic cells within the brain during toxoplasmic encephalitis." *PLoS Pathog* **7**(9): e1002246.

John GR, Lee SC, Song X, Rivieccio M and Brosnan CF (2005). "IL-1-regulated responses in astrocytes: relevance to injury and recovery." *Glia* **49**(2): 161-176.

Johnson-Leger C, Aurrand-Lions M and Imhof BA (2000). "The parting of the endothelium: miracle, or simply a junctional affair?" *J Cell Sci* **113 (Pt 6)**: 921-933.

Johnson Z, Proudfoot AE and Handel TM (2005). "Interaction of chemokines and glycosaminoglycans: a new twist in the regulation of chemokine function with

opportunities for therapeutic intervention." *Cytokine Growth Factor Rev* **16**(6): 625-636.

Jolly RD, Brown S, Das AM and Walkley SU (2002). "Mitochondrial dysfunction in the neuronal ceroid-lipofuscinoses (Batten disease)." *Neurochemistry International* **40**(6): 565-571.

Jones C, Virji M and Crocker PR (2003). "Recognition of sialylated meningococcal lipopolysaccharide by siglecs expressed on myeloid cells leads to enhanced bacterial uptake." *Mol Microbiol* **49**(5): 1213-1225.

Jones KJ, Serpe CJ, Byram SC, Deboy CA and Sanders VM (2005). "Role of the immune system in the maintenance of mouse facial motoneuron viability after nerve injury." *Brain Behav Immun* **19**(1): 12-19.

Junt T, Moseman EA, Iannacone M, Massberg S, Lang PA, Boes M, Fink K, Henrickson SE, Shayakhmetov DM, Di Paolo NC, van Rooijen N, Mempel TR, Whelan SP and von Andrian UH (2007). "Subcapsular sinus macrophages in lymph nodes clear lymph-borne viruses and present them to antiviral B cells." *Nature* **450**(7166): 110-114.

Kaczmarski W, Wisniewski KE, Golabek A, Kaczmarski A, Kida E and Michalewski M (1999). "Studies of membrane association of CLN3 protein." *Mol Genet Metab* **66**(4): 261-264.

Kakkis ED, Muenzer J, Tiller GE, Waber L, Belmont J, Passage M, Izykowski B, Phillips J, Doroshow R, Walot I, Hoft R and Neufeld EF (2001). "Enzyme-replacement therapy in mucopolysaccharidosis I." *N Engl J Med* **344**(3): 182-188.

Kama R, Robinson M and Gerst JE (2007). "Btn2, a Hook1 ortholog and potential Batten disease-related protein, mediates late endosome-Golgi protein sorting in yeast." *Mol Cell Biol* **27**(2): 605-621.

Kansas GS (1996). "Selectins and their ligands: current concepts and controversies." *Blood* **88**(9): 3259-3287.

Kaplan A, Fischer D, Achord D and Sly W (1977). "Phosphohexosyl recognition is a general characteristic of pinocytosis of lysosomal glycosidases by human fibroblasts." *J Clin Invest* **60**(5): 1088-1093.

Karman J, Ling CY, Sandor M and Fabry Z (2004). "Initiation of immune responses in brain is promoted by local dendritic cells." *Journal of Immunology* **173**(4): 2353-2361.

Kataoka T, Takaku K, Magae J, Shinohara N, Takayama H, Kondo S and Nagai K (1994). "Acidification is essential for maintaining the structure and function of lytic granules of CTL. Effect of concanamycin A, an inhibitor of vacuolar type H(+)-ATPase, on CTL-mediated cytotoxicity." *J Immunol* **153**(9): 3938-3947.

Katz ML, Shibuya H, Liu PC, Kaur S, Gao CL and Johnson GS (1999). "A mouse gene knockout model for juvenile ceroid-lipofuscinosis (Batten disease)." *Journal of Neuroscience Research* **57**(4): 551-556.

Kawakami N, Nagerl UV, Odoardi F, Bonhoeffer T, Wekerle H and Flugel A (2005). "Live imaging of effector cell trafficking and autoantigen recognition within the

unfolding autoimmune encephalomyelitis lesion." *Journal of Experimental Medicine* **201**(11): 1805-1814.

Kawamata T, Akiyama H, Yamada T and McGeer PL (1992). "Immunological reactions in Amyotrophic-Lateral-Sclerosis brain and spinal-cord tissue." *American Journal of Pathology* **140**(3): 691-707.

Kay GW, Palmer DN, Rezaie P and Cooper JD (2006). "Activation of Non-neuronal Cells within the Prenatal Developing Brain of Sheep with Neuronal Ceroid Lipofuscinosis." *Brain Pathology* **16**(2): 110-116.

Kebir H, Kreymborg K, Ifergan I, Dodelet-Devillers A, Cayrol R, Bernard M, Giuliani F, Arbour N, Becher B and Prat A (2007). "Human TH17 lymphocytes promote blood-brain barrier disruption and central nervous system inflammation." *Nat Med* **13**(10): 1173-1175.

Keeling KM, Brooks DA, Hopwood JJ, Li P, Thompson JN and Bedwell DM (2001). "Gentamicin-mediated suppression of Hurler syndrome stop mutations restores a low level of alpha-L-iduronidase activity and reduces lysosomal glycosaminoglycan accumulation." *Hum Mol Genet* **10**(3): 291-299.

Keene JA and Forman J (1982). "Helper activity is required for the in vivo generation of cytotoxic T lymphocytes." *J Exp Med* **155**(3): 768-782.

Kelm Sr, Pelz A, Schauer R, Filbin MT, Tang S, Bellard M-Ed, Schnaar RL, Mahoney JA, Hartnell A, Bradfield P and Crocker PR (1994). "Sialoadhesin, myelin-associated glycoprotein and CD22 define a new family of sialic acid-dependent adhesion molecules of the immunoglobulin superfamily." *Current Biology* **4**(11): 965-972.

Kennedy MA (2010). "A brief review of the basics of immunology: the innate and adaptive response." *Vet Clin North Am Small Anim Pract* **40**(3): 369-379.

Kerschensteiner M, Stadelmann C, Dechant G, Wekerle H and Hohlfeld R (2003). "Neurotrophic cross-talk between the nervous and immune systems: implications for neurological diseases." *Ann Neurol* **53**(3): 292-304.

Khatami M (2011). "Unresolved inflammation: 'immune tsunami' or erosion of integrity in immune-privileged and immune-responsive tissues and acute and chronic inflammatory diseases or cancer." *Expert Opinion on Biological Therapy* **11**(11): 1419-1432.

Kida E, Kaczmarski W, Golabek AA, Kaczmarski A, Michalewski M and Wisniewski KE (1999). "Analysis of intracellular distribution and trafficking of the CLN3 protein in fusion with the green fluorescent protein in vitro." *Mol Genet Metab* **66**(4): 265-271.

Kida S, Pantazis A and Weller RO (1993). "CSF drains directly from the subarachnoid space into the nasel lymphatics in the rat - anatomy, histology and immunological significance." *Neuropathology and Applied Neurobiology* **19**(6): 480-488.

Kielar C, Maddox L, Bible E, Pontikis CC, Macauley SL, Griffey MA, Wong M, Sands MS and Cooper JD (2007). "Successive neuron loss in the thalamus and cortex in a mouse model of infantile neuronal ceroid lipofuscinosis." *Neurobiology of Disease* **25**(1): 150-162.

Kielar C, Wishart TM, Palmer A, Dihanich S, Wong AM, Macauley SL, Chan CH, Sands MS, Pearce DA, Cooper JD and Gillingwater TH (2009). "Molecular correlates of axonal and synaptic pathology in mouse models of Batten disease." *Human Molecular Genetics* **18**(21): 4066-4080.

Kielian T (2012). Effects of CLN3 loss on inflammasome activation in microglia. O. P. 12. *13th International Conference on Neuronal Ceroid Lipofuscinoses (Batten Disease) (NCL 2012)*, Royal Holloway College, London, UK.

Kieseier BC and Goebel HH (1994). "Characterization of T-cell subclasses and NK-cells in lysosomal disorders by immuno-electron microscopy." *Neuropathol Appl Neurobiol* **20**(6): 604-608.

Kieseier BC, Wisniewski KE, Park E, Schuller-Levis G, Mehta PD and Goebel HH (1997). "Leukocytes in neuronal ceroid-lipofuscinoses: function and apoptosis." *Brain Dev* **19**(5): 317-322.

Kim SJ, Zhang Z, Lee YC and Mukherjee AB (2006). "Palmitoyl-protein thioesterase-1 deficiency leads to the activation of caspase-9 and contributes to rapid neurodegeneration in INCL." *Hum Mol Genet* **15**(10): 1580-1586.

Kim SJ, Zhang Z, Sarkar C, Tsai PC, Lee YC, Dye L and Mukherjee AB (2008). "Palmitoyl protein thioesterase-1 deficiency impairs synaptic vesicle recycling at nerve terminals, contributing to neuropathology in humans and mice." *J Clin Invest* **118**(9): 3075-3086.

Kim SU and de Vellis J (2005). "Microglia in health and disease." *J Neurosci Res* **81**(3): 302-313.

Kimura S and Goebel HH (1988). "Light and electron microscopic study of juvenile neuronal ceroid-lipofuscinosis lymphocytes." *Pediatr Neurol* **4**(3): 148-152.

Kimura T and Griffin DE (2000). "The role of CD8(+) T cells and major histocompatibility complex class I expression in the central nervous system of mice infected with neurovirulent Sindbis virus." *J Virol* **74**(13): 6117-6125.

Kinashi T (2005). "Intracellular signalling controlling integrin activation in lymphocytes." *Nat Rev Immunol* **5**(7): 546-559.

King IL, Dickendesher TL and Segal BM (2009). "Circulating Ly-6C+ myeloid precursors migrate to the CNS and play a pathogenic role during autoimmune demyelinating disease." *Blood* **113**(14): 3190-3197.

Kivisakk P, Mahad DJ, Callahan MK, Trebst C, Tucky B, Wei T, Wu LJ, Baekkevold ES, Lassmann H, Staugaitis SM, Campbell JJ and Ransohoff RM (2003). "Human cerebrospinal fluid central memory CD4(+) T cells: Evidence for trafficking through choroid plexus and meninges via P-selectin." *Proceedings of the National Academy of Sciences of the United States of America* **100**(14): 8389-8394.

Klaas M and Crocker P (2012). "Sialoadhesin in recognition of self and non-self." *Seminars in Immunopathology*: 1-12.

Klein D, Bussow H, Fewou SN and Gieselmann V (2005a). "Exocytosis of storage material in a lysosomal disorder." *Biochem Biophys Res Commun* **327**(3): 663-667.

Klein RS, Lin E, Zhang B, Luster AD, Tollett J, Samuel MA, Engle M and Diamond MS (2005b). "Neuronal CXCL10 directs CD8+ T-cell recruitment and control of West Nile virus encephalitis." *J Virol* **79**(17): 11457-11466.

Kobsar I, Oetke C, Kroner A, Wessig C, Crocker P and Martini R (2006). "Attenuated demyelination in the absence of the macrophage-restricted adhesion molecule sialoadhesin (Siglec-1) in mice heterozygously deficient in P0." *Molecular and Cellular Neuroscience* **31**(4): 685-691.

Koide J and Engleman EG (1990). "Differences in surface phenotype and mechanism of action between alloantigen-specific CD8+ cytotoxic and suppressor T-cell clones." *Journal of Immunology* **144**(1): 32-40.

Kornfeld S (1992). "Structure and function of the mannose 6-phosphate/insulinlike growth factor II receptors." *Annu Rev Biochem* **61**: 307-330.

Kornfeld S and Mellman I (1989). "The biogenesis of lysosomes." *Annu Rev Cell Biol* **5**: 483-525.

Koubek K (2008). "[Human leukocyte differentiation antigens and CD classification]." *VnitrÌ†ni lekarÌ†stvi* **54**(4): 402-409.

Kousi M, Lehesjoki AE and Mole SE (2012). "Update of the mutation spectrum and clinical correlations of over 360 mutations in eight genes that underlie the neuronal ceroid lipofuscinoses." *Human mutation* **33**(1): 42-63.

Kovacs AD and Pearce DA (2008). "Attenuation of AMPA receptor activity improves motor skills in a mouse model of juvenile Batten disease." *Exp Neurol* **209**(1): 288-291.

Kovacs AD, Saje A, Wong A, Szenasi G, Kiricsi P, Szabo E, Cooper JD and Pearce DA (2011). "Temporary inhibition of AMPA receptors induces a prolonged improvement of motor performance in a mouse model of juvenile Batten disease." *Neuropharmacology* **60**(2-3): 405-409.

Kovacs AD, Weimer JM and Pearce DA (2006). "Selectively increased sensitivity of cerebellar granule cells to AMPA receptor-mediated excitotoxicity in a mouse model of Batten disease." *Neurobiol Dis* **22**(3): 575-585.

Kovács GG, Höftberger R, Majtényi K, Horváth R, Barsi P, Komoly S, Lassmann H, Budka H and Jakab G (2005). "Neuropathology of white matter disease in Leber's hereditary optic neuropathy." *Brain* **128**(1): 35-41.

Krakowski ML and Owens T (2000). "Naive T lymphocytes traffic to inflamed central nervous system, but require antigen recognition for activation." *European Journal of Immunology* **30**(4): 1002-1009.

Kratzer R, Mauvais FX, Burgevin A, Barilleau E and van Endert P (2010). "Fusion Proteins for Versatile Antigen Targeting to Cell Surface Receptors Reveal Differential Capacity to Prime Immune Responses." *Journal of Immunology* **184**(12): 6855-6864.

Kreijtz JH, Fouchier RA and Rimmelzwaan GF (2011). "Immune responses to influenza virus infection." *Virus Res* **162**(1-2): 19-30.

Kreutzberg GW (1996). "Microglia: a sensor for pathological events in the CNS." *Trends Neurosci* **19**(8): 312-318.

Krishnamoorthy G, Saxena A, Mars LT, Domingues HS, Mentele R, Ben-Nun A, Lassmann H, Dornmair K, Kurschus FC, Liblau RS and Wekerle H (2009). "Myelin-specific T cells also recognize neuronal autoantigen in a transgenic mouse model of multiple sclerosis." *Nat Med* **15**(6): 626-632.

Kroner A, Ip CW, Thalhammer J, Nave KA and Martini R (2010). "Ectopic T-Cell Specificity and Absence of Perforin and Granzyme B Alleviate Neural Damage in Oligodendrocyte Mutant Mice." *American Journal of Pathology* **176**(2): 549-555.

Kumamoto Y, Higashi N, Denda-Nagai K, Tsuiji M, Sato K, Crocker PR and Irimura T (2004). "Identification of sialoadhesin as a dominant lymph node counter-receptor for mouse macrophage galactose-type C-type lectin 1." *J Biol Chem* **279**(47): 49274-49280.

Kuronen M, Lehesjoki AE, Jalanko A, Cooper JD and Kopra O (2012). "Selective spatiotemporal patterns of glial activation and neuron loss in the sensory thalamocortical pathways of neuronal ceroid lipofuscinosis 8 mice." *Neurobiol Dis* **47**(3): 444-457.

Kwidzinski E, Bunse J, Aktas O, Richter D, Mutlu L, Zipp F, Nitsch R and Bechmann I (2005). "Indolamine 2,3-dioxygenase is expressed in the CNS and down-regulates autoimmune inflammation." *FASEB J* **19**(10): 1347-1349.

Kyttala A, Ihrke G, Vesa J, Schell MJ and Luzio JP (2004). "Two motifs target Batten disease protein CLN3 to lysosomes in transfected nonneuronal and neuronal cells." *Mol Biol Cell* **15**(3): 1313-1323.

Kyttala A, Lahtinen U, Braulke T and Hofmann SL (2006). "Functional biology of the neuronal ceroid lipofuscinoses (NCL) proteins." *Biochim Biophys Acta* **1762**(10): 920-933.

Lachmann R (2010). "Treatments for lysosomal storage disorders." *Biochem Soc Trans* **38**(6): 1465-1468.

Lake BD and Cavanagh NPC (1978). "Early-juvenile Batten disease recognizable subgroup distinct from other forms of Batten disease - Analysis of 5 patients." *Journal of the Neurological Sciences* **36**(2): 265-271.

Lake BD, Steward CG, Oakhill A, Wilson J and Perham TGM (1997). "Bone marrow transplantation in late infantile Batten disease and juvenile Batten disease." *Neuropediatrics* **28**(1): 80-81.

Lane SC, Jolly RD, Schmechel DE, Alroy J and Boustany RM (1996). "Apoptosis as the mechanism of neurodegeneration in Batten's disease." *J Neurochem* **67**(2): 677-683.

Larsen M, Arnaud L, Hie M, Parizot C, Dorgham K, Shoukry M, Kemula M, Barete S, Derai D, Sauce D, Amoura Z, Pene J, Yssel H and Gorochov G (2011). "Multiparameter grouping delineates heterogeneous populations of human IL-17 and/or IL-22 T-cell producers that share antigen specificities with other T-cell subsets." *Eur J Immunol* **41**(9): 2596-2605.

Lasiecka ZM and Winckler B (2011). "Mechanisms of polarized membrane trafficking in neurons - Focusing in on endosomes." *Molecular and Cellular Neuroscience* **48**(4): 278-287.

Lassmann H (2011). "Mechanisms of neurodegeneration shared between multiple sclerosis and Alzheimer's disease." *J Neural Transm* **118**(5): 747-752.

Lassmann H, Bruck W and Lucchinetti C (2001). "Heterogeneity of multiple sclerosis pathogenesis: implications for diagnosis and therapy." *Trends Mol Med* **7**(3): 115-121.

Laudanna C, Kim JY, Constantin G and Butcher E (2002). "Rapid leukocyte integrin activation by chemokines." *Immunol Rev* **186**: 37-46.

Laugel B, Cole DK, Clement M, Wooldridge L, Price DA and Sewell AK (2011). "The multiple roles of the CD8 coreceptor in T cell biology: opportunities for the selective modulation of self-reactive cytotoxic T cells." *J Leukoc Biol* **90**(6): 1089-1099.

Lavi E, Suzumura A, Murasko DM, Murray EM, Silberberg DH and Weiss SR (1988). "Tumor necrosis factor induces expression of MHC class-I antigens on mouse astrocytes." *Journal of Neuroimmunology* **18**(3): 245-253.

Le W, Rowe D, Xie W, Ortiz I, He Y and Appel SH (2001). "Microglial activation and dopaminergic cell injury: an in vitro model relevant to Parkinson's disease." *J Neurosci* **21**(21): 8447-8455.

Leblond V, Autran B and Cesbron JY (1997). "The SCID mouse mutant: Definition and potential use as a model for immune and hematological disorders." *Hematology and Cell Therapy* **39**(5): 213-221.

Lee JA, Beigneux A, Ahmad ST, Young SG and Gao FB (2007a). "ESCRT-III dysfunction causes autophagosome accumulation and neurodegeneration." *Curr Biol* **17**(18): 1561-1567.

Lee JP, Jeyakumar M, Gonzalez R, Takahashi H, Lee PJ, Baek RC, Clark D, Rose H, Fu G, Clarke J, McKercher S, Meerloo J, Muller FJ, Park KI, Butters TD, Dwek RA, Schwartz P, Tong G, Wenger D, Lipton SA, Seyfried TN, Platt FM and Snyder EY (2007b). "Stem cells act through multiple mechanisms to benefit mice with neurodegenerative metabolic disease." *Nat Med* **13**(4): 439-447.

Lee SC, Liu W, Dickson DW, Brosnan CF and Berman JW (1993). "Cytokine production by human fetal microglia and astrocytes. Differential induction by lipopolysaccharide and IL-1 beta." *J Immunol* **150**(7): 2659-2667.

Lee SHC, Liu W, Brosnan CF and Dickson DW (1992). "Characterization of primary fetal dissociated Central-Nervous-System cultures with an emphasis on microglia." *Laboratory Investigation* **67**(4): 465-476.

Lee YB, Nagai A and Kim SU (2002). "Cytokines, chemokines, and cytokine receptors in human microglia." *J Neurosci Res* **69**(1): 94-103.

Lefrancois L (2006). "Development, trafficking, and function of memory T-cell subsets." *Immunological Reviews* **211**: 93-103.

Lehtovirta M, Kyttala A, Eskelinen EL, Hess M, Heinonen O and Jalanko A (2001). "Palmitoyl protein thioesterase (PPT) localizes into synaptosomes and synaptic vesicles in neurons: implications for infantile neuronal ceroid lipofuscinosis (INCL)." *Hum Mol Genet* **10**(1): 69-75.

Lerner TJ, Boustany RMN, Anderson JW, Darigo KL, Schlumpf K, Buckler AJ, Gusella JF, Haines JL, Kremmidiotis G, Lensink IL, Sutherland GR, Callen DF, Taschner PEM, Devos N, Vanommen GJB, Breuning MH, Doggett NA, Meincke LJ, Liu ZY, Goodwin LA, Tesmer JG, Mitchison HM, Orawe AM, Munroe PB, Jarvela IE, Gardiner RM and Mole SE (1995). "Isolation of a novel gene underlying Batten-Disease, CLN3." *Cell* **82**(6): 949-957.

Levine B and Klionsky DJ (2004). "Development by self-digestion: molecular mechanisms and biological functions of autophagy." *Dev Cell* **6**(4): 463-477.

Levite M (2008). "Neurotransmitters activate T-cells and elicit crucial functions via neurotransmitter receptors." *Curr Opin Pharmacol* **8**(4): 460-471.

Lewinsohn DM, Bargatze RF and Butcher EC (1987). "Leukocyte-endothelial cell recognition - evidence of a common molecular mechanism shared by neutrophils, lymphocytes, and other leukocytes." *Journal of Immunology* **138**(12): 4313-4321.

Ley K, Laudanna C, Cybulsky MI and Nourshargh S (2007). "Getting to the site of inflammation: the leukocyte adhesion cascade updated." *Nat Rev Immunol* **7**(9): 678-689.

Li L, Lundkvist A, Andersson D, Wilhelmsson U, Nagai N, Pardo AC, Nodin C, Stahlberg A, Aprico K, Larsson K, Yabe T, Moons L, Fotheringham A, Davies I, Carmeliet P, Schwartz JP, Pekna M, Kubista M, Blomstrand F, Maragakis N, Nilsson M and Pekny M (2008). "Protective role of reactive astrocytes in brain ischemia." *J Cereb Blood Flow Metab* **28**(3): 468-481.

Li MO, Sanjabi S and Flavell RA (2006). "Transforming growth factor-beta controls development, homeostasis, and tolerance of T cells by regulatory T cell-dependent and -independent mechanisms." *Immunity* **25**(3): 455-471.

Lidington EA, McCormack AM, Yacoub MH and Rose ML (1998). "The effects of monocytes on the transendothelial migration of T lymphocytes." *Immunology* **94**(2): 221-227.

Liedtke W, Edelmann W, Chiu FC, Kucherlapati R and Raine CS (1998). "Experimental autoimmune encephalomyelitis in mice lacking glial fibrillary acidic protein is characterized by a more severe clinical course and an infiltrative central nervous system lesion." *Am J Pathol* **152**(1): 251-259.

Lim A and Kraut R (2009). "The Drosophila BEACH family protein, blue cheese, links lysosomal axon transport with motor neuron degeneration." *J Neurosci* **29**(4): 951-963.

Lim M (2011). "Treating inflammation in childhood neurodegenerative disorders." *Developmental Medicine and Child Neurology* **53**(4): 298-304.

Lim MJ, Alexander N, Benedict JW, Chattopadhyay S, Shemilt SJ, Guerin CJ, Cooper JD and Pearce DA (2007a). "IgG entry and deposition are components of the neuroimmune response in Batten disease." *Neurobiol Dis* **25**(2): 239-251.

Lim MJ, Alexander N, Benedict JW, Chattopadhyay S, Shemilt SJA, Guerin CJ, Cooper JD and Pearce DA (2007b). "IgG entry and deposition are components of the neuroimmune response in Batten disease." *Neurobiology of Disease* **25**(2): 239-251.

Lim MJ, Beake J, Bible E, Curran TM, Ramirez-Montealegre D, Pearce DA and Cooper JD (2006). "Distinct patterns of serum immunoreactivity as evidence for multiple brain-directed autoantibodies in juvenile neuronal ceroid lipofuscinosis." *Neuropathology and Applied Neurobiology* **32**(5): 469-482.

Lin D, Donsante A, Macauley S, Levy B, Vogler C and Sands MS (2007). "Central nervous system-directed AAV2/5-mediated gene therapy synergizes with bone marrow transplantation in the murine model of globoid-cell leukodystrophy." *Mol Ther* **15**(1): 44-52.

Ling CY, Sandor M and Fabry Z (2003). "In situ processing and distribution of intracerebrally injected OVA in the CNS." *Journal of Neuroimmunology* **141**(1-2): 90-98.

Linthorst GE, Hollak CE, Donker-Koopman WE, Strijland A and Aerts JM (2004). "Enzyme therapy for Fabry disease: neutralizing antibodies toward agalsidase alpha and beta." *Kidney Int* **66**(4): 1589-1595.

Liu J, Gong N, Huang X, Reynolds AD, Mosley RL and Gendelman HE (2009). "Neuromodulatory activities of CD4+CD25+ regulatory T cells in a murine model of HIV-1-associated neurodegeneration." *J Immunol* **182**(6): 3855-3865.

Liu XF, Fawcett JR, Thorne RG, DeFor TA and Frey WH (2001). "Intranasal administration of insulin-like growth factor-I bypasses the blood-brain barrier and protects against focal cerebral ischemic damage." *Journal of the Neurological Sciences* **187**(1-2): 91-97.

Liu Y, Liu H, Kim BO, Gattone VH, Li J, Nath A, Blum J and He JJ (2004). "CD4-independent infection of astrocytes by human immunodeficiency virus type 1: requirement for the human mannose receptor." *J Virol* **78**(8): 4120-4133.

Liu Y, Teige I, Birnir B and Issazadeh-Navikas S (2006). "Neuron-mediated generation of regulatory T cells from encephalitogenic T cells suppresses EAE." *Nat Med* **12**(5): 518-525.

Lloyd E, Somera-Molina K, Van Eldik LJ, Watterson DM and Wainwright MS (2008). "Suppression of acute proinflammatory cytokine and chemokine upregulation by post-injury administration of a novel small molecule improves long-term neurologic outcome in a mouse model of traumatic brain injury." *J Neuroinflammation* **5**: 28.

Lo D, Feng L, Li L, Carson MJ, Crowley M, Pauza M, Nguyen A and Reilly CR (1999). "Integrating innate and adaptive immunity in the whole animal." *Immunol Rev* **169**: 225-239.

Lobsiger CS and Cleveland DW (2007). "Glial cells as intrinsic components of non-cell-autonomous neurodegenerative disease." *Nat Neurosci* **10**(11): 1355-1360.

Loeffler C, Dietz K, Schleich A, Schlaszus H, Stoll M, Meyermann R and Mittelbronn M (2011). "Immune surveillance of the normal human CNS takes place in

dependence of the locoregional blood-brain barrier configuration and is mainly performed by CD3+/CD8+lymphocytes." *Neuropathology* **31**(3): 230-238.

Lois C and Alvarezbuylla A (1994). "Long-distance neuronal migration in the adult mammalian brain." *Science* **264**(5162): 1145-1148.

Lonnqvist T, Vanhanen SL, Vettenranta K, Autti T, Rapola J, Santavuori P and Saarinen-Pihkala UM (2001). "Hematopoietic stem cell transplantation in infantile neuronal ceroid lipofuscinosis." *Neurology* **57**(8): 1411-1416.

Loos M, Dihne M and Block F (2003). "Tumor necrosis factor-alpha expression in areas of remote degeneration following middle cerebral artery occlusion of the rat." *Neuroscience* **122**(2): 373-380.

Lovatt D, Sonnewald U, Waagepetersen HS, Schousboe A, He W, Lin JH, Han X, Takano T, Wang S, Sim FJ, Goldman SA and Nedergaard M (2007). "The transcriptome and metabolic gene signature of protoplasmic astrocytes in the adult murine cortex." *J Neurosci* **27**(45): 12255-12266.

Lucocq J (2007). "Efficient quantitative morphological phenotyping of genetically altered organisms using stereology." *Transgenic Research* **16**(2): 133-145.

Luiro K, Kopra O, Blom T, Gentile M, Mitchison HM, Hovatta I, Tornquist K and Jalanko A (2006). "Batten disease (JNCL) is linked to disturbances in mitochondrial, cytoskeletal, and synaptic compartments." *J Neurosci Res* **84**(5): 1124-1138.

Luiro K, Kopra O, Lehtovirta M and Jalanko A (2001). "CLN3 protein is targeted to neuronal synapses but excluded from synaptic vesicles: new clues to Batten disease." *Hum Mol Genet* **10**(19): 2123-2131.

Lull ME and Block ML (2010). "Microglial activation and chronic neurodegeneration." *Neurotherapeutics* **7**(4): 354-365.

Luse S (1958). "Ultrastructure of reactive and neoplastic astrocytes." *Lab Invest* **7**(4): 401-417.

Luzio JP, Pryor PR and Bright NA (2007). "Lysosomes: fusion and function." *Nat Rev Mol Cell Biol* **8**(8): 622-632.

Lyly A, Marjavaara SK, Kyttala A, Uusi-Rauva K, Luiro K, Kopra O, Martinez LO, Tanhuanpaa K, Kalkkinen N, Suomalainen A, Jauhiainen M and Jalanko A (2008). "Deficiency of the INCL protein Ppt1 results in changes in ectopic F1-ATP synthase and altered cholesterol metabolism." *Hum Mol Genet* **17**(10): 1406-1417.

Lynch MA and Mills KHG (2011). "Immunology meets neuroscience - Opportunities for immune intervention in neurodegenerative diseases." *Brain, Behavior, and Immunity*(0).

Macauley SL, Pekny M and Sands MS (2011). "The Role of Attenuated Astrocyte Activation in Infantile Neuronal Ceroid Lipofuscinosis." *The Journal of Neuroscience* **31**(43): 15575-15585.

Macauley SL, Roberts MS, Wong AM, McSloy F, Reddy AS, Cooper JD and Sands MS (2012). "Synergistic effects of central nervous system-directed gene therapy and

bone marrow transplantation in the murine model of infantile neuronal ceroid lipofuscinosis." *Annals of Neurology* **71**(6): 797-804.

Macauley SL, Wozniak DF, Kielar C, Tan Y, Cooper JD and Sands MS (2009). "Cerebellar pathology and motor deficits in the palmitoyl protein thioesterase 1-deficient mouse." *Experimental Neurology* **217**(1): 124-135.

MacDonald HR (2002). "Immunology. T before NK." *Science* **296**(5567): 481-482.

Maddon PJ, Littman DR, Godfrey M, Maddon DE, Chess L and Axel R (1985). "The isolation and nucleotide-sequence of a cDNA-encoding the T-cell surface protein-T4 - a new member of the immunoglobulin gene family." *Cell* **42**(1): 93-104.

Magesh S, Ando H, Tsubata T, Ishida H and Kiso M (2011). "High-Affinity Ligands of Siglec Receptors and their Therapeutic Potentials." *Current Medicinal Chemistry* **18**(23): 3537-3550.

Magnus T, Schreiner B, Korn T, Jack C, Guo H, Antel J, Ifergan I, Chen L, Bischof F, Bar-Or A and Wiendl H (2005). "Microglial expression of the B7 family member B7 homolog 1 confers strong immune inhibition: implications for immune responses and autoimmunity in the CNS." *J Neurosci* **25**(10): 2537-2546.

Majed HH, Chandran S, Niclou SP, Nicholas RS, Wilkins A, Wing MG, Rhodes KE, Spillantini MG and Compston A (2006). "A novel role for Sema3A in neuroprotection from injury mediated by activated microglia." *J Neurosci* **26**(6): 1730-1738.

Mao Q, Foster BJ, Xia H and Davidson BL (2003). "Membrane topology of CLN3, the protein underlying Batten disease." *FEBS Lett* **541**(1-3): 40-46.

Maria B L (1993). "Restricted proliferation and migration of postnatally generated neurons derived from the forebrain subventricular zone." *Neuron* **11**(1): 173-189.

Marino G, Madeo F and Kroemer G (2011). "Autophagy for tissue homeostasis and neuroprotection." *Curr Opin Cell Biol* **23**(2): 198-206.

Marsh JL and Thompson LM (2006). "Drosophila in the study of neurodegenerative disease." *Neuron* **52**(1): 169-178.

Martinez-Pomares L and Gordon S (2012). "CD169+ macrophages at the crossroads of antigen presentation." *Trends in Immunology* **33**(2): 66-70.

Martinez-Pomares L, Kosco-Vilbois M, Darley E, Tree P, Herren S, Bonnefoy JY and Gordon S (1996). "Fc chimeric protein containing the cysteine-rich domain of the murine mannose receptor binds to macrophages from splenic marginal zone and lymph node subcapsular sinus and to germinal centers." *J Exp Med* **184**(5): 1927-1937.

Mason DW, Charlton HM, Jones AJ, Lavy CB, Puklavec M and Simmonds SJ (1986). "The fate of allogeneic and xenogeneic neuronal tissue transplanted into the third ventricle of rodents." *Neuroscience* **19**(3): 685-694.

Masopust D and Picker LJ (2012). "Hidden memories: frontline memory T cells and early pathogen interception." *J Immunol* **188**(12): 5811-5817.

Matheny HE, Deem TL and Cook-Mills JM (2000). "Lymphocyte migration through monolayers of endothelial cell lines involves VCAM-1 signaling via endothelial cell NADPH oxidase." *J Immunol* **164**(12): 6550-6559.

Mathey EK, Derfuss T, Storch MK, Williams KR, Hales K, Woolley DR, Al-Hayani A, Davies SN, Rasband MN, Olsson T, Moldenhauer A, Velhin S, Hohlfeld R, Meinl E and Linington C (2007). "Neurofascin as a novel target for autoantibody-mediated axonal injury." *J Exp Med* **204**(10): 2363-2372.

Matthews AE, Lavi E, Weiss SR and Paterson Y (2002). "Neither B cells nor T cells are required for CNS demyelination in mice persistently infected with MHV-A59." *Journal of Neurovirology* **8**(3): 257-264.

Matyszak MK, Denis-Donini S, Citterio S, Longhi R, Granucci F and Ricciardi-Castagnoli P (1999). "Microglia induce myelin basic protein-specific T cell anergy or T cell activation, according to their state of activation." *Eur J Immunol* **29**(10): 3063-3076.

Matyszak MK and Perry VH (1996a). "A comparison of leucocyte responses to heat-killed bacillus Calmette-Guerin in different CNS compartments." *Neuropathol Appl Neurobiol* **22**(1): 44-53.

Matyszak MK and Perry VH (1996b). "The potential role of dendritic cells in immune-mediated inflammatory diseases in the central nervous system." *Neuroscience* **74**(2): 599-608.

McCaughan KK, Brown CM, Dalphin ME, Berry MJ and Tate WP (1995). "Translational termination efficiency in mammals is influenced by the base following the stop codon." *Proc Natl Acad Sci U S A* **92**(12): 5431-5435.

McClintock MK, Jacob S, Zelano B and Hayreh DJ (2001). "Pheromones and vasanas: the functions of social chemosignals." *Nebraska Symposium on Motivation. Nebraska Symposium on Motivation* **47**: 75-112.

McCormack AL, Thiruchelvam M, Manning-Bog AB, Thiffault C, Langston JW, Cory-Slechta DA and Di Monte DA (2002). "Environmental risk factors and Parkinson's disease: Selective degeneration of nigral dopaminergic neurons caused by the herbicide paraquat." *Neurobiology of Disease* **10**(2): 119-127.

McCown TJ (2005). "Adeno-associated virus (AAV) vectors in the CNS." *Current Gene Therapy* **5**(3): 333-338.

McEver RP and Cummings RD (1997). "Perspectives series: cell adhesion in vascular biology. Role of PSGL-1 binding to selectins in leukocyte recruitment." *J Clin Invest* **100**(3): 485-491.

McGaha TL, Chen Y, Ravishankar B, van Rooijen N and Karlsson MC (2011). "Marginal zone macrophages suppress innate and adaptive immunity to apoptotic cells in the spleen." *Blood* **117**(20): 5403-5412.

McGeer EG and McGeer PL (2003). "Inflammatory processes in Alzheimer's disease." *Progress in Neuro-Psychopharmacology and Biological Psychiatry* **27**(5): 741-749.

McGeer PL, Itagaki S, Akiyama H and McGeer EG (1988). "Rate of cell-death in Parkinsonism indicates active neuropathological process." *Annals of Neurology* **24**(4): 574-576.

McLin JP and Steward O (2006). "Comparison of seizure phenotype and neurodegeneration induced by systemic kainic acid in inbred, outbred, and hybrid mouse strains." *European Journal of Neuroscience* **24**(8): 2191-2202.

McMahon EJ, Bailey SL, Castenada CV, Waldner H and Miller SD (2005). "Epitope spreading initiates in the CNS in two mouse models of multiple sclerosis." *Nat Med* **11**(3): 335-339.

McMenamin PG (1999). "Distribution and phenotype of dendritic cells and resident tissue macrophages in the dura mater, leptomeninges, and choroid plexus of the rat brain as demonstrated in wholemount preparations." *J Comp Neurol* **405**(4): 553-562.

McMenamin PG, Wealthall RJ, Deverall M, Cooper SJ and Griffin B (2003). "Macrophages and dendritic cells in the rat meninges and choroid plexus: three-dimensional localisation by environmental scanning electron microscopy and confocal microscopy." *Cell Tissue Res* **313**(3): 259-269.

Medana I, Martinic MA, Wekerle H and Neumann H (2001). "Transection of major histocompatibility complex class I-induced neurites by cytotoxic T lymphocytes." *Am J Pathol* **159**(3): 809-815.

Medana IM, Gallimore A, Oxenius A, Martinic MM, Wekerle H and Neumann H (2000). "MHC class I-restricted killing of neurons by virus-specific CD8+ T lymphocytes is effected through the Fas/FasL, but not the perforin pathway." *Eur J Immunol* **30**(12): 3623-3633.

Medina DL, Fraldi A, Bouche V, Annunziata F, Mansueto G, Spampanato C, Puri C, Pignata A, Martina JA, Sardiello M, Palmieri M, Polishchuk R, Puertollano R and Ballabio A (2011). "Transcriptional Activation of Lysosomal Exocytosis Promotes Cellular Clearance." *Dev Cell* **21**(3): 421-430.

Medzhitov R and Janeway CA, Jr. (1997). "Innate immunity: the virtues of a nonclonal system of recognition." *Cell* **91**(3): 295-298.

Medzhitov R and Janeway CA, Jr. (1998). "Innate immune recognition and control of adaptive immune responses." *Semin Immunol* **10**(5): 351-353.

Meikle PJ, Hopwood JJ, Clague AE and Carey WF (1999). "Prevalence of lysosomal storage disorders." *Jama-Journal of the American Medical Association* **281**(3): 249-254.

Meinl E, Aloisi F, Ertl B, Weber F, de Waal Malefyt R, Wekerle H and Hohlfeld R (1994). "Multiple sclerosis. Immunomodulatory effects of human astrocytes on T cells." *Brain* **117 (Pt 6)**: 1323-1332.

Mellman I (1996). "Endocytosis and molecular sorting." *Annu Rev Cell Dev Biol* **12**: 575-625.

Mellman I, Turley S and Steinman R (1998). "Antigen processing for amateurs and professionals." *Trends Cell Biol* **8**(6): 231-237.

Melville SA, Wilson CL, Chiang CS, Studdert VP, Lingaas F and Wilton AN (2005). "A mutation in canine CLN5 causes neuronal ceroid lipofuscinosis in Border collie dogs." *Genomics* **86**(3): 287-294.

Melzer N, Meuth SG and Wiendl H (2009). "CD8+ T cells and neuronal damage: direct and collateral mechanisms of cytotoxicity and impaired electrical excitability." *The FASEB Journal* **23**(11): 3659-3673.

Mendiratta SK, Martin WD, Hong S, Boesteanu A, Joyce S and Van Kaer L (1997). "CD1d1 mutant mice are deficient in natural T cells that promptly produce IL-4." *Immunity* **6**(4): 469-477.

Metzger D, Clifford J, Chiba H and Chambon P (1995). "Conditional site-specific recombination in mammalian cells using a ligand-dependent chimeric Cre recombinase." *Proc Natl Acad Sci U S A* **92**(15): 6991-6995.

Meuer SC, Schlossman SF and Reinherz EL (1982). "Clonal analysis of human cytotoxic lymphocytes-T - T4 and T8+ effector-cells recognize products of different major histocompatibilty complex regions." *Proceedings of the National Academy of Sciences of the United States of America-Biological Sciences* **79**(14): 4395-4399.

Miceli MC and Parnes JR (1991). "The roles of CD4 and CD8 in T cell activation." *Semin Immunol* **3**(3): 133-141.

Michelucci A, Heurtaux T, Grandbarbe L, Morga E and Heuschling P (2009). "Characterization of the microglial phenotype under specific pro-inflammatory and anti-inflammatory conditions: Effects of oligomeric and fibrillar amyloid-beta." *J Neuroimmunol* **210**(1-2): 3-12.

Milà M (2012). Glial dysfunction in Infantile Neuronal Ceroid Lipofuscinosis (INCL). BSc thesis, King's College London.

Mildner A, Mack M, Schmidt H, Bruck W, Djukic M, Zabel MD, Hille A, Priller J and Prinz M (2009). "CCR2+Ly-6Chi monocytes are crucial for the effector phase of autoimmunity in the central nervous system." *Brain* **132**(Pt 9): 2487-2500.

Miller MD and Krangel MS (1992). "Biology and biochemistry of the chemokines - a family of chemotactic and inflammatory cytokines." *Critical Reviews in Immunology* **12**(1-2): 17-46.

Milligan CE, Cunningham TJ and Levitt P (1991). "Differential immunochemical markers reveal the normal distribution of brain macrophages and microglia in the developing rat brain." *J Comp Neurol* **314**(1): 125-135.

Minagar A, Shapshak P, Fujimura R, Ownby R, Heyes M and Eisdorfer C (2002). "The role of macrophage/microglia and astrocytes in the pathogenesis of three neurologic disorders: HIV-associated dementia, Alzheimer disease, and multiple sclerosis." *J Neurol Sci* **202**(1-2): 13-23.

Minghetti L, Ajmone-Cat MA, De Berardinis MA and De Simone R (2005). "Microglial activation in chronic neurodegenerative diseases: roles of apoptotic neurons and chronic stimulation." *Brain Res Brain Res Rev* **48**(2): 251-256.

Mitchison HM, Bernard DJ, Greene ND, Cooper JD, Junaid MA, Pullarkat RK, de Vos N, Breuning MH, Owens JW, Mobley WC, Gardiner RM, Lake BD, Taschner PE and Nussbaum RL (1999). "Targeted disruption of the Cln3 gene provides a mouse model for Batten disease. The Batten Mouse Model Consortium [corrected]." *Neurobiol Dis* **6**(5): 321-334.

Mitchison HM, Lim MJ and Cooper JD (2004). "Selectivity and types of cell death in the neuronal ceroid lipofuscinoses (NCLs)." *Brain Pathology* **14**(1): 86-96.

Mitter D, Reisinger C, Hinz B, Hollmann S, Yelamanchili SV, Treiber-Held S, Ohm TG, Herrmann A and Ahnert-Hilger G (2003). "The synaptophysin/synaptobrevin interaction critically depends on the cholesterol content." *J Neurochem* **84**(1): 35-42.

Mix E, Goertsches R and Zett UK (2006). "Immunoglobulins--basic considerations." *J Neurol* **253 Suppl 5**: V9-17.

Miyake Y, Asano K, Kaise H, Uemura M, Nakayama M and Tanaka M (2007). "Critical role of macrophages in the marginal zone in the suppression of immune responses to apoptotic cell-associated antigens." *J Clin Invest* **117**(8): 2268-2278.

Mizukami H, Mi YD, Wada R, Kono M, Yamashita T, Liu YJ, Werth N, Sandhoff R, Sandhoff K and Proia RL (2002). "Systemic inflammation in glucocerebrosidase-deficient mice with minimal glucosylceramide storage." *Journal of Clinical Investigation* **109**(9): 1215-1221.

Moalem G, Gdalyahu A, Shani Y, Otten U, Lazarovici P, Cohen IR and Schwartz M (2000). "Production of neurotrophins by activated T cells: implications for neuroprotective autoimmunity." *J Autoimmun* **15**(3): 331-345.

Mocali A, Cedrola S, Della Malva N, Bontempelli M, Mitidieri VA, Bavazzano A, Comolli R, Paoletti F and La Porta CA (2004). "Increased plasma levels of soluble CD40, together with the decrease of TGF beta 1, as possible differential markers of Alzheimer disease." *Exp Gerontol* **39**(10): 1555-1561.

Mole S (2004). "Neuronal ceroid lipofuscinoses (NCL)." *Eur J Paediatr Neurol* **8**(2): 101-103.

Mole SE, Williams RE, Goebel HH and (Editors) (2011). The neuronal ceroid lipofuscinoses (Batten disease). *Oxford, UK*, Oxford University Press.

Mombaerts P (1995). "Lymphocyte development and function in T-cell receptor and RAG-1 mutant mice." *International reviews of immunology* **13**(1): 43-63.

Mombaerts P, Iacomini J, Johnson RS, Herrup K, Tonegawa S and Papaioannou VE (1992). "RAG-1-deficient mice have no mature B and T lymphocytes." *Cell* **68**(5): 869-877.

Mondino A and Jenkins MK (1994). "Surface-proteins involved in T-cell costimulation." *Journal of Leukocyte Biology* **55**(6): 805-815.

Monteiro VG, Lobato CS, Silva AR, Medina DV, de Oliveira MA, Seabra SH, de Souza W and DaMatta RA (2005). "Increased association of Trypanosoma cruzi with sialoadhesin positive mice macrophages." *Parasitol Res* **97**(5): 380-385.

Mor F, Quintana F, Mimran A and Cohen IR (2003). "Autoimmune encephalomyelitis and uveitis induced by T cell immunity to self beta-synuclein." *J Immunol* **170**(1): 628-634.

Morrison RS, De Vellis J, Lee YL, Bradshaw RA and Eng LF (1985). "Hormones and growth factors induce the synthesis of glial fibrillary acidic protein in rat brain astrocytes." *J Neurosci Res* **14**(2): 167-176.

Mosmann TR, Cherwinski H, Bond MW, Giedlin MA and Coffman RL (1986). "Two types of murine helper T cell clone. I. Definition according to profiles of lymphokine activities and secreted proteins." *J Immunol* **136**(7): 2348-2357.

Mosmann TR and Coffman RL (1989). "TH1 and TH2 cells: different patterns of lymphokine secretion lead to different functional properties." *Annu Rev Immunol* **7**: 145-173.

Mosser DM and Edwards JP (2008). "Exploring the full spectrum of macrophage activation." *Nat Rev Immunol* **8**(12): 958-969.

Mott RT, Ait-Ghezala G, Town T, Mori T, Vendrame M, Zeng J, Ehrhart J, Mullan M and Tan J (2004). "Neuronal expression of CD22: novel mechanism for inhibiting microglial proinflammatory cytokine production." *Glia* **46**(4): 369-379.

Mrass P, Takano H, Ng LG, Daxini S, Lasaro MO, Iparraguirre A, Cavanagh LL, von Andrian UH, Ertl HCJ, Haydon PG and Weninger W (2006). "Random migration precedes stable target cell interactions of tumor-infiltrating T cells." *Journal of Experimental Medicine* **203**(12): 2749-2761.

Muerkoster S, Rocha M, Crocker PR, Schirrmacher V and Umansky V (1999). "Sialoadhesin-positive host macrophages play an essential role in graft-versus-leukemia reactivity in mice." *Blood* **93**(12): 4375-4386.

Mullereberhard HJ (1988). "The molecular basis of target-cell killing by human-lymphocytes and of killer cell self-protection." *Immunological Reviews* **103**: 87-98.

Munroe ME (2009). "Functional roles for T cell CD40 in infection and autoimmune disease: The role of CD40 in lymphocyte homeostasis." *Seminars in Immunology* **21**(5): 283-288.

Murtaugh MP and Foss DL (2002). "Inflammatory cytokines and antigen presenting cell activation." *Veterinary Immunology and Immunopathology* **87**(3-4): 109-121.

Murthy VN and Stevens CF (1998). "Synaptic vesicles retain their identity through the endocytic cycle." *Nature* **392**(6675): 497-501.

Muzio L, Martino G and Furlan R (2007). "Multifaceted aspects of inflammation in multiple sclerosis: the role of microglia." *J Neuroimmunol* **191**(1-2): 39-44.

Myer DJ, Gurkoff GG, Lee SM, Hovda DA and Sofroniew MV (2006). "Essential protective roles of reactive astrocytes in traumatic brain injury." *Brain* **129**(Pt 10): 2761-2772.

Nagata S (1996). "Apoptosis: Telling cells their time is up." *Current Biology* **6**(10): 1241-1243.

Nakanishi Y, Lu B, Gerard C and Iwasaki A (2009). "CD8(+) T lymphocyte mobilization to virus-infected tissue requires CD4(+) T-cell help." *Nature* **462**(7272): 510-513.

Nedergaard M, Ransom B and Goldman SA (2003). "New roles for astrocytes: redefining the functional architecture of the brain." *Trends Neurosci* **26**(10): 523-530.

Neufeld EF (1991). "Lysosomal storage diseases." *Annu Rev Biochem* **60**: 257-280.

Neumann H (2001). "Control of glial immune function by neurons." *Glia* **36**(2): 191-199.

Neumann H, Medana IM, Bauer J and Lassmann H (2002). "Cytotoxic T lymphocytes in autoimmune and degenerative CNS diseases." *Trends in Neurosciences* **25**(6): 313-319.

Neumann H, Schmidt H, Cavalie A, Jenne D and Wekerle H (1997). "Major histocompatibility complex (MHC) class I gene expression in single neurons of the central nervous system: differential regulation by interferon (IFN)-gamma and tumor necrosis factor (TNF)-alpha." *J Exp Med* **185**(2): 305-316.

Neumann H and Wekerle H (1998). "Neuronal control of the immune response in the central nervous system: Linking brain immunity to neurodegeneration." *Journal of Neuropathology and Experimental Neurology* **57**(1): 1-9.

Neumann J, Gunzer M, Gutzeit HO, Ullrich O, Reymann KG and Dinkel K (2006). "Microglia provide neuroprotection after ischemia." *FASEB J* **20**(6): 714-716.

Nicholson SM, Haynes LM, Vanderlugt CL, Miller SD and Melvold RW (1999). "The role of protective CD8+ T cells in resistance of BALB/c mice to Theiler's murine encephalomyelitis virus-induced demyelinating disease: regulatory vs. lytic." *J Neuroimmunol* **98**(2): 136-146.

Nielsen CH and Leslie RG (2002). "Complement's participation in acquired immunity." *J Leukoc Biol* **72**(2): 249-261.

Nijssen PC, Ceuterick C, van Diggelen OP, Elleder M, Martin JJ, Teepen JL, Tyynela J and Roos RA (2003). "Autosomal dominant adult neuronal ceroid lipofuscinosis: a novel form of NCL with granular osmiophilic deposits without palmitoyl protein thioesterase 1 deficiency." *Brain Pathol* **13**(4): 574-581.

Nimmerjahn A, Kirchhoff F and Helmchen F (2005). "Resting microglial cells are highly dynamic surveillants of brain parenchyma in vivo." *Science* **308**(5726): 1314-1318.

Nishimura M, Wakana S, Kakinuma S, Mita K, Ishii H, Kobayashi S, Ogiu T, Sado T and Shimada Y (1999). "Low frequency of Ras gene mutation in spontaneous and gamma-ray-induced thymic lymphomas of scid mice." *Radiat Res* **151**(2): 142-149.

Nixon RA and Cataldo AM (1995). "The endosomal-lysosomal system of neurons: new roles." *Trends Neurosci* **18**(11): 489-496.

Nixon RA and Cataldo AM (2006). "Lysosomal system pathways: genes to neurodegeneration in Alzheimer's disease." *Journal of Alzheimer's disease : JAD* **9**(3 Suppl): 277-289.

Norment A and Littman D (1988). "Human CD8 binds class I MHC molecules." *FASEB Journal* **2**(4): 3341.

Nutku E, Aizawa H, Hudson SA and Bochner BS (2003). "Ligation of Siglec-8: a selective mechanism for induction of human eosinophil apoptosis." *Blood* **101**(12): 5014-5020.

O'Reilly MK and Paulson JC (2009). "Siglecs as targets for therapy in immune-cell-mediated disease." *Trends Pharmacol Sci* **30**(5): 240-248.

Obara M, Szeliga M and Albrecht J (2008). "Regulation of pH in the mammalian central nervous system under normal and pathological conditions: facts and hypotheses." *Neurochem Int* **52**(6): 905-919.

Odoardi F, Sie C, Streyl K, Ulaganathan VK, Schlager C, Lodygin D, Heckelsmiller K, Nietfeld W, Ellwart J, Klinkert WE, Lottaz C, Nosov M, Brinkmann V, Spang R, Lehrach H, Vingron M, Wekerle H, Flugel-Koch C and Flugel A (2012). "T cells become licensed in the lung to enter the central nervous system." *Nature* **488**(7413): 675-679.

Oetke C, Vinson MC, Jones C and Crocker PR (2006). "Sialoadhesin-Deficient Mice Exhibit Subtle Changes in B- and T-Cell Populations and Reduced Immunoglobulin M Levels." *Mol. Cell. Biol.* **26**(4): 1549-1557.

Oettinger MA, Schatz DG, Gorka C and Baltimore D (1990). "RAG-1 and RAG-2, adjacent genes that synergistically activate V(D)J recombination." *Science* **248**(4962): 1517-1523.

Ohmi K, Greenberg DS, Rajavel KS, Ryazantsev S, Li HH and Neufeld EF (2003). "Activated microglia in cortex of mouse models of mucopolysaccharidoses I and IIIB." *Proceedings of the National Academy of Sciences of the United States of America* **100**(4): 1902-1907.

Ohtsubo K and Marth JD (2006). "Glycosylation in cellular mechanisms of health and disease." *Cell* **126**(5): 855-867.

Olson JK, Girvin AM and Miller SD (2001). "Direct activation of innate and antigen-presenting functions of microglia following infection with Theiler's virus." *J Virol* **75**(20): 9780-9789.

Omari KM and Dorovini-Zis K (2003). "CD40 expressed by human brain endothelial cells regulates CD4+T cell adhesion to endothelium." *Journal of Neuroimmunology* **134**(1-2): 166-178.

Orban PC, Chui D and Marth JD (1992). "Tissue- and site-specific DNA recombination in transgenic mice." *Proc Natl Acad Sci U S A* **89**(15): 6861-6865.

Oswald MJ, Palmer DN, Kay GW, Barwell KJ and Cooper JD (2008). "Location and connectivity determine GABAergic interneuron survival in the brains of South Hampshire sheep with CLN6 neuronal ceroid lipofuscinosis." *Neurobiol Dis* **32**(1): 50-65.

Oswald MJ, Palmer DN, Kay GW, Shemilt SJA, Rezaie P and Cooper JD (2005). "Glial activation spreads from specific cerebral foci and precedes neurodegeneration in presymptomatic ovine neuronal ceroid lipofuscinosis (CLN6)." *Neurobiology of Disease* **20**(1): 49-63.

Ousman SS and David S (2000). "Lysophosphatidylcholine induces rapid recruitment and activation of macrophages in the adult mouse spinal cord." *Glia* **30**(1): 92-104.

Owens T, Bechmann I and Engelhardt B (2008). "Perivascular spaces and the two steps to neuroinflammation." *J Neuropathol Exp Neurol* **67**(12): 1113-1121.

Padilla-Lopez S and Pearce DA (2006). "Saccharomyces cerevisiae lacking Btn1p modulate vacuolar ATPase activity to regulate pH imbalance in the vacuole." *J Biol Chem* **281**(15): 10273-10280.

Page LJ, Darmon AJ, Uellner R and Griffiths GM (1998). "L is for lytic granules: lysosomes that kill." *Biochim Biophys Acta* **1401**(2): 146-156.

Pais TF, Figueiredo C, Peixoto R, Braz MH and Chatterjee S (2008). "Necrotic neurons enhance microglial neurotoxicity through induction of glutaminase by a MyD88-dependent pathway." *J Neuroinflammation* **5**: 43.

Palmer DN, Fearnley IM, Walker JE, Hall NA, Lake BD, Wolfe LS, Haltia M, Martinus RD and Jolly RD (1992). "Mitochondrial ATP synthase subunit c storage in the ceroid-lipofuscinoses (Batten disease)." *Am J Med Genet* **42**(4): 561-567.

Palmer DN, Oswald MJ, Westlake VJ and Kay GW (2002). "The origin of fluorescence in the neuronal ceroid lipofuscinoses (Batten disease) and neuron cultures from affected sheep for studies of neurodegeneration." *Arch Gerontol Geriatr* **34**(3): 343-357.

Pan T, Kondo S, Le W and Jankovic J (2008). "The role of autophagy-lysosome pathway in neurodegeneration associated with Parkinson's disease." *Brain* **131**(Pt 8): 1969-1978.

Pape KA, Catron DM, Itano AA and Jenkins MK (2007). "The humoral immune response is initiated in lymph nodes by B cells that acquire soluble antigen directly in the follicles." *Immunity* **26**(4): 491-502.

Parkinson-Lawrence EJ, Shandala T, Prodoehl M, Plew R, Borlace GN and Brooks DA (2010). "Lysosomal Storage Disease: Revealing Lysosomal Function and Physiology." *Physiology* **25**(2): 102-115.

Partanen S, Haapanen A, Kielar C, Pontikis C, Alexander N, Inkinen T, Saftig P, Gillingwater TH, Cooper JD and Tyynela J (2008). "Synaptic changes in the thalamocortical system of cathepsin D-deficient mice: A model of human congenital neuronal ceroid-lipofuscinosis." *Journal of Neuropathology and Experimental Neurology* **67**(1): 16-29.

Parton RG and Dotti CG (1993). "Cell biology of neuronal endocytosis." *Journal of Neuroscience Research* **36**(1): 1-9.

Parviainen L (2012). Mutant glia impair health of neurons in Juvenile NCL. 13th International Conference on Neuronal Ceroid Lipofuscinoses (Batten Disease) (NCL 2012). O. P. 11. *Royal Holloway College, London, UK.*

Patterson WP and Caldwell CW (1992). "CD45 expression and up-regulation in monocytes." *Clinical Research* **40**(3): A694-A694.

Paul S and Lombroso PJ (2003). "Receptor and nonreceptor protein tyrosine phosphatases in the nervous system." *Cellular and Molecular Life Sciences* **60**(11): 2465-2482.

Paul WE and Seder RA (1994). "Lymphocyte responses and cytokines." *Cell* **76**(2): 241-251.

Paulson JC, Macauley MS, Kawasaki N and Annals NYAS (2012). Siglecs as sensors of self in innate and adaptive immune responses. Glycobiology of the Immune Response. Oxford, Blackwell Science Publ. **1253:** 37-48.

Pavlov VA and Tracey KJ (2004). "Neural regulators of innate immune responses and inflammation." *Cell Mol Life Sci* **61**(18): 2322-2331.

Paxinos G and Franklin B (2001). The Mouse Brain in Stereotaxic Coordinates. *San Diego*, CA: Academic Press.

Payes A, Zanon RG, Pierucci A and Oliveira ALR (2008). "MHC class I upregulation is not sufficient to rescue neonatal alpha motoneurons after peripheral axotomy." *Brain Research* **1238**: 23-30.

Pearce DA, Ferea T, Nosel SA, Das B and Sherman F (1999). "Action of BTN1, the yeast orthologue of the gene mutated in Batten disease." *Nat Genet* **22**(1): 55-58.

Pearce DA and Sherman F (1998). "A yeast model for the study of Batten disease." *Proc Natl Acad Sci U S A* **95**(12): 6915-6918.

Pears MR, Cooper JD, Mitchison HM, Mortishire-Smith RJ, Pearce DA and Griffin JL (2005). "High resolution 1H NMR-based metabolomics indicates a neurotransmitter cycling deficit in cerebral tissue from a mouse model of Batten disease." *J Biol Chem* **280**(52): 42508-42514.

Pekny M and Nilsson M (2005). "Astrocyte activation and reactive gliosis." *Glia* **50**(4): 427-434.

Pellerin L, Bouzier-Sore AK, Aubert A, Serres S, Merle M, Costalat R and Magistretti PJ (2007). "Activity-dependent regulation of energy metabolism by astrocytes: an update." *Glia* **55**(12): 1251-1262.

Penna G, Vulcano M, Roncari A, Facchetti F, Sozzani S and Adorini L (2002). "Cutting edge: Differential chemokine production by myeloid and plasmacytoid dendritic cells." *Journal of Immunology* **169**(12): 6673-6676.

Perea G, Navarrete M and Araque A (2009). "Tripartite synapses: astrocytes process and control synaptic information." *Trends Neurosci* **32**(8): 421-431.

Peress NS, Perillo E and Fenstermacher JD (1989). "Circumventricular organs in chronic serum sickness: a model for cerebral lupus." *Biol Psychiatry* **26**(4): 397-407.

Perry VH (2004). "The influence of systemic inflammation on inflammation in the brain: implications for chronic neurodegenerative disease." *Brain Behav Immun* **18**(5): 407-413.

Perry VH, Bell MD, Brown HC and Matyszak MK (1995). "Inflammation in the nervous system." *Curr Opin Neurobiol* **5**(5): 636-641.

Perry VH, Crocker PR and Gordon S (1992). "The blood-brain barrier regulates the expression of a macrophage sialic acid-binding receptor on microglia." *Journal of Cell Science* **101**(1): 201-207.

Perry VH and Gordon S (1988). "Macrophages and microglia in the nervous system." *Trends Neurosci* **11**(6): 273-277.

Persaud-Sawin DA and Boustany RM (2005). "Cell death pathways in juvenile Batten disease." *Apoptosis* **10**(5): 973-985.

Persidsky Y, Ramirez SH, Haorah J and Kanmogne GD (2006). "Blood-brain barrier: structural components and function under physiologic and pathologic conditions." *J Neuroimmune Pharmacol* **1**(3): 223-236.

Peters C, Braun M, Weber B, Wendland M, Schmidt B, Pohlmann R, Waheed A and von Figura K (1990). "Targeting of a lysosomal membrane protein: a tyrosine-containing endocytosis signal in the cytoplasmic tail of lysosomal acid phosphatase is necessary and sufficient for targeting to lysosomes." *EMBO J* **9**(11): 3497-3506.

Peters PJ, Borst J, Oorschot V, Fukuda M, Krahenbuhl O, Tschopp J, Slot JW and Geuze HJ (1991). "Cytotoxic T lymphocyte granules are secretory lysosomes, containing both perforin and granzymes." *J Exp Med* **173**(5): 1099-1109.

Petty MA and Lo EH (2002). "Junctional complexes of the blood–brain barrier: permeability changes in neuroinflammation." *Progress in Neurobiology* **68**(5): 311-323.

Phan TG, Green JA, Gray EE, Xu Y and Cyster JG (2009). "Immune complex relay by subcapsular sinus macrophages and noncognate B cells drives antibody affinity maturation." *Nat Immunol* **10**(7): 786-793.

Phares TW, Stohlman SA, Hwang M, Min B, Hinton DR and Bergmann CC (2012). "CD4 T Cells Promote CD8 T Cell Immunity at the Priming and Effector Site during Viral Encephalitis." *Journal of Virology* **86**(5): 2416-2427.

Phillips SN, Muzaffar N, Codlin S, Korey CA, Taschner PE, de Voer G, Mole SE and Pearce DA (2006). "Characterizing pathogenic processes in Batten disease: use of small eukaryotic model systems." *Biochim Biophys Acta* **1762**(10): 906-919.

Pillai S, Netravali IA, Cariappa A and Mattoo H (2012). "Siglecs and immune regulation." *Annu Rev Immunol* **30**: 357-392.

Pirko I, Chen Y, Lohrey AK, McDole J, Gamez JD, Allen KS, Pavelko KD, Lindquist DM, Dunn RS, Macura SI and Johnson AJ (2012). "Contrasting roles for CD4 vs. CD8 T-cells in a murine model of virally induced "T1 black hole" formation." *Plos One* **7**(2): e31459.

Pluchino S, Zanotti L, Rossi B, Brambilla E, Ottoboni L, Salani G, Martinello M, Cattalini A, Bergami A, Furlan R, Comi G, Constantin G and Martino G (2005). "Neurosphere-derived multipotent precursors promote neuroprotection by an immunomodulatory mechanism." *Nature* **436**(7048): 266-271.

Polikov VS, Hong JS and Reichert WM (2010). "Soluble factor effects on glial cell reactivity at the surface of gel-coated microwires." *J Neurosci Methods* **190**(2): 180-187.

Pollard JW (2009). "Trophic macrophages in development and disease." *Nat Rev Immunol* **9**(4): 259-270.

Pontikis CC, Cella CV, Parihar N, Lim MJ, Chakrabarti S, Mitchison HM, Mobley WC, Rezaie P, Pearce DA and Cooper JD (2004). "Late onset neurodegeneration in the Cln(3-/-) mouse model of juvenile neuronal ceroid lipofuscinosis is preceded by low level glial activation." *Brain Research* **1023**(2): 231-242.

Pontikis CC, Cotman SL, MacDonald ME and Cooper JD (2005). "Thalamocortical neuron loss and localized astrocytosis in the Cln3(triangle ex7/8) knock-in mouse model of Batten disease." *Neurobiology of Disease* **20**(3): 823-836.

Powell LD and Varki A (1995). "I-type lectins." *J Biol Chem* **270**(24): 14243-14246.

Presta M, Urbinati C, Dell'era P, Lauro GM, Sogos V, Balaci L, Ennas MG and Gremo F (1995). "Expression of basic fibroblast growth factor and its receptors in human fetal microglia cells." *Int J Dev Neurosci* **13**(1): 29-39.

Prinz M, Priller J, Sisodia SS and Ransohoff RM (2011). "Heterogeneity of CNS myeloid cells and their roles in neurodegeneration." *Nat Neurosci* **14**(10): 1227-1235.

Puranam KL, Guo WX, Qian WH, Nikbakht K and Boustany RM (1999). "CLN3 defines a novel antiapoptotic pathway operative in neurodegeneration and mediated by ceramide." *Mol Genet Metab* **66**(4): 294-308.

Qiao X, Lu JY and Hofmann SL (2007). "Gene expression profiling in a mouse model of infantile neuronal ceroid lipofuscinosis reveals upregulation of immediate early genes and mediators of the inflammatory response." *BMC Neurosci* **8**: 95.

Quan N and Herkenham M (2002). "Connecting cytokines and brain: A review of current issues." *Histology and Histopathology* **17**(1): 273-288.

Raivich G, Bohatschek M, Kloss CUA, Werner A, Jones LL and Kreutzberg GW (1999). "Neuroglial activation repertoire in the injured brain: graded response, molecular mechanisms and cues to physiological function." *Brain Research Reviews* **30**(1): 77-105.

Rakheja D, Narayan SB, Pastor JV and Bennett MJ (2004). "CLN3P, the Batten disease protein, localizes to membrane lipid rafts (detergent-resistant membranes)." *Biochem Biophys Res Commun* **317**(4): 988-991.

Ramirez-Montealegre D and Pearce DA (2005). "Defective lysosomal arginine transport in juvenile Batten disease." *Human Molecular Genetics* **14**(23): 3759-3773.

Ramon y Cajal S (1928). Degeneration and Regeneration of the Nervous System. *London, UK*, Oxford University Press.

Ransohoff RM and Brown MA (2012). "Innate immunity in the central nervous system." *J Clin Invest* **122**(4): 1164-1171.

Ransohoff RM, Kivisakk P and Kidd G (2003). "Three or more routes for leukocyte migration into the central nervous system." *Nature Reviews Immunology* **3**(7): 569-581.

Ransohoff RM and Perry VH (2009). "Microglial physiology: unique stimuli, specialized responses." *Annu Rev Immunol* **27**: 119-145.

Ransohoff RM and Tani M (1998). "Do chemokines mediate leukocyte recruitment in post-traumatic CNS inflammation?" *Trends Neurosci* **21**(4): 154-159.

Rapola J (1994). "Lysosomal storage diseases in adults." *Pathol Res Pract* **190**(8): 759-766.

Raposo G, Fevrier B, Stoorvogel W and Marks MS (2002). "Lysosome-related organelles: a view from immunity and pigmentation." *Cell Struct Funct* **27**(6): 443-456.

Reijerkerk A, Lakeman KAM, Drexhage JAR, van het Hof B, van Wijck Y, van der Pol SMA, Kooij G, Geerts D and de Vries HE (2012). "Brain endothelial barrier passage by monocytes is controlled by the endothelin system." *Journal of Neurochemistry* **121**(5): 730-737.

Reinke E and Fabry Z (2006). "Breaking or making immunological privilege in the central nervous system: the regulation of immunity by neuropeptides." *Immunol Lett* **104**(1-2): 102-109.

Rempel H, Calosing C, Sun B and Pulliam L (2008). "Sialoadhesin expressed on IFN-induced monocytes binds HIV-1 and enhances infectivity." *Plos One* **3**(4): e1967.

Rensing-Ehl A, Malipiero U, Irmler M, Tschopp J, Constam D and Fontana A (1996). "Neurons induced to express major histocompatibility complex class I antigen are killed via the perforin and not the Fas (APO-1/CD95) pathway." *Eur J Immunol* **26**(9): 2271-2274.

Revilla C, Poderoso T, Martinez P, Alvarez B, Lopez-Fuertes L, Alonso F, Ezquerra A and Dominguez J (2009). "Targeting to porcine sialoadhesin receptor improves antigen presentation to T cells." *Vet Res* **40**(3): 14.

Richards MH, Getts MT, Podojil JR, Jin YH, Kim BS and Miller SD (2011). "Virus expanded regulatory T cells control disease severity in the Theiler's virus mouse model of MS." *J Autoimmun* **36**(2): 142-154.

Richartz-Salzburger E, Batra A, Stransky E, Laske C, Kohler N, Bartels M, Buchkremer G and Schott K (2007). "Altered lymphocyte distribution in Alzheimer's disease." *Journal of Psychiatric Research* **41**(1-2): 174-178.

Rinne JO, Ruottinen HM, Nagren K, Aberg LE and Santavuori P (2002). "Positron emission tomography shows reduced striatal dopamine D1 but not D2 receptors in juvenile neuronal ceroid lipofuscinosis." *Neuropediatrics* **33**(3): 138-141.

Rivest S (2009). "Regulation of innate immune responses in the brain." *Nature Reviews Immunology* **9**(6): 429-439.

Roberts MS, Macauley SL, Wong AM, Yilmas D, Hohm S, Cooper JD and Sands MS (2012). "Combination small molecule PPT1 mimetic and CNS-directed gene therapy as a treatment for infantile neuronal ceroid lipofuscinosis." *J Inherit Metab Dis*.

Roberts N, CruzOrive LM, Bourne M, Herfkens RJ, Karwoski RA and Whitehouse GH (1997). "Analysis of cardiac function by MRI and stereology." *Journal of Microscopy-Oxford* **187**: 31-42.

Rogers J, Mastroeni D, Leonard B, Joyce J, Grover A, Giacinto Bagetta MTC and Stuart AL (2007). Neuroinflammation in Alzheimer's Disease and Parkinson's Disease: Are Microglia Pathogenic in Either Disorder? International Review of Neurobiology, Academic Press. **Volume 82:** 235-246.

Romagnani S (1997). "The Th1/Th2 paradigm." *Immunology Today* **18**(6): 263-266.

Rosenberg GA (2002). "Matrix metalloproteinases in neuroinflammation." *Glia* **39**(3): 279-291.

Rothstein JD, Dykes-Hoberg M, Pardo CA, Bristol LA, Jin L, Kuncl RW, Kanai Y, Hediger MA, Wang Y, Schielke JP and Welty DF (1996). "Knockout of glutamate transporters reveals a major role for astroglial transport in excitotoxicity and clearance of glutamate." *Neuron* **16**(3): 675-686.

Rousselet E, Callebert J, Parain K, Joubert C, Hunot S, Hartmann A, Jacque C, Perez-Diaz F, Cohen-Salmon C, Launay JM and Hirsch EC (2002). "Role of TNF-alpha receptors in mice intoxicated with the parkinsonian toxin MPTP." *Exp Neurol* **177**(1): 183-192.

Rubartelli A and Lotze MT (2007). "Inside, outside, upside down: damage-associated molecular-pattern molecules (DAMPs) and redox." *Trends Immunol* **28**(10): 429-436.

Rubtsov YP, Rasmussen JP, Chi EY, Fontenot J, Castelli L, Ye X, Treuting P, Siewe L, Roers A, Henderson WR, Jr., Muller W and Rudensky AY (2008). "Regulatory T cell-derived interleukin-10 limits inflammation at environmental interfaces." *Immunity* **28**(4): 546-558.

Saftig P and Klumperman J (2009). "Lysosome biogenesis and lysosomal membrane proteins: trafficking meets function." *Nat Rev Mol Cell Biol* **10**(9): 623-635.

Saha A, Kim SJ, Zhang Z, Lee YC, Sarkar C, Tsai PC and Mukherjee AB (2008). "RAGE signaling contributes to neuroinflammation in infantile neuronal ceroid lipofuscinosis." *FEBS Lett* **582**(27): 3823-3831.

Saha A, Sarkar C, Singh SP, Zhang ZJ, Munasinghe J, Peng SY, Chandra G, Kong EY and Mukherjee AB (2012). "The blood-brain barrier is disrupted in a mouse model of infantile neuronal ceroid lipofuscinosis: amelioration by resveratrol." *Human Molecular Genetics* **21**(10): 2233-2244.

Sakaguchi S (2000). "Regulatory T cells: key controllers of immunologic self-tolerance." *Cell* **101**(5): 455-458.

Sakaguchi S (2004). "Naturally arising CD4+ regulatory t cells for immunologic self-tolerance and negative control of immune responses." *Annu Rev Immunol* **22**: 531-562.

Sakurai K, Iizuka S, Shen JS, Meng XL, Mori T, Umezawa A, Ohashi T and Eto Y (2004). "Brain transplantation of genetically modified bone marrow stromal cells corrects CNS pathology and cognitive function in MPS VII mice." *Gene Ther* **11**(19): 1475-1481.

Salgame P, Abrams JS, Clayberger C, Goldstein H, Convit J, Modlin RL and Bloom BR (1991). "Differing lymphokine profiles of functional subsets of human CD4 and CD8 T-cell clones." *Science* **254**(5029): 279-282.

Salonen T, Hellsten E, Horelli-Kuitunen N, Peltonen L and Jalanko A (1998). "Mouse palmitoyl protein thioesterase: gene structure and expression of cDNA." *Genome Res* **8**(7): 724-730.

Sands MS and Davidson BL (2006). "Gene therapy for lysosomal storage diseases." *Mol Ther* **13**(5): 839-849.

Sands MS, Vogler C, Torrey A, Levy B, Gwynn B, Grubb J, Sly WS and Birkenmeier EH (1997). "Murine mucopolysaccharidosis type VII: long term therapeutic effects of enzyme replacement and enzyme replacement followed by bone marrow transplantation." *J Clin Invest* **99**(7): 1596-1605.

Sann S, Wang Z, Brown H and Jin Y (2009). "Roles of endosomal trafficking in neurite outgrowth and guidance." *Trends Cell Biol* **19**(7): 317-324.

Santavuori P (1988). "Neuronal ceroid-lipofuscinoses in childhood." *Brain Dev* **10**(2): 80-83.

Santavuori P, Heiskala H, Autti T, Johansson E and Westermarck T (1989). "Comparison of the clinical courses in patients with juvenile neuronal ceroid lipofuscinosis receiving antioxidant treatment and those without antioxidant treatment." *Adv Exp Med Biol* **266**: 273-282.

Santavuori P, Lauronen L, Kirveskari E, Aberg L, Sainio K and Autti T (2000). "Neuronal ceroid lipofuscinoses in childhood." *Neurological Sciences* **21**(3): S35-S41.

Santavuori P, Rapola J, Sainio K and Raitta C (1982). "A variant of Jansky-Bielschowsky disease." *Neuropediatrics* **13**(3): 135-141.

Santavuori P, Vanhanen SL, Sainio K, Nieminen M, Wallden T, Launes J and Raininko R (1993). "Infantile neuronal ceroid-lipofuscinosis (INCL): diagnostic criteria." *J Inherit Metab Dis* **16**(2): 227-229.

Sapara A, Cooke M, Fannon D, Francis A, Buchanan RW, Anilkumar APP, Barkataki I, Aasen I, Kuipers E and Kumari V (2007). "Prefrontal cortex and insight in schizophrenia: A volumetric MRI study." *Schizophrenia Research* **89**(1-3): 22-34.

Sappington RM, Pearce DA and Calkins DJ (2003). "Optic Nerve Degeneration in a Murine Model of Juvenile Ceroid Lipofuscinosis." *Investigative Ophthalmology & Visual Science* **44**(9): 3725-3731.

Saraste J and Kuismanen E (1992). "Pathways of protein sorting and membrane traffic between the rough endoplasmic reticulum and the Golgi complex." *Semin Cell Biol* **3**(5): 343-355.

Sasaki N, Toki S, Chowei H, Saito T, Nakano N, Hayashi Y, Takeuchi M and Makita Z (2001). "Immunohistochemical distribution of the receptor for advanced glycation end products in neurons and astrocytes in Alzheimer's disease." *Brain Res* **888**(2): 256-262.

Sattler R and Rothstein JD (2006). "Regulation and dysregulation of glutamate transporters." *Handb Exp Pharmacol*(175): 277-303.

Sauer B and Henderson N (1988). "Site-specific DNA recombination in mammalian cells by the Cre recombinase of bacteriophage P1." *Proc Natl Acad Sci U S A* **85**(14): 5166-5170.

Saunders NR, Ek CJ, Habgood MD and Dziegielewska KM (2008). "Barriers in the brain: a renaissance?" *Trends Neurosci* **31**(6): 279-286.

Sawkar AR, Adamski-Werner SL, Cheng WC, Wong CH, Beutler E, Zimmer KP and Kelly JW (2005). "Gaucher disease-associated glucocerebrosidases show mutation-dependent chemical chaperoning profiles." *Chem Biol* **12**(11): 1235-1244.

Sayed BA, Christy AL, Walker ME and Brown MA (2010). "Meningeal Mast Cells Affect Early T Cell Central Nervous System Infiltration and Blood-Brain Barrier Integrity through TNF: A Role for Neutrophil Recruitment?" *Journal of Immunology* **184**(12): 6891-6900.

Scalabrino G (2009). "The multi-faceted basis of vitamin B12 (cobalamin) neurotrophism in adult central nervous system: Lessons learned from its deficiency." *Prog Neurobiol* **88**(3): 203-220.

Schadee-Eestermans IL, Hoefsmit EC, van de Ende M, Crocker PR, van den Berg TK and Dijkstra CD (2000). "Ultrastructural localisation of sialoadhesin (siglec-1) on macrophages in rodent lymphoid tissues." *Immunobiology* **202**(4): 309-325.

Schaeffer M, Han SJ, Chtanova T, van Dooren GG, Herzmark P, Chen Y, Roysam B, Striepen B and Robey EA (2009). "Dynamic Imaging of T Cell-Parasite Interactions in the Brains of Mice Chronically Infected with Toxoplasma gondii." *Journal of Immunology* **182**(10): 6379-6393.

Schall TJ, Bacon K, Toy KJ and Goeddel DV (1990). "Selective attraction of monocytes and T lymphocytes of the memory phenotype by cytokine RANTES." *Nature* **347**(6294): 669-671.

Schall TJ, Jongstra J, Dyer BJ, Jorgensen J, Clayberger C, Davis MM and Krensky AM (1988). "A human T cell-specific molecule is a member of a new gene family." *J Immunol* **141**(3): 1018-1025.

Schatz DG, Oettinger MA and Baltimore D (1989). "The V(D)J recombination activating gene, RAG-1." *Cell* **59**(6): 1035-1048.

Schenten D and Medzhitov R (2011). "The control of adaptive immune responses by the innate immune system." *Adv Immunol* **109**: 87-124.

Schlett K (2006). "Glutamate as a modulator of embryonic and adult neurogenesis." *Current Topics in Medicinal Chemistry* **6**(10): 949-960.

Schlissel M, Constantinescu A, Morrow T, Baxter M and Peng A (1993). "Double-strand signal sequence breaks in V(D)J recombination are blunt, 5'-phosphorylated, RAG-dependent, and cell cycle regulated." *Genes Dev* **7**(12B): 2520-2532.

Schmid D and Munz C (2005). "Immune surveillance of intracellular pathogens via autophagy." *Cell Death Differ* **12 Suppl 2**: 1519-1527.

Schmiedt ML, Blom T, Blom T, Kopra O, Wong A, von Schantz-Fant C, Ikonen E, Kuronen M, Jauhiainen M, Cooper JD and Jalanko A (2012). "Cln5-deficiency in mice leads to microglial activation, defective myelination and changes in lipid metabolism." *Neurobiology of Disease* **46**(1): 19-29.

Schmitz C and Hof PR (2005). "Design-based stereology in neuroscience." *Neuroscience* **130**(4): 813-831.

Schnell L, Fearn S, Klassen H, Schwab ME and Perry VH (1999). "Acute inflammatory responses to mechanical lesions in the CNS: differences between brain and spinal cord." *European Journal of Neuroscience* **11**(10): 3648-3658.

Schroder R and Linke RP (1999). "Cerebrovascular involvement in systemic AA and AL amyloidosis: a clear haematogenic pattern." *Virchows Arch* **434**(6): 551-560.

Schroeter M and Jander S (2005). "T-cell cytokines in injury-induced neural damage and repair." *NeuroMolecular Medicine* **7**(3): 183-195.

Schuler W, Weiler IJ, Schuler A, Phillips RA, Rosenberg N, Mak TW, Kearney JF, Perry RP and Bosma MJ (1986). "Rearrangement of antigen receptor genes is defective in mice with severe combined immune deficiency." *Cell* **46**(7): 963-972.

Schultz ML, Tecedor L, Chang M and Davidson BL (2011). "Clarifying lysosomal storage diseases." *Trends in Neurosciences* **34**(8): 401-410.

Schulz M and Engelhardt B (2005). "The circumventricular organs participate in the immunopathogenesis of experimental autoimmune encephalomyelitis." *Cerebrospinal Fluid Res* **2**: 8.

Schwab N, Bien CG, Waschbisch A, Becker A, Vince GH, Dornmair K and Wiendl H (2009). "CD8+ T-cell clones dominate brain infiltrates in Rasmussen encephalitis and persist in the periphery." *Brain* **132**(Pt 5): 1236-1246.

Schwartz M and Kipnis J (2005). "Protective autoimmunity and neuroprotection in inflammatory and noninflammatory neurodegenerative diseases." *Journal of the Neurological Sciences* **233**(1-2): 163-166.

Schwartz RH, Yano A and Paul WE (1978). "Interaction between antigen-presenting cells and primed T-lymphocytes - assessment of IR gene-expression in antigen-presenting cell." *Immunological Reviews* **40**: 153-180.

Scriver CR, Sly WS, Childs B, Beaudet AL, Valle D, Kinzler KW and Vogelstein B (2001). The Metabolic and Molecular Bases of Inherited Disease. *New York*, McGraw-Hill Professional.

Seder RA and Ahmed R (2003). "Similarities and differences in CD4(+) and CD8(+) effector and memory T cell generation." *Nature Immunology* **4**(9): 835-842.

Seehafer SS, Ramirez-Montealegre D, Wong AMS, Chan CH, Castaneda J, Horak M, Ahmadi SM, Lim MJ, Cooper JD and Pearce DA (2011). "Immunosuppression alters disease severity in juvenile Batten disease mice." *Journal of Neuroimmunology* **230**(1-2): 169-172.

Segura E and Villadangos JA (2009). "Antigen presentation by dendritic cells in vivo." *Curr Opin Immunol* **21**(1): 105-110.

Seifert G, Schilling K and Steinhauser C (2006). "Astrocyte dysfunction in neurological disorders: a molecular perspective." *Nat Rev Neurosci* **7**(3): 194-206.

Seifert U, Maranon C, Shmueli A, Desoutter JF, Wesoloski L, Janek K, Henklein P, Diescher S, Andrieu M, de la Salle H, Weinschenk T, Schild H, Laderach D, Galy A, Haas G, Kloetzel PM, Reiss Y and Hosmalin A (2003). "An essential role for

tripeptidyl peptidase in the generation of an MHC class I epitope." *Nat Immunol* **4**(4): 375-379.

Seitz RJ, Heininger K, Schwendemann G, Toyka KV and Wechsler W (1985). "The mouse blood-brain barrier and blood-nerve barrier for IgG: a tracer study by use of the avidin-biotin system." *Acta Neuropathol* **68**(1): 15-21.

Sellers RS, Clifford CB, Treuting PM and Brayton C (2012). "Immunological Variation Between Inbred Laboratory Mouse Strains: Points to Consider in Phenotyping Genetically Immunomodified Mice." *Veterinary Pathology* **49**(1): 32-43.

Serafini B, Rosicarelli B, Magliozzi R, Stigliano E, Capello E, Mancardi GL and Aloisi F (2006). "Dendritic cells in multiple sclerosis lesions: Maturation stage, myelin uptake, and interaction with proliferating T cells." *Journal of Neuropathology and Experimental Neurology* **65**(2): 124-141.

Serody JS, Burkett SE, Panoskaltsis-Mortari A, Ng-Cashin J, McMahon E, Matsushima GK, Lira SA, Cook DN and Blazar BR (2000). "T-lymphocyte production of macrophage inflammatory protein-1alpha is critical to the recruitment of CD8(+) T cells to the liver, lung, and spleen during graft-versus-host disease." *Blood* **96**(9): 2973-2980.

Serpe CJ, Coers S, Sanders VM and Jones KJ (2003). "CD4+ T, but not CD8+ or B, lymphocytes mediate facial motoneuron survival after facial nerve transection." *Brain Behav Immun* **17**(5): 393-402.

Seta N and Kuwana M (2007). "Human circulating monocytes as multipotential progenitors." *Keio Journal of Medicine* **56**(2): 41-47.

Settembre C, Fraldi A, Rubinsztein DC and Ballabio A (2008). "Lysosomal storage diseases as disorders of autophagy." *Autophagy* **4**(1): 113-114.

Seyerl M, Kirchberger S, Majdic O, Seipelt J, Jindra C, Schrauf C and Stockl J (2010). "Human rhinoviruses induce IL-35-producing Treg via induction of B7-H1 (CD274) and sialoadhesin (CD169) on DC." *Eur J Immunol* **40**(2): 321-329.

Shacka JJ (2012). "Mouse models of neuronal ceroid lipofuscinoses: Useful pre-clinical tools to delineate disease pathophysiology and validate therapeutics." *Brain Research Bulletin* **88**(1): 43-57.

Shedlock DJ and Shen H (2003). "Requirement for CD4 T cell help in generating functional CD8 T cell memory." *Science* **300**(5617): 337-339.

Shevach EM (2002). "CD4+ CD25+ suppressor T cells: more questions than answers." *Nat Rev Immunol* **2**(6): 389-400.

Shigetomi E, Bowser DN, Sofroniew MV and Khakh BS (2008). "Two forms of astrocyte calcium excitability have distinct effects on NMDA receptor-mediated slow inward currents in pyramidal neurons." *J Neurosci* **28**(26): 6659-6663.

Shinkai Y, Rathbun G, Lam KP, Oltz EM, Stewart V, Mendelsohn M, Charron J, Datta M, Young F, Stall AM and et al. (1992). "RAG-2-deficient mice lack mature lymphocytes owing to inability to initiate V(D)J rearrangement." *Cell* **68**(5): 855-867.

Shoenfeld Y, Beresovski A, Zharhary D, Tomer Y, Swissa M, Sela E, Zimran A, Zevin S, Gilburd B and Blank M (1995). "Natural autoantibodies in sera of patients with Gauchers-Disease." *Journal of Clinical Immunology* **15**(6): 363-372.

Shresta S, Pham CTN, Thomas DA, Graubert TA and Ley TJ (1998). "How do cytotoxic lymphocytes kill their targets?" *Current Opinion in Immunology* **10**(5): 581-587.

Shrikant P and Benveniste EN (1996). "The central nervous system as an immunocompetent organ - Role of glial cells in antigen presentation." *Journal of Immunology* **157**(5): 1819-1822.

Shyng C (2012). A small molecule anti-inflammatory enhances the therapeutic effects of AAV-mediated CNS-directed gene therapy for infantile neuronal ceroid lipofuscinosis. 13th International Conference on Neuronal Ceroid Lipofuscinoses (Batten Disease) (NCL 2012) O. P. 43. *Royal Holloway College, London, UK.*

Siintola E, Lehesjoki AE and Mole SE (2006). "Molecular genetics of the NCLs -- status and perspectives." *Biochim Biophys Acta* **1762**(10): 857-864.

Simard M and Nedergaard M (2004). "The neurobiology of glia in the context of water and ion homeostasis." *Neuroscience* **129**(4): 877-896.

Simon MI, Strathmann MP and Gautam N (1991). "Diversity of G proteins in signal transduction." *Science* **252**(5007): 802-808.

Sims TN and Dustin ML (2002). "The immunological synapse: integrins take the stage." *Immunol Rev* **186**: 100-117.

Siso S, Jeffrey M and Gonzalez L (2010). "Sensory circumventricular organs in health and disease." *Acta Neuropathologica* **120**(6): 689-705.

Sitter B, Autti T, Tyynela J, Sonnewald U, Bathen TF, Puranen J, Santavuori P, Haltia MJ, Paetau A, Polvikoski T, Gribbestad IS and Hakkinen AM (2004). "High-resolution magic angle spinning and 1H magnetic resonance spectroscopy reveal significantly altered neuronal metabolite profiles in CLN1 but not in CLN3." *J Neurosci Res* **77**(5): 762-769.

Sleat DE, Gin RM, Sohar I, Wisniewski K, Sklower-Brooks S, Pullarkat RK, Palmer DN, Lerner TJ, Boustany RM, Uldall P, Siakotos AN, Donnelly RJ and Lobel P (1999). "Mutational analysis of the defective protease in classic late-infantile neuronal ceroid lipofuscinosis, a neurodegenerative lysosomal storage disorder." *Am J Hum Genet* **64**(6): 1511-1523.

Sofroniew MV (2005). "Reactive astrocytes in neural repair and protection." *Neuroscientist* **11**(5): 400-407.

Sofroniew MV (2009). "Molecular dissection of reactive astrogliosis and glial scar formation." *Trends Neurosci* **32**(12): 638-647.

Sofroniew MV, Howe CL and Mobley WC (2001). "Nerve growth factor signaling, neuroprotection, and neural repair." *Annu Rev Neurosci* **24**: 1217-1281.

Sofroniew MV and Vinters HV (2010). "Astrocytes: biology and pathology." *Acta Neuropathol* **119**(1): 7-35.

Soghoian DZ and Streeck H (2010). "Cytolytic CD4(+) T cells in viral immunity." *Expert Rev Vaccines* **9**(12): 1453-1463.

Sondhi D, Hackett NR, Peterson DA, Stratton J, Baad M, Travis KM, Wilson JM and Crystal RG (2007). "Enhanced survival of the LINCL mouse following CLN2 gene transfer using the rh.10 rhesus macaque-derived adeno-associated virus vector." *Mol Ther* **15**(3): 481-491.

Song JW, Misgeld T, Kang H, Knecht S, Lu J, Cao Y, Cotman SL, Bishop DL and Lichtman JW (2008). "Lysosomal activity associated with developmental axon pruning." *J Neurosci* **28**(36): 8993-9001.

Springer TA (1994). "Traffic signals for lymphocyte recirculation and leukocyte emigration: the multistep paradigm." *Cell* **76**(2): 301-314.

Sriram K, Miller DB and O'Callaghan JP (2006). "Minocycline attenuates microglial activation but fails to mitigate striatal dopaminergic neurotoxicity: role of tumor necrosis factor-alpha." *J Neurochem* **96**(3): 706-718.

Sta M, Sylva-Steenland RMR, Casula M, de Jong J, Troost D, Aronica E and Baas F (2011). "Innate and adaptive immunity in amyotrophic lateral sclerosis: Evidence of complement activation." *Neurobiology of Disease* **42**(3): 211-220.

Stadelmann C, Wegner C and Brueck W (2011). "Inflammation, demyelination, and degeneration - Recent insights from MS pathology." *Biochimica et Biophysica Acta (BBA) - Molecular Basis of Disease* **1812**(2): 275-282.

Staropoli JF, Haliw L, Biswas S, Garrett L, Holter SM, Becker L, Skosyrski S, Da Silva-Buttkus P, Calzada-Wack J, Neff F, Rathkolb B, Rozman J, Schrewe A, Adler T, Puk O, Sun M, Favor J, Racz I, Bekeredjian R, Busch DH, Graw J, Klingenspor M, Klopstock T, Wolf E, Wurst W, Zimmer A, Lopez E, Harati H, Hill E, Krause DS, Guide J, Dragileva E, Gale E, Wheeler VC, Boustany R-M, Brown DE, Breton S, Ruether K, Gailus-Durner V, Fuchs H, de Angelis MH and Cotman SL (2012). "Large-Scale Phenotyping of an Accurate Genetic Mouse Model of JNCL Identifies Novel Early Pathology Outside the Central Nervous System." *Plos One* **7**(6): e38310.

Starr TK, Jameson SC and Hogquist KA (2003). "Positive and negative selection of T cells." *Annu Rev Immunol* **21**: 139-176.

Stein TD, Fedynyshyn JP and Kalil RE (2002). "Circulating autoantibodies recognize and bind dying neurons following injury to the brain." *J Neuropathol Exp Neurol* **61**(12): 1100-1108.

Steinman RM (1991). "The dendritic cell system and its role in immunogenicity." *Annu Rev Immunol* **9**: 271-296.

Stence N, Waite M and Dailey ME (2001). "Dynamics of microglial activation: a confocal time-lapse analysis in hippocampal slices." *Glia* **33**(3): 256-266.

Stephenson LM, Miller BC, Ng A, Eisenberg J, Zhao Z, Cadwell K, Graham DB, Mizushima NN, Xavier R, Virgin HW and Swat W (2009). "Identification of Atg5-dependent transcriptional changes and increases in mitochondrial mass in Atg5-deficient T lymphocytes." *Autophagy* **5**(5): 625-635.

Sterka D, Jr., Rati DM and Marriott I (2006). "Functional expression of NOD2, a novel pattern recognition receptor for bacterial motifs, in primary murine astrocytes." *Glia* **53**(3): 322-330.

Stevens B, Allen NJ, Vazquez LE, Howell GR, Christopherson KS, Nouri N, Micheva KD, Mehalow AK, Huberman AD, Stafford B, Sher A, Litke AM, Lambris JD, Smith SJ, John SW and Barres BA (2007). "The classical complement cascade mediates CNS synapse elimination." *Cell* **131**(6): 1164-1178.

Stinchcombe JC and Griffiths GM (1999). "Regulated secretion from hemopoietic cells." *J Cell Biol* **147**(1): 1-6.

Stockinger B and Veldhoen M (2007). "Differentiation and function of Th17 T cells." *Curr Opin Immunol* **19**(3): 281-286.

Stoll G and Jander S (1999). "The role of microglia and macrophages in the pathophysiology of the CNS." *Prog Neurobiol* **58**(3): 233-247.

Stone DK, Reynolds AD, Mosley RL and Gendelman HE (2009). "Innate and Adaptive Immunity for the Pathobiology of Parkinson's Disease." *Antioxidants & Redox Signaling* **11**(9): 2151-2166.

Storch S, Pohl S, Quitsch A, Falley K and Braulke T (2007). "C-terminal prenylation of the CLN3 membrane glycoprotein is required for efficient endosomal sorting to lysosomes." *Traffic* **8**(4): 431-444.

Stout RD (1993). "Macrophage activation by T cells: cognate and non-cognate signals." *Curr Opin Immunol* **5**(3): 398-403.

Streit WJ (2002). "Microglia as neuroprotective, immunocompetent cells of the CNS." *Glia* **40**(2): 133-139.

Streit WJ, Graeber MB and Kreutzberg GW (1988). "Functional plasticity of microglia: a review." *Glia* **1**(5): 301-307.

Streit WJ, Mrak RE and Griffin WS (2004). "Microglia and neuroinflammation: a pathological perspective." *J Neuroinflammation* **1**(1): 14.

Streit WJ and Xue QS (2009). "Life and death of microglia." *J Neuroimmune Pharmacol* **4**(4): 371-379.

Stromhaug PE and Klionsky DJ (2001). "Approaching the molecular mechanism of autophagy." *Traffic* **2**(8): 524-531.

Suda T, Okazaki T, Naito Y, Yokota T, Arai N, Ozaki S, Nakao K and Nagata S (1995). "Expression of the Fas ligand in cells of T cell lineage." *J Immunol* **154**(8): 3806-3813.

Sukardi H, Chng HT, Chan ECY, Gong ZY and Lam SH (2011). "Zebrafish for drug toxicity screening: bridging the in vitro cell-based models and in vivo mammalian models." *Expert Opinion on Drug Metabolism & Toxicology* **7**(5): 579-589.

Sun DM, Whitaker JN, Huang ZG, Liu D, Coleclough C, Wekerle H and Raine CS (2001). "Myelin antigen-specific CD8(+) T cells are encephalitogenic and produce severe disease in C57BL/6 mice." *Journal of Immunology* **166**(12): 7579-7587.

Suopanki J, Tyynela J, Baumann M and Haltia M (1999). "The expression of palmitoyl-protein thioesterase is developmentally regulated in neural tissues but not in nonneural tissues." *Mol Genet Metab* **66**(4): 290-293.

Suzuki K (1998). "Twenty five years of the "psychosine hypothesis": a personal perspective of its history and present status." *Neurochem Res* **23**(3): 251-259.

Suzuki K (2003). "Globoid cell leukodystrophy (Krabbe's disease): Update." *Journal of Child Neurology* **18**(9): 595-603.

Suzuki K, Johnson AB, Marquet E and Suzuki K (1968). "A case of juvenile lipidosis: electron microscopic, histochemical and biochemical studies." *Acta Neuropathol* **11**(2): 122-139.

Svensson M, Marsal J, Ericsson A, Carramolino L, Broden T, Marquez G and Agace WW (2002). "CCL25 mediates the localization of recently activated CD8alphabeta(+) lymphocytes to the small-intestinal mucosa." *J Clin Invest* **110**(8): 1113-1121.

Tai CY, Kim SA and Schuman EM (2008). "Cadherins and synaptic plasticity." *Curr Opin Cell Biol* **20**(5): 567-575.

Takahashi K, Donovan MJ, Rogers RA and Ezekowitz RA (1998). "Distribution of murine mannose receptor expression from early embryogenesis through to adulthood." *Cell Tissue Res* **292**(2): 311-323.

Takano T, Kang J, Jaiswal JK, Simon SM, Lin JH, Yu Y, Li Y, Yang J, Dienel G, Zielke HR and Nedergaard M (2005). "Receptor-mediated glutamate release from volume sensitive channels in astrocytes." *Proc Natl Acad Sci U S A* **102**(45): 16466-16471.

Tamaki SJ, Jacobs Y, Dohse M, Capela A, Cooper JD, Reitsma M, He D, Tushinski R, Belichenko PV, Salehi A, Mobley W, Gage FH, Huhn S, Tsukamoto AS, Weissman IL and Uchida N (2009). "Neuroprotection of host cells by human central nervous system stem cells in a mouse model of infantile neuronal ceroid lipofuscinosis." *Cell Stem Cell* **5**(3): 310-319.

Tammen I, Houweling PJ, Frugier T, Mitchell NL, Kay GW, Cavanagh JA, Cook RW, Raadsma HW and Palmer DN (2006). "A missense mutation (c.184C>T) in ovine CLN6 causes neuronal ceroid lipofuscinosis in Merino sheep whereas affected South Hampshire sheep have reduced levels of CLN6 mRNA." *Biochim Biophys Acta* **1762**(10): 898-905.

Tanaka K, Tanahashi N, Tsurumi C, Yokota KY and Shimbara N (1997). "Proteasomes and antigen processing." *Adv Immunol* **64**: 1-38.

Tanaka R, Komine-Kobayashi M, Mochizuki H, Yamada M, Furuya T, Migita M, Shimada T, Mizuno Y and Urabe T (2003). "Migration of enhanced green fluorescent protein expressing bone marrow-derived microglia/macrophage into the mouse brain following permanent focal ischemia." *Neuroscience* **117**(3): 531-539.

Tardy C, Sabourdy F, Garcia V, Jalanko A, Therville N, Levade T and Andrieu-Abadie N (2009). "Palmitoyl protein thioesterase 1 modulates tumor necrosis factor alpha-induced apoptosis." *Biochim Biophys Acta* **1793**(7): 1250-1258.

Taub DD and Oppenheim JJ (1994). "Chemokines, inflammation and the immune system." *Therapeutic immunology* **1**(4): 229-246.

Terman A, Kurz T, Navratil M, Arriaga EA and Brunk UT (2010). "Mitochondrial turnover and aging of long-lived postmitotic cells: the mitochondrial-lysosomal axis theory of aging." *Antioxid Redox Signal* **12**(4): 503-535.

Thelen M, Damme M, Schweizer M, Hagel C, Wong AM, Cooper JD, Braulke T and Galliciotti G (2012). "Disruption of the autophagy-lysosome pathway is involved in neuropathology of the nclf mouse model of neuronal ceroid lipofuscinosis." *Plos One* **7**(4): e35493.

Thomas ML (1989). "The leukocyte common antigen family." *Annual Review of Immunology* **7**: 339-369.

Thomas WE (1992). "Brain macrophages: evaluation of microglia and their functions." *Brain Res Brain Res Rev* **17**(1): 61-74.

Thorne RG, Pronk GJ, Padmanabhan V and Frey Ii WH (2004). "Delivery of insulin-like growth factor-I to the rat brain and spinal cord along olfactory and trigeminal pathways following intranasal administration." *Neuroscience* **127**(2): 481-496.

Tian GF, Azmi H, Takano T, Xu Q, Peng W, Lin J, Oberheim N, Lou N, Wang X, Zielke HR, Kang J and Nedergaard M (2005). "An astrocytic basis of epilepsy." *Nat Med* **11**(9): 973-981.

Tian L, Rauvala H and Gahmberg CG (2009). "Neuronal regulation of immune responses in the central nervous system." *Trends in Immunology* **30**(2): 91-99.

TIBDC (1995). "Isolation of a novel gene underlying Batten disease, CLN3. The International Batten Disease Consortium (TIBDC)." *Cell* **82**(6): 949-957.

Toft-Hansen H, Buist R, Sun XJ, Schellenberg A, Peeling J and Owens T (2006). "Metalloproteinases control brain inflammation induced by pertussis toxin in mice overexpressing the chemokine CCL2 in the central nervous system." *J Immunol* **177**(10): 7242-7249.

Toft-Hansen H, Fuchtbauer L and Owens T (2011). "Inhibition of Reactive Astrocytosis in Established Experimental Autoimmune Encephalomyelitis Favors Infiltration by Myeloid Cells Over T Cells and Enhances Severity of Disease." *Glia* **59**(1): 166-176.

Togo T, Akiyama H, Iseki E, Kondo H, Ikeda K, Kato M, Oda T, Tsuchiya K and Kosaka K (2002). "Occurrence of T cells in the brain of Alzheimer's disease and other neurological diseases." *Journal of Neuroimmunology* **124**(1-2): 83-92.

Tonegawa S (1983). "Somatic generation of antibody diversity." *Nature* **302**(5909): 575-581.

Town T, Tan J, Flavell RA and Mullan M (2005). "T-cells in Alzheimer's disease." *NeuroMolecular Medicine* **7**(3): 255-264.

Townsend A and Bodmer H (1989). "Antigen recognition by class I-restricted T lymphocytes." *Annu Rev Immunol* **7**: 601-624.

Trajkovic V, Vuckovic O, Stosic-Grujicic S, Miljkovic D, Popadic D, Markovic M, Bumbasirevic V, Backovic A, Cvetkovic I, Harhaji L, Ramic Z and Mostarica Stojkovic M (2004). "Astrocyte-induced regulatory T cells mitigate CNS autoimmunity." *Glia* **47**(2): 168-179.

Tran EH, Hoekstra K, van Rooijen N, Dijkstra CD and Owens T (1998). "Immune Invasion of the Central Nervous System Parenchyma and Experimental Allergic Encephalomyelitis, But Not Leukocyte Extravasation from Blood, Are Prevented in Macrophage-Depleted Mice." *The Journal of Immunology* **161**(7): 3767-3775.

Trapani JA, Davis J, Sutton VR and Smyth MJ (2000). "Proapoptotic functions of cytotoxic lymphocyte granule constituents in vitro and in vivo." *Current Opinion in Immunology* **12**(3): 323-329.

Trigylidas T, Baronia B, Vassilyadi M and Ventureyra ECG (2008). "Posterior fossa dimension and volume estimates in pediatric patients with Chiari I malformations." *Childs Nervous System* **24**(3): 329-336.

Trinchieri G (1995). "Interleukin-12 - A proinflammatory cytokine with immunoregulatory functions that bridge innate resistance and antigen-specific adaptive immunity." *Annual Review of Immunology* **13**: 251-276.

Troost D, Vandenoord JJ and Dejong J (1990). "Immunohistochemical characterization of the inflammatory infiltrate in Amyotrophic-Lateral-Sclerosis." *Neuropathology and Applied Neurobiology* **16**(5): 401-410.

Trouw LA and Daha MR (2011). "Role of complement in innate immunity and host defense." *Immunol Lett* **138**(1): 35-37.

Tuxworth RI, Vivancos Vr, O'Hare MB and Tear G (2009). "Interactions between the juvenile Batten disease gene, CLN3, and the Notch and JNK signalling pathways." *Human Molecular Genetics* **18**(4): 667-678.

Tyynela J, Cooper JD, Khan MN, Shemilts SJ and Haltia M (2004). "Hippocampal pathology in the human neuronal ceroid-lipofuscinoses: distinct patterns of storage deposition, neurodegeneration and glial activation." *Brain Pathol* **14**(4): 349-357.

Tyynela J, Palmer DN, Baumann M and Haltia M (1993). "Storage of saposins A and D in infantile neuronal ceroid-lipofuscinosis." *FEBS Lett* **330**(1): 8-12.

Tyynela J, Suopanki J, Santavuori P, Baumann M and Haltia M (1997). "Variant late infantile neuronal ceroid-lipofuscinosis: pathology and biochemistry." *J Neuropathol Exp Neurol* **56**(4): 369-375.

Ueno M, Akiguchi I, Hosokawa M, Shinnou M, Sakamoto H, Takemura M and Higuchi K (1997). "Age-related changes in barrier function in mouse brain .2. Accumulation of serum albumin in the olfactory bulb of SAM mice increased with aging." *Archives of Gerontology and Geriatrics* **25**(3): 321-331.

Ueno M, Akiguchi I, Hosokawa M, Shinnou M, Sakamoto H, Takemura M and Higuchi K (1998). "Ultrastructural and permeability features of microvessels in the olfactory bulbs of SAM mice." *Acta Neuropathologica* **96**(3): 261-270.

Ueno M, Dobrogowska DH and Vorbrodt AW (1996). "Immunocytochemical evaluation of the blood-brain barrier to endogenous albumin in the olfactory bulb and pons of senescence-accelerated mice (SAM)." *Histochem Cell Biol* **105**(3): 203-212.

Umansky V, Beckhove P, Rocha M, Kruger A, Crocker PR and Schirrmacher V (1996). "A role for sialoadhesin-positive tissue macrophages in host resistance to lymphoma metastasis in vivo." *Immunology* **87**(2): 303-309.

Unanue ER (1984). "Antigen-presenting function of the macrophage." *Annual Review of Immunology* **2**: 395-428.

Urban D, Thanabalasingam U, Stibenz D, Kaufmann J, Meyborg H, Fleck E, Grafe M and Stawowy P (2011). "CD40/CD4OL interaction induces E-selectin dependent leukocyte adhesion to human endothelial cells and inhibits endothelial cell migration." *Biochem Biophys Res Commun* **404**(1): 448-452.

Uusi-Rauva K, Luiro K, Tanhuanpaa K, Kopra O, Martin-Vasallo P, Kyttala A and Jalanko A (2008). "Novel interactions of CLN3 protein link Batten disease to dysregulation of fodrin-Na+, K+ ATPase complex." *Exp Cell Res* **314**(15): 2895-2905.

Van Breedam W, Delputte PL, Van Gorp H, Misinzo G, Vanderheijden N, Duan X and Nauwynck HJ (2010). "Porcine reproductive and respiratory syndrome virus entry into the porcine macrophage." *J Gen Virol* **91**(Pt 7): 1659-1667.

van de Berg PJ, van Leeuwen EM, ten Berge IJ and van Lier R (2008). "Cytotoxic human CD4+ T cells." *Current Opinion in Immunology* **20**(3): 339-343.

van den Berg TK, Brevé JJ, Damoiseaux JG, Döpp EA, Kelm S, Crocker PR, Dijkstra CD and Kraal G (1992). "Sialoadhesin on macrophages: its identification as a lymphocyte adhesion molecule." *The Journal of Experimental Medicine* **176**(3): 647-655.

van den Berg TK, Nath D, Ziltener HJ, Vestweber D, Fukuda M, van Die I and Crocker PR (2001). "Cutting Edge: CD43 Functions as a T Cell Counterreceptor for the Macrophage Adhesion Receptor Sialoadhesin (Siglec-1)." *The Journal of Immunology* **166**(6): 3637-3640.

van den Berg TK, van Die I, de Lavalette CR, Dopp EA, Smit LD, van der Meide PH, Tilders FJ, Crocker PR and Dijkstra CD (1996). "Regulation of sialoadhesin expression on rat macrophages. Induction by glucocorticoids and enhancement by IFN-beta, IFN-gamma, IL-4, and lipopolysaccharide." *J Immunol* **157**(7): 3130-3138.

van der Spoel AC, Mott R and Platt FM (2008). "Differential sensitivity of mouse strains to an N-alkylated imino sugar: glycosphingolipid metabolism and acrosome formation." *Pharmacogenomics* **9**(6): 717-731.

van der Vliet HJJ, Molling JW, von Blomberg BME, Nishi N, Kolgen W, van den Eertwegh AJM, Pinedo HM, Giaccone G and Scheper RJ (2004). "The immunoregulatory role of CD1d-restricted natural killer T cells in disease." *Clinical Immunology* **112**(1): 8-23.

Varki A and Angata T (2006). "Siglecs--the major subfamily of I-type lectins." *Glycobiology* **16**(1): 1R-27R.

Velinov M, Dolzhanskaya N, Gonzalez M, Powell E, Konidari I, Hulme W, Staropoli JF, Xin W, Wen GY, Barone R, Coppel SH, Sims K, Brown WT and Zuchner S (2012). "Mutations in the gene DNAJC5 cause autosomal dominant Kufs disease in a proportion of cases: study of the Parry family and 8 other families." *Plos One* **7**(1): e29729.

Verkruyse LA and Hofmann SL (1996). "Lysosomal targeting of palmitoyl-protein thioesterase." *J Biol Chem* **271**(26): 15831-15836.

Vesa J, Hellsten E, Verkruyse LA, Camp LA, Rapola J, Santavuori P, Hofmann SL and Peltonen L (1995). "Mutations in the palmitoyl protein thioesterase gene causing infantile neuronal ceroid lipofuscinosis." *Nature* **376**(6541): 584-587.

Virmani T, Gupta P, Liu X, Kavalali ET and Hofmann SL (2005). "Progressively reduced synaptic vesicle pool size in cultured neurons derived from neuronal ceroid lipofuscinosis-1 knockout mice." *Neurobiol Dis* **20**(2): 314-323.

Vitale C, Romagnani C, Falco M, Ponte M, Vitale M, Moretta A, Bacigalupo A, Moretta L and Mingari MC (1999). "Engagement of p75/AIRM1 or CD33 inhibits the proliferation of normal or leukemic myeloid cells." *Proc Natl Acad Sci U S A* **96**(26): 15091-15096.

Vitner EB, Platt FM and Futerman AH (2010). "Common and uncommon pathogenic cascades in lysosomal storage diseases." *J Biol Chem* **285**(27): 20423-20427.

Vogt J, Paul F, Aktas O, Muller-Wielsch K, Dorr J, Dorr S, Bharathi BS, Glumm R, Schmitz C, Steinbusch H, Raine CS, Tsokos M, Nitsch R and Zipp F (2009). "Lower motor neuron loss in multiple sclerosis and experimental autoimmune encephalomyelitis." *Ann Neurol* **66**(3): 310-322.

Volterra A and Meldolesi J (2005). "Astrocytes, from brain glue to communication elements: the revolution continues." *Nat Rev Neurosci* **6**(8): 626-640.

von Gunten S, Yousefi S, Seitz M, Jakob SM, Schaffner T, Seger R, Takala J, Villiger PM and Simon HU (2005). "Siglec-9 transduces apoptotic and nonapoptotic death signals into neutrophils depending on the proinflammatory cytokine environment." *Blood* **106**(4): 1423-1431.

von Schantz C, Kielar C, Hansen SN, Pontikis CC, Alexander NA, Kopra O, Jalanko A and Cooper JD (2009). "Progressive thalamocortical neuron loss in Cln5 deficient mice: Distinct effects in Finnish variant late infantile NCL." *Neurobiology of Disease* **34**(2): 308-319.

Vorbrodt AW, Dobrogowska DH, Ueno M and Tarnawski M (1995). "A quantitative immunocytochemical study of blood-brain barrier to endogenous albumin in cerebral cortex and hippocampus of senescence-accelerated mice (SAM)." *Folia Histochem Cytobiol* **33**(4): 229-237.

Voskuhl RR, Peterson RS, Song B, Ao Y, Morales LBJ, Tiwari-Woodruff S and Sofroniew MV (2009). "Reactive Astrocytes Form Scar-Like Perivascular Barriers to Leukocytes during Adaptive Immune Inflammation of the CNS." *The Journal of Neuroscience* **29**(37): 11511-11522.

Wada R, Tifft CJ and Proia RL (2000). "Microglial activation precedes acute neurodegeneration in Sandhoff disease and is suppressed by bone marrow transplantation." *Proc Natl Acad Sci U S A* **97**(20): 10954-10959.

Wake H, Moorhouse AJ, Jinno S, Kohsaka S and Nabekura J (2009). "Resting microglia directly monitor the functional state of synapses in vivo and determine the fate of ischemic terminals." *J Neurosci* **29**(13): 3974-3980.

Wakim LM, Gebhardt T, Heath WR and Carbone FR (2008). "Cutting edge: local recall responses by memory T cells newly recruited to peripheral nonlymphoid tissues." *J Immunol* **181**(9): 5837-5841.

Walkley SU (2007). "Pathogenic mechanisms in lysosomal disease: a reappraisal of the role of the lysosome." *Acta Paediatr Suppl* **96**(455): 26-32.

Walkley SU (2009). "Pathogenic cascades in lysosomal disease-Why so complex?" *J Inherit Metab Dis* **32**(2): 181-189.

Walkley SU and Vanier MT (2009). "Secondary lipid accumulation in lysosomal disease." *Biochim Biophys Acta* **1793**(4): 726-736.

Walter BA, Valera VA, Takahashi S and Ushiki T (2006). "The olfactory route for cerebrospinal fluid drainage into the peripheral lymphatic system." *Neuropathol Appl Neurobiol* **32**(4): 388-396.

Wasser CR, Ertunc M, Liu X and Kavalali ET (2007). "Cholesterol-dependent balance between evoked and spontaneous synaptic vesicle recycling." *J Physiol* **579**(Pt 2): 413-429.

Watt SM, Gschmeissner SE and Bates PA (1995). "PECAM-1 - Its expression and function as a cell-adhesion molecule on hematopoietic and endothelial cells." *Leukemia & Lymphoma* **17**(3-4): 229-244.

Watts C (2001). "Antigen processing in the endocytic compartment." *Curr Opin Immunol* **13**(1): 26-31.

Weaver CT, Harrington LE, Mangan PR, Gavrieli M and Murphy KM (2006). "Th17: an effector CD4 T cell lineage with regulatory T cell ties." *Immunity* **24**(6): 677-688.

Wei H, Zhang Z, Saha A, Peng S, Chandra G, Quezado Z and Mukherjee AB (2011). "Disruption of adaptive energy metabolism and elevated ribosomal p-S6K1 levels contribute to INCL pathogenesis: partial rescue by resveratrol." *Hum Mol Genet* **20**(6): 1111-1121.

Weimer JM, Benedict JW, Elshatory YM, Short DW, Ramirez-Montealegre D, Ryan DA, Alexander NA, Federoff HJ, Cooper JD and Pearce DA (2007). "Alterations in striatal dopamine catabolism precede loss of substantia nigra neurons in a mouse model of juvenile neuronal ceroid lipofuscinosis." *Brain Res* **1162**: 98-112.

Weimer JM, Benedict JW, Getty AL, Pontikis CC, Lim MJ, Cooper JD and Pearce DA (2009). "Cerebellar defects in a mouse model of juvenile neuronal ceroid lipofuscinosis." *Brain Research* **1266**: 93-107.

Weimer JM, Custer AW, Benedict JW, Alexander NA, Kingsley E, Federoff HJ, Cooper JD and Pearce DA (2006). "Visual deficits in a mouse model of Batten disease are

the result of optic nerve degeneration and loss of dorsal lateral geniculate thalamic neurons." *Neurobiol Dis* **22**(2): 284-293.

Wekerle H, Linington C, Lassmann H and Meyermann R (1986). "Cellular immune reactivity within the CNS." *Trends in Neurosciences* **9**(6): 271-277.

Wekerle H, Sun D, Oropeza-Wekerle RL and Meyermann R (1987). "Immune reactivity in the nervous system: modulation of T-lymphocyte activation by glial cells." *J Exp Biol* **132**: 43-57.

Weller RO, Kida S and Zhang ET (1993). Pathways of fluid drainage from the brain - morphological aspects and immunological significance in rat and man. *Udine*, Edizioni Centauro.

West MJ (1993). "New stereological methods for counting neurons." *Neurobiology of Aging* **14**(4): 275-285.

West MJ (2001). "Design based stereological methods for estimating the total number of objects in histological material." *Folia morphologica* **60**(1): 11-19.

West MJ, Slomianka L and Gundersen HJG (1991). "Unbiased stereological estimation of the total number of neurons in the subdivisions of the rat hippocampus using the optical fractionator." *Anatomical Record* **231**(4): 482-497.

West MJ and Thomas Sutula AP (2002). Design-based stereological methods for counting neurons. Progress in Brain Research, Elsevier. **Volume 135:** 43-51.

Westermarck T, Aberg L, Santavuori P, Antila E, Edlund P and Atroshi F (1997). "Evaluation of the possible role of coenzyme Q10 and vitamin E in juvenile neuronal ceroid-lipofuscinosis (JNCL)." *Mol Aspects Med* **18 Suppl**: S259-262.

Wiedemann A, Depoil D, Faroudi M and Valitutti S (2006). "Cytotoxic T lymphocytes kill multiple targets simultaneously via spatiotemporal uncoupling of lytic and stimulatory synapses." *Proc Natl Acad Sci U S A* **103**(29): 10985-10990.

Wiesel M and Oxenius A (2012). "From crucial to negligible: Functional CD8(+) T-cell responses and their dependence on CD4(+) T-cell help." *European Journal of Immunology* **42**(5): 1080-1088.

Wiesel M, Walton S, Richter K and Oxenius A (2009). "Virus-specific CD8 T cells: activation, differentiation and memory formation." *APMIS* **117**(5-6): 356-381.

Wilcox WR (2004). "Lysosomal storage disorders: the need for better pediatric recognition and comprehensive care." *J Pediatr* **144**(5 Suppl): S3-14.

Wilhelmsson U, Bushong EA, Price DL, Smarr BL, Phung V, Terada M, Ellisman MH and Pekny M (2006). "Redefining the concept of reactive astrocytes as cells that remain within their unique domains upon reaction to injury." *Proc Natl Acad Sci U S A* **103**(46): 17513-17518.

Wilhelmsson U, Li L, Pekna M, Berthold CH, Blom S, Eliasson C, Renner O, Bushong E, Ellisman M, Morgan TE and Pekny M (2004). "Absence of glial fibrillary acidic protein and vimentin prevents hypertrophy of astrocytic processes and improves post-traumatic regeneration." *J Neurosci* **24**(21): 5016-5021.

Williams A, Piaton G and Lubetzki C (2007). "Astrocytes--friends or foes in multiple sclerosis?" *Glia* **55**(13): 1300-1312.

Williams AF and Barclay AN (1988). "The immunoglobulin superfamily--domains for cell surface recognition." *Annu Rev Immunol* **6**: 381-405.

Williams RE, Aberg L, Autti T, Goebel HH, Kohlschutter A and Lonnqvist T (2006). "Diagnosis of the neuronal ceroid lipofuscinoses: an update." *Biochim Biophys Acta* **1762**(10): 865-872.

Williams RE and Mole SE (2012). "New nomenclature and classification scheme for the neuronal ceroid lipofuscinoses." *Neurology* **79**(2): 183-191.

Wilschanski M, Yahav Y, Yaacov Y, Blau H, Bentur L, Rivlin J, Aviram M, Bdolah-Abram T, Bebok Z, Shushi L, Kerem B and Kerem E (2003). "Gentamicin-induced correction of CFTR function in patients with cystic fibrosis and CFTR stop mutations." *N Engl J Med* **349**(15): 1433-1441.

Wilson EH, Harris TH, Mrass P, John B, Tait ED, Wu GF, Pepper M, Wherry EJ, Dzierzinski F, Roos D, Haydon PG, Laufer TM, Weninger W and Hunter CA (2009). "Behavior of Parasite-Specific Effector CD8(+) T Cells in the Brain and Visualization of a Kinesis-Associated System of Reticular Fibers." *Immunity* **30**(2): 300-311.

Wilson EH, Weninger W and Hunter CA (2010). "Trafficking of immune cells in the central nervous system." *Journal of Clinical Investigation* **120**(5): 1368-1379.

Winchester B, Vellodi A and Young E (2000). "The molecular basis of lysosomal storage diseases and their treatment." *Biochem Soc Trans* **28**(2): 150-154.

Wininger AF (2012). Magnetic resonance volumetrics, diffusion tensor imaging and spectroscopy as biomarkers to assess efficacy of gene therapy in a canine model for LINCL. 13th International Conference on Neuronal Ceroid Lipofuscinoses (Batten Disease) (NCL 2012), Royal Holloway College, London, UK, Oral presentation 41.

Wong AM, Rahim AA, Waddington SN and Cooper JD (2010). "Current therapies for the soluble lysosomal forms of neuronal ceroid lipofuscinosis." *Biochem Soc Trans* **38**(6): 1484-1488.

Wong GHW, Bartlett PF, Clarklewis I, Battye F and Schrader JW (1984). "Inducible expression of H-2 and IA antigens on brain-cells." *Nature* **310**(5979): 688-691.

Worgall S, Sondhi D, Hackett NR, Kosofsky B, Kekatpure MV, Neyzi N, Dyke JP, Ballon D, Heier L, Greenwald BM, Christos P, Mazumdar M, Souweidane MM, Kaplitt MG and Crystal RG (2008). "Treatment of late infantile neuronal ceroid lipofuscinosis by CNS administration of a serotype 2 adeno-associated virus expressing CLN2 cDNA." *Hum Gene Ther* **19**(5): 463-474.

Wraith JE (2004). "The clinical presentation of lysosomal storage disorders." *Acta Neurol Taiwan* **13**(3): 101-106.

Wu C, Rauch U, Korpos E, Song J, Loser K, Crocker PR and Sorokin LM (2009). "Sialoadhesin-Positive Macrophages Bind Regulatory T Cells, Negatively

Controlling Their Expansion and Autoimmune Disease Progression." *Journal of Immunology* **182**(10): 6508-6516.

Wu YP, Matsuda J, Kubota A and Suzuki K (2000). "Infiltration of hematogenous lineage cells into the demyelinating central nervous system of twitcher mice." *Journal of Neuropathology and Experimental Neurology* **59**(7): 628-639.

Wyss-Coray T and Mucke L (2002). "Inflammation in neurodegenerative disease--a double-edged sword." *Neuron* **35**(3): 419-432.

Yamada S, Depasquale M, Patlak CS and Cserr HF (1991). "Albumin outflow into deep cervical lymph from different regions of the rabbit brain." *American Journal of Physiology* **261**(4): H1197-H1204.

Yamashima T and Oikawa S (2009). "The role of lysosomal rupture in neuronal death." *Prog Neurobiol* **89**(4): 343-358.

Yanagawa M, Tsukuba T, Nishioku T, Okamoto Y, Okamoto K, Takii R, Terada Y, Nakayama KI, Kadowaki T and Yamamoto K (2007). "Cathepsin E deficiency induces a novel form of lysosomal storage disorder showing the accumulation of lysosomal membrane sialoglycoproteins and the elevation of lysosomal pH in macrophages." *J Biol Chem* **282**(3): 1851-1862.

Yeh TH, Lee da Y, Gianino SM and Gutmann DH (2009). "Microarray analyses reveal regional astrocyte heterogeneity with implications for neurofibromatosis type 1 (NF1)-regulated glial proliferation." *Glia* **57**(11): 1239-1249.

Yoon DH, Kwon OY, Mang JY, Jung MJ, Kim do Y, Park YK, Heo TH and Kim SJ (2011). "Protective potential of resveratrol against oxidative stress and apoptosis in Batten disease lymphoblast cells." *Biochem Biophys Res Commun* **414**(1): 49-52.

York MR, Nagai T, Mangini AJ, Lemaire R, van Seventer JM and Lafyatis R (2007). "A macrophage marker, Siglec-1, is increased on circulating monocytes in patients with systemic sclerosis and induced by type I interferons and toll-like receptor agonists." *Arthritis Rheum* **56**(3): 1010-1020.

Yuan H, Gaber MW, McColgan T, Naimark MD, Kiani MF and Merchant TE (2003). "Radiation-induced permeability and leukocyte adhesion in the rat blood-brain barrier: modulation with anti-ICAM-1 antibodies." *Brain Res* **969**(1-2): 59-69.

Zaffaroni M, Gallo L, Ghezzi A and Cazzullo CL (1991). "CD4+ Lymphocyte subsets in the cerebrospinal-fluid of Multiple-Sclerosis and noninflammatory neurological diseases." *J Neurol* **238**(4): 209-211.

Zeman W and Dyken P (1969). "Neuronal ceroid-lipofuscinosis (Batten's disease): relationship to amaurotic family idiocy?" *Pediatrics* **44**(4): 570-583.

Zeromski J, Mozer-Lisewska I and Kowala-Piaskowska A (2011). "Innate and adaptive immunity in viral infections." *Central European Journal of Immunology* **36**(4): 298-302.

Zhang ET, Richards HK, Kida S and Weller RO (1992). "Directional and compartmentalized drainage of interstitial fluid and cerebrospinal fluid from the rat-brain." *Acta Neuropathologica* **83**(3): 233-239.

Zhang H, Wang FW, Yao LL and Hao AJ (2011). "Microglia--friend or foe." *Front Biosci (Schol Ed)* **3**: 869-883.

Zhang J, Zhao J, Jiang WJ, Shan XW, Yang XM and Gao JG (2012). "Conditional gene manipulation: Cre-ating a new biological era." *J Zhejiang Univ Sci B* **13**(7): 511-524.

Zhang L, Sheng R and Qin Z (2009). "The lysosome and neurodegenerative diseases." *Acta Biochim Biophys Sin (Shanghai)* **41**(6): 437-445.

Zhang Z, Butler JD, Levin SW, Wisniewski KE, Brooks SS and Mukherjee AB (2001). "Lysosomal ceroid depletion by drugs: therapeutic implications for a hereditary neurodegenerative disease of childhood." *Nat Med* **7**(4): 478-484.

Zhang Z, Lee YC, Kim SJ, Choi MS, Tsai PC, Saha A, Wei H, Xu Y, Xiao YJ, Zhang P, Heffer A and Mukherjee AB (2007). "Production of lysophosphatidylcholine by cPLA2 in the brain of mice lacking PPT1 is a signal for phagocyte infiltration." *Hum Mol Genet* **16**(7): 837-847.

Zhang Z, Lee YC, Kim SJ, Choi MS, Tsai PC, Xu Y, Xiao YJ, Zhang P, Heffer A and Mukherjee AB (2006). "Palmitoyl-protein thioesterase-1 deficiency mediates the activation of the unfolded protein response and neuronal apoptosis in INCL." *Hum Mol Genet* **15**(2): 337-346.

Zheng J, Yan T, Feng Y and Zhai Q (2010). "Involvement of lysosomes in the early stages of axon degeneration." *Neurochem Int* **56**(3): 516-521.

Zheng Y, Rozengurt N, Ryazantsev S, Kohn DB, Satake N and Neufeld EF (2003). "Treatment of the mouse model of mucopolysaccharidosis I with retrovirally transduced bone marrow." *Mol Genet Metab* **79**(4): 233-244.

Zhu J and Paul WE (2010). "Heterogeneity and plasticity of T helper cells." *Cell Res* **20**(1): 4-12.

Zhu J, Yamane H and Paul WE (2010). "Differentiation of effector CD4 T cell populations (*)." *Annu Rev Immunol* **28**: 445-489.

Zhu JF and Paul WE (2008). "CD4 T cells: fates, functions, and faults." *Blood* **112**(5): 1557-1569.

Zipp F and Aktas O (2006). "The brain as a target of inflammation: common pathways link inflammatory and neurodegenerative diseases." *Trends Neurosci* **29**(9): 518-527.

Zola H, Swart B, Banham A, Barry S, Beare A, Bensussan A, Boumsell L, D. Buckley C, BÃ¼hring H-Jr, Clark G, Engel P, Fox D, Jin B-Q, Macardle PJ, Malavasi F, Mason D, Stockinger H and Yang X (2007). "CD molecules 2006 â€" Human cell differentiation molecules." *Journal of Immunological Methods* **319**(1-2): 1-5.

Zozulya AL, Ortler S, Lee J, Weidenfeller C, Sandor M, Wiendl H and Fabry Z (2009). "Intracerebral Dendritic Cells Critically Modulate Encephalitogenic versus Regulatory Immune Responses in the CNS." *Journal of Neuroscience* **29**(1): 140-152.

Appendices

Appendix I

Volume measurements in Infantile and Juvenile NCL brains

To be able to convert total lymphocyte counts into lymphocyte density values (see **Figure 21** and **Figure 27** in **Chapter 3**), we performed volume measurements of the entire brain volume and each rostrocaudally defined brain level of *Ppt1*$^{-/-}$, *Cln3*$^{-/-}$ and age-matched wildtype brains using the unbiased Cavalieri method (see **section 2.6a** in **Chapter 2**). To date, previous volume measurements in *Ppt1*$^{-/-}$ or *Cln3*$^{-/-}$ mice only focused on regions that may be involved in these diseases, and no overall assessment of brain volume or how it was affected at different rostrocaudal levels has been attempted ((Bible *et al.*, 2004; Pontikis *et al.*, 2005); JD Cooper, personal communication). Therefore, this rostrocaudal approach represented a new way of analysing regional atrophy in NCL brains, with which we could confirm and extend previous findings (Bible *et al.*, 2004; Pontikis *et al.*, 2005; Kielar *et al.*, 2007).

a) Reduced brain volume in *Ppt1*$^{-/-}$ mice

The total volume of each *Ppt1*$^{-/-}$ brain and the volume of each rostrocaudal level I to V (see **Table 6** and **Figure 14** in **Chapter 2**) were measured in Nissl stained sections using the Cavalieri method. By adopting this approach we were able to describe for the first time the rostrocaudal distribution of atrophy within the brain of 1, 3, 5 and 7 month old animals. This added a new perspective to our previously neuroanatomically based description of regional atrophy in these mice (Kielar *et al.*, 2007), and also allowed us to calculate lymphocyte density at each rostrocaudal level.

Compared to our previous analysis (Kielar *et al.*, 2007), our rostrocaudal level based analysis revealed that a significant reduction in total brain volume could already be detected from 5 months onwards in *Ppt1*$^{-/-}$ mice, compared to age-matched controls (**Appendix I: Figure 77A**). In terms of the rostrocaudal breakdown, these volume differences appeared initially in level III (forebrain with hippocampal structures) and II (forebrain from begin of cortex to first appearance of hippocampus) between 3 to 5 months of age, becoming more widespread throughout almost the entire brain at 7 months of age (**Appendix I: Figure 77B**). These regionally specific susceptibilities of levels III and II correlate with the brain regions of the thalamus, hippocampus and somatosensory cortex of *Ppt1*$^{-/-}$ mice that appear to be affected earliest. Therefore, speculatively, these volume changes could be explained by neuron loss, which

succeeds pronounced astrocytosis and microglial activations in these brain regions (Kielar *et al.*, 2007).

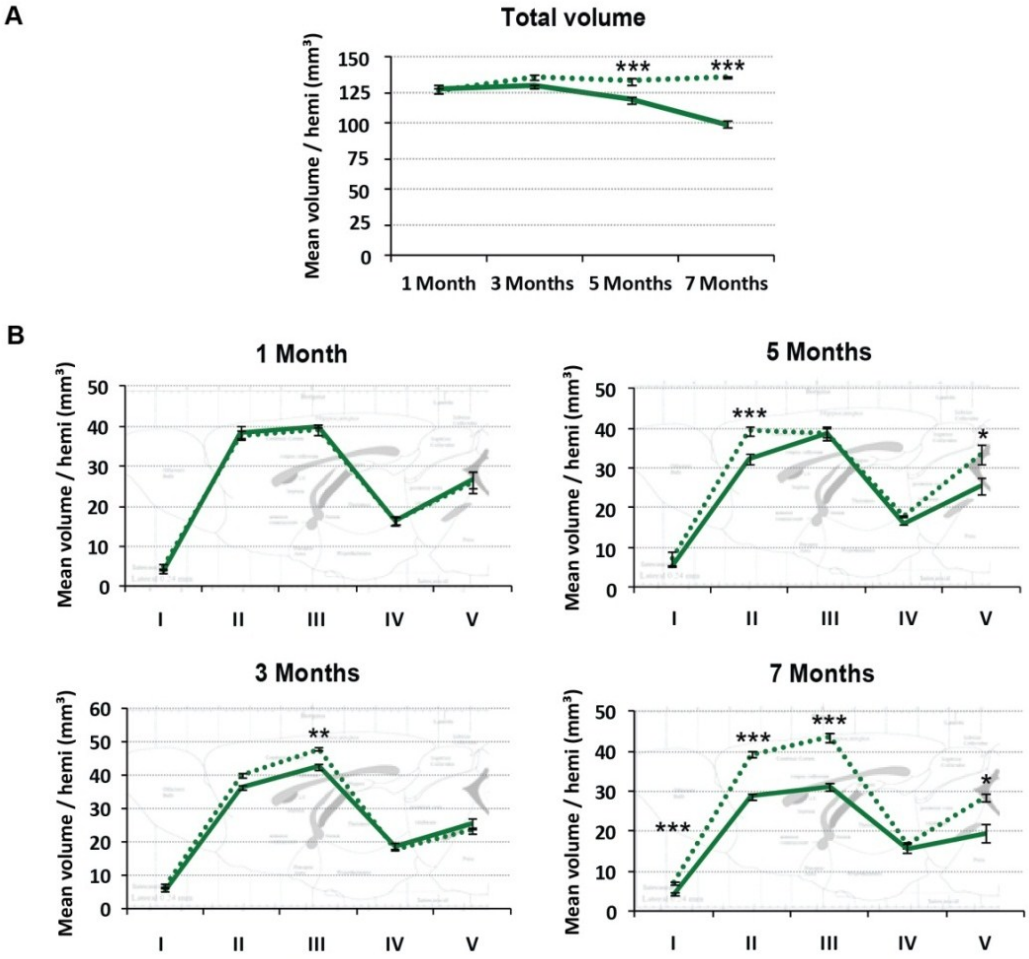

Appendix I: Figure 77. Progressive reduction in the volume of *Ppt1*$^{-/-}$ brains. Unbiased Cavalieri estimates of total brain volume (A) and regional brain volume (B) of *Ppt1*$^{-/-}$(—) and age-matched wildtype (WT) (····) mice at 1, 3, 5 and 7 months of age, calculated as mean volume/hemisphere in mm^3. (A) A significant decrease in total brain volume was seen from 5 months onwards in mutant compared to WT mice. (B) Rostrocaudal effects upon regional volume were revealed in regional volume measurements. A significant decrease in regional volume was seen from 3 months onwards in mutant animals compared to WT mice - starting in level III and level II until finally spreading throughout the brain. Brain levels: I = Olfactory bulb, II = Forebrain until *hippocampus*, III = Hippocampal forebrain, IV = Midbrain with *superior colliculus*, V = Midbrain with *pons*. Statistics: Two-way ANOVA with Bonferroni post hoc test, *p<0.05, **p<0.01, ***p<0.001. Data shown as mean ± SEM, n =5.

b) Reduced brain volume in *Cln3*$^{-/-}$ mice

To be able to calculate the mean lymphocyte density of each T-cell subset (CD8+ve cytotoxic T-cells and CD4+ve T-helper cells) throughout the brain, the same volumetric analysis performed in *Ppt1*$^{-/-}$ mice (see **section a** above) was applied to Nissl stained sections from *Cln3*$^{-/-}$ mice and wildtype controls at 6.5, 12 and 21

months of age. This allowed us to define changes in whole brain volume and rostrocaudal levels I to V (see **Table 6** and **Figure 14** in **Chapter 2**) at these ages.

A significant reduction in total brain volume was first detected at 21 months of age in *Cln3*$^{-/-}$ mice compared to age-matched controls (see **Appendix I: Figure 78A**). By breaking the brain into rostrocaudal levels, we determined that this reduced volume at 21 months of age occurred mostly within level III, which includes the thalamus, hippocampus and somatosensory cortex – all regions that show an early immune reaction in terms of astrocytosis and microglial activation (see **Appendix I: Figure 78B**).

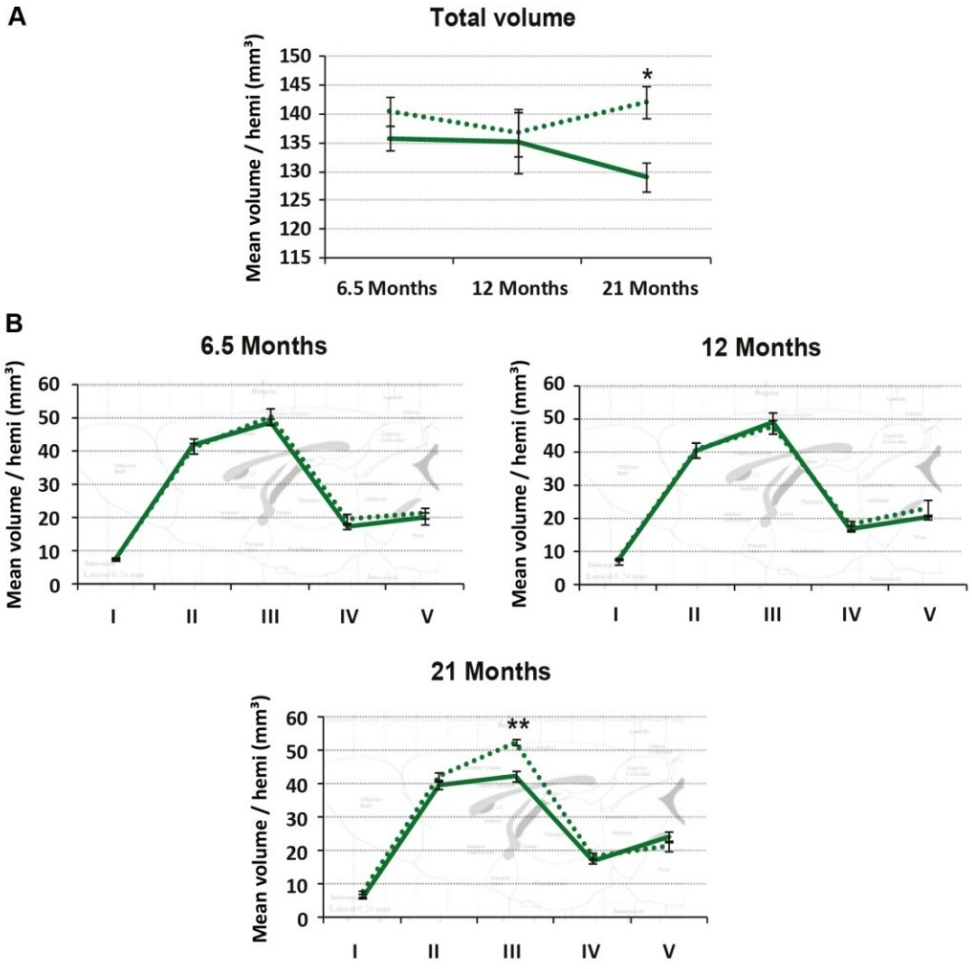

Appendix I: Figure 78. Late onset reduction in the volume of *Cln3*$^{-/-}$ brains. Unbiased Cavalieri estimates of total brain volume (A) and regional brain volume (B) of *Cln3*$^{-/-}$(—) and age-matched wildtype (WT) (····) mice at 6.5, 12 and 21 months of age, calculated as mean volume/hemisphere in mm^3. (A) A significant decrease in total brain volume was only seen at 21 months of age in mutant compared to WT mice. (B) Rostrocaudal effects upon regional volume were revealed in regional volume measurements. A significant decrease in regional volume was seen at level III of 21 months old mutant mice compared to WT mice. Brain levels: I = Olfactory bulb, II = Forebrain until *hippocampus*, III = Hippocampal forebrain, IV = Midbrain with *superior colliculus*, V = Midbrain with *pons*. Statistics: Two-way ANOVA with Bonferroni post hoc test, *p<0.05, **p<0.01. Data shown as mean ± SEM, n =5.

Taken together, the volume measurements presented in this study not only enabled the calculation of lymphocyte density of both subsets of T-cells, but also revealed a new rostrocaudal perspective to the volumetric changes in *Ppt1*$^{-/-}$ and *Cln3*$^{-/-}$ mice. With our new approach we were able to demonstrate an earlier onset of volume changes in *Ppt1*$^{-/-}$ mice with regional volume reductions already seen at 3 months of age, and entire brain volume changes at 5 months of age compared to findings of previous studies ((Bible *et al.*, 2004; Kielar *et al.*, 2007); JD Cooper, personal communication). Furthermore, as our study included the oldest *Cln3* deficient brains analysed so far, our volumetric data on 21 month old *Cln3*$^{-/-}$ mice represent the first time that entire (and regional) brain volume reductions have been demonstrated in aged JNCL mice.

Appendix II

Increased neuron survival in the cortex of *Ppt1*$^{-/-}$/*Rag-1*$^{-/-}$ mice

After demonstrating significantly increased neuron survival in the thalamic *ventral posterior nucleus* (*VPM/VPL*) of *Ppt1*$^{-/-}$/*Rag-1*$^{-/-}$ mice at 3 months of age, compared to age-matched *Ppt1*$^{-/-}$ mice (see **Figure 40** in **Chapter 4**), we extended our analysis to the primary barrelfield of the somatosensory cortex (*S1BF*) which receives projections from *VPM/VPL*. Progressive neuron loss in the *S1BF* has previously been shown to occur subsequent to events within the thalamus (Kielar *et al.*, 2007). Furthermore, our data demonstrated that weaker glial activation occurs in the *S1BF* of *Ppt1*$^{-/-}$ mice, compared to the thalamus (see **Figure 33**, **Figure 35**, **Figure 37** and **Figure 39** in **Chapter 4**). Thus, we wanted to investigate what effect this lack of lymphocytes has on neuron survival in the *S1BF*, as an example of a brain region that contains less glial activation and is affected later in disease progression.

We quantified the number of lamina V neurons in *S1BF* of 3, 5 and 7 month old *Ppt1*$^{-/-}$, *Ppt1*$^{-/-}$/*Rag-1*$^{-/-}$, *Rag-1*$^{-/-}$ and wildtype mice using the unbiased optical fractionator method (see **section 2.6c** in **Chapter 2**). This analysis incorporated the same mice that have been characterised in **Chapter 4**, but these cortical neuron counts were conducted by Steven Duckett within the scope of his MSc project.

Whereas at 3 months of age no statistical difference was detected in the number of lamina V *S1BF* neurons between any of the genotypes, *Ppt1*$^{-/-}$ mice displayed a progressive loss of these neurons from 5 months onwards (see **Appendix II: Figure 79**). In contrast, the neuron loss of *Ppt1*$^{-/-}$/*Rag-1*$^{-/-}$ double knockout mice was rescued by the absence of adaptive immune cells at 5 months of age (see **Appendix II: Figure 79B**). Likewise, the number of lamina V *S1BF* neurons in these double mutant mice did not differ from those of wildtype mice at this time point. However, by 7 months of age this protective effect did not persist, and there was no difference in the number of lamina V *S1BF* neurons between *Ppt1*$^{-/-}$/*Rag-1*$^{-/-}$ double knockout and *Ppt1*$^{-/-}$ mice, with both strains of mutant mice showing similar, significant degrees of neuron loss compared to age matched control mice (see **Appendix II: Figure 79C**).

These data revealed that the genetic removal of adaptive immune cells also leads to reduced neuron loss in the *S1BF* sub-region of the cortex, but in a delayed manner, compared to events in the thalamus (see **Figure 40** in **Chapter 4**). These findings are consistent with our *S1BF* thickness and cortical volume measurements in **Chapter 4**,

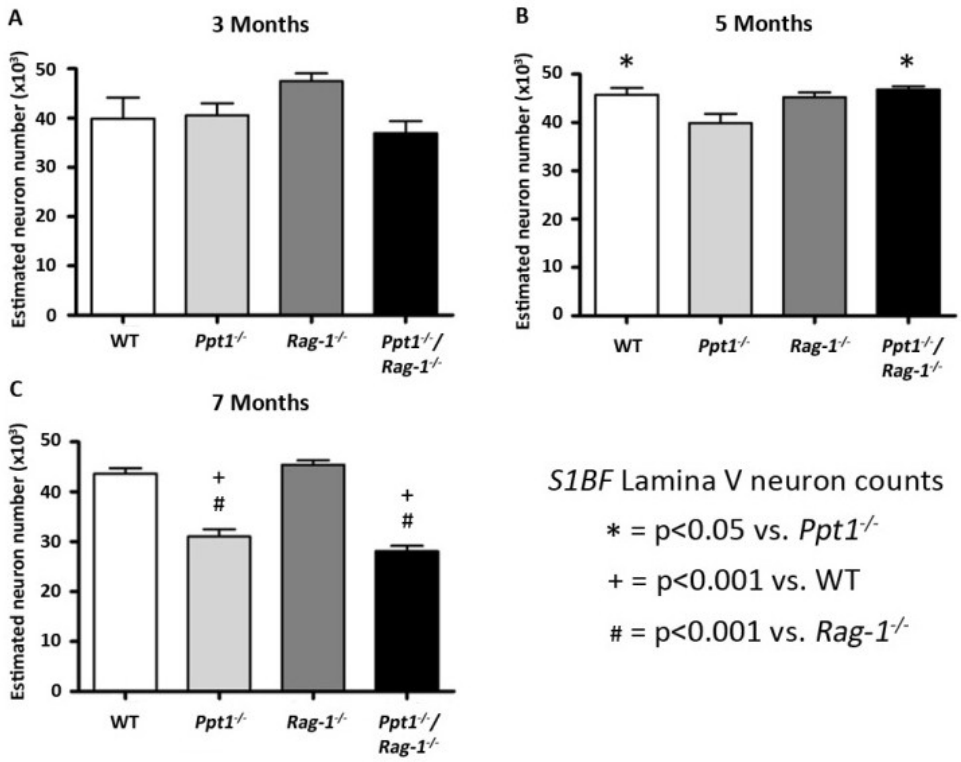

Appendix II: Figure 79. Progressive neuron loss in lamina V of the somatosensory barrel field (*S1BF*) cortex of *Ppt1*$^{-/-}$ and *Ppt1*$^{-/-}$*/Rag-1*$^{-/-}$ double knockout mice. Unbiased optical fractionator estimates of number of Nissl stained cortical neurons in lamina V of the *S1BF* of *Ppt1*$^{-/-}$, *Ppt1*$^{-/-}$*/Rag-1*$^{-/-}$, *Rag-1*$^{-/-}$ and age-matched wildtype (WT) control mice at different stages of disease progression ((A) 3, (B) 5 and (C) 7 months). Neuron loss was significantly slowed down in *Ppt1*$^{-/-}$*/Rag-1*$^{-/-}$ mice compared to single mutant *Ppt1* mice. Significantly more neurons were present in *Ppt1*$^{-/-}$*/Rag-1*$^{-/-}$ mice at 5 months of age, compared to *Ppt1*$^{-/-}$ mice. Whereas no difference between the genotypes could be detected at 3 months of age, *Ppt1*$^{-/-}$ mice displayed significant neuron loss from 5 months onwards, compared to WT mice. In contrast, the number of lamina V neurons in *Ppt1*$^{-/-}$*/Rag-1*$^{-/-}$ mice resembled WT values until 5 months of age, and only showed significant loss at 7 months of age. *Rag-1*$^{-/-}$ and WT mice showed no significant difference in neuron numbers at any age. Statistics: One-way ANOVA with Bonferroni post hoc test, * indicate significance compared to *Ppt1*$^{-/-}$ mice ($p<0.05$), + indicate significance compared to WT mice ($p<0.001$), # indicate significance compared to *Rag-1*$^{-/-}$ mice ($p<0.001$). Data shown as mean ± SEM, n =5. (Graph adapted from S Duckett, MSc thesis.)

which demonstrated a similar delay in disease progression in *Ppt1*$^{-/-}$*/Rag-1*$^{-/-}$ mice, compared to *Ppt1*$^{-/-}$ mice (see **Figure 41** and **Figure 42** in **Chapter 4**). In other words, collectively these data confirmed that the adaptive immune cells have a pathogenic influence on neuron survival, not only in the thalamus, but also in the *S1BF* cortex of *Ppt1*$^{-/-}$ mice. However, in general adaptive immune cells seem to have a similar effect on neuron survival in both brain regions. In the thalamus and the *S1BF* of *Ppt1*$^{-/-}$*/Rag-1*$^{-/-}$ mice neuron survival was only improved at the time point when neuron loss would normally start in this brain region of *Ppt1*$^{-/-}$ mice, and this beneficial effect on neurodegeneration vanished with disease progression. Thus, our cortical data on neuron survival also highlight that, in addition to adaptive immune responses, other driving forces must contribute to disease pathogenesis in INCL mice (see **section 7.4** in **Chapter 7** for discussion).